Fuel Cell Systems

Symposia sponsored by the
Division of Fuel
Chemistry at the 145th
and 146th Meetings
of the American Chemical Society
New York, N.Y., Sept. 12–13, 1963
Philadelphia, Pa., April 6–7, 1964

George J. Young, and Henry R. Linden,
Symposia Chairmen

ADVANCES IN CHEMISTRY SERIES **47**

AMERICAN CHEMICAL SOCIETY
WASHINGTON, D.C. 1965

Publication Date: January 1, 1969 | doi: 10.1021/ba-1965-0047.fw001

In Fuel Cell Systems; Young, G., el al.;
Advances in Chemistry; American Chemical Society: Washington, DC, 1969.

Publication Date: January 1, 1969 | doi: 10.1021/ba-1965-0047.fw001

Copyright © 1965

American Chemical Society

All Rights Reserved

Library of Congress Catalog Card 65–16399

PRINTED IN THE UNITED STATES OF AMERICA

American Chemical Society
Library
1155 16th St., N.W.
Washington, D.C. 20036

In Fuel Cell Systems; Young, G., el al.;
Advances in Chemistry; American Chemical Society: Washington, DC, 1969.

Advances in Chemistry Series

Robert F. Gould, *Editor*

Advisory Board

Fred Basolo

Raymond F. Boyer

Jack Halpern

George W. Irving

Amel R. Menotti

C. M. Sliepcevich

Leo H. Sommer

Fred R. Whaley

William A. Zisman

AMERICAN CHEMICAL SOCIETY

APPLIED PUBLICATIONS

Publication Date: January 1, 1969 | doi: 10.1021/ba-1965-0047.fw001

Publication Date: January 1, 1969 | doi: 10.1021/ba-1965-0047.fw001

FOREWORD

ADVANCES IN CHEMISTRY SERIES was founded in 1949 by the American Chemical Society as an outlet for symposia and collections of data in special areas of topical interest that could not be accommodated in the Society's journals. It provides a medium for symposia that would otherwise be fragmented, their papers distributed among several journals or not published at all. Papers are reviewed critically according to ACS editorial standards and receive the careful attention and processing characteristic of ACS publications.

PREFACE

During the past decade, research and development work on fuel cells has grown tremendously. The total number of programs in late 1963 was cited as being at least 200 (*1*). Hydrogen-oxygen fuel cells have emerged from the research laboratory and are finding functional applications in space programs. Fuel cells based on light hydrocarbons are being intensively investigated and subjected to engineering design and development. Work on fuel cells for industrial, motive, residential, and portable power units is being conducted on an increasing scale. Support for this is being provided by both government and private sources; however, much of it is being supplied by the Federal Government for military reasons and in the Gemini and Apollo programs of the National Aeronautics and Space Administration. Although fuel cells are finding important uses in military and space applications, significant commercial applications are believed to be at least 10 years away. (*2*)

Progress achieved with fuel cells is being reported on an increasing scale both at technical society meetings and in technical publications. For example, in 1959 eight papers and one patent appeared in *Chemical Abstracts;* four years later, in 1963 the number had grown to 60 papers and 43 patents. This increased interest has also been reflected in the technical programs of the Division of Fuel Chemistry at the National Meetings of the American Chemical Society. To date, three symposia have been held by the Division and interest has continued at a high level. Authors from the United States and abroad have presented papers. Papers presented during the first symposium at the 136th National Meeting of the American Chemical Society, September 1959, in Atlantic City, were published in book form in 1960 (*3*). Those presented during the second symposium, held jointly with the Division of Petroleum Chemistry at the 140th National Meeting, September 1961, in Chicago, were also published in book form in 1963 (*4*). Papers presented during the third symposium at the 145th National Meeting of the American Chemical Society, September 1963, in New York, together with selected papers from the Symposium on Gas Generation held April 1964, at the 147th National Meeting in Philadelphia, form the basis of the present volume. Dr. G. J. Young organized and served as Chairman of the Fuel Cell Symposium; Dr. H. R. Linden organized and served as Chairman of the Symposium on Gas Generation.

Publication Date: January 1, 1969 | doi: 10.1021/ba-1965-0047.pr001

In Fuel Cell Systems; Young, G., el al.;
Advances in Chemistry; American Chemical Society: Washington, DC, 1969.

With a continuing high level of interest in fuel cells, specific aspects of their development and application could well be the basis for future symposia sponsored by the Division of Fuel Chemistry.

(*1*) Chopey, N. P., *Chemical Engineering*, May 25, 1964, p. 125.
(*2*) Cohn, E. M., *Mining Engineering*, September 1964, p. 75.
(*3*) "Fuel Cells," Vol. I, G. J. Young, Ed., Reinhold Publishing Co., New York, 1960.
(*4*) "Fuel Cells," Vol. II, G. J. Young, Ed., Reinhold Publishing Co., New York, 1963.

J. D. CLENDENIN
R. A. GLENN

Monroeville, Pa.
January 1965

Publication Date: January 1, 1969 | doi: 10.1021/ba-1965-0047.pr001

In Fuel Cell Systems; Young, G., el al.;
Advances in Chemistry; American Chemical Society: Washington, DC, 1969.

NASA's Fuel Cell Program

ERNST M. COHN

National Aeronautics and Space Administration, Washington, D. C., 20546

Publication Date: January 1, 1969 | doi: 10.1021/ba-1965-0047.ch001

NASA's fuel-cell program spans the range from basic research to hardware. University grants cover studies of potentials of zero charge, deactivation of catalysts with time, differences between chemical and electrochemical catalysis, porous electrodes, and basics of biochemical fuel cells. Basic engineering research concerns pulsed operation of fuel cells with mechanical pulsing. Applied research on heat and mass-transfer device includes dual-membrane fuel cell, one with aqueous caustic electrolyte retained in an asbestos matrix, and an inorganic membrane. Two kinds of regenerative systems are being investigated—an electrolytically regenerative hydrogen-oxygen cell and a thermally regenerative potassium concentration cell. The ion-exchange-membrane power package for Gemini and the molten KOH system for Apollo are well under way.

The goal of NASA's fuel cell program is to obtain lightweight, dependable power sources for a variety of needs. These may include communication; command and control; guidance; radar; image acquisition, processing, and transmission; data handling and storage; life support; experiments on planetary surfaces and environment; and power for surface-exploration vehicles.

Among the major factors to be considered in designing space type fuel cells are: (1) the need for very high reliability, since chances for repair are extremely limited even on manned missions; (2) high energy and power densities, because it costs between $1000 and $5,000 to put a pound of substance into space, and our lift capabilities are limited while power requirements keep increasing; (3) the space environment (where

In Fuel Cell Systems; Young, G., el al.;
Advances in Chemistry; American Chemical Society: Washington, DC, 1969.

gravity is absent) and the planet surface (which varies from that on earth), where radiation and meteoroids present hazards, where temperatures can fluctuate widely, and where there is no atmosphere providing oxygen to act as a heat sink.

Work is now in progress on the low-temperature fuel cell, using an ion-exchange membrane as electrolyte, which will power the Gemini spacecraft (Figure 1) and on two versions of the intermediate-temperature modified Bacon fuel cell for the Apollo vehicle and its Lunar Excursion Module (Figure 2). These developments represent the first functional uses of fuel cells. Such multi-million dollar programs (about $50 million) for developing flight equipment far eclipse the more moderate research and development program of NASA. The former are the responsibility of the Office of Manned Space Flight, the latter of the Office of Advanced Research and Technology (OART).

Publication Date: January 1, 1969 | doi: 10.1021/ba-1965-0047.ch001

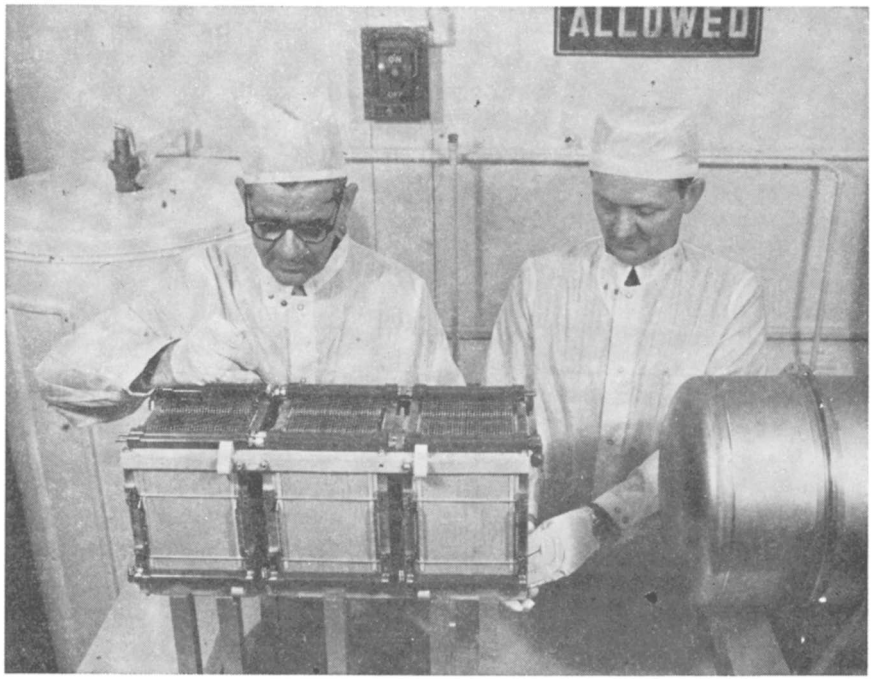

Figure 1. Interior and cannister of Gemini fuel cell

In fiscal year 1964, OART spent about $1.8 million on fuel cell projects ranging from basic research to prototype development. At this time, I can select only a few examples of our work to illustrate the range of problems it covers and to give some of the reasons for undertaking these projects.

On a NASA grant, Professor Bockris and his co-workers at the University of Pennsylvania are studying the dynamic behavior of porous electrodes, potentials of zero charge, and differences between chemical and electrochemical catalysis, among other topics. As part of their work on direct energy conversion in general, they are also exploring the fundamentals of bioelectrochemistry. From these studies we hope to acquire information useful for all kinds of fuel cell systems. I shall return to biochemical fuel cells later.

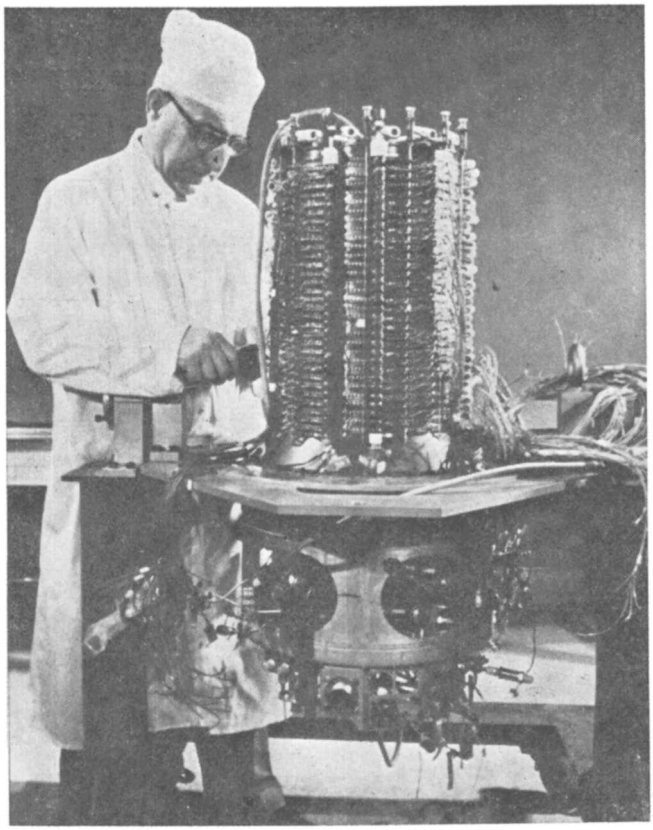

Figure 2. Module of Apollo fuel cell

An interesting hybrid between conventional batteries and fuel cells is advanced by Bernard Gruber. He proposes to impregnate a dry tape with anodic and cathodic material, one on each side, and add electrolyte just before running the tape through two current collectors. In this manner, one can activate the ingredients immediately before use, thus making possible indefinite storage as well as combinations of normally incompatible materials. This work is well underway at Monsanto and

Publication Date: January 1, 1969 | doi: 10.1021/ba-1965-0047.ch001

promises to yield high-energy-density electrochemical power sources that may compete with both primary batteries and primary fuel cells. The need for storable reactants—for emergency use or energy-depot purposes—might also be met by developing fuel cells with multi-chemical capabilities which might utilize residual or excess amounts of rocket propellants, such as UDHM and nitrogen tetroxide (Figure 3).

In devising space power systems, we must consider not only the power source but also the equipment it runs. As a crude rule of thumb, we may assume 25% of the output will be needed as alternating current, 25% as direct current, and the remainder as either a.c. or d.c. Further-

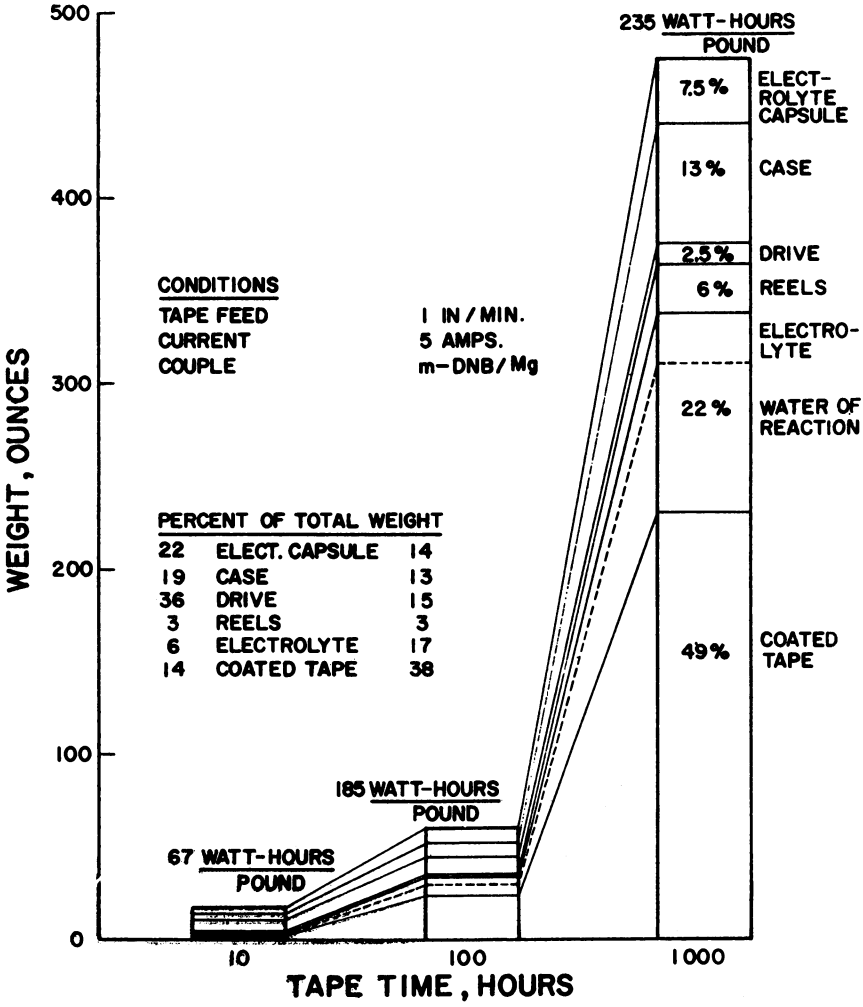

Figure 3. Projected energy densities for magnesium/m-dinitrobenzene dry tape fuel cells

Publication Date: January 1, 1969 | doi: 10.1021/ba-1965-0047.ch001

more, various devices will be operated at different voltages. Thus, power "conditioning" is an important factor in considering the electrical system as a whole. Mechanical and/or electric pulsing of fuel cells (Figure 4)—now being studied on grant as well as contract—may yield several kinds of advantages: longer operating life, improved resistance to poisoning of catalysts, lower concentration polarization, and greater output from the fuel cell battery. Better circuit control and higher conversion efficiency from the over-all system may be obtained by quasi-a.c. operation. Needless to say, such benefits, particularly as concerns the fuel cell proper, might be even greater in ground applications where hydrocarbons or alcohols are used directly as anodic fuels.

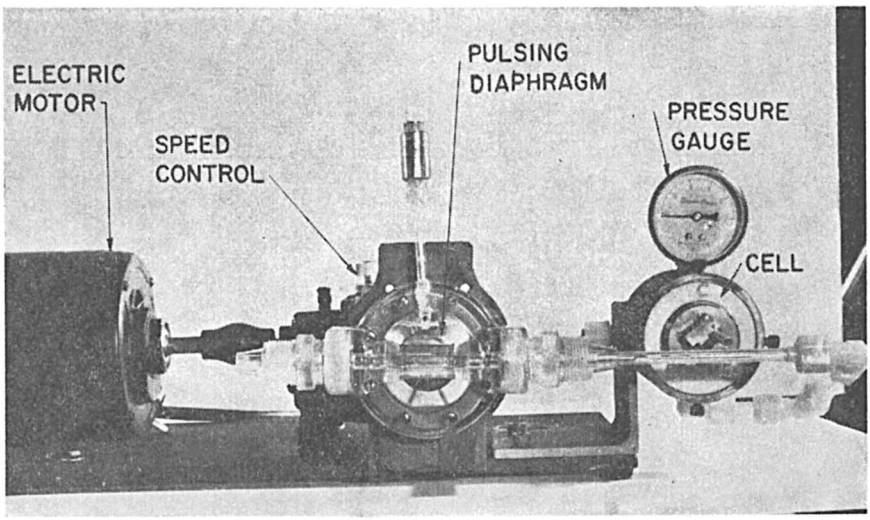

Figure 4. Equipment for mechanical pulsing of fuel cells

Research on high performance, thin electrodes that promise drastic cuts in fuel cell weight and volume should benefit both earth and space applications. Over the last two years or so we have progressed from about 150 lbs./kw. to about 70 lbs./kw., exclusive of fuel and fuel tankage; 30-40 lbs./kw. for fuel cell plus auxiliaries now appears to be in sight.

Work underway at Allis-Chalmers is directed not only at obtaining a space type, low-temperature, hydrogen-oxygen fuel cell, with an asbestos retainer for the electrolyte, but is also concerned with finding a simple and reliable method for removing heat and water with the minimum of mechanical moving parts and minimum need for parasitic power (Figure 5). This could be done by evaporating water through a capillary membrane adjacent to the electrodes. The cavity behind the membrane should be evacuated to a pressure corresponding to the vapor pressure

Publication Date: January 1, 1969 | doi: 10.1021/ba-1965-0047.ch001

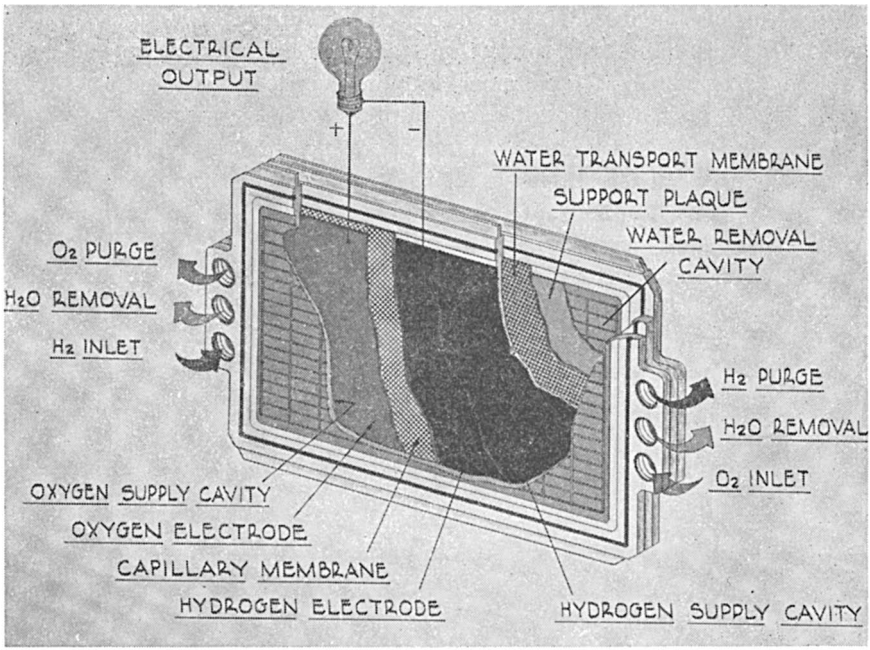

Figure 5. Schematic diagram of fuel cell with passive water removal system

of the KOH electrolyte at its operating temperature (about 200° F.). Feasibility of such an arrangement has been demonstrated. Control is simple, and temperature is not a critical factor.

Primary fuel cells are those through which reactants are passed only once. They are useful in space for only limited periods because the product of power and duration (= energy) determines the amount of fuel and oxidant that must be carried aloft. For extended missions, therefore, other primary sources of energy must be used. In connection with solar and nuclear energy sources and conversion devices, fuel cells may be used for energy storage, as secondary power sources during darkness (solar primary power), during emergencies, and during periods of peak-power demand. Among the methods of regenerating reactants from products, only electrolysis and thermal treatment have shown promise. Even so, it is not yet clear whether regenerative fuel cells will be competitive with secondary batteries or other secondary conversion devices.

At present, we have only one effort under way on a secondary or regenerative fuel cell: a low-temperature hydrogen-oxygen cell with electrolytic decomposition of water. It might be useful in connection with solar energy in a synchronous satellite. Here the disadvantages of inefficiency—as compared with a secondary battery—may be compensated

Publication Date: January 1, 1969 | doi: 10.1021/ba-1965-0047.ch001

by weight savings effected by storing energy in the form of $H_2 + O_2$ instead of metal + metal oxide.

Biochemical fuel cells captured the public imagination some time ago. Further exploration of this 50-year-old concept has indicated rather severe power density and energy density limitations for such cells. Nevertheless, biocells are likely to find special uses as energy-saving waste disposals for extended space flights, during which human waste must be reprocessed for attaining a closed or nearly closed ecology. NASA has supported a three-fold attack on this problem by sponsoring basic, applied, and developmental studies, aimed at finding materials and conditions to dispose of human waste. Since the power consumed by such a device would undoubtedly exceed the theoretical—let alone the realizable—power output, this biocell was obviously not intended to produce power. Even so, it became apparent that the low power densities would require weights and volumes of equipment completely out of proportion to any possible benefits. Resuming applied research would become attractive only if much more active enzymes or organisms were developed, if efficient charge-transfer media were found, or if it could be proved that direct electron transfer from enzyme or organism to electrode can take place. If something like a one hundred-fold increase in power density can be achieved in biocells, they might be re-evaluated for this purpose. Similarly, biocells might be used to solve problems of water pollution, and the power produced would be a welcome byproduct.

What do we expect from space-type fuel cells? Our immediate, prime considerations are high power density and reliability. The Gemini and Apollo fuel cells, for example, will be about $^1/_6$ to $^1/_{10}$ the weight of the best available primary batteries that are capable of delivering the same total amount of energy. Furthermore, the water product, an additional bonus not available from batteries, will be used by the astronauts.

Other requirements may become important for different space applications. Longevity and ease of maintenance, for example, could well be the desiderata for fuel cells used at a lunar station or depot. Ease of packaging, storing, and converting chemicals to active species (say, hydrogen and oxygen) may determine what types of fuel cell will be best for propulsion on the moon or for powering space suits.

Apart from requiring a variety of fuel cells, each optimized for a particular task, we expect to see a much more sophisticated operation of fuel cell systems. Increasing attention is already being directed toward optimization of controls and operating conditions. Each system must be optimized to take advantage of the leeway permitted by its size, components, and operating variables.

Fuel cells must become truly integrated into the systems of which they will be parts. I already mentioned biochemical fuel cells as primary chemical reactors, and the Gemini and Apollo fuel cells as sources of

Publication Date: January 1, 1969 | doi: 10.1021/ba-1965-0047.ch001

potable water. Not only byproduct chemicals, but also byproduct heat could be useful. Once we have reliable information about the composition of the lunar surface, we may need to develop fuel cells particularly suited for lunar purposes and independent of supplies from earth.

This brief discussion of NASA's fuel cell program indicates some of the difficulties we face and how we attempt to overcome them. Our task is to provide NASA with reliable, optimized fuel cell power that will be applicable to many different jobs under a great variety of space and planetary conditions. Virtually all of the information obtained in its pursuit should be as useful for earth-bound as for space type fuel cells. Thus, we hope not only to solve a part of the space power problem, but also to contribute to advancing fuel cell technology that will benefit our economy.

RECEIVED April 27, 1964.

Publication Date: January 1, 1969 | doi: 10.1021/ba-1965-0047.ch001

Fuel Cell Electrodes for Acid Media

WALTER G. TASCHEK

U. S. Army Electronics Research and Development Laboratories, Fort Monmouth, N.J.

Publication Date: January 1, 1969 | doi: 10.1021/ba-1965-0047.ch002

Investigations have been conducted toward developing high drain fuel cell electrodes for acid media. Activated carbon electrodes have been prepared, wetproofed with paraffin or Teflon, and catalyzed with platinum. The wetproofing agent was applied by immersion or electrodeposition and the catalyst applied by chemical decomposition of H_2PtCl_6 solutions. Half cell studies with hydrogen anodes and oxygen (air) cathodes have shown that electrochemical performance is essentially the same for paraffin and Teflon-treated electrodes; however, the life of the Teflon-treated electrodes under equal conditions of load is greater than that for paraffin-treated electrodes. An equation that describes the cathode's polarization behavior for heterogeneous porous electrodes expresses a simple relationship between current density and polarization and is valid in the range of practical current densities.

The long range goal of fuel cell research is the development of fuel cell batteries operating directly or indirectly on inexpensive fuels—for example, hydrocarbons, and air as the oxidant. The batteries must operate at high efficiency at practical current densities and have long operational life if they are to compete with present forms of power generation. The batteries must employ electrolytes which are not affected by carbon dioxide. For this approach, acid electrolytes are mandatory. Consequently, a part of our program is concerned with liquid acid electrolytes. Also, the development of an efficient air cathode operating under these conditions is necessary.

In Fuel Cell Systems; Young, G., el al.;
Advances in Chemistry; American Chemical Society: Washington, DC, 1969.

Original work on hydrogen and oxygen electrodes for acid media was reported in 1962 (*3*). It was found that by means of a new preparation technique for catalyzed, activated carbon electrodes, wetproofed with paraffin, high performance of hydrogen anodes and oxygen cathodes could be obtained. The life of the paraffin wetproofed electrodes was short. Initial tests made with Teflon wetproofed electrodes showed performances close to that of paraffin wetproofed electrodes.

In continuation of this work, investigations have been conducted on hydrogen, oxygen, and air electrodes operating in liquid, acid media. Various electrode preparation techniques have been used, employing paraffin and Teflon as wetproofing agents. The electrochemical performance of the electrodes has been measured over extended periods of operation.

The carbon electrodes used in these investigations were supplied by Speer Carbon Co., grade 7716, dimensions $1 \times 1 \times {}^1/_8$ inch.

The preparation techniques used most extensively were:

Publication Date: January 1, 1969 | doi: 10.1021/ba-1965-0047.ch002

Paraffin-Treated Electrodes (A)

Activation. The raw carbon electrodes were weighed and then fired in a carbon dioxide atmosphere at 800° C. for eight minutes. After that, the electrodes were cooled in a stream of carbon dioxide to prevent air oxidation of the hot carbon. Finally, the electrodes were weighed and their weight loss calculated. A 7 to 10% weight loss was desired.

Wetproofing. The activated carbon electrodes were immersed in a wetproofing solution for ${}^1/_2$ hour. The wetproofing solution contained 2 grams of paraffin per 100 ml. of petroleum ether. The electrodes were then dried by drawing air through the pores for several hours. This was accomplished by means of a water aspirator. The activated and wetproofed electrodes were then ready for catalyzation with platinum.

Catalyzation. A solution of H_2PtCl_6 were prepared containing from 50 to 100 mg. of platinum per ml. of solution. The volume of solution which was necessary to cover the electrodes with 2 mg. of platinum per sq. cm. of geometric electrodes surface was measured. The electrodes were heated in an oven at 200° C. The solution was then applied to the surface of the hot electrodes with a brush. Finally, the electrodes were placed in a vacuum oven at 150° to 175° C. for several hours.

Teflon-Treated Electrodes (Teflon Applied by Immersion) (B)

Activation. Same as with paraffin-treated electrodes.

Wetproofing. The activated electrodes were immersed for 15 minutes in a dispersion containing 10 ml. of Teflon 41-BX per 100 ml. of water. Prior to drying, the excess of Teflon resin was rinsed from the carbon surface with distilled water. The electrodes were then dried as in the

In Fuel Cell Systems; Young, G., el al.;
Advances in Chemistry; American Chemical Society: Washington, DC, 1969.

case of paraffin wetproofing. Teflon 41-BX is a fluorocarbon resin of hydrophobic negatively charged particles in an aqueous medium of pH = 10. The average size of the resin particles is about 0.2 micron. The dispersion was obtained from E. I. DuPont de Nemours & Co. (*1*).

Catalyzation. Same as with paraffin-treated electrodes.

Teflon-Treated Electrodes (Teflon applied by electrodeposition) (C)

Activation. Same as with paraffin-treated electrodes.

Wetproofing. The activated electrode was placed in the electrodeposition bath containing 4 ml. of Teflon 41-BX per 100 ml. water. A d.c. power supply connected to a variable resistor served as the source of current. The electrode to be wetproofed was the anode (+) and a platinum strip was the cathode (—). A potential of 6 volts was applied across the electrodes and the resulting current was about 65 ma. The distance between the anode and cathode was 1 to 2 inches. Direct current passing through the dispersion of Teflon 41-BX caused the negatively charged dispersed particles to migrate toward the positive carbon anode by electrophoresis. The particles were discharged and deposited there. The only occurrence at the platinum cathode was the evolution of hydrogen gas. It was observed that a heavier deposit of Teflon was formed at the carbon surface facing away from the cathode.

Catalyzation. Same as with paraffin-treated electrodes. The carbon surface clean of Teflon deposits was catalyzed.

A diagram of the cell used to test electrodes is shown in Figure 1. The electrolyte used in all tests was 5*N* sulfuric acid. All cells were operated at room temperature. Gas pressures of hydrogen, oxygen, and air were maintained at the bubble pressure of the electrode. The bubble pressure was defined as the minimum pressure required to maintain visible bubbling at the electrode-electrolyte interface. The interrupter technique described by Kordesch and Marko was used to eliminate the IR drop in potential measurements (*2*). A saturated calomel electrode was used as the reference electrode.

An equation was found that described the polarization behavior of the porous gas diffusion type oxygen (or air) electrodes. The equation is given by:

$$\eta = ai^b$$

η is the polarization in volts; i is the current density in amp. per square centimeter, and a and b are constants of the equation. The equation was found to be valid in the range of current densities from 5×10^{-4} to 10^{-1} amp./sq. cm. Its validity could be established for 19 out of 21 current voltage curves using various electrodes. By plotting the polarization and the current density on a log-log plot, the constants a and b can be readily

Publication Date: January 1, 1969 | doi: 10.1021/ba-1965-0047.ch002

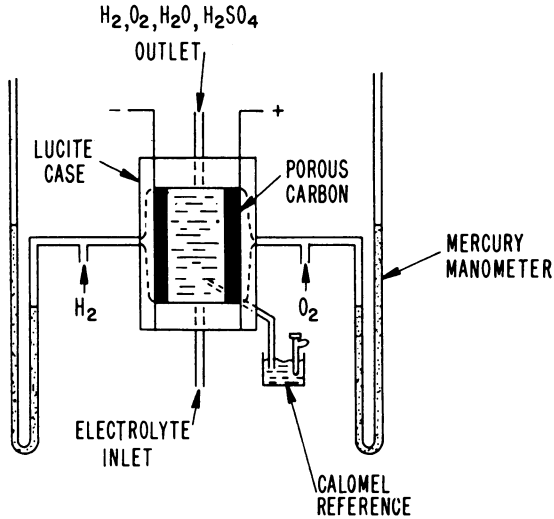

Figure 1. Schematic drawing of experimental cell

evaluated. The log-log plot of the polarization versus the current density was obtained by superimposing the measured potential values on the polarization ordinate and assigning an arbitrary open-circuit potential of 1.1 volts for oxygen and air electrodes versus the standard hydrogen electrode (SHE). We used arbitrary open-circuit potential since the experimental open-circuit potentials are difficult to reproduce from one electrode to the next. The range of the experimental open-circuit potentials observed was about 0.8 volt to 1.1 volts. This range is probably caused by mixed potentials whose values depend on various factors. The reversible open-circuit potential of 1.229 volts was not chosen because related investigations indicate the presence of another reaction mechanism(*4*).

In Figure 2 a conventional Tafel plot is compared with a log η *vs.* log i plot representing a typical set of data. It can be observed that there is no straight line portion in the Tafel plot. The log η *vs.* log i plot shows that equation $\eta = ai^b$ is valid for practical ranges of current density. Deviations occur below current densities of 5×10^{-4} amp./sq. cm. and above current densities of 10^{-1} amp./sq. cm. For low polarizations, small errors in experimental measurements are magnified because of the structure of the log-log plot. Above 10^{-1} amp./sq. cm. apparent effects of high concentration polarization are observed.

Determination of the constants a and b in the equation shows that low polarization is associated with low a values and high b values for b values less than one. No b values greater than one were observed. The high, low, and average values of a, b, and the limiting current density I_1 are given in Table I and show the differences arising from different

Publication Date: January 1, 1969 | doi: 10.1021/ba-1965-0047.ch002

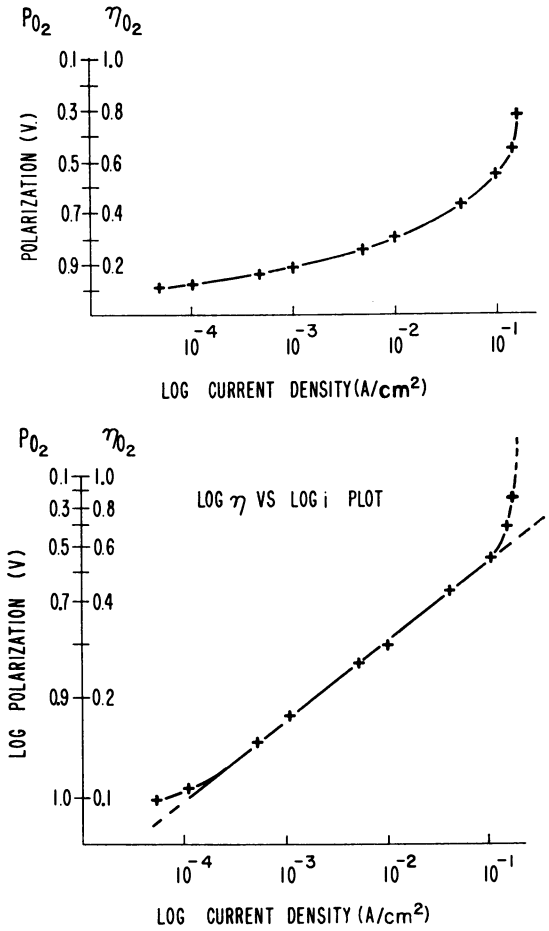

Figure 2. Tafel vs. log η–log i plot

Publication Date: January 1, 1969 | doi: 10.1021/ba-1965-0047.ch002

preparation techniques. The table was compiled from nine trials of *A*, four trials of *B*, and four trials of *C*. No significant deviations were observed in average *a* values for the three preparation techniques, although there was considerable variation in these values from one electrode to the next. Close agreement was found in all *b* values for techniques *A* and *B*,

Table I. Tabulation of *a*, *b*, and I_1 Values

Preparation Technique	*a*	*a, Average*	*b*	*b, Average*	I_1, *Amp./ Sq. Cm.*	I_1, *Amp./ Sq. Cm., Average*
A	0.72–1.10	0.90	0.12–0.145	0.13	0.07–0.3	0.19
B	0.87–1.05	0.96	0.13–0.14	0.13	0.08–0.2	0.12
C	0.59–1.15	0.89	0.13–0.22	0.18	0.05–0.1	0.08

but C showed higher b values and more variation from one electrode to another. However, technique C was connected with strong effects of concentration polarization above current drains of 50 ma. per sq. cm.

The hydrogen electrodes tested showed low polarization in the order of 50 mv. up to 100 ma./sq. cm. No limiting current densities could be observed over the range of current density investigated.

Life tests were conducted on hydrogen and oxygen electrodes with paraffin and Teflon treated electrodes. The electrodes were operated for eight hours per day. Figure 3 shows the results. Life tests of hydrogen electrodes showed nearly constant performance over all operation periods.

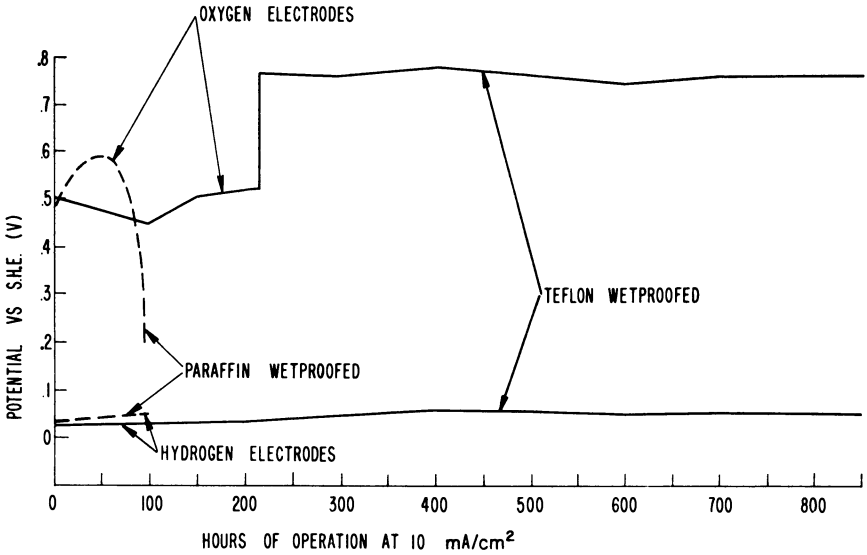

Figure 3. Life tests

With Teflon-treated oxygen electrodes, over 850 hours of operation were obtained at 10 ma./sq. cm. without loss in performance. Previously with paraffin treated electrodes, only 80 hours of operation at 10 ma./sq. cm. were obtained before the oxygen cathode failed. It was observed that after 230 hours of operation, the Teflon-treated electrodes showed a sharp rise in performance. This potential jump from 0.52 to 0.76 volt *vs.* SHE resulted from an increase of the oxygen gas pressure from 0.13 atm. to 0.35 atm. At the start of the test the bubble pressure for the oxygen electrode was 0.13 atm. This pressure was maintained for 230 hours of operation. It was then observed that the bubble pressure rose to 0.35 atm. The bubble pressure then remained stable from 296 to 850 hours of operation.

From these results it is evident that at relatively low drains of 10

Publication Date: January 1, 1969 | doi: 10.1021/ba-1965-0047.ch002

ma./sq. cm., Teflon wetproofing does not impede the electrodes performance but increases the life of the electrodes considerably over that of paraffin wetproofed electrodes.

In addition to the constant performance test, complete current-voltage curves were taken at zero, 296, and 800 hours. Figure 4 shows the curves for the oxygen electrodes in a log η *vs.* log i plot. The curves show that a values decreased, b values increased, and I_1 values increased during the course of the life test. This means an increase in performance with aging of the electrode. This can be expected since the Teflon wetproofing initially prevents the electrolyte from making extended contact with the electrode surface. As the life test continues, the electrode surface becomes more wetted and the performance improves. This is shown in the table in Figure 4. A decrease in the a value and a considerable increase in the b and I_1 values are observed from zero to 296 hours. After that, little change in these values was observed.

Publication Date: January 1, 1969 | doi: 10.1021/ba-1965-0047.ch002

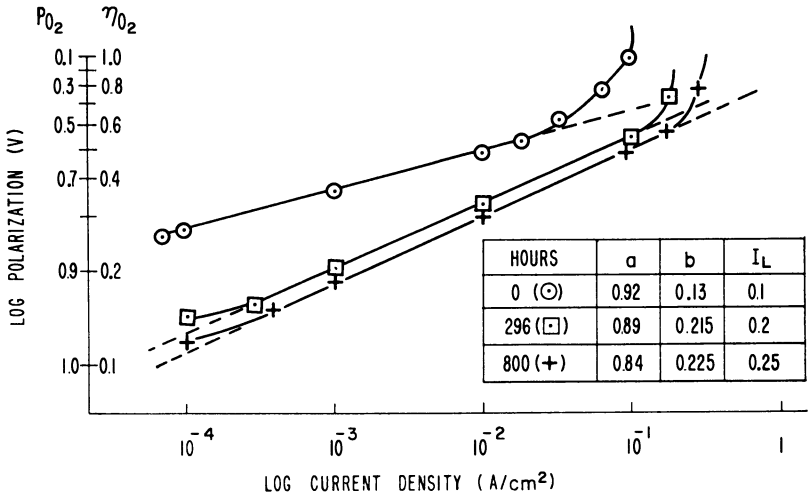

Figure 4. Log η–log i plot as function of time

Further, current voltage curves were taken for air cathodes and compared with curves obtained with pure oxygen. Paraffin and Teflon-treated electrodes were used. First, a current-voltage curve was taken of the hydrogen-oxygen cell. Then, after thoroughly flushing the cathode with air for several hours, the second current voltage curve was taken of the hydrogen-air cell. The results are shown in Figure 5. In both cases the oxygen electrode performed better than the air electrode. The performance of the Teflon-treated electrode decreased only slightly when air was used instead of oxygen. In the case of the paraffin wetproofing, the air performance was poor.

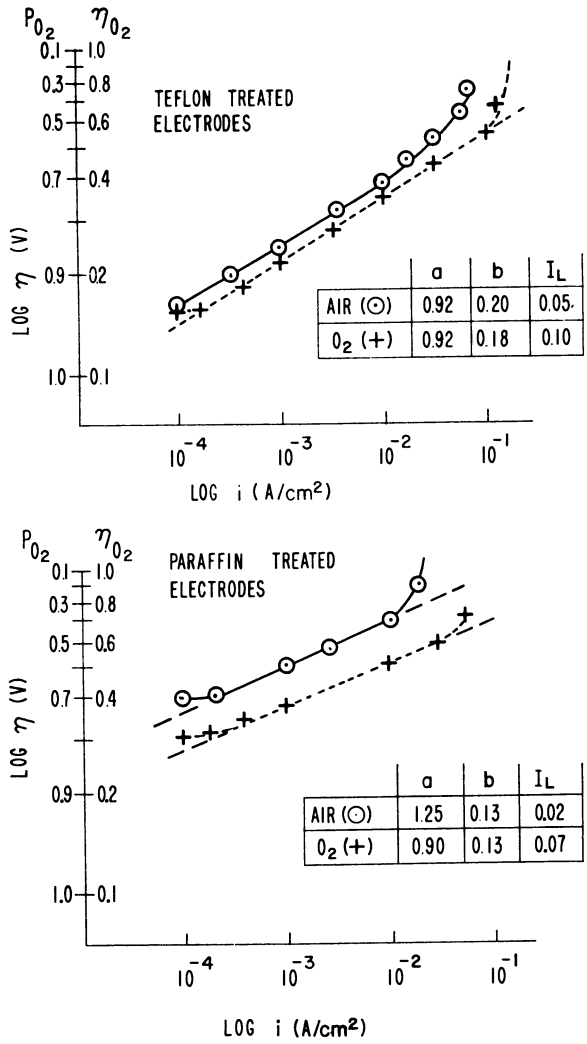

Figure 5. Air vs. oxygen

In conclusion:

1. Paraffin wetproofed electrodes show high initial performance but do not have long life.
2. Teflon wetproofed electrodes (by immersion) show excellent life characteristics without loss of electrochemical performance.
3. Teflon wetproofed electrodes (by electrodeposition) show high performance at low current densities but have low limiting current densities. Life of the electrodes has not been established.
4. Polarization of oxygen (or air) electrodes can be described by the equation $\eta = ai^b$. The equation is valid for the range of current densities investigated.

Publication Date: January 1, 1969 | doi: 10.1021/ba-1965-0047.ch002

Literature Cited

(1) E. I. DuPont de Nemours & Co., Inc., Wilmington, Del., "Teflon," Inform. Bull. No. X-916, Polychemicals Dept.
(2) Kordesch, K., Marko, A., *J. Electrochem. Soc.* **107**, 480 (1960).
(3) Taschek W. G., Wynn, J. E., Proc. 16th Annual Power Sources Conference, 12 (1962), PSC Publications Committee.
(4) Wynn, J. E., Extended Abstract No. **25**, Battery Division, 120th Meeting Electrochemical Society (1961).

RECEIVED February 17, 1964.

Publication Date: January 1, 1969 | doi: 10.1021/ba-1965-0047.ch002

3

Electrochemical Characteristics of Graded Porosity Carbon Electrodes

EDWARD A. HEINTZ, RONALD W. MAREK and WILLIAM E. PARKER

Speer Carbon Co.
A Division of Air Reduction Co., Inc., Niagara Falls, N.Y.

Publication Date: January 1, 1969 | doi: 10.1021/ba-1965-0047.ch003

A series of carbon electrodes possessing a porosity gradient of different pore size distributions has been prepared by carefully controlling fabricating conditions. When these materials were tested in a laboratory hydrogen-oxygen fuel cell using an acid electrolyte, the reaction at the oxygen electrode (the cathode) depended on the particular porosity facing the electrolyte. Generally, this conclusion is valid only for a given electrode material as no over-all correlation between electron change and pore size could be made. Paraffin as a wetproofing agent on these materials inhibits the reduction of oxygen at a carbon electrode by both polarographic methods and by decreased fuel cell performance. The oxidation of hydrogen at a carbon electrode in acid media appears to be fairly straightforward.

For the past several years Speer has conducted a comprehensive investigation of porous carbon electrode materials for use in fuel cells. Much of the information obtained from this study has been presented in various reports and papers (*12–20*). One result of this prior work has been the development of techniques for fabricating, from given formulations, carbon materials in which permeability and macropore distribution can be consistently and predictably varied over wide ranges.

A logical extension of this finding was to prepare carbon electrode materials which exhibit a pore size gradient across their thickness. By further refining these techniques, bodies have been fabricated which con-

In Fuel Cell Systems; Young, G., el al.;
Advances in Chemistry; American Chemical Society: Washington, DC, 1969.

tain a prechosen number of layers of selected pore size distributions. The evenness of these strata and their mutual compatibility during processing is remarkable. To avoid extraneous variation, all layers of each sample are taken from the same formulation and, indeed, from the same basic mix.

The physical properties of these carbon electrodes and their electrochemical characteristics in fuel cell operation are presented below.

Electrode Preparation

A formulation of petroleum coke and coal tar pitch was selected for the initial fabrication of these novel materials. A lignin sulfate derivative marketed under the trade name "Orzan" was used as an additive. The latter is employed as a means of increasing the porosity of the baked carbon through exfoliation during the baking process. The materials were intimately mixed at 135° C. and crushed to desired size when cooled. The sized materials were then placed in very even layers in a molding die in the chosen sequence and thickness. All samples were molded and baked under uniform conditions to yield electrodes of two or three zones of predictable permeability and macropore distribution. The physical properties of these samples are given in Table I.

Measuring the contact angle of the electrode with the electrolyte is very useful. When a liquid is placed in contact with a solid which it does not wet, a definite angle of contact between the two phases may be observed. For complete nonwetting this angle of contact would be 180°. However, for all practical considerations, if the contact angle exceeds 90°, the liquid will not enter into capillaries of the solid to any appreciable degree. Conversely, a contact angle of 0° indicates that complete wetting occurs and flooding of the capillary pores of the porous solid readily occurs. Contact angle, therefore, is a useful criteria for determining the degree of wetting of porous carbon materials. The tilting plate technique, as described by Fowkes and Harkins (*2*), was chosen as the method most suitable for this application.

Polarization characteristics of carbon electrodes have been determined with the laboratory size hydrogen-oxygen fuel cell identical to that described by Taschek in another article in this monograph (*23*). The entire system was reduced to thermal equilibrium at 25.0 ± 0.2° C. prior to measuring the electrode polarization in order to remove temperature dependent processes from consideration. Sulfuric acid (3.0*N*) was employed as the electrolyte. The electrode preparation procedure was varied only in the application of wetproofing where desired. Some electrodes were wetproofed by treating with a solution of 2 grams of paraffin per 100 ml. of petroleum ether (b.p. range 30–60° C.) and allowed to dry in air. This was normally followed by catalyzing with 2 mg. of platinum black per square centimeter of geometrical surface area as

Publication Date: January 1, 1969 | doi: 10.1021/ba-1965-0047.ch003

Table I. Properties of Graded

Sample	Thickness, inches			Permeability, darcys		
	Zone I	Zone II	Zone III	Zone I	Zone II	Zone III
1	0.031	0.031	0.031	1.38	0.45	0.14
2	0.031	0.031	0.031	1.38	0.45	0.05
3	0.125	0.031	..	1.38	0.14	..
4	0.125	0.031	..	1.38	0.05	..
5	0.031	0.031	0.031	1.38	1.16	0.76
6	0.031	0.031	0.031	0.24	0.14	0.09
7	0.031	0.031	0.031	1.38	0.76	0.14
8	0.031	0.031	0.031	1.38	0.76	0.05
9	0.031	0.031	0.031	1.38	0.05	1.38
10	0.031	0.031	0.031	0.05	1.38	0.05
11	0.031	0.031	0.031	1.38	0.45	0.33
12	0.125	0.031	..	1.38	0.33	..
1-Pt[2]	0.031*	0.031	0.031	1.38*	0.45	0.14
2-Pt[2]	0.031	0.031*	0.031	1.38	0.45*	0.14
3-Pt[2]	0.031	0.031	0.031*	1.38	0.45	0.14*
1-Ch[3]	0.031	0.031	0.031	0.26	0.35	0.24
2-Ch[3]	0.031	0.031	0.031	0.24	0.27	0.26
3-Ch[3]	0.031	0.031	0.031	0.26	0.23	0.35

[1] Contact angle with water is a qualitative measure of the hydrophilic (wetting) character of the material; the lower the angle the more hydrophillic the material. The charcoal materials are both quite porous and hydrophillic.
[2] Samples 1-Pt through 3-Pt were fabricated in similar fashion except that 2 mg. of platinum black per square centimeter of geometrical surface were added to the

recommended by Taschek (*23*). Where no wetproofing was applied, the pretreatment proceeded directly to the catalyzing step. No activation of electrode materials was employed so that the possibility of masking the effects and interactions of electrode process variables and raw materials could be obviated. The electrodes were studied with a 1 × 1-inch surface in contact with the aqueous electrolyte.

A modified Kordesch-Marko bridge circuit (*8*) was constructed for interrupting the current during measurement of the electrode potential. This bridge circuit provides for the measurement of combined polarization due to activation and concentration by eliminating the influence of resistance polarization.

Gas Pressure Studies

The pressures of hydrogen and oxygen were varied so that the electrical output could be determined as a function of gas pressure. The maximum pressure used was just less than that needed to cause rapid continuous gas bubbling from the surface of the electrode. The maximum pressure varied with the particular surface facing the electrolyte and the gas involved. In this work that quantity has been termed the "bubble pressure." The description of the porosity gradients for the materials studied (Table I) shows that a variety of two- and three-layered materials have been prepared. Some have a very coarse zone on one face which

Publication Date: January 1, 1969 | doi: 10.1021/ba-1965-0047.ch003

Porosity Electrode Materials

Probable pore diameter range, microns (μ)			*Contact angle,*[1] *°*			*Surface area, sq. m./gram*		
Zone I	*Zone II*	*Zone III*	*Zone I*	*Zone II*	*Zone III*	*Zone I*	*Zone II*	*Zone III*
9–>90	5–25	3–7	77.0	32.5	28.0	37.4	56.7	137.7
9–>90	5–25	3–4	77.0	32.5	27.0	37.4	56.7	158.2
9–>90	3–7	..	77.0	28.0	..	37.4	137.7	..
9–>90	3–4	..	77.0	27.0	..	37.4	158.2	..
9–>90	8–40	8–20	77.0	79.5	30.0	37.4	71.0	43.3
6–14	3–7	3–6	34.5	28.0	39.0	46.5	137.7	181.0
9–>90	8–20	3–7	77.0	30.0	28.0	37.4	43.3	137.7
9–>90	8–20	3–4	77.0	30.0	77.0	37.4	43.3	158.2
9–>90	3–4	9–>90	77.0	27.0	77.0	37.4	158.2	37.4
3–4	9–>90	3–4	27.0	77.0	27.0	158.2	37.4	158.2
9–>90	5–25	3–5	77.0	32.5	37.5	37.4	56.7	129.3
9–>90	3–5	..	77.0	37.5	..	37.4	129.3	..
9–>90*	5–25	3–7	77.0*	32.5	28.0	37.4*	56.7	137.7
9–>90	5–25*	3–7	77.0	32.5*	28.0	37.4	56.7*	137.7
9–>90	5–25	3–7*	77.0	32.5	28.0*	37.4	56.7	137.7*
1.5–20	1–7	0.9–6	41.5	11.0	16.0	..	..	..
0.9–6	0.9–6	0.9–6	16.0	35.0	27.0	..	..	..
0.9–6	0.9–5	1–6	27.0	26.0	25.0	..	..	..

zone marked with an asterisk. These materials were processed under conditions identical to the first set.
[1] Samples 1-Ch through 3-Ch of Table I were identical to Samples 1 through 12 except for substitution of a hardwood charcoal for the petroleum coke used as the filler material to obtain very porous, hydrophilic materials.

Publication Date: January 1, 1969 | doi: 10.1021/ba-1965-0047.ch003

decreases to a finer zone on the opposite face; some are "uniformly coarse" or "uniformly fine"; and some have a coarse zone sandwiched between two fine zones or vice versa. Each material was evaluated with both the "fine" (F) and the "coarse" (C) side facing the electrolyte. The first six materials listed in Table I were also tested in the experimental fuel cell in both a wetproofed (WP) and nonwetproofed (NWP) condition. The next 12 materials were tested only in the nonwetproofed condition.

The observed current density at 0.3 volt polarization and the bubble pressure appear to vary with the surface facing the electrolyte and the application of wetproofing to the electrode material. These data are summarized in Table II for samples 1 through 12. In a nonwetproofed condition, the graded electrodes usually yield a higher current density at a lower fuel gas pressure when the finer porosity zone faces the electrolyte. In all but Sample 6, better performance is attained when the materials are *not* wetproofed. Even in sample 6 the nonwetproofed fine zone yields higher current densities on the fine side. This could be interpreted as evidence of increased available active carbon surface together with improved catalyst proximity to this active surface. Sample 6 is the most "uniformly fine" material (or perhaps most like a standard nongraded electrode) and in this case wetproofing with paraffin was beneficial.

Another possibility is that the wetproofing treatment inhibits the total

Table II. Current Density at O.3 v. Polarization and Bubble Pressure as a Function of Wetproofing and Porosity of Electrode Surface

	Current density, ma./sq. cm.		*Pressure*[1]		*Current Density, ma./sq. cm.*		*Pressure*[1]	
Sample[2]	H_2[3]	O_2	H_2	O_2	H_2	O_2	H_2	O_2
	Wetproofed				*Nonwetproofed*			
1F	17.3	31.0	25.8	26.7	28.5	50	37.6	19.7
1C	12.8	13.5	2.1	7.3	23.0	29.5	1.6	1.4
2F	4.4	8.2	103.3	98.1	28.0	70	1.6	99.5
2C	7.3	3.9	101.1	95.7	12.2	18.9	16.3	1.7
3F	1.66	0.93	96.2	97.5	8.4	20	26.7	26.0
3C	15.5	10.00	1.9	48.2	11.8	9.5	1.4	1.1
4F	2.40	1.37	6.3	98.7	9.9	4.6	71.6	73.3
4C	2.75	0.61	3.1	1.7	3.8	1.0	52.4	47.0
5F	2.1	2.24	2.90	37.4	12.5	3.1	55.5	37.5
5C	2.9	0.76	30.0	1.1	5.4	1.3	33.6	32.6
6F	44.0	70	54.1	81.8	9.4	15	31.9	48.3
6C	29.8	1.11	1.6	35.1	15.4	3.35	47.0	2.4
7F	..	..	..	..	16.0	0.6	78.4	70.0
7C	..	..	..	..	..	..	..	..
8F	..	..	..	..	9.2	2.9	67.0	53.5
8C	..	..	..	..	..	0.7	58.0	41.5
9C	..	..	..	..	15.0	1.0	68.8	50.8
10F	..	..	..	..	11.3	21.0	95.8	71.7
11F	..	..	..	..	22.0	14.1	31.2	30.9
11C	..	..	..	..	23.0	5.8	31.0	26.5
12F	..	..	..	..	17.3	2.3	80.3	84.5
12C	..	..	..	..	13.5	..	40.0	46.2

[1] In cm. of dibutyl phthalate.
[2] *F* = fine side facing electrolyte; *C* = coarse side (see Table I).
[3] H_2 = hydrogen electrode; O_2 = oxygen electrode.

contact of catalyst with the electrode and electrolyte because part of the catalyzing treatment involves a reheating of the electrode to a temperature well above the melting point of the hydrophobic agent (paraffin). During the heat treatment, while the paraffin is molten, it is probable that a fraction of the catalyst is also wetproofed. If this occurs, then the wetproofed, catalyzed electrode can be regarded as less active than a nonwetproofed, catalyzed electrode and may even result in a somewhat different electrochemical response. To test this hypothesis the following series of experiments was performed:

A series of 5 mm. carbon disks from the same bulk sample and prepared from identical materials as the graded porosity electrodes were sealed into the end of a glass tube. An electrical contact was made on the inside of the tube to the surface of the carbon. The tube was connected to a source of oxygen and placed in a 3*N* sulfuric acid solution as part of a conventional polarographic system in which the carbon disks were the working electrodes. Oxygen pressure was then applied so that a bubble of oxygen was allowed to escape from the carbon disk into the solution at a rate no greater than once every 5 seconds. The potential was then scanned in a cathodic direction using a Sargent Model XXI recording polarograph over the range +0.3 to −1.2 volt *vs* SCE. Four different electrodes were used: an untreated carbon electrode; a catalyzed but nonwetproofed electrode; a catalyzed and wetproofed electrode; and an electrode which was only wetproofed.

Publication Date: January 1, 1969 | doi: 10.1021/ba-1965-0047.ch003

The first material gave $E_{1/2}$ values which corresponded to the reduction of oxygen to peroxide and the reduction of peroxide to hydroxide. The second material was so active that the size of the disk had to be cut down to 2-mm. diameter to hold the current response on scale for the same two reductions. Electrode No. 3 gave only a poorly defined response for the second reduction, the first being entirely absent. The last material showed hydrogen evolution as the only electrode reaction. The presence of the wetproofing material inhibited the polarographic response, in probably the same manner in which the fuel cell process is retarded. Wetproofing is therefore detrimental to optimum electrochemical performance. However, some exceptions to this behavior have been noted, as for Sample 6, where the wetproofed sample showed a better electrochemical response. In all other samples wetproofing has a definite inhibiting effect on electrochemical performance. Because of this, it was decided to omit the wetproofing step from the evaluation of all remaining graded porosity electrode materials.

One interesting interpretation of these results can be made by utilizing the capillary transport theory proposed by Hunger (*6*). The force (pressure, p) needed to move the gas through a wetproofed capillary (pore) can be expressed as a function of the radius (r) of the pore, the surface tension (γ) of the electrolyte and the contact angle (θ) of the meniscus formed between the electrolyte and the porous body. This relationship is expressed by a form of the Washburn equation (*21*):

$$p = \frac{2\gamma \cos \theta}{r} \tag{1}$$

When p is the maximum pressure which can be applied to the porous body while still maintaining some electrolyte within the capillary—that is, the bubble pressure—then a limiting value of the pore radius, r, can be calculated for a particular carbon electrode material. The results of such a series of calculations for the first 12 graded porosity materials listed in Table I are given in Table III. A comparison of these calculated pore radii with predicted pore diameter range (Table I) leads to some interesting conclusions. It is apparent, from the comparison of the predicted and calculated pore sizes that the position of the reaction interface—that is, the common point in the interior of the electrode material where the gas, electrolyte, and electrode meet—varies from one electrode material to another. In some the electrolyte apparently diffuses well into the body of the electrode material as is shown by materials 1-WP, 2-WP, 3-WP, 6-WP and 1-NWP, in which the calculated limiting pore radii appear not to be in the zone facing the electrolyte but rather into the middle or opposite outer zone. In most instances it is also apparent that the reaction interface is not on the apparent surface of electrode material but

Publication Date: January 1, 1969 | doi: 10.1021/ba-1965-0047.ch003

well within the body of the electrode. For the nonwetproofed materials the calculated limiting pore radii are smaller when the finer zone faces the electrolyte than when the coarser zone is in the reacting position. This is true for all the materials except Sample 1, which shows the opposite effect. When the materials are wetproofed, however, the paraffin tends to close some of the smaller pores on the finer zone as most of the calculated limiting pore radii are larger than or about the same magnitude as the values obtained for the coarser zone. For those materials which have not been wetproofed the position of the reaction interface depends on the material. Table III shows that when the fine zone of Sample 1 is facing the electrolyte, the limiting pore radius is 15.35μ indicating that the reaction interface is at least in the middle zone or at the interface between the coarser and middle zone. When the coarser side faces the electrolyte the limiting pore radius decreases to an extent that the reaction interface must be in the fine zone. Thus the electrolyte appears to diffuse through two zones into the finer zone to react with the fuel gas. For Sample 1, when the coarse zone faces the electrolyte, the presence or absence of a hydrophobic paraffin coating makes little difference with respect to the position of the reaction interface. Apparently, the interface location is a function of the diffusability of both the fuel gas and the electrolyte, as well as the factors given in Equation 1. In Sample 2 the untreated material is easily wet by the electrolyte as evidenced by the low contact angles (F-28°, C-77°). When the material possesses a hydrophobic film on the surface, however, there appears to be deeper penetration of the electrolyte from the fine side than when this film is absent. The small limiting pore radius of 1.30μ is well within the 3 to 4μ diameter range expected for the unwetproofed fine zone of Sample 2. This low limiting pore radius indicates that the reaction interface is apparently at or just under the geometrical surface; in the fine zone. Apparently, the hydrophobic film present in wetproofed materials is not the only controlling factor influencing the diffusion of the electrolyte and the position of the reaction interface. Sample 6 gives a very unusual limiting pore radius for both its fine and coarse zones. When the fine zone faces the electrolyte it is quite apparent that the reaction interface can only be in the fine zone. When the coarse zone faces the electrolyte, the calculated limiting pore radius is larger than the pores expected to be present in the material. Either the reaction is occurring at the "real surface" of the electrode or the material has developed unusually large and unexpected pores during fabrication. Samples 7 through 12 show limiting pore radii which are consistent with the pore size of the zone facing the electrolyte. Because Samples 9 and 10 are made up of a fine zone sandwiched between two identical coarse zones and a coarse zone sandwiched between two identical fine zones, respectively, it is impossible to determine which zone contains the reaction interface.

Publication Date: January 1, 1969 | doi: 10.1021/ba-1965-0047.ch003

Table III. Electron Change (Δn) Values and Calculated Limiting Pore Radii for the Oxygen Electrode

Sample[1]	Limiting pore radius, μ	Bubble pressure, atm.	E_0[2] at 1 atm. vs. NHE[4]	Δn[3]	Open-circuit voltage	
					H_2 electrode	O_2 electrode
1-F-WP	5.56	0.0730	..	NNB	−0.026	0.886
1-C-WP	4.17	0.0975	0.797	3.38	−0.043	0.816
2-F-WP	5.45	0.0745	0.810	2.27	−0.034	0.905
2-C-WP	4.18	0.0970	..	..	−0.039	0.770
3-F-WP	4.12	0.0985	..	NNB	−0.028	0.878
3-C-WP	4.10	0.0900	..	NNB	−0.046	0.666
4-F-WP	4.06	0.1000	0.785	0.83	−0.039	0.859
4-C-WP	21.20	0.0191	0.782	3.48	−0.031	0.811
5-F-WP	8.08	0.0502	0.808	2.27	−0.022	0.842
5-C-WP	14.00	0.0290	..	NNB	−0.023	0.869
6-F-WP	8.60	0.0471	0.832	0.75	−0.014	0.855
6-C-WP	4.93	0.0825	0.786	2.82	−0.016	0.889
1-F-NWP	15.35	0.0199	0.737	2.20	−0.017	0.857
1-C-NWP	3.41	0.0972	0.843	4.18	−0.035	0.845
2-F-NWP	1.30	0.1005	0.817	2.56	−0.020	0.929
2-C-NWP	9.18	0.0360	0.765	1.42	−0.018	0.827
3-F-NWP	2.76	0.0354	..	NNB	−0.017	0.944
3-C-NWP	6.33	0.0523	..	NNB	−0.034	0.904
4-F-NWP	1.76	0.0740	0.832	3.87	−0.027	0.928
4-C-NWP	6.85	0.0480	..	NNB	−0.042	0.939
5-F-NWP	3.32	0.0380	0.970	0.94	−0.040	0.879
5-C-NWP	9.95	0.0333	1.025	0.89	−0.025	0.939
6-F-NWP	1.77	0.0645	..	NNB	−0.016	0.897
6-C-NWP	20.60	0.0248	0.730	1.42	−0.017	0.859
7-F-NWP	5.50	0.0707	0.772	1.59	−0.019	0.934
7-C-NWP						
8-F-NWP	2.40	0.0540	..	NNB	−0.021	0.976
8-C-NWP	7.83	0.0420	0.793	2.60	−0.027	0.947
9-C-NWP	6.40	0.0515	0.985	0.76	−0.020	0.900
10-F-NWP	1.79	0.0725	0.887	0.92	−0.011	0.811
11-F-NWP	3.72	0.0311	0.789	4.20	−0.019	0.769
11-C-NWP	12.26	0.0268	..	NNB	−0.026	0.781
12-F-NWP	1.36	0.0855	0.929	0.77	−0.008	0.848
12-C-NWP	7.00	0.0468	..	NNB	−0.030	0.845

[1] F = fine side facing electrolyte; C = coarse side (Table I).
[2] E_0 = value obtained by extrapolation of a plot of log P_{O_2} against potential to the value for P_{O_2} equal to 1 atm. (Figure 1); average E_0 = 0.832 *vs.* NHE.
[3] NNB = Non-Nernstian behavior.
[4] NHE = Normal Hydrogen Electrode.

Publication Date: January 1, 1969 | doi: 10.1021/ba-1965-0047.ch003

It has been suggested (*7*) that the concentration of the catalyst in a preferential location within the body of the material may influence the observed variation of the position of the limiting pore radius. To test this possibility, a series of materials duplicating Sample 1 were prepared in which 2 mg. of platinum black per square centimeter of geometrical surface area was added to one zone per sample. These materials were then examined in the fuel cell in the same manner as the other graded porosity materials. If the location of the catalyst exerts a preferential effect then the calculated limiting pore radii should be in the range of the zone which contains the catalyst. Sample 1 was chosen because its three zones represent a coarse, medium, and fine porosity. The results of this study are summarized on Table IV in which Sample 1-Pt contains

the catalyst in the coarse zone, Sample 2-Pt contains the catalyst in the middle zone, and Sample 3-Pt has the catalyst in the fine zone. The results are, at best, inconclusive as to the relationship between limiting pore radius and catalyst position. Sample 1-Pt definitely shows that the limiting pore radius and thus, the reaction interface, is not in the fine zone, regardless of which side faces the electrolyte. However, the values obtained for the limiting radius leave considerable doubt as to whether the reaction interface is in the coarse (outside) or middle zone. For Samples 2-Pt and 3-Pt the location of the reaction interface appears to depend on which side of the electrode is facing the electrolyte. The values obtained for the limiting pore radius suggest that the reaction interface appears to be located in the zone facing the electrolyte. If diffusion into the bulk of the electrode material does occur, then these calculated radius values strongly suggest that the deepest electrolyte penetration is only into the middle zone. A similar conclusion can be obtained by inspection of the limiting pore radii given for the nonwetproofed samples in Table III.

Table IV. Electron Change (Δn) Values and Calculated Limiting Pore Radii for the Oxygen Electrode at Platinum Loaded Materials

Sample	*Limiting pore radius, μ*	*Bubble pressure, atm.*	*E_0 at 1 atm.*[1] *vs NHE*	Δn	*Open-circuit voltage at bubble pressure*	
					H_2 electrode	*O_2 electrode*
1-Pt-F	5.30	0.0242	0.857	3.50	−0.191	0.831
1-Pt-C	7.06	0.0465	1.042	1.26	−0.179	0.944
2-Pt-F	3.76	0.0345	1.015	3.75	−0.062	0.902
2-Pt-C	12.00	0.0273	1.000	2.15	−0.196	0.961
3-Pt-F	3.13	0.0413	0.962	2.73	−0.139	0.934
3-Pt-C	17.00	0.0193	1.070	2.64	−0.206	0.916

[1] Average E_0 = 0.991 v. *vs.* NHE.

The presence of a foreign hydrophobic material like paraffin apparently alters the physical as well as the electrochemical nature of the electrode material by filling up the smaller pores as well as covering the entire material with a fine film. In this respect, the bubble pressures are usually higher for a given material when it has been treated with paraffin. This can be explained if it is assumed that the wetproofing treatment tends to fill the smaller pores, reduce the diameter of the larger pores, and, perhaps, reduce the number of complete routes through the material in which a gas or electrolyte can flow.

Two standard, single-layered electrode materials made from the same raw materials as the graded porosity electrodes were also run at varying gas pressures. These results are given in Table V. Both these materials were wetproofed before testing. The finer material has the larger limiting pore radius, indicating that some of the smaller pores were filled with paraffin. These data are admittedly limited, but the electron change

Publication Date: January 1, 1969 | doi: 10.1021/ba-1965-0047.ch003

values correspond to a peroxide or hydroperoxide mechanism at the reaction interface. This corresponds rather well with the assumed change using the layered, graded porosity materials described previously.

Table V. Properties and Electrochemical Performance of Standard Electrodes

Sample	13	14[1]
Permeability, darcys	0.285	0.366
Probable pore diameter, μ	2–9	1.5–9
Calculated limiting pore radius, μ	3.60	2.22
Bubble pressure, atm.		
H_2 electrode	0.0395	0.0520
O_2 electrode	0.0350	0.0550
E_0 at 1 atm. *vs.* NHE	0.840	0.892
Δn	1.8	2.5
Open circuit voltage		
H_2 electrode	−0.017	−0.016
O_2 electrode	0.859	0.782

[1] Basal planes of crystallites in this sample orientated perpendicular to surface of material; other sample orientation is parallel.

The open-circuit voltages (OCV) of the materials listed in Tables III, IV, and V provided some intriguing results. For the materials in Table III, the non-wetproofed materials generally have a higher OCV than the wetproofed materials. Also, when the finer zone of a given electrode faces the electrolyte a higher OCV is obtained regardless of the presence or absence of a hydrophobic agent. There are some exceptions to this, as for example Sample 5, but these occur in the materials in which the graded porosity is less extreme. The addition of platinum to the various layers during fabrication appears to enhance the values of the open circuit voltages. While the data in Table V are limited, the trend with respect to the fine-coarse OCV relationship is consistent with that of the other materials.

Table VI gives the electrochemical performance of the charcoal materials. Unlike the former materials, charcoal-based carbons are easily "wet" by aqueous solutions. Thus the limiting pore radius at the bubble pressure indicates a large amount of diffusion within the electrode by the electrolyte. The bubble pressures are all very low indicating the probable existence of a large number of continuous pores through the material.

The finer materials described in Table VI (increasing sample number corresponds to increasing fineness) give higher oxygen electrode current densities at lower polarization in the nonwetproofed condition. The hydrogen electrode showed little correlation with respect to electrochemical performance and fineness of the electrode material. Generally, higher current densities at lower polarizations are obtained for nonwetproofed materials for both the hydrogen and oxygen electrodes. This indicates that there is an inhibiting effect caused by the wetproofing agent on

Publication Date: January 1, 1969 | doi: 10.1021/ba-1965-0047.ch003

Table VI. Electron Change (Δn) Values and Calculated Limiting Pore Radii for the Oxygen Electrode at Charcoal Materials

Sample	Limiting pore radius, μ	Bubble pressure, atm.	E_0 at 1 atm.[1] vs. NHE	Δn[2]	Open-circuit voltage at bubble pressure	
					H_2	O_2
1-Ch-C	4.92	0.0222	0.740	1.65	−0.022	0.799
1-Ch-F	10.01	0.0141	0.595	1.45	−0.043	0.699
2-Ch-C	3.81	0.0370	0.727	3.81	−0.019	0.749
2-Ch-F	7.65	0.0170	0.820	5.80	−0.016	0.839
3-Ch-C	7.52	0.0173	0.675	3.92	−0.022	0.699
3-Ch-F	7.07	0.0187	..	NNB	−0.022	0.739

	Current density at 0.3 v. polarization and bubble pressure, ma./sq. cm.	
	H_2 electrode	O_2 electrode
1-Ch-C	4.6	17.5
1-Ch-F	5.2	4.5
2-Ch-C	4.5	6.0
2-Ch-F	6.2	..
3-Ch-C	5.2	4.8
3-Ch-F	4.7	6.8

[1] Average E_0 = 0.771 v. *vs.* NHE.
[2] NNB = Non-Nernstian behavior.

charcoal materials similar to the effect described for electrodes made from other fillers. The effect would be expected to be greater for the charcoal filler materials than for the standard filler materials in that the untreated materials are very hydrophilic. When these easily wet materials are treated with the paraffin in the wetproofing process, great changes might be expected in electrochemical performance. However, the open circuit voltages of these charcoal-based materials give a reverse response to wetproofing compared to the other materials in this study. Usually, nonwetproofed materials have higher open-circuit voltages than wetproofed materials. In the charcoal-based electrodes, wetproofed samples gave superior performance for both the hydrogen and oxygen electrodes.

Electrode Kinetics

While both the hydrogen (anode) and oxygen (cathode) electrodes showed definite bubble pressures which varied with the particular electrode material, only the oxygen electrode showed a large variation in open-circuit potential with gas pressure. The variation in OCV of the hydrogen electrode was of the order 5 millivolts or less for hundredfold changes in pressure. This is probably because the reaction at the hydrogen electrode is a simple one-electron change given by

$$\tfrac{1}{2}H_2 \rightarrow H^+ + e^- \quad (2)$$

or if the molecule is considered to react in a step wise fashion, then

$$H_2 \rightarrow H_2^+ + e^- \quad (3)$$

Publication Date: January 1, 1969 | doi: 10.1021/ba-1965-0047.ch003

The existence of H_2^+ is considered to be very transitory (9, 22) so that the possibility of a long half-life can be discounted. Gaseous hydrogen also has a rate of diffusion some four times greater than oxygen and is considerably more soluble in an aqueous electrolyte of low pH than is oxygen.

Oxygen, on the other hand, has the possibility of undergoing several reactions at the cathode, all of which vary in the electron change per mole of oxygen. Under the proper conditions one mole of oxygen can add one electron to form the perhydroxyl ion as shown by

$$O_2 + e^- \rightarrow O_2^- \tag{4}$$

Oxygen can also add two electrons to form the doubly charged peroxide ion

$$O_2 + 2e^- \rightarrow O_2^{=} \tag{5}$$

And, finally, oxygen can add four electrons to form the oxide ion

$$O_2 + 4e^- \rightarrow 2O^{=} \tag{6}$$

A general reaction covering all three cases takes the form

$$O_2 + xX + ne^- \rightarrow yYO \tag{7}$$

in which n is the electron change, X is a species such as C, Pt, or H^+ present in the system, and YO is either a surface carbon-oxygen complex or some compound with Pt (PtO or PtO_2) or H^+ (HO_2, H_2O_2, HO_2^-, or H_2O). Substituting the factors of Equation 7 into the Nernst equation gives

$$E = E'_0 + \frac{RT}{nF} \ln \left[\frac{a_X^x P_{O_2}}{a_{YO}^y} \right] \tag{8}$$

in which a signifies the activity of the various reactants and products, P_{O_2} is the pressure in atmospheres of gaseous oxygen and the other symbols have their usual electrochemical significance. If only the pressure of oxygen (P_{O_2}) is varied then a_X^x and a_{YO}^y becomes constant and E'_0 will equal E_0, the standard electrode potential. Substituting the numerical values for the constants in Equation 8 and reducing to $\log_{10}$ the equation becomes

$$E = E_0 + \frac{0.059}{n} \log P_{O_2} \tag{9}$$

at 298.16° K. A plot of the observed potential versus the log of P_{O_2} should yield a straight line with a slope equal to $n/0.059$. Further, at $P_{O_2} = 1$ atm., E equals E_0. Such a plot for a typical electrode is shown in Figure

Publication Date: January 1, 1969 | doi: 10.1021/ba-1965-0047.ch003

1. Thus, it should be possible to obtain an indication as to which of the reactions given in Equations 4, 5, and 6 may be occurring at the cathodic reaction interface. Such an approach has been used recently in a study of the rest potentials of the oxygen-platinum-acid system (5).

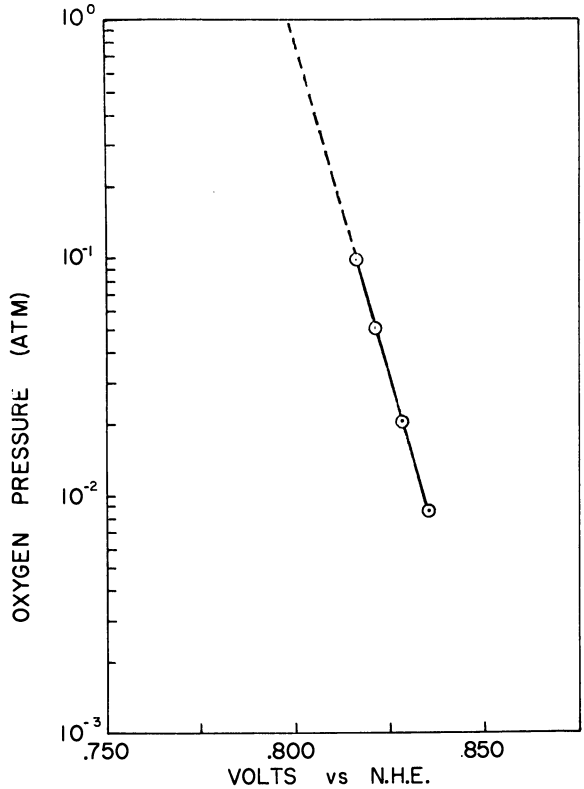

Figure 1. Log O_2 pressure vs. observed potential—sample 1-C-WP

Δn values calculated by this technique (Tables III, IV, V, VI) show that some of the carbons tested gave a non-Nernstian behavior pattern—that is, log P_{O_2} *vs.* E observed lines not linear. For wetproofed samples (Table III), the Δn value is predominantly in the 3 to 4 electron region, when the coarser side of the carbon body is facing the aqueous electrolyte. This is an indication that the reaction occurring at the gas-electrode-aqueous interface (the reaction interface) is due to the reduction of oxygen directly to the dinegative state (an oxide ion). On the finer side, however, the electron change is in the 1 to 2 region indicating formation of perhydroxyl (O_2^-), peroxide ($O_2^=$) or hydroperoxide (HO_2^-) at the reaction interface. For the nonwetproofed materials, the

Publication Date: January 1, 1969 | doi: 10.1021/ba-1965-0047.ch003

predominant electron change is in the 1 to 2 range, indicating the formation of perhydroxyl or more probably hydroperoxide intermediates at the pH values employed in this study. There appears to be no rigorous relationship between limiting pore radii or bubble pressure and the Δn values in the materials under study. The average E_0 value is 0.832 $\pm$ 0.059 volt *vs.* the Normal Hydrogen Electrode, using data from a standard source of electrode potentials (*10*). This value does not correspond to the formation of HO_2, H_2O_2, or H_2O. The average E_o, as well as the individual values, do, however, fall well within the range of the listed values for the formation of some substituted quinones. The formation of such a species on the surface of a carbon body is quite possible as the presence has been determined on certain carbons by polarographic (*4*) and spectrophotometric (*3, 24*) techniques. The fact that the E_0 values have a wide variation indicates the influence of various functional groups, in different positions relative to the quinone groups, on the standard potential.

When platinum black is incorporated into the electrode materials during the fabricating process the electron change values appear to be radically different. In these materials the reaction at the interface seems to proceed directly to the oxide ion rather than through the intermediate, less negative, perradical as shown in Table IV. The E_0 value for electrodes containing platinum black is 0.991 $\pm$ 0.054 volt *vs.* the NHE, a good indication that a different reaction is occurring since the value is quite different from that found for similar materials catalyzed in the standard manner. For the quinone-hydroquinone system, higher E_0 values indicate more highly substituted aromatic structures similar to those which could be expected on a carbon surface.

The use of charcoal as a filler material results in electron change values which depend, to a degree, on the pore size of the electrode. The data for samples with coarser pores indicates reduction of the oxygen to a peroxide or hydroperoxide stage. The average E_0 obtained for these materials is 0.711 $\pm$ 0.063 volt *vs.* the NHE, indicating the presence of less complicated aromatic ring structures (*10*) on the surface. The calculated limiting pore radii of these materials vary only slightly from one material to another, even though the expected change is a twentyfold variation. This could be the result of the wetting of these materials by the electrolyte, as shown by their extremely low contact angles.

The wide range in E_0 values obtained could well be due to the nature of the porous electrode material. In comparison with solid, impermeable electrode materials, porous electrodes possess a larger (by orders of magnitude) contact area per unit volume of electrolyte, reactant and electrode. Because of this there can be a range of reactions, occurring at different reaction rates, within the pores. The distribution of these reactions and the predominance of one or more of these will be a function of the physical structure of the electrode matrix as well as

Publication Date: January 1, 1969 | doi: 10.1021/ba-1965-0047.ch003

the environment in which the electrode material is placed (*1, 11*). Also, because of the porous nature of the electrode material, concentrations of reacting species are constant only at the instant the circuit is closed (commencement of current flow) so that reaction distributions can be quite nonuniform within the electrode matrix. Thus linear polarization may occur only at very low over-potentials where the electrode reaction is initiated. As the reaction interface proceeds further into the matrix of the electrode, the predominating electrode reaction becomes less uniform in its distribution and more complex in its nature. The wide variation in electron change values (Δn) can be considered as evidence for the complexity of the reactions at the reaction interface on a "carbon surface." The Δn and E_o values given in Tables III, IV, V, and VI are most probably those for the rate-controlling step at the reaction interface so that it is quite probable that some carbons have surface properties which enhance the formation of one quinone intermediate over another. On a given carbon the formation of a simple quinone group

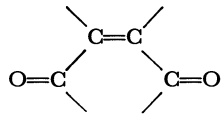

may occur. On a second carbon or at another reaction site on the same carbon, the formation of a degenerate quinone grouping such as

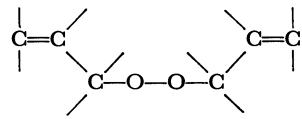

could be favored prior to a rearrangement to the quinone grouping. Considerably more experimental work is needed before a firmly supported mechanism can be postulated.

No attempt was made to interpret the electrochemical data in terms of Tafel slopes (*9*) derived from activation polarization data (since linear polarizations were obtained only at very low overpotentials at the initiation of the electrode reaction) because of the heterogeneous nature of a porous electrode. In addition, other investigators have also reported (*25*) that fuel cell systems do not yield linear polarization curves.

Conclusions

The electroreduction of oxygen at a porous carbon cathode in 3.0*N* sulfuric acid in a fuel cell system appears to proceed through a quinone-hydroquinone reaction based on the comparison of measured potentials with standard potentials. The initial step in the reduction of oxygen may proceed via a one electron change to hydroperoxyl (HO_2), a two

Publication Date: January 1, 1969 | doi: 10.1021/ba-1965-0047.ch003

electron change to peroxide (H_2O_2) or hydroperoxide (HO_2^-), or a four electron change to water (H_2O), depending on the particular carbon material serving as the electrode. When the electrode material has been wetproofed the reduction is directly to the oxide ($\Delta n \sim 4$) state when the coarser side faces the electrolyte and to either the perhydroxyl or hydroperoxide ($\Delta n \sim 1$ or 2) when the finer one is facing the electrolyte.

For nonwetproofed materials the electron change is apparently a function of the particular electrode surface facing the aqueous electrolyte, perhaps indicating the relative ease of formation of one substituted quinone-hydroquinone group versus another. No direct correlation between pore size distribution and electron change values is apparent. Generally, however, zones of finer porosity tend to give higher Δn values than coarser when a platinum black catalyst has been fabricated into the electrode material. This could be due, in part, to the increased resistance offered by the electrode matrix to diffusion resulting in more complete oxygen reaction.

The limiting pore radii of the graded porosity electrodes were calculated to define the position of the reaction interface within the electrode matrix. When the materials had been wetproofed by the addition of paraffin, the reaction interface was probably in the same location regardless of which porosity zone faced the electrolyte. This could result if the wetproofing process plugged the smaller pores in the electrode, producing an electrode material without a porosity gradient. For nonwetproofed materials, the limiting pore radii showed that the reaction interface was located closer to the zone facing the electrolyte. This is an indication that the aqueous electrolyte does not penetrate the electrode matrix as deeply as the gas in the graded porosity materials. There was no correlation of electron change or extrapolated standard potential with the calculated limiting pore radii. When hardwood charcoal was substituted for petroleum coke as a filler material, the extrapolated standard potential indicates that a less substituted quinone-hydroquinone system may be present at the surface. Since the limiting pore radii for these materials were not appreciably different from the petroleum coke materials, it appears that material differences are the principle contributory factors to this effect.

Publication Date: January 1, 1969 | doi: 10.1021/ba-1965-0047.ch003

Literature Cited

(1) Euler, J., and Nonnenmacher, W., *Electrochim. Acta.* **2**, 268 (1960).
(2) Fowkes, F., and Harkins, W., *J. Am. Chem. Soc.* **62**, 3377 (1940).
(3) Garten, V. A., Weiss, D. E., and Willis, J. B., *Australian J. Chem.* **10**, 295 (1957).
(4) Hallum, J., and Drushel, H. V., *J. Phys. Chem.* **62**, 110 (1958).
(5) Hoare, J. P., *J. Electrochem. Soc.* **109**, 858 (1962).

(6) Hunger, H., "Investigation of the Hydrogen-Oxygen Fuel Cell," USASRDL, Tech. Rept. **2001,** Dec. 15, 1958.
(7) Hunger, H., USAELRDL, private communication.
(8) Kordesch K., and Marko, A., *J. Electrochem. Soc.* **107,** 480 (1960).
(9) Kortum, G., and Bockris, J. O'M., "Textbook of Electrochemistry," pages 418–60, Elsevier Publishing Co., New York, 1951.
(10) Latimer, W. L., "Oxidation States of the Elements and Their Potentials in Aqueous Solution," Prentice-Hall, Inc., New York, 1952.
(11) Newman, J. S., and Tobias, C. W., *J. Electrochem. Soc.* **109,** 1183 (1962).
(12) Parker, W. E., Marek, R. W., and Heintz, E. A., "Fuel Cell Electrode Materials," USAELRDL, Contract No. DA 36–039 SC-88954, Rept. 1, March 1, 1962–May 31, 1962.
(13) *Ibid.*, Rept. **2,** June 1, 1962–Aug. 31, 1962.
(14) *Ibid.*, Rept. **3,** Sept. 1, 1962–Nov. 30, 1962.
(15) *Ibid.*, Rept. **4,** Dec. 1, 1962–Feb. 28, 1963.
(16) Parker, W. E., and Rusinko, F., Jr., "Development of Electrode Materials for Fuels Cells," USASRDL, Contract No. DA 36-039 SC-85356, Rept. 1, July 1, 1960–Sept. 30, 1960.
(17) Parker, W. E., Rusinko, F., Jr., and Marek, R. W., "Development of Electrode Materials for Fuel Cells," USASRDL, Contract No. DA 36-039 SC-85356, Rept. **2,** Oct. 1, 1960–Dec. 31, 1960.
(18) *Ibid.*, Rept. **3,** Jan. 1, 1961–March 31, 1961.
(19) *Ibid.*, Rept. **4,** April 1, 1961–June 30, 1961.
(20) *Ibid.*, Rept. **5,** July 1, 1961–Sept. 20, 1961.
(21) Ritter, H. L., and Drake, L. C., *Ind. Eng. Chem.* **17,** 782 (1945).
(22) Stern, M., and Geary, A. L., *J. Electrochem. Soc.* **104,** 56 (1957).
(23) Taschek, W., ADVAN. CHEM. SERIES, **47,** 9 (1965).
(24) Test, R. E., and Hansen, R. S., "Acid Base Properties of Carbon Black Surfaces," AEC Rep. **IS-341,** May 1961.
(25) VanWinkle, J., and Carson, W. N., *Electrochem. Tech.* **1,** 18 (1963).

RECEIVED February 17, 1964. This work has been partially supported by USAELRDL, Power Sources Branch, Fort Monmouth, New Jersey.

Publication Date: January 1, 1969 | doi: 10.1021/ba-1965-0047.ch003

In Fuel Cell Systems; Young, G., el al.;
Advances in Chemistry; American Chemical Society: Washington, DC, 1969.

Polarization at Porous Flow-Through Electrodes

LEONARD G. AUSTIN, PIERRE PALASI, and RICHARD R. KLIMPEL

Fuel Technology Department, Pennsylvania State University, University Park, Pa.

The combined equations of electrokinetics, mass transport, and ohmic resistance for dissolved reactants flowing through a porous electrode have been computed in dimensionless variable form. It was assumed that radial mass transfer and axial diffusion effects are negligible. Experimental results using a redox couple show general agreement with the predicted values but indicate that axial diffusion may be significant at high current densities. Several soluble fuels and oxidants have been tested through electrodes of packed platinum black and abnormally low limiting currents are observed at high current densities. This may be due to the poisoning of platinum with surface adsorbed oxygen, discharged at the anodic potentials used.

Publication Date: January 1, 1969 | doi: 10.1021/ba-1965-0047.ch004

The flow-through electrode is an electrochemical system which has received little attention. It is of primary interest in redox fuel cells (*1*, *8*, *16*) where a dissolved ionic fuel (or oxidant) is to react at an electrode. In such a system, where liquid is circulated through the cell, it is clearly much better to force the fresh liquid through the electrode and take spent liquid from the exit side. The electrode then acts as a separator between fresh and spent liquid and, more important, the mass transport of reactant to the electrode can be easily controlled. By forcing electrolyte through the electrode, it is no longer necessary to rely on diffusion of fuel to the electrode, and, consequently, the mass transport problems of non flow-through electrodes can be considerably diminished. Similarly, for fuels or oxidants such as methanol, hydrazine, and nitric acid, which can be dissolved in high concentrations in the electrolyte, it may be desirable to use flow-through electrodes (*9*, *13*, *14*).

The concentration of reactant and rate of flow determine the maxi-

In Fuel Cell Systems; Young, G., el al.;
Advances in Chemistry; American Chemical Society: Washington, DC, 1969.

mum current which can be drawn since it is not possible to draw more current than the corresponding amount of reactant put in per second. The speed of electrochemical reaction, in the form of the exchange current for the reaction (2), is important in determining the polarization at a given current. In addition, the ohmic voltage gradient in the electrolyte in the pores of the electrode also affects the polarization.

Perskaya and Zaidenman (*15*) gave the basic mathematical form of the process. However, they solved the equation only for low current density, low polarization conditions, where the approximation $\exp(\alpha nF\eta/RT) = 1 + \alpha nF\eta/RT$ applies. In our analysis we have found that this can only rarely be applied. The treatment we give explains reasonably well the whole current-voltage range of their experimental results and also explains the experimental results of Bond and Singman (*5*). However, the assumptions made in the theory are not generally valid, and the breakdown of the theory is demonstrated and discussed.

Publication Date: January 1, 1969 | doi: 10.1021/ba-1965-0047.ch004

Physical System and Assumptions

The physical system studied consists of a uniform, porous, plane electrode with reactant dissolved in electrolyte flowing into the left hand face; unreacted reactant and dissolved product flow out of the right hand face (Figure 1). The reaction could be a simple redox reaction such as $Fe^{2+} \rightleftarrows Fe^{3+} + e^-$. In a redox cell employing a separator the circuit is completed within the cell by hydrogen ion flowing from the anode to the cathode. The following assumptions are made.

The flow is uniform through the electrode. This is very nearly true for a small experimental electrode, but it may not be so for a large electrode.

Ohmic loss in the material of the electrode is negligible. This will be a good approximation for properly constructed electrodes of metal or carbon.

The reaction at the external faces of the electrode is small compared to the total reaction. The external faces can be considered as extensions of the internal area and the assumption would only be false in the limit where the internal area became small.

The pores of the electrode are small in radius compared to their length so that negligible concentration gradients exist across the radius of the pore. In other words, the pore radius is so small the radial diffusion is rapid enough to maintain uniform concentration across the pore radius; the only concentration changes will be linear along the axis of the pore. With this assumption, the variation of laminar flow rate across the pore radius is of no consequence. This assumption is discussed later in more detail.

The porous electrode has its pores so well interlinked that it can be considered to act as a homogenous system, with variation of conditions at a given penetration applying only over small regions. Electrodes must be constructed so that no major cracks or pinholes exist.

The flow rate is great enough that axial mass transfer of reactant and product by diffusion is negligible compared to mass transfer by the bulk flow. For concentrated electrolytes it may also be assumed that the specific conductivity of the electrolyte remains constant.

The streaming potential is small when compared to other effects, which will be true when strong electrolytes are used.

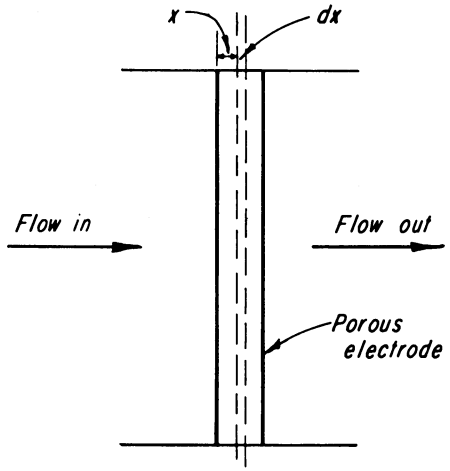

Figure 1. Illustration of system studied.

A less easily justified assumption is that the electrochemical reaction at the pore surface is a simple reaction with the rate form (2)

$$i = i_0[(R/R_i)e^{\eta/b} - (P/P_i)e^{-\eta/b}] \quad (1)$$

R_i, P_i are the entering concentrations (assumed equivalent to activities) of the reactant and product; i, i_0 refer to unit area of the pore surface, (see list of nomenclature). Equation 1 may apply to simple redox reactions, but one would expect, for example, dissolved methyl alcohol fuel to have a more complex form. At open circuit conditions, with no current flow, R and P are constant through the electrode and equal to R_i and P_i, and they determine the theoretical potential. However, if the basic exchange current is small, then impurities in the feed may give rise to leakage current, and a mixed potential may be obtained. A sufficient rate of flow will prevent diffusion of a disturbing material from the other electrode, but any impurities in the feed are being constantly replaced. Thus, very low current density measurements and open circuit potentials may not correspond to ideal values.

Theory

Consider unit face area of the electrode. Let the velocity of flow through the electrode be v, cc per square centimeter of face per second.

Publication Date: January 1, 1969 | doi: 10.1021/ba-1965-0047.ch004

Consider element dx in Figure 1. The amount of reactant flowing in per second is Rv and the amount flowing out is $[R + (dR/dx)dx]\ v$. The amount of R reacted to P in the element per second, is given by

$$di/nF = i_0[(R/R_i)e^{\eta/b} - (P/P_i)e^{-\eta/b}](S/nF)dx \tag{2}$$

n is the total number of electrons involved for each complete reaction; S is the reacting area per unit volume of electrode. At steady state $R_i + P_i = R + P$, therefore

$$-dR/dx = (i_0S/vnF)\left[R\left\{\frac{e^{\eta/b}}{R_i} + \frac{e^{-\eta/b}}{P_i}\right\} - \frac{(R_i + P_i)}{P_i}e^{-\eta/b}\right] \tag{3}$$

If the specific resistance of the electrolyte is ρ', the porosity of the electrode ϵ and the tortuosity factor q (6) then, by Ohm's law,

$$(\rho' q/\epsilon)i = d\eta/dx$$

or

$$i = (1/\rho)\ d\eta/dx \tag{4}$$

where ρ is understood to include the porosity and tortuosity factors.

The complete solution to the problem is given by the solution of Equations 3 and 4. We could not, however, obtain an analytical solution. Computed results are presented later, but it is informative to consider a limiting condition which has an analytical solution. The limiting condition is that the ohmic drop within the electrolyte in the pores is negligible. The effect of ohmic drop can be considered as a disturbance of this limiting condition.

Case 1. Ohmic Effects Neglected.

Neglecting ohmic drop, Equation 3 can be integrated from $x = 0$, $R = R_i$ to x, $R = R$

$$(i_0S/vnF)x = \frac{1}{(\epsilon^{\eta/b}/R_i) + (e^{-\eta/b}/P_i)} \ln\left[\frac{(e^{\eta/b} - e^{-\eta/b})}{(R/R_i)e^{\eta/b} - [(R_i + P_i - R)/P_i]e^{-\eta/b}}\right] \tag{5}$$

When $x = L$, the thickness of the electrode, $R = R_f$, the final concentration of reactant issuing from the right face of the electrode. The current per square centimeter of electrode is $i = nFv\ (R_i - R_f)$ and the limiting density is clearly given by

$$i_L = nFvR_i$$

Thus

$$i/i_L = 1 - R_f/R_i = \text{degree of conversion} \tag{7}$$

Publication Date: January 1, 1969 | doi: 10.1021/ba-1965-0047.ch004

Eliminating R_f between Equations 5 and 7

$$i/i_L = (e^{\eta/b} - e^{-\eta/b})(1 - e^{-(LSi_o/i_L)f})/f \quad (8)$$

where $f = e^{\eta/b} + (R_i/P_i)e^{-\eta/b}$.

This is the equation relating current to polarization and it includes the parameters of i_o, S, L, v, R_i, P_i.

At low polarization the approximation $\exp(\eta/b) = 1 + \eta/b$ can be used. Then, when LSi_O/i_L is small, that is, the reaction has a relatively low exchange current,

$$i = LSi_o(n_1F/RT)\eta \quad (9)$$

(n_1 is the electron transfer in the rate controlling step, usually 1). This is the normal linear form of i versus η, and physically it represents the interior of the electrode being used at uniform concentration, with an effective area of SL per sq. cm. of electrode planar area. Alternatively, if LSi_O/i_L is large, that is, the exchange current is high by comparison with the limiting current,

$$\eta = (2.3RT/nF) \log\left[\frac{(1 + \gamma i/i_L)}{(1 - i/i_L)}\right], \gamma = R_i/P_i \quad (10)$$

This is again an expected result; it corresponds to pure concentration polarization.

For irreversible conditions [(R_i/P_i) exp $(-\eta/b)$ negligible compared to exp(η/b)],

$$i/i_L = 1 - e^{-(SLi_o/i_{r_1})e^{\eta/b}}$$

or

$$\eta/2.3b = \log\left[\log\left\{\frac{i_L}{i_L - i}\right\}\right] - \log [SLi_o/2.3i_L] \quad (11)$$

When i is much less than the limiting current a normal Tafel equation is obtained

$$\eta/2.3b = \log i - \log(SLi_o) \quad (12)$$

Case 2. Ohmic Effects Included.

Combining Equations 4 and 7 gives

$$d^2\eta/dx^2 = \rho i_o S\left[R_t\left(1 - \frac{i}{\rho i_L}\frac{d\eta}{dx}\right)\left(\frac{e^{\eta/b}}{R_i} + \frac{e^{-\eta/b}}{P_i}\right) - \left(\frac{R_i + P_i}{P_i}\right)e^{-\eta/b}\right]. \quad (13)$$

This is the basic equation relating polarization to distance into the electrode. One limiting case can be treated analytically. For high rates of

Publication Date: January 1, 1969 | doi: 10.1021/ba-1965-0047.ch004

flow, high electrolyte resistance, and low fractional currents such that the concentrations R and P can be assumed constant through the electrode, the equation reduces to

$$d^2\eta/dx^2 = \rho i_o S(e^{\eta/b} - e^{-\eta/b})$$

This has been treated by Ksenzhek and Stender (11) and Austin (3, 4).

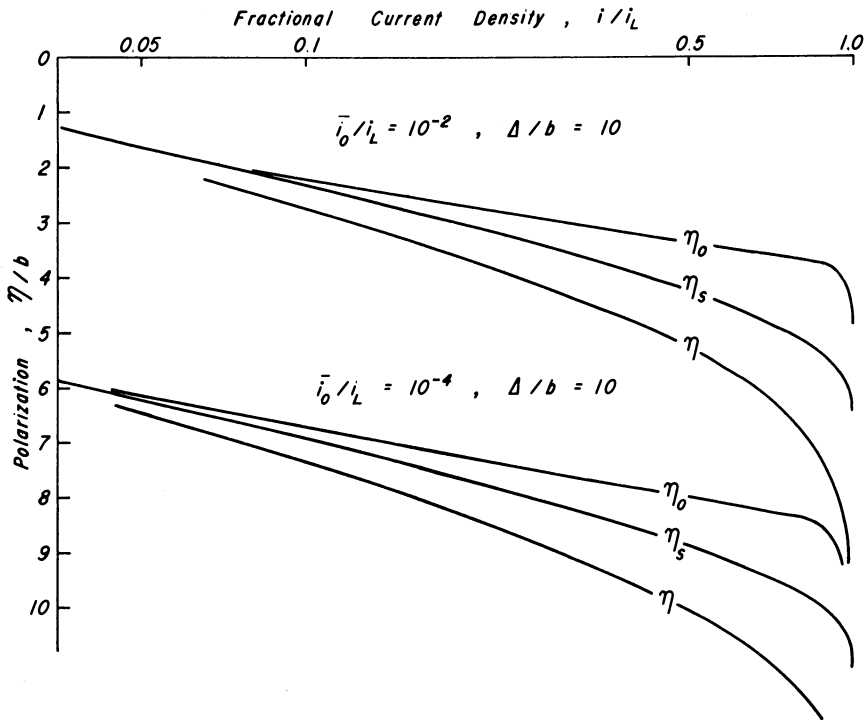

Figure 2. Relation of current to polarization for flow-through electrode.

Equation 13 was put into a form suitable for numerical integration as follows. Reduced values of η, x are defined by $\bar{\eta} = \eta/b, \bar{x} = x/L$. It is also convenient to let $\Delta = i_L \rho L$. Δ *is the* maximum possible ohmic loss through the electrode and is obtained under conditions where the reaction is completed in a differential element at $x = 0$, so that all the ions supporting i_L have to be transported from L *to* $x = 0$ (or $x = 0$ to L). This can only occur at large total polarization. A reduced Δ is defined by $\bar{\Delta} = \Delta/b$, and $i_o SL$ is replaced by $\bar{i}_o$. Then,

$$d^2\bar{\eta}\, d\bar{x}^2 = (\bar{i}_o/i_L)\bar{\Delta}[(1 - (1/\bar{\Delta})d\bar{\eta}/d\bar{x})(e^{\bar{\eta}} + e^{-\bar{\eta}}) - (1 + \gamma)e^{-\bar{\eta}}]. \quad (14)$$

The boundary conditions are $\eta = \eta_o$ at $x = 0$ and $\eta = \eta_L$ *at* $\bar{x} = 1$, where η

Publication Date: January 1, 1969 | doi: 10.1021/ba-1965-0047.ch004

is the polarization at the right hand face of the electrode. The total current density from the electrode is

$$i/i_L = (1/\bar{\Delta})\ (d\bar{\eta}/d\bar{x})_{\bar{x}\,=\,1} \tag{15}$$

Equation 14 was solved by integrating once, putting into finite difference form and re-iteratively computing; $d\bar{\eta}/d\bar{x}$ at $x = 1$ was obtained and i/i_L found from Equation 15. It is readily shown that for irreversible conditions the shape of the curves is independent of the value of $\bar{i}_o/i_L$ (for a given Δ value), but the curves are shifted bodily to higher polarizations at lower $\bar{i}_o/i_L$ values according to

$$\Delta\eta_{12} = 2.3b \log [(\bar{i}_o/i_L)_1/(\bar{i}_o/i_L)_2] \text{ volts} \tag{16}$$

where $\Delta\eta_{12}$ is the change in polarization (at all currents in the irreversible region) in going from $(\bar{i}_o/i_L)_1$ to $(\bar{i}_o/i_L)_2$.

It must be realized that the results of the computations are quite general since they are given in reduced form. Even if an analytical solution existed (in the form of an infinite series, for example) it would be so complex that the meaning of the solution would not be apparent until values were computed for given conditions. No restriction exists to the computed values except they are in reduced form, so that the scales do not represent voltage and current directly but voltage in multiples of b and current as a fraction of i_L.

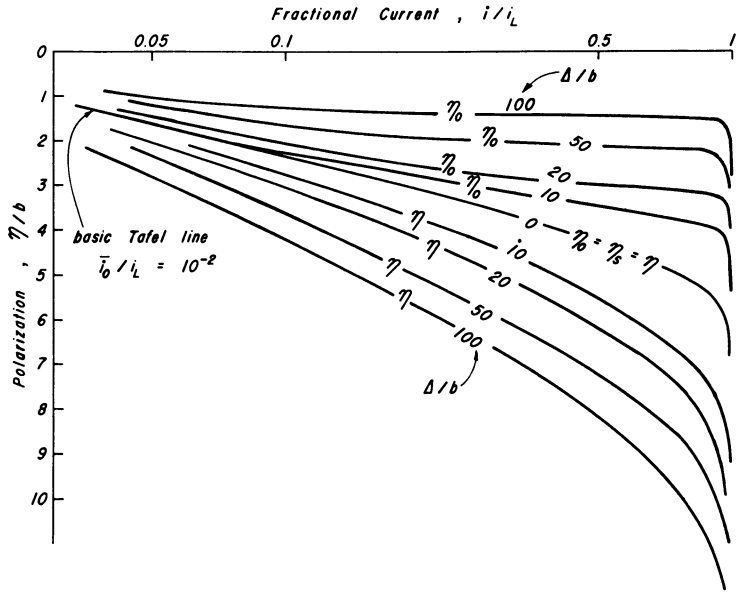

Figure 3. Effect of ohmic resistance on polarization of flow-through electrode.

Publication Date: January 1, 1969 | doi: 10.1021/ba-1965-0047.ch004

Results of Computations.

The equations were solved on an IBM 7074 digital computer. Figures 2, 3, and 4 show the results of computations of the full equation, allowing for ohmic resistance. To avoid confusion, the η calculated for the case of no ohmic effect is termed η_s, the polarization at the entering face is termed η_0 and the polarization of practical importance, at the exit face, is termed η.

The physical picture of the effect of ohmic voltage gradient which emerges from the solution of the equations is as follows. The flowing electrolyte, with a high concentration of fuel, enters at one face and,

Publication Date: January 1, 1969 | doi: 10.1021/ba-1965-0047.ch004

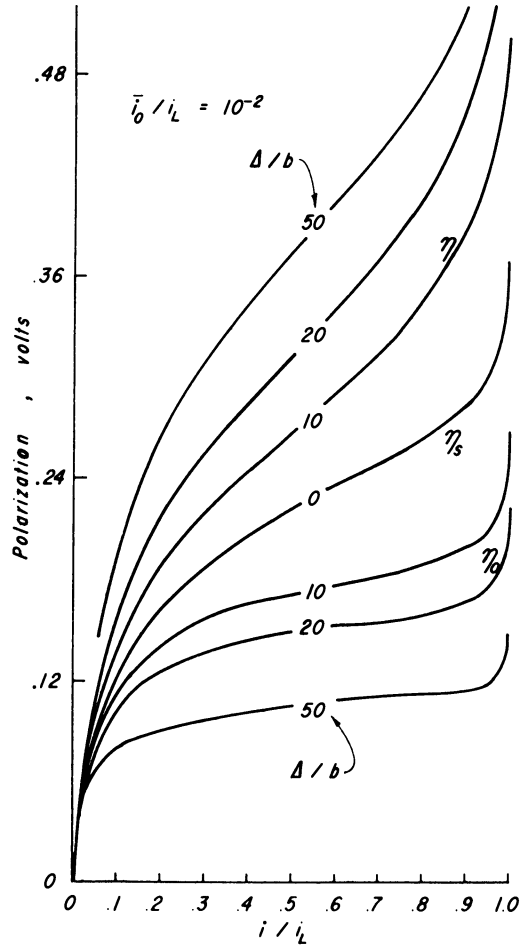

Figure 4. Results of Figure 3 for a Tafel coefficient of 0.12 volts.

with a suitable polarization, it starts to react. The ionic transfer through the electrolyte, which maintains charge balance, gives rise to an ohmic voltage gradient. This ohmic effect increases the polarization at further penetration into the electrode, and the reaction rate is increased. Therefore, as the fuel flows through the electrode, it is consumed more and more rapidly, which increases the cumulative ion transfer, which causes increased ohmic effect, which increases the rate of consumption and so on. Thus for a large value of Δ (the index of ohmic effect) the reaction is concentrated towards the exist face of the electrode. This is shown in Figure 5 for $\bar{\Delta} = 100$ and currents of 0.84 and 0.23 of the limiting current. For the larger value, most of the reaction occurs in the final one-tenth of the electrode. For the lower value, most of the reaction occurs in the final three-tenths. An effect of this concentration of the reaction in a zone towards the exit face is that radial mass transfer limitations across the pore may come into play sooner than would be expected if reaction were more uniformly distributed through the pore.

The curves in Figure 2 are calculated for a Δ/b value of 10. Examining the curves for $i_0/i_L = 10^{-2}$ it is seen that η_0 and η lie on either side of the η_s curve. This is as expected, because the ohmic voltage gradient in the electrode speeds up the reaction toward the exit face; therefore, the initial activation polarization η_0 has to be less to give a certain i/i_L value. As expected, the η_0 value at low current density (but reaction still irreversible) approaches η_s, both being given by a Tafel form. Because the increase in polarization from entrance to exit in the electrode causes the reaction to proceed faster towards the exit, the mean distance which the current carrying ions have to traverse is strongly weighted to be near to the exit face, giving a relatively small ohmic drop. Of course, as the limiting current is approached very closely, all of the reaction occurs towards the entrance face giving the complete ohmic drop. This condition is only reached as the polarization becomes very large.

It can be seen, therefore, that the simpler analytical Equation 8 is of value since it predicts the main features of the process. The ohmic effect is a secondary effect. Figure 2 shows that a decrease in the basic parameter i_0/i_L causes a bodily shift of the curves, with no difference in shape; as expected, decrease of i_0/i_L by a factor of 10 bodily shifts the polarization curve by $2.3b$ volts. (The 2.3 arises because b is $RT/\alpha n_1 F$, whereas the normal Tafel coefficient is $2.3RT/\alpha n_1 F$.) For a one electron process at room temperature the shift would be about 0.12 volts, assuming α to be 1/2.

The effect of change of Δ is shown in Figure 3. The results were computed for $\Delta/b = 0$, 10, 20, 50 and 100. This covers most of the range likely to be encountered for electrodes of reasonable porosity and

Publication Date: January 1, 1969 | doi: 10.1021/ba-1965-0047.ch004

strongly conducting electrolytes. Figure 4 shows the polarization for a one electron rate controlling step at room temperature where the normal Tafel coefficient would be 0.12 volts. For a given limiting current (given by the flow rate and concentration of reactant), the important parameters are the effective exchange current i_o, the effective ohmic resistance of the electrolyte in the pores and αn_1, determined principally by the number of electrons transferred in the rate controlling step. The ohmic effect, represented by Δ, does not give a linear effect on the polarization. For example, in going from $\Delta/b = 10$ to $\Delta/b = 50$, the difference between η and η_s over the practical range is increased much less than five times. This is to be expected since the higher ohmic voltage gradient forces the reaction to occur nearer the exit face.

Publication Date: January 1, 1969 | doi: 10.1021/ba-1965-0047.ch004

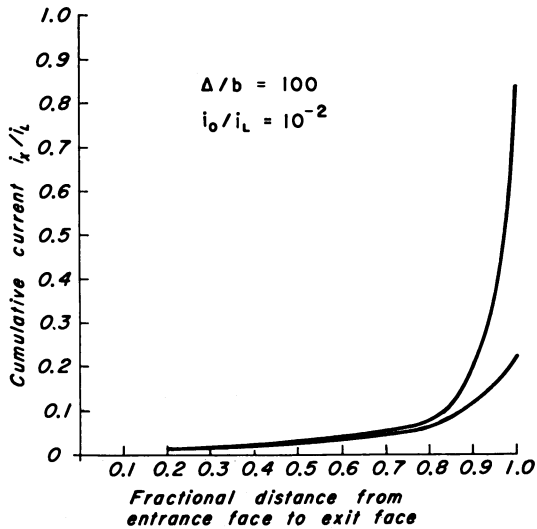

Figure 5. Cumulative reaction through a flow-through electrode.

Figure 6 shows the results plotted for limiting currents in the ratios 1:2:5, but with the same i_o. This would correspond to a given electrode and fuel at different flow rates. Note that Δ/b will vary in the same ratio while i_o/i_L will vary as the inverse of the ratio. Figure 6 shows that the initial portions of the curves are almost identical. The figures may be compared with the experimental results given below.

Experimental Results.

To test whether the theory could explain, in a qualitative manner, results for dissolved fuels such as methanol, a porous electrode made of

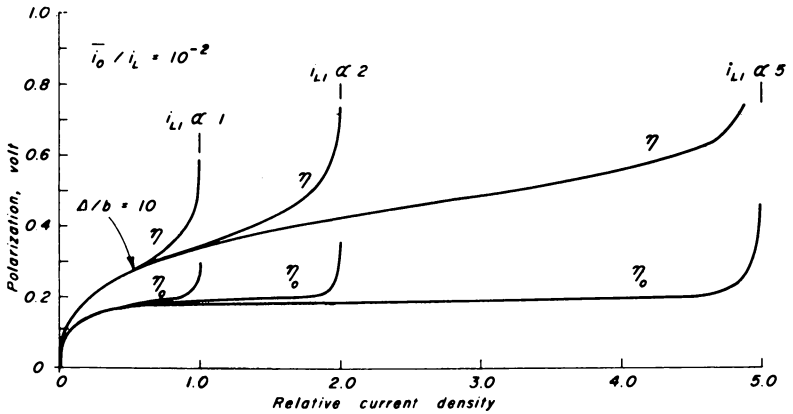

Figure 6. Computed effect of increasing flow rate.

platinum black was used. The use of this catalytic material made it possible to reach the limiting currents at voltages before the oxygen evolution potential. A known weight of platinum black was compressed between two 80 mesh screens of bright platinum. For the thicker electrodes made with a greater weight of platinum black, a third screen was used in the center of the electrode (100 mg. per sq. cm. of platinum black gave about 1 mm. thickness). The electrode was clamped in a Lucite holder to give compression of the powder. The ohmic resistance through the electrode material was found to be negligible. A fritted glass disc was used at the entrance face of the electrode to provide a rigid backing and to ensure even flow distribution. A counter electrode of platinum screen was mounted in the Lucite tube, in line with the porous electrode. The cell was run vertically with the reactant dissolved in the electrolyte entering at the bottom, flowing through the fritted disc and the platinum black electrode, up past the counter-electrode (at which hydrogen was evolved) and out to a collector for flow rate measurement. Evolved gases were taken off from the top of the cell. The voltage between the electrode and the entering electrolyte was measured against a saturated calomel electrode. The electrode-electrolyte voltage at the exit face was also measured against the saturated calomel electrode, by extrapolation to the electrode face of measurements at two known positions downstream.

Blank measurements made without a dissolved reactant showed negligible current densities between hydrogen evolution potentials and oxygen evolution potentials.

The most stable and reproducible results were obtained when the stannous-stannic redox couple, was used as a reactant. Other work (*12*) has shown that this couple gives a Tafel form at potentials more anodic than about 0.05 volts *vs.* S.C.E., with a slope of 0.14 volt per current

Publication Date: January 1, 1969 | doi: 10.1021/ba-1965-0047.ch004

decade at 25° C. Figure 7 shows typical results for two different flow rates. The solid curve shows the exit face polarization *vs.* current, and the broken curve shows the entrance face polarization *vs.* current. From a plot of the results according to Equation 11 it was estimated that the apparent exchange current was 1.7 ma. per sq. cm. and the Tafel slope about 0.14. The values could not be determined precisely because: (a) a line corresponding to η_s has to be drawn between the entrance face and exit face polarization curves, and uncertainty is present as to the best position for this line; (b) the higher current density portions of the curve deviate from the expected curves (see discussion of results); and (c) the low current values were in a region where the Tafel slope of the $Sn^{2+} \rightarrow Sn^{4+}$ reaction is changing (*12*). However these values were used to compute the η_s values for the two limiting currents; the comparison between computed and experimental results is shown in Figure 8. It can be seen that the experimental curves bracket the computed curve in the expected manner except at values of current density approaching the limiting current density (see discussion of results).

Publication Date: January 1, 1969 | doi: 10.1021/ba-1965-0047.ch004

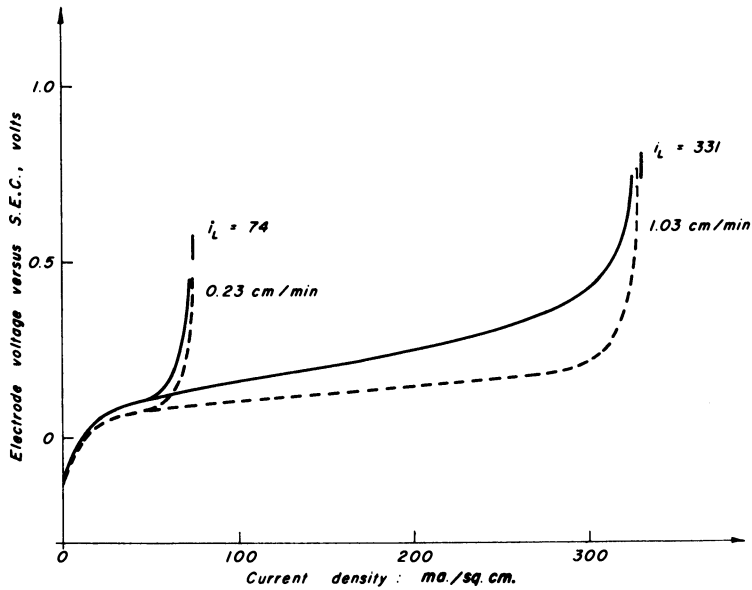

Figure 7. Anodic reaction, 0.1M stannous chloride, 0.1M stannic chloride, 4M HCl, 250 mg/cm² Pt black.

Some typical results using dissolved fuel are shown in Figures 9 to 16. All tests were made at room temperature. The broken lines represent the inlet voltage and the solid lines the exit voltage where the latter is

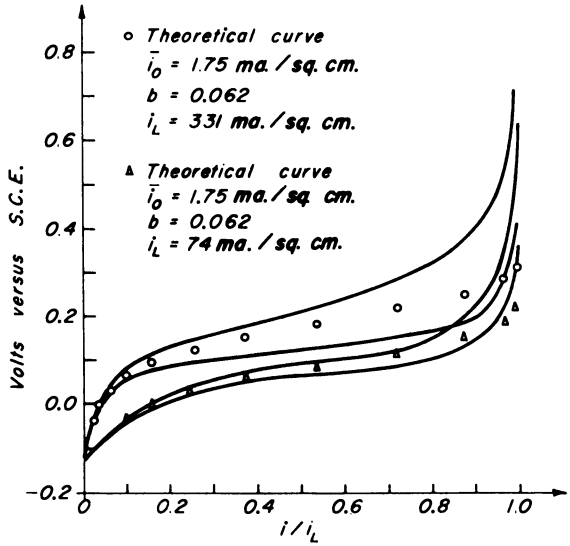

Figure 8. Comparison of simple (no ohmic effect) theoretical curves with experimental results of Fig. 7.

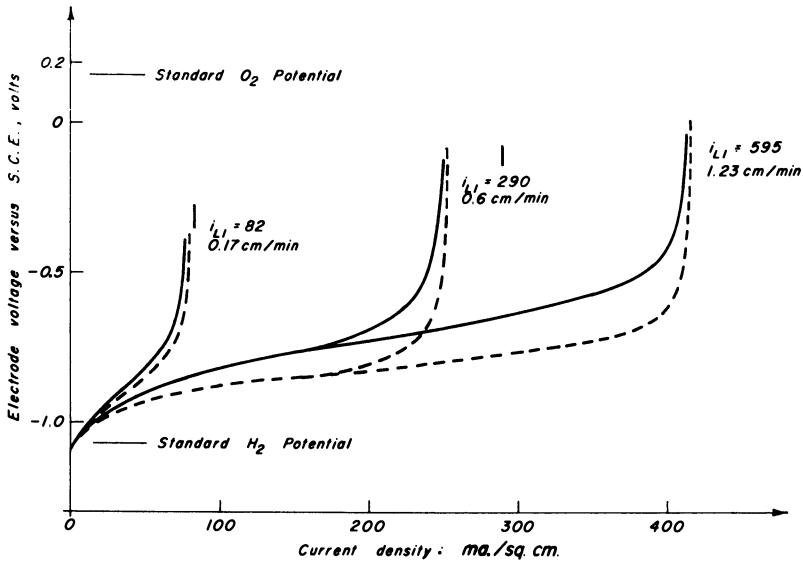

Figure 9. 0.05M Methanol, 4M KOH, 500 mg/cm² Pt black.

the curve which shows the full voltage loss at the electrode. In general the curves were reasonably stable, and providing the voltage was not taken too near to oxygen evolution, it was usually possible to go up and

American Chemical Society
Library
1155 16th St., N.W.
Washington, D.C. 20036

In Fuel Cells; Young, G. J., et al.;
Advances in Chemistry; American Chemical Society: Washington, DC, 1969.

Publication Date: January 1, 1969 | doi: 10.1021/ba-1965-0047.ch004

down the curve without hysteresis (although slow drift was observed for times of 20 minutes or so). It is obvious that the results fro this type of electrode cannot be completely explained by the simple theory developed previously. In general, the limiting currents obtained at the higher flow rates were less than those expected from the amount of reactant being forced through the electrode. Figure 17 shows results for methanol, formaldehyde (with methanol stabilizer) and potassium formate in alkaline solution. Similar results were obtained in 32% sulfuric acid solution. Other results are summarized in Table 1.

Table I. Expected and Observed Values of Limiting Current

Fuel	*n*	*Molar Concn. of Fuel*	*Electrolyte*	*Mg./ Sq. Cm. of Pt. Black*	*Flow Rate, Cm./ Min.*	i_{L1} *Ma./ Sq. Cm.*	i_{L2} *Ma./ Sq. Cm.*	i_{L2}/i_{L1}
Methanol	6	0.1	4*M* KOH	40	0.10	97	117	1.2
					0.57	54	220	0.4
					1.67	161	335	0.2
				200	0.17	161	215	1.3
					0.57	546	497	0.9
			3*M* H_2SO_4	80	0.12	113	90	0.8
					0.40	386	230	0.6
					1.00	965	330	0.3
KBH_4	8	0.02	4*M* KOH	80	0.20	52	50	1.0
					0.43	112	112	1.0
					2.50	642	380	0.6
					4.00	1030	500	0.5
		0.1			0.20	278	258	1.07
					0.47	600	595	1.0
Ammonia	3	0.1	4*M* KOH	70	0.23	113	138	1.2
					0.60	290	296	1.0
					2.00	955	344	0.4
		0.5			0.17	400	498	1.25
Hydrazine	4	0.02	4*M* KOH	80	0.43	57	80	1.4
					1.37	176	150	0.9
					2.00	258	200	0.8
		0.1			0.30	192	200	1.04
					0.60	385	384	1.0
					1.00	640	620	0.97
Hydrogen peroxide	2	0.2	4*M* KOH	130	0.2	128	84	.7
					0.67	426	250	.6
					1.07	682	352	.5
			7*M* H_2SO_4		0.23	150	152	1.0
					0.67	426	304	.7

Limiting Currents.

There are at least three possible reasons why the limiting currents observed at high flow rates are less than those predicted. Firstly, radial

Publication Date: January 1, 1969 | doi: 10.1021/ba-1965-0047.ch004

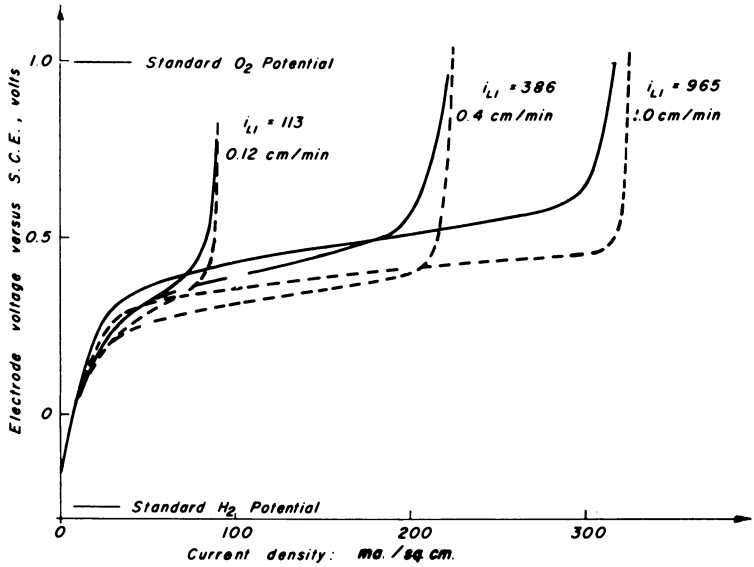

Figure 10. 0.1M Methanol, 3M H_2SO_4, 80 mg/cm² Pt black.

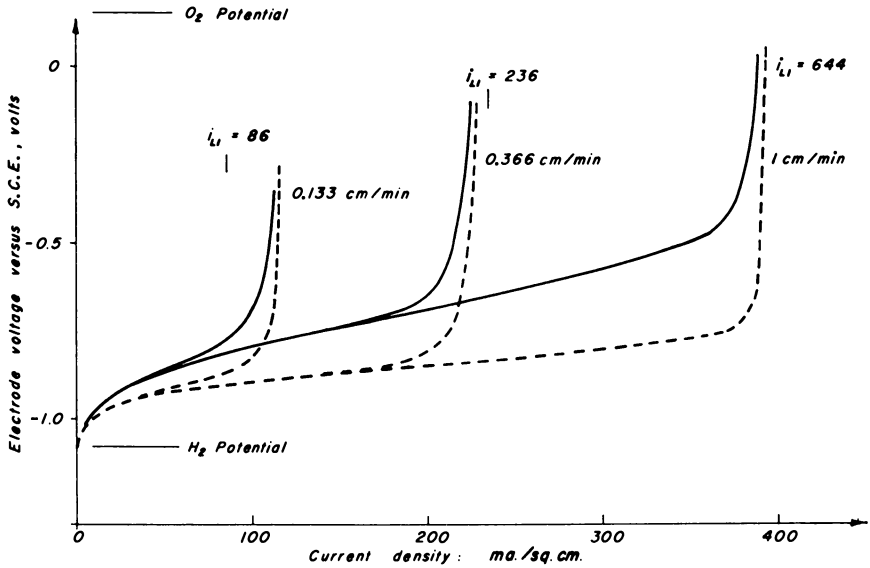

Figure 11. 0.2M Potassium formate, 4M KOH, 230 mg/cm² Pt black.

mass transport hindrance across the pores of the electrode might be significant. Secondly, the reaction may involve a non-electrochemical step which can become rate controlling—e.g., a slow chemisorption, surface rearrangement or dissociation in the bulk of the electrolyte. Thirdly, the

Publication Date: January 1, 1969 | doi: 10.1021/ba-1965-0047.ch004

platinum may become less active as potential is increased owing to the formation of oxide on the surface. A limiting current would be reached when the change in voltage deactivated the surface (and hence reduced the electrochemical rate) at the same rate at which it accelerated the electrochemical reaction.

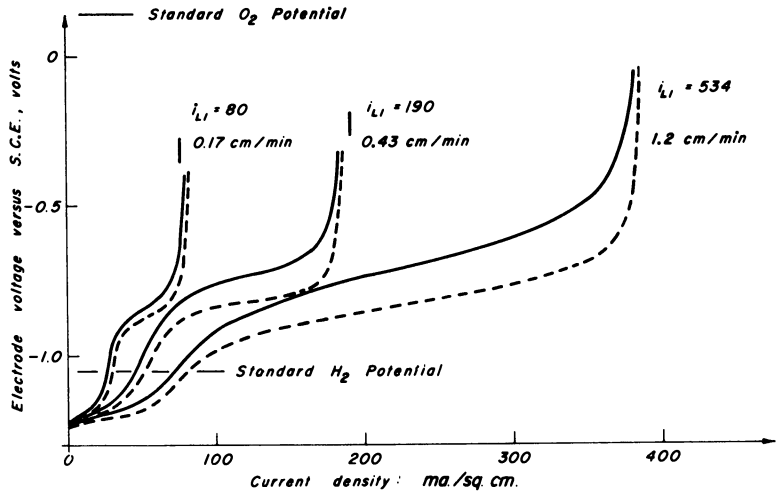

Figure 12. 0.05M Formaldehyde (0.0125 methanol as stabilizer), 4M KOH, 250 mg/cm² Pt black.

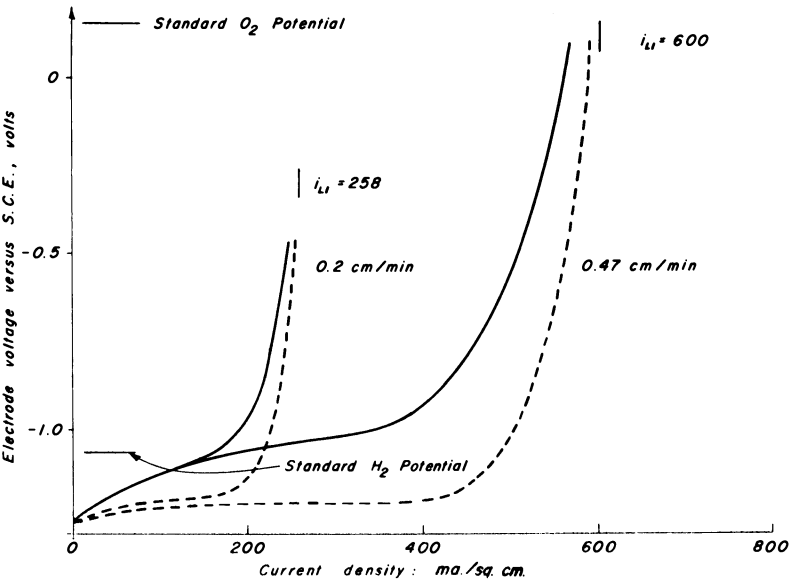

Figure 13. 0.1M KBH_4, 4M KOH, 80 mg/cm² Pt black

Publication Date: January 1, 1969 | doi: 10.1021/ba-1965-0047.ch004

Considering the first possibility, that of radial mass transport, the problem can be solved with sufficient accuracy by considering the mass transfer analogy to radial heat transfer in laminar flow systems. The solution for laminar flow, for a fixed concentration at the wall and for fully developed velocity and concentration profiles, is given by (17)

$$Nu = hD/k = 3.66$$

$$\text{Rate per unit area} = h(R_m - R_w) \tag{17}$$

D is the pore diameter; k is the mass transfer coefficient, which is the diffusion coefficient of the reactant in this case; R_m is the mass flow mean concentration of reactant, and R_w is the concentration at the wall of the pore. The assumption of negligible entrance effects, and fully developed flow, is probably reasonably good because of the very low Reynold's numbers of flow in fine pores. A limiting current is clearly reached when $R_w = 0$ at all points along the wall of the pore. Let A be the specific geometric area of the walls of pores, in sq. cm. of area per cu. cm. of electrode (note that A does not necessarily equal S). Then the differential current density in an element dx at the condition where $R_w = 0$ is

$$di = nF\ 3.66(k/D)AR_m dx$$

At the same time

$$di = nFv\ dR$$

$$i = nFv(R_i - R_m)$$

$$i_{L_1} = nFvR_i$$

Therefore,

$$R_m = (i_{L_1} - i)/nFv$$

and

$$\int_o^{i_{L_2}} (1/(i_{L_1} - i))di = 2.66(Ak/Dv) \int_o^L dx$$

or

$$i_{L_2}/i_{L_1} = 1 - e^{-3.66(AkL/vD)} \tag{18}$$

Thus the ratio of the observed limiting current i_{L2} to that of the expected limiting current i_{L1} is given by Equation 18 where A/D is an unknown factor. An estimate of the ratio of limiting currents can be made by taking L as 0.1 cm, k as 10^{-5} cm. sq./second, v as 1 cm. per minute, A as 500 sq. cm. per cc., and D as 10 microns. The exponent of the exponential term is then approximately —120, and the radial mass transport effect

Publication Date: January 1, 1969 | doi: 10.1021/ba-1965-0047.ch004

would be negligible. This theoretical result was tested by measuring the limiting currents obtained with the redox couple $Sn^{2+} \rightleftharpoons Sn^{4+}$ in 4*N* HCl. Figure 18 shows that the predicted and experimental values are in perfect agreement even at current densities of 500 ma./sq. cm. This proves that radial mass transfer cannot be giving rise to the limiting currents observed in Figure 17 since the same effect would be expected for the redox couple (a lower diffusion coefficient for organic molecules would be amply compensated by the increase in the number of Faradays per gram mole).

The second possibility, that of a chemisorption rate limitation, can be analyzed by assuming that the limiting rate of chemisorption is given by

$$\text{Rate per unit area} = k_1 R, \text{ gram moles per sq. cm. second}$$

This follows from a chemisorption equation when $\theta \rightarrow 0$, $1-\theta \rightarrow 1$. k_1 is the rate constant. The treatment then follows as before giving

$$i_{L_2}/i_{L_1} = 1 - e^{-Sk_1L/v} \tag{19}$$

A similar possibility, of a dissociation before discharge, is similarly handled by assuming a dissociation rate of

$$\text{Rate per unit volume} = k_2 R$$

A limiting rate is obtained when the reaction is irreversible and the product of reaction is removed, by electrochemical reaction, as fast as it is formed. Then the differential current density is given by

$$di = nFk_2R \epsilon \, dx$$

and, as before,

$$i_{L_2}/i_{L_1} = 1 - e^{-(k_2\epsilon L/v)} \tag{20}$$

Thus these three possibilities all give rise to a form

$$i_{L_2}/i_{L_1} = 1 - e^{-(JL/v)} \tag{21}$$

where the exponent includes L/v in all cases, but J has a different physical meaning for the different cases.

It is known (*7*) that at anodic potentials greater than about 0.6 to 0.8 volt *vs.* S.H.E. oxygen is placed on platinum electrodes as a surface complex. It has been shown (*18*) that this oxygen has an appreciable poisoning effect on the reaction of hydrocarbons at the electrode. Figures 9 to 13 show that where complete oxidation can occur at potentials less anodic than this oxygen discharge region, the actual limiting current is close to the theoretical value. For higher flow rates where the exit polarization for complete reaction has to be higher (Figure 6), the electrode potential reaches the region of oxygen complex formation on platinum and the theoretical limiting current is then not obtained. This explanation, proposed by Schlatter (*19*), appears to be the most reasonable

Publication Date: January 1, 1969 | doi: 10.1021/ba-1965-0047.ch004

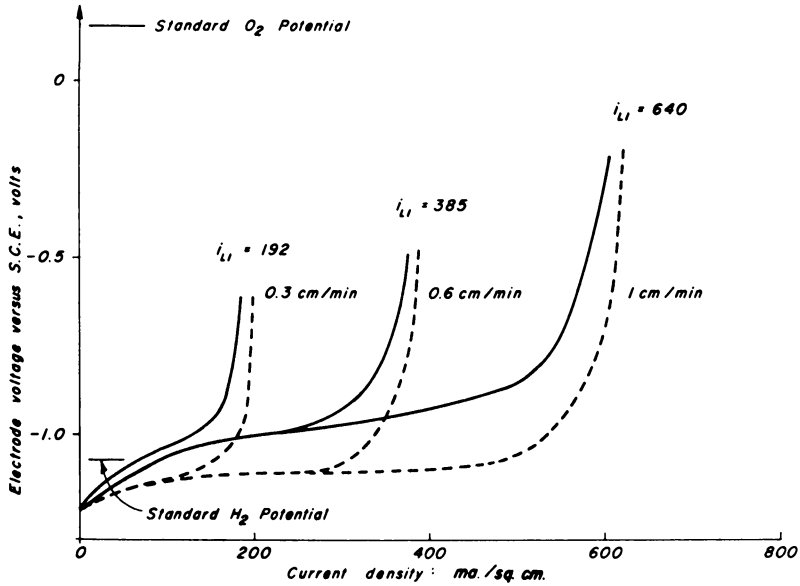

Figure 14. 0.1M N_2H_4, 4M KOH, 80 mg/cm² Pt black.

reason why the limiting currents at high flow rates are less than expected.

Discussion of Results

Results obtained with redox couples have consistently shown that at high current densities, the polarizations obtained as the limiting current is approached are higher than predicted by the theory, especially the entrance face polarization. Figure 5 shows that near the limiting current, the reaction is concentrated in a thin zone in the electrode. The concentration of reactant goes from the initial value to a small value over a short distance; therefore the diffusion gradient along the axis of a pore is large, and a diffusion term should be included in the basic equation. This would have the effect of forcing the entrance face polarization to be larger to give a required current, with a corresponding increase in exit face polarization.

The standard reversible potential of methanol in alkaline solution is about -1.15 volts *vs.* S.C.E., for the over-all reaction $CH_3OH + 8OH^- \rightarrow CO_3^= + 6H_2O + 6e^-$. Figure 9 shows that oxidation started at about this voltage. [Experimental open circuit potentials are not expected to correspond exactly to theoretical standard state values because the conditions are not usually standard state and because potentials are usually mixed potentials with the hydrogen evolution reaction.] The increase in exit and entrance face polarization with current density was greater than that expected from theory, and it is probable that the

Publication Date: January 1, 1969 | doi: 10.1021/ba-1965-0047.ch004

reaction has more than one rate controlling step. In sulfuric acid solution, evolution of carbon dioxide was observed using methanol fuel. The polarization required to obtain the same current densities as in alkali solution (under comparable conditions of concentration, flow rate, etc.) was about 0.3 to 0.4 volt greater for acid. However, the polarization curves were relatively flat, suggesting a one step rate control.

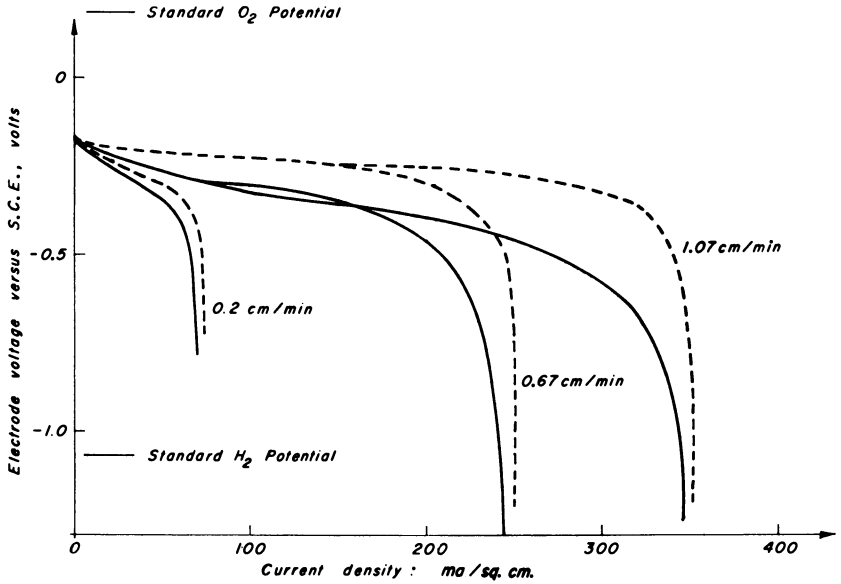

Figure 15. 0.2M H_2O_2, 4M KOH, 130 mg/cm² Pt black.

Figure 12 shows the results for formaldehyde stabilized with methanol. The initial open circuit voltage *vs.* S.C.E. for the possible reactions are

(1) $HCHO + 6OH^- \rightarrow CO_3^= + 4H_2O + 4e^-$ — 1.3 volts.

(2) $HCHO + 2OH^- \rightarrow HCOOH + H_2O + 2e^-$ — 1.1 volts.

(3) $HCOOH + 4OH^- \rightarrow CO_3^= + 3H_2O + 2e^-$ — 1.5 volts.

If formaldehyde went to formate, followed by a slow reaction of formate (2 fast, 3 slow), the concentration of formate would build up to give roughly equal amounts of formaldehyde and formate. Then the voltage at low current would be expected to be controlled by Reaction 2 and to be near or more positive than −1.1 volts. This was not observed since the voltage at low current was near −1.25 volts. If the formate produced was rapidly oxidized to carbonate (2 slow, 3 fast), the voltage would be near (or more positive than) −1.30 volts; however, the results of formate

Publication Date: January 1, 1969 | doi: 10.1021/ba-1965-0047.ch004

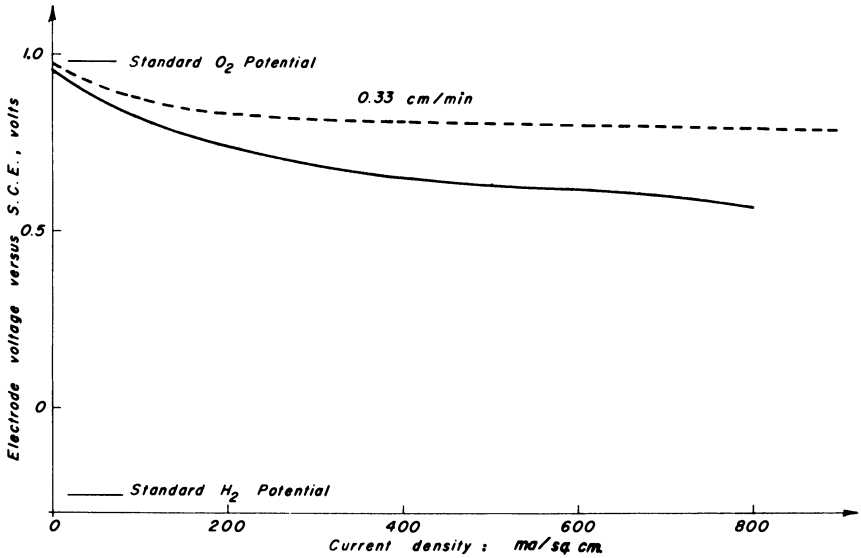

Figure 16. 2M HNO_3, 7M H_2SO_4, 80 mg/cm² Pt black.

oxidation (Figure 11)show that formate oxidation is not rapid at these voltages. Therefore it is concluded that the potential determining reaction is Reaction 1, which gives complete oxidation to carbonate without desorption of formate as a necessary step. (In acid electrolyte carbon dioxide evolution was observed at current densities as low as 1 ma./sq.cm., indicating some complete oxidation near the open circuit potential.) On the other hand, the initial waves in the curves of Figure 12 do not correspond to four electron consumption or indeed to two electron consumptions. Although the formaldehyde oxidation is rapid at about 0.2 volts more negative potentials than those required to give comparable rates with methanol or formate, it seems that all of the formaldehyde present cannot be consumed at these voltages. Presumably, some of the formaldehyde which reacts with the surface is released as formate before it is further oxidized. In addition, it is well known that platinum is a good catalyst for the reaction

$$(4)\quad 2HCHO + OH^- \rightarrow CH_3OH + HCOO^-.$$

Both the methanol and the formate require much more positive potentials to react. If the curves in Figures 11 and 12 are superimposed on Figure 9, it is found that the formate oxidation curves at comparable conditions roughly coincide with the methanol oxidation curves and that the second waves in the formaldehyde results also correspond to these values. Therefore it may be concluded that methanol and formate react at comparable rates at a given voltage; formaldehyde reacts much more quickly,

Publication Date: January 1, 1969 | doi: 10.1021/ba-1965-0047.ch004

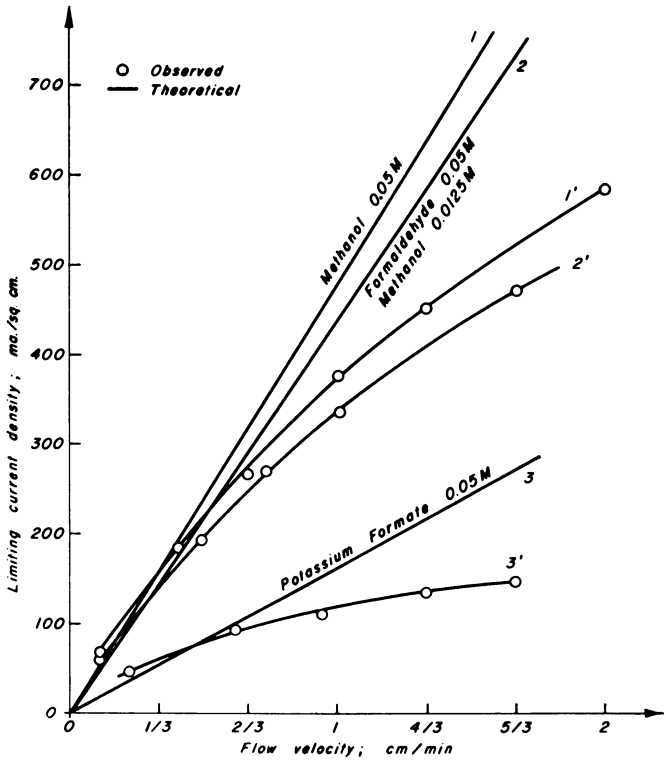

Figure 17. Observed and theoretical limiting current densities for various fuels (4M KOH), 250 mg/cm² Pt black.

but considerable amounts of it are converted to formate and methanol which in turn react only slowly,

$$\text{Methanol} \xrightarrow{\text{slow}} \text{formaldehyde} \xrightarrow{\text{fast}} \text{formate} \xrightarrow{\text{slow}} \text{carbonate}$$

If the formate oxidation were much slower than the methanol, two waves in the voltage-current plot would be observed. However, since they are of comparable rate, methanol reacts to give appreciable concentrations of formate in the electrode, which then further reacts as the voltage increases. The two waves fuse into one long curve.

Complete electrochemical oxidation of borohydride in alkali is

$$BH_4^- + 8OH^- \rightarrow BO_2^- + 6\ H_2O + 8e^-$$

with a reversible potential of about —1.5 volts *vs.* S.C.E. Decomposition at open circuit was observed in our system ($BH_4^- + 2H_2O \rightarrow BO_2^- + 4H_2$), but on appreciable current drain the evolution of gas from the electrode exterior ceased and a limiting current corresponding to eight electrons was observed at suitable flow rates. The open circuit potential lay be-

Publication Date: January 1, 1969 | doi: 10.1021/ba-1965-0047.ch004

tween the hydrogen evolution potential and the borohydride potential, at about —1.20 to —1.25 volts. It is clear from the results that potassium borohydride is an extremely effective fuel, and it was possible, using higher concentrations, to obtain several amperes per square centimeters at significant voltages *vs.* the theoretical oxygen electrode potential. Similarly, decomposition was observed to occur when high concentrations of hydrazine were in contact with the platinum black electrode ($N_2H_4 \rightarrow N_2 + 2H_2$). This decomposition was negligible up to 0.1*M* concentrations, but could be clearly observed at 0.5*M* concentrations. The over-all electrochemical oxidation is:

$$N_2H_4 + 4OH^- \rightarrow N_2 + 4H_2O + 4e^-$$

with a reversible standard state potential of —1.40 volts *vs.* S.C.E. The observed open circuit potential is 0.2 volt less than this, but the curves are relatively flat and hydrazine is a very effective fuel.

Publication Date: January 1, 1969 | doi: 10.1021/ba-1965-0047.ch004

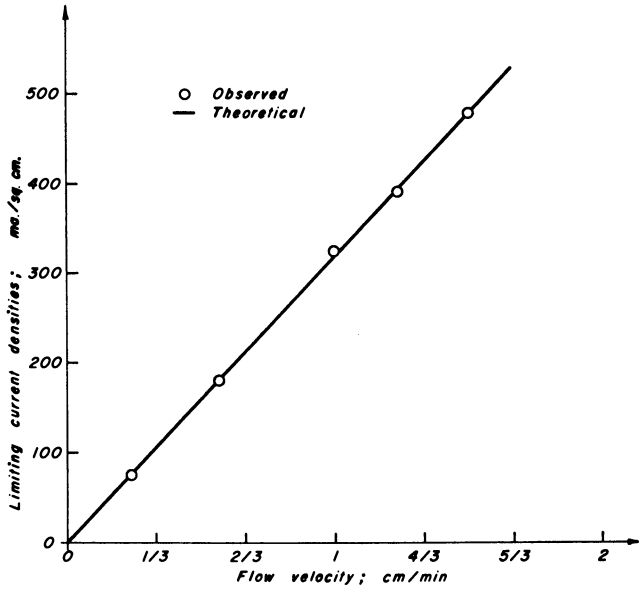

Figure 18. Observed and theoretical limiting current densities for Sn^{2+} (0.1M) → Sn^{4+} (0.1M), 4N HCl, 250 mg/cm² Pt black.

Conclusions

The theory of polarization at porous flow-through electrodes developed above appears to be reasonably satisfactory for simple redox reactions. However, as expected, it is not satisfactory for complex reactions.

In particular, in many cases the observed limiting currents at high current densities (high concentrations and flow rates) were much less than the theoretical values for complete reaction. This is not due to mass transfer effects within the electrode; it is due either to rate-limiting non-electrochemical steps or to oxidative poisoning of the platinum electrode.

Using platinum black flow-through electrodes at room temperature it was found that, at appropriate flow rates, methanol could be completely oxidized to carbonate in alkaline solution or carbon dioxide in acid solution. Tests on formaldehyde and potassium formate in basic solution showed that the formaldehyde is relatively rapidly oxidized compared to methanol while formate is only slightly more readily oxidized. On the same type of electrode, potassium borohydride could be completely utilized giving eight electrons per molecule and hydrazine could be utilized to nitrogen giving four electrons per molecule. The evolution of gas did not hinder the performance of the electrode. The reactions of hydrogen peroxide and nitric acid were found to be complex.

Publication Date: January 1, 1969 | doi: 10.1021/ba-1965-0047.ch004

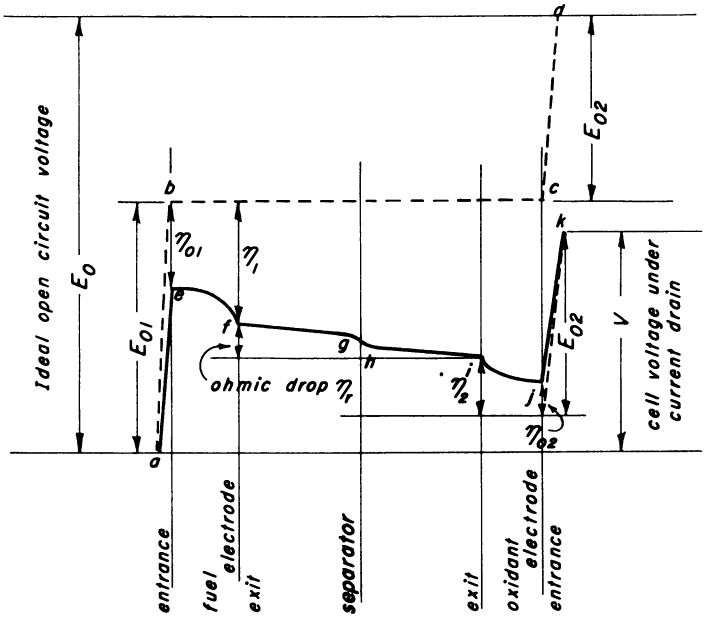

Figure 19. Illustration of voltage gradients within cell.

The voltage in a fuel cell consisting of two flow-through electrodes using fuel and oxidant is illustrated in Figure 19. Line *ab* represents the voltage change between the electrode potential at *a* and the electrolyte at *b*, at ideal zero current conditions; *cd* is the voltage change from the electrolyte to the cathode under these conditions. Under load, *eb* is the loss of voltage η_0, owing to initial activation polarization on the fuel

electrode while η_1 is the total polarization through the electrode. The line *fghi* represents the ohmic voltage gradients through the free electrolyte, *gh* being that across a separator. *ijk* is the equivalent cathode voltage curve to *gef* for the anode. The terminal voltage is now V, where $V = E_o - (\eta_1 + \eta_r + \eta_2)$. The results presented in the figures show only η_1 values *vs.* current density for the given fuels.

Nomenclature

A = specific geometric area of pore walls
b = $RT/\alpha n_1 F$
D = pore diameter
f = $\exp(\eta/b) + \gamma\exp(-\eta/b)$
F = Faraday
i = current density
i_o = true exchange current density
i_o = $i_o SL$, apparent exchange current density for the electrode
i_L = limiting current density
i_{L_1} = $nFvR_i$, expected limiting current density
i_{L_2} = obtained limiting current density
J = defined by Equations 18, 19, 20, 21
k = mass transfer coefficient of reactant, cm. sq./second
k_1 = specific rate constant for chemisorption
k_2 = rate constant for dissociation
L = thickness of electrode, cm.
n_1 = number of electrons involved in the rate controlling step
Nu = Nusselt number
P = concentration (activity) of product at distance x in the electrode
P_i = initial value of P, at $x = 0$
q = tortuosity factor for conduction in electrolyte in the pores of the electrode
R = concentration (activity) of reactant at distance x in the electrode
R_i = initial value R, at $x = 0$
RT = gas constant times absolute temperature
S = effective specific area of electrode interior, sq. cm./cu. cm.
v = velocity of flow of feed, cm./sec.
x = distance into electrode from entrance face
$\bar{x}$ = x/L
α = transfer coefficient in the direction of reaction
Δ = $i_L \rho L$, maximum ohmic polarization
$\bar{\Delta}$ = Δ/b
ϵ = porosity of the electrode
η = polarization
$\bar{\eta}$ = η/b
η_o = polarization at entrance face
η_s = polarization with negligible internal ohmic effect
γ = ratio of inlet reactant concentration to inlet product concentration
ρ = effective specific resistance of electrolyte in the pores, ohm. cm.
ρ' = true specific resistance of the electrolyte

Publication Date: January 1, 1969 | doi: 10.1021/ba-1965-0047.ch004

Acknowledgments

The work reported here has been performed for the Harry Diamond Laboratories, Washington, D.C., under contract DA49-186-502-ORD-917. Grateful acknowledgment is made to the U. S. Army Materiel Command for permission to publish the work.

Literature Cited

(1) Austin, L. G., "Fuel Cells" in "Selected Papers on New Techniques for Energy Conversion," Sumner Levine ed., Dover, New York, 1964.
(2) Austin, L. G., *Proc. Inst. Elec. Electronic Eng.*, **51**, 820 (1963).
(3) Austin, L. G., *Trans. Faraday Soc. (London)*, **60**, (499), 1319-24 (1964).
(4) Austin, L. G., Lerner, H., *Electrochim. Acta*, **9**, 1469 (1964).
(5) Bond, A. P., Singman, D., "Electrode Kinetics of Oxidation-Reduction Couples," Diamond Ordnance Fuze Laboratories, Washington, D. C. 1960.
(6) Carman, P. C., "Flow of Gases through Porous Media," Academic Press, New York, 1956.
(7) Frumkin, A. N., *Advan. Electrochem. Electrochem. Eng.* **3**, P. Delahay, ed., Interscience, New York, 1963.
(8) General Electric Co., Aircraft Accessory Turbine Dept., "Research on Low Temperature Fuel Cell Systems," Progr. Rept. 8, ASTIA No. **AD 243 474** (1960).
(9) Guillou, M., "Repartitions couplees due potential et des concentrations dans les cellules electrochemique," thesis presented to Faculté des Sciences de l'Université de Paris, 1963.
(10) Guillou, M., Buvet, R., *Electrochim. Acta* **8**, 489 (1963).
(11) Ksenzhek, O. S., Stander, V. V., *Dokl. Akad. Nauk. SSSR*, **106**, 487 (1956); **107**, 280 (1956); *Zh. Prikl. Khim.* **32**, 110, 1959.
(12) Lerner, H., Austin, L. G., Rept. **6**, Harry Diamond Laboratories, AMC., Washington, D. C., September 1962.
(13) Lockheed Missiles and Space Co., "Basic Studies on Fuel Cell Systems," Quart. Rept. **III** and **IV**, ASTIA Nos. **AD 273 702, AD 278 353** (November 1961 to May 1962).
(14) Monsanto Research Corp., "Compact Power Fuel Cell," Rept. **ASD-TDR-62-42**, ASTIA No. **AD 282 862** (June 1962).
(15) Perskaya, R. M., Zaidenman, I. A., *Proc. Acad. Sci. U.S.S.R., Phys. Chem. Sect.* **115**, 513 (1957).
(16) Posner, A. M., *Fuel* **34**, 330 (1955).
(17) Rohsenow, W. M., Choi, H. Y., "Heat, Mass and Momentum Transfer," p. 141, Prentice Hall, Englewood Cliffs, N. J., 1961.
(18) Schlatter, M. J., ADVAN CHEM. SER. No. **47**, 292 (1965).
(19) Schlatter, M. J., California Research Corp., private communication, 1963.

RECEIVED February 17, 1964.

Publication Date: January 1, 1969 | doi: 10.1021/ba-1965-0047.ch004

In Fuel Cell Systems; Young, G., el al.;
Advances in Chemistry; American Chemical Society: Washington, DC, 1969.

Nonporous Hydrogen Depolarized Anode for Fuel Cells

HARRY G. OSWIN and STEWART M. CHODOSH

Leesona Moos Laboratories, Great Neck, N. Y.

Publication Date: January 1, 1969 | doi: 10.1021/ba-1965-0047.ch005

This nonporous diffusion anode has been developed to the stage where reproducibility and simplicity of manufacture have been amply demonstrated. Its extreme thinness and ability to handle high current densities make it suitable for very high power density systems. Further the ability of the alloy to handle impure streams of hydrogen and its low susceptibility to poisoning show that it is extremely suitable for use with reformer streams using cheap hydrocarbons, methanol, or ammonia as fuel. Its ability to operate in alkaline or acid electrolyte makes it a versatile anode. In addition, it can operate at negative, zero, or positive differential pressures.

A solid nonporous diffusion-type anode has been developed which permits efficient utilization of impure hydrogen from reformed carbonaceous gas streams. This anode obviates some of the limitations of conventional porous structures, such as stringent quality control during anode manufacture, critical differential operating pressure, and contamination of the electrolyte by impurities in the hydrogen gas stream.

Conventional Porous Anodes

Conventional porous anodes require control of the three-phase anode/fuel/electrolyte interface to stabilize the system and maintain an acceptable level of polarization. Three ways presently used to achieve such control are:

1. The biporous electrode structure developed by F. T. Bacon (*1*) essentially consists of two porous structures. One faces the electrolyte having a mean pore size smaller than that of the coarse-pore structure

In Fuel Cell Systems; Young, G., el al.;
Advances in Chemistry; American Chemical Society: Washington, DC, 1969.

facing the gas phase. Thus, by careful control of the differential pressure applied across the electrode, a stable interface is maintained somewhere within the electrode. If a certain differential pressure is exceeded, bubbling will commence at the largest pore in the fine-pore layer.

2. The homoporous electrode structure, such as described by Justi (*4*), is used in a bubbling condition. Again, a certain differential pressure is required at which an acceptable rate of bubbling occurs through some of the larger pores, while a stable interface is maintained in pores of smaller diameter.

3. Waterproofing the electrode structure consists of applying a waterproof layer to the surface of the porous structure. This apparently prevents gross flooding of the larger pores. Likewise, electrodes can be constructed by incorporating waterproofing agents such as Teflon or Kel-F into a finely dispersed metal powder which is then fabricated into a porous layer.

These electrodes have disadvantages such as the difficulty of controlling bubbling on waterproofed or homoporous structures with the consequent loss of fuel and its attendant dangers. In biporous structures, stringent quality control during manufacture is essential to achieve reproducibility. It was apparent some years ago that a nonporous hydrogen diffusion anode would eliminate many of these problems and have unique advantages of its own. The ability of palladium to diffuse hydrogen was recognized long ago, and an extensive literature is concerned with this phenomenon.

There are references (*8*) in the literature relating to the "electrochemical extraction" of hydrogen from palladium. Recently, it was shown that the rate of absorption of hydrogen by palladium could be increased by covering the palladium surface with transition metal hydrides (*9*). However, only a small amount of work (*5–7*) has been carried out on palladium alloy electrodes, which are more stable mechanically than pure palladium in the presence of hydrogen (*3*).

The work described here, therefore, was carried out with the intent of developing a reliable, nonporous anode for fuel cell applications. It was considered desirable to develop an anode capable of extracting hydrogen at low partial pressures from impure (reformed hydrocarbons) gas streams.

Physical and Electrochemical Mechanisms Involved

The processes occurring in the solid nonporous diffusion-type electrodes are shown in Figure 1. The first stage involves chemisorption and dissociation of the hydrogen accompanied by the formation of metal hydrogen bonds at the surface. The hydrogen then diffuses as a proton interstitially through the bulk metal; the nature of the diffusion mechanism

Publication Date: January 1, 1969 | doi: 10.1021/ba-1965-0047.ch005

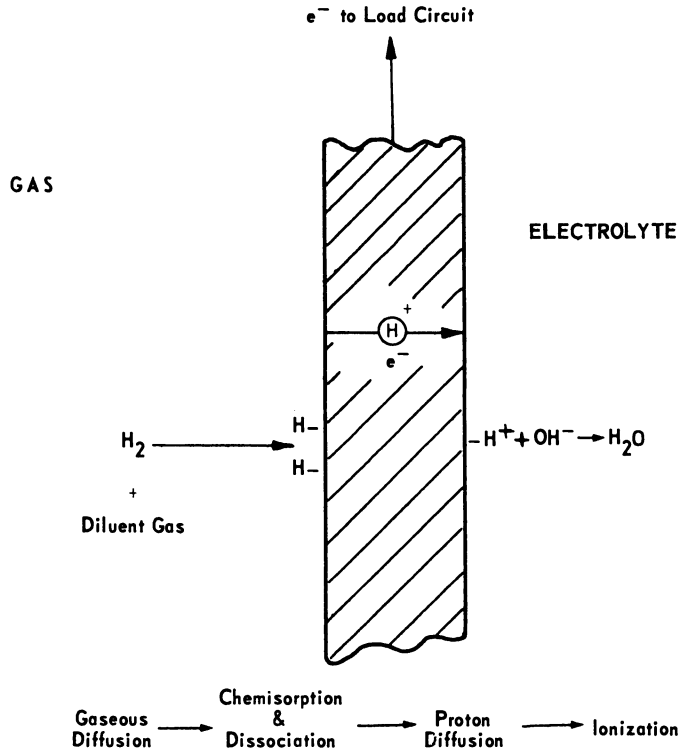

Figure 1. Sequence of mechanisms involved at nonporous anode

at grain boundaries is not defined. On reaching the electrolyte surface of the membrane, the protons emerge into specific bound surface states from which they are removed by the potential difference across the double layer. Thus, the total process involves three distinct activation energies—activation energy of dissociation; activation energy of the bulk diffusion process; and the activation energy for the transfer of protons at the electrolyte interface.

There exists a concentration gradient of protons across the membrane which provides the driving force for the diffusion process. Part of the investigation has been to determine the role of these various processes and the rate-controlling mass-transfer mechanisms.

Experimental Procedures

The electrochemical data were obtained under controlled conditions of temperature and pressure using "half cells" in most cases. The cathode of the cell consisted of a platinum gauze from which hydrogen was evolved.

Publication Date: January 1, 1969 | doi: 10.1021/ba-1965-0047.ch005

Certain of the early feasibility studies and the scale-up studies were conducted on cells containing oxygen depolarized cathodes. During the feasibility stage, some of the electrodes investigated consisted of tubular structures of the type used for gaseous diffusion and separation of hydrogen. It had been hoped that these could be incorporated into concentric type cells giving high power density per unit volume, but the many problems associated with fabricating, sealing, and gasketing biporous tubular cathodes resulted in the use of more suitable designs. It was also extremely difficult to calculate current-density distributions in cells using circular cross-section electrodes (tubes) unless the surrounding cathode was exactly concentric.

Polarization data are quoted on the E* scale—that is, using a reversible hydrogen electrode in the same electrolyte as a reference. Electrode dimensions were in most cases 1-inch diameter flat membranes; in scale-up studies, 3-inch, 5-inch, 6-inch square electrodes were used. Except where stated otherwise, the alloy used was 75% palladium–25% silver.

The electrolytes consisted of USP grades of potassium hydroxide, sulfuric acid, and phosphoric acid, from room temperature to 250° C.

Luggin capillaries were used to measure the potential at the electrode surface. All of the data presented herein (except in Figure 6) are steady-state polarizations and do not include any values derived from galvanostatic transients. Thus, all electrode IR drops—that is those caused by conductor resistances—are included in the measurements.

Publication Date: January 1, 1969 | doi: 10.1021/ba-1965-0047.ch005

Feasibility Studies

Initial feasibility studies were conducted on 25%Ag/75%Pd alloy membranes at temperatures up to 250° C. Limiting currents up to several amps/sq. cm. were observed and polarizations of the order 150 mv. were obtained over the current density range 200 to 400 amps/sq. ft. However, at lower temperatures occasional irreproducibility and varying rates of surface poisoning prompted a study of surface treatment and preparation.

Effects of Surface Pretreatment

The effects of surface preparation—for example, the effect of treating gas and electrolyte surfaces, separately and in combination—are shown in Figure 2. In order to demonstrate the surface effects, pretreatment polarization values are shown for various membranes at 150° C. Pretreatment of the electrolyte surface has a significant effect on the activation polarization and has resulted in a more active surface, either by lowering the activation energy of the process or by increasing the number of sites available.

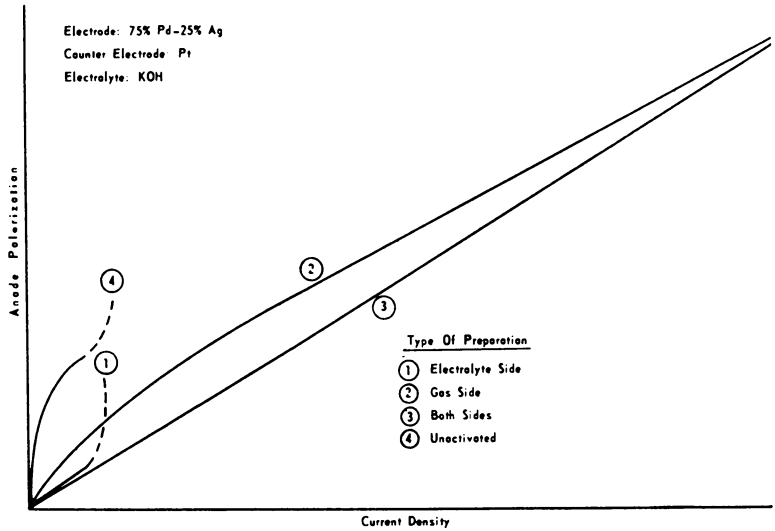

Figure 2. Effect of surface preparation on polarization of membrane anode

Limiting currents are not affected, however. Activation of the gas surface demonstrates a marked effect on the limiting current density obtainable from the membranes, confirming our suspicion that the surface absorption and dissociation processes constituted a rate-controlling mechanism.

It is of interest to note also that pretreatment of the gas-side surface has an effect on the "activation-polarization" region as well as on limiting currents. This is accounted for by the increased diffusion of hydrogen to the electrolyte surface, resulting in a greater concentration of hydrogen in the double layer. This increases the pre-exponential factor in the rate equation, resulting in higher currents at a given polarization value. The combination of pretreating the gas and electrolyte sides results in an electrode having both high limiting currents and low polarization.

Diffusion studies, conducted concurrently, confirmed the results of the electrochemical investigation—namely, at lower temperatures the surface processes were rate controlling. However, limiting currents are always somewhat larger than those predicted from diffusion experiments. The probable explanation of this anomaly is that on polarizing the electrode, a very low partial pressure of hydrogen exists at the electrolyte interface.

Taking a very simple view, the electrochemical process eliminates the recombination step: $H + H \rightarrow H_2$. The removal of hydrogen from the surface under conditions of polarization can be far more rapid than desorption of hydrogen into the gas phase.

Publication Date: January 1, 1969 | doi: 10.1021/ba-1965-0047.ch005

The investigation of surface treatment indicates clearly that the "electrolyte-surface" is potential-controlling while the "gas-surface" is rate controlling.

From a practical point of view, this phase of the investigation resulted in methods of preparing the diffusion electrodes with extremely good reproducibility and with a minimum need for quality control procedures.

Having easily reproducible electrodes available, a series of parametric investigations was conducted.

Temperature Dependence

The effects of temperature on polarization and limiting currents are shown in Figure 3 over the range from room temperature to 200° C. Although at room temperature polarization is considerably increased, limiting currents of the order of 300 to 400 ma./sq. cm. are still obtainable, and the electrode can provide adequate starting power from ambient. Above 100° C. the measurement of limiting current becomes difficult because of the very high current values involved. For example, measurements at 200° C. have indicated limiting currents in the region of 3500 to 4000 amps/sq. ft.; it is virtually impossible to measure such high limiting currents with accuracy.

Publication Date: January 1, 1969 | doi: 10.1021/ba-1965-0047.ch005

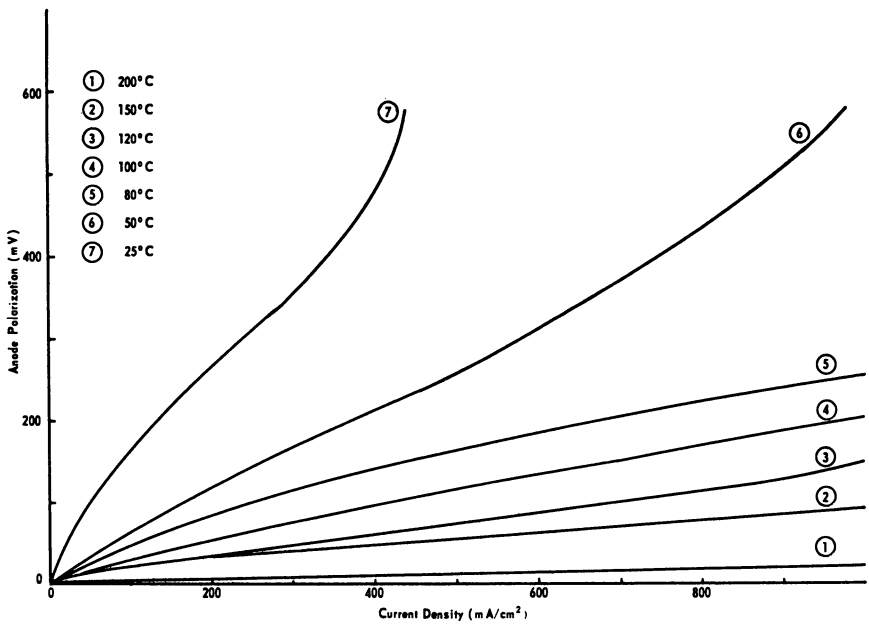

Figure 3. Polarization of palladium-silver/hydrogen anode as function of temperature

Durability of Anodes

Many anodes of various sizes have been investigated for periods up to 500 hours under varying load conditions. Corrosion appears to be the only factor controlling electrode durability. However, since the corrosion potential of the palladium/silver alloy is 800 mv. positive to hydrogen, only complete poisoning of the electrode surface can result in such excessive polarization and subsequent corrosion. It has been our experience that by using the electrolytes mentioned here and commercially pure gases, this situation does not arise, and no theoretical limit to the lifetime of the electrodes appears to exist.

Effect of Electrolyte Composition

The effect of electrolyte concentration has been studied. There is no apparent effect on polarization or limiting current over the composition ranges of interest. Naturally, the specific resistivity of the electrolyte varies and this can affect the over-all polarization of the cell. This variability with electrolyte concentration indicates the minimum importance of concentration polarization at the surface due to electrolyte species. Polarization in acidic or basic electrolytes is similar.

Limiting Effects of Hydrogen Partial Pressure

A study of the partial pressure effects of hydrogen (Figure 4) indicated that partial pressure has little or no effect on polarization until limiting current density regions are approached. Significant current densities can be sustained at partial pressures of hydrogen as low as 1 p.s.i.a. In connection with our original concept for a solid diffusion-anode capable of operating with impure hydrogen streams, this is an extremely important finding since it determines the degree of utilization of the fuel. For example, if the limiting current density acceptable is 150 ma./sq.cm., then the partial pressure of hydrogen in the purge gas—that is the gas being discarded from behind the electrode—would be approximately 1 p.s.i.a. If the in-going partial pressure of hydrogen is atmospheric (15 p.s.i.a.), this would represent about 93% utilization of the hydrogen. An in-going partial hydrogen pressure of 25 p.s.i.a. would result in 96% fuel utilization.

Effects of Membrane Thickness

The effects of membrane thickness on the polarization and limiting current are shown on Figure 5. The effects on polarization at current densities below the limiting current density region are negligible. Limiting current density, however, is an inverse function of thickness for a

Publication Date: January 1, 1969 | doi: 10.1021/ba-1965-0047.ch005

given partial pressure of hydrogen. This indicates that performance, as well as economics, can be improved by the use of extremely thin membranes.

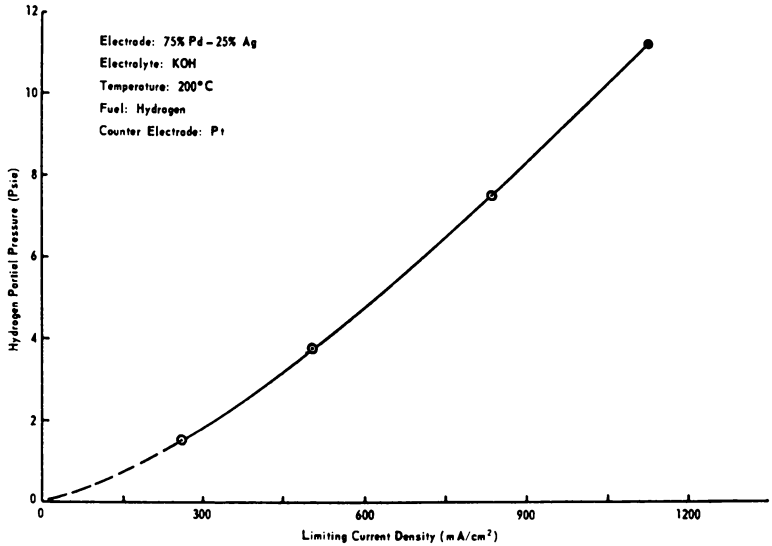

Figure 4. Limiting current density of palladium-silver/hydrogen anode as function of hydrogen partial pressure

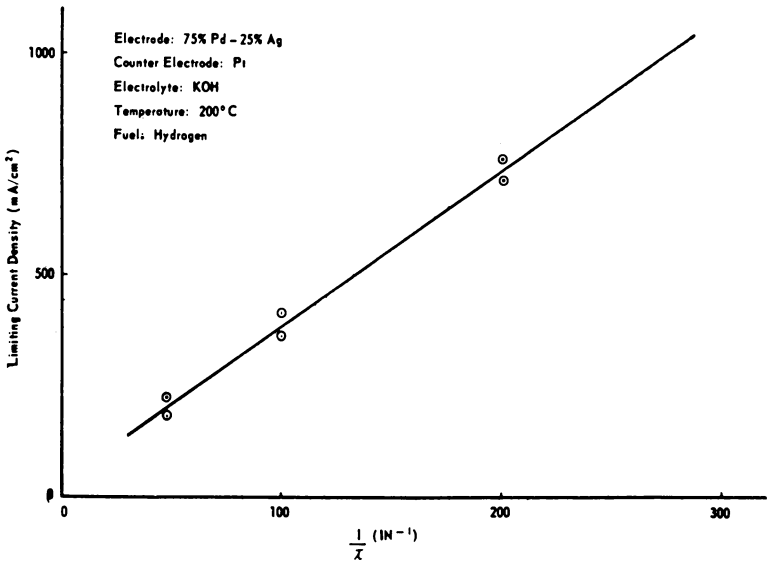

Figure 5. Limiting current density as function of anode thickness

Publication Date: January 1, 1969 | doi: 10.1021/ba-1965-0047.ch005

Study of Poisoning Effects

A comprehensive study of poisoning has been conducted. Poisoning of the electrode/electrolyte interface is of course affected (as are all metal surfaces) by excessive amounts of heavy metal ions and chloride ions; but in all cases, using USP grades of electrolyte and distilled water, no deterioration in electrode performance has been observed under working conditions.

A comprehensive study of poisoning of the gas surface has been made, including the effects of hydrocarbons, CH_3OH, HCHO, HCOOH, CO, CO_2, NH_3, N_2, and water in the hydrogen-containing streams. By control of the flow rates and conditions on the gas side of the membrane, none of these has been observed to cause significant polarization effects. Also, if a reformer stream is used for the fuel cell we do not expect the membrane to be any more susceptible to poisoning than the reforming catalyst, which may, in fact, selectively remove some of the undesirable materials, such as sulfur, and trace metals, such as vanadium. Carbon deposition on the gas surface has never been observed.

Generally, we can expect sulfur poisoning to become more important at lower temperatures. Although sulfur is recognized as an important poisoning agent, the nature of its poisoning effect will depend upon the form in which it exists in the gas stream; pertinent data will soon be available.

An interesting effect, which is a form of poisoning, has been reported by Darling (2). In the course of studies of hydrogen diffusion through palladium, Darling observed that even when using electrolytic hydrogen of high purity, a constant diffusion rate could only be maintained by "purging" the high-pressure side of the membrane. We observed the same phenomenon with "pure" hydrogen using the Pd/Ag anode. If the gas-vents were closed, a steady increase in polarization ensued. An experiment in which the "pure" (electrolytic) hydrogen was first diffused through Pd/Ag anode resulted in the disappearance of the phenomenon. It can only be concluded that an impurity is present in small quantities. Since the "Darling effect" is observed over a temperature range from ambient to 600° C., it is likely that the impurity does not chemisorb or physically adsorb. Most probably it accumulates in surface micropores, restricting hydrogen diffusion to active sites on the metal surface of such pores and cracks.

Electrochemical Characteristics of the Solid Diffusion Electrode

Polarization values for the electrode at 200° C., derived by transient techniques, are plotted semilog in Figure 6. It would appear that the electrode exhibits Tafel behavior. Unfortunately, because of the large currents involved, it has not been possible to study the electrode

Publication Date: January 1, 1969 | doi: 10.1021/ba-1965-0047.ch005

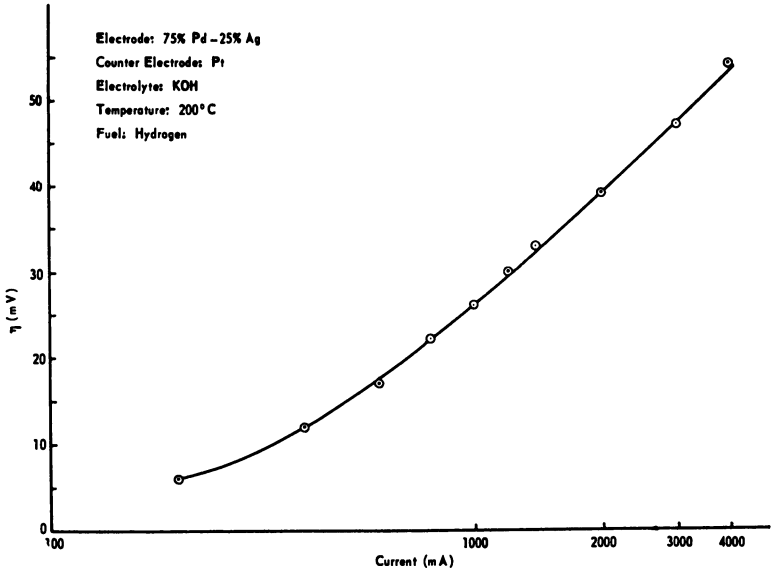

Figure 6. Tafel plot of palladium-silver/hydrogen anode

polarization far into the linear Tafel region; IR contributions become excessively large. Essentially, at practical current densities the electrode polarization is in the nonlinear Tafel region.

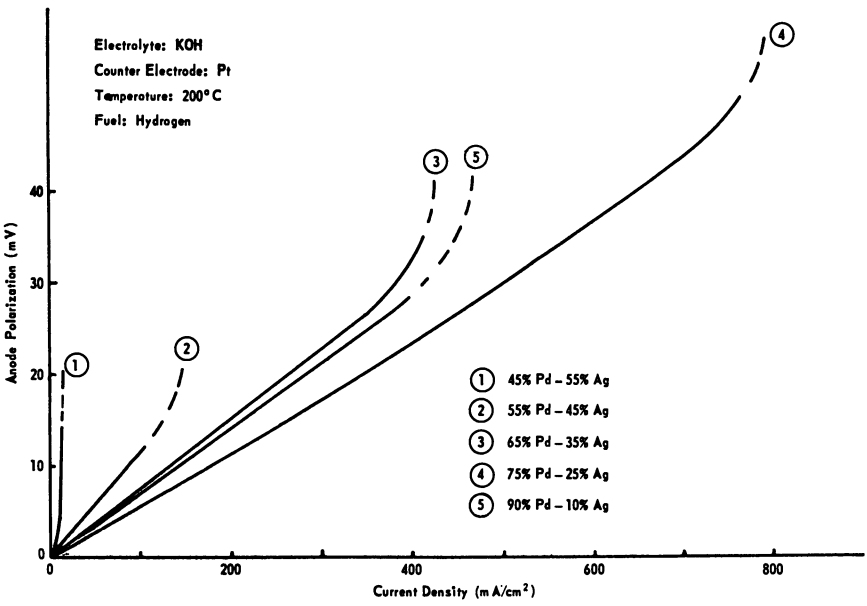

Figure 7. Anode polarization as function of membrane composition

Publication Date: January 1, 1969 | doi: 10.1021/ba-1965-0047.ch005

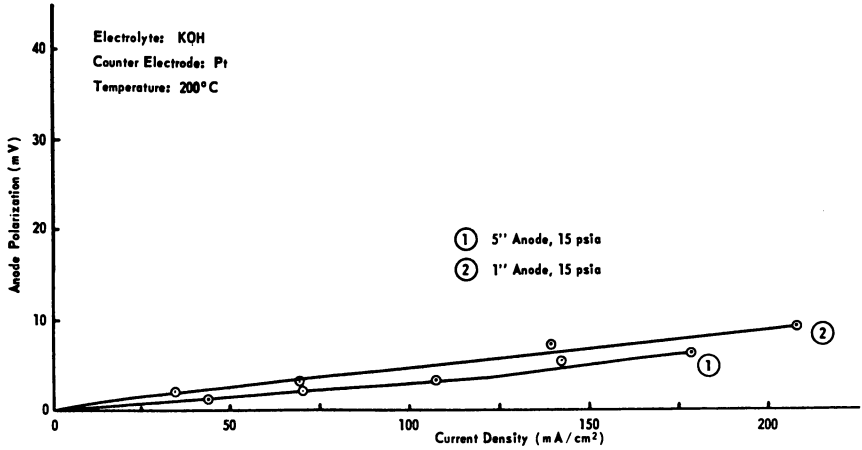

Figure 8. Scale-up effects on 1- and 5-inch diameter anodes

Effect of Membrane Composition

The effects of various alloy compositions were studied, and results are shown in Figure 7. The 25% Ag/75% Pd alloy demonstrates superior polarization and higher limiting currents than all other compositions studied; there appears to be little economic advantage at this stage to increasing the amount of silver in the alloy.

Scale-up Studies

Scale-up studies have been conducted on electrodes from 1-inch diameter to 6-inch square size. Results are shown in Figure 8 for electrodes of 1- and 5-inch diameter. The differences in polarization behavior are insignificant.

Acknowledgment

The authors acknowledge the technical contribution and experimental studies of Mr. F. Malaspina and the results of the diffusion studies conducted by Mr. N. I. Palmer.

Literature Cited

(1) Bacon, F. T., Brit. Patent **667,298** (1952).
(2) Darling, A. S., *Platinum Metals Rev.* **2**, 16 (1958).
(3) Hunter, J. B., Ibid., **4**, 130 (1960).
(4) Justi, E., U. S. Patent **2,860,175** (1958).
(5) Kussner, A., *Z. Elektrochemie* **66**, 675 (1963).
(6) Kussner, A., *Z. Physikalische Chemie,* **36**, 383 (1963).

Publication Date: January 1, 1969 | doi: 10.1021/ba-1965-0047.ch005

(7) Oswin, H. G., U. S. Patent 3,092,517 (1963).
(8) Vetter, K. J., "Electrochemische Kinetik," pp. 492–96, Springer-Verlag, Berlin, 1961.
(9) Wickes, E., Kussner, A., Otto, K., Actes du Deuxieme Congres International de Catalyse, Paris, 1960, p. 1035.

RECEIVED February 17, 1964.

Publication Date: January 1, 1969 | doi: 10.1021/ba-1965-0047.ch005

Theory of Polarization of Porous Electrodes

KAREL MICKA

J. Heyrovsky's Polarographic Institute, Prague, Czechoslovakia

Publication Date: January 1, 1969 | doi: 10.1021/ba-1965-0047.ch006

A theory of polarization of porous electrodes with constant current is given under the assumption that concentration changes of depolarizer and supporting electrolyte are negligible. No restrictions are made as to the pore geometry, specific resistances of electrode and electrolyte, and polarization of the solid-liquid interface, the electrode being regarded as a macrohomogeneous superposition of two continua, a solid and a liquid one. Some special cases are discussed briefly—namely, small or large specific electrode resistance, small and large polarization. It is shown that the same theory can be applied under reasonable assumptions to the case where the depolarizer is in the gaseous phase, i. e. to a gaseous porous electrode. Some implications as to the structure of the latter are presented.

The problem of polarization of porous electrodes with relation to the resistance of the electrode material was solved first by Coleman (*1*) in the case of cylindrical cathodes of Leclanché elements. In his differential equation, a supposition is implicitly included that the faradayic current, u, is directly proportional to polarization of manganese dioxide particles. Therefore, Coleman's expression for faradayic current as a function of distance from electrode surface is substantially in accord with that of Euler and Nonnenmacher (*3*) who assumed a linear polarization curve of manganese dioxide electrode. Daniel-Bek (*2*) was the first to deduce fundamental differential equations in the form which is used nowadays. He gave the solution for two limiting cases—that the faradayic current is an exponential or linear function of polarization. Finally, Newman and Tobias (*6*) solved the differential equations under the assumption that the

In Fuel Cell Systems; Young, G., el al.;
Advances in Chemistry; American Chemical Society: Washington, DC, 1969.

faradayic current is an exponential function of polarization and their results are substantially in accord with those of Daniel-Bek.

The latter assumption is valid only when the thickness of the electrode (the "pore length") is small, the electrolyte conductivity high, and the current large. These restrictions are severe enough, and it is therefore desirable to get a more general solution which would be applicable in any case. Such a solution can indeed be obtained in a relatively simple way.

Mathematics

Let us consider a porous electrode flooded with electrolyte and backed by a metallic conductor of negligible resistivity (Figure 1). Experimental conditions are chosen such that the depolarizer and supporting electrolyte concentrations within the pores can be considered as constant. This applies (for a limited time interval) when the electrode material itself undergoes electrode reaction or when the electrolyte is forced to flow sufficiently rapidly through the pores. Also, a physical model of a gaseous porous electrode was proposed (*7*) for which the following theory is applicable (*4*).

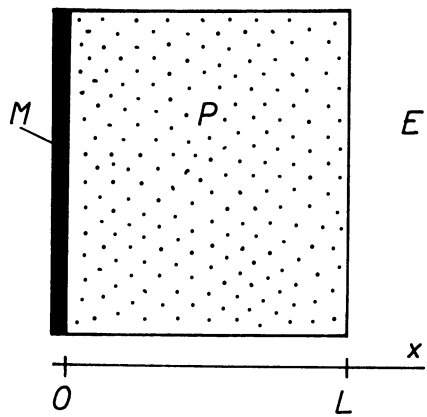

Figure 1. Schematic cross section of a porous electrode.
M = metallic conductor; E = electrolyte; P = porous matter

It is unnecessary to make any assumptions concerning the structure of the porous electrode except that this structure is sufficiently fine to be regarded as macrohomogeneous. Thus, the electrode may be described as a superposition of two continua—a solid and a liquid one (*6*). A more detailed analysis of this idea is given in another paper (*5*).

For potential, φ_1, of the electrode material, Ohm's law holds:

Publication Date: January 1, 1969 | doi: 10.1021/ba-1965-0047.ch006

$$\frac{d\varphi_1}{dx} = -\rho_1 i_1 \tag{1}$$

where ρ_1 is the specific resistance of the porous electrode matrix and i_1 is the electronic current density corresponding to unit area of the electrode cross section perpendicular to the x-axis.

An analogous equation holds for the potential, φ_2, of the electrolyte:

$$\frac{d\varphi_2}{dx} = -\rho_2 i_2 \tag{2}$$

where ρ_2 is the resistance of the electrolyte contained in one cubic centimeter of the electrode—that is, the specific resistance of the "electrolyte matrix"—and i_2 is the ionic current density corresponding again to unit area of the electrode section. Finally according to Daniel-Bek (*2*) we may write the following equation for the faradayic current density, D, on the inner pore surface:

$$\frac{di_2}{dx} = SD \tag{3}$$

where S is the active surface area of a cubic centimeter of the electrode—that is, the area on which the electrode reaction takes place. Let us choose for D the following function of polarization (overvoltage), E:

$$D = i_0\left(\exp\frac{\beta nFE}{RT} - \exp\frac{-\alpha nFE}{RT}\right) \tag{4}$$

in which $E = \varphi_1 - \varphi_2$ fulfills the condition that $E = 0$ when $D = 0$; i_0 is the exchange current density for reaction Red $\rightleftarrows$ Ox + ne, equal to nFk^0_e $[\mathrm{Ox}]^\beta$ $[\mathrm{Red}]^\alpha$, k^0_e being the standard rate constant of the electrode reaction proper. Other symbols have their usual meaning.

Boundary conditions for Equations 1 to 3 are:

$$x = 0\colon\ i_1 = I, \tag{5}$$

$$x = L\colon\ \ i_1 = 0,\ \varphi_2 = 0, \tag{6}$$

and the conservation law of current

$$i_1 + i_2 = I. \tag{7}$$

For an anodic current, $I > 0$, $E > 0$, and $D > 0$; for a cathodic current, inverse relations apply.

The problem defined by Equations 1 to 7 can be reduced to a single differential equation. Subtracting Equation 2 from 1 yields

$$\frac{dE}{dx} = \rho_2 i_2 - \rho_1 i_1 = (\rho_1 + \rho_2)i_2 - \rho_1 I. \tag{8}$$

Publication Date: January 1, 1969 | doi: 10.1021/ba-1965-0047.ch006

When differentiating the latter formula and combining the result with Equations 3 and 4, we get

$$\frac{d^2E}{dx^2} = i_0S(\rho_1 + \rho_2)\left(\exp\frac{\beta nFE}{RT} - \exp\frac{-\alpha nFE}{RT}\right) \tag{9}$$

Let us now introduce the following parameters:

$$u = \alpha nFE/RT = aE,\ \lambda = 1/\sqrt{2ai_0S(\rho_1 + \rho_2)},\ I_0 = 2/a\lambda\rho_2. \tag{10}$$

Equation 9 then becomes

$$2\lambda^2\frac{d^2u}{dx^2} = \exp\left(\frac{\beta}{\alpha}u\right) - \exp(-u). \tag{11}$$

Multiplying Equation 11 by du/dx and integrating, we obtain

$$\lambda^2\left(\frac{du}{dx}\right)^2 = \frac{\alpha}{\beta}\exp\left(\frac{\beta}{\alpha}u\right) + \exp(-u) - C \tag{12}$$

where the integration constant $C > 0$ is defined by the condition that when $du/dx = 0$, then the absolute value of dimensionless polarization $|u|$, attains its minimum $|u_m|$:

$$C = \frac{\alpha}{\beta}\exp\left(\frac{\beta}{\alpha}u_m\right) + \exp(-u_m). \tag{13}$$

The solution of Equation 12 may be written in the form

$$s(x - x_m) = \lambda\int_{u_m}^{u}\frac{du}{\sqrt{\frac{\alpha}{\beta}\exp\left(\frac{\beta}{\alpha}u\right) + \exp(-u) - C}} \tag{14}$$

in which s denotes the sign of du/dx and x_m is the value of x for which $u = u_m$.

The integral on the right-hand side of Equation 14 cannot, in general, be expressed by elementary or other known functions; however, it can be reduced to an elliptic integral of the first kind when α/β attains one of the following values: $^1/_2$, 1, 2. In practical cases, α/β usually will not be appreciably different from unity. Instead of Equation 9, we may therefore write an approximate one:

$$\frac{d^2E}{dx^2} \approx 2i_0S(\rho_1 + \rho_2)\sinh aE \tag{9'}$$

in which $a = \beta nF/RT$ when $E > 0$, and $a = \alpha nF/RT$ when $E < 0$. Thus, instead of Equation 14 we obtain

$$s(x - x_m) = \frac{\lambda}{\sqrt{2}}\int_{u_m}^{u}\frac{du}{\sqrt{\cosh u - \cosh u_m}} \tag{14'}$$

Publication Date: January 1, 1969 | doi: 10.1021/ba-1965-0047.ch006

By substitution

$$\cos \psi = (\sinh \tfrac{1}{2}u_m)/\sinh \tfrac{1}{2}u,\ k = 1/\cosh \tfrac{1}{2}u_m \tag{15}$$

Equation 14′ takes the form of the final solution

$$|x - x_m| = \lambda k F(k, \psi) \tag{16}$$

in which $F(k, \psi)$ denotes the elliptic integral of the first kind with the modulus k and amplitude ψ

$$F(k, \psi) = \int_0^{\psi} \frac{d\psi}{\sqrt{1 - k^2 \sin^2 \psi}} \tag{17}$$

Formally, Equation 16 is analogous to that which Winsel (8) derived for the case of $\rho_1 = 0$.

The faradayic current as a function of distance, x, from the metallic conductor is given by

$$D/D_m = \cos^{-2}\psi \sqrt{1 - k^2 \sin^2 \psi_1} \tag{18}$$

ψ being defined by Equation 16 as

$$\sin \psi = sn\left(\frac{|x - x_m|}{k\lambda}, k\right), \tag{19}$$

where *sn* denotes Jacobi's elliptic function. Further D_m stands for $2i_0 \sinh u_m$, so that $|D_m|$ represents the minimum absolute value of D.

An important measurable quantity is the potential, $\varphi_{1,0}$ of the metallic conductor at the end of the pores *vs.* the electrolyte potential at $x = L$. For this we obtain:

$$a\varphi_{1,0} = a \frac{\rho_1 E_0 + \rho_2 E_L}{\rho_1 + \rho_2} + \frac{2\rho_1}{\rho_1 + \rho_2} \frac{L}{\lambda} \frac{I}{I_0} \tag{20}$$

where E_0 and E_L are the values of E for $x = 0$ and $x = L$, respectively, which fulfill the following relationship:

$$\cosh aE_L - \cosh aE_0 = \tfrac{1}{2}a^2\lambda^2 I^2(\rho_2^2 - \rho_1^2). \tag{21}$$

The value of E_L can be computed from the equation

$$\sinh \tfrac{1}{2}aE_L = \frac{I}{I_0 \sin \psi_L} \tag{22}$$

where ψ_L is the solution of the equation

$$\frac{L}{k\lambda} = F(k,\psi_0) + F(k,\psi_L) \tag{23}$$

with $tg\ \psi_0 = (\rho_1/\rho_2) tg\psi_L$, and $k = 1/\sqrt{1 + I^2/I_0^2 tg^2\psi_L}$.

Publication Date: January 1, 1969 | doi: 10.1021/ba-1965-0047.ch006

Some Limiting Cases

When the pores are short so that $L < {}^1/_2\pi k\lambda$ and the current is large, then $k << 1$ and the expression for faradayic current becomes:

$$D/D_m = \cos^{-2}\frac{x - x_m}{k\lambda}. \tag{24}$$

In this case the polarization of the electrode is large so that the hyperbolic sine in Equation 9 may be substituted by an exponential function. Equation 24 can be shown to correspond exactly to the solution given by Newman and Tobias (*6*).

When, on the contrary, the pores are long and the current is small so that $|I| << I_0\sinh(L/2\lambda)$, Equation 18 becomes

$$D/D_m = \cosh\frac{x - x_m}{\lambda}\sqrt{k^2 + (1 - k^2)\cosh^2\frac{x - x_m}{\lambda}}. \tag{25}$$

When, in addition, the polarization of the electrode is small so that the hyperbolic sine in Equation 9′ may be substituted by a linear function, we can set $k = 1$ in Equation 25 to obtain a simple formula which, after suitable rearrangement, can be shown to correspond exactly to the solution given by Euler and Nonnenmacher (*3*).

When the specific resistances of both phases, electrode and electrolyte, are equal, then Equation 21 yields simply $E_0 = E_L$ so that the polarization at one end of the pores is equal to that at the other. Further $x_m = {}^1/_2L$—that is the minimum absolute value of polarization corresponds to the middle of the electrode. Hence, the faradayic current distribution in the electrode is symmetrical. Equation 20 becomes

$$a\varphi_{1,0} = {}^1/_2aE_L + \frac{L}{\lambda}\frac{I}{I_0} \tag{26}$$

When the specific resistance of the electrode is negligible so that $\rho_1/\rho_2 \approx 0$ we have the case already discussed by Winsel (*8*); then $\varphi_{1.0} = E_L$, $x_m = 0$. On the contrary, when the specific resistance of the electrode is very large so that $\rho_1/\rho_2 \to \infty$ we have $\varphi_{1.0} = E_0$, $x_m = L$. The results of Winsel (*8*) can be applied in this case if we introduce an independent variable, $x' = L - x$. In other words, we consider the end of the pores as the beginning and vice versa.

An interesting and very simple case is when the specific resistances of both phases are equal and, simultaneously, the pores are long or the current is small. This means $E_m \to 0$, $k \to 1$. Then we can express $\varphi_{1.0}$ simply as a function of the current, I:

$$a\varphi_{1,0} = 2\,\text{arcsinh}\left(\frac{I}{I_0}\operatorname{cotgh}\frac{L}{2\lambda}\right) + \frac{L}{\lambda}\frac{I}{I_0} \tag{27}$$

Publication Date: January 1, 1969 | doi: 10.1021/ba-1965-0047.ch006

whence it can be seen that the electrode polarization, $\varphi_{1,0}$ is directly proportional to the total current when $|I| << I_0$.

Results

In general, faradayic current distribution—that is, D/D_m as a function of x depends on three dimensionless parameters—namely I/I_0, L/λ, and ρ_1/ρ_2. Figure 2 shows current distribution curves for several values of ρ_1/ρ_2 and for $I/I_0 = 1$, $L/\lambda = 4.46$. Other curves can easily be derived from those in Figure 2 by setting $\rho'_1 = \rho_2$, $\rho'_2 = \rho_1$, and $x' = L - x$. In fact Equations 18 and 20 are invariant with respect to that simple transformation (*4*). The parameter I_0 is, of course, transformed to $I'_0 = I_0 \rho_2/\rho_1$.

Publication Date: January 1, 1969 | doi: 10.1021/ba-1965-0047.ch006

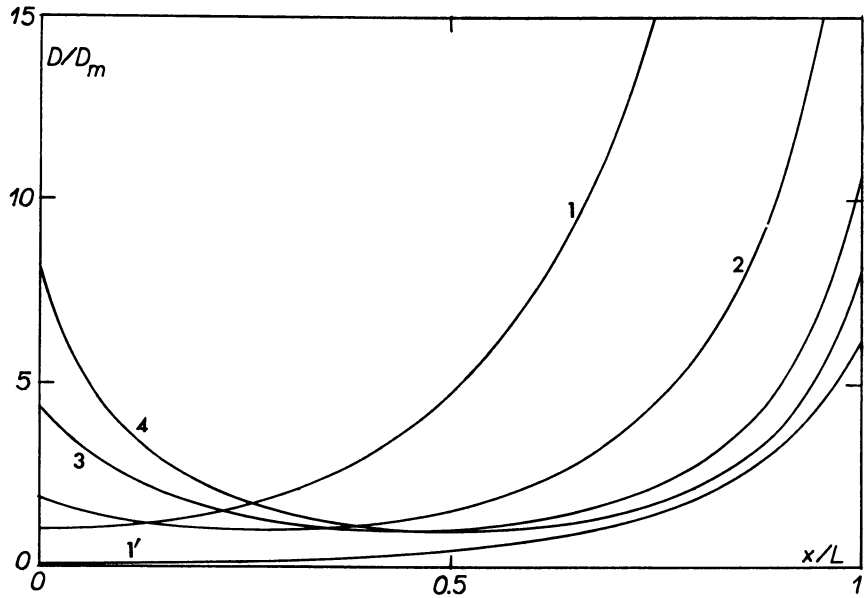

Figure 2. Current distribution curves in dependence on the parameter ρ_1/ρ_2 1. $\rho_1/\rho_2 = 0$; 2. $\rho_1/\rho_2 = 0.1$; 3. $\rho_1/\rho_2 = 0.5$; 4. $\rho_1/\rho_2 = 1.0$. $L/\lambda = 4.462$, and $I/I_0 = 1$ for all curves. Curve 1' corresponds to curve 1 with the vertical scale reduced to 1:10.

The coordinate x_m denoting the place of minimum absolute value of polarization within the pores is constant only in the case that the current is small and E_m approaches zero. However, with increasing current x_m approaches $^1/_2L$ independently of the value of ρ_1/ρ_2—supposing that the latter is larger than zero and finite. An an example, for $L/\lambda = 1$ and $\rho_1/\rho_2 = 0.1$ the following values were computed:

I/I_0:	0.1	0.1	1.0	5.0	10	20	50
x_m/L:	0.1021	0.1024	0.1178	0.1961	0.2635	0.3356	0.4178

The fact that the polarization curve depends on the previously mentioned parameters means that its general equation may be written in the form

$$\frac{I}{I_0} = f\left(\frac{L}{\lambda}, \frac{\rho_1}{\rho_2}, a\varphi_{1,0}\right). \tag{28}$$

Some important conclusions can be drawn from this equation without taking care of the exact analytical expression of the function, f. The value of $a = \alpha nF/RT$ depends only on the kind of electrode reaction in question, and it can be considered as constant. When the electrode polarization and other parameters of function f are constant the ratio I/I_0 must also be constant. Let us set $L/\lambda = A$, $I/I_0 = {}^1/_2B$. Then

$$L = A\lambda = A/\sqrt{2ai_0S(\rho_1 + \rho_2)}, \tag{29}$$

$$I = {}^1/_2BI_0 = \frac{B}{a\rho_2}\sqrt{2ai_0S(\rho_1 + \rho_2)}. \tag{30}$$

Hence, when the specific active surface area, S, is increased by a factor of q^2, the thickness of the electrode, L, can be reduced by the factor of q and nevertheless the current increases by the factor q, the polarization and other conditions being the same.

On the basis of a physical model of a gaseous porous electrode proposed by Pshenichnikov (7), it is possible to adapt the above theory to such an electrode. According to this author, the electrode process takes place in a thin electrolyte film on the inner surface of pores that are filled with gas (hydrogen). The electrode material (nickel powder and Raney nickel) itself is penetrated by a large number of micropores which are filled with electrolyte (a highly concentrated potassium hydroxide solution). In addition, some electrode pores are also filled with electrolyte. Figure 3 is simplified for better understanding. It is of course not necessary to assume that the pores are linear and parallel to each other as Pshenichnikov did. His assumption that polarization is very small can be abandoned as well.

Obviously, concentrations of the depolarizer (hydrogen) and of the supporting electrolyte can be considered as constant during large time intervals, the water of reaction being removed by diffusion and evaporation. Our theoretical conclusions therefore can be applied to this case after setting S = inner surface of pores that are filled with gas, $\rho_1 = 0$, ρ_2 = resistance of pores filled with electrolyte. The latter quantity may be expressed as

$$\rho_2 = \frac{\rho}{v_e} l_p \tag{31}$$

ρ being the specific resistance of the electrolyte, v_e the volume of pores

Publication Date: January 1, 1969 | doi: 10.1021/ba-1965-0047.ch006

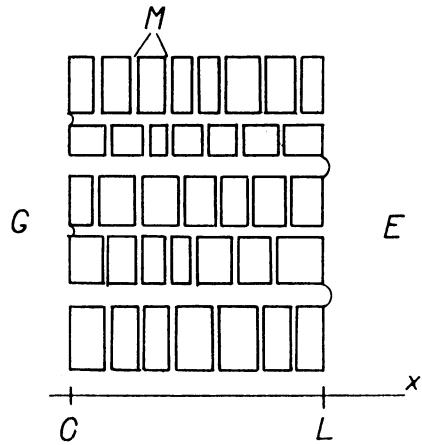

Figure 3. Schematic cross section of a gaseous porous electrode

G-gas; E-electrolyte; M-micropores. The finely porous covering layer is not included as it does not play any role in current generation.

Publication Date: January 1, 1969 | doi: 10.1021/ba-1965-0047.ch006

filled with electrolyte in unit volume of the electrode, and l_p a factor larger than unity ("tortuosity" factor). Thus, Equation 30 takes the form

$$I = B\sqrt{\frac{2i_0}{al_p\rho}}\sqrt{Sv_e} \tag{32}$$

The value of the product Sv_e depends on the pore size distribution characterizing the electrode in question and on the gas pressure. The form of the pore size distribution curve of pores filled with electrolyte exerts no influence on v_e neither on S; therefore, we must consider only the pore size distribution of pores filled with gas (*4*). Obviously these pores should be as fine as possible to make S as large as possible. On the other hand a limitation arises from gas pressure which should not be too high, being given by the well known formula $(2\sigma/r)\cos\theta$ in which r denotes the smallest effective radius of pores that are filled with gas.

By comparison of current densities, I, pore size distribution curves, and the square root of the product Sv_e, it appears that Pshenichnikov's physical model (*7*) of a gaseous porous electrode is sound and that the use of our generalized theory to describe the function of such an electrode is justified.

Literature Cited

(1) Coleman, J. J., *Trans. Electrochem. Soc.* **90**, 545 (1946).
(2) Daniel-Bek, V. S., *Zhur. Fiz. Khim.* **22**, 697 (1948).

(3) Euler, J., Nonnenmacher, W., *Electrochim. Acta* **2**, 268 (1960).
(4) Micka, K., *Collection Czech. Chem. Commun.*, in press.
(5) *Ibid.* **29**, 1998 (1964).
(6) Newman, J. S., Tobias, Ch. W., *J. Electrochem. Soc.* **109**, 1183 (1962).
(7) Pshenichnikov, A. G., *Dokl. Akad. Nauk SSSR* **148**, 1121 (1963).
(8) Winsel, A., *Z. Elektrochem.* **66**, 287 (1962).

RECEIVED February 17, 1964.

Publication Date: January 1, 1969 | doi: 10.1021/ba-1965-0047.ch006

In Fuel Cell Systems; Young, G., el al.;
Advances in Chemistry; American Chemical Society: Washington, DC, 1969.

7

Diffusion Polarization in Air Channels

Electrochemical Reduction of Oxygen (Air)

HENRI J. R. MAGET and EUGENE A. OSTER

Fuel Cell Laboratory, General Electric Co., West Lynn, Mass.

Publication Date: January 1, 1969 | doi: 10.1021/ba-1965-0047.ch007

Current density distributions in electrodes operating by gas diffusion into restricted rectangular cross-sectional channels are largely affected by channel geometry. The ratio edge current/center channel current can be as large as 4, resulting practically in nonuniform surface conditions—(temperature, concentration). Semiempirical equations allow calculation of position-dependent current-voltage relationships.

Rates of cathodic oxygen reduction—that is, cell currents—are dependent on partial pressures of the oxidant if rate-controlling steps involve the concentration or partial pressure of oxygen. This is likely to be observed since reaction rates will be either liquid film or gas diffusion controlled. However, cases can arise where removal of the reaction product may be hindered by slow transport processes, thus resulting in, possibly, appreciably lower rates. This could be the case of water removal from the catalyst surface of an oxygen electrode. If local current densities are either dependent on partial pressures of oxygen or water, it will become necessary to establish a relationship predicting such local current densities and to design electrode geometries favorable to uniform current distribution, and as a result, uniform distribution of the main influential variables affecting oxygen electrode performance. Such considerations, however, would imply knowledge of limiting current densities.

In establishing over-all oxygen electrode capabilities for fuel cell application, one of the important variables is the limiting current density. Although these limiting currents are not simply dependent on some limited parameters—that is, electrode activity, electrode structure, electrolyte properties, local temperatures, and anisotropic current density distributions—actual measurements are valuable if some reproducible

In Fuel Cell Systems; Young, G., el al.;
Advances in Chemistry; American Chemical Society: Washington, DC, 1969.

characteristics can be controlled—that is, catalytic activity, electrode structure, electrolyte properties. Thus, measurements are valuable for a specifically designed system, as related to limiting current densities, and very generally applicable to any air electrode current collector design, if the geometry is influential on, and descriptive of, the limiting currents.

The ultimate goal—that is, quantitative description of current-voltage relationships as a function of main variables—can be, in principle, attained from experimental studies, involving the determination of limiting current densities at discrete positions on the air electrode, placed in a channel through which the reaction air is diffusing or flowing. Also necessary are the establishment of the rate-controlling process for known channel geometries in the high current density range (corresponding to .85 to 0.5 volt); the derivation of relationships describing the current-voltage behavior over practical operational ranges; the transport phenomena explaining polarization potentials at these practical currents; and the experimental values of open-circuit potentials. If all these equilibrium conditions, rates, and processes are known, a reasonable analytical description of local as well as over-all currents and potentials, can be expected.

It is conceivable then, that limiting currents can be associated with channel geometry and that diffusional processes in restricted channels become small enough (rate-controlling).

The purpose of the work described here was to obtain experimental results and interpretation to explain polarization in channels of defined geometry and to establish influential parameters which would affect electrode performance. In order to establish applicability of a self-breathing air electrode (without forced convective air-flow) for low current densities, experimental investigations were started on straight air channels. Since the diffusion polarization becomes quite severe at high current densities, these electrodes can not operate near limiting currents. To minimize large polarization contributions, the electrode must operate under forced-flow conditions. Experimental results on current distribution in air-electrode channels under forced-flow conditions were reported elsewhere (*1*).

Publication Date: January 1, 1969 | doi: 10.1021/ba-1965-0047.ch007

Experimental Equipment

The system chosen for experimental investigation was based on platinum black electrodes bound to a solid-matrix electrolyte (cation exchange membranes). Such a system offered multiple advantages in preparing discretely separated small electrodes and displaying good and uniform contact with the electrolyte. The individual electrodes included metallic screens to increase surface conductivity.

Reference potential measurements were based on a Luggin-type

capillary-saturated calomel electrode (SCE) system, specially developed for application to ion exchange membrane electrolytes (2). A low-leakage capillary was placed against the membrane and sulfuric acid used to establish the bridge with the calomel electrode. In all cases, the ion exchange membrane extended outside of the apparatus for potential measurements. Effects of capillary positions were investigated by placing the tip against and within the membrane. No appreciable differences were observed.

The ten segmented electrodes allowed the determination of limiting currents as a function of position and represented values for discrete electrode sizes. In many instances, the data presented represent smooth interpolation of position-dependent limiting currents.

Investigations were conducted under galvanostatic operating conditions. Voltage current curves were obtained for individual electrode segments while all segments were under operating conditions. From these measurements it was possible to obtain local electrode currents of nearly uniform potential for all segments. The equipment is shown in Figure 1. All experimental work was conducted on air channels 6.35 cm. long and 1.27 cm. wide. Channel height could be varied by changing a removable Lucite bar placed on the channel top. Thus, channel heights could be 0.16, 0.32, 0.64, or 1.27 cm. The channel was mounted on an air electrode and placed in a large Lucite box to avoid small air flow sweeps over the air electrode. Both channel ends were open to allow for oxygen diffusion.

Publication Date: January 1, 1969 | doi: 10.1021/ba-1965-0047.ch007

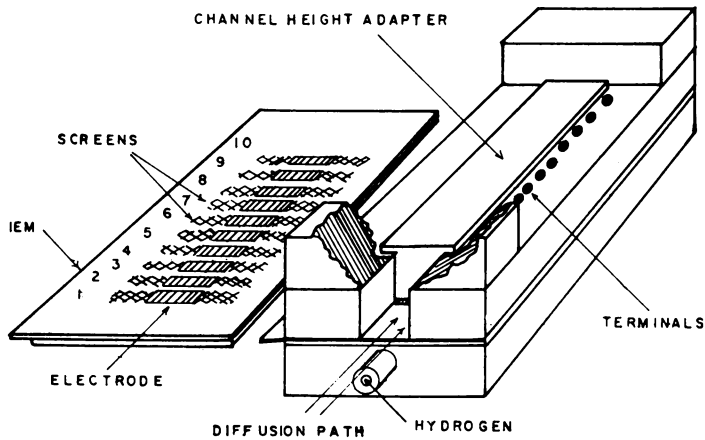

Figure 1. Experimental device for measuring local currents in air channels of variable geometry

To determine local current densities, the air electrode was manufactured by placing ten parallel electrode/screen strips on an ion ex-

change membrane. Gaps of 0.16 cm. between electrodes allowed for electrical insulation of the various electrodes. Electrode dimensions were (1.27 × 0.48) sq. cm. with an actual area of 0.60 ± 0.05 sq. cm. The ion exchange membrane extended out of the channel for reference potential measurements and stainless steel rods contacted the screens for current pickup.

The counter electrode (hydrogen electrode) was prepared in a similar manner. Catalytic electrodes faced each other across the electrolyte (membrane).

The two ends of the self-breathing channel were open, thus displaying planar symmetry for either side of the channel center cross-section. Closing one channel end actually corresponded to doubling the channel length. Single electrode failure would not affect results appreciably, since experimental results could be obtained from mirror-image electrode.

Publication Date: January 1, 1969 | doi: 10.1021/ba-1965-0047.ch007

Experimental Results

Representative single electrode polarization characteristics are presented in Figure 2 for a channel height of 0.32 cm. These polarization curves represent the largest changes from the edge to center electrodes for the smallest channel height investigated. Limiting current densities for the channel edges (edges of electrode 1 and 10) should be about 130 to 140 ma./sq. cm., as determined independently for electrodes exposed to semi-infinite air space (3). Thus, the local limiting currents should increase very sharply, precisely at the channel edges. Figure 2 indicates that appreciable polarization is encountered as soon as measurements are conducted slightly away from the channel edge. Larger currents are observed for all electrodes for increasing channel height. For 1.27 cm. channels, very little polarization is observed even at current densities near limiting values—130 to 140 ma./sq. cm. Polarization is less severe for all electrodes at small local currents, as expected.

Channel heights affect polarization characteristics to a large degree—that is, limiting currents for center electrodes are 22 and 35 ma. for 0.16 and 0.32 cm. channels, respectively. These currents correspond to oxygen partial pressures of 0.07 and 0.1, respectively, as determined independently by determining the effect of oxygen partial pressure on limiting currents (3). For identical polarization potentials (as determined from polarization curves) current density distributions display minima for inner electrodes and can be extrapolated to edge values of limiting currents of 130 to 140 ma./sq. cm.

Current density distributions for channel heights of 0.32 and 0.16 cm. for various applied potentials are shown in Figures 3 and 4. Edge currents can become two to four times larger than center currents, but display much more uniform distribution for lower electrode polarization—

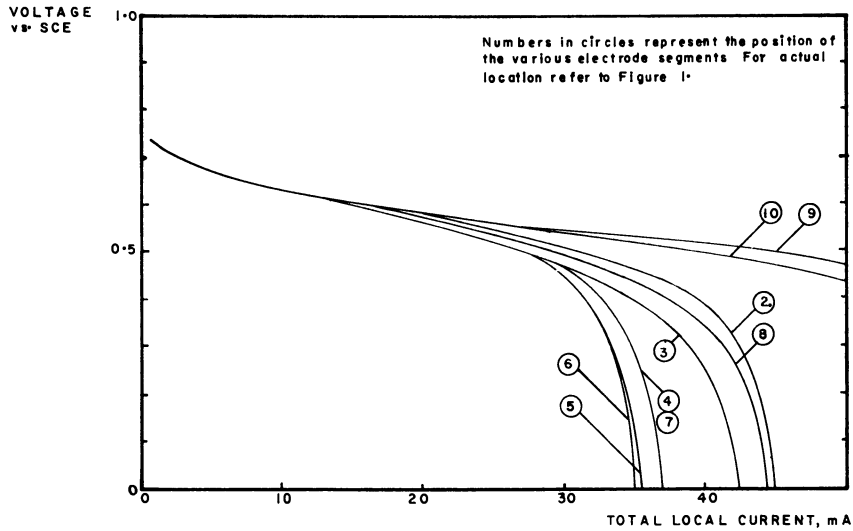

Figure 2. Polarization characteristics of individual electrodes for 10 parallel electrodes

Channel height, 0.32 cm.; electrode surface, 0.6 sq. cm.

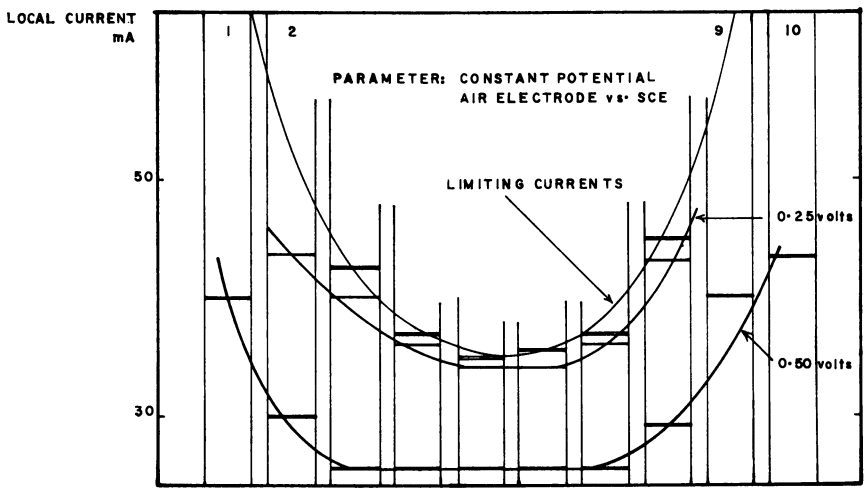

Figure 3. Current distribution for individual electrodes in the self-breathing channel

Channel height, 0.32 cm.; electrode surface, 0.6 sq. cm.

Publication Date: January 1, 1969 | doi: 10.1021/ba-1965-0047.ch007

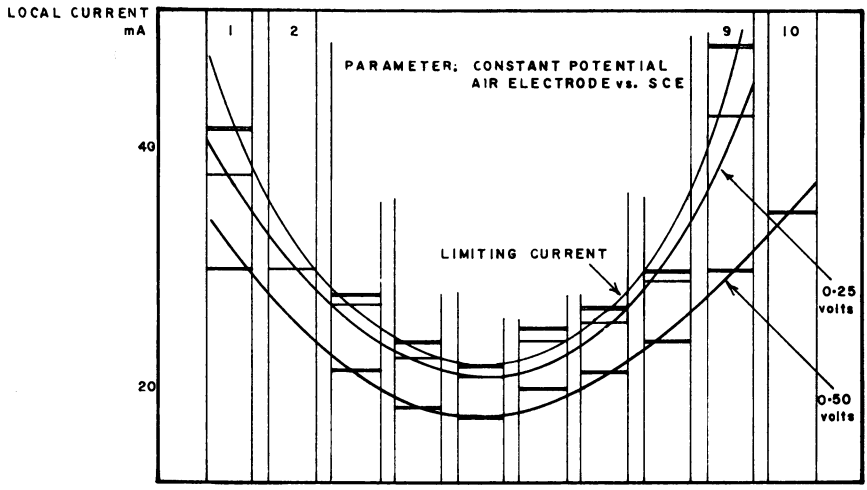

Figure 4. Current distribution for individual electrodes in the self-breathing channel

Channel height, 0.16 cm.; electrode surface, 0.6 sq. cm.

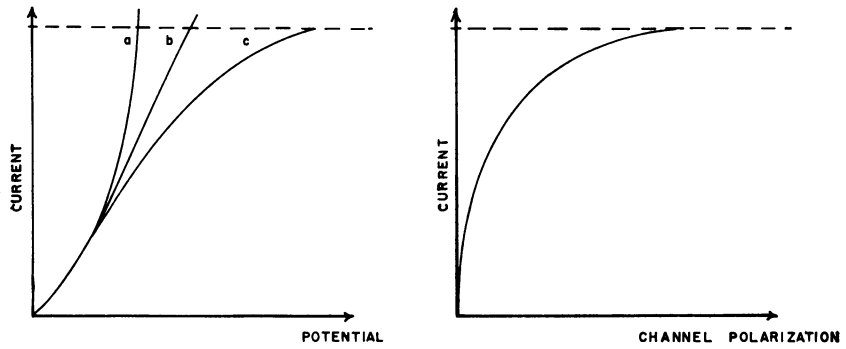

Figure 5. Single-electrode diffusion polarization

i_d = *diffusion-limited current channel polarization*
η_d = *Ea-Ewce = actual voltage minus voltage in absence of channel effects*

that is, 0.5 volts *vs.* SCE for 0.32 cm. channel.

Interpretation of Individual Polarization Curves

Current potential behavior for the investigated systems is shown in Figure 5.

Figure 5*A* represents polarization characteristics as observed in absence and presence of diffusion polarization (including activation polarization, in absence of ohmic contribution, which are generally eliminated). Figure 5*B* represents strictly diffusion polarization terms in absence of

Publication Date: January 1, 1969 | doi: 10.1021/ba-1965-0047.ch007

other possible polarization. The shape of curve 5*B* suggests the following empirical relationship between current and channel polarization:

$$(1 - i/i_L) = e^{-a(E^0 - E)} \tag{1}$$

in which all variables but E^0 are position-dependent; i and i_L represent actual and limiting position-dependent currents, respectively. The constant (a) must be evaluated. E^0 represents the air electrode potential in absence of channel polarization, E the electrode potential and $E^0 - E = \eta_d$ represents the channel polarization.

It follows from Equation 1 that:

$$\ln(1 - i/i_L) = -a(E^0 - E) = -a\eta_d \tag{2}$$

By differentiation:

$$\frac{d\eta_d}{di} = \frac{1}{a\, i_L(1 - i/i_L)} \tag{3}$$

with

$$\left(\frac{d\eta_d}{di}\right) \to \infty \text{ as } i \to i_L$$

and

$$R_d(x) = \left(\frac{d\eta_d}{di}\right)_{i=0} = \frac{1}{a\, i_L(x)} \tag{4}$$

If Equation 1 is applicable, it would follow that slope $(d\eta_d/di)$ at $i = 0$ should be inversely proportional to the limiting current for each electrode segment. In fact, these slopes can be determined and are dependent on the electrode position. (Figure 2 does not present these voltage variations at low local currents for reasons of clarity. However, results are presented in Table I). From Equation 2 and for $i = 0$:

$$\frac{\Delta\eta_d}{\Delta i} = \frac{\Delta E^0}{\Delta i} - \frac{\Delta E}{\Delta i} = R_d(x) \tag{2a}$$

$\Delta E^0/\Delta i$ was determined from experimental results obtained for a channel height of 0.64 cm., which displayed no channel polarization contribution as reported in Figure 6, and for which the position independent slope was determined to be $\Delta E^0/\Delta i = R = 4$. The coefficient (a) can then be evaluated from:

$$a = \frac{i_L}{R - (\Delta E/\Delta i)_{i=0}} \tag{4a}$$

The evaluation of (a) from the experimental results is reported in Table I. Since i_L (x) displays a regular decrease up to channel center, Equa-

Publication Date: January 1, 1969 | doi: 10.1021/ba-1965-0047.ch007

tion 4 is expected to display an increase from channel edge to center. Figure 6 presents smoothed experimental results for channel heights of 0.16, 0.32, and 0.64 cm. As suggested by Equation 4 and experimentally observed, the diffusional resistance displays:

- No diffusional resistance at the channel edges, at least as related to electrode geometry.
- Maximum diffusional resistance for center electrodes.
- Increased resistance for reduced channel cross-section.

Since the coefficient (a) has the dimensions of volt^{-1}, it is suggested to identify (a) with $\alpha nF/RT$, in which case $\alpha n = 0.24$ to 0.27.

Table I. Determination of (a) from Experimental Data

Electrode osition	*Limiting current, i_L, amps*	*$1/i_L$, amps^{-1}*	*$\left(\frac{\Delta V}{\Delta I}\right)_{exp}$, ohm*	*$\left(\frac{\Delta V}{\Delta I} - R\right)$, ohm*	*$\frac{i_L}{(\Delta V/\Delta I - R)}$ volts^{-1}*
		Channel height: 0.16 cm.			
1	0.041	..	..	..	..
2	..	..	..	..	..
3	0.028	35.8	7.3	3.3	10.8
4	0.024	41.7	7.8	3.8	11.0
5	0.022	45.5	8.2	4.2	10.8
6	0.025	40.0	8.1	4.1	9.8
7	0.027	38.0	7.9	3.9	9.7
8	0.030	33.3	7.3	3.3	10.1
9	0.050	20.0	6.1	2.1	9.6
				Average (a) =	10.4
		Channel height: 0.32 cm.			
1	..	..	..	..	..
2	0.045	22.2	6.0	2.0	11.1
3	0.043	23.2	6.7	2.7	8.6
4	0.037	27.0	7.1	3.1	9.0
5	0.035	28.6	7.3	3.3	8.7
6	0.035	28.6	7.3	3.3	8.7
7	0.037	27.0	7.1	3.1	9.0
8	0.044	22.7	6.8	2.8	8.2
				Average (a) =	9.0

A current-voltage relationship can now be obtained from Equation 1, if $i_L\,(x)$ can be obtained as a function of channel parameters.

Evaluation of $i_L\,(x)$

For steady state conditions, it is now necessary to approximate current density distributions over the electrode surface by assuming a mass transfer process which accounts for channel geometry and yields position-dependent transport rates simulating current distributions. This approach will not elucidate the transport mechanism but allow evaluations of $i_L\,(x)$, which then can be used in Equation 1 describing current-potential behavior of the electrode.

Channel conditions are not easy to define since electrode surface

Publication Date: January 1, 1969 | doi: 10.1021/ba-1965-0047.ch007

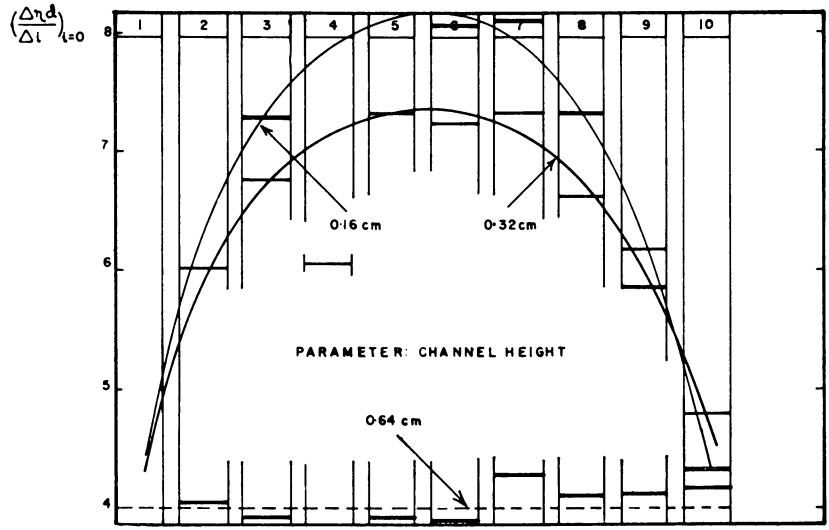

Figure 6. Slopes ($\Delta V/\Delta I$) for various electrodes in the self-breathing air electrode channel

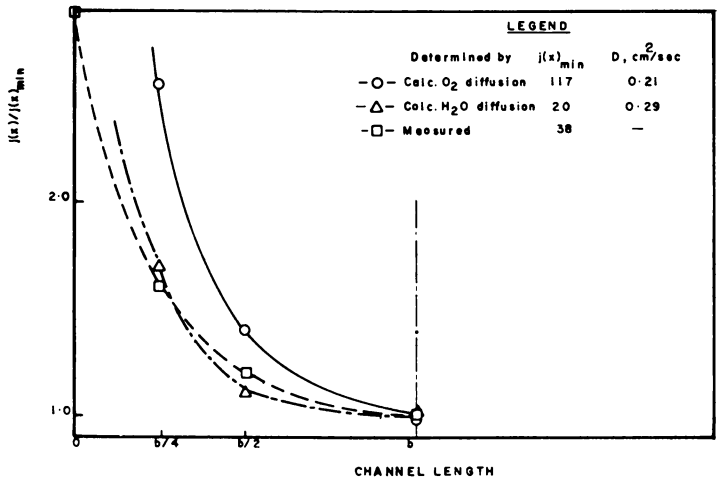

Figure 7. Current distribution in 0.16 cm. channel

concentrations as well as temperature distributions are not known. However, it will be assumed that the temperature is uniform; that the surface concentration of oxygen is small (equal to 0); and that the liquid water is in equilibrium with a saturated gas phase at the electrode temperature. In the following derivations, convection will be neglected, and transport

Publication Date: January 1, 1969 | doi: 10.1021/ba-1965-0047.ch007

rates will be evaluated for the moving gas phase components—that is, oxygen and water. Under these conditions:

$$\nabla^2 C_i = 0 \tag{5}$$

$$\sum_i C_i = 1 \tag{6}$$

C_i represents the concentration in the three component gas phase. In the two-dimensional channel, y represents the distance above the electrode surface ($y = 0$ at the surface and $y = y_0$ at the top of the channel), and x is the direction parallel to the electrode surface ($x = 0$ and $x = 2b$ at channel edges). Boundary conditions are:

$$C_i(0, y) = C_i(2b, y) = C^i$$

At the electrode surface:

$$C_{O_2}(x, 0) = 0; \; C_W(x, 0) = f(T); \; C_{N_2}(x, 0) = 1 - f(T)$$

Furthermore it will be assumed that:

$$\left(\frac{dC_{O_2}}{dy} = \frac{dC_{N_2}}{dy}\right)_{y = y_0} = 0$$

Oxygen Transport Rates. With these boundary conditions the concentration distribution for oxygen becomes:

$$C_{O_2} = C^\circ \left[1 - \sum_{n=1} A_n \sin \alpha_n x (\cosh \alpha_n y - th\alpha_n y_0 sh\alpha_n y)\right] \tag{7}$$

where $A_n \dfrac{(-1)^n - 1}{b\alpha_n}$ and $\alpha_n = \dfrac{n\pi}{2b}$

The local current densities which can be associated with this concentration are obtained from:

$$j(x)_{O_2} = -nFD_{O_2}\left(\frac{dC_{O_2}}{dy}\right) y = 0 \tag{8}$$

For air, with $D_{O_2} = 0.21$ sq. cm./sec., the following expression has been obtained:

$$j(x)_{O_2} = 0.235 \sum_{n = 1,3\ldots} \sin(n\pi x/2b) th(n\pi y_0/2b) \tag{9}$$

and plotted in Figure 7. The calculated values deviate appreciably from experimental results.

Water Transport Rates:

1. With the previous boundary conditions, in addition to

$$(dC_W/dy)_{y=y0} = 0,$$

similar expressions as Equations 7 and 9 can be derived, yielding transport rate distributions appreciably lower than measured.

Publication Date: January 1, 1969 | doi: 10.1021/ba-1965-0047.ch007

2. If the temperature at $y = y_0$ is lower than at $y = 0$ and if gas phase saturation is assumed, the following boundary condition is introduced: $(C_W)_{y = y_0} = g(T)$. For these conditions the concentration distribution for water becomes:

$$C_W = \sum_{n=1} A_n \sin \alpha_n x \times \left[\frac{g(T) - f(T) \cosh \alpha_n y_0}{\text{sh } \alpha_n y_0} \text{ sh } \alpha_n y + f(T) \cosh \alpha_n y \right] \quad (10)$$

The current distribution associated with this concentration profile, as obtained from Equation 8, for $D_w = 0.29$ sq. cm./sec. becomes:

$$j(x)_w = 0.031 \sum_{n = 1,3,\ldots} \sin (n \pi x/2b) \left[\frac{1 - \cosh \alpha_n y_0}{\text{sh } \alpha_n y_0} \right] \quad (11)$$

and is plotted in Figure 7 for the specific limiting condition of $g(T) = F(T) = 30$ mm. Hg (vapor pressure of water at 30°C.).

Some calculated data obtained from Equations 9 and 11 are presented in Table II and compared with experimental results. The nearest approximation to experimental data is based on an assumed water diffusion-controlled process simulating limiting current density distributions.

Table II. Local Current Density for Channel Height of 0.16 Cm.

	Electrode position (total channel length 2b)	*Local current density j(x), ma./sq. cm.*	$j(x)/j(x)_{min}$	*Minimum current density* $j(x)_{min}$
Oxygen diffusion	*b*	117	1.0	...
	b/2	163	1.41	117
	b/4	298	2.55	...
Water diffusion	*b*	20	1.0	...
	b/2	22	1.1	20
	b/4	35	1.7	...
Measured	*b*	38	1.0	...
	b/2	44	1.2	38
	b/4	61	1.6	...
	0	110	2.9	...

Restriction of channel cross-section—that is, channel height—may result in appreciable reduction in gas-phase transport rates. If air-breathing electrodes were to be utilized in practice, only low current densities could be supported for channel heights less than 0.6 cm. In fact, disk-type electrodes would offer appreciable advantages over rectangular cross-sectional channels. In all cases, but at relatively low currents, the surface concentrations, thus current densities and heat rejection, would be nonuniform, resulting in time-variance of the interfaces rather difficult to control. The results obtained here suggest applicability up to about 25 ma./sq. cm. at ambient temperature in a design where air-

Publication Date: January 1, 1969 | doi: 10.1021/ba-1965-0047.ch007

electrodes would be disposed face-to face and separated by air-channels such that $y_0 \geq 0.6$ cm. Higher uniform current densities will require creation of convection (as a chimney effect) or, better yet, operation under forced flow conditions.

Literature Cited

(1) Maget, H., presented before the Symposium on Mass Transport in Electrochemical Processes, The Electrochemical Society, Spring Meeting 1964, Toronto, Can.
(2) U.S. Army Signal Corps, R&D Labs., Ft. Monmouth, N.J., Rept. 2, "Ion Exchange Membrane Fuel Cell," September 1962.
(3) *Ibid.*, Final Technical Rept.

RECEIVED February 17, 1964. This work was a part of contract DA-36-039-AMC-00095(E), 1962-63, with the U.S. Army Electronics Research and Development Laboratory, Fort Monmouth, N.J.

Publication Date: January 1, 1969 | doi: 10.1021/ba-1965-0047.ch007

A New Fuel Cell Anode Catalyst

RAYMOND J. JASINSKI

Research Division, Allis-Chalmers Manufacturing Co.,[1] Milwaukee, Wis.

There are a number of possible commercial applications for hydrogen-air fuel cells—for example, the on-the-site fuel cell oxidation of by-product hydrogen. One of the principal items which affects the capital cost of the fuel cell power plant itself is the cost of the anode and cathode catalysts. A new nonnoble metal hydrogen anode catalyst—nickel boride—has been developed. This material possesses a high surface area—20 sq. meters/gram—and is active in chemisorbing hydrogen. A hydrogen-oxygen fuel cell employing this catalyst operated continuously for 1200 hours at 32 ma./sq. cm. The initial cell voltage was 0.78 volt.

Publication Date: January 1, 1969 | doi: 10.1021/ba-1965-0047.ch008

The operating cost of a fuel cell power plant is determined primarily by the cost of the fuel. Although hydrogen is generally a more expensive fuel than methanol or propane, there are a number of situations in which fuel cells operating on hydrogen could be economical. An example of this is the on-the-site fuel cell oxidation of by-product hydrogen obtained from commercial processes, such as the electrolytic production of chlorine.

One of the principal items which affects the capital cost of the fuel cell power plant itself is the cost of the anode and cathode catalysts. The majority of the ambient temperature, hydrogen-oxygen fuel cells described in the literature have employed noble metals such as platinum and palladium. These metals are expensive, and some question has been raised regarding an adequate natural abundance of the elements (*12*).

There are two alternatives to developing inexpensive catalyst-anodes: Either reduce the amounts of the noble metal catalyst on the electrode to about 1 mg./sq. inch of electrode or employ less expensive nonnoble metal catalysts.

[1] Present address: Tyco Laboratories, Inc., Waltham 54, Mass.

In Fuel Cell Systems; Young, G., el al.;
Advances in Chemistry; American Chemical Society: Washington, DC, 1969.

The latter approach has been followed, for example, by E. Justi (7), who successfully constructed hydrogen anodes starting with the Raney alloy (Ni_2Al_3). It would appear, however, that the economic advantage of employing less expensive metals, such as nickel and aluminum, is more than offset by the relatively involved, and hence costly, procedure of electrode preparation. Furthermore, the problem of adapting these procedures to the preparation of large electrodes for the construction of fuel cell power plants may limit the applications of this catalyst.

This article discusses the use of a new material, nickel boride, as a hydrogen anode. The existence of catalytic activity is described as well as some of the general chemical properties of nickel boride. No attempt is made, at this stage, to present a detailed electrochemical characterization of the material.

Publication Date: January 1, 1969 | doi: 10.1021/ba-1965-0047.ch008

The properties of nickel boride as an anode in the hydrazine-oxygen cell and the potassium borohydride–oxygen cell have been discussed elsewhere (*6*). It was shown that, for these cells, the nickel boride catalyst-anodes were approximately 0.1 volt more effective than a palladium catalyst for the direct fuel cell oxidation of hydrazine and potassium borohydride. The same comparison holds true for platinum anodes.

The chemical hydrogenation properties of this catalyst have been discussed only briefly in the literature. Nickel boride has been reported to be superior in catalytic activity to Raney nickel and more resistant to fatigue in the hydrogenation of safrole, furfural, and benzonitrile (*9*). Some of the properties of this material have also been described in the Russian literature (*5*). More recently, H. C. Brown (*2*) has discussed the hydrogenation of olefins by nickel boride.

Nickel boride can be formed by heating nickel oxide to 700° to 1000° C. in a stream of boron trichloride and hydrogen (*3*). Another method of preparation involves electrolysis of nickel oxide "dissolved in variable quantities of alkali tetraborates" (*8*). The compound can also be formed directly from the elements by diffusing powdered boron into the reduced nickel (*4*). However, the most convenient method has been that developed by Schlesinger (*11*) in which nickel boride is formed by combining solutions of potassium borohydride and a nickel salt. This technique has also been employed by Paul, Buisson, and Joseph (*9*).

Chemisorption Properties

Nickel boride, prepared by the Schlesinger method, is formed in an atmosphere of hydrogen, produced by the decomposition of the excess potassium borohydride on the catalyst surface. As a result, there can be a considerable quantity of hydrogen chemisorbed on the material so that in some cases it may be pyrophoric. No difficulty was experienced in handling the electrodes. It is dersiable, however, that contact with air be held to a minimum.

The chemisorption of hydrogen on nickel boride was studied as a function of temperature. (The sample employed in these experiments had a surface area of 15 sq. meters/gram, as determined from the adsorption of nitrogen at —196° C.) Adsorbed hydrogen was removed by evacuating the sample at 200° C. to a pressure of less than one micron. Heating at this temperature has only a minor effect on surface area. The adsorption of hydrogen at a pressure of 1 atmosphere, as a function of temperature, is shown in Table I.

Table I. Adsorption of Hydrogen on Nickel Boride

Temperature, ° C.	*Volume Adsorbed (STP), Cc./Gram*
—196	0.6
0	3.5
25	3.4
150	3.2
275	2.3

The variation of the quantity of hydrogen adsorbed with temperature, as shown in Table I, is characteristic of activated adsorption. At —196° C., the hydrogen has insufficient energy to overcome the energy barrier for adsorption. At the higher temperatures (275° C.), there is sufficient energy to break the chemical bonds holding the hydrogen to the surface of the solid and the quantity of gas adsorbed decreases.

However, the drop in hydrogen adsorption at 275° C. is complicated somewhat by the fact that the catalyst has probably undergone some sintering, thus lowering the over-all surface area.

The shape of the hydrogen adsorption isotherm suggests that, at a pressure of 360 mm., a monolayer has been achieved. From the volume of hydrogen adsorbed, it is possible to obtain an approximate value for the fraction of the total nickel boride surface available for hydrogen chemisorption.

It was assumed in the calculations that the surface of the catalyst had the same atom ratio as the bulk compound—that is, 2Ni:1B. An effective radius of the nickel atoms of 1.30 A. was chosen from the literature (*14*). The radius of the boron atoms was chosen as 0.89 A. (*13*). It was also assumed that the hydrogen dissociated upon adsorption and that one hydrogen atom adsorbed per nickel atom. Finally, it was assumed that all the hydrogen adsorbing at room temperature chemisorbed on the catalyst surface and did not diffuse into the lattice. With these assumptions, it can be shown that the nickel atoms adsorbing hydrogen account for 10 sq. meters/gram. Taking into account the boron on the surface raises this value to 12 sq. meters/gram.

This surface area, computed from the hydrogen adsorption isotherm, is of the same order as that obtained from nitrogen adsorption, 15.2 sq.

Publication Date: January 1, 1969 | doi: 10.1021/ba-1965-0047.ch008

meters/gram. The lack of a closer correspondence in area as computed by the two isotherms could be due to a number of factors. According to Beeck (*1*), the use of nitrogen adsorption to determine the area of nickel or iron catalysts generally leads to a value which is too high, because of a small amount of nitrogen chemisorption. The somewhat arbitrary choice of the nickel atom radius, representative of Ni in Ni_2B, has an influence on the surface area computed from hydrogen adsorption—that is, $\pm$ 0.1 A. is equivalent to $\pm$ 1.5 sq. meters/gram.

Nevertheless these data do indicate that a major portion of the nickel boride surface is active in absorbing hydrogen, a necessary, but not sufficient, property of a hydrogen anode catalyst.

A preliminary study was also made of the physical structure of the catalyst as a function of sintering temperature. A second sample of nickel boride was heated under vacuum to successively higher temperatures. The surface area of the sample was determined between heat treatments from the nitrogen adsorption isotherm.

The sample was first degassed at ambient temperature until a constant pressure of less than 1 micron was reached. A nitrogen adsorption isotherm, measured at —195° C., indicated a surface area of 22.5 sq. meters/gram. The boride was then heated under vacuum to 200° C. and held at a pressure of less than 1 micron for four hours. A second nitrogen isotherm indicated a surface area of 21.3 sq. meters/gram. The decrease is small, indicating little, if any, sintering of the nickel boride. Next, the sample was heated to 350° C. for $17^1/_2$ hours at a pressure of less than 1 micron. The surface area dropped to 13.3 sq. meters/gram. Finally the sample was heated to 475° C. for $2^1/_2$ hours. The final surface area was 6.38 sq. meters/gram. These data are plotted in Figure 1.

Very little chemisorption of hydrogen was noted on the nickel boride sample after sintering at 350° C. The sample was cooled to 25° C., and the hydrogen isotherm measured. After evacuating to a pressure of $< 1\mu$ at this temperature to remove only physically adsorbed hydrogen, another hydrogen isotherm was measured. The two isotherms were identical, indicating at most, weakly adsorbed hydrogen. This loss of a large number of active sites during sintering is confirmed by electrochemical data. Fuel cells containing nickel boride anodes which had been sintered at 500° C. did not attain a voltage greater than 0.4 volt, while the samples sintered at 400° C. attained a cell voltage of 1 volt but only very slowly.

Apparently, the activity of the electrocatalyst was more sensitive to heat treatments than would be expected simply from changes in surface area. A 3×3 inch anode, generating approximately 10 ma./sq. cm., must have at least 10^{19} hydrogen atoms chemisorbing and reacting per second. The minimum current involved in the voltmeter reading of 1 volt was approximately 10^{-6} amps—10^{13} hydrogen atoms reacting per second. A catalyst-anode sintered at 500° C. achieved an open-circuit voltage of

Publication Date: January 1, 1969 | doi: 10.1021/ba-1965-0047.ch008

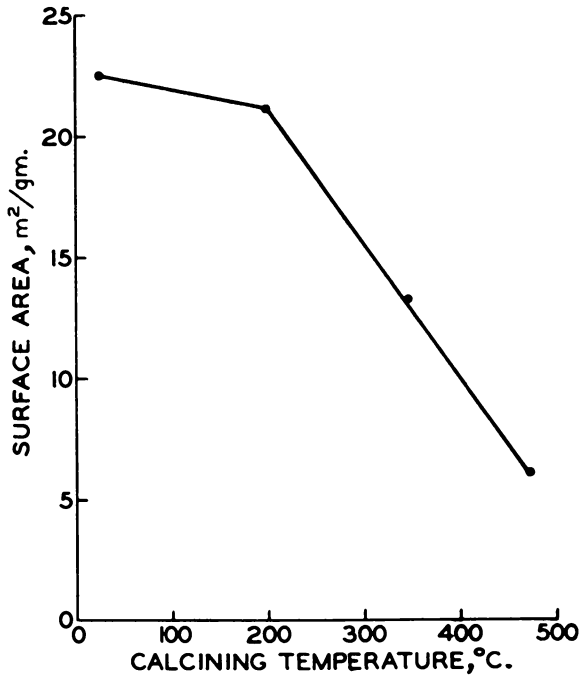

Figure 1. Variation in surface area with sintering temperature

only 0.4 volt. Assuming a direct proportionality between the rate of reaction and the number of active sites, there must have been a decrease by a factor of 10^6 in the number of active sites upon sintering at 500° C. The surface area, however, was decreased only by a factor of four. This conclusion is also apparent from a comparison of the hydrogen chemisorption after sintering at 350° C. with the loss of surface area. The chemisorption of hydrogen was reduced to a negligible value, while the surface area had decreased by a factor of four.

Therefore, the use of total surface area as an indicator of active catalyst site concentration in formulations of electrochemical reaction rates is a very tenuous procedure. A more valid approach would be the use of the hydrogen adsorption isotherm "surface area." This is not intended to imply an identity but rather a proportionality between the number of sites adsorbing hydrogen and the number of catalytically active sites.

Anodic Oxidation of Hydrogen

Nickel boride was studied as a hydrogen anode catalyst in two forms—first as the powder and then supported on a porous nickel plaque. The powder was prepared by combining a basic solution of 5% potassium boro-

Publication Date: January 1, 1969 | doi: 10.1021/ba-1965-0047.ch008

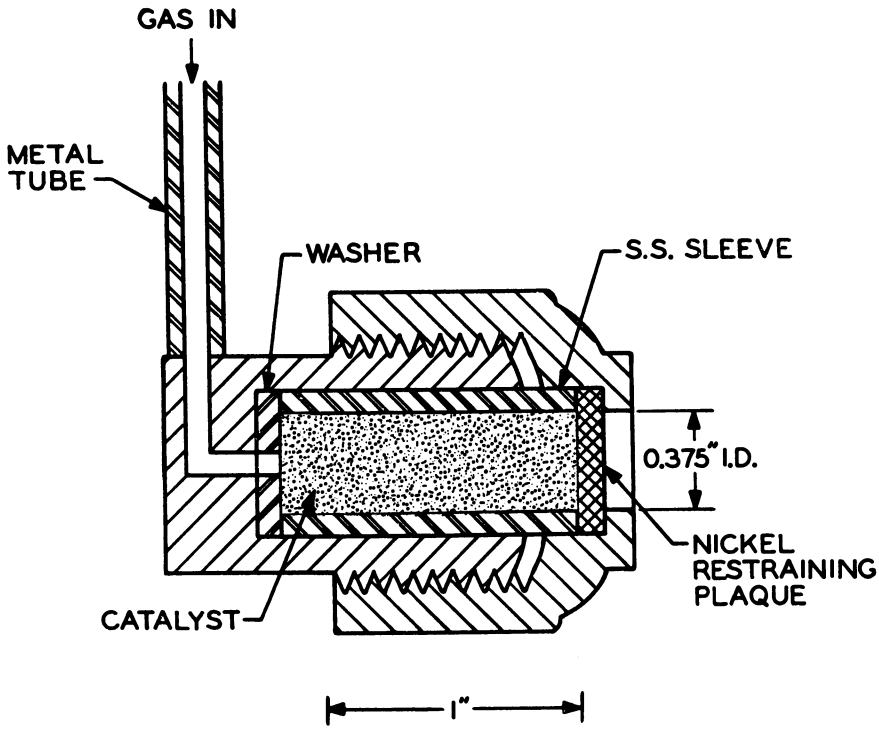

Figure 2. Catalyst test electrode

hydride with a dilute aqueous solution of a nickel salt—for example, nickel acetate. A voluminous black precipitate formed immediately and was accompanied by a rapid evolution of hydrogen gas. The details of the procedure are all well documented (*9*) and insoluble nickel boride is the sole solid reaction product. As a check on the procedure, a sample of this material was analyzed and shown to have a Ni/B atom ratio of 2.05. The plaque-electrode was formed by depositing nickel boride in the voids of a porous sintered nickel plaque. The substrate, commercially available, measured $3 \times 3 \times 0.03$ inches.

Since the nickel boride is an electrical conductor, it was possible to study the catalyst directly—that is, it was not necessary to first support the catalyst on a conducting substrate. The catalyst was formed into a plug and placed in the catalyst test electrode shown in Figure 2. The fuel gas was passed down the metal tube, through the catalyst plug, and into the "free" electrolyte. Studying the catalyst in this form alleviated many of the problems involved in operating hydrogen-oxygen fuel cells, such as maintaining the proper moisture balance in the cell. The two electrodes were "driven" with the commutator (*10*) hence the voltages measured were free of internal resistance (IR) loss. In such a system,

Publication Date: January 1, 1969 | doi: 10.1021/ba-1965-0047.ch008

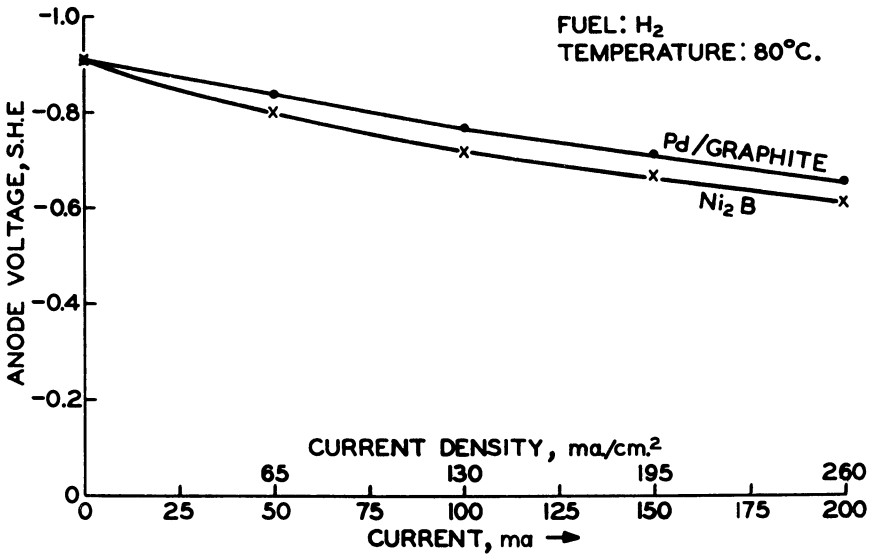

Figure 3. Anodic oxidation of hydrogen by nickel boride and by palladium black

hydrogen was consumed at the anode, and water was electrolyzed at the auxiliary electrode. A saturated calomel electrode, connected to the cell by a salt bridge, was used as the reference electrode. The entire cell was mounted in a constant temperature bath maintained at 80° C. A typical voltage-current curve obtained for a nickel boride "plug" hydrogen anode is shown in Figure 3. A curve recorded under similar conditions for 1:1 palladium black–graphite mixture is included for comparison purposes. It is apparent that the nickel boride anode is sufficiently active to support high current densities.

A test electrode was then operated at a constant load of 65 ma./sq. cm. and the anode voltage recorded as a function of time. These data are summarized in Figure 4. There is apparently a small fall-off in performance over the first 200 hours—that is, from —0.87 to —0.83 volt. The voltage then remained constant for the next 700 hours, at which time the test was terminated. It is apparent from these data that nickel boride is capable of extended performance as a hydrogen anode catalyst.

The nickel boride catalyst was then evaluated in complete fuel cells of the Allis-Chalmers design, shown in Figure 5. It was possible to apply the active powder directly to the surface of the capillary membrane, and a number of cells of this type were built. Since this procedure is inefficient in the use of catalysts, it was desirable to employ a support to more efficiently disperse the catalyst across the electrode. As mentioned, a porous, sintered nickel plaque (3×3×0.03 inches) was used for this purpose with the nickel boride catalyst deposited in the pores of the

Publication Date: January 1, 1969 | doi: 10.1021/ba-1965-0047.ch008

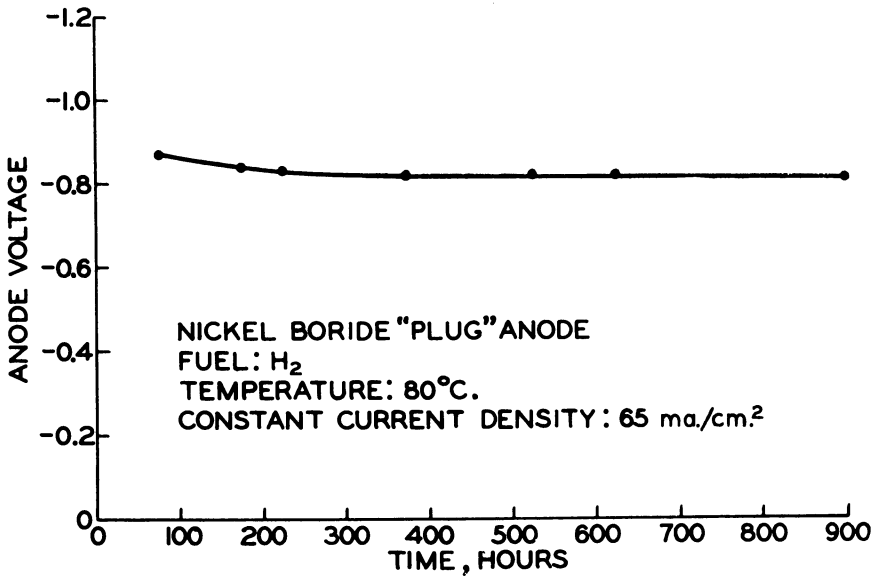

Figure 4. Extended operation of a nickel boride hydrogen electrode

substrate. A voltage-current curve obtained for a fuel cell employing such an anode is shown in Figure 6. The cell temperature in this case was 78° C. It was possible to support a load of approximately 70 ma./sq. cm. at a cell voltage of 0.7 volt. Improvements in cell and electrode design have increased this performance to 100 ma./sq. cm. at 0.7 volt.

The plaque type of electrode structure employed in these experiments is satisfactory for a demonstration of the existence of electrocatalytic activity. However, it is difficult to obtain more than a general estimate of the catalyst loading—that is, the weight of catalyst per unit geometric area. Obviously this information is necessary before an exact evaluation of catalyst cost is possible. Further experiments have confirmed that the use of nickel boride as a hydrogen anode does markedly reduce the anode catalyst cost.

Extended Performance Tests

The fuel cell data shown in Figure 6 describe the initial performance of the catalyst electrodes—that is, the voltage-current characteristics obtained during the first day or two of operation. However, fuel cell electrodes generally show some loss in activity with time, as shown in Figure 4. This effect was also studied with a fuel cell of the type shown in Figure 5, employing an anode of nickel boride deposited within a porous nickel substrate. The initial performance was essentially that described by the voltage-current curve of Figure 6.

Publication Date: January 1, 1969 | doi: 10.1021/ba-1965-0047.ch008

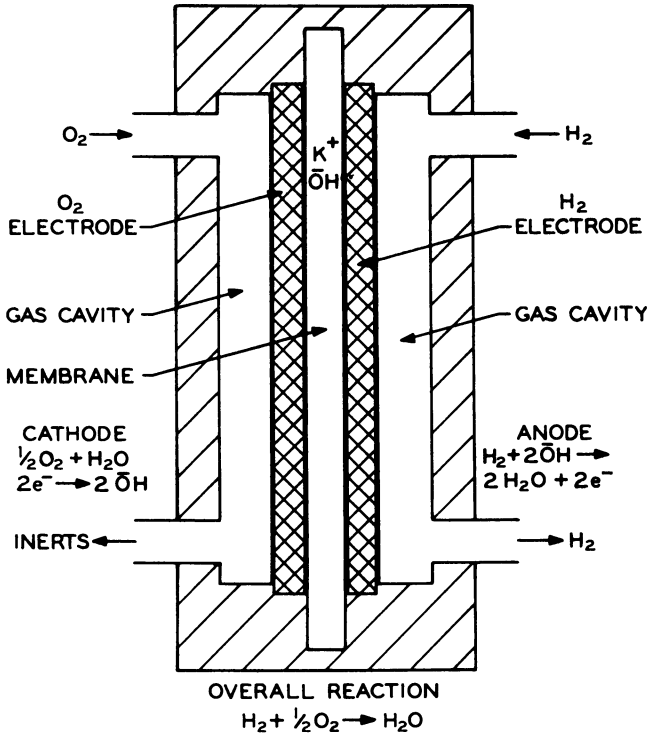

Figure 5. Allis-Chalmers hydrogen-oxygen capillary membrane fuel cell

Before discussing the extended performance data, it is necessary to briefly mention the subject of fuel cell "controls". The principal problem, common to all hydrogen-oxygen fuel cells, centers on maintaining the proper water balance in the cell. It is desirable to withdraw from the operating fuel cell only that amount of water produced by the fuel cell reaction. If an excess is removed, the cell will dry out; if insufficient water is removed, the electrode will flood or the electrolyte will be diluted. In either case, the extended performance of the hydrogen-oxygen fuel cell would be adversely affected.

A high operating current density provides for a high rate of water production, and the problem of maintaining the proper amount of water in the cell becomes more severe. The life test on the nickel boride hydrogen anode was carried out at a relatively low current density—that is, 32 ma./sq. cm. At this level, the rate of water production was determined to be sufficiently low so as not to require an involved water monitoring system. The moisture in the cell was controlled empirically by adjusting the hydrogen flow rate to establish either a wetting or a desiccative condition as needed. The variation in cell voltage with time is shown in

Publication Date: January 1, 1969 | doi: 10.1021/ba-1965-0047.ch008

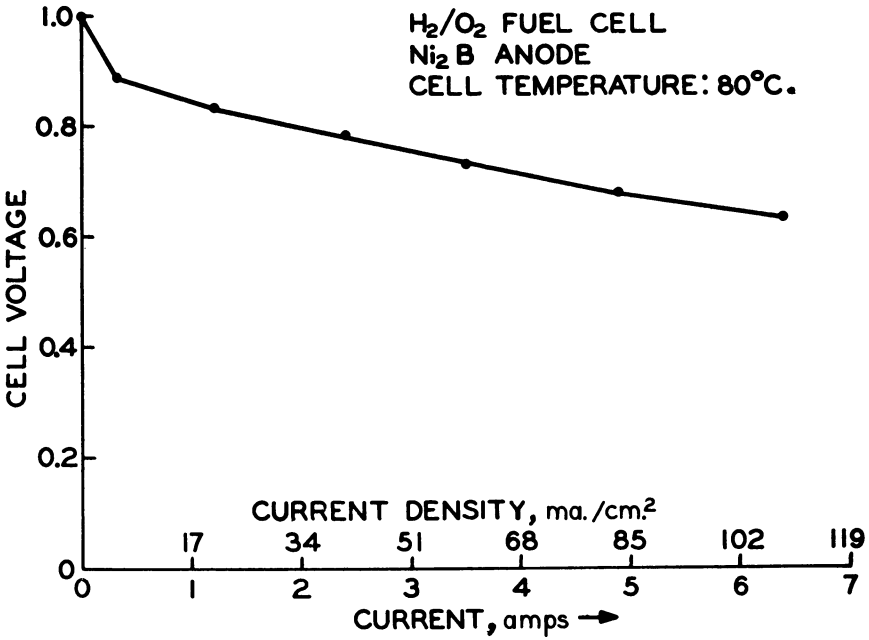

Figure 6. Voltage-current characteristics of a hydrogen-oxygen fuel cell employing a nickel boride anode

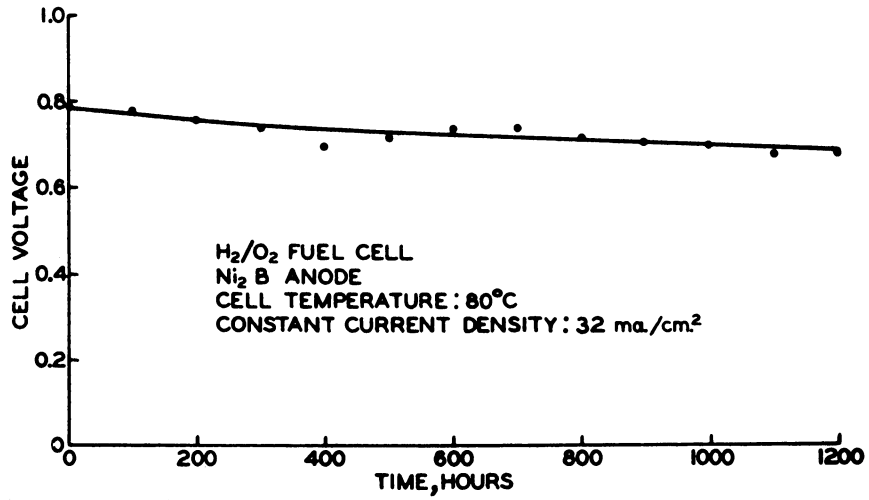

Figure 7. Extended operation of a H_2/O_2 fuel cell employing a nickel boride anode

Figure 7 for a cell operated in this manner for 1200 hours. There appears to be a small, gradual fall-off in cell performance with time. Comparing these data with those of Figure 4, most of the fall-off after the first 200

Publication Date: January 1, 1969 | doi: 10.1021/ba-1965-0047.ch008

hours must be ascribed to problems of cell control. Nevertheless, the data are sufficient to establish that it is possible to construct large nickel boride catalyst-electrodes which are capable of extended operation as hydrogen anodes.

The data presented were taken with 3 × 3 inch electrodes. No difficulty has been experienced in adapting the preparative procedures to 6 × 4 inch nickel boride catalyst-anodes. The use of electrodes of this size in the hydrazine-oxygen fuel cell has already been described (*6*).

Acknowledgment

The author wishes to acknowledge the efforts of James Huff in obtaining the gas adsorption data and the efforts of David Cary in carrying out the extended performance tests. The catalyst test electrode was developed with the assistance of Phil Horwitz and Larry Swette.

Publication Date: January 1, 1969 | doi: 10.1021/ba-1965-0047.ch008

Literature Cited

(1) Beeck, O., "Advance in Catalysis," Vol. 2., Academic Press, New York, 1950.
(2) Brown, C. A., Brown, H. C., *J. Am. Chem. Soc.* **85,** 1003 (1963).
(3) Deiss, W. J., Blum, P., *Compt. rend.* **244,** 464 (1957).
(4) Fruchant, R., Michel, A., *Bull. Soc. Chim. France* **1959,** 422.
(5) Iverdovskii, I. P., Tupitsyn, I. F., *Problemy Kinetiki i Kataliza, Akad. Nauk, S.S.S.R. Inst. Fiz. Khim., Soreshscanie, Moscow* **9,** 86 (1956).
(6) Jasinski, R., presented at 123rd Meeting Electrochemical Society, Pittsburgh, Pa., April 15, 1963.
(7) Justi, E., Pilkuhn, M., Schiebe, W., and Winsel, A., "High Drain Diffusion–Electrodes Operating at Ambient Temperature and Low Pressure," *Akad. Wiss, Lit.* (Mainz) *Abhand. Math. Nat. Klasse*, No. 8, Komm Verlag Steiner, Wiesbaden, 1959.
(8) Marion, S., *Bull. Soc. Chim., France,* **1957,** 522.
(9) Paul, R., Buisson, P., Joseph, N., *Ind. Eng. Chem.* **44,** 100 (1952).
(10) Pollnow, G., Kay, R., *J. Electrochem. Soc.* **109,** 648 (1962).
(11) Schlesinger, H. I., U. S. Patent **2,461,611** (Jan. 9, 1945).
(12) Slaughter, J., presented at 121st Meeting Electrochemical Society, Los Angeles, Calif., May 1962.
(13) Sneed, M. C., Brasted, R. C., "Comprehensive Inorganic Chemistry," **7,** D. Van Nostrand Co., N.J. (1958).
(14) Well, A. F., "Structural Inorganic Chemistry," Clarendon Press, Oxford, 1962.

RECEIVED February 17, 1964.

9

Thin Fuel Cell Electrodes

R. G. HALDEMAN, W. P. COLMAN, S. H. LANGER, and W. A. BARBER

Stamford Research Laboratories, American Cyanamid Co., Stamford, Conn.

Publication Date: January 1, 1969 | doi: 10.1021/ba-1965-0047.ch009

An experimental investigation was made of the structure and performance of thin electrodes consisting of platinum and platinum-carbon supported on metal screens. Platinum loadings were in the range 1 to 9 mg./sq. cm. The electrodes were shown to have a very open structure consisting of aggregates of platinum black bonded by Teflon fibrils. Gas adsorption and electrochemical measurements indicate virtually the entire surface area of the platinum black to be available for reaction. The electrodes were tested in both acid- and base-equilibrated matrix cells. Initial polarization and life-testing data were obtained. The effect of temperature and operation on air were studied. These electrodes were capable of sustaining high current densities and show considerable promise for use in lightweight, high performance fuel cell batteries.

There is considerable current interest in lightweight high performance electrodes for low temperature hydrogen-oxygen fuel cells. Electrode performance characteristics are of critical importance in potential application of fuel cells in space, communications, marine and ground power (*12*). The present work is directed toward development of electrode structures for "equilibrated matrix" cells since these have compact structure and are capable of operation at high current densities (*6*). Electrodes suitable for this system should be useful also in the ion exchange membrane fuel cell and, with some modification, in the free electrolyte fuel cell.

The electrode system chosen consisted of catalytic materials spread on thin metal screens and bonded and waterproofed with Teflon. This general type of fuel cell electrode has been investigated previously by

In Fuel Cell Systems; Young, G., el al.;
Advances in Chemistry; American Chemical Society: Washington, DC, 1969.

Elmore and Tanner (*1*) and by Grubb (*3, 4*). Here, we characterize in some detail the physical and electrochemical properties of two electrode modifications in which platinum is incorporated as a black (Type A) and as supported on carbon (Type B).

Procedures

The initial evaluation work was carried out in 1-inch diameter (5 sq. cm. active area) matrix cells. Life testing was conducted in 2 × 2 inch cells. Components of these cells were similar to those of plastic cells previously described (*4*), except that for most of the work reported here metal faceplates of nickel or gold-plated nickel were used. For the alkaline system (5*N* KOH) asbestos was found to be a suitable matrix material, while for the acid system (5*N* H_2SO_4) glass-fiber paper performed satisfactorily. Cell matrix thickness was 10 to 20 mils and cell internal resistance as measured by an a.c. bridge fell within the range 0.2 to 0.4 ohm/sq. cm. for both base and acid cells.

In obtaining polarization data, two minutes at steady potential were required at each load before moving to the next higher current. Product water was removed by flow of sufficient dry hydrogen and oxygen (or air), about equally divided, to remove water as fast as it was formed. Close control of water balance was particularly critical in life testing, which was carried out on a continuous basis.

Unless otherwise indicated, performance data are given for cells having the same electrode material at anode and cathode.

Electrodes

For the equilibrated matrix system electrodes have been developed consisting of a porous layer of platinum black or platinum supported on carbon, mixed with a binder-waterproofing agent (Teflon) and spread uniformly on and supported by a wire mesh screen. The thickness of the electrode and the catalyst loading can be varied by using screens of differing mesh and wire diameter. Electrodes of area up to 1 sq. ft. have been prepared. The range of composition of the two major electrode variations studied is indicated in Table I. Preferred compositions are roughly midway in the range indicated.

Table I. Thin Fuel Cell Electrodes

	Thickness, Mils	*Platinum, Mg./Sq. Cm.*	*Carbon, Mg./Sq. Cm.*	*Teflon Binder, Mg./Sq. Cm.*	*Support Screen*
Type A	4–8	7–10	None	1.0–3.5	Ni or Ta
Type B	4–8	0.5–4.0	8–12	1.0–3.5	Ni or Ta

Publication Date: January 1, 1969 | doi: 10.1021/ba-1965-0047.ch009

In Type A no extender is used. Thus, with screens in the range 50 to 100 mesh and 0.002 to 0.004 inch wire diameter, platinum loadings are typically in the range 7 to 10 mg./sq. cm. and electrode thickness 0.004 to 0.008 inch. Resistivity is nearly that of the support screens. In Type B electrodes, platinum is deposited, usually by borohydride reduction, on a carbon or graphite extender. Electrodes of this type may contain 0.5 to 4 mg. Pt/sq. cm. electrode area and have the same thickness and resistivity characteristics as Type A electrodes. Nickel screens are used for base cells, tantalum screens for acid cells.

Characterization of Electrode Structures

The electrode structures were investigated by electron microscopy and by surface area measurements using electrochemical and adsorption techniques.

Microscopy. Type A electrodes were examined by electron microscopy. In a typical study, material from the surface of an electrode was extracted by the gelatin stripping method. After the stripped gelatin film was vacuum coated with silica and the gelatin removed, the silica layer remaining was a partial replica of the original surface and a medium for entrapping the stripped fragments of material that were originally a part of the electrode surface. Figure 1 shows that the platinum black of the

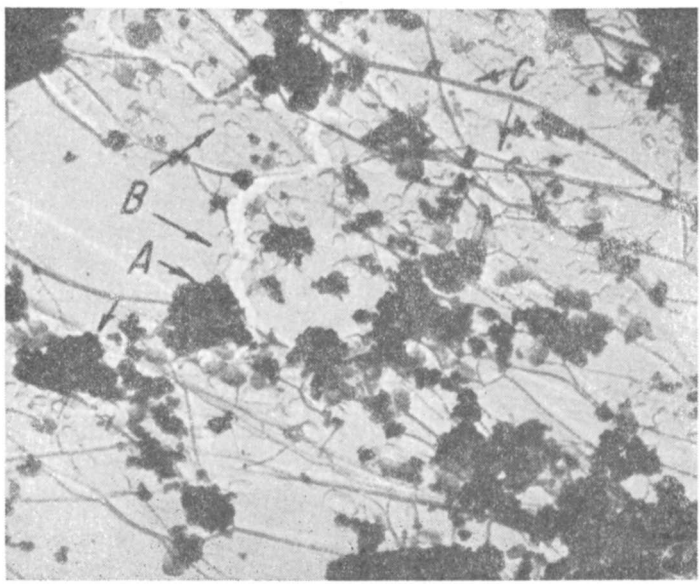

Figure 1. Electronmicrograph (10,000x) of silica replica of surface of Type A electrode showing Pt aggregates at A; Teflon latex particles at B; and Teflon fibrils at C

Publication Date: January 1, 1969 | doi: 10.1021/ba-1965-0047.ch009

electrode was in the form of loosely packed aggregates (*A*) with fibrils (*C*) of Teflon interspersed. These are believed to bind the platinum aggregates together as well as to provide water repellancy. The field also shows the presence of Teflon latex particles (*B*). This study reveals a high degree of dispersion of platinum aggregates and indicates that the Teflon does not occlude or cover any significant fraction of the platinum surface. This conclusion is consistent with surface area measurements.

Surface Area Studies. Surface area studies were made on a typical Type A electrode both by electrochemical and low temperature krypton adsorption measurements (BET method). A galvanostatic oxidation technique was used in the electrochemical measurements (*11*). As shown in Table II, surface area values obtained by the two methods on this electrode are in approximate agreement, indicating that essentially the same platinum surface is available for electrochemical reaction as for gas adsorption. Further, krypton adsorption measurements indicate roughly the same surface area for platinum in the electrode as in the black. Also, the electrochemical surface area of the electrode had not changed after 1200 hours of continuous operation in a fuel cell.

Table II. Surface Area of Type A Electrodes

	Area: Sq. M./Gram Platinum	
	Electro-chemical	*Krypton adsorption*
Initial	33	26
After 1200 hours on test	33	..
Pt black	..	28

Performance of Type A Electrodes

Comprehensive studies were made with the platinum black–metal screen electrodes, since these were found to be capable of sustaining very high current densities at low polarization.

Acid System. Figure 2 shows typical polarization curves for 50-mesh tantalum screen electrodes containing 9 mg. Pt/sq. cm. and 25 wt. % Teflon as used on both sides of hydrogen-oxygen and hydrogen-air cells. Measurements were made at 30° and 70° C. The electrolyte consisted of 5*N* H_2SO_4 in a glass fiber matrix. The polarization curve for hydrogen-oxygen at 30° C. indicates a working potential of about 0.74 volt at 200 ma./sq. cm. and 0.65 volt at 400 ma./sq. cm. Similar curves have been found to be approximately linear to current densities of more than 1000 ma./sq. cm.

As indicated in Figure 2, an increase in temperature of about 40° C. produces a relatively small increase in cell working potential. Thus, at 200 ma./sq. cm. the increase is about 30 mv., most of which can be accounted for by decrease in the internal resistance of the cell, and indicates a rather small effect of temperature on electrode activity.

Publication Date: January 1, 1969 | doi: 10.1021/ba-1965-0047.ch009

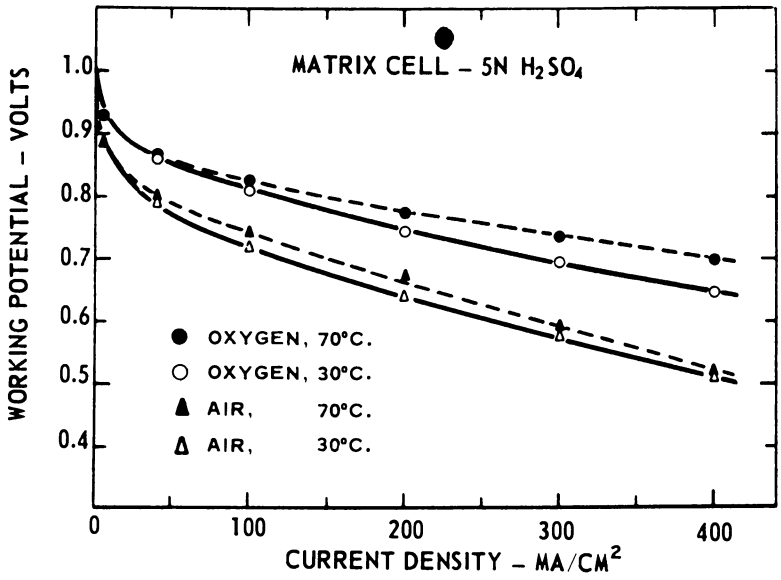

Figure 2. Performance of Type A electrodes—acid system

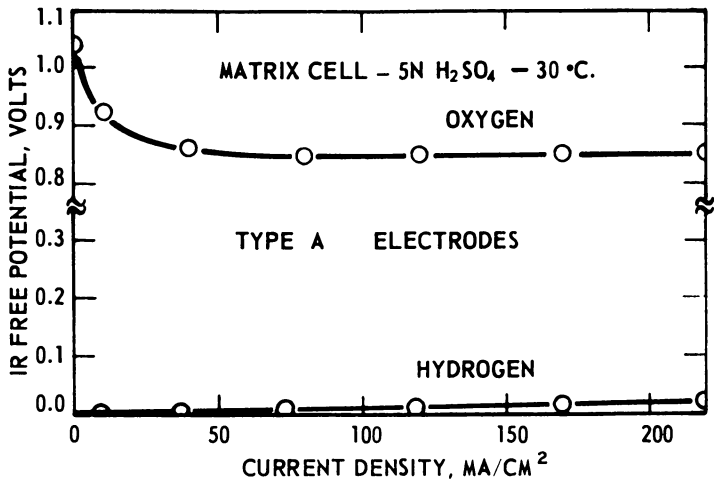

Figure 3. Individual electrode polarization

When the cell is operated on air instead of oxygen, a substantial decrease in working voltage occurs—for example, 100 mv. at 200 ma./sq. cm. Equivalent effects are observed at 30° and 70° C. The voltage decrease conforms roughly to that predicted in the theory of diffusion electrodes as developed by Heath and Sweeney (2) for the effect of partial pressure (P) of reactant gas on current density in a gas diffusion electrode:

Publication Date: January 1, 1969 | doi: 10.1021/ba-1965-0047.ch009

$$\frac{i}{i'} = \left(\frac{P}{P'}\right)^{1/2}$$

For the fivefold reduction in oxygen partial pressure, as occurs in changing from oxygen to air, the current density should be diminished by a factor of about 2.2. This corresponds approximately to our observations. But this rule does not apply as well in the case of the base cells.

Single electrode polarization data were obtained for a typical cell operated at ambient temperature. The electrolyte matrix was extended out of the cell into a reservoir containing acid of the same concentration as in the cell and a reference hydrogen electrode. Measurement of the potential of each of the working electrodes relative to the reference electrode was made using a Kordesch-Marko bridge to eliminate the contribution of internal resistance (7). The results of these measurements are shown in Figure 3. The oxygen electrode polarizes rapidly at low current densities. At current densities greater than 50 ma./sq. cm., the oxygen electrode potential remains nearly constant at about 0.85 volt *vs.* the reference hydrogen electrode. The working hydrogen electrode polarizes approximately linearly to 20 to 30 mv. at 200 ma./sq. cm.

Some indication of life performance has been obtained with these platinum-on-tantalum screen electrodes in the hydrogen-oxygen system at ambient temperature. The electrodes have been operated continuously for over 1000 hours at current densities up to 150 ma./sq. cm. without evidence of deterioration after an initial drop of 30 to 50 mv. over the first 100 hours.

Base System. Extensive studies have been made of platinum black–Teflon mixtures spread on 100-mesh nickel screens. Standard loadings were 9 mg. Pt/sq. cm. and 25 wt. % Teflon. Figure 4 shows initial polarization with hydrogen-oxygen and hydrogen-air for the system consisting of these electrodes with 5*N* KOH in a matrix cell. The hydrogen-oxygen polarization curve indicates a cell working potential of 0.77 volt at 200 ma./sq. cm. at 30° C. This curve is nearly linear to 1000 ma./sq. cm. Thus, these electrodes are capable of sustaining very high electrochemical rates in the alkaline system.

The effect of temperature on performance of the base cell is also indicated in Figure 4. At 200 ma./sq. cm., the working potential at 70° C. is 40 to 50 mv. higher than at 30° C. Again, this improvement in performance may be attributed largely to a decrease in cell internal resistance.

The decrease in cell working potential on substitution of air for oxygen is considerably less than was observed for the acid cells. Thus, at 200 ma./sq. cm., the additional polarization was only 40 to 50 mv. at both 30° and 70° C. At constant potential it is apparent that the ratios of current densities for oxygen *vs.* air are substantially less than the 2.2

Publication Date: January 1, 1969 | doi: 10.1021/ba-1965-0047.ch009

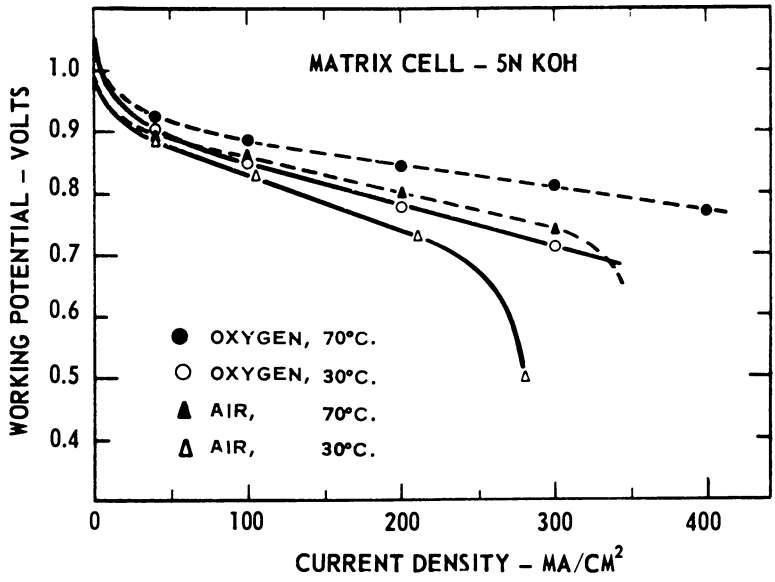

Figure 4. Performance of Type A electrodes–base system

factor previously mentioned. In contrast, Hartner *et al* (5) found that $i \propto P_{O_2}^{1/2}$ for porous cathodes operating in 75 wt. % potassium hydroxide at 200° C. The reasons for these divergent observations and their implications in leading to still better air electrode performance must await further research.

Single electrode polarization data for the base cell are similar to the acid cell and will not be reproduced here. Relative to corresponding measurements in the acid system, polarization was 30 to 40 mv. less at the oxygen electrode and 10 to 20 mv. more at the hydrogen electrode.

Studies of Type B Electrodes

Type B electrodes represent an approach to more effective utilization of catalytic materials. Carbons added to the formulation act as extenders and substrates for the spreading of platinum or other activating ingredient. Excellent control of distribution of catalyst and waterproofing agent is achieved.

Choice of Carbons. As the result of a survey of over 75 carbons, several promising carbons were found with good chemical stability and high catalytic activity when platinized. For these purposes, lower surface area, finely divided graphites or graphitized carbons give superior performance. One such carbon is Cyanamid 99% graphite, which is a by-

Publication Date: January 1, 1969 | doi: 10.1021/ba-1965-0047.ch009

product of the manufacture of calcium cyanamide from calcium carbide. Some properties of this material are given in Table III.

Table III. Properties of Cyanamid 99% Graphite

Purity	99.0 wt. %
Impurities	SiO_2, CaO, Fe_2O_3, Al_2O_3
Particle size	Approx. 0.25 to 2.0 microns
Surface area	11.4 Sq. m./gram
Conductivity[1]	50 Mho/cm.
Bulk density[1]	1.28 Gram/cc.
% Porosity[1]	40%
Structure (x-ray)	Graphitic

[1] Measured at 200 p.s.i.

Publication Date: January 1, 1969 | doi: 10.1021/ba-1965-0047.ch009

This material can be compacted into a rather uniform porous structure having a conductivity characteristic of graphite. Its surface area and pore structure are such that no appreciable amount of catalytic material remains buried in tiny inaccessible pores.

Base System. Electrodes were prepared from platinized Cyanamid 99% graphite by methods analogous to those used for Type A electrodes. Waterproofing level was held at about 15%. Platinum loadings of 1 and 2.5 mg./sq. cm. on appropriate screens were obtained. Electrode thickness was approximately 0.007 inch. Figure 5 shows the performances of these electrodes in the base-type matrix cell. Platinum loadings on each side are indicated in the table in lower part of the graph. It is evident

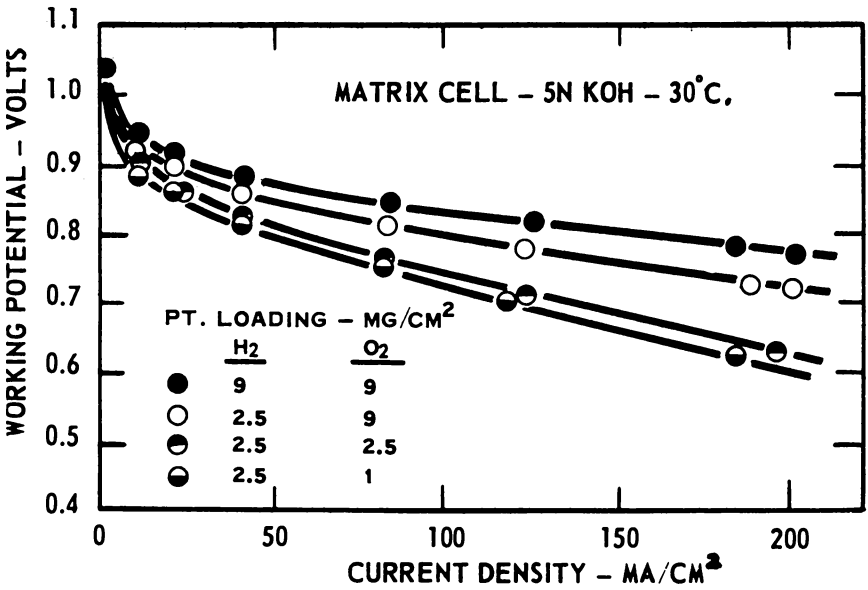

Figure 5. Performance of Type B electrodes–base system

that reduction of platinum loading at either electrode produces some loss in performance. However, even at a total loading of 3.5 mg./sq. cm. for both sides, the loss in cell potential is only about 100 mv. at 100 ma./sq. cm. It is believed that substantial improvement in performance by improved methods of platinization can be achieved.

Discussion

Based on the performance and physical characteristics of Type A and Type B electrodes, we can project that cells constructed with these electrodes will have very desirable weight and volume characteristics. The polarization data in Figures 2 to 5 indicate that for cells operating at 150 amps/sq. ft., power levels of 80 to 120 watts/sq. ft. could be achieved on either oxygen or air. A typical electrolyte matrix with two thin electrodes would have a total thickness of about 0.030 inch and a weight of about 0.3 lb./sq. ft. At 100 watts/sq. ft., total electrode-electrolyte weight would be about 3 lb./kw. If it is assumed that individual cells could be stacked four to the inch, power densities in excess of 3 kw./cu. ft. of battery (exclusive of auxiliaries) should be feasible.

A power density of 100 watts/sq. ft. can probably be achieved in the near future with a platinum usage of about 2 grams/sq. ft. of cell area (including both electrodes). This represents an investment in platinum of about $60/kw. Moreover, the major part of this platinum value can be recovered when the useful life of the battery has ended. Since electrode preparation techniques seem to be amenable to large scale production, eventual total electrode cost will depend primarily on cost of materials. Further, it is anticipated that lower cost catalytic materials can be formulated into effective electrodes of similar structure. In conclusion, it should be pointed out that the use of platinum screen electrodes is not limited to standard fuel cell applications. Type A electrodes have proved useful in gas purification cells (*8*, *9*), electrogenerative hydrogenation cells (*10*) and electrolysis cells.

Publication Date: January 1, 1969 | doi: 10.1021/ba-1965-0047.ch009

Acknowledgment

The authors are indebted to J. S. Mayell who made the electrochemical surface area measurements and to M. C. Botty who performed the electron microscopy.

Literature Cited

(1) Elmore, G. V., and Tanner, H. A., *J. Electrochem. Soc.* **108**, 69 (1961).
(2) "Fuel Cells," W. Mitchell, Jr., ed., pp. 94–98, Academic Press, New York, 1963.
(3) Grubb, W. T., "*Proc. 16th Ann. Power Sources Conf.*," pp. 31–34, (PSC Publications Committee, P.O. Box 891, Red Bank, N. J.).

(4) Grubb, W. T., and Michalske, C. J., *J. Electrochem. Soc.* **111,** 477 (1964).
(5) Hartner, A. J., Vertes, M. A., Medina, V. E., and Oswin, H. G., ADVAN. CHEM. SER. **47,** 141 (1965).
(6) Kirkland, T., and Jasinski, R., *Trans. IEEE Ind. Electr.* **10,** 111 (1963).
(7) Kordesch, K. V., and Marko, A., *J. Electrochem. Soc.* **107,** 480 (1960).
(8) Langer, S. H., and Haldeman, R. G., *J. Phys. Chem.* **68,** 962 (1964).
(9) Langer, S. H., and Haldeman, R. G., *Science* **142,** No. 3589, p. 225 (1963).
(10) Langer, S. H., and Landi, H. P., *J. Am. Chem. Soc.* **86,** 4694 (1964).
(11) Mayell, J. S., and Langer, S. H., *J. Electrochem. Soc.* **111,** 438 (1964).
(12) *"Proc. 16th Ann. Power Sources Conf.,"* Panel discussion on future of fuel cells, pp. 80–104 (PSC Publications Committee, P.O. Box 891, Red Bank, N. J.).

RECEIVED February 17, 1964.

Publication Date: January 1, 1969 | doi: 10.1021/ba-1965-0047.ch009

In Fuel Cell Systems; Young, G., el al.;
Advances in Chemistry; American Chemical Society: Washington, DC, 1969.

10

Current Density and Electrode Structure in Fuel Cells

H. A. LIEBHAFSKY, E. J. CAIRNS, W. T. GRUBB, and L. W. NIEDRACH

General Electric Research Laboratory, Schenectady, N. Y.

Publication Date: January 1, 1969 | doi: 10.1021/ba-1965-0047.ch010

Continued progress on fuel cells requires a better understanding of electrode structure. A survey of pertinent information has contributed to this end, but it has shown that the effect of electrode structure on cell performance will be difficult to isolate even after the badly needed extensive experimental work has been done. We believe that investigations of complete fuel cells will lead most directly to successful fuel batteries. Therefore, data for complete fuel cells are emphasized in this survey.

The effect of electrode structure on the current density obtainable at a given voltage in a fuel cell is second only to that of the electrocatalysts. The two effects are difficult to separate, and their relative importance changes with current density and voltage. As a permissible oversimplification, one may say that the effect of electrode structure on current density is mainly physical. In the fuel cell of Figure 1, the electrode must serve functions that at first sight appear mutually self-exclusive: It must join yet separate the reacting gas and the electrolyte. It must join them that they may react; it must separate them to prevent massive transfer of gas into electrolyte or of electrolyte into gas.

The physical burden imposed upon the electrode varies with the electrolyte and with the gases reacting. For a given electrolyte, the burden is least when access of reactant gas is unhindered by the presence of other substances, as in the favorable case in which hydrogen or oxygen reacts, and water is easily rejected as liquid. The burden increases when the oxygen must be taken from air or when hydrazine is oxidized with the formation of nitrogen. Because intermediate compounds may form, the burden can be even greater when hydrocarbons are oxidized.

The relationship between electrode structure and current density can be approached via simple models and via electrode kinetics. The models aid in the understanding of transport processes, and the kinetic studies

In Fuel Cell Systems; Young, G., el al.;
Advances in Chemistry; American Chemical Society: Washington, DC, 1969.

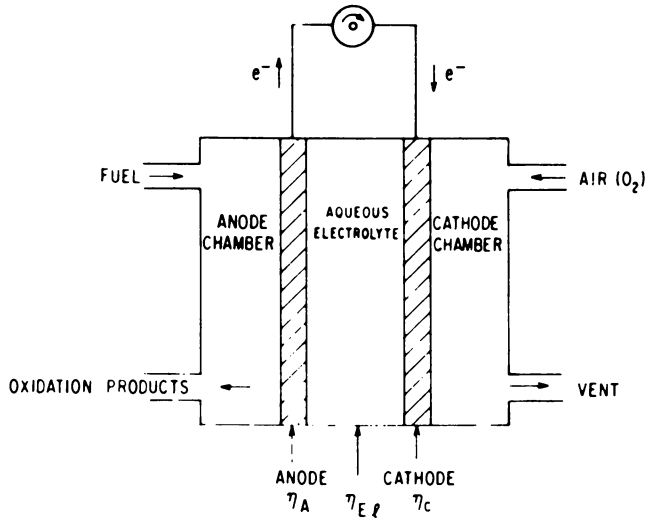

Figure 1. Schematic diagram of type of fuel cell considered

Electrodes are envisaged as permeable to some degree by the gases and the free electrolyte. Electrodes relying on hydrogen diffusion through a solid—for example Pd-Ag alloys—are thus excluded

are important because the current density is the rate of the over-all electrode reaction per unit area, expressed in electrical units; for a unidirectional reaction

$$\text{Current density} = k(A)(B), \text{ etc. } e^{-\frac{(Q - k'\epsilon)}{RT}} \quad (1)$$

where (A) (B), etc. are related to the concentrations of species involved in the rate-determining step; Q = an energy of activation; ϵ = a voltage term that increases with current density; and k' = a multiplicative constant analogous to NF in the thermodynamic relation $\Delta G = -NFE$. Because fuel-cell electrodes are complex, and the processes occurring there are not well understood, models and mechanisms are mainly of qualitative use.

To be satisfactory, a fuel cell must be acceptable in at least these four respects:

1. Current density—voltage relationship
2. Stoichiometry
3. Reaction per pass
4. Life

The electrodes in a satisfactory cell must have a structure that meets this severe set of requirements, and the electrodes in addition should have a fifth property—versatility—by which we mean, for example, that the cathode should operate satisfactorily on both oxygen and air and that

Publication Date: January 1, 1969 | doi: 10.1021/ba-1965-0047.ch010

the anode should operate satisfactorily on a number of fuels, some of which might be liquid.

A satisfactory current density–voltage relationship means low overvoltage, and it is well known that the overvoltage,

$$\eta = E_r - E_a \tag{2}$$

increases with current density. (E_r = the reversible electromotive force; E_a = the actual cell voltage as measured at the terminals.) Equation 1 is limited in usefulness because it is difficult to tell what part of η belongs in this equation and because it is difficult to formulate the process that gives rise to ϵ.

Yet, it is advisable to use overvoltage in the study of electrode structure. The usual procedure in attempting to understand overvoltage is to subdivide it according to processes. We propose for the complete fuel cell that η be subdivided initially according to location as follows:

$$\eta = \eta_A + \eta_C + \eta_{El} \tag{3}$$

where the subscripts, in order, mean anode, cathode, and electrolyte. Once the overvoltage (η) at a given current density (i) is known, appropriate measurements with Luggin capillaries give η_A and η_C, thus establishing η_{El} by difference. More than one measurement may be needed for an electrode because electrodes are not always uniform; also, the overvoltage and its components will vary with current density.

To make Equation 3 more useful in the study of electrode structure, it is advisable to establish what fraction of each component of η is attributable to resistive losses. (The most important of these resistive losses will occur in the electrolyte, but there will be contributions from metallic conductors and from films on the electrodes. For simplicity's sake, the resistance of metallic conductors will be assumed negligible and solid films will be assumed absent.) By using interrupter techniques on the complete cell and on the Luggin capillary circuit for each electrode, one should be able to obtain η'_{El} by difference from the equation

$$\eta' = \eta'_A + \eta'_C + \eta'_{El} \tag{4}$$

where the singly primed values are the overvoltages of Equation 3 less the electrolyte resistances as eliminated by the interrupter. The individual resistance terms are then obtained by difference—for example, $\eta_A - \eta'_A$ gives the electrolyte resistance in the anode. If η'_{El} exceeds zero, concentration gradients are to be looked for in the bulk electrolyte.

It is advisable further to establish the effect of changing gas composition on overvoltage (and hence on current density). This can be done as follows for the anode chamber as example:

Establish η'_A (Equation 4) for one set of conditions—say, pure fuel gas at 1 atmosphere total pressure. At this total pressure, change condi-

Publication Date: January 1, 1969 | doi: 10.1021/ba-1965-0047.ch010

tions in the anode chamber by using an inert diluent to reduce the partial pressure of fuel gas to 0.1 atmosphere. Then obtain η''_A (analogous to η'_A) for the changed conditions. Comparison of η'_A and η''_A gives the information sought.

Instead of comparing overvoltages for a fixed current density, one may wish to compare current densities at a fixed value of a particular overvoltage; this can be done if the data available permit interpolation.

The difficulty of using Equation 1 to interpret the processes in a working fuel cell is clear from Figure 2, in which the effect of temperature on current density is shown at fixed values of η' for several carbonaceous fuel cells. Equation 1 obviously cannot be the rate law that

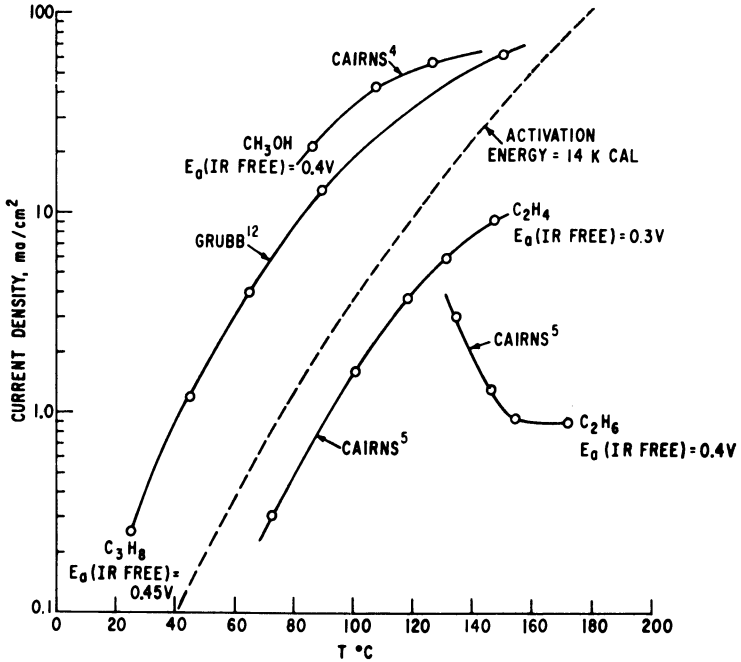

Figure 2. Unpublished performance data for fuel cells with carbonaceous fuels, illustrating complexity of temperature coefficients

Fuels and electrolytes: methanol and cesium carbonate solution (4); propane and concentrated phosphoric acid (12); ethane and ethylene, each with cesium carbonate solution (5)

governs the current density in working fuel cells under all conditions. To realize why this is true, we need only remember that the step most important in determining current density in such cells may be physical, not electrochemical, and that the relative importance of any step may change with current density.

Publication Date: January 1, 1969 | doi: 10.1021/ba-1965-0047.ch010

In this situation, it becomes advisable to investigate simpler rate laws such as

$$\text{Current density} = f[(M)(N) \ldots] \tag{5}$$

the study being made at fixed, appropriate values of overvoltage, temperature, and of the bulk concentrations (M) and (N)—for example, (M) and (N) could be pressures of reacting gases. In this study, the subdivision of overvoltage into its components, as outlined previously, would prove helpful; in particular, values of η' and η'' could be used to test the validity of the simple relation (a special case of Equation 5):

$$\text{Limiting current density} = k_1(P) \tag{6}$$

where P is the partial pressure of the gas reacting at an electrode.

Publication Date: January 1, 1969 | doi: 10.1021/ba-1965-0047.ch010

Importance of Electrolyte Films On the Electrode

While it has long been realized that too much electrolyte on or in a porous electrode will decrease current density by "drowning" the electrode, the idea that a film of electrolyte can actually increase current density, though not new, is only now gaining wide acceptance.

In 1842, Grove (*10*) said of his fuel cell: "As the chemical or catalytic action . . . . . could only be supposed to take place with ordinary platina foil, at the line or watermark where the liquid, gas, and platina met, the chief difficulty was to obtain anything like a notable surface of action." The "line" later came to be called the three-phase boundary. The contrast of line with surface is provocative.

Grove found that:

It was desirable to increase electrode surface by electrodepositing platinum.

Submerged electrodes were inactive.

Partially exposed electrodes were active.

Washing exposed portions of electrodes restored activity that had decreased.

Mond and Langer (*16*), relying heavily upon Grove, said that they needed to keep their platinum black "comparatively dry" to obtain active electrodes. Accordingly, they used their electrolyte "in a quasisolid form, viz., soaked up by a porous nonconducting material, in a similar way as has been done in the so-called dry piles and batteries."

Schmid (*20*), who deserves major credit for what are commonly called "gas-diffusion" electrodes, first sought to increase the current from a hydrogen anode by mechanically pulsating the electrolyte (Grove's "washing") to achieve rapidly alternating exposures of electrode area to electrolyte and to hydrogen. Unsatisfied, he proceeded to his "funda-

mental experiment," which consisted in measuring the current at a hydrogen anode as a function of electrode area exposed to the gas. The current increased to a limiting value as this exposed area increased. Schmid learned subsequently that this result had been obtained in about 1909 by Nobis (*19*), who seems not to have appreciated its full significance. Nobis' results (Table I) were almost identical with Schmid's, who (in contrast to Nobis) did not bubble hydrogen through the electrolyte. Schmid recognized that an electrode could carry a film of electrolyte, but he thought such a film would reduce performance by preventing intimate contact of hydrogen with the electrode.

Table 1. Increase of Current With Increased Exposed Electrode Area (*19*)

Width of exposed area, mm.	*Current, ma.*
3.0	10
2.0	10
1.5	9
1.0	7
0.5	3

In 1957, Wagner (*21*) said of an oxygen cathode:

Since reactants and reaction products occur in three different phases, a reaction at the three-phase boundary gas-electrode-electrolyte may be anticipated. The number of sites along a three-phase boundary . . . . is in general very much smaller than the number of sites along the two-phase boundary electrode-electrolyte. Consequently, one may anticipate that the cathodic process takes place by virtue of the following steps, viz., (1) dissolution of oxygen molecules in the electrolyte at the gas-electrolyte interface, (2) diffusion of oxygen molecules in the electrolyte from the gas-electrolyte interface to the electrode-electrolyte interface, (3) cathodic reduction involving dissolved oxygen molecules and electrons as reactants and oxygen ions as reaction products at the electrode-electrolyte interface.

This quotation shows clearly that a three-phase boundary on an electrode is unlikely to be the important seat of reaction and that a film of electrolyte on the electrode can lead to increased current. The results of Nobis (Table I) and of Schmid fit into the picture sketched by Wagner, if one assumes the presence on the exposed portion of the electrode of an electrolyte film limited in effective extent to a fixed distance above the electrolyte level and that current density in such experiments would then increase with exposed electrode area only so long as there was a concomitant increase in the effective area of electrolyte film.

Weber, Meissner, and Sama (*22*) also measured total current on an electrode positioned at various heights (h) above the level of the undisturbed electrolyte. Their electrode was a copper cathode, and the reacting gas was oxygen. With increasing values of h, the total current increased to a maximum value I_{max}, which was reached at the largest value of h for which the emerged part of the electrode was still covered by the

Publication Date: January 1, 1969 | doi: 10.1021/ba-1965-0047.ch010

electrolyte meniscus. At comparable meniscus heights for this emerged part when completely wetted, the current for a nickel cathode or a silver cathode was the same as that for a copper cathode; this points to the diffusion of oxygen through the electrolyte (20% potassium hydroxide) as the rate-determining step.

Recently, Will (*23*) measured the total current (I) from a hydrogen anode (the outer lateral surface of a platinum tube 1.2 cm. long and 0.635 cm. in diameter) as a function of l_1, the height of the upper edge of the anode above the top of the undisturbed electrolyte. The anode was driven by an impressed voltage of 0.4 volt. In two experiments, he obtained the results in Figure 3. The salient features of the curves are:

1. The low residual currents, independent of l_1 below $l_1 = 0.13$ cm., which are due to the diffusion-limited oxidation of hydrogen on the submerged portion of the anode (*23*). This residual current is about twice as great in 1*N* as in 8*N* sulfuric acid, because hydrogen at a given pressure diffuses more rapidly through the dilute electrolyte (*23*).

2. Beyond $l_1 = 0.13$ cm., the current increases rapidly to I_{max} near $l_1 = 0.26$ cm. For our purposes, $\Delta I/\Delta l_1$ is considered constant over this range of l_1. The average current density calculated from I_{max} is about 30 ma. /sq. cm. for the emerged part of the anode.

3. For 8*N* sulfuric acid I_{max} is 1.25 as great as for 1*N* sulfuric acid.

4. The gradual decrease in I beyond I_{max} is caused by a decrease in residual current owing to decrease of submerged anode area (*23*).

The significance of Will's results rests on the assumption that I_{max} is reached because the rate of the electrochemical reaction is limited by the rate of diffusion of hydrogen through the electrolyte film. Investigations are necessary to find out whether the limiting currents (i_L) observed in fuel cells are due to this cause. One way of doing this is by varying the pressure of reacting gas at different current densities (Equation 4).

Experiments like those of Will are significant for the fuel cell because they show that the electrolyte films exist, and they provide data for estimating their maximum thickness. The diffusion of hydrogen through a static film of 8*N* sulfuric acid cannot support a current density of 30 ma./sq. cm. if the length of the diffusion path greatly exceeds 1 micron (10^{-4} cm.). For this calculation, $i_L = N\ F\ D\ C_o/\delta$ or, numerically, $i_L = 3.044 \times 10^{-3}\ (1/\delta\ (\text{cm.}))\ (\text{ma./sq. cm.})$ for H_2 in 8*N* H_2SO_4 at 25° C. For $\delta = 1 \times 10^{-4}$ cm., $i_L = 30.44$ ma./sq. cm. The desirability of varying the gas pressure in investigations such as these is also evident, for this is the most convincing way to prove that the rate-determining step is the diffusion of the gas as a molecule (Equation 6). It seems that diffusion through visible portions of the meniscus cannot contribute greatly to the current.

The (approximate) constancy of $\Delta I/\Delta l_1$ can be reconciled with hydrogen diffusion through an electrolyte film as the rate-determining step if

Publication Date: January 1, 1969 | doi: 10.1021/ba-1965-0047.ch010

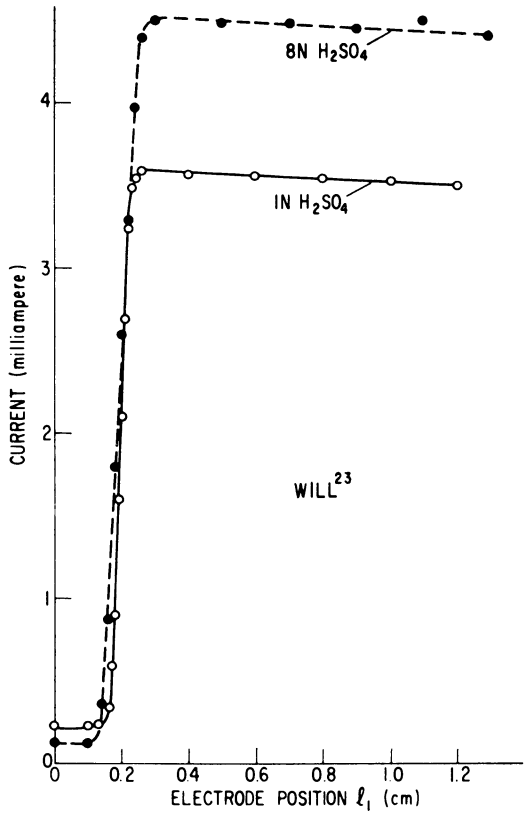

Figure 3. Experiments (23) to show total current at a cylindrical platinum anode immersed ($l_1 = 0$) and at various positions with emergent height shown on abcissa

Note abrupt transition to region of maximum current. Intercept on ordinate represents current due to hydrogen dissolved in electrolyte. Rapid rise in current was attributed mainly to formation of a thin film of electrolyte on emergent portion. Slight decrease in maximum current results from a decrease in immersed area

one assumes that, for each increment of l_1, the area covered by film stands in constant ratio to the area covered by meniscus.

In Figure 3, there is an abrupt change of slope in the region of I_{max}. This behavior can be interpreted as follows: In Equation 3, η_A contains a resistive component that acts vertically along the film (23) so that we may write

$$0.4 = \eta = \eta_A + \text{const.} \tag{7}$$

$$\eta_A \epsilon + \eta_{IR(film)} + \text{const. (see Equation 1)} \tag{8}$$

Publication Date: January 1, 1969 | doi: 10.1021/ba-1965-0047.ch010

The resistive component in Equation 8 increases with the area of electrolytically active film on an anode like Will's. When it has increased so far that η_A can no longer supply ϵ to drive the anodic reaction, this reaction ceases. Because ϵ is small—say, 0.01 volt or so (*23*)—a small increase in $\eta_{IR(film)}$ (a small change in l_1) suffices to bring this about—hence the abrupt change of slope.

If all this is true, increased electrolyte conductivity should increase I_{max}. Obviously it does but by more than Figure 3 indicates. If the reduced diffusion rate of hydrogen (see the residual currents) in 8*N* sulfuric acid is taken into account, the estimated increase is $2 \times 1.25 = 2.50$, which compares favorably with 4, this being the ratio of conductivities for 8*N* and 1*N* sulfuric acid (*23*).

Will found that I_{max} increased with the roughness of the electrode and that only rough electrodes gave true steady-state values of I. Experiments by Bikerman (*2*) are important in this connection:

Stainless steel plates of six standard finishes were coated with oil and suspended vertically. The amount of oil remaining on a plate was measured after suitable time intervals by weighing the plate on an analytical balance. The relation between this amount and the average height (h_{rms}) of surface hills, as determined by two commercial stylus instruments, was ascertained; at a first approximation, the liquid drained at such a rate as if a layer, h_{rms} thick and adjacent to the solid, did not participate in the flow.

The values of h_{rms} ranged from 0.2 micron to between 3 and 4 microns; the thickness of the immobile layer from 0.26 micron to about the same upper limit; the correlation is surprisingly good. Because h_{rms} increases with roughness, we assume that the thickness of the electrolyte film on Will's rough electrodes did also. If it did, the net effect on I is not easily predictable; the electrochemically active area would increase because of the roughness, and the mean diffusion path for hydrogen might be shortened, even though a thicker electrolyte layer on a smooth surface implies a longer path.

All of these investigations point to the importance of films on completely wetted fuel cell electrodes. Temperature and electrolyte concentrations within these films will not be uniform, and films on anodes will differ from films on cathodes. The local potential gradient may well influence the thickness of the films. Lack of uniformity will contribute to the dynamic character of the electrode, and because of this dynamic character, it would be difficult to apply to the fuel cell information obtained from model electrodes.

The two-phase boundary between the films and the electrode appears to be Grove's "notable surface of action," and a good electrode structure would seem to be one that provides a large area of electrolytically active two-phase boundary. Other things being equal (which they seldom are), this effective area increases with the conductivity of the electrolyte.

Publication Date: January 1, 1969 | doi: 10.1021/ba-1965-0047.ch010

The case for electrolyte films on completely wetted electrodes seems conclusive. But there are important electrodes that are not completely wetted; on different areas of these, the contact angles with the electrolyte can have values ranging from zero to about 100°. Such electrodes either contain nonmetallic components—for example, Teflon—or they have been made electrolyte-repellent by surface treatment: In either case the electrode and electrolyte are kept separate by controlled wetting. Even so, the existence of effective electrolyte films is a highly plausible working hypothesis.

High current density per unit of geometric area would seem to require a large effective area of electrolyte film. A completely hydrophobic static electrode cannot provide the film that is needed. The current density for geometric area would increase at such an electrode with (1) the length of three-phase boundary and (2) the effective area of contact between electrode and electrolyte in bulk. Both of these usually increase with the amount of actual electrode surface—that is, with electrode porosity and electrode thickness. But porosity and thickness cannot be increased indefinitely without undesirable consequences. To mention only the consequence immediately important here, increase of porosity and of thickness must eventually lead to diffusion barriers when an inert gas is present —for example, nitrogen in an air cathode or carbon dioxide produced at a hydrocarbon anode. When gaseous diffusion is rate-determining, Equation 6 can be expected under the simplest conditions to take the form

$$\text{Limiting current density} = k_2(P)/(P_T) \qquad (6a)$$

where P (as in Equation 6) is the partial pressure of the gas reacting at the electrode, and P_T is the total pressure. The limiting current density will be reduced by the presence of the diffusion barrier, and k_2 should be most nearly constant when $P_T >> P$.

Of course, no one attempts to make a completely hydrophobic fuel cell electrode. Instead, the aim is to obtain controlled wetting—that is, contact angles low enough toward the electrolyte side to provide the effective film area needed for respectable current densities. If, as seems reasonable, the electrode is dynamic, transient film formation will occur, and this will also promote the diffusion of reacting gas.

The aim of controlled wetting is to keep bulk gas and electrolyte separate while permitting gas and electrolyte to join for reaction (9). To understand how this is done in a working fuel cell, one must remember that fuel cell electrodes contain pores of many sizes and orientations and that they are more highly dynamic systems than the simpler electrodes used in these investigations. Even though different kinds of areas are involved, the 30 ma./sq. cm. obtained on a vertical platinum anode by Will can be used as a rough bench mark to assess the effectiveness of the more complex electrode structures. Thus, the highest current densities

Publication Date: January 1, 1969 | doi: 10.1021/ba-1965-0047.ch010

obtained on fuel cell electrodes at room temperature approach 1000 ma./sq. cm. The formation of electrolyte films will be less influenced by gravity in an electrode with pores of all orientations (including the horizontal) than for the vertical electrodes of the simple experiments. This fact and the increased opportunities for movement of electrolyte and for evaporation and condensation caused by thermal gradients and convection currents will contribute to make the fuel cell electrode a dynamic system and to producing the "washing action" that Grove found desirable.

The three-phase boundary is no longer a useful concept. Maximizing the three-phase boundary, the surface, or the micropore volume may lead to improved electrode structures, but that does not establish any of them as the significant parameter in the operation of the electrode. Also, if diffusion of a gas through an electrolyte film is likely to be important for all fuel-cell electrodes when reactions at the electrode-electrolyte interface are rapid, is it not advisable to use "gas diffusion electrode" as a name for all such electrodes instead of restricting it to gas electrodes of some particular kind?

The aqueous film that seems to exist on electrodes of ion exchange membrane cells may differ from the films described here. Figure 4 shows the results of experiments by Christianson and Hovious (*6*), in which each electrode faced a surface ΔT degrees below electrode temperature and water distilled from electrode to surface during cell operation. They found that current density at fixed cell-voltage passed through a maximum

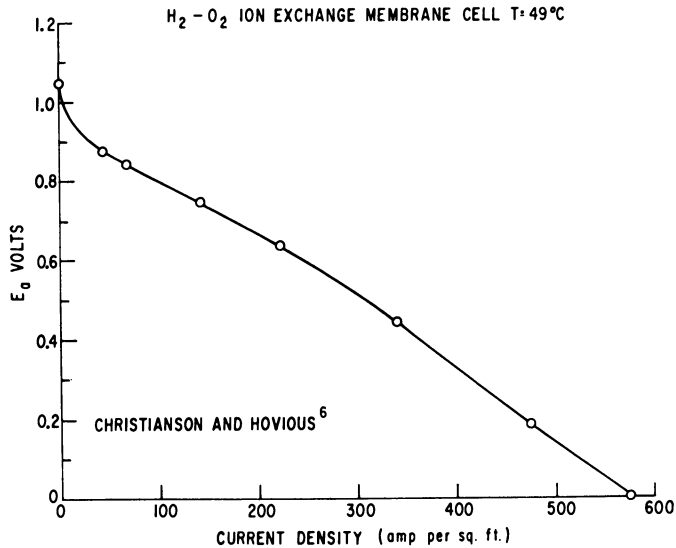

Figure 4. Current density–voltage curve (6) for ion exchange membrane fuel cell operated to optimize film formation. Note high current density at short-circuit

Publication Date: January 1, 1969 | doi: 10.1021/ba-1965-0047.ch010

as ΔT (and the rate of distillation) increased. Figure 4 shows such maximum current densities, all obtained by keeping ΔT at optimum values maintained through a servolink between ΔT and the current density.

The current density maximum exists because the electrode is at optimum water content. Too much water gives an aqueous film that hinders diffusion; too little water could have several effects. Perhaps too little water reduces the film area needed for high current density, but this explanation must be tentative because not enough is known about the interface between the electrode and the ion exchange membrane. The large absolute value (near 600 amp/sq. ft.) of the maximum current density in Figure 4 is a record for this kind of fuel cell.

Publication Date: January 1, 1969 | doi: 10.1021/ba-1965-0047.ch010

Electrode Structure, Current Density, and Overvoltage

The problem of using overvoltage to assess the effect of electrode structure on current density for the complete fuel cell cannot be satisfactorily solved because we do not know how to subdivide η. What follows is merely a beginning.

Guided by electrochemistry, we write

$$E_a = E_r - a \log i - bi + c \log \left(\frac{i_L - i}{i_L} \right) - d = E_r - \eta \qquad (9)$$

or,

$$\eta = a \log i + bi - c \log \left(\frac{i_L - i}{i_L} \right) + d \qquad (9a)$$

as a semi-empirical approximation to the general relationship in a complete fuel cell between current density (i) and E_a (or η) at current densities high enough to make the reverse reaction negligible.

The new symbols in Equation 9 and their reasonable values for hydrogen-oxygen cells are:

a = the Tafel slope, 2.3 $RT/\alpha NF$, usually in the range 0.03 to 0.12 volt for 298° K.
b = internal resistance, about 3×10^{-4} k.-ohm/sq. cm. for a cell of 3 mm. electrode spacing and 1 ohm-cm. electrolyte. (Resistance of metallic conductors assumed negligible.)
c = a thermodynamic proportionality constant, ideally 2.3 RT/NF.
d = the difference between E_r and E_a at unit current density taken as about 0.2 volt at 1 ma./sq. cm.

Further,

$$1.\ bi = \eta - \eta' = (\eta_A - \eta'_A) + (\eta_C - \eta'_C) + (\eta_{El} - \eta'_{El}) \text{ (See Equations 3 and 4)} \qquad (10)$$

2. For a given electrode reaction, i_L is the limiting current density—that is, the maximum current density obtainable in a given set of conditions no matter how much η is increased—even if η is made to exceed E_r in absolute value by imposing an external voltage source. Such limiting currents in fuel cells are often due to the slowness of one or more concurrent mass transport processes such as the diffusion of a reactant gas through the electrolyte film on an electrode, the diffusion of gas through gas, or the transport of an ion or molecule (especially water) of the electrolyte on, within, or outside an electrode.

3. Because Equation 9 applies only when the reverse reaction is negligible at each electrode, it was convenient to take

$$d = E_r - E_a \approx \eta \text{ at } i = 1 \text{ ma./sq. cm.} \tag{11}$$

The curve C in Figure 5 represents Equation 9 with a, b, c, and d having these values.

To facilitate comparison with experiment, Equation 9 is differentiated:

$$-\frac{dE_a}{di} = +\frac{d\eta}{di} = \underset{\text{I}}{+\frac{a}{2.303i}} + \underset{\text{II}}{b} + \underset{\text{III}}{\frac{c}{2.303\,(i_L - i)}} \tag{12}$$

where the Roman numerals define Regions I, II, and III for the current density-voltage curve defined by Equation 9.

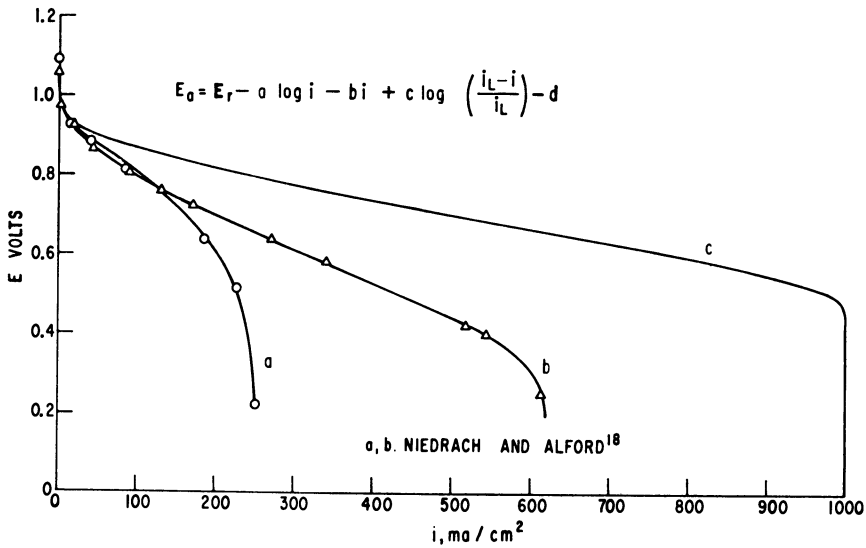

Figure 5. Simplified analysis of current density–voltage data according to method in text

Curve c is an idealized case. Curves a and b show that method adequately represents results for hydrogen-air cells (Table II)

Publication Date: January 1, 1969 | doi: 10.1021/ba-1965-0047.ch010

The overvoltage is the intensity factor in the energy terms required to overcome the various kinds of irreversibility. The rate at which the required overvoltage must be increased to increase current density is different in each region:

In Region I, the rate is inversely proportional to i.
In Region II, the rate is independent of i.
In Region III, as i approaches i_L, the rate increases very rapidly, which means that a situation is being approached in which increasing η can produce no further increase in i.

General experience with fuel cells justifies the following generalizations about the three regions.

At low current densities, the first (or Tafel) term predominates, and this defines Region I. Here electrode structure helps to determine current density because it governs the size of the effective electrode area, but the characteristics of the electrochemical reaction are of overriding importance. The current density in Region I is usually below the useful range in a working fuel cell.

In Region II, where the voltage–current density curve is linear, the effect of internal resistance is overriding. This effect (see Equation 10) derives from the bulk electrolyte and the electrodes. Within the electrodes, it results from the resistance of retained bulk electrolyte and of electrolyte films. A good electrode structure will not contribute materially to b in Equation 12. (Solid films, if present on the electrode, could make such a contribution.)

It is clear from Equations 9 and 12 that Region III will terminate steeply at i_L as i approaches i_L. Electrode structure will have a pronounced effect on i_L, which therefore qualifies as a figure of merit for assessing electrodes. For electrodes of equal activity, the higher i_L, the better the structure. For curve C of Figure 5, $i_L = 1000$ ma./sq. cm. (1 amp./sq. cm.), a reasonable value at room temperature and pressure, has been assumed.

To summarize: The current density–voltage curve has been divided into three regions according to the rate at which current density increases with increasing overvoltage. In each region the process deserving major emphasis is the one that requires the largest increment of overvoltage to maintain the desired steady-state operation of the fuel cell.

Electrode structure influences current density differently in the three regions. In Region I, this influence results because electrode structure determines the area effective for electrode reaction; in Region II, because electrode structure can affect IR; in Region III, because electrode structure can affect the rate of a mass transport process that eventually determines i_L.

If electrolyte films on electrodes are important, then rate laws such

Publication Date: January 1, 1969 | doi: 10.1021/ba-1965-0047.ch010

as Equations 5 and 6, which emphasize the importance of mass transport, need extensive investigation.

Interpretation of Cell Data

Let us see how far the ideas presented here can be used to interpret current density–voltage data for complete cells. Because the data in the literature are incomplete, the interpretations cannot be definitive, but they do suggest where further work is needed.

Figure 6 shows data that cannot be interpreted in terms of Equation 9 because the cells are unstable—that is, they do not reach true steady states at the higher current densities—and the dotted lines pointing to the origin are meant to show that E_a and i both decrease with time. Furthermore, the current densities are very low, the highest being only 4 ma./sq. cm. All these data lie well within Region I, and anodic reactivity appears to be limited by low temperature and not primarily by electrode structure. Indeed, similar behavior has been observed with propane-oxygen in ion-exchange membrane cells (*1, 7*).

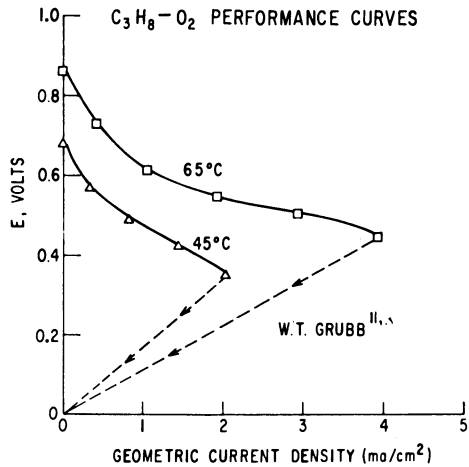

Figure 6. Early current density–voltage curves too unstable for analysis

Sulfuric acid electrolyte [11]

Figure 7 contains data calculated from results presented by Kordesch (*14*) in 1959 for carbon electrodes. Clearly, Equation 6 holds, and it holds also in more recent work by Clark (*7*). Under the simplest possible conditions, such results might mean that diffusion of molecular oxygen through an electrolyte film is rate-determining. Because the simplest conditions do not obtain, further work is necessary before valid conclusions can be drawn.

Publication Date: January 1, 1969 | doi: 10.1021/ba-1965-0047.ch010

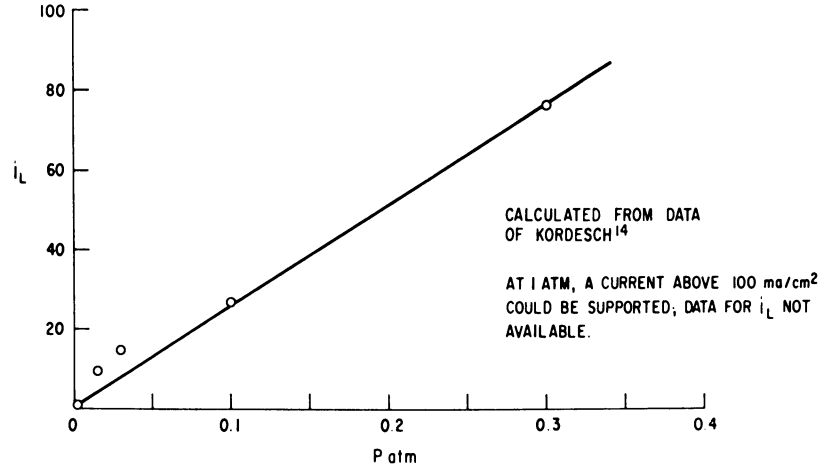

Figure 7. Limiting current densities (14) calculated from measurements on an oxygen cathode of carbon

Clark's way of obtaining i_L also differs from ours, but this difference may be ignored. His highest value—i_L = 2000 ma./sq. cm. for oxygen at 1 atm.—is noteworthy both because it is so high and because it still lies on the line conforming to Equation 6. Another noteworthy result is that an unwetproofed electrode gave i_L lower by some 20% than a wetproofed one, but this leads to no quantitative conclusions because different electrodes were used. The difficulty of forming extensive electrolyte films on incompletely wet electrodes leads us to believe that the dynamic character of the carbon electrodes must be important in making the high i_L values possible.

Figure 8 contains results for the oxygen and air operation of hydrogen fuel cells with Shell Oil Co. electrodes.

As is well known, these electrodes are usually prepared by reinforcing a metal layer evaporated onto a Porvic membrane. During operation, the metal faces the gas chamber (Figure 1). The metal layer is no doubt rough and partially penetrates the pores. The electrolyte, which gains access to the metal through the pores, thus has every chance to form effective electrolyte films on the metal. The electrode structure is versatile in that it can serve for the anode with a fuel dissolved in the electrolyte of a cell the cathode of which has a similar structure and reduces gaseous oxygen, both electrodes being carried by the same Porvic membrane.

The data in Figure 8 do not extend to high enough current densities for the application of Equation 9. They show d to be 0.23 volt—a reasonable value for a hydrogen-oxygen cell. Limiting current densities cannot be computed. At the same η (or E_a), current densities are lower

Publication Date: January 1, 1969 | doi: 10.1021/ba-1965-0047.ch010

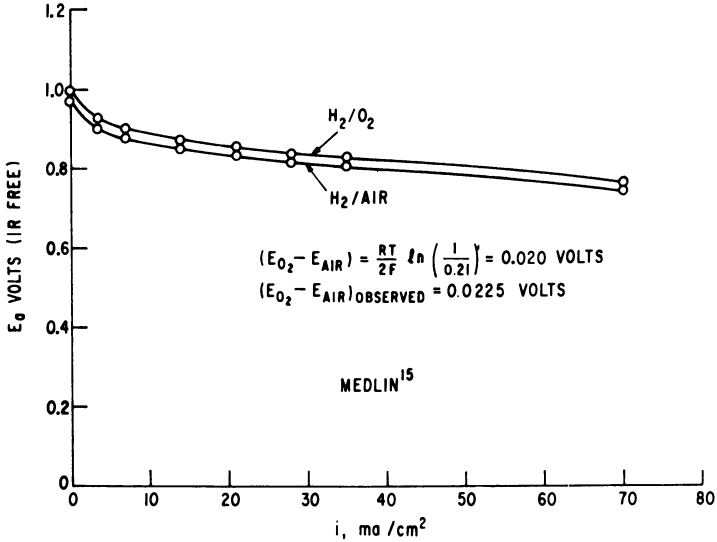

Figure 8. Current density–voltage curves obtained at Thorton Research Centre, Shell Ltd.

Difference between curves for air and oxygen was interpreted as agreeing with two-electron mechanism for cathodic reaction

for air than for oxygen, but they are clearly not proportional to oxygen pressure. This means that we cannot assume diffusion of oxygen through the electrolyte film to be rate-determining. Instead, we shall assume that the difference between the oxygen and the air curve is due to a displacement of the electrochemical equilibrium (*8*)

$$2e^- + O_2 + H_2O \rightleftharpoons HO_2^- + OH^- \qquad (13)$$

The resulting calculated change in cell voltage is given in Figure 8, and it is in excellent agreement with the change observed, which is virtually constant for the entire range of current densities. That this interpretation should hold at $i = 0$ is not so surprising; after all, the value $E_r = 1.23$ volts for the hydrogen-oxygen electrode is never reached in hydrogen fuel cells. But what is surprising is that the interpretation should be valid for current densities above 100 ma./sq. cm., as the authors cited have concluded it is. After all, the electrons participate in Reaction 13, and they are being rapidly withdrawn at these current densities. Note, however, that the calculation we have made involves only the oxygen pressure—not all the substances in the electrochemical equilibrium. We might therefore have a situation in which the chemical potential of the electrons is identical for oxygen and for air at the same current density, while that of HO_2^- remains nearly the same because there is no change in the rate of the reaction

Publication Date: January 1, 1969 | doi: 10.1021/ba-1965-0047.ch010

$$HO_2^- = OH^- + {}^1/_2\,O_2 \qquad (14)$$

by which it is removed. In that case, the only difference between the two curves would be in the chemical potential of oxygen, which, being lower in air, gives rise to the calculated change in E_a.

We proceed now to the analysis of current density–voltage curves in terms of Equation 9 or 9a. This analysis rests on the assumption that the curves can be divided into three regions defined by Equation 9, and it makes use of the four adjustable parameters *a*, *b*, *c*, and *d*, assumed to be constant for the entire curve, which is an assumption not likely to be realized. There is no doubt that any current density–voltage curve likely to be found can be fitted with four adjustable parameters at one's disposal.

Nevertheless, the fitting was done for six cases, region by region, and Equation 9a with the parameters in Table II does represent the experimental curves satisfactorily—that is, within a few hundredths of a volt over the range of current densities. Attempts at closer fitting are not justified; for one thing, the experimental data at high current densities are uncertain owing to the difficulty of maintaining well-defined experimental conditions.

Table II. Parameters for Equation 9a

	Cell	*a*, volts	*b*, k.-ohm/sq. cm.[b]	*c*, volts	i_L, ma./sq. cm.	*d*, volts	See Figure No.
1.	H_2–air (model)	0.05	3.0×10^{-4}	0.0296	1000	0.23[f]	5
2.	H_2–air (*18*)	0.031	5.9×10^{-4}	0.285	255	0.24	5
3.	H_2–air (*18*)	0.102	5.7×10^{-4}	0.088	620	0.16	5, 10
4.	CH_3OH–O_2 (*4*)	0.345	4.8×10^{-3}	0.076	403[g]	0.20	13
5.	C_3H_8–O_2 (*13*)	0.161	1.5×10^{-3}	...	[g]	0.35	13
6[a].	H_2–O_2 (*7*)	0.126	1.6×10^{-4}	[d]	[d]	0.07	9
7[a].	Zn–O_2 (*7*)	0.122	[c]	0.175	1211	...	11

[a] In applying Equation 9a, insert 0.1 *i* for No. 6 and 7.
[b] The units are kilo-ohms as an offset to milliamperes/sq. cm.
[c] Data for estimation of b are not available.
[d] No indication of diffusion limitation up to highest value of *i* cited.
[e] Highest observed *i* was 390 ma./sq. cm. at $\eta > E_r$.
[f] All values for No. 1 are reasonable assumed values.
[g] In later experiments on propane, i_L exceeded 500 ma./sq. cm. at $\eta > E_r$.

The results in Table II deserve consideration except for the values of *b*, which are not significant because they are not necessarily minimum values. All the General Electric results (No. 2-5, inclusive) were obtained with Niedrach-Alford electrodes (*18*) about 10 mils thick with platinum black as electrocatalyst; they should be comparable among themselves for the purpose of showing the effectiveness of this electrode structure for the different fuels.

As here defined, *d* is the value of η at unit current density. On Niedrach-Alford electrodes, hydrogen and methanol gave about the same value of *d;* that for propane was considerably higher. Bacon electrodes

Publication Date: January 1, 1969 | doi: 10.1021/ba-1965-0047.ch010

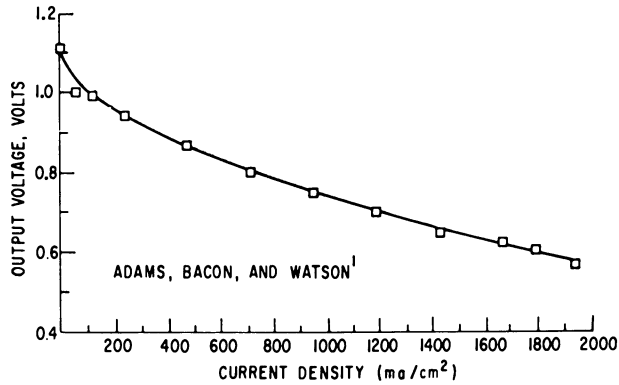

Figure 9. Current density–voltage curve showing high current density obtained in a Bacon hydrogen-oxygen cell

Publication Date: January 1, 1969 | doi: 10.1021/ba-1965-0047.ch010

give a notably small d for hydrogen under conditions that favor high reactivity. Experiments on isolated anodes are needed to establish how much of d is attributable, in each test to the anode reaction.

The high value of a for methanol in Table II may be related to its oxygen content. With both propane and methanol, anodic oxidation was complete, and carbon dioxide and water were rejected as gases. Perhaps the difficulty of rejecting carbon dioxide at the anode is responsible for the lower values of i_L observed with carbonaceous fuels.

The constant, c, together with the absolute value of i_L governs the sharpness of the downward break. All values of c in Table II exceed the theoretical value 2.3 RT/NF. In No. 2, which shows the highest value of c, the electrodes were known to be less permeable to gas than in No. 3 and 4; and this suggests that the difference between c and 2.3 RT/NF may in general be due to restricted permeability.

Table II should be regarded as a promising guide to further investigations. Such investigations could well proceed along the lines laid out by Equations 3 and 4. If successful, they should reveal the effect of electrode structure on parameters a, b, c, and d.

The Bacon cell (Table II, No. 6 and Figure 9) gives outstanding performance among those tested. As is well known, this cell does not use controlled wetting to keep gases and electrolyte apart but relies on the dual-layer structure in which the layer of smaller pores faces the electrolyte that fills them. The reactive zone is near the boundary of the two layers. The surface-active properties of the strongly alkaline electrolyte provide excellent opportunity for electrolyte film formation, and the low resistance of the electrolyte makes a large fraction of this film area effective for promoting electrode reactions. Rapid rates for these reactions are further favored by high pressure and high temperature. As Table II shows, the values of d and of b are the smallest given, and the value of a

is intermediate. There is not even a hint of a limiting current density up to 2000 amp./sq. ft., and this very high current density is attained at a sacrifice of only about half of E_r.

The difference in operating conditions considered, it is clear that the Niedrach-Alford electrode is not far behind the Bacon electrode in performance on hydrogen and oxygen (Figure 10). To be sure, it uses platinum instead of nickel or nickel oxide as electrocatalyst, but it operates at a much lower pressure and temperature. Like the Bacon electrode, it shows no indication of a limiting current for oxygen over the current-density range investigated, which terminates just over 1000 ma./sq. cm. with E_a near 20% of E_r. The outstanding characteristic of the Niedrach-Alford electrode is the excellent performance it gives on air, for which i_L has the high value of 620 ma./sq. cm. for one electrode and 255 for another, the second being of lower permeability (Table II). If we assume that there is no nitrogen diffusion barrier at i_L and that Equation 6 applies, i_L for operation on oxygen can be estimated as 620 (1/0.21) or about 3000 ma./sq. cm.; if, as is likely, some nitrogen barrier does exist, the estimated i_L is even higher. In addition to its other advantages, the Niedrach-Alford electrode is highly versatile as it shows good performance on a wide variety of fuels, gaseous and liquid hydrocarbons included.

Satisfactory operation on air is, we believe, a hallmark of good electrode structure, and we suggest that it be adopted as one criterion for judging electrode performance.

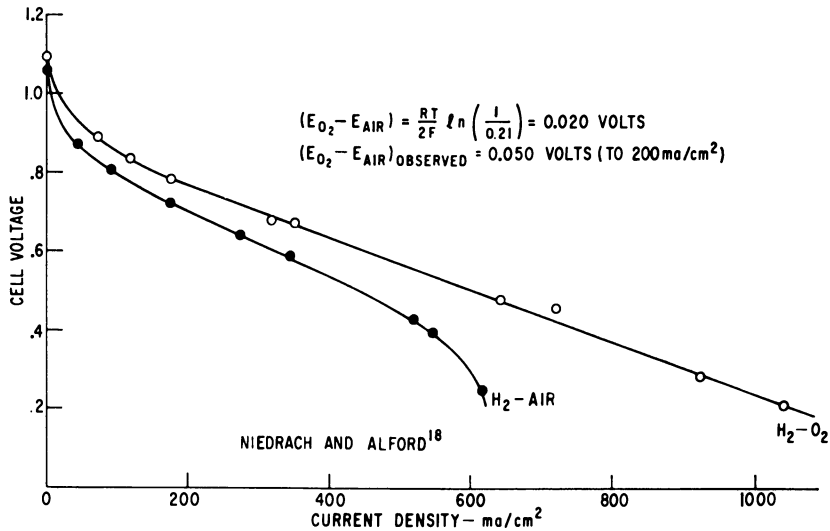

Figure 10. Comparative current density–voltage curves (18) for operation on oxygen and on air in a cell with sulfuric acid as electrolyte

Note high current density achieved with air and absence of a limiting current during operation with oxygen

Publication Date: January 1, 1969 | doi: 10.1021/ba-1965-0047.ch010

Figure 10, compared with Figure 8, shows that the interpretation built around Reaction 13 is not valid over the entire current-density range, for ΔE_a increases continuously from about 0.02 volt at $i = 0$ to about 0.1 volt in the region (near 600 ma./sq. cm.) where the $E_a - i$ curve begins to turn down sharply. This behavior suggests that the interpretation designed for the Shell electrodes is valid here at $i = 0$ but that with the Niedrach-Alford electrode diffusion barriers begin to become important even at low current densities and continue to grow in importance until i_L is reached. Further work is required before these diffusion barriers can be interpreted in terms of Equation 6 or 6a.

The work of Clark (7) shows the seriousness of the nitrogen diffusion barrier for thick carbon electrodes. Clark seems to have made his electrodes unusually thick to make prominent the diffusion barriers he wished to study. As his anodes were zinc, these diffusion barriers are associated with the cathodes. We could not find thicknesses cited by Clark but we estimate 1 cm. as the thickness of the electrode in his Figure 2.

Experiments by Clark with oxygen have been mentioned. Of his nitrogen-oxygen experiments, we show the simpler set in Figure 11. In these experiments, P was held constant at 0.205 atm. of oxygen, and P_T increased with the nitrogen content. The data of Figure 11 were shown by Clark (in his Figure 11) to have the inverse dependence of i_L on P_T called for by Equation 6a; i_L was taken as the value of i near 0.9 volt (dotted line in Figure 11). Such experiments should be done on electrodes such as Shell and Niedrach-Alford, for which the length of gaseous diffusion path is much shorter.

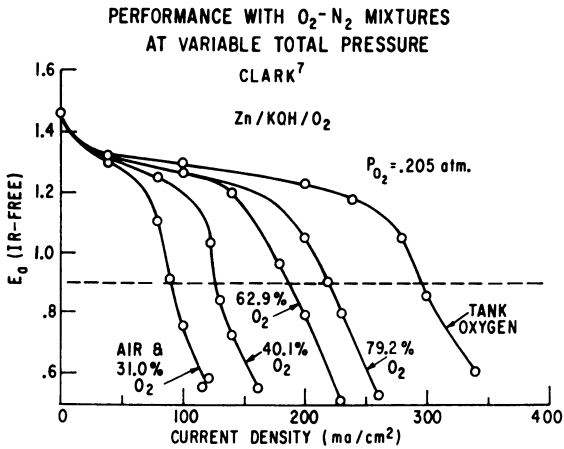

Figure 11. Limiting current densities (7) obtained with various oxygen-nitrogen mixtures at constant partial pressure of oxygen

Note decrease of limiting current with increasing nitrogen content

Publication Date: January 1, 1969 | doi: 10.1021/ba-1965-0047.ch010

Figure 12 shows the more complex results obtained by Clark (7) on oxygen-nitrogen mixtures at a fixed total pressure near 1 atm. The linear portion of the curve could be explained as was Figure 11, but the sharp upward rise could not. Figure 12 also shows that a small amount of nitrogen added to pure oxygen is more effective in reducing limiting current density than the linear region would lead one to expect. Two possible explanations come to mind: Nitrogen preferentially blocks the pores most electrochemically active, and nitrogen accumulates more rapidly at the active areas when the current density is high. Any complete explanation must consider the rate at which nitrogen leaves the neighborhood of these areas, but much further work will have to be done before a complete, definitive explanation can be attempted.

The lowering of i_L by the presence of nitrogen for carbon electrodes has been abundantly demonstrated by Clark (7). In Figure 11, i_L for air is about 100 ma./sq. cm. or about one third that for oxygen. Carbon electrodes like his are at a disadvantage in air operation because the gas diffusion path is too long; thinner electrodes could of course be used in fuel batteries.

The length of gaseous diffusion path seems a rational criterion for judging electrode structure. Again, everything else being equal, a short diffusion path is desirable. This holds true not only when nitrogen is present but even more when the partial pressure of water is appreciable. When the length of gaseous diffusion path and the thickness are proportional (often they are not), the relation between thickness and limiting current density seems worth establishing (7).

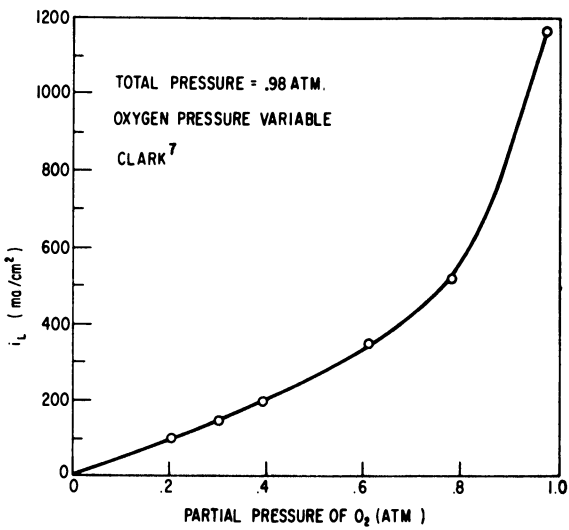

Figure 12. Limiting current densities (7) obtained with oxygen-nitrogen mixtures at constant total and variable oxygen pressure

Publication Date: January 1, 1969 | doi: 10.1021/ba-1965-0047.ch010

After everything is said and done, we believe that thin electrodes are likely to be better than thick ones and that any good electrode structure must provide an adequate effective area of electrolyte film.

Finally, Figure 13 shows current density–voltage curves for the two carbonaceous fuels of Table II. With hydrogen as fuel, one may assume that the cathode behavior predominantly determines i_L. With carbonaceous fuels, one may assume that anode behavior has a considerably greater influence. The data in Figure 13 are presented in a form to emphasize the difference in the anodic behavior of methanol and propane.

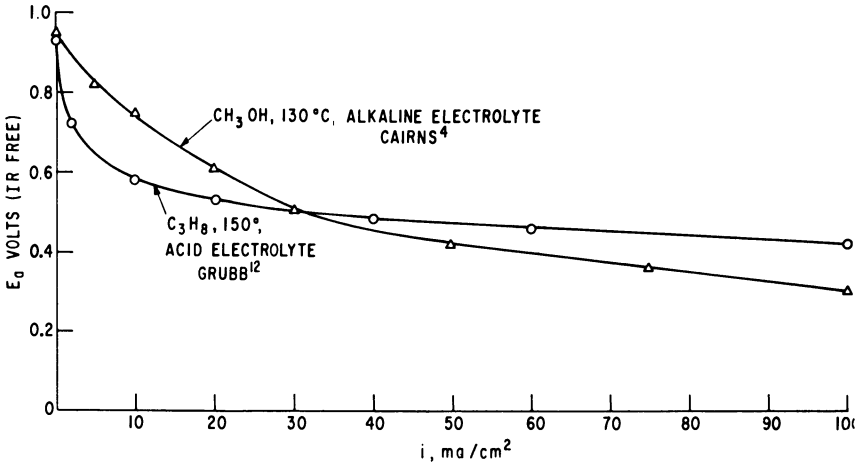

Figure 13. Current density–voltage curve for methanol-oxygen cell, cesium carbonate solution as electrolyte (4); and propane-oxygen cell, concentrated phosphoric acid as electrolyte (12)

Note difference in shapes of curves, which must be due to differences in anode processes (Table II)

Conclusions

1. The investigation of electrode structure must acquire a scientific basis if progress in fuel cells is to continue. The influence of electrode structure on fuel cell performance is difficult to isolate. The fuel cell program must be surveyed broadly to assess this influence.

2. It appears established that Grove's "notable surface of action" on metallic fuel cell electrodes is the effective area of electrolyte film on the electrode. This area will vary markedly with electrode structure. Such films are presumably important also on electrodes where gas and electrolyte are kept apart by controlled wetting, but the evidence is less convincing.

3. The concept of the "three-phase boundary" as the seat of reaction in working fuel cells should be abandoned. "Gas diffusion electrode" should be dropped as a name for a particular kind of gas electrode.

4. The electrolyte films in question are thin and bound to be unstable. The working fuel cell electrode must consequently be thought of

Publication Date: January 1, 1969 | doi: 10.1021/ba-1965-0047.ch010

as a highly dynamic system, and this increases the difficulty of making useful models for such systems.

5. Current density–voltage curves for working fuel cells need to be analyzed to establish how the overvoltage of the cell is allocated among the different processes occurring in the fuel cell. An attempt at such analysis has been made for several representative fuel cells by dividing the current density–voltage curve into three regions. Electrode structure influences performance differently in each region. The results of the attempt at analysis are encouraging, but it seems likely that more significant results will have to await further experiments.

6. In doing such experiments, it seems desirable to obtain overvoltage measurements at the anode, at the cathode, and for the electrolyte region between. Such measurements need to be made for different electrode structures over the entire current density range and at varying pressures of reacting and inert gases.

Publication Date: January 1, 1969 | doi: 10.1021/ba-1965-0047.ch010

Acknowledgment

The authors wish to thank Dr. Keith R. Williams and others in the Shell organization for permission to use the results in Figure 8.

Literature Cited

(1) Adams, A. M., Bacon, F. T., and Watson, R. G. H., in "Fuel Cells," Chapter 4, Mitchell, W., Jr., Academic Press, New York, 1963.
(2) Bikerman, J. J., *J. Colloid Sci.* **11**, 299 (1956).
(3) Brit. Patent No. 874,283 (1961).
(4) Cairns, E. J., and Bartosik, D. C., Electrochemical Society, Toronto Meeting, May 1964; Extended Abstracts of Theoretical Div., Abstract No. 214; *J. Electrochem. Soc.*, **111**, 1205 (1964).
(5) Cairns, E. J., and Macdonald, D. I., Electrochemical Society, New York Meeting, Sept. 30–Oct. 3, 1963; Extended Abstracts of Battery Div., No. 30; *Electrochem. Technol.* **2**, 65 (1964).
(6) Christianson, C. C., and Hovious, T. C., Direct Energy Conversion Operation, General Electric Co., Lynn, Mass., unpublished results.
(7) Clark, M. B., Electrochemical Society, Boston Meeting, Sept. 1962; Extended Abstracts of the Battery Div., p. 34.
(8) Davies, M. O., Clark, M., Yeager, E., and Hovorka, F., *J. Electrochem. Soc.* **106**, 56 (1959).
(9) Faris, S. R., *Nature* **199**, 754 (1963).
(10) Grove, W. R., *Phil. Mag.* and *J. Science* **21**, 417 (1842).
(11) Grubb, W. T., Proc. 16th Annual Power Sources Conference, Atlantic City, N. J., May 1962, p. 31.
(12) Grubb, W. T., *J. Electrochem. Soc.* **111**, 1015 (1964).
(13) Grubb, W. T., *Nature* **201**, 699 (1964).
(14) Kordesch, K., in "Fuel Cells," Chapter 2, Young, G. J., ed., Reinhold Publishing Corp., New York, 1960.
(15) Medlin, W. V., private commun. March 19, 1963.
(16) Mond, L., and Langer, C., *Proc. Roy. Soc.* (*London*) **46**, 296 (1889).
(17) Niedrach, L. W., *J. Electrochem. Soc.* **109**, 1092 (1962).
(18) Niedrach, L. W., and Alford, H. R., *Ibid.*, in press.
(19) Nobis A., dissertation, Dresden, 1909.
(20) Schmid, A., "Die Diffusionsgaselektrode," Ferdinand Enke, Stuttgart, 1923.
(21) Wagner, C., private communication to H. A. Liebhafsky, 1957.

(22) Weber, H. C., Meissner, H. P., and Sama, D. A., *J. Electrochem. Soc.* **109,** 884 (1962).
(23) Will, F. G., *Ibid.*, **110,** 145 (1963).

RECEIVED March 25, 1964. In part, this work was made possible by the support of the Advanced Research Projects Agency (Order No. 247) through the United States Army Engineer Research and Development Laboratories under Contract DA-44-099-ENG-4909.

Publication Date: January 1, 1969 | doi: 10.1021/ba-1965-0047.ch010

In Fuel Cell Systems; Young, G., el al.;
Advances in Chemistry; American Chemical Society: Washington, DC, 1969.

11

Effects of Oxygen Partial Pressure on Fuel Cell Cathodes

A. J. HARTNER, M. A. VERTES, V. E. MEDINA, and H. G. OSWIN

Leesona Moos Laboratories, Community Drive, Great Neck, N. Y.

Publication Date: January 1, 1969 | doi: 10.1021/ba-1965-0047.ch011

The study of transport and electrochemical processes occurring at the oxygen cathode is of fundamental importance in fuel cell development. Since the polarization of the oxygen depolarized cathode is the major factor contributing to cell inefficiency in hydrogen/air fuel cells, an improvement in the polarization would lead to higher power densities.

Polarization is minimized by employing porous electrodes having a high ratio of reaction area to apparent electrode area. The liquid electrolyte then partially permeates the pores of the electrode, and the balancing gas pressure on the reverse side of the cathode establishes a liquid meniscus zone. This zone is usually referred to as the three-phase interface. The effect of the partial pressure of oxygen on this electrode/electrolyte/gas interface has been studied using hydrophilic electrodes throughout the study.

Experimental

During this study, the meniscus was established by partly immersing a flat-plate electrode into the electrolyte. This arrangement was preferred because of the inability to define accurately the reaction zone in a porous electrode. As shown by the experimental arrangement used in Figure 1, slight current contributions that would arise if the electrode were immersed in the electrolyte were minimized by allowing the electrode to just contact the electrolyte surface. The partial pressure of oxygen was varied both by varying total system pressure and by using inert diluents.

The difficulty (*4*) in defining the utilized area of the meniscus prevents the expression of rate/unit area. For this reason we express current densities in μA. per linear centimeter of the interface.

Materials used for the flat-plate electrodes were platinum, gold, silver,

In Fuel Cell Systems; Young, G., el al.;
Advances in Chemistry; American Chemical Society: Washington, DC, 1969.

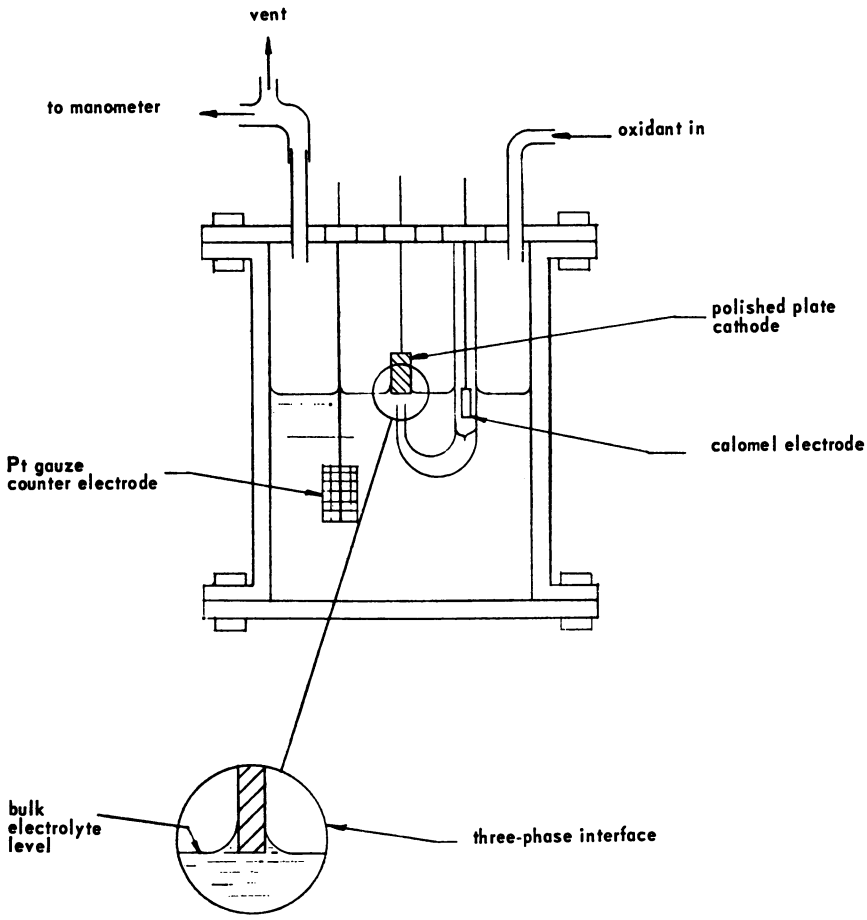

Figure 1. Experimental arrangement

Publication Date: January 1, 1969 | doi: 10.1021/ba-1965-0047.ch011

and palladium, and correlations obtained were confirmed using porous electrodes. Standard potential-current measurements were made in the p_{O_2} range—0.10 to 10 atm. A Wenking potentiostat was used for controlled potential experiments. To prevent disturbance of the interface, the electrolyte was not stirred while measurements were taken.

Effect of P_{O_2} on OCV and Polarization

According to Weber, Meissner, and Sama (3), the rate limiting step for a partially immersed depolarized oxygen cathode is mass-transport of oxygen through the liquid meniscus zone where the partial pressure of oxygen is a major mass-transport parameter. The partial pressure of oxygen affects both the open circuit voltage (OCV) and potential at

In Fuel Cell Systems; Young, G., el al.;
Advances in Chemistry; American Chemical Society: Washington, DC, 1969.

constant current. Although changes in OCV that were observed (Figure 2) were anticipated in accordance with the Nernst equation, the changes in current at constant potential merit attention since mass-transport is now involved. Figure 2 shows that polarization decreases with higher oxygen partial pressure. This polarization decrease is less marked with increasing p_O values.

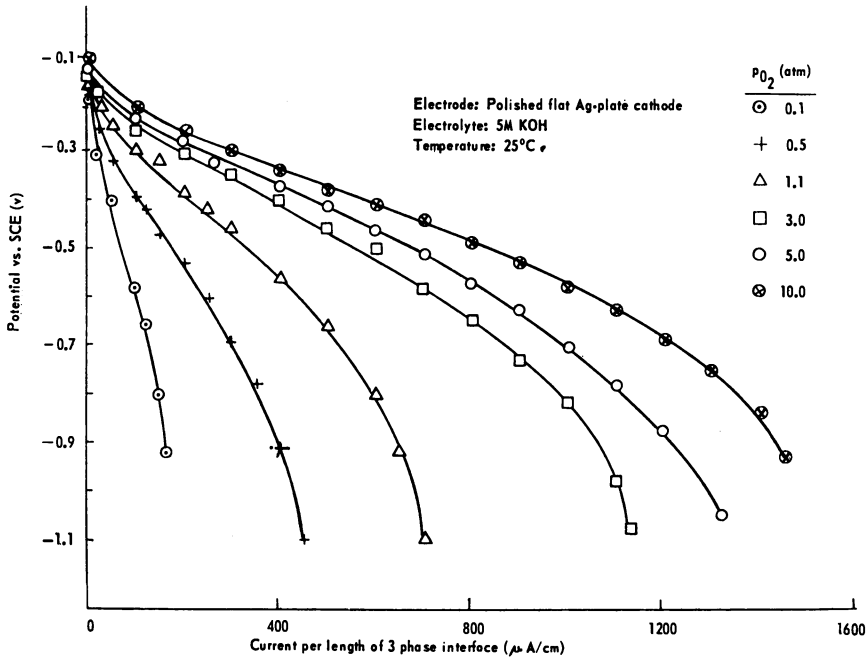

Figure 2. Polarization of flat-plate electrode partially immersed in potassium hydroxide electrolyte

A better understanding of the diminishing effect of the partial pressure of oxygen on polarization can be derived when p_{O_2} or log p_{O_2} values are plotted against polarization at constant current density (Figures 3 and 4).

The nonlinear relation between polarization and p_{O_2} can be examined in terms of the concentration polarization and mass transfer parameters. The current (i) obtainable from the transport of oxygen through an electrolyte layer can be expressed by the following equation:

$$i_c = DZF \frac{C_1 - C_2}{\delta} \quad (1)$$

For a limiting current (i_l), $C_2 = 0$ and

$$i_l = DZF\,(C_1/\delta) \quad (2)$$

Publication Date: January 1, 1969 | doi: 10.1021/ba-1965-0047.ch011

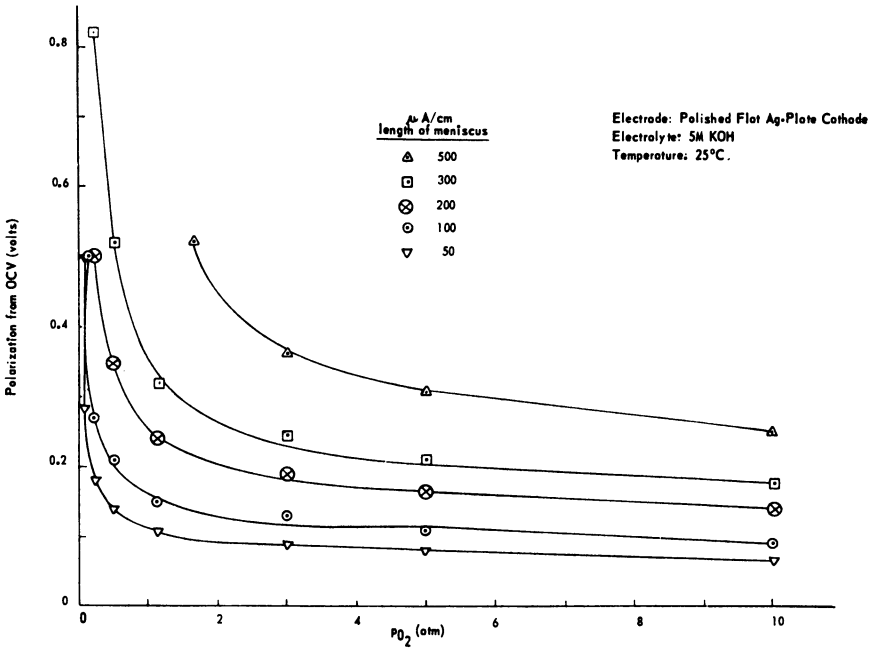

Figure 3. Polarization from OCV vs p_{o_2} for a flat-plate electrode partially immersed in potassium hydroxide electrolyte

The relation of concontration polarization (η_C) at a current (i_C) and limiting current (i_l) is given by:

$$\eta_C = \frac{2.303\ RT}{ZF} \log \frac{i_l}{i_l - i_C} \tag{3}$$

Equation 2 implies that limiting current can be increased by: increasing D—for example increasing temperature; decreasing δ (through agitation); and increasing C_1. In the experiments reported here, D and δ were kept constant by maintaining constant temperature and preventing agitation of the electrolyte, leaving C_1 as variable.

At constant current, the term $(C_1 - C_2)$ will be constant (see Equation 1), and Equation 3 becomes:

$$\eta_C = \frac{2.303\ RT}{ZF} \log \frac{C_1}{C_1 - K_1} \tag{4}$$

The concentration of oxygen at the gas/liquid interface (C_1) is a function of p_{O_2}. Therefore:

$$\eta_C = \frac{2.303\ RT}{ZF} \log \frac{f(p_{O_2})}{f(p_{O_2}) - K_1} \tag{5}$$

and: $lim\ (\eta_C) = 0$, if $f(p_{O_2})$ approaches infinity.

Publication Date: January 1, 1969 | doi: 10.1021/ba-1965-0047.ch011

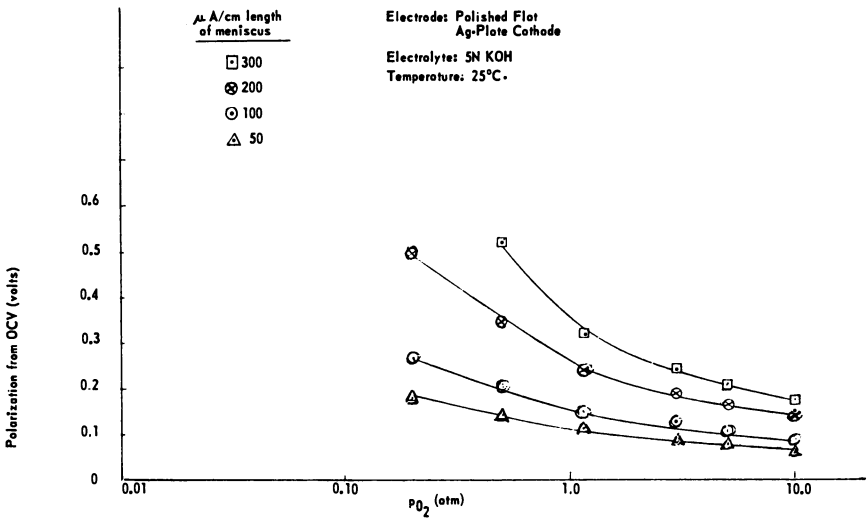

Figure 4. Polarization from OCV vs. p_{O_2} for a flat-plate electrode partially immersed in potassium hydroxide

The curves shown in Figures 3 and 4 follow the trend indicated by Equation 5. In addition, our experimental results show that activated porous nickel structures exhibit the same dependence on the partial pressure of oxygen as the flat-plate cathodes. The relationship was further verified with porous silver electrodes.

Thus, while the flat-plate structure is an idealized model of the porous cathodes used in fuel cells, the relationship between p_{O_2} and i_E appears to be the same as observed with porous electrodes.

Effect of P_{O_2} on Equipotential Current (i_E)

The four catalysts tested (Pt, Pd, Ag, and Au) yielded identical currents on flat-plate electrodes. These currents were measured at —0.8 volt against the open-circuit potential of the cathode. The open-circuit potentials measured against the standard calomel electrode fell within the range of less than 50 mv. Thus, the fixed potential at which limiting current was arbitrarily measured represents a fixed potential *vs.* the reversible H_2/H^+ electrode in the same electrolyte: approximately 200 to 250 mv. (E^*). This potential was chosen to eliminate the contribution of hydrogen evolution, or deposition currents.

In the initial experiments, the partial pressure of oxygen was varied and the corresponding i_E values were observed. The i_E — p_{O_2} data obtained were plotted, using log coordinates (Figure 5, curve 2) giving a straight line described by the equation $i_E = A \log p_{O_2} + B$, where A is 0.5 and B is 740 (μA./cm.). This means that i_E is independent of the

Publication Date: January 1, 1969 | doi: 10.1021/ba-1965-0047.ch011

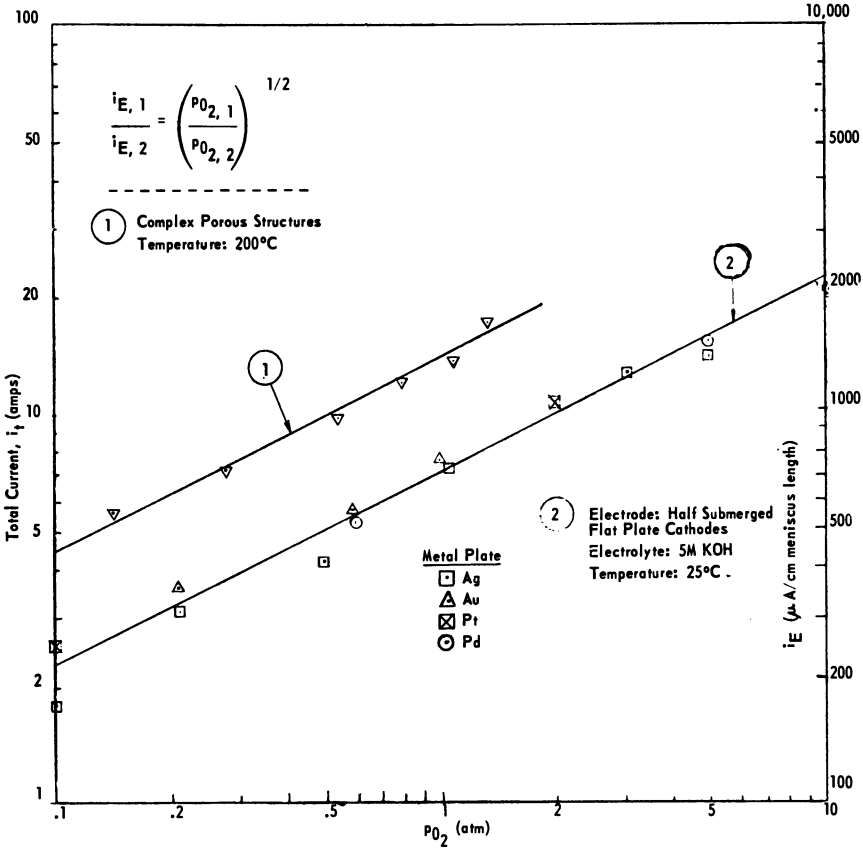

Figure 5. i_E vs. p_{O_2} for various electrodes

four catalytic materials and varies according to the one-half power of the partial pressure of oxygen. This relationship predicts i_E for any p_{O_2} within the range studied—that is,

$$\frac{i_{E,1}}{i_{E,2}} = \left(\frac{p_{O_2,1}}{p_{O_2,2}}\right)^{1/2} \tag{6}$$

where $i_{E,1}$ and $i_{E,2}$ are the maximum equipotential current obtainable for a flat-plate cathode at the same temperature and electrolyte concentration at $p_{O_2,1}$ and $p_{O_2,2}$, respectively.

From these data, it could be concluded that the four metals tested have identical catalytic activity; this is unlikely. At the experimental conditions (800 mv. polarization from OCV where the OCV is -0.17 ± 0.02 volt [*SCE*] at $p_{O_2} = 1$ atm.), the catalytic activity no longer, we believe, significantly affects current, since at potentials 800 mv. from the rest potential, the electron-transfer process is no longer itself rate-controlling.

Publication Date: January 1, 1969 | doi: 10.1021/ba-1965-0047.ch011

Constant-potential currents from porous structures follow the relationship expressed by Equation 6. Figure 5, line 1, shows data derived using a porous structure which exhibits negligible activation-polarization and reversible behavior at 200° C. Values of i_E vary with the one-half power of the partial pressure of oxygen.

Oxygen Transport

If catalytic activity is not a current-controlling factor at 200 to 250 mv., E^* mass-transport of oxygen to the catalytic sites must be involved. The likeliness of alternate transport mechanisms—for example, diffusion through the bulk of the liquid or migration of adsorbed oxygen along the unwetted portion of the electrode—was ruled out earlier, and the transport of oxygen to the catalytic sites through the electrolyte in the immediate vicinity of the three-phase interface was established (3).

There are two possible rate-controlling steps in such a case. One is the diffusion of dissolved oxygen through the liquid in the meniscus zone, and the other is interphase mass-transfer of oxygen from the gas to the liquid phase. Where diffusion in the liquid phase is rate-controlling, the liquid surface in contact with the gas is saturated with oxygen, and a linear variation of current with p_{O_2} should exist.

Investigating this liquid phase diffusion rate-controlled case, Reti (2) performed an experiment in the course of which he presaturated electrolytes with oxygen at various partial pressures. He then pumped the electrolytes through silver or platinum screen electrodes. Under constant hydrodynamic conditions (flow rate and temperature), he indeed found a linear relationship between equipotential currents and the partial pressure of oxygen in the presaturating gas. Since in Reti's experiment there was no liquid/gas interface, diffusion through the liquid is the only mass-transfer process (governed by Fick's Law).

If diffusion through the liquid is limiting in a three-phase system, we would expect, therefore, a linear relation between i_E and p_{O_2} rather than the observed dependence of i_E or $(p_{O_2})^{1/2}$.

Equipotential Current and Oxygen Solubility

With potassium hydroxide of varying concentration, the maximum obtainable current decreased with increasing electrolyte concentration. It is known that oxygen solubility (at constant partial pressure of oxygen) decreases with increasing potassium hydroxide concentration, and the data have been analyzed to determine the importance of this parameter.

The first step was to check whether Equation 6 is valid at all potassium hydroxide concentrations. If so, it can be used to calculate the maximum current obtainable (i_E) at any other oxygen partial pressure value.

American Chemical Society
Library
1155 16th St., N.W.
Washington, D.C. 20036

In Fuel Cell Systems; Young, G. J., et al.;
Advances in Chemistry; American Chemical Society: Washington, DC, 1969.

Publication Date: January 1, 1969 | doi: 10.1021/ba-1965-0047.ch011

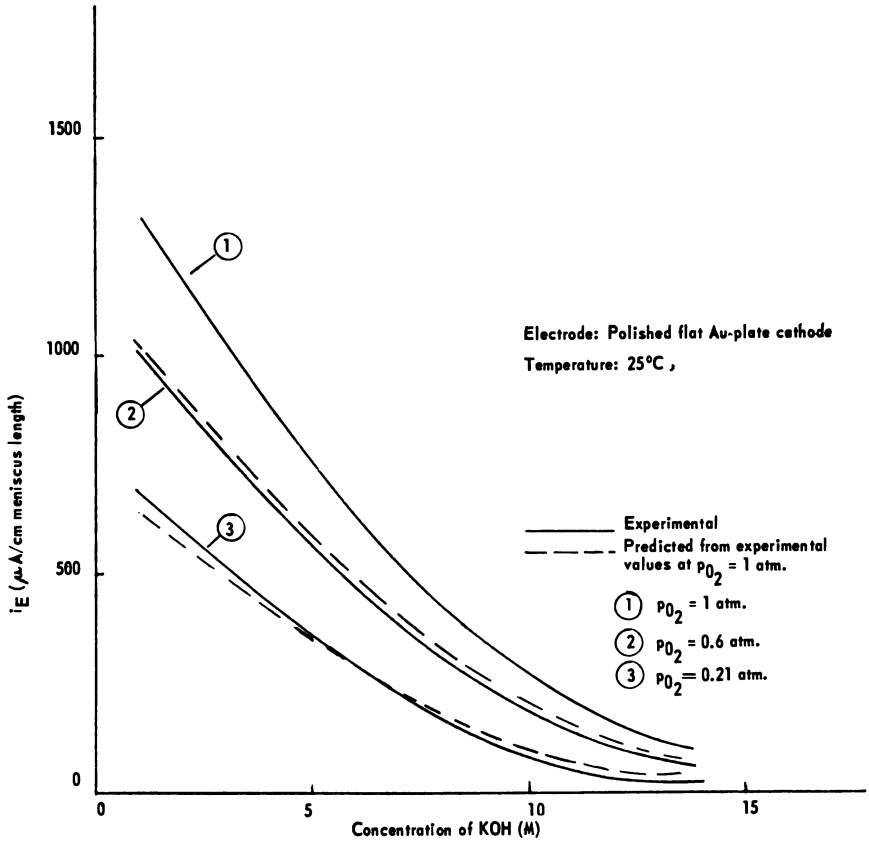

Figure 6. i_E vs. concentration of potassium hydroxide for a flat-plate electrode

This has been accomplished, and the results are illustrated by Figure 6. The solid lines in this figure, representing experimental data measured at various partial pressures of oxygen, show that the maximum obtainable current decreases with increasing potassium hydroxide concentration, as expected by decreasing solubility. The broken lines of the same figure were calculated from the data obtained at $p_{O_2} = 1$ atm., using Equation 6, and represent maximum obtainable currents at lower partial pressures of oxygen. Calculated and measured values agree well.

Investigating further the effect of oxygen solubility, studies were made at constant equilibrium concentrations of oxygen in the electrolyte. These constant concentrations were achieved by either varying the partial pressure of oxygen at a fixed electrolyte concentration, or varying the electrolyte concentration at a fixed partial pressure of oxygen.

At equal equilibrium concentrations of oxygen in potassium hydroxide at a given p_{O_2} (C^*) the i_E currents obtained are approximately equal (Table I). Because data for solubility of oxygen in potassium hydroxide

Publication Date: January 1, 1969 | doi: 10.1021/ba-1965-0047.ch011

is unavailable, the equilibrium concentration values had to be extrapolated (*1*), which may explain the small deviations between the currents obtained at nominally equal oxygen concentrations.

Table I. i_E Obtained for Various C* Values in KOH Electrolyte

Electrode: polished flat gold plate; temperature: 25° C.

C_{KOH} = 1 *Molar*			p_{O_2} = 1 atm.		
p_{O_2}, atm.	C^*, ml./l.	i_E, μA./cm.[a]	C_{KOH}, M.	C^*, ml./l.	i_E, μA./cm.[a]
1	22.2	1320	...	...	...
0.6	13.32	1008	2.18	13.32	1130
0.21	4.66	685	2.5	4.66	700

[a] Length of meniscus.

Publication Date: January 1, 1969 | doi: 10.1021/ba-1965-0047.ch011

It is well known that in the case of transport of a slightly soluble gas into a liquid, the bulk of the resistance is in the liquid phase. Because of this limitation, the bulk liquid near the transfer zone does not reach the equilibrium saturation as predicted using Henry's Law. If we plot equipotential current (i_E) against the equilibrium solubility of oxygen (C^*) at various electrolyte concentrations, we obtain a relationship similar to the one previously shown—that is, $i_E = A' \log C^* + B'$, where the experimentally obtained A' value is 0.48; this compares well with the previously obtained 0.5 value (Figure 7). Since actual solubility data are scarce, the use of extrapolated C^* values may account for this deviation.

Prediction of Performance

The current density *vs.* partial pressure of oxygen relationship developed in Equation 6, can be used to predict electrode polarization over the linear portion of the potential *vs.* current density ($E - i$) curves. This is the case, for example, for the highly active complex porous electrode structures shown in curve 1 of Figure 5.

If the slope of a linear $E - i$ curve at $p_{O_2, 1}$ is b_1, then at a given polarization (η):

$$b_1 = \eta/i_1$$

and similarly, of another linear $E - i$ curve at $p_{O_2, 2}$

$$b_2 = \eta/i_2$$

and

$$\left(\frac{i_1}{i_2}\right)_\eta = \frac{b_2}{b_1} \text{ and } \left(\frac{\eta_2}{\eta_1}\right)_i = \frac{b_2}{b_1}$$

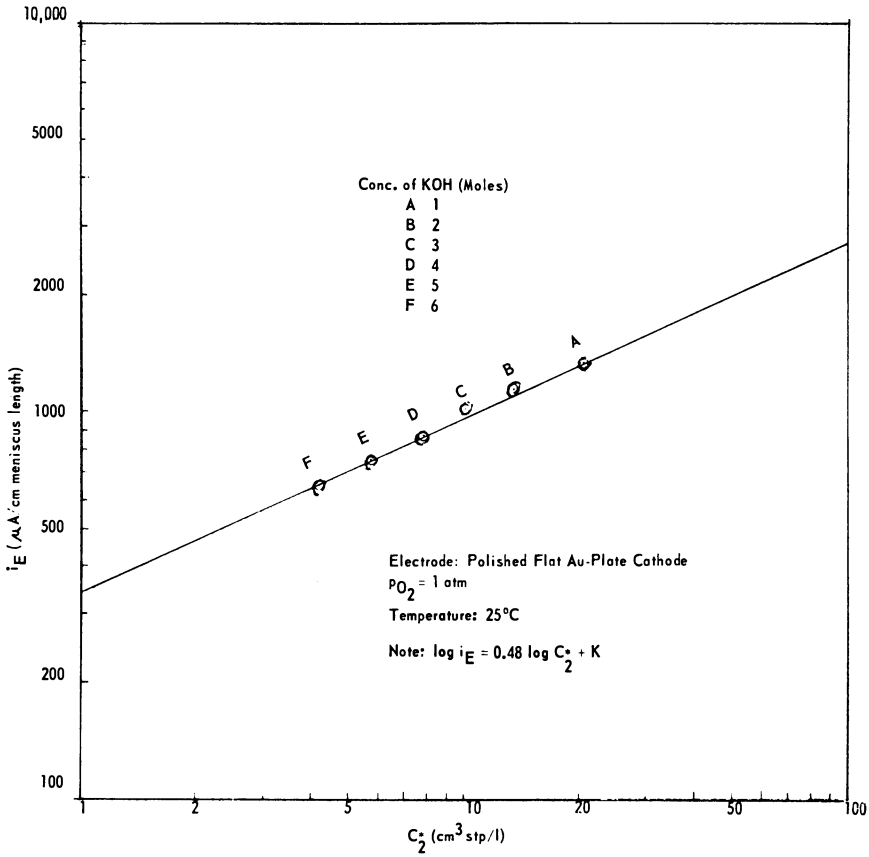

Figure 7. i_E vs. C for flat-plate electrode*

Thus from Equation 6

$$\left(\frac{\eta_2}{\eta_1}\right)_t = \left(\frac{i_1}{i_2}\right)_\eta = \left(\frac{p_{O_2,\,1}}{p_{O_2,\,2}}\right)^{1/2} \tag{7}$$

or

$$\eta = Ji(p_{O_2})^{-1/2} \tag{8}$$

Lines calculated by Equation 8 together with experimental points are shown in Figure 8.

Conclusions

The data presented show the effect of oxygen partial pressure on the polarization and equipotential current at partially immersed flat-plate cathodes. Polarization-oxygen partial pressure dependence for the flat-

Publication Date: January 1, 1969 | doi: 10.1021/ba-1965-0047.ch011

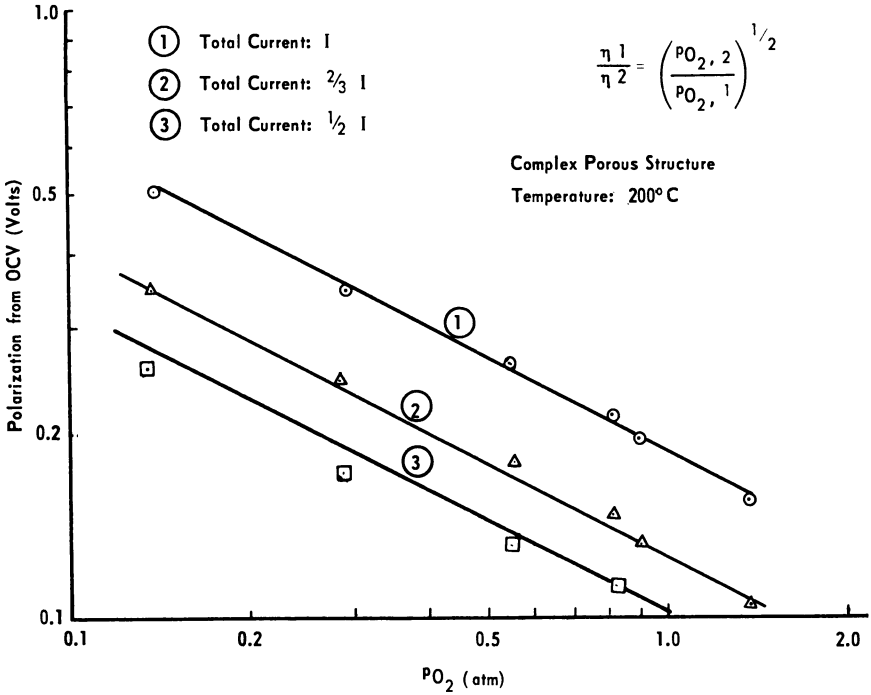

Figure 8. Polarization vs. p_{O_2}

plate electrodes is valid for complex porous structures as well. A marked decrease in electrode polarization was observed at the lower p_{O_2} range—0.1 to 2 atm. Beyond this range the polarization decrease is not as marked. Therefore, extremely high p_{O_2} values are ineffective in obtaining minimum cathode polarization for practical fuel cell operation.

The following equations are very useful for predicting cathode currents under different operating conditions if the cathode current is known for one condition, and there are no other experimental data available:

$$\frac{i_{E,1}}{i_{E,2}} = \left(\frac{C^*_1}{C^*_2}\right)^{1/2}$$

When the same electrolyte concentration is used,

$$\frac{i_{E,1}}{i_{E,2}} = \left(\frac{p_{O_2,1}}{p_{O_2,2}}\right)^{1/2}$$

These equations are valid for complex porous structures only when the activation polarization is small and diffusion (both ionic and gaseous) limitations and the electrical resistance of the structure are negligible.

There are two possible explanations of the nonlinear relation between current and partial pressure of oxygen. The first assumes that the rate-

Publication Date: January 1, 1969 | doi: 10.1021/ba-1965-0047.ch011

controlling step is interphase mass-transport of oxygen at the gas/liquid interface. This is supported by the finding that at the same polarization, four different metals yielded identical currents at the same oxygen partial pressure. Unless one assumes identical catalytic activity for all four (Pt, Pd, Ag, and Au), the reason for the phenomenon must be mass-transport limitations.

On the other hand, the dependence of i_E on $(p_{O_2})^{1/2}$ can apparently be extended to $(C_{O_2})^{1/2}$, thus indicating that the rate of solution of oxygen at the gas/liquid interface is probably not a current-limiting step. The dependence of i_E on $(C_{O_2})^{1/2}$ clearly cannot be explained by a limiting bulk-diffusion process. It seems most likely that it could reflect the rate-dependence on a surface process involving scission of the oxygen bond. The decomposition of peroxide species or surface oxide formation may be implicit in this relationship. A detailed study of this system is needed before the observed dependence of i_E on $(p_{O_2})^{1/2}$ can be satisfactorily explained.

Publication Date: January 1, 1969 | doi: 10.1021/ba-1965-0047.ch011

Nomenclature

A = proportionality constant
b = slope of linear $E - i$ curve
C^* = equilibrium concentration of O_2 in KOH electrolyte at a given p_{O_2} (ml. of O_2 at standard pressure/liter of electrolyte)
C_1 = concentration of O_2 at the gas/liquid interface
C_2 = concentration of O_2 at the electrode surface
D = diffusivity coefficient (unit area/unit time)
F = the Faraday constant
i_C = the current obtained at potential η_C
i_E = current obtained at a fixed potential from open circuit
i_l = limiting current
J = proportionality constant
N = number of moles of O_2 diffusing per unit area–unit time
P_{O_2} = partial pressure of O_2 (atm.)
R = the ideal gas constant
T = temperature (° K.)
Z = No. of electrons transferred during the reaction
δ = thickness of the diffusion layer
μ = vicosity
η = polarization (volts)

Literature Cited

(1) International Critical Tables, Vol. 3, p. 271, McGraw-Hill Book Co., New York, 1928.
(2) Reti, A. R., "Rate Limiting Step on Fuel Cell Electrodes," D.Sc. thesis, MIT Cambridge, Mass., June 1962.
(3) Weber, H. C., Meissner, H. P., and Sama, D. A., *J. Electrochem. Soc.*, **109**. 10, 884–9 (1962).
(4) Will, F. G., *J. Electrochem. Soc.*, **110**, 2, 145–160 (1963).

RECEIVED February 17, 1964

12

The Nitric Acid-Oxygen Redox Electrode in Acid Electrolyte

JOSEPH A. SHROPSHIRE and BARRY L. TARMY

Esso Research and Engineering Co. Linden, N. J.

Publication Date: January 1, 1969 | doi: 10.1021/ba-1965-0047.ch012

The performance and mechanism of a fuel cell oxygen cathode were studied, using low concentrations of nitric acid as a redox intermediate in sulfuric acid. Electrode performance using either carbon or noble metal electrodes is superior to that attainable by direct electrochemical reduction of oxygen or air in acid solution. Mechanism studies showed that the reaction is autocatalytic with the actual electrochemical reaction being the reduction of nitrous acid to nitric oxide and the rate limiting step involving the chemical reduction of nitric acid with nitric oxide. Regeneration of nitric acid by oxidation of nitric oxide and subsequent hydrolysis of nitrogen dioxide proceeds at rates that would require 0.1 lb/kwh. of nitric acid in actual fuel cell operation on air.

One approach to developing a satisfactory oxygen or air electrode for a fuel cell operating in an acid electrolyte is to use a so-called redox electrode. Such a system utilizes the more favorable electrochemical activity of a secondary oxidant with the electrochemical reduction products regenerated chemically by oxygen or air. In this manner it is possible to obtain higher electrical performance than by direct electrochemical reduction of oxygen. This increased performance is particularly significant in operating air electrodes, where high concentrations of nitrogen seriously affect electrode efficiency. Recent reports have cited the use of Br^{-}—Br_2 and Ce^{+4}—Ce^{+3} for this purpose (*7*, *8*). However, these systems have shown serious limitations in practical operation.

This paper describes the performance and mechanism of operation of another redox cathode, one based on the reduction of nitric acid in

In Fuel Cell Systems; Young, G., el al.;
Advances in Chemistry; American Chemical Society: Washington, DC, 1969.

sulfuric acid. Previous investigators have studied the cathode reaction on platinum in HNO_3/HNO_2 systems under various conditions (*4, 5, 6, 9*). However, none of these considered the possibility of using this system as a redox oxygen electrode. Furthermore, with the acid concentrations used, the presence of nitric acid could seriously impair the performance of a fuel electrode. With the intent of avoiding this difficulty, a study has been made of the redox behavior of low concentrations of nitric acid in sulfuric acid electrolyte.

Experimental

All electrochemical measurements described here were made in conventional glass cells with either parallel or coaxial electrode arrangements. Anode and cathode compartments were separated by either glass frits or cationic exchange membranes. Noble metal and carbon electrodes were used, and performance in most cases was obtained during operation against a "driven" counterelectrode, power being supplied by 6–12 volt regulated D.C. sources. All solutions were prepared using C.P. grade sulfuric (96.5%) and nitric (70%) acids diluted with deionized water of conductivity 10^{-6} mho/cm. Electrode voltages were measured against commercial saturated calomel electrodes equipped with Luggin capillary probes. Voltages and currents were measured with Keithley electrometers of 10^{14} ohms input impedance.

More specific details, when necessary, are in the text. All electrode potentials reported herein are referred to the standard hydrogen electrode (N.H.E.), and sign conventions conform to the adopted standards. No attempt has been made to correct the voltage measurements for liquid junction and thermal potentials, the magnitude of which may be significant in strong acids, about 50 to 100 mv.

Performance of the HNO_3 Redox Electrode

The initial performance tests, using platinized-carbon oxygen electrodes in 3.7*M* H_2SO_4 at 80–82° C., indicated that the addition of 0.2*M* HNO_3 to the sulfuric acid electrolyte resulted in large improvements in performance as measured by conventional voltage–log current plots. Further tests indicated that these improvements were not limited to carbon based electrodes alone but were also attainable with noble metal electrodes. The performance, an example of which is shown in Figure 1, was found to be independent of the supply of primary oxidant, i.e., oxygen or air, but did depend on both nitric acid and sulfuric acid concentrations.

Typical *E*-log *I* plots showed little evidence of a well defined Tafel slope. At temperatures above 50° C., open circuit potentials as high as 0.92 volt *vs.* the calomel reference were obtained. Neglecting liquid

Publication Date: January 1, 1969 | doi: 10.1021/ba-1965-0047.ch012

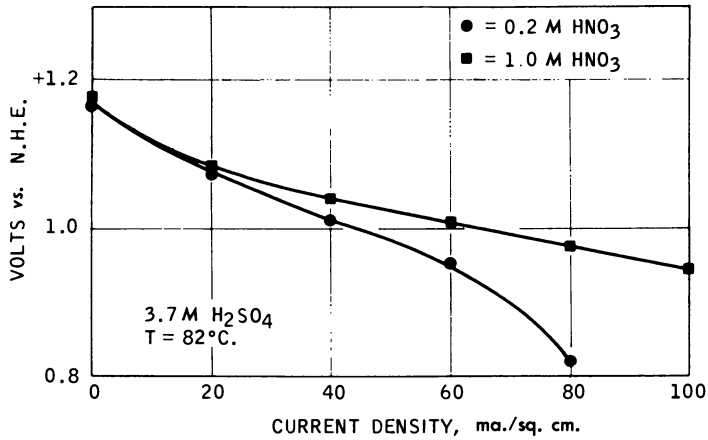

Figure 1. Typical performance of nitric acid-oxygen electrode

junction and thermal potentials, this is equivalent to 1.16 volts *vs.* N.H.E. High performance in a fresh electrolyte was shown to occur only at temperatures in excess of 50° C., but accumulation of reduction products with continued operation enabled the return of the system to 25° C. with retention of relatively high performance levels.

Furthermore, coulometric determinations in the experiments with oxygen showed that the number of coulombs involved was far greater than that needed to account for reduction of all nitric acid in the system. Thus a redox cycle exists, consisting of an electrochemical reduction of some species in the nitric acid system and the reoxidation of the products by oxygen.

Concentration Variables. A concentration variable study was carried out in which performance (E *vs.* log I) and limiting currents were determined for a series of electrolyte compositions covering the range of 0.2-1.0M HNO_3 at a sulfuric acid concentration of 3.7M, and 0.5-3.7M H_2SO_4 at a nitric acid concentration of 0.2M. The results of this study showed that limiting currents depend linearly not only on nitric acid concentration (Figure 2), but also on the proton activity in the system neglecting the contribution from the nitric acid (Figure 3). It was also observed that for these systems limiting currents decreased with increasing agitation of the electrolyte. The data, therefore, are reported with respect to a fixed rate of gas flow agitation or at quiescent conditions. Similar observations of decreasing limiting currents with increasing agitation were made by previous investigators in HNO_3/HNO_2 systems (*4*, *9*).

Effect of Temperature. Variation of the nitric acid electrode activity with temperature was studied in the range of 50°−106° C. Limiting currents were measured with the electrolyte solution presaturated

Publication Date: January 1, 1969 | doi: 10.1021/ba-1965-0047.ch012

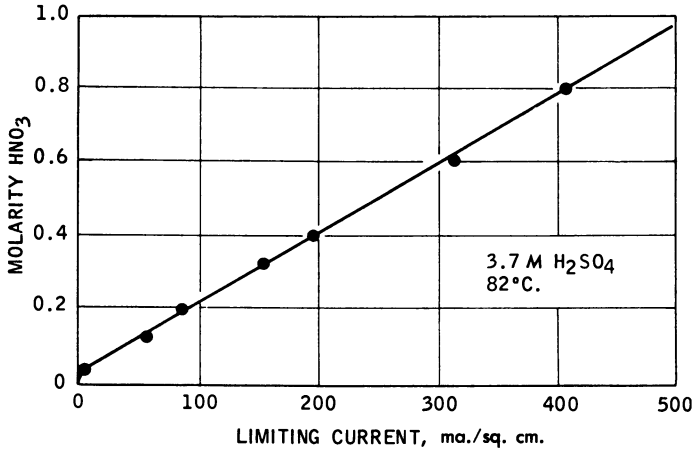

Figure 2. Dependence of limiting currents on nitric acid concentration

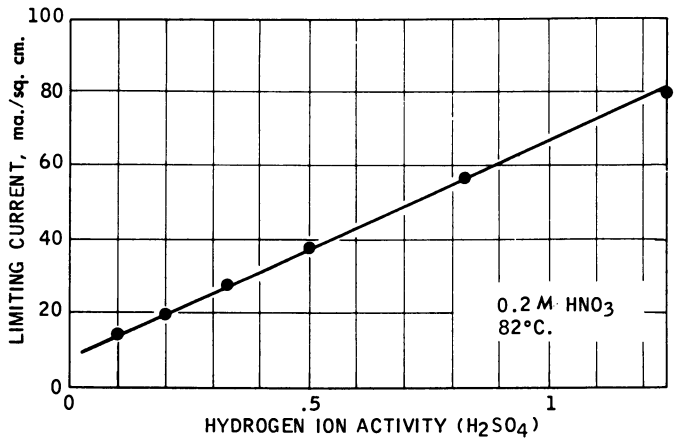

Figure 3. Dependence of limiting currents on hydrogen ion activity

with either oxygen, nitrogen or nitric oxide. The data provided a straight-line plot of log limiting current *vs.* reciprocal absolute temperature (Figure 4) with a slope corresponding to an activation energy of about 10 kcal./mol for all three gases. An activation energy of this magnitude indicates a chemical rate-limited rather than diffusion-limited current. The absolute level of the limiting currents varied, however, among the three gases used. This effect will be discussed in a later section.

Publication Date: January 1, 1969 | doi: 10.1021/ba-1965-0047.ch012

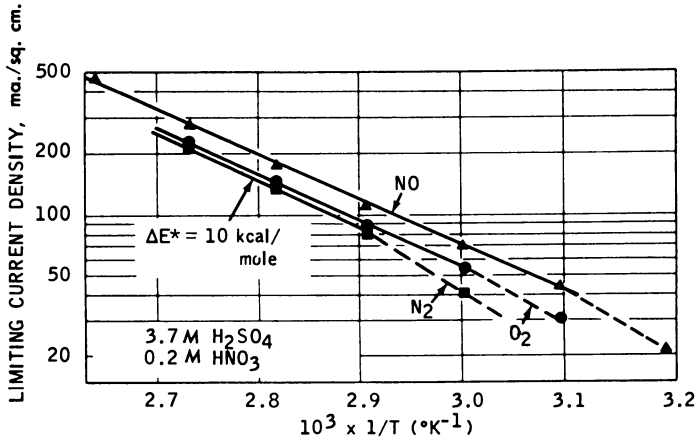

Figure 4. Temperature dependence of limiting current

Mechanism Studies

These data suggest a relatively complex reaction mechanism. Furthermore, it was felt that the practical development of this redox system for fuel cell use would require a complete knowledge of the reduction and regeneration reactions. Consequently, studies were directed toward establishing the reduction mechanism and determining the reaction products.

Cathodic Transients. A system was assembled to investigate the response of an electrode to constant current pulses during the nitric acid reduction reaction. Current pulses were applied to the electrode in a 3.7*M* H_2SO_4-0.2*M* HNO_3 electrolyte at 82° C. Constancy of current ($< 1\%$) was obtained using a high voltage (175 v.) D.C. regulated power supply and a high series resistance. Voltage transients, measured against a saturated calomel electrode-Luggin capillary arrangement, were displayed on a Tektronic 545A oscilloscope (Type D-D.C. Preamp.) and photographed. Input impedance of this oscilloscope (10^6 ohms) represented an insignificant load in the voltage measuring circuit.

Voltage-time variations at constant current can be analyzed in terms of the transition time, τ. This transition time is a function of concentrations, diffusion coefficients, and current density for reactions under diffusion control (3). It is measured from the inception of the reaction wave to its inflection (see Figure 8) and can be used analytically as a measure of concentration of a reacting species.
Thus,

$$i\tau^{1/2} = \frac{\pi^{1/2} n F C_R \mathfrak{D}^{1/2}}{2}$$

Publication Date: January 1, 1969 | doi: 10.1021/ba-1965-0047.ch012

where C_R is the bulk concentration of the reaction species and all other symbols have their usual significance.

Initial experiments with this technique confirmed that nitric acid itself was not directly reduced. Under conditions where diffusion controlled transition times for nitric acid reduction would be expected to begin at about +0.95 volt *vs.* N.H.E. and to exceed 10 seconds duration, observed transition times at this level were less than 0.1 second. Transients at currents slightly less than that required for complete polarization showed autocatalytic behavior. Typically, the electrode polarized several tenths of a volt and rapidly recovered to more positive voltages, all at constant current load (Figure 5). The reaction wave at more negative potentials in Figure 5-A disappeared upon degassing with nitrogen.

Publication Date: January 1, 1969 | doi: 10.1021/ba-1965-0047.ch012

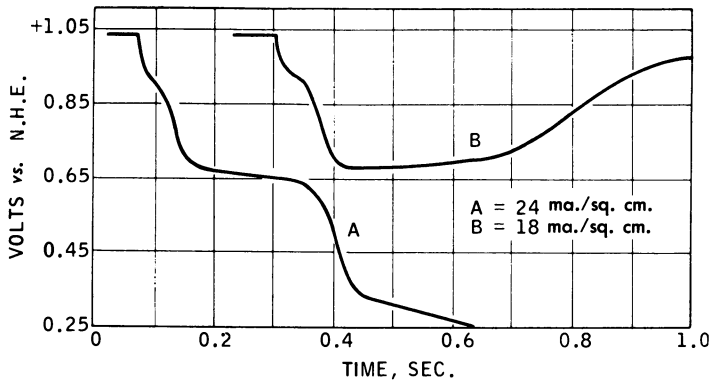

Figure 5. Typical voltage transients at constant current
A. Current in excess of limiting current
B. Current less than limiting current

The extreme autocatalytic nature of the electrode reaction was further emphasized by transients observed following extended periods of cathodization and under conditions of repetitive current pulses. An electrode placed in a fresh electrolyte solution extensively sparged with oxygen polarized completely to hydrogen evolution potential upon application of a 1 ma./sq. cm. current pulse. Upon slowly increasing the current from zero, however, a level of 5 ma./sq. cm. was easily obtained. After 5 minutes cathodization at this level followed by several seconds at open circuit, the electrode withstood a current pulse of 66 ma./sq. cm. with equilibrium polarization of only 0.1 volt (Figure 6). A gradually improving response could be observed with repetitive current pulses in a fresh solution as shown in Figure 7.

Based on the high temperature dependence of the limiting currents and absence of a well-defined Tafel slope, a reduction reaction with

chemical rate-limitation is indicated. The dependence of limiting currents on nitric acid concentration, in conjunction with the autocatalytic behavior, suggests that this rate limiting step involves reaction of a product species with the nitric acid itself to produce the electrochemical reactant.

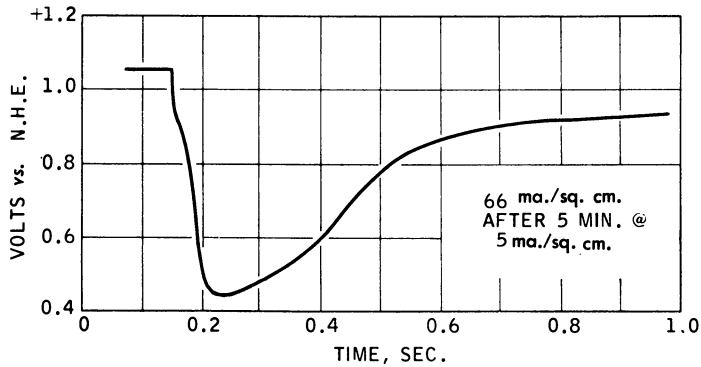

Figure 6. Response to high loads after preconditioning

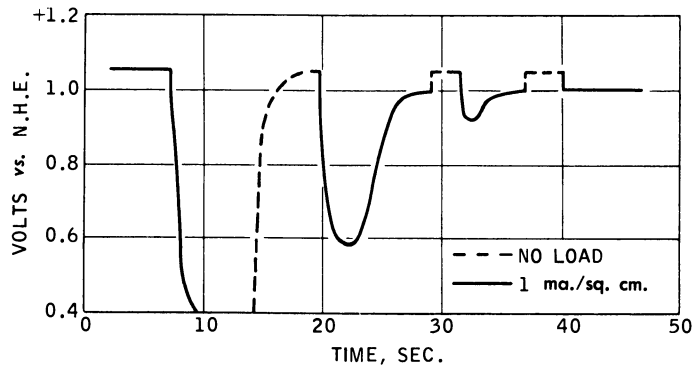

Figure 7. Response to repetitive load

Product Identification. To clarify the mechanism and assess the possibilities of this system as an efficient redox electrode, experiments were run to establish the identity of the reaction products. A cell with 3.7*M* H_2SO_4-0.2*M* HNO_3 electrolyte containing a large auxiliary cathode was used for reaction with nitric acid. Another electrode (0.27 sq. cm. in area) was placed in close proximity and used as a product detection device. At desired intervals this electrode was supplied with an anodic current pulse to reoxidize the product material present. The potential transient produced was recorded photographically from the oscilloscope trace. A typical transient found for product reoxidation is shown in

Publication Date: January 1, 1969 | doi: 10.1021/ba-1965-0047.ch012

Figure 8. Using this technique, it was possible to follow the build-up of product and its rate of disappearance under conditions of oxygen or nitrogen sparging. It was found that the product was removed during both nitrogen and oxygen sparging but that removal occurred more rapidly with oxygen sparge, suggesting reaction with oxygen. The data obtained are shown in Figure 9, where $1/i_\tau^{1/2}$ is recorded versus sparge time. This quantity, as previously described, is proportional to reciprocal concentration $(1/C_R)$ of the reacting species.

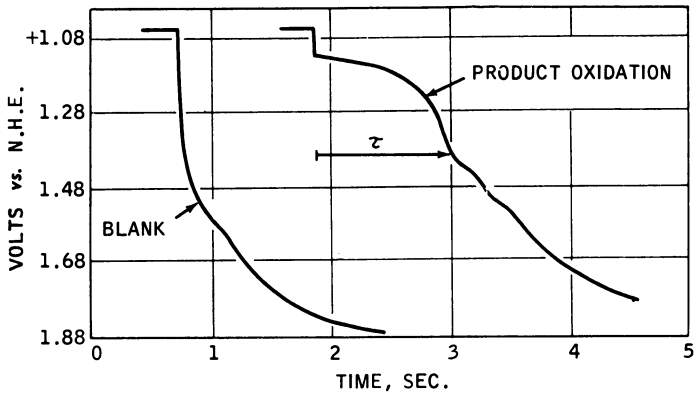

Figure 8. Transient observed during product reoxidation

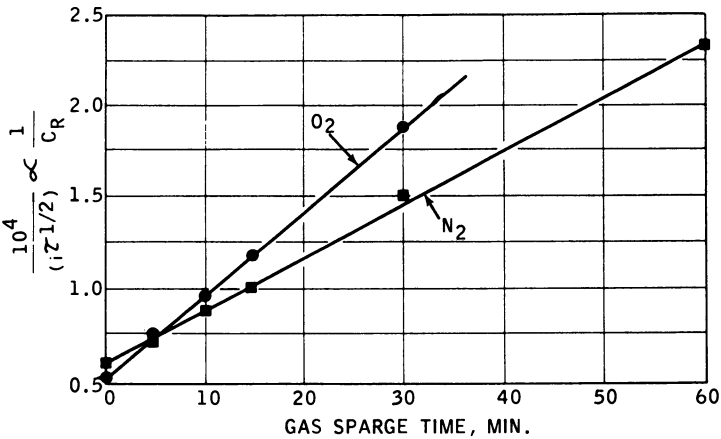

Figure 9. Removal of product by gas sparging

This evidence strongly indicated nitric oxide as the electrochemical reaction product. This conclusion was confirmed by observations on transients obtained in an air-free 3.7*M* H_2SO_4 solution saturated with nitric oxide gas. Transients obtained in this system were identical to those

Publication Date: January 1, 1969 | doi: 10.1021/ba-1965-0047.ch012

of Figure 8. Furthermore, saturation of the H_2SO_4-HNO_3 electrolyte with nitric oxide caused the complete absence of all autocatalytic effects previously observed.

The effect of temperature on limiting current in this latter system was shown in Figure 4. The increase in limiting currents in this nitric oxide equilibrated solution over those obtained with oxygen and nitrogen also affirms the role of nitric oxide as the electrochemical product which participates in the chemical rate limiting step. Limiting currents with nitric oxide are not disproportionately high, however, since electrochemical nitric oxide evolution at the limiting current is sufficient essentially to saturate the solution in the vicinity of the electrode.

Proposed Mechanism. Based on the observed behavior, the overall mechanism of the cathodic reaction in the 3.7*M* H_2SO_4-0.2*M* HNO_3 electrolyte would seem best suited by the following scheme:

$$H^+ + NO_3^- \rightleftarrows HNO_3 \text{ (undissociated)} \quad (1)$$

$$HNO_3 + 2NO + H_2O \rightarrow 3\ HNO_2 \text{ (slow, chemical rate-limiting)} \quad (2)$$

$$3\ (HNO_2 + H^+ + e^- \rightarrow H_2O + NO) \text{ (electron transfer)} \quad (3)$$

$$4\ H^+ + NO_3^- + 3\ e^- \rightarrow 2\ H_2O + NO \text{ (overall)} \quad (4)$$

As previously indicated, the rate limiting step is the slow chemical production of nitrous acid, the electrochemical reactant. Reaction 3 is assumed to operate reasonably reversibly, with the potential at any given current density being fixed by the local ratio of nitrous acid and nitric oxide activities. Since autocatalysis was found to exist over the 100-fold range of currents studied, the chemically limited reaction is considered always controlling. At the limit of the chemical reaction rate, the concentration of nitrous acid at the electrode surface falls to zero, and the potential increases until another reaction potential is reached. This scheme takes full account of the observed dependence of limiting current on stirring since excess agitation tends to remove the product, nitric oxide, making it unavailable for reaction 2 near the surface. The dependence of limiting current on both nitric acid and sulfuric acid concentration probably indicates that nitric acid is undissociated in reaction 2.

Minc (5) has studied polarization curves for platinum electrodes in nitric acid. He found that the high positive potential cathode process takes place only in solutions of nitric acid at concentrations sufficient to contain appreciable amounts of the nonionized form of nitric acid. His work indicates a linear relation between the log of the concentration of the nonionized form and electrode voltage at constant current values in the Tafel region. In our high proton activity solutions, it is expected that significant quantities of nonionized nitric acid also exist. Thus,

Publication Date: January 1, 1969 | doi: 10.1021/ba-1965-0047.ch012

equilibrium of Reaction 2 at low current densities would result in a similar dependence on acid concentration.

The mechanism proposed here differs from the one advanced by Vetter (*9*) to account for similar effects in the system HNO_3/HNO_2 at 25° C. That investigator, following the earlier work of Beinert *et al* (*1*), measured anodic and cathodic polarization curves in various HNO_3/HNO_2 systems. He concluded that the reduced species of the reactive electrochemical couple was nitrous acid or a species in rapid equilibrium with nitrous acid (e.g., NO, NO^-_2, etc.). Vetter derived a mechanism involving the reduction of nitrogen dioxide to nitrous acid and entrance of the product nitrous acid into a rate limiting chemical step analogous to Reaction 2. The distinction between these mechanisms rests on two observations:

1. Since there is little likelihood of further reduction beyond nitric oxide (the observed product), the reaction wave in Figure 5-A which is removed by degassing must represent nitrogen dioxide reduction. This is reinforced by the fact that spontaneous reversion to the low polarization level of activity ($\sim +$ 0.97 volt *vs.* N.H.E.) occurs upon reaching this reaction plateau. Such behavior would occur if this reaction level represented another source of nitrous acid, i.e., by a one-electron electrochemical reduction of nitrogen dioxide. Thus, if insufficient nitrous acid is available to support the reaction at the low polarization level, the system has a built-in "safety" for electrochemical nitrous acid production at the higher polarization, if sufficient nitrogen dioxide is present in solution.

2. As was indicated earlier, saturation of degassed 3.7*M* H_2SO_4 with nitric oxide gas alone produced an anodic transient identical to that observed for the product of the cathodic reaction. Moreover, this oxidation wave of nitric oxide, and the observed cathodic reaction wave are symmetrical about the observed rest potential of the system. It would then appear that nitric oxide, rather than nitrous acid, is the reduced component to the reversible couple operating at this potential. The reduction wave in Figure 5-A, presumed to be nitrogen dioxide, occurs at much less positive potentials.

Vetter's work was carried out at 25° C. and in general much higher nitric acid concentrations than were employed in this study. Thus there need be no direct relationship between the behavior observed in these systems. At low nitric acid concentrations Ellingham (*6*) points out the importance of Reaction 2 in determining the equilibrium between nitric oxide and nitric acid.

Regeneration

With no regard to the mechanisms involved, it has been definitely

Publication Date: January 1, 1969 | doi: 10.1021/ba-1965-0047.ch012

established that the net product of the cathode reaction is gaseous nitric oxide. Thus the problem of completing the redox cycle by conversion of nitric oxide to nitric acid then becomes a process well known in the nitric acid production industry (2).

The reaction goes by the scheme:

$$2\,NO + O_2 \rightarrow 2\,NO_2 \quad (5)$$

$$3\,NO_2 + H_2O \rightleftharpoons 2\,HNO_3 + NO \quad (6)$$

Reaction 5 is a classical termolecular reaction with negative energy of activation, favored by low temperature and high pressure. Reaction 6 at normal pressures is not limiting but suffers the drawback that nitric oxide is produced, thus requiring infinite reaction space for completion of Reactions 5 and 6. On a practical basis, however, sufficient nitric oxide conversion is obtained by maximizing gas contact times before and during hydrolysis.

Using standard methods of contacting the nitric oxide produced at the electrode with oxygen and the electrolyte, it is possible to regenerate nitric acid to the extent that the electrochemical cathode process of nitric acid reduction may be carried out for periods of time equal to several times the coulombic equivalent of nitric acid added. However, under carefully optimized oxygen regeneration conditions, it has been possible in our laboratories to pass currents at low polarization equal to 225 times the coulombic equivalent of the nitric acid lost from the system. Under comparable conditions, this number with air is about 30. Operation at this regeneration efficiency reduces the amount of nitric acid make-up to a small quantity, about 0.1 lb./kw. hour.

Compatibility

Although it is not the purpose of this paper to deal with the operation of entire fuel cell systems, a few words concerning compatibility seem appropriate. Owing to the highly active oxidizing nature of the cathode reactant, it is necessary to carry out the cathode reaction at the lowest possible nitric acid concentration consistent with the current required. A nitric acid concentration of 0.2*M* is sufficient to obtain currents of 75-100 ma./sq. cm.

The effect of nitric acid on the opposing electrode generally will be less with highly electroactive anode fuels. Thus, a fuel such as hydrogen will suffer least. Deleterious effects seem to arise primarily from accumulation of intermediate species in the nitric acid systems, e.g. nitrous acid, nitrogen dioxide, and thus, efficient regeneration on the cathode side increases compatibility. For instance, addition of nitric acid at concentrations below 0.6*M* directly to a separated anolyte compartment causes no deleterious effects at an operating methanol elec-

Publication Date: January 1, 1969 | doi: 10.1021/ba-1965-0047.ch012

trode. Effects were evident, however, at 0.25*M* when an operating nitric acid cathode was not separated from the anode compartment and reduction products were allowed to accumulate. Presence of fuel did not appear to effect operation of the nitric acid cathode in the systems tested.

Summary

The use of nitric acid in a fuel cell cathode redox cycle improves performance over that generally achieved with direct electrochemical reduction of oxygen. The system provides equal electrical performance using either oxygen or air since oxygen is not involved directly in the electrochemical reaction. The product of cathode reaction in this system is gaseous nitric oxide and efficiency of the redox cycle depends on its reconversion to nitric acid. While both oxygen and air provide high levels of regeneration, oxygen, as would be expected, shows superiority. A consistent mechanism has been advanced to account for all aspects of the cathode reaction in this system. Basic rate limitation in the electrochemical reduction appears to be a chemical step involving the reaction of nitric oxide and nitric acid.

The redox concept, as applied here, can of course be extended in principle to improve any electrode reaction where reactants exhibit low electroactivity. The conditions require that the redox intermediate be less easily reduced (or more difficultly oxidized) in theory than the oxidant (or fuel) species to be replaced. Thus, while actually exhibiting more electrochemical activity than the oxidant or fuel to be replaced, the chemical regeneration of the intermediate is still feasible. For most practical fuel cell systems, the redox intermediate would thus be restricted to those couples exhibiting reversible potentials not more than about 0.2 volt less positive (or 0.2 volt more positive) than the oxidants (or fuels) to be replaced.

Publication Date: January 1, 1969 | doi: 10.1021/ba-1965-0047.ch012

Acknowledgment

This research is part of the Energy Conversion Project sponsored by the Advanced Research Projects Agency, Department of Defense. The contract, DA 36-039 SC-89156, was administered by the United States Army Electronics Research and Development Laboratory.

Some of the data presented was obtained by Esso Research and Engineering Co. prior to the inception of this contract. The authors wish to acknowledge the efforts of their colleagues who contributed to this work, in particular A. W. Moerikofer, and to express their appreciation to Esso Research and Engineering Co. for permitting its publication.

Literature Cited

(1) Beinert, H., Bonhoeffer, K. F., *Z. Elektrochem. Angew. Physik. Chem.* **47,** 538 (1941).
(2) Chilton, T. H., "Manufacture of Nitric Acid by the Oxidation of Ammonia," *Chem. Eng. Progr. Monograph, Ser.* **56,** No. 3, (1960).
(3) Delahay, Paul, "New Instrumental Methods in Electrochemistry," p. 184, Interscience, New York, 1954.
(4) Ellingham, H. J. T., *J. Chem Soc.*, **1932,** 1565.
(5) Minc, S., Jasielski, S., *Roczniki Chem.*, **28,** 109 (1954).
(6) Monk, R. G., Ellingham, H. J. T., *J. Chem. Soc.*, **1935,** 125.
(7) Reneke, W. E., "Air Regeneration of Bromine-Bromide Fuel Cell Catholyte," Office of Technical Services **AD 273299** (1961).
(8) Stein, B. R., "Status Report on Fuel Cells," pp. 60–2, *Ibid.*, **PB 151804** (1959).
(9) Vetter, K., *Z. Physik. Chem.*, **194** 199–206 (1950).

RECEIVED February 17, 1964.

Publication Date: January 1, 1969 | doi: 10.1021/ba-1965-0047.ch012

13

Technology of Hydrogen-Oxygen Carbon Electrode Fuel Cells

LAWRENCE M. LITZ and KARL V. KORDESCH

Parma Research Laboratory, Union Carbide Corp., Parma, Ohio

Publication Date: January 1, 1969 | doi: 10.1021/ba-1965-0047.ch013

The translation of successful laboratory systems to useful practical devices often presents a variety of technological problems. This article presents some of the important considerations involved in producing rugged, long life, high current density batteries based on the carbon electrode fuel cell. Integration of advanced battery and systems engineering principles with new developments in thin, carbon-based electrodes is leading to battery power densities of approximately 20 pounds per kw. and complete power plants, excluding the fuel supply, of the order of 40 pounds per kw. depending on the size.

Intensive work over the past several years continues to sustain the advantages of carbon electrode fuel cell batteries in terms of low cost, commercially interesting systems. Laboratory studies have shown that Union Carbide carbon fuel cell anodes and cathodes have rather flat polarization curves through current densities of several hundred amperes per square foot and limiting current densities on the order of thousands of amperes per square foot (*1*). Oxygen electrodes have attained lives of the order of 4000 hours at current densities of 200 amp./sq. ft. and hydrogen electrodes over 2000 hours at 100 amp./sq. ft. in life tests involving daily probing to 350 amp./sq. ft. However, limitations imposed by mass transport phenomena, heat rejection, and water rejection can make it difficult to fully realize this electrochemical potentiality in large batteries.

While high performance obtained with selected systems under optimized conditions presents a goal to be sought after, practical operating considerations usually require that, for large production units, a more nominal level be chosen. For the Union Carbide carbon electrode fuel

In Fuel Cell Systems; Young, G., el al.;
Advances in Chemistry; American Chemical Society: Washington, DC, 1969.

cell battery, as of mid-1963, the proposed continuous operating level for long life is 50 amp./sq. ft. for hydrogen-oxygen batteries operating between 25° and 80° C. with 6*N* to 14*N* potassium hydroxide electrolyte. Overload levels of two to three times this value are easily sustained for several hours at a time, and momentary transient currents of the order of 400 amp./sq. ft., such as are required for motor starting, have been repeatedly drawn from large batteries. A motor starting power of 9 kw. has been drawn without detrimental effect from a nominal 1.25-kw. battery even after storage on open circuit for over two months following the initial break-in and use period.

The aqueous potassium hydroxide electrolyte coupled with these carbon electrodes permits instantaneous start-up at temperatures as low as −10° C., a very desirable feature for many applications. Further, the broad electrolyte concentration range which may be tolerated permits wide swings in power demand. The accompanying variations in electrolyte volume are accommodated by providing appropriate reservoir capacity.

Evans (*1*) has recently discussed vibration, shock, and acceleration

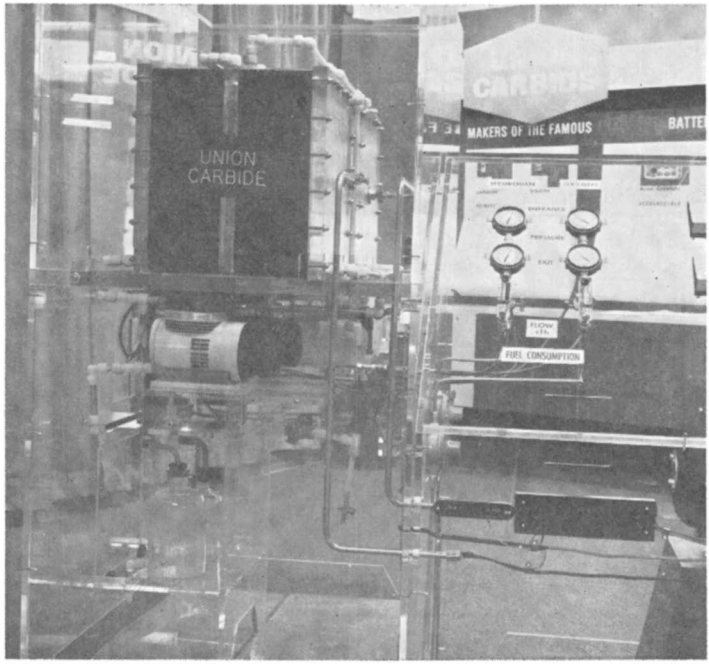

Figure 1. Baked carbon H_2-O_2 fuel cell power supply—1.25-kw.

tests performed on operating carbon electrode batteries which have demonstrated their ruggedness and their ability to withstand mechanical

Publication Date: January 1, 1969 | doi: 10.1021/ba-1965-0047.ch013

abuse without sustaining damage. The severity of these tests was well in excess of the launch requirements for the Agena B rocket. Some of the cells used in these environmental experiments have been kept on life tests for periods of the order of 7000 hours, the majority of the time at 65 to 100 amp./sq. ft., to demonstrate that exposure to such rigors does not affect the long life expectancy of these units.

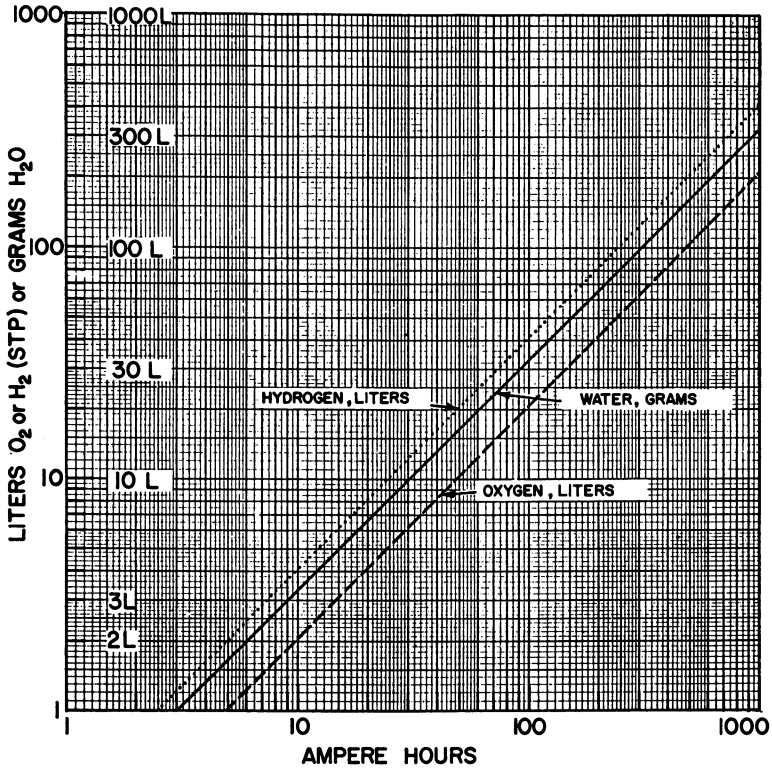

Figure 2. Gas use and water production rate

Design Criteria

Union Carbide carbon electrodes provide a high caliber fuel cell electrochemical system. To make proper use of these electrodes, they must be built into potentially low cost batteries of minimum weight and volume with adequate gas and electrolyte flow distribution and heat and water removal systems. Such a battery should be easily assembled and be dimensionably stable over the desired temperature and pressure operating range.

The quantities of reactants, products, and heat involved in even a 1-kw. battery are sizable. Figure 1 shows a nominal 1.25-kw., 32-cell, series-connected carbon electrode power supply. Such a system, operating

Publication Date: January 1, 1969 | doi: 10.1021/ba-1965-0047.ch013

at its design level of 46.5 amp. (50 amp./sq. ft. of available electrode surface), will typically exhibit an average terminal voltage of 0.84 volt per cell. At this operating level, referring to Figure 2, each cell will consume, per hour, 9.7 liters of oxygen and 19.4 liters of hydrogen to produce 15.6 grams of water. In one 24-hour day, this amounts to a usage, for the 32-cell battery, of 263 cubic feet of oxygen and 526 cubic feet of hydrogen. About 26.5 pounds of water (more than 3 gallons) will be formed during this day. The heat output, referring to Figure 3, will be 3360 B.t.u., or about 850 kcal., per hour. (The curves of Figure 3 assume that all of the energy of the hydrogen-oxygen reaction not withdrawn as electrical energy at the battery terminals will appear as heat.) The feed systems, by-product water removal, and heat rejection systems must not only be designed to handle the indicated quantities but must be capable of taking care of the several-fold overloads which such a battery can provide.

Publication Date: January 1, 1969 | doi: 10.1021/ba-1965-0047.ch013

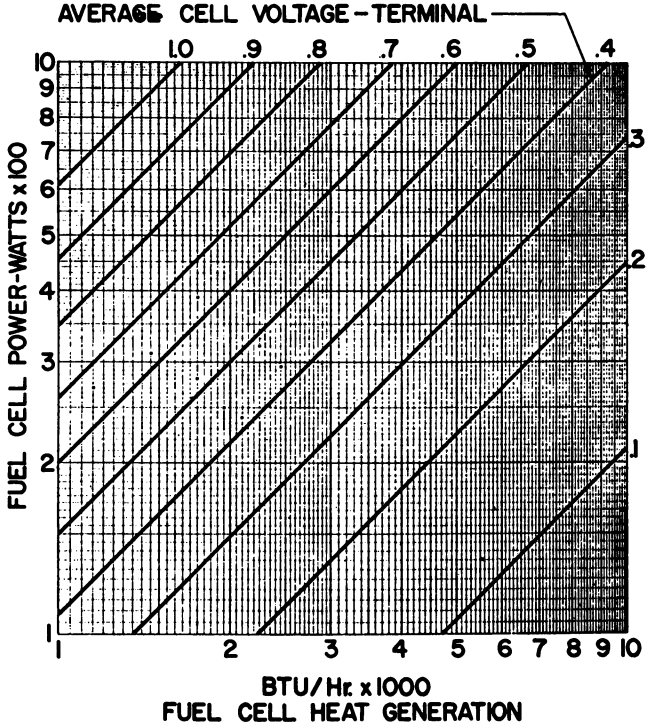

Figure 3. Heat generation versus power based on standard heat of formation for H_2O (liquid) at 25° C.

Gas and Electrolyte Feed. Design studies of our larger battery systems have established the desirability of recirculating both the hydrogen

In Fuel Cell Systems; Young, G., el al.;
Advances in Chemistry; American Chemical Society: Washington, DC, 1969.

and oxygen as a means of transporting the water formed in the battery to an external condenser. Such recirculation also assists in maintaining uniform gas composition and flow to each cell in a power supply. Electrolyte recirculation through a heat exchanger is a convenient means of maintaining temperature control in large battery systems. This affords heat removal directly from the working surface of the electrodes giving, obviously, better temperature uniformity and, thereby, better operating characteristics than other heat-removal techniques.

In assembling a set of cells into a battery, the gas flow (and electrolyte flow, where used) can be so arranged as to feed each cell in series from one to the other or to feed a set of cells in parallel from a given manifold. The prime advantage of the series flow system is that the same rate of fluid flow is guaranteed through each cell. In the parallel system, blockage of one sort or another may raise the flow resistance into a particular cell and thereby cause that cell to be partially or completely bypassed. Such a situation can adversely affect the performance of the blocked cell and may even cause it to fail. The series flow approach has the disadvantages of higher pressure drop, increase in the concentration of any impurities as the flow proceeds from the inlet to the outlet of the battery, and an increase in temperature of the feed material from the first to the last cell. Such difficulties were particularly evident in early series flow models. All of our present systems utilize the parallel flow arrangement for both gases and liquids.

The first parallel-flow models were built with comparatively large ports feeding each cell from the common inlet and outlet manifolds. While this permitted operation with very low pressure drop in the flow system, it also introduced significant maldistribution of both gases and electrolyte from one cell to another. Temperature differences as great as 25° C. were experienced from one cell to another in a 13-cell parallel flow module operating at 50 amp./sq. ft., and even more drastic temperature excursions occurred at higher operating levels. Blocked gas ports resulted in a build-up in the gaseous inerts to the point where the blocked cell would drop in potential far enough to be driven as an electrolysis cell by adjoining cells.

A solution to the problem of maldistribution of electrolyte and gas flow was reached by inserting orifices in the feed manifold to increase the normal pressure drop between the feed manifold and the cell. These orifices were designed to ensure that the variations in flow resistance from cell to cell were small compared to the pressure drop across the orifices. This pressure drop was also sufficient to clear the electrolyte exit ports of stray gas bubbles and the gas exit ports of any liquid blocks. A criterion used in sizing the orifices was that set by Richardson (*2*) in his analysis of fluid flow distributors. For equal distribution to each unit in a parallel system, he suggests that the pressure drop

Publication Date: January 1, 1969 | doi: 10.1021/ba-1965-0047.ch013

down the entire feed manifold should not exceed 1% of the pressure drop across the individual orifices.

Temperature operating levels are typically set by (a) electrode voltage, electrochemical stability, and operating range; (b) limitations of the framing materials and the magnitude of strains set up between the shell and the electrode proper; (c) water transpiration requirements; and (d) the ability to maintain the required thermal balances in both normal and overload operating modes. The optimum temperature range for present state-of-the-art batteries is approximately 50° to 70° C. although satisfactory operation is attainable considerably above and below this range.

To optimize the water transpiration capabilities, it is desirable to operate near the top temperature of the useful operating range so as to maximize the water partial pressure. For this reason, electrolyte flow rates through the battery are usually chosen which will permit the electrolyte to enter the cell relatively warm and to exit with only a moderate temperature increase; 10° C. has been set as a practical and easily maintained increase. Figure 4 shows the required flow to hold this ΔT as a function of the cell's terminal voltage and current, assuming all of the heat is removed via the electrolyte. (A considerable fraction of the heat generated in an operating battery may be removed as heat of evaporation and sensible heat if water transpiration is employed. In addition, there are the usual conductive, convective, and radiative heat losses from the battery surface.) These flow data and the expected operating levels must be taken into account in determining the feed port size.

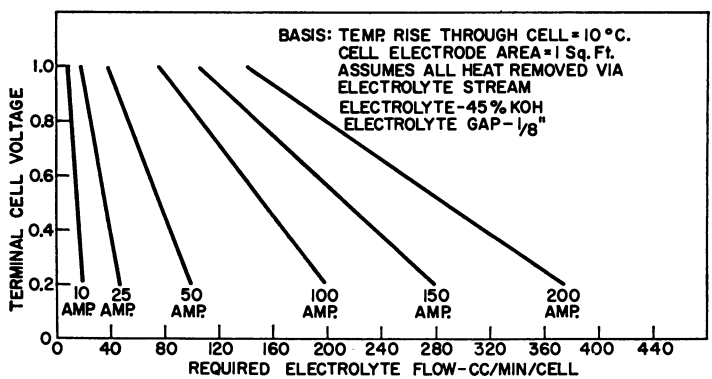

Figure 4. Electrolyte flow required for temperature control as a function of cell voltage and current

Gas distribution studies across the electrode face have been made on single cells. The gas feeds into a distribution header covering one-

Publication Date: January 1, 1969 | doi: 10.1021/ba-1965-0047.ch013

half the plate width. To ascertain the flow distribution, filter paper strips, soaked in phenolphthalein indicator solution, were placed across various sections of the plate as shown in Figure 5. The feed gas was made ammoniacal by passing it over an ammonium hydroxide solution prior to entering the cell. Motion pictures were taken to show the gas distribution as indicated by the color change (colorless to pink) in the indicator tape as the gas flowed over it. Summarized in Table I is the time requirements for the gas to completely cover the electrode surface of the current unit as a function of flow rate. The gas space in this system was $10^{7}/_{8}$ inches wide by 13 inches high by $^{1}/_{16}$ inch thick.

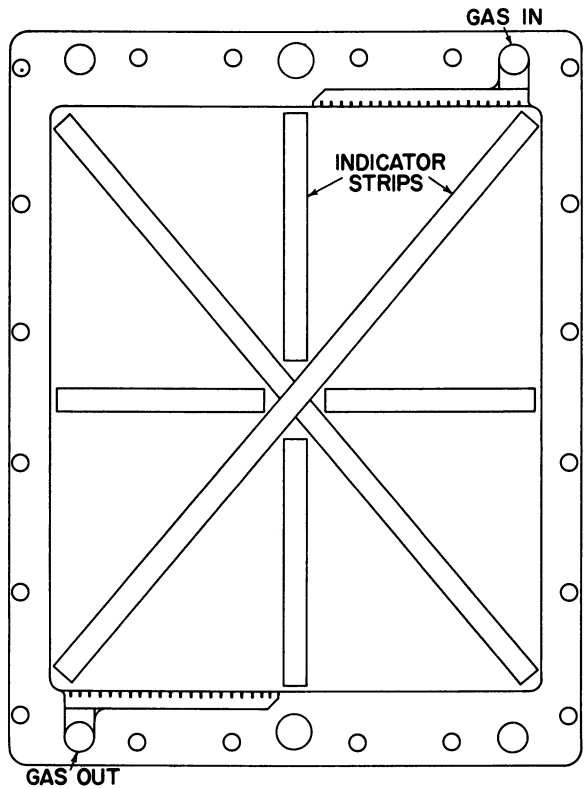

Figure 5. Test arrangement for gas distribution studies

At flow rates of 50 to 400 cc./min. the flow pattern characteristically moves in a frontal fashion from the inlet diagonally to the outlet. The total width is covered in about the same time period as one-half the length. The last section to be covered is the lower right area. At flow rates of 600 to 2000 cc./min. the total electrode is covered very

Publication Date: January 1, 1969 | doi: 10.1021/ba-1965-0047.ch013

rapidly. Therefore, to ensure complete sweeping of the electrode surface and provide good mixing of the use and feed gases, a minimum recirculation gas rate of approximately 600 cc./min. should be used. The use rate at 50 amp./sq. ft. is about 160 cc./min. of oxygen and 320 cc./min. of hydrogen.

Table I. Gas Distribution Analysis ($^1/_{16}$-inch Gas Space)

Gas flow rate, cc./min.	*Time to cover total face, seconds*
50	400
100	335
200	210
400	60
800	15
2000	13

Gas Purge Requirements. Most feed gas supplies will contain some impurities. For example, typical commercial tank oxygen will contain about 0.5% inerts, while tank hydrogen will have about 0.05% impurities. As these gases are consumed in the cell, the inert impurities will tend to accumulate unless they are purged. The effect of oxygen concentration on the output of the $^1/_4$-inch carbon cathode is indicated by the difference in voltage attained on operation with air and with pure oxygen as shown in the curves of Figure 6. Operation of a cell at 50 amp./sq. ft. using either a 90/10% mixture of oxygen-nitrogen or pure oxygen showed no significant difference. At higher current densities, half-cell tests did indicate a concentration effect. These cathode tests were run continuously at 200 amp./sq. ft. with periodic spot checks at higher levels. At 300 amp./sq. ft. the cathodes supplied with the 90% oxygen mixture showed approximately 40 millivolts lower voltage than those supplied by 99.5% oxygen.

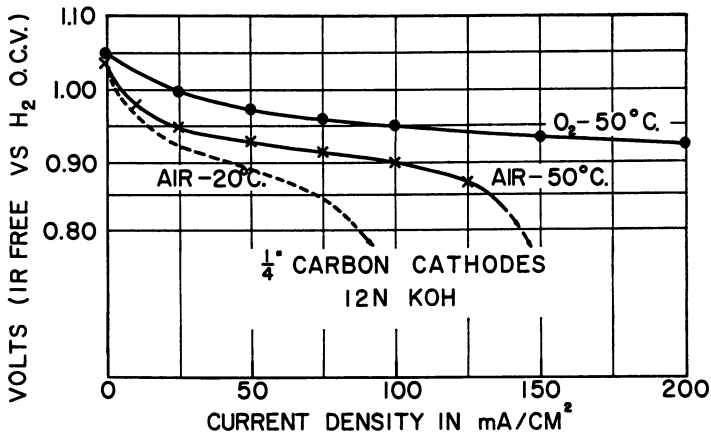

Figure 6. Cathode performance on air and on oxygen

Publication Date: January 1, 1969 | doi: 10.1021/ba-1965-0047.ch013

Figure 7 gives the equilibrium gas composition as a function of continuous purge rate based on these supply purity figures. If the purity level is to be held at 95%, a hydrogen purge of the order of 1% of the use rate will be required and an oxygen purge rate of about 10% of the use rate under steady state conditions.

It should again be emphasized that if the only gas flow out of the cell is the purge, the possibility exists of accumulating fairly high concentrations of inerts over some area of the surface of large electrodes due to variations in the gas flow pattern. This may locally cause excessive concentration polarization resulting in a nonuniform distribution of current over the face of the electrode. Gas recirculation helps avoid this problem.

Resistive Power Losses. It is important to minimize internal resistance in any battery design. Not only does the internal resistance result in a loss of available power which may be obtained from the terminals of a battery, but it also gives rise to heat which must be dissipated. The items involved, in order of significance for these systems in which the current flow is perpendicular to the face of the electrode, are (a) the resistance of the electrolyte; (b) the contact drops between the electrode, the metal mesh contact member, and the metal current collector plate; and (c) the resistance of the electrode itself.

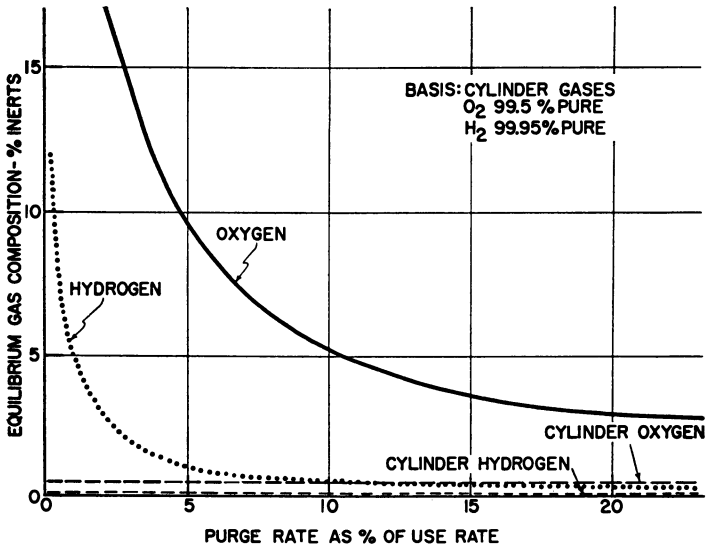

Figure 7. Equilibrium gas composition versus purge rate

The typical order of magnitude of the voltage drops due to these factors in an operating Union Carbide fuel cell with 1/4-inch thick electrodes is presented in Figure 8. Voltages involving the electrodes were

Publication Date: January 1, 1969 | doi: 10.1021/ba-1965-0047.ch013

Publication Date: January 1, 1969 | doi: 10.1021/ba-1965-0047.ch013

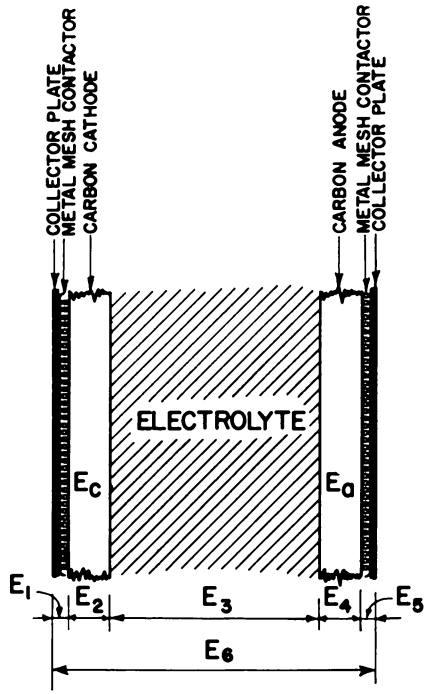

Figure 8. Voltage drop distribution in 1/4-inch carbon electrode fuel cells

Typical voltage drops based on initial cell Performance
Temperature = 45° C.; Open-circuit voltage = 1.06 volt

	Voltage drop, volts	
	50 amp./sq. ft	200 amp./sq. ft.
E_1	0.002–0.005	0.008–0.02
E_2	<0.0002	<0.0008
E_3 ($^1/_8$-inch gap. calcd.)	0.030	0.120
E_4	<0.0002	<0.0008
E_5	0.002–0.005	0.008–0.02
E_6 (total IR)	0.035–0.040	0.138–0.162
E_c (polarization)	0.130–0.150	0.200–0.220
E_a (polarization)	0.030–0.040	0.080–0.100
Cell voltage	0.86 –0.83	0.68 –0.63

obtained potentiometrically using needles inserted through the rubber frames as probes. The greatest potential drop is associated with polarization voltage losses of the electrodes. Resistive losses in contacts and in the electrodes are very small. The electrolyte contributes the greatest IR loss, accounting for up to 15% of the total loss in the present system at 50 amp./sq. ft. loads and up to 30% at 200 amp./sq. ft.

Reduction of the electrolyte IR loss may be achieved through reduction in electrolyte gap thickness, increase in operating temperature, or reduction in normality of the potassium hydroxide. The influence of temperature is shown in Figure 9, where the IR drop is plotted against current density at four different operating temperatures. Its significance is evident from the fact that at the overload current of 200 amp./sq. ft., an increase in operating temperature from 35° to 60° C. results in roughly a 0.07 volt increase in cell voltage, corresponding to more than 0.5 volt for an eight-cell battery. The greatest factor is thickness. Again comparing 200 amp./sq. ft. operation, a reduction in the $^1/_8$-inch electrolyte gap to $^1/_{16}$-inch would improve the voltage by 0.060 volt per cell at 45° C. The effect of the resistive losses on terminal voltage is shown in Figure 10, where the polarization of a $^1/_4$-inch carbon electrode fuel cell with $^1/_{16}$-inch gap is measured with and without the resistive components. This figure also illustrates the flat IR free polarization curve obtained with the Union Carbide electrodes.

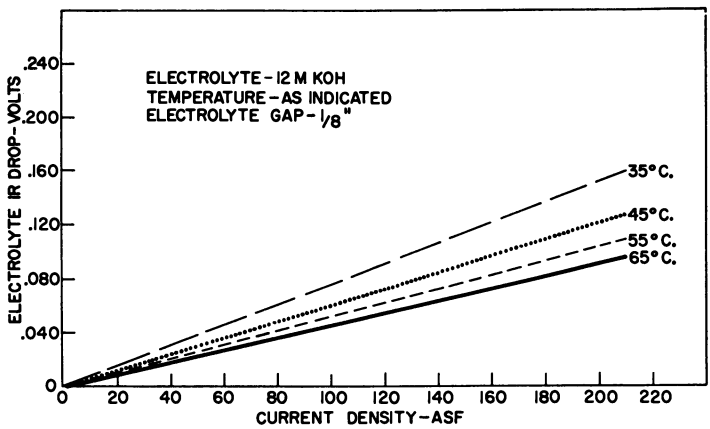

Figure 9. Electrolyte voltage drop versus temperature

Parasitic Currents in the Electrolyte System. Another source of power loss in any series-connected battery system having a common electrolyte manifold is the internal current which flows through this manifold between the individual cells. A mathematic analysis of the various resistance and potential components of the circuits involved in such batteries has been made and fed into a computer program to calculate these currents as a function of the number of cells and cell position. Measurements of these internal currents in an actual system compared very well with those calculated from this program. The magnitude of this current in a 12-cell, 12 x 14 inch battery is indicated in Figure 11. The dashed line indicates the effect of inserting the inlet orifices

Publication Date: January 1, 1969 | doi: 10.1021/ba-1965-0047.ch013

between the inlet manifold and the cell. The parasitic losses were cut in half by introducing this high resistance path.

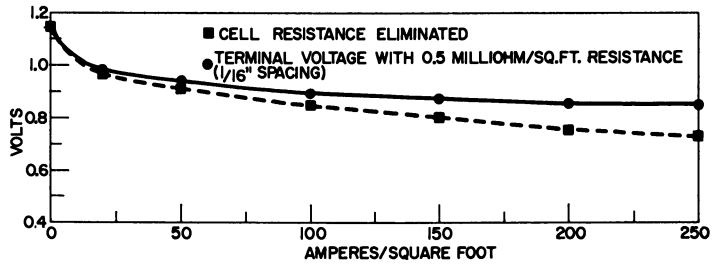

Figure 10. Polarization curve of hydrogen-oxygen fuel cell
Atmospheric pressure, 60° 1/4-inch carbon electrodes

Water Transpiration. The desirability of removing the water by transpiration through the electrodes into the gas stream has been mentioned. Fractional factorial experiments have been carried out to determine the effects of temperature, gas flow rate, electrolyte concentration, and current density on the rate of water transpiration through a number of types of carbon electrodes. Some of the experimental data from this work are presented in Table II. The influence of temperature on the vapor pressure of water over the system was by far the dominant one. Variations in the electrolyte flow rate had only a slight effect as did variations in the gas flow rate above rates equivalent to approximately fifteen times the use rate.

Table II. Fractional factorial experiment with seven-cell fuel module

Load level, amp./sq. ft.[a]	*Gas flow rate,*[b] *cu. ft./hr.*	*KOH flow rate,*[b] *gal./hr.*	*Water transpired, ml./hr.*	*Gas flow rate, cu. ft./hr.*	*KOH flow rate, gal./hr.*	*Water transpired, ml./hr.*
	Anodes—45° C.			Anodes—60° C.		
0	20	10	0.75	38	10	5.79
42	20	5	1.62	20	10	6.45
42	38	10	1.16	38	5	6.80
62	20	10	2.05	20	5	5.60
62	38	5	1.46	38	10	4.33
	Cathodes—45° C.			Cathodes—60° C.		
0	16	10	0.68	29	10	3.59
42	16	5	0.21	16	10	2.61
42	29	10	0.0	29	5	4.11
62	16	10	0.25	16	5	4.0
62	29	5	0.61	29	10	2.98

[a] Temperature and battery load measurements are within ±3% of indicated value.
[b] Gas and electrolyte recirculation rates are within ±10%.

Current density also had very little effect on the transpiration rate in the range 0 to 62 amp./sq. ft. This is an interesting fact since it is

Publication Date: January 1, 1969 | doi: 10.1021/ba-1965-0047.ch013

known from the basic electrochemistry of the system that water is generated at the hydrogen electrode and consumed at the oxygen electrode. This should result in a dilution of the electrolyte in the anode and a concentration in the cathode, with this change being a function of the current density and the porous character of the electrode. It was found that the anode did transpire roughly twice as much water as did the cathode, but, particularly at higher temperatures, this seemed to occur whether the system was at open circuit or under load.

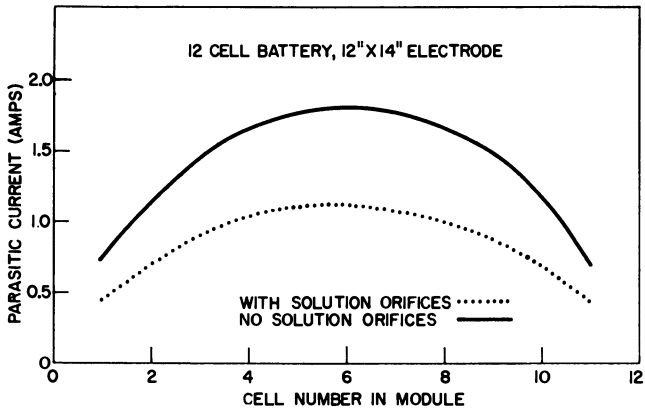

Figure 11. Internal leakage current in a series battery

Another set of experiments was carried out to determine the current density limit as defined by the maximum water transpiration rate for the standard $^1/_4$-inch carbon electrode system in terms of the temperature of a 12*N* potassium hydroxide electrolyte. The results are shown in Table III. Operation with more dilute electrolyte or with thinner or more porous electrodes will increase these limiting values at any given operating temperature.

Table III. Limiting Current Density in Terms of Equivalent Water Removal

Condenser (gas) temperature: 20° C.
Electrolyte: 12*N* KOH
Gas Flow: Above 10 cu. ft./hr./sq. ft.
Electrode Material: $^1/_4$-inch standard baked carbon

Temperature, ° C.	35	50	65	80	100
Water removal rate (current density equivalent, ma./sq. cm.	10	30	60	100	180

Self-Regulation. In previous paragraphs the authors have illustrated some of the ranges within which the various fuel cell operating parameters are optimum. An important feature of the present Union Carbide fuel cell is that these ranges are broad enough and their interaction on one another in such direction that the batteries tend to

Publication Date: January 1, 1969 | doi: 10.1021/ba-1965-0047.ch013

be self-regulating—that is, deviations from steady-state operating conditions tend to change conditions to restore an equilibrium condition.

For example, assume that the battery is operating at a steady state in which the voltage, current, temperature, and flow rates are fixed, and water is being removed at a rate equal to the rate of production so that the electrolyte concentration is invariant. The system is now in a state of dynamic equilibrium, and a change from these steady state conditions will automatically tend to be corrected. A decrease in battery temperature, for example, increases the internal resistance, increases the polarization loss, lowers the rate of electrolyte evaporation, and lowers the temperature difference between the battery and the heat sink, thus lowering the heat loss. Each of these effects separately and jointly tend to raise the battery temperature back toward the original steady-state value.

Consider now a change in operating requirements—for example, a 50% increase in the output power load. The voltage will drop slightly, and the current will increase by slightly more than 50%. The rate of water production will increase in proportion to the current, tending to dilute the electrolyte and increase the water partial pressure. The increase in heat generation will increase the battery temperature until the new ΔT between the battery and the heat sink establishes a new steady-state temperature. At the higher battery temperature, water is removed more rapidly at the same fixed gas recirculation rate, aided in this tendency by the electrolyte dilution. The net effect is to establish a new temperature distribution and new electrolyte concentration in which steady state would be maintained.

There are practical limitations on this principal of self-regulation since, for a particular setting of the flow rates of electrolyte or of the power level, the steady-state conditions toward which the system tends may be outside the desirable range of fuel cell operating parameters. For example, a call for maximum power output over an extended period combined with normal electrolyte circulation rates may easily produce a new steady-state battery temperature exceeding the maximum rating temperature of the materials of construction. For this reason, a maximum temperature thermostatic control is normally provided as the only operational control in Union Carbide fuel cell power plants.

Battery Construction

Up to this point, the important basic physical and electrochemical fuel cell parameters have been presented. In the following sections, the methods and principles used in actual construction of successful fuel cell power supplies are discussed.

Publication Date: January 1, 1969 | doi: 10.1021/ba-1965-0047.ch013

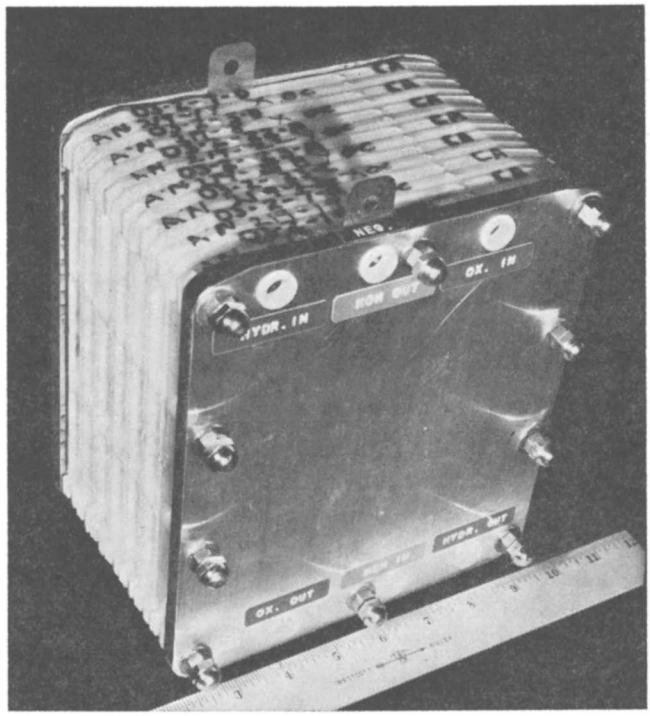

Figure 12. Anode end of 6 x 6 inch battery

Battery Size. For power supplies greater than few watts, it is desirable that the electrodes be of some substantial area to minimize weight and volume associated with assembly materials and manifolding. The two larger sizes which have been used to date as standard by Union Carbide are (1) the nominal 6 x 6-inch illustrated in Figure 12, which has an active electrode area of approximately 0.20 sq. ft.; and (2) the nominal 12 x 14-inch battery illustrated in Figure 1, which has an active electrode area of approximately 0.93 sq. ft.

For most fuel cell battery systems, the size limitation is often defined by the available electrode fabrication facility. However, distribution of feed gases uniformly across the electrode face and removal of heat becomes increasingly more difficult as the electrode area increases, and these features plus framing and other construction problems may introduce a practical size limit. Building up a large power supply from a set of smaller modules rather than one large one permits replacement of a weak unit which otherwise might have made it necessary to remove the entire battery.

Basic Cell Design. A bipolar electrode unit cell forms the basic unit from which the Union Carbide fuel cell batteries are constructed.

Publication Date: January 1, 1969 | doi: 10.1021/ba-1965-0047.ch013

Figure 13 indicates the present 6 x 6-inch system, with Figure 13*A* indicating the electrolyte flow path and porting and Figure 13*B*, the gas flow path and porting. The dark circles are the O-ring cross sections. The actual components, in the order of their assembly, are shown in Figure 14. These include, from left to right, the framed anode, the nickel mesh contactor, a nickel-plated copper gas barrier, a Neoprene insulator sheet, a second gas barrier, nickel mesh contactor, and the cathode. The appropriate passages and porting are molded into the polystyrene frame members to handle the necessary electrolyte, hydrogen and oxygen feed and discharge streams.

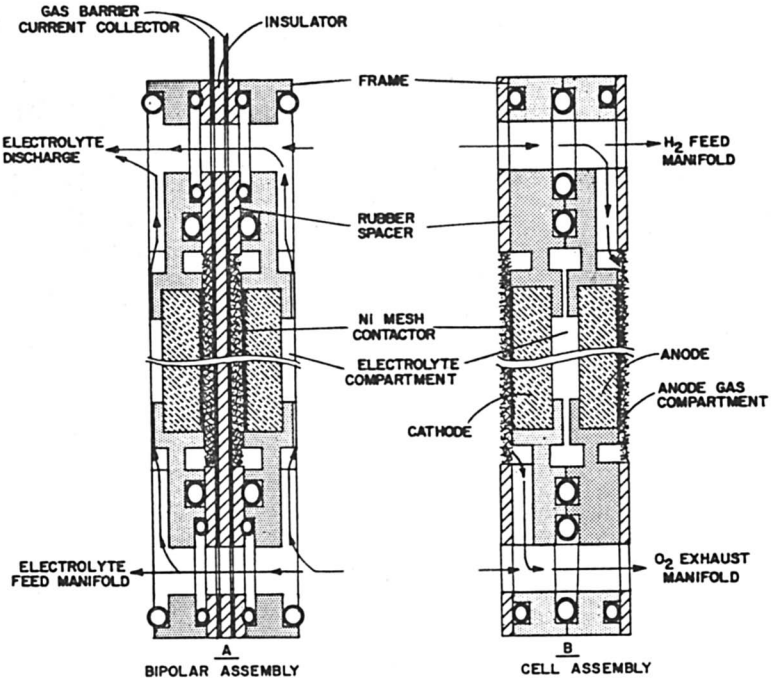

Figure 13. Unit cell design

The framed electrode to the left shows the electrolyte face to which the electrolyte is fed through two small ports located inside of the protruding loops in the O-ring. From there, the electrolyte passes upward through a series of small distributor slots and across the electrode face and out of a similar configuration at the top of the frame. The inlet and exit holes in this frame form the manifold down the length of the multicell battery when a number of electrodes are placed together in the battery structure. The woven nickel wire mesh is surrounded by a $^1/_{16}$-inch thick Neoprene gasket. This nickel mesh provides a gas-per-

Publication Date: January 1, 1969 | doi: 10.1021/ba-1965-0047.ch013

meable electrical contact between the back of the carbon electrode and the metal gas barrier which separates the oxygen from the hydrogen gas spaces. In this particular construction, used primarily for laboratory studies, a second gas barrier is included which is separated from the first barrier by a thin rubber insulator sheet, properly ported to permit gas and electrolyte flow through the manifold. This double barrier permits connecting the cells of such an assembly either in parallel or in series and also permits shunting an individual cell, should it decline in performance.

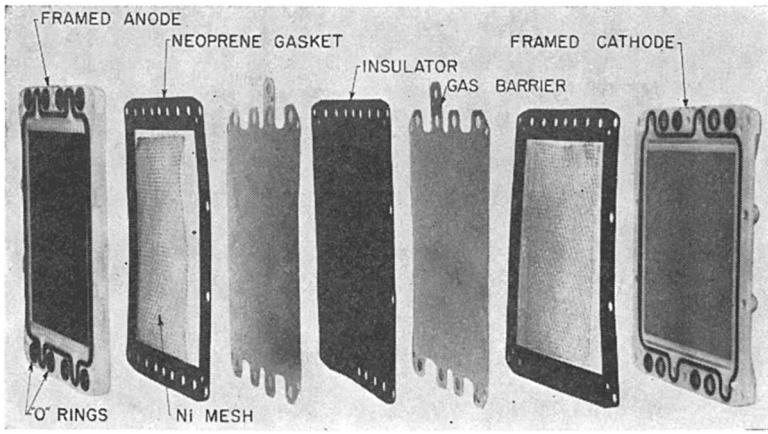

Figure 14. Battery components

In this modification of the manifold, two ports are used to carry each of the fluids involved. For example, on the cathode (on the right of Figure 14), the first and fourth upper ports carry oxygen into the cell. The oxygen stream exits at the bottom of the frame through the third and sixth ports, diagonally across the electrode face. Hydrogen is fed to the anode through the third and sixth ports at the top of the cell and is discharged from the first and fourth ports at the bottom. The electrolyte flows into ports two and five at the bottom of the electrode and out of the ports two and five at the top. Both the cathode and anode frames are identical. When placed with the gas faces toward each other as in Figure 13*B*, separated by the gas barrier, each gas is sent through its separate port without intermingling.

Battery Assembly. The various components are assembled into individual bipolar units and then the appropriate units are assembled on metal tie rods with suitable end plates to form the finished battery. Drilled and tapped holes in the end plates permit ready coupling to the external gas and electrolyte systems through standard fittings. To meet the usual requirements of voltages on the order of 6, 12, 24, or 28 volts

Publication Date: January 1, 1969 | doi: 10.1021/ba-1965-0047.ch013

d.c., a package size using seven to nine cells to provide nominally 6 or 7 volts has been chosen as standard although other combinations can of course be assembled.

Electrode Framing. For the 6 x 6-inch size, the ported frame is injection molded directly around the carbon electrode providing an appreciable economy in the generation of the finished assembly. For the larger 12 x 14-inch size, a rubber frame is used; this also contains the necessary manifolding. This frame is molded separately and then snapped on over the electrode. Techniques for utilizing the lower cost injection molded system for this large size have proved difficult to develop because of the strains introduced in the molding operation. Built-in raised ribs coupled with the elasticity of the rubber provide the required seals, thus eliminating the O-ring insertion problems involved in the 6 x 6-inch unit and thereby simplifying the assembly operation.

Another approach, which has proved successful on smaller sized units, involves casting an epoxy shell completely around the entire battery assembly. Such a unit, built with $^1/_4$-inch carbon electrodes

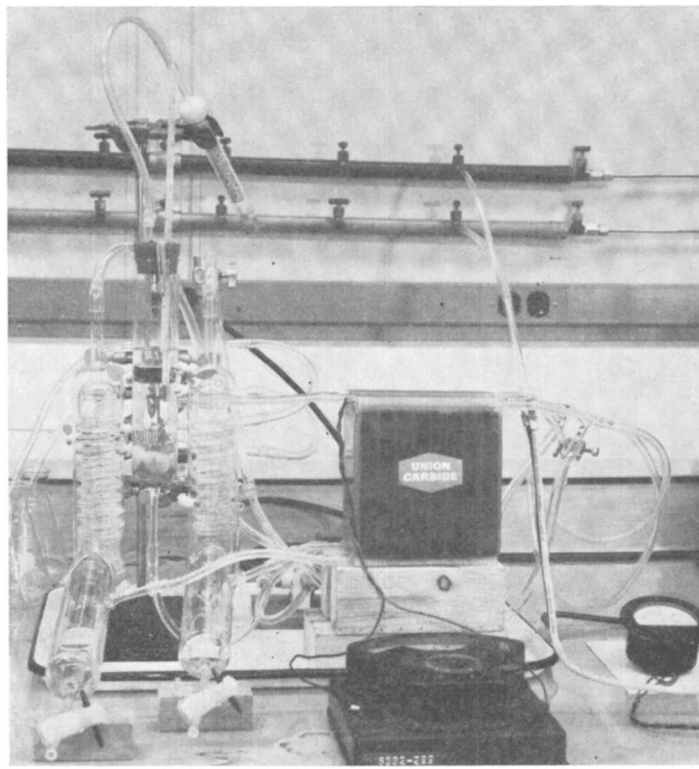

Figure 15. Epoxy potted 1/4-inch carbon electrode battery

Publication Date: January 1, 1969 | doi: 10.1021/ba-1965-0047.ch013

and measuring roughly 3 x 5 x 6-inches is shown in Figure 15. It weighs about 3 pounds and will deliver 20 watts at 50 amp./sq. ft.

Thin "Fixed-Zone" Carbon Electrode Batteries. A promising development aimed at drastically reducing the weight and volume of carbon electrode fuel cells is the "fixed-zone" electrode. This electrode is so named because its construction generates a succession of layers of markedly different repellency toward the electrolyte. This results in electrolyte penetration to a fixed depth. A sketch of one form of this construction is shown in Figure 16. The catalyzed carbon layer is readily wet, the nickel phase highly repellent but porous. Electrodes of this construction weigh one third to one fourth as much as the standard $^1/_4$-inch carbon and can be made in thickness from $^1/_{64}$ to $^1/_{16}$-inch. An important advantage gained with these electrodes is their ability to transpire water at roughly three times the rate of the $^1/_4$-inch carbon permitting invariant electrolyte operation as high as 200 amp./sq. ft. Increased performance on air is also obtained.

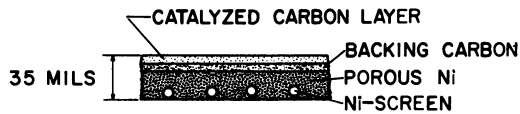

Figure 16. Cut through a thin fixed-zone electrode

This type of electrode is particularly amenable to the potted epoxy type construction. Figure 17 is a photograph of a 50 watt, 16-cell air-battery made with the thin "fixed-zone" electrodes. It has twice the number of electrodes, but the weight is the same as that of the battery of Figure 15. This particular 6-volt battery is built with pairs of cells connected electrically in parallel and eight sets of these in series. In this manner, a longer life expectancy is obtained as compared with a purely series-connected battery, since the more active cell can carry a larger share of the total current than the weaker one of the pair at the common polarization level. This tends to prolong the life of the weaker ones and thereby of the battery unit.

Air-Breathing Batteries. Most of the work done to date with carbon electrodes has utilized hydrogen and oxygen. It is obvious, however, that operation of fuel cells utilizing oxygen from the air is of major importance for most potential commercial as well as certain noncommercial applications. Two significant limitations are imposed in such a consideration: (a) the dilution of the oxygen by inert nitrogen; and (b) the presence of a few hundredths of a per cent of carbon dioxide. The influence of the inert diluent was discussed previously. The problem of the carbon dioxide requires either a carbon dioxide rejecting electrolyte or a system

Publication Date: January 1, 1969 | doi: 10.1021/ba-1965-0047.ch013

with some significant tolerance for carbon dioxide. Our present Union Carbide system falls in the latter class.

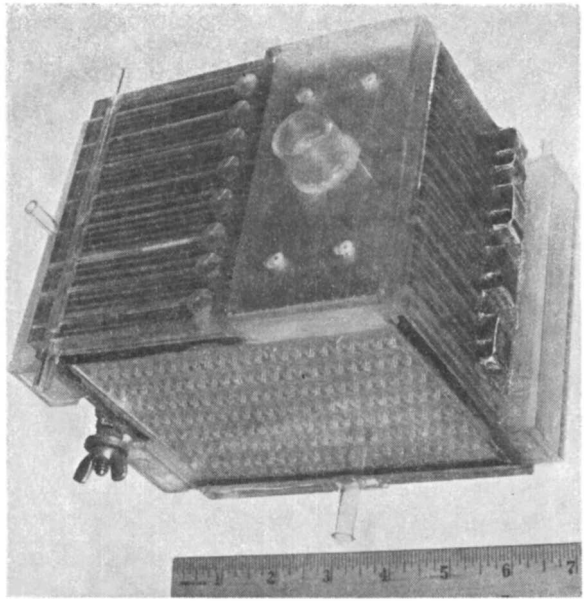

Figure 17. Epoxy potted thin electrode battery

Carbon electrode cells, such as those shown in Figure 18 were still operating after 4000 to 5000 hours in normal laboratory air, even though a potassium hydroxide electrolyte is used. Referring to Figure 6, for the particular $^1/_4$-inch carbon electrodes used for these measurements, the polarization on operation in air at 50° C. is only about 50 mv. lower than in oxygen over most of the range to 100 ma./sq. cm. Construction of such air-breathing units may be considerably different than that for hydrogen-oxygen batteries. The free accessibility of air eliminates the need for the oxygen positive pressure recirculation and feed system. Normal convection and diffusion readily supplies the necessary volume of air. The high repellency of the Union Carbide air cathode permits operation under conditions where the hydraulic head is considerably greater than the external air pressure without gross intrusion of the electrolyte into the electrode pores.

A feature of the particular concentric triangular construction of the cells in Figure 18 is that the inner anode triangle is smaller than the outer cathode. This gives a larger cathode area and thereby reduced polarization of the critical electrode for a given anode size, weight, and current density. The triangular cell also permits close packing of the units in the generation of multicell batteries.

Publication Date: January 1, 1969 | doi: 10.1021/ba-1965-0047.ch013

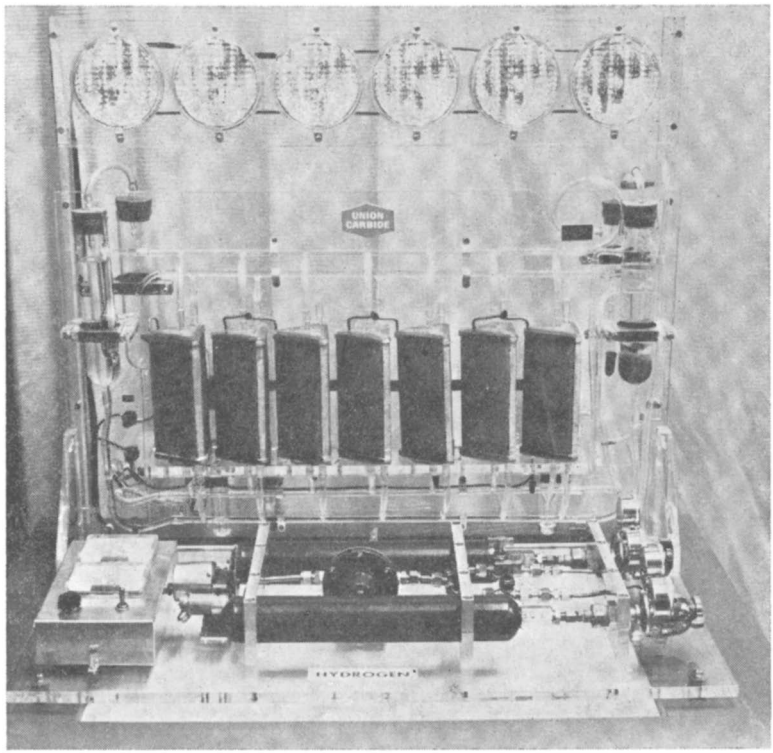

Figure 18. Triangular air-hydrogen cells

Publication Date: January 1, 1969 | doi: 10.1021/ba-1965-0047.ch013

Power Density

Variations in electrode and cell thickness and frame and case design have been shown to yield significantly different weights and sizes to batteries of a given power level. The several hydrogen-oxygen systems discussed here are shown in Table IV to compare their relative power densities at 50 amp./sq. ft.

Table IV. Battery Power Densities

Figure No.	*Frame or shell*	*Electrode thickness, inch*	*Size, inches*	*No. cells*	*Weight, lb./kw.*[a]	*Size, cu. ft./ kw.*
1	Rubber	1/4	12 × 14	32	176	2.3
12	Plastic	1/4	6 × 6	8	350	2.9
15	Epoxy	1/4	3 × 5	8	150	2.6
17	Epoxy	Thin	3 × 5	8	62.5	0.87

[a] Without electrolyte.

Changes in the number of cells per end plate will vary these numbers somewhat. Higher current densities will, of course, lower these numbers almost linearly. The 12 x 14 inch battery, for example, will de-

liver 1 kw. from 53 pounds of battery at 200 amp./sq. ft. or, in delivering the 400 amperes motor starting load, its weight to power ratio was only 30 pounds per kw. Larger batteries are being designed with the thin electrodes. These will weigh approximately 20 lb/kw. and have a volume of about 0.5 cu. ft/kw. utilizing a current density of 50 amp./sq. ft. Complete power plants built with such batteries will weigh between 25 and 50 pounds per kilowatt depending on the power level and rated current density. These figures do not include the fuel supply.

Acknowledgment

The authors wish to acknowledge the efforts of their coworkers and of George R. Drengler and George E. Smith in particular for much of the engineering work reported in this paper. Our appreciation is also due the Air Force's Wright-Patterson Aeronautical Systems Division and the Navy's Bureau of Ships for their support of a portion of this effort under their contracts No. AF 33(616)-7256 and NObs 78633, respectively.

Literature Cited

(1) Evans, G. E., "Fuel Cells," CEP Tech. Manual, Am. Inst. Chem. Engr., 1963, pp. 6–10.
(2) Richardson, D. R., *Chem. Eng.* **68**, 83 (May 1, 1961).

RECEIVED June 22, 1964.

Publication Date: January 1, 1969 | doi: 10.1021/ba-1965-0047.ch013

14

Fuel Cells Incorporating Ion Exchange Membranes

Current State of Development

CARL BERGER

Astropower Laboratory, Douglas Aircraft Co., Newport Beach, Calif.

Publication Date: January 1, 1969 | doi: 10.1021/ba-1965-0047.ch014

The current state of development of ion exchange membrane fuel cells is reviewed with a discussion of approximate upper limits of performance and particular emphasis on the actual operation of such devices at the present time. The fuel cells analyzed are the single membrane fuel cell, the hydrogen-bromine fuel cell, and the dual membrane fuel cell. There are substantial differences between anticipated performances and those actually realized. Much of this is due to the problems inherent in removal of product water and represents definitive engineering limitations. Projections are made with respect to power and volume densities achievable in the foreseeable future. Suggestions are presented relative to fruitful avenues of research and development in the future.

The upsurge of interest in the last several years in fuel cell research is abundantly documented in the literature found in scientific, engineering, and business articles. The work reported here concerns applications of semipermeable membranes—in particular, ion-membrane fuel cells. Most representative of this group are the single membrane fuel cell *(16)*, the dual membrane fuel cell *(5)*, and a significant hybrid, the gas-liquid single membrane fuel cell *(6)*.

It may be of value to review briefly the advantages and disadvantages of an ion-membrane fuel cell in comparison with fuel cells with porous electrodes in contact with liquid electrolytes. Some of the advantages are:

1. Construction of electrode-catalyst configurations is simplified—the

In Fuel Cell Systems; Young, G., el al.;
Advances in Chemistry; American Chemical Society: Washington, DC, 1969.

exact sizing of electrode pores, the criticality of catalyst deposition, and the requirements for waterproofing are all minimized.

2. There is no loss of gaseous reactants due to pore inexactitude. The gaseous reactants cannot be lost to the electrolyte but simply rebound back into the catalyst structure or the gas compartment if they do not react.

3. Compactness.

4. Light weight.

The disadvantages of the ion-membrane fuel cell are:

1. Moderate current densities at practical voltage levels have been achievable although the compactness of configurations mitigates this problem to some extent.

2. Heat removal is more difficult than in systems where an electrolyte can be circulated—e.g., approximately 30 to 50% of the realizable power in a fuel cell ends up as heat. The hydrogen-bromine fuel cell (HBFC) and the dual membrane fuel cell (DMFC) described here represent compromises instituted to overcome this problem.

3. The most highly developed ion-membrane fuel cells are organic and therefore sensitive to heat even when in an aqueous environment. The hydrolysis of the ionic groups in the organic matrix (in the presence of catalyst) is a possibility. The probability of such an occurrence would increase with elevation in temperature.

4. Water removal from electrode-catalyst sites represents a variable difficult to control quantitatively and directly influences voltage output.

The basic membrane used in the three generalized configurations described here are of two physical species—a homogeneous fabric supported polymer (*19*) and a grafted polymeric type (*1*). In both cases the polymers are sulfonated polystyrenes cross linked to a greater or lesser extent. The mechanism of operation of the membrane, however, differs appreciably in the three types of fuel cells (Figure 1). All of the fuel cells shown in Figure 1 have been amply described in the literature (*4–6, 12, 13, 16*).

The single membrane fuel cell (Figure 1*A*) uses hydrogen and oxygen as reactants. Hydrogen is converted to H^+ at the anode, electromigrates through the membrane, and unites with a reduced oxygen species at the cathode to form water, which must be removed.

In the hydrogen-bromine fuel cell (Figure 1*B*), the anode reaction is

$$H_2 \rightarrow 2H^+ + 2e$$

and the cathode reaction

$$Br_2 + 2e \rightarrow 2Br^-$$

The net result of the reaction is the formation of hydrogen bromide in the aqueous catholyte.

Publication Date: January 1, 1969 | doi: 10.1021/ba-1965-0047.ch014

In the dual membrane fuel cell (Figure 1C), the anode and cathode reactions are identical to those in the single membrane fuel cell. The difference in these cells is that in the former a layer of sulfuric acid is found between two membranes which serves to level out membrane water balance problems and functions importantly as a heat transfer fluid.

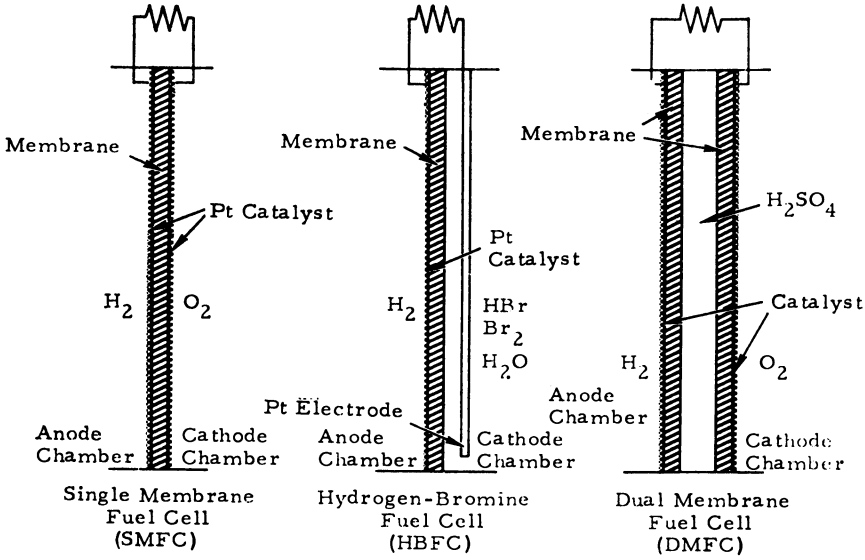

Figure 1. Three representative ion-membrane fuel cells

Single Membrane Fuel Cell

The single membrane fuel cell (SMFC) is the system which has been most intensively investigated in the last few years. The membrane used in this case is a completely water leached ion-membrane where all of the electrical transport is due to the migration of H^+ ion formed at the anode from one sulfonic acid group to another until water is formed at the cathode.

If the ion exchange membrane is considered a polymer network of a linear or branched variety crosslinked at various sites and swollen with solvent, an adequate physical network can be envisioned for the transport of solute. It is apparent in envisioning this network as a "solid gel" that the velocity of H^+ ion in this network will be altered and if, as the theory of aqueous electrolytes indicates, the velocities of ions in "gel" structures is a function of the increased viscosity of the internal solvent phase (8), then it follows that a quasi-Stokes frictional resistance to flow (F)

$$F = 6\pi\eta r \tag{1}$$

where η = viscosity r = radius of migrating particle

Publication Date: January 1, 1969 | doi: 10.1021/ba-1965-0047.ch014

should be increased producing slower ionic migration whether the forces are purely those of diffusion or electromigration. In electromigration, this retardation will be manifested by lower ionic mobilities. For example, the ionic mobility of H^+ ion in an aqueous electrolyte is about 362 x 10^{-5} cm./sec. in contrast to a velocity of H^+ ion in sulfonated phenol formaldehyde resin of about 19 x 10^{-5} cm./sec. (*8*).

If one accepts as an operating basis that the SMFC is now utilizing the optimum catalysts obtainable for the hydrogen-oxygen system and that practical operating voltages much greater than 0.93 volt are not likely to be obtained (*26*) (a fact that the writer concurs in as a result of his experience in development of hydrogen-oxygen fuel cells), then theoretically the net power that can be obtained will be a function of the ionic mobility of the H^+ ion over a given transit thickness.

Approximate calculations may be of some value in guiding us with respect to the limiting current densities that can be achieved in a leached H^+ transport system. Using the approach of Kortum and Bockris *(21)* and Spiegler and Coryell (*28*), the limiting current density of a leached membrane system may be defined as

$$\delta = \frac{R}{Z_t F} \cdot \frac{\lambda TC}{l_L} \tag{2}$$

where

δ = thickness of diffusion layer
R = constant
Z_t = valence
F = Faraday
λ = ionic mobility
C = gram ions/mole
l_L = limiting current

Substituting appropriate values

δ = thickness of diffusion layer = thickness of membrane = 0.0165 cm.

$$\lambda_{H^+ \text{membrane}} = \lambda_{0.1\ H^+ \text{solution}} = 35 \text{ ohms}^{-1} \text{ sq. cm.}$$

$$C = 0.6 \text{ gram ion/liter}$$

we find l_L = c. 330 ma./ sq. cm.

The writer recognizes that Equation 2 holds strictly for cases at infinite dilution and that the utilization of ion exchange capacity as a concentration term is only approximate, but, for our purposes the approximation is sufficient.

Another means of corroborating the order of magnitude of l_L is to use experimental data of resistances of membranes in the H^+ form in calculat-

Publication Date: January 1, 1969 | doi: 10.1021/ba-1965-0047.ch014

ing achievable current density limits. The data presented by Grubb (*15*) on the specific resistance of ion exchange membranes yields on Ohm's Law calculation for a membrane thickness of 0.0165 cm. current densities in the range of 400 ma./sq. cm. Finally, it is of value to note that Maget *(13)*, in his extrapolations of limiting current density for SMFC, projects values of the order of 500 ma./sq. cm.

It can be assumed, based on the preceding approximations, that high current densities are achievable by the SMFC and indeed laboratory evidence *(25)* indicates that such is the case in single cell test units. It may then be valid to initiate thinking of thin ion membranes (<0.02 cm.) as diffusion barriers through which, in theory, large amounts of current can flow in a fashion analogous to the thin diffusion barriers in stirred aqueous electrolytes.

Candidly, while the preceding analysis is of interest in small, single cell test configurations, engineering factors have played a critical role in limiting the achievements of higher power densities in multiple fuel cell configurations. First, the necessity of uniform rapid water removal at high current densities, which must be performed by gas circulation or a combination of condensation and capillary wick action is unsatisfactory *(12)*. Inability to remove water uniformly and rapidly enough can cause voltage fluctuations in individual cells and can in fact "drown" electrodes causing failure. Another important engineering problem is the removal of heat generated in the membrane. The removal of heat can be performed in a number of ways, but in all cases involves transit through a gaseous phase. In any case, it is our conviction that if the heat generated could be conducted into a fluid medium, the heat transfer considerations related to the rapidity of heat removal and energy expended for such transfer would be more favorable from over-all systems considerations. It is interesting to note that in larger multiple-cell power sources, that heat transfer fluids will most likely be introduced into cell separators to carry away large quantities of waste heat.

Publication Date: January 1, 1969 | doi: 10.1021/ba-1965-0047.ch014

Hydrogen-Bromine Fuel Cell

The hydrogen-bromine fuel cell (HBFC), a secondary fuel cell device (*5*), represents an attempt to overcome the engineering difficulties inherent in one aspect of the SMFC, particularly heat transfer problems. A comparison of the heat transfer coefficients of oxygen, hydrogen, and water indicates the advantages of using aqueous solutions of bromine-hydrobromic acid as a catholyte for the HBFC.

In addition the bromine–hydrobromic acid electrode is a highly reversible couple compared to the oxygen electrode in the SMFC. Oster (*25*) indicates that a certain activation loss of 0.35 to 0.40 volt occurs at the oxygen electrode in the SMFC. Calculations and experimental data

(5, 7, 10) show that activation overvoltage for the HBFC on discharge can be described as follows:

$$\eta = \frac{0.059}{0.6} \log i + \frac{0.059}{0.6} \log (3.10^{-3}) \quad (3)$$

where

η = activation overvoltage
i = current density in amps/sq. cm.

Therefore, at 100 amps/sq. cm. on a plain electrode surface, the activation overvoltage for reduction of bromine to bromide ion is equal to —0.05 volt.

However, a disadvantage of the bromine–hydrobromic acid couple is that the equivalent weight of bromine is considerably greater than oxygen, an important consideration in a practical engineering sense. This is mitigated to some extent by other considerations. For instance, when electrical regeneration of secondary fuel cells is called for, the higher voltage efficiency of the HBFC requires less weight of solar cells for recharging than a comparable secondary SMFC operating at the same voltage.

Once again our analysis of the maximum current density limitation will be based on the membrane as the limiting factor in fuel cell performance. It is also assumed that the anode and cathode are not limiting with respect to current flow.

A closer look at the ionic species involved in the performance of this cell is warranted before proceeding further inasmuch as this is an important factor in determining practical cell performance. The over-all reaction of the cell is

$$H_2 + Br_3^- \rightleftarrows 2H^+ + 3Br^- \quad E_0 = 1.056 \quad (4)$$

The voltage of the cell can be determined by the Nernst relationship

$$E = E^0 - \frac{RT}{nF} \ln \frac{[H^+]^2}{[H_2]} \frac{[Br^-]^3}{[Br_3^-]} \quad (5)$$

Equation 5 implies that the major portion of the bromine exists in solution as Br_3^-. Since the equilibrium constant for $Br_2 + Br^- \rightleftharpoons Br_3^-$ is 17, and the equilibrium constant for $Br_3^- + Br_2 \rightleftharpoons Br_5^-$ is 0.055, it appears that at concentrations in the applicable catholyte range $H^+ = 6$, $Br^- = 6$, $Br_2 = 1 - 2$, the assumption is justified; for example, at $Br_2 = 1$, $Br_3^- = 0.99$ and $Br_5^- = 6 \times 10^{-4}$.

Proceeding onward to explore the nature of the discharge process at the anode, the ideal situation is where only H^+ and Br^- are in the membrane and Br_3^- is excluded. If this is the case $t_{H^+} + t_{Br^-} = 1$, and hydrogen ion formed at the anode is neutralized by Br^-. Clearly, if Br_3^-

Publication Date: January 1, 1969 | doi: 10.1021/ba-1965-0047.ch014

can diffuse into the membrane and migrate toward the anode, loss of electrical energy can result from the reaction of hydrogen and bromine complex at the noble metal catalyst electrode. It is exactly this problem that Berger and coworkers (5) found to be a limiting factor in cell life. A reformulation of the membrane in order to decrease the mean intramolecular diameter of the membrane was successful in limiting the diffusion of Br_3^- into the membrane and led to long cycling lives of greater than 9000 charge-discharge cycles.

One marked difference between the SMFC and the HBFC is that major transport in the latter is a function of the absorbed hydrobromic acid in the membrane rather than the H^+ ion in equilibrium with the fixed ionic sites of the leached ion exchange membrane. Let us assume that 6*N* hydrobromic acid and 2*N* bromine catholyte solution are in equilibrium with a cation membrane and, if we assume that the migration of bromine into the membrane is strongly hindered, then an imbibition of 2 to 3 milliequivalents of hydrogen bromide per milliliter of membrane volume can be approximated (*20*).

If we assume as previously discussed that the limiting factor in l_L is the membrane itself, then we can fix a number of limiting conditions. For the bromine electrode

$$l_d = \frac{DnF(C)}{(1 - t_-)\delta} \tag{6}$$

or

$$l_d \cong 1.8\ (10^{-1})\ C \text{ amp./sq. cm. } (7) \tag{7}$$

where

$D = 4.10^{-5}$ sq. cm./sec.
$n = 2$ electrons
$F =$ Faraday
$t \cong 0.15$ (max.)
$\delta = 0.05$ cm. (max.)

At solution normality of 6*N* we have an activity (C) of about 2 to 3 (*22*) and therefore could expect a limiting current density of about 360 to 540 ma./sq. cm. even without considering surface roughness factors. The surface factor assumption is reasonable since smooth platinum was utilized for the cathode. We now turn to an analysis of the limiting current at the membrane-anode interface.

Presuming that the hydrogen electrode has its diffusion layer in the form of a membrane upon which the catalyst is imbedded, the diffusion barrier will be a membrane into which H^+ ion is discharged and which

Publication Date: January 1, 1969 | doi: 10.1021/ba-1965-0047.ch014

must be neutralized with electromigrating Br^-. The calculation of the limiting current for the hydrogen electrode may be expressed as (23)

$$l_d = \frac{DnF\,(C)}{(1 - t_+)\delta} \tag{8}$$

or

$$l_d \cong \frac{4 \times 10^{-6} \times (1)\ 96{,}500 \times C}{(1 - 0.85)(0.0165)\ 1000} \tag{9}$$

where

$D = 4 \times 10^{-6}$ sq. cm./sec. (7) $\quad t_+ = 0.85$
$n = 1 \quad \delta = 0.0165$ cm.
$F =$ Faraday

Assuming that the concentration of hydrogen bromide in the membrane has a limiting value of about 2.5 meq. of hydrogen bromide per ml. of resin and that the activity coefficient of 2.5N hydrobromic acid is about 1.2, an effective activity of 2.4 is obtained. Substituting this value into (9) $l_d =$ 325 ma./sq.cm.

Both of the limiting currents derived for the bromine electrode and the hydrogen electrode are deemed to be within conservative limits—for example, the roughness factors have been assumed to be one. Once again we recognize that the value of l_d is approximate, but it is of particular interest when compared to experimentally achievable results (Figure 2).

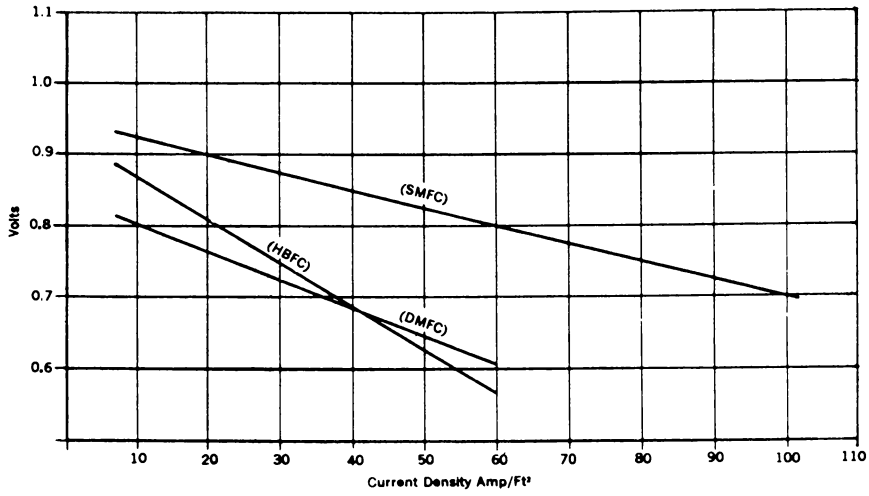

Figure 2. Comparison of discharge curves for SMFC, HBFC, and DMFC

Publication Date: January 1, 1969 | doi: 10.1021/ba-1965-0047.ch014

Dual Membrane Fuel Cell

An effective combination of the best aspects of membrane and free electrolyte fuel cell system is found in the dual membrane fuel cell (DMFC), where the hydrogen and the oxygen electrodes are both placed against cation membranes and a 6*N* sulfuric acid solution interposed between the membranes. It is clear that if we once again make the assumption that ionic diffusion in the membrane is limiting, then limiting current calculations may be performed for both membranes.

$$l_a = \frac{4 \times 10^{-6} \times 1 \times 96{,}500 \times C}{0.15 \times 0.0165 \times 10^3} \tag{10}$$

or

$$l_a \leqq 0.156\ C$$
$$l_a \leqq 94 \text{ ma./sq. cm.}$$

The assumptions made in this case are similar to those in the HBFC. It is assumed that the diffusion coefficient will be equivalent to or less than hydrogen bromide and that the transference number of H^+ is slightly greater than for the HBFC. We have also made the assumption that similar quantities of sulfuric acid are imbibed but that the activity of 2 to 3*N* sulfuric acid is much lower (*17*). There is one factor here, however, which is not present in the HBFC. A film of water forms at the oxygen cathode, the tendency of which is to migrate into the 6*N* liquid electrolyte between the membranes. In practice, interestingly enough, this is borne out by the fact that all the water formed is found ultimately in the central compartment. The film of water which forms can not be removed as rapidly as it is in the SMFC because of the osmotic forces in the membrane and the electrolyte tending to draw the water toward the central electrolyte compartment. The presence of this water film causes significant IR losses and is a limiting factor in the operation of the DMFC.

Engineering Considerations

The approximations presented with reference to current density limitations are of interest when compared to the practical achievements with each type of fuel cell. A graph of fuel cell operating characteristics, based on available publications for the three fuel cells is shown in Figure 2 (*2, 3, 5, 18, 25*).

Single Membrane Fuel Cell. The SMFC shows the most advanced operational capability of the three configurations discussed. An important reason for this is that a great deal more research and development has

Publication Date: January 1, 1969 | doi: 10.1021/ba-1965-0047.ch014

been committed to this concept. Although current densities as high as 150 ma./sq. cm. have been achieved, a number of practical limitations appear to limit gains for the SMFC in multiple fuel cell configurations.

1. Water removal from the area of the oxygen electrode must be carefully controlled so that enough water is removed from each cell of a multiple-cell unit to keep the electrode from drowning or more practically to keep all single cell voltages in a multiple series configuration from widely diverging and tending to instability of cell output (*12*).

The removal of water from the electrode surface in the present apparatus is accomplished by the condensation on a bipolar cell separator of the moisture from the electrode surface. Water removal is effected by a difference in temperature (c. 5 to 10° F.) between the electrode surface and the cell separator. It is clear that the rate of product removal from the reaction site will vary with the temperature differential, fuel gas temperature, and other factors related to the heat removal system. In light of these complicated engineering problems, the writer projects that current densities of about 50 to 75 ma./sq. cm. at 0.78 to 0.72 volt appear to be achievable in multiple units within the next 12 to 18 months, but it is not likely that operating current densities of greater than 100 ma./sq. cm. will be achieved within the next 30 months unless important breakthroughs in engineering know-how occur. This does not appear to be an important limitation at present, since it is likely that operational current densities in the range 25 to 50 ma./sq. cm. will suffice for the initial space missions for which this fuel cell is designated.

2. Some 30 to 50% of the total energy generated in the SMFC results in heat which must be dissipated. This can be affected by heat transfer through metal cell separators with radiative heat loss to space or the recirculation of fuel gas (H_2) to pick up heat and moisture with subsequent cooling and condensation and finally the use of a separate liquid circulation system to remove heat from the separator plate area. If the last approach is used for units in the 1 to 5 kw. range (*27*), then it appears that the weight and volume of the circulation system would at least equal the electrolyte inventory required in the HBFC or the DMFC. In addition, in contrast to the DMFC, the water recovery system for the SMFC requires a separate subsystem for transport and recovery of water, an important factor in decreasing over-all reliability and in adding weight to the system.

3. Reproducibility and the quality control appears to be an important engineering area where more research must be performed. The leached membrane used in the SMFC must have an absolute homogeneity of physical and chemical characteristics to avoid areas of intense heating and uneven water formation and removal. This is avoided to a great extent by the HBFC and DMFC since the electrolyte imbibed by the membranes

Publication Date: January 1, 1969 | doi: 10.1021/ba-1965-0047.ch014

in this system serves as a leveling factor for physical properties and water balance problems.

4. Another possible problem area is the hydrolysis of sulfonic acid groups in the ion exchange matrix, particularly in the presence of noble metal catalysts.

Hydrogen-Bromine Fuel Cell. The HBFC limiting diffusion current is relatively high as indicated (>300 ma./cm.), and when used as a secondary battery, charge acceptance efficiency is high compared to the SMFC system. This is due to the considerable irreversibilities encountered on charging a leached hydrogen-oxygen (SMFC) system compared to the HBFC where overvoltage is a minor consideration. In practical systems this calls for a 20 to 30% greater power requirement for recharging at a given current density (*5*). The major factor which has held back the rapid development of this concept has been the lack of solid advances in membrane technology. Recently (*5*), advances have been made which augur well for the development of this cell. It will continue to suffer, however, from one basic limitation. To prevent the migration of Br_3^- into the membrane, the network of the ion exchange membrane must be made less porous—that is penetration of Br_3^- must be decreased. The consequence of restricting the Br_3^- penetration is a "tighter" internal structure which decreases ionic mobility. It therefore seems unlikely that effective operation of greater than 50 to 60 ma./sq. cm. at 0.62 to 0.57 volt will be achieved in multiple configurations of HBFC in the next 36 months. The maximums could probably be improved by 30 to 50% if substantially more effort is devoted to this type of device than is presently contemplated. It is likely, however, that fuel cell optimization studies will indicate that values of about 30 ma./sq. cm. and 0.72 volt are appropriate for design considerations at the present time. Since these values are satisfactory for secondary battery operation, practical applications in such areas (weather satellites) may be envisioned.

Dual Membrane Fuel Cell. Various experimental considerations indicate the advantages of the DMFC. The membranes are continually in equilibrium with 6*N* sulfuric acid, thereby eliminating problems related to water balance and drying of membranes (*4*). Moreover, the removal of generated heat can be efficiently performed by circulation of the electrolyte. Finally, since water formed at the cathode migrates into the central electrolyte reservoir (*6*), we essentially eliminate the water transfer system required in the SMFC, eliminate complexity, and increase reliability.

Factors detrimental to the achievement of higher operating current densities in the device are the probable low activity of equilibrated sulfuric acid in the membrane, thereby lowering the conductivity substantially as compared to hydrobromic acid of the same concentration in the membrane. Most importantly, the formation of water film on the oxygen

Publication Date: January 1, 1969 | doi: 10.1021/ba-1965-0047.ch014

electrode-membrane interface, suggests a limiting factor, the diffusion rate of the water from the interface into the membrane and the central reservoir. The water film appears to have a definitive means of leaving the area of the oxygen electrode by ordinary mass diffusional processes. If one assumes a diffusion constant of an order equivalent to that used in calculating limiting currents in membranes and circumvents the ambiguities of working with activities at membrane interfaces, then a rate of diffusion of sulfuric acid through the membrane to the oxygen electrode interface of about 8 to 16 ma./sq. cm. for a membrane 0.050 cm. thick or values of about 24 to 48 ma./sq. cm. for membranes 0.0165 cm. thick can be calculated. These values agree rather well with the data obtained during the course of a research program devoted to the DMFC (*6*). It appears likely that using thinner membranes and with sufficient membrane development, current densities of 40 to 50 ma./sq. cm. at 0.67 to 0.63 volt can be achieved in multiple configuration within the next few years. Improvement in this system could be obtained by providing a more open polymer network; however, laboratory efforts (*29*) have indicated that improved current density obtained this way causes increased "osmotic" leakage of electrolyte into the gas compartments. When this occurs, steps must be taken to remove the fluid so that continuous effective performance of the fuel cell can be maintained. This, of course, would decrease the over-all efficiency and reliability of the DMFC.

Because of the simplicity and ruggedness of this fuel cell, the DMFC units have been offered commercially to industry and government since 1962 (*18*).

Publication Date: January 1, 1969 | doi: 10.1021/ba-1965-0047.ch014

Conclusions

The writer has taken operating parameters that he feels may be achieved within the next 12 months for multiple fuel cells of the three general classes of devices discussed here. One must bear in mind that one of these (HBFC), is fundamentally used as a secondary battery. Of particular interest are projections of approximate weight, volume, and power density based on estimates of reasonable voltages and current densities. There are shown in Table I.

Table I. Volume and Weight Factors

Type	*Voltage*	*Amps/ sq. ft.*	*Thickness, inches*	*Pounds/ sq. ft.*	*Volume, cu. ft.*	*Watts/ sq. ft.*	*Kw./ cu. ft.*	*Watts/lb*
SMFC	0.72	75	0.205	1.37	0.0171	55.0	3.2	40.2
DMFC	0.72	30	0.194	1.97	0.0162	21.6	1.33	10.97
HBFC	0.72	30	0.165	1.67	0.0138	21.6	1.56	12.92

It is important to reiterate the basis on which the calculations were made:

1. The weights and dimensions refer to a unit cell with no instrumen-

tation, electrolyte holdup, water removal, or any other system factors considered. For instance, it is clear that in long missions requiring primary cells, the increased weight of fuel needed will tend to improve markedly the watt-hours/lb. obtained from a given system. It is because of this variability of missions in space, on land, or in the sea that no attempt has been made to go beyond the unit cell structure in analysis. Table I however, should be of value as a general starting point for systems analysis and is presented in nonmetrical units for engineering convenience.

2. The SMFC and DMFC are primary cells and therefore not strictly comparable with HBFC.

3. The SMFC has been the object of a far greater investment of time and effort than either the DMFC or the HBFC. It is almost certain that the values of watts/lb. and kw./cu. ft. for the latter two would increase two to four times with an intensive development effort. Projections made in this paper assume that the development of neither the DMFC nor HBFC will be at as high a level in the next 30 months as has been the case with the SMFC.

It may be of value, to suggest possible research and development concepts that appear promising in the improvement of ion membrane fuel cells.

1. First, because of processing advances in producing thinner membranes (*1*) the membrane may be regarded as less of a structural electrolyte and more as a diffusion barrier up against an electrode. In this conceptual framework, we find that the membrane, for instance, can be regarded as a means for producing low cost porous electrodes since thin membrane barriers will lessen the need for the elegant procedures used at present for preparation of metal and carbon electrodes. Moreover, such electrode membrane systems could be used in various electrolytes, aqueous and nonaqueous. Finally, if very thin membranes are used (<0.01 cm.), there should be little difficulty in eventually sustaining current densities in excess of 200 ma./sq. cm. at reasonable voltage levels.

2. Inorganic membrane systems have strong potential as intermediate temperature range (100° to 200° C.) solid electrolytes both as cationic and anionic systems. Recent results (*9, 24*) indicate that inorganic membranes with resistivities of 10 to 12 ohm-cm. have been formulated.

3. Research relevant to attaining a high level of quality control for membranes and membrane electrode assemblies would appear to be of much value in promoting the commercial manufacture of multiple unit fuel cells.

4. The exploration of the advantages in using liquid ion exchangers would appear to be of value (*11*).

5. The possibility of using foamed ion exchange membranes to

Publication Date: January 1, 1969 | doi: 10.1021/ba-1965-0047.ch014

achieve low electrical resistance lightweight membranes should be considered.

6. Although considerable effort has been expended in recent years in basic membrane research (*1, 8, 14, 15, 20, 26, 28*), intensified and well planned efforts may yet bring important break-throughs in this field.

Acknowledgment

The writer wishes to acknowledge his debt to those individuals who have been his coworkers in the past on various fuel cell projects—R. Lurie, H. Viklund, V. Masse, F. Leitz, S. Jain, and H. Perry—and to the agencies which have provided support for these activities—the National Aeronautics and Space Agency and the United States Air Force. The writer also wishes to acknowledge the useful discussions with Dr. D. H. McClelland of Astropower relevant to theoretical considerations.

Publication Date: January 1, 1969 | doi: 10.1021/ba-1965-0047.ch014

Literature Cited

(1) American Machine and Foundry Co., AMFion C-60.
(2) *Ibid.*, Curve calculated presuming use of AMFion C-313 membrane for dual membrane fuel cell.
(3) *Ibid.*, Curve calculated presuming use of AMFion C-313 membrane for hydrogen-bromic fuel cell.
(4) Berger, C., Lurie, M. R., Shuman, R. J., and Viklund, H. J., Contract No. DA-44-009-ENG-4554, Final Report U.S. Engineering and Development Laboratory, Ft. Belvoir, Va.
(5) Berger, C., Lurie, M. R., Viklund, H. J., Contract AF19 (604)-8508 (1960-1962).
(6) Berger, C., Perry, H., Jain, S., Leitz, F., TRW Subcontract RD 236560 to Ionics, Inc. (1962).
(7) Chang, F. L., and Wick, H., *Z. Phys. Chem.*, **A172,** 448 (1935).
(8) Despic, A., and Hills, J. C., *Trans. Faraday Soc.* **51,** 1260 (1960).
(9) Douglas Aircraft Co., Astropower Lab, Internal Project No. **8017-1.**
(10) *Ibid.*, Internal Report (1963).
(11) *Ibid.*, Tech Paper, "Liquid Ion Exchangers for Fuel Cells."
(12) General Electric Co., AF33(616)-8159 (1961-1962).
(13) General Electric Co., Contract No. DA-36-039-AMC-00095 (E) (Oct. 1, 1962) U.S. ERDL, Ft. Belvoir, Va.
(14) Gregor, H. P., *J. Am. Chem. Soc.*, **73,** 642 (1951).
(15) Grubb, W. T., *J. Phys. Chem.* **63,** 55 (1959).
(16) Grubb, W. T., and Niedrach, L. W., *J. Electrochem. Soc.* **107,** 133 1960).
(17) Harned, H. S., and Owen, B.B., "Physical Chemistry of Electrolytic Solutions," 3rd ed. p. 137, Reinhold Publishing Co. (1958).
(18) Ionics, Inc., Bull. **FC101.**
(19) *Ibid.*, Nepton CR-61.
(20) Juda, W., Rosenberg, N. W., Marinsky, J. A., and Kasper, A. A., *J. Am. Chem. Soc.* **74,** 3736 (1952).
(21) Kortum, G., and Bockris, J. O'M., "Textbook of Electrochemistry," Vol. II, p. 403. Elsevier Publishing Co. (1951).
(22) *Ibid.*, p. 661.
(23) *Ibid.*, p. 704.

(24) National Aeronautics and Space Administration, Contract NAS 7-150, Astropower, Inc. (1962).
(25) Oster, E. A., "Ion Exchange Membrane Fuel Cells," 16th Annual Power Sources Conference, p. 22–24.
(26) Popat, P. V., Contract No. DA-44-009-ENG-3371, (Nov 1, 1959—Nov. 30, 1961).
(27) Schanz, J. L., and Bullock, E. K., ARS, Space Power System Conference, (Sept. 1962).
(28) Spiegler, K. S., and Coryell, C., *J. Phys. Chem.* **57**, 687 (1953).
(29) Thompson Ramo Wooldridge, Inc., Final Report ER-5728, Contract NAS-3-2551, Jan. 15, 1964.

RECEIVED February 17, 1964.

Publication Date: January 1, 1969 | doi: 10.1021/ba-1965-0047.ch014

Performance of Hydrogen-Bromine Fuel Cells

WERNER GLASS and G. H. BOYLE[1]

Ionics, Inc. 152 Sixth Street, Cambridge 42, Mass.

Both the exoenergetic formation of hydrogen bromide from the elements and the endoenergetic dissociation of hydrogen bromide into hydrogen and bromine can be carried out reversibly in a fuel cell. Platinum, tantalum, niobium, and tri- or tetrafluoroethylene polymers are acceptable materials of construction. Aqueous hydrogen bromide is the best solubilizer for bromine. Properties of hydrogen bromide–bromine-water solutions were determined in considerable detail. A special low water content ion exchange membrane minimized diffusive attack of bromine on the anode and permitted cell life to be extended to well over a year. The effective internal resistance of present cells is still high (~8 ohm-sq. cm.). Further work will be aimed at decreasing this resistance.

Publication Date: January 1, 1969 | doi: 10.1021/ba-1965-0047.ch015

The hydrogen-bromine cell is intended to serve as a secondary cell—that is, electrical energy can be obtained from a "discharge" reaction:

$$H_2 + Br_2 \rightarrow 2HBr + \text{electrical energy}$$

and electrical energy can be stored as chemical potential by means of a "charge" reaction:

$$2HBr + \text{electrical energy} \rightarrow H_2 + Br_2$$

The energy is stored within the electrolyte reservoir in the form of dissolved bromine and in the hydrogen reservoir in the form of hydrogen gas. The total watt-hours of storage provided depends primarily on the size of the reservoirs, not on the size of the cell itself.

The advantage that the hydrogen-bromine system has over most

[1] Present address, P. R. Mallory & Co., Burlington, Mass.

In Fuel Cell Systems; Young, G., el al.;
Advances in Chemistry; American Chemical Society: Washington, DC, 1969.

other fuel cell systems (hydrogen-oxygen, for example) is that the charge reaction can be carried out without any detectable electrode overpotential and that the discharge reaction can be carried out without any detectable electrode polarization, (3). As a result, the reactions

$$H_2 + Br_2 \rightleftarrows 2HBr + \text{electrical energy}$$

can be made to approach thermodynamic reversibility closely. The hydrogen-bromine system thus has the promise of being a very efficient energy storage and supply system.

Obviously, the hydrogen-bromine system currently also has disadvantages relative to the hydrogen-oxygen secondary fuel cell system (3). These disadvantages are chiefly:

1. Higher equivalent weight of oxidant (Br_2 + solubilizer *vs.* O_2).
2. Higher corrosivity (Br_2 + HBr *vs.* O_2 + KOH or H_2SO_4).
3. Higher state of the art ohmic cell resistance.
4. Open-circuit voltage dependent on degree of charge of the oxidant reservoir.

The last of these disadvantages—variable open-circuit voltage—can be handled in any actual multicell battery by suitable solid-state switching devices that select the number of cells required at any given time. The factors affecting the other disadvantages—equivalent weight, corrosivity, ohmic resistance—were studied.

The hydrogen-bromine cell under development in this laboratory uses bromine solubilized in liquid electrolyte (3). A platinum electrode is immersed in the electrolyte. The electrolyte compartment is separated from the hydrogen compartment by a proton-transferring ion exchange membrane. The hydrogen compartment contains a catalytically active electrode which is pressed against the ion exchange membrane.

The reactions that occur can be summarized stoichiometrically as follows:

$$\text{In the electrolyte compartment, } 2HBr \underset{\text{discharge}}{\overset{\text{charge}}{\rightleftarrows}} Br_2 + 2H^+ + 2e^-$$

$$\text{In the hydrogen compartment, } 2H^+ + 2e^- \underset{\text{discharge}}{\overset{\text{charge}}{\rightleftarrows}} H_2$$

The reactions as written represent only the over-all stoichiometry and not the actual mechanisms or states involved. For example, the bromine in the electrolyte compartment is presumably present primarily in the complexed form (as Br^-_3 or Br^-_5) in conjunction with an anion from the solution.

All the major components of a hydrogen-bromine cell presented problems that had to be solved before a truly reliable, efficient, long-lived

Publication Date: January 1, 1969 | doi: 10.1021/ba-1965-0047.ch015

hydrogen-bromine secondary fuel cell system could be developed. The problems involved were grouped into cell construction problems; electrode problems; electrolyte problems; and membrane problems.

Cell Construction Problems

The hydrogen-bromine system corrodes most materials. A materials testing study showed that acceptable metals include platinum, platinum-iridium, titanium-palladium, tantalum, or niobium. Of the organic plastics, tri- or tetrafluoroethylene polymers such as Teflon, Halon, or Kynar were adequately bromine resistant.

Electrode Problems

Stable, reproducible, low resistance electrodes are needed. Various compositions and methods of manufacture were tried. Electrodes were evaluated by their performance in test cells (*2*).

Initially the platinized graphite felt or cloth electrode was studied to determine the important variables affecting the life and performance of this component of the cell. Following this work, a pressed platinum black on platinum or titanium screen electrode was developed which proved superior to the previous graphite base electrode. Further work along this line led to the development of a sintered type of platinum black electrode.

Electrolyte Problems

As a hydrogen-bromine cell is discharged, bromine is removed from the electrolyte and hydrogen bromide substituted. No more than 26.8 amp-hours can be drawn out of the cell per gram-equivalent of bromine used. Weight considerations inherent in aerospace applications make it imperative that each gram-mole of bromine be dissolved in as little as possible of "unproductive" solvent. Water alone is a poor solvent. More than 2.4 kg. would be needed to dissolve a gram-equivalent of bromine, resulting in a total electrolyte weight of nearly 2.5 kg. per 26.8 amp-hours. Moreover, a cell could not reasonably be run all the way down to zero bromine content so that the effective current-producing capacity of the 2.5 kg. of electrolyte would be less than 26.8 amp.-hours.

A way around the poor solubility of bromine in water is to use a "solubilizer" (*2*). Any halide ion, x^-, will solubilize an appreciable quantity of bromine. Presumably the bromine is complexed as Br_2x^-, $(2Br_2)x^-$, or even more brominated forms. If the halide is a bromide, the corresponding complex ions are Br^-_3, Br^-_5, etc.

The possible halide solubilizers screened included bromides of hy-

Publication Date: January 1, 1969 | doi: 10.1021/ba-1965-0047.ch015

Table I. Effect of Solubilizer

Solubilizing agent	Charged State: Molality, Agent	Molality, Br_2	Open-circuit volts	Cell resistance, ohm-sq. cm.: On Charge	On discharge
HBr	2.64	3.66	0.985	8.25	7.75
NaBr	3.41	3.66	0.946	28.1	21.75
LiBr	3.04	3.66	1.017	65.0	39.5
KBr	2.86	3.66	1.043	26.2	25.0
NH_4Br	2.76	3.66	1.017	35.6	31.5

drogen, sodium, potassium, lithium, ammonia, cesium, and strontium and hydrogen and sodium chlorides (HBr, NaBr, KBr, LiBr, NH_4Br, CsBr, $SrBr_2$, HCl, and NaCl). Certain of these solubilizers were checked in cells containing a "charged" electrolyte—that is, water, solubilizers, and bromine—and a substantially "discharged" electrolyte (water, solubilizer, some bromine and the remaining bromine as hydrogen bromide). The system based on the most promising solubilizer (hydrogen bromide), was examined in considerable detail.

Cells were run with electrolytes using hydrogen, lithium, sodium, potassium, and ammonium bromides as solubilizing agents. Bromine was found to form an insoluble precipitate in solutions of tetraethyl ammonium bromide. Upon addition of bromine to a cesium bromide solution a precipitate was formed which appeared to dissolve with agitation but settled out again on standing. This precipitate is believed to be insoluble cesium tribromide. Attempts were made to run cells with a "fully charged" electrolyte as well as with a "substantially discharged" electrolyte. The fully charged electrolytes contained enough solubilizer to solubilize 3.66 moles of bromine per kg. of water. The substantially discharged electrolytes contained the same molality of solubilizer—0.5 mole Br_2/kg. H_2O and an additional $2(3.66\text{-}0.5) = 6.32$ moles HBr/kg. H_2O. Precipitates formed when the "substantially discharged" versions of the potassium and ammonium bromide solubilized electrolytes were prepared. Results of the remaining tests are summarized in Table I.

Table I shows that the cell resistance, when the electrolyte is in the charged state, is much higher for the salt-solubilized cells (20 to 65 ohm-sq. cm.) than for the hydrogen-bromine solubilized one (approximately 8 ohm-sq. cm.). Presumably the lack of protons in the ion exchange membrane between the gas and electrolyte compartments results in a serious hindrance to current flow. This lack of protons is especially noticeable when the resistance is measured with a charging current impressed on the cell.

When the electrolyte is in a substantially discharged state—that is, with appreciable amounts of hydrogen bromide present, very little difference in cell potential or cell resistance is found for different solubilizers.

Publication Date: January 1, 1969 | doi: 10.1021/ba-1965-0047.ch015

on Cell Performance

Discharged State					
Molality			Open-circuit, volts	Cell resistance, ohm-sq. cm.	
Agent	HBr	Br_2		On charge	On discharge
← 8.96 →		0.50	0.743	14.0	16.75
3.41	6.32	0.50	0.784	16.25	16.0
3.04	6.32	0.50	0.779	16.5	18.25
...	...	...	...	...	...
...	...	...	...	...	...

Apparently 6.32 molal hydrogen bromide is adequate to ensure a ready supply of protons in the membrane even in the presence of 3 molal sodium or lithium bromides.

Salt solubilizers thus do not show any advantage over hydrogen bromide as a solubilizer.

HBr–Br_2–H_2O System Properties

The importance of the liquid electrolyte hydrogen bromide–bromine–water system to the hydrogen bromine fuel cell led to a study of the properties of the liquid system itself as well as to a study of its interaction with an ion exchange membrane and in a hydrogen-bromine fuel cell.

The density, electrical conductivity, and relative electropotential of various hydrogen bromide–bromine–water solutions were determined in an attempt to gain some insight into the nature of their constituents. To facilitate the experimental work, 19 specific solutions were chosen for study. The composition of these 19 solutions is shown in Figure 1. The solutions are also grouped in Table II.

The density data obtained for the hydrogen bromide–bromine–water at 30° C. are plotted in Figure 2. The plot shows density, grams/ml. *vs.* the total milli-equivalent of bromine per gram of water. The points fall very close to a single curve–that is, the volume contribution of each bromine atom remains pretty much the same whether it is present as HBr or Br^-_3 or Br^-_5. Thus a Br^-_3 is just about three times as big as a hydrogen bromide. This appears to be a reasonable state of affairs.

Electrical conductivity data were obtained at 0° C., 30° C., and 60° C. and are listed, *inter alia,* in Table III. Cross-plots of the data obtained at a given temperature permitted the drawing of contours of lines of constant conductivity in the hydrogen bromide molality/bromine molality plane. Such plots are shown in Figures 3 and 4. These plots are working plots–that is, they give the value of the conductivity to be expected for any composition. However, they do not permit ready interpretation of the effect of composition changes on conductivity. Such interpretation can be more readily obtained when the data are plotted as specific conductance with respect to hydrogen bromide normality, Λ_{HBr} (mhos/cm.cube)/

Publication Date: January 1, 1969 | doi: 10.1021/ba-1965-0047.ch015

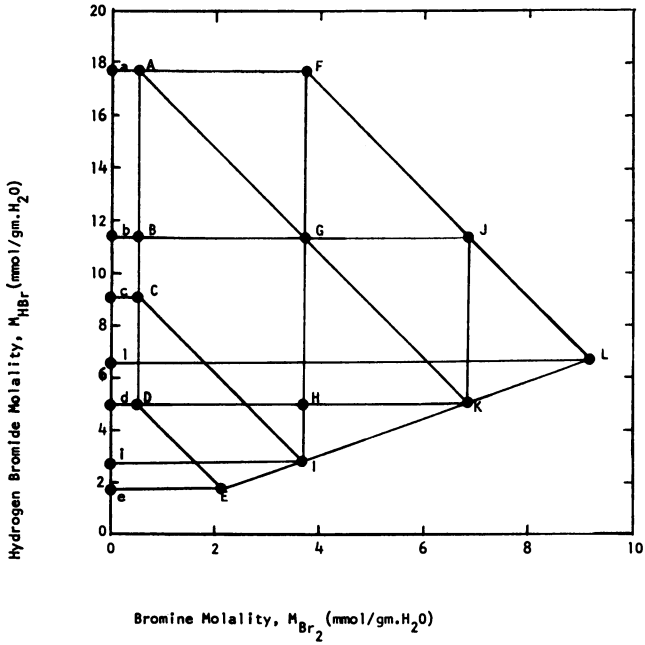

Figure 1. Experimental scheme of solutions investigated

Table II. Experimental Scheme

Family Type	*Solutions*[a]
Constant Br_2 molality	● a,b,c,d,e,i,l ● A,B,C,D, ● F,G,H,I ● J,K
Constant HBr molality	● a,A,F ● b,B,G,J ● c,C ● l,L ● d,D,H,K ● i,I ● e,E
Constant bromine + bromide (charge-discharge line)	● F,J,L ● A,G,K ● B,H ● C,I ● D,E
Saturation line	● E,I,K,L

[a] See Figure 1.

(mmoles HBr/ml.) *vs.* the hydrogen bromide molality, M_{HBr} (mmoles HBr/grams H_2O).

The choice of this coordinate system deserves some discussion. The conductance measurement is basically a volumetric one–that is, it meas-

Publication Date: January 1, 1969 | doi: 10.1021/ba-1965-0047.ch015

ures the ease with which current can traverse a given geometric path. Thus it is reasonable to use a volumetric concentration (normality) when defining Λ, the specific conductance. Λ is thus a measure of the conducting ability per dissolved molecule. Λ_{HBr} is the specific conductance with respect to dissolved hydrogen bromide only. It is thus a measure of the conducting ability per dissolved hydrogen bromide molecule. The dissolved bromine, complexed or otherwise, would not be expected to have any significant conducting ability.

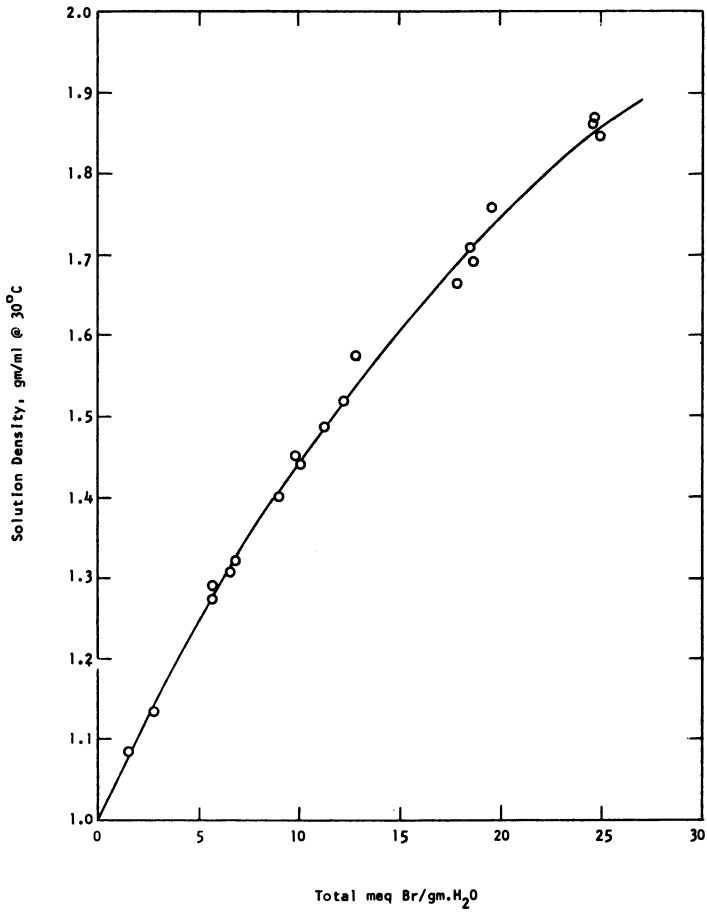

Figure 2. Density of hydrogen bromide–water–bromine solutions at 30° C.

One can expect the conducting ability per molecule of dissolved hydrogen bromide (Λ_{HBr}) to depend on the degree of ionization of hydrogen bromide. This again should depend on the environment in which the hydrogen bromide finds itself. Empirically it was found that the

Publication Date: January 1, 1969 | doi: 10.1021/ba-1965-0047.ch015

Table III. Properties of

Solution	Normality, meq./ml. N_{HBr}	N_{Br_2}	Molality, mmole/g. H_2O M_{HBr}	M_{Br_2}	Potential[a], volts 30°C.	60°C.
a	12.17	0	17.9	0	...	...
b	8.74	0	11.2	0	...	...
c	7.26	0	8.93	0	...	...
d	4.97	0	5.69	0	...	...
e	1.54	0	1.61	0	...	...
i	2.48	0	2.69	0	...	...
l	5.63	0	6.59	0	...	...
A	11.85	0.696	17.58	0.516	0.572	0.541
B	8.57	0.734	11.19	0.478	0.692	0.664
C	7.13	0.795	8.95	0.499	0.748	0.718
D	4.89	0.916	5.74	0.538	0.844	0.811
E	1.42	3.62	1.60	2.04	1.076	1.050
F	10.86	4.42	17.71	3.61	0.609	0.584
G	7.75	4.87	11.20	3.53	0.704	0.693
H	4.34	5.70	5.67	3.59	0.880	0.853
I	2.14	5.80	2.64	3.57	1.032	1.004
J	7.06	8.46	11.25	6.73	0.729	0.705
K	3.88	9.53	5.68	6.97	0.895	0.872
L	4.15	11.22	6.67	9.01	0.888	0.855

[a] EMF measured against H_2 electrode.

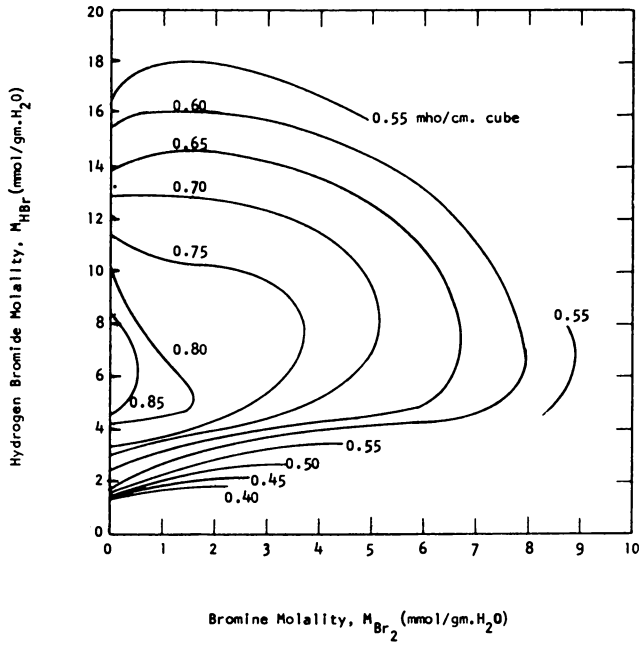

Figure 3. Conductivity of hydrogen bromide–water–bromine solutions at 30° C.

Publication Date: January 1, 1969 | doi: 10.1021/ba-1965-0047.ch015

HBr-Br_2-H_2O System

Conductivity (K), mhos/cm.cube			*Specific conductance* $(\Lambda_{HBr})\ K/N_{HBr}$			$\left(\frac{\Lambda_0}{\Lambda_{30}}\right)$	$\left(\frac{\Lambda_{60}}{\Lambda_{30}}\right)$	*Density* ρ_{30}°C. *g./ml.*
0°C.	30°C.	60°C.	0°C.	30°C.	60°C.			
...	0.495	0.636	...	0.041	0.053	...	1.28	1.665
0.502	0.733	0.960	0.058	0.084	0.110	0.685	1.31	1.485
0.548	0.834	1.078	0.075	0.115	0.148	0.656	1.29	1.400
0.582	0.880	1.184	0.117	0.177	0.238	0.660	1.35	1.275
0.321	0.530	0.682	0.208	0.344	0.443	0.605	1.29	1.085
0.431	0.691	1.920	0.174	0.279	0.370	0.623	1.33	1.135
0.613	0.880	1.198	0.109	0.157	0.213	0.695	1.36	1.310
...	0.551	0.720	...	0.047	0.061	...	1.31	1.690
0.560	0.725	0.896	0.065	0.085	0.105	0.775	1.23	1.520
...	0.763	0.945	...	0.107	0.132	...	1.24	1.440
0.613	0.858	1.112	0.125	0.175	0.227	0.715	1.30	1.320
...	0.393	0.505	...	0.275	0.356	...	1.28	1.290
...	0.431	0.669	...	0.048	0.062	...	1.26	1.845
0.456	0.714	0.904	0.059	0.093	0.116	0.640	1.27	1.710
0.498	0.725	0.936	0.115	0.167	0.216	0.688	1.29	1.575
...	0.512	0.645	...	0.238	0.303	...	1.26	1.450
0.422	0.599	0.824	0.060	0.085	0.117	0.715	1.40	1.870
0.393	0.624	0.802	0.102	0.161	0.207	0.630	1.28	1.760
0.365	0.536	0.720	0.088	0.129	0.173	0.680	1.34	1.865

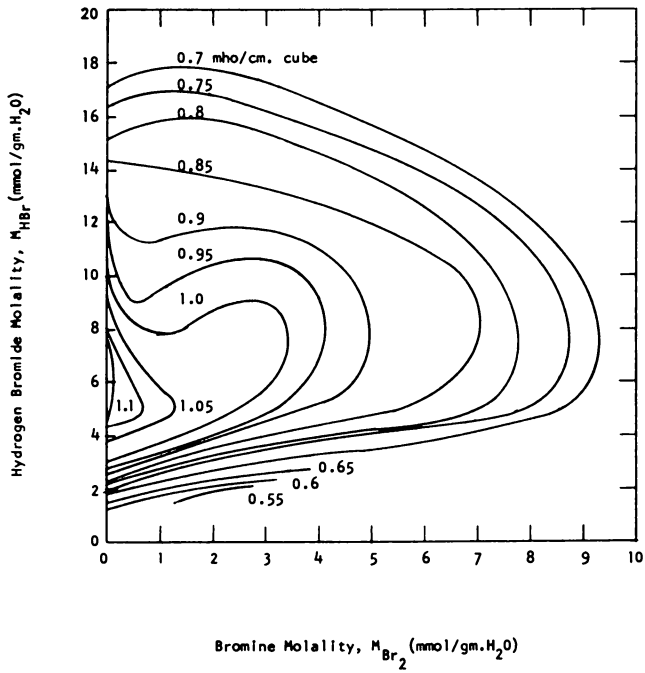

Figure 4. Conductivity of hydrogen bromide–water–bromine solutions at 60° C.

Publication Date: January 1, 1969 | doi: 10.1021/ba-1965-0047.ch015

best correlation of Λ_{HBr} with the environment was obtained when this environment is defined by M_{HBr}, the hydrogen bromide molality, a measure of the ratio of hydrogen bromide to water present in the solution. Figure 5 shows a plot of Λ_{HBr} *vs.* M_{HBR}.

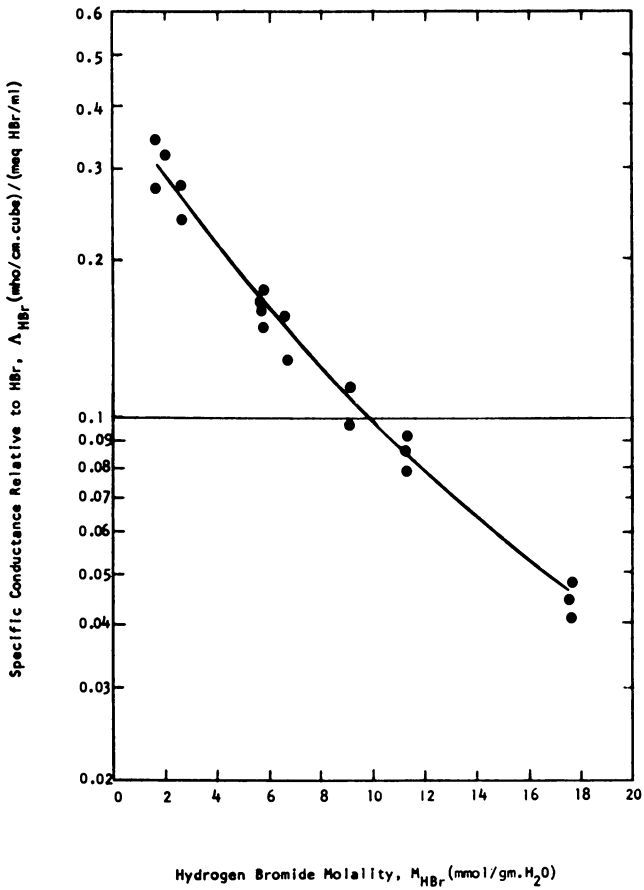

Figure 5. Specific conductance vs. hydrogen bromide molality at 30° C.

The higher M_{HBr}—that is, the higher the hydrogen bromide–water ratio of the solution, the lower Λ_{HBr}, the conducting ability per dissolved hydrogen bromide molecule. This decline in specific conductance with increasing molality is indicative of the expected decrease in ionization. As a first approximation, at a given temperature, a single curve of Λ_{HBr} is obtained *vs.* M_{HBr} independent of the amount of the bromine dissolved. This implies that the available conducting species remain the same both with regard to number and mobility as the bromine content is varied. (Com-

Publication Date: January 1, 1969 | doi: 10.1021/ba-1965-0047.ch015

pensating changes in number on the one hand and in mobility on the other could also account for the rough consistency of Λ_{HBr} but it is hard to see how increasing the bromine content could increase either one of these two factors.) From the viewpoint of electrolytic conductivity then, the dissolved bromine acts primarily as an inert "extender," serving to separate the current carrying species and thus reducing the conductivity (K) without reducing the specific conductance (Λ_{HBr}). From a practical stoichiometric viewpoint, of course, the amount of bromine present in the solution is of great importance because it determines the further discharge capability of the solution.

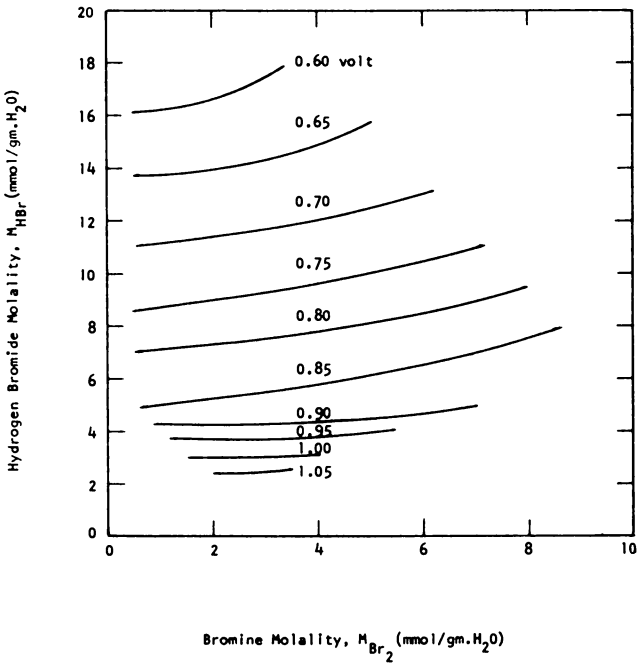

Figure 6. Potential vs. hydrogen electrode at 30° C.

The effect of temperature can be isolated by calculating the ratio of the values of Λ_{HBr} at two different temperatures for the same solution. This has been done and the results also listed in Table III. The values of $\Lambda_{60}/\Lambda_{30}$ are fairly constant and average about 1.31 while Λ_0/Λ_{30} averages about 0.68. The three ratios—$\Lambda_{60}/\Lambda_{30} = 1.31$; $\Lambda_{30}/\Lambda_{30} = 1.00$; and $\Lambda_0/\Lambda_{30} = 0.68$—correspond to a temperature coefficient with the reasonable magnitude of 2 kcal./mole if Λ_{HBr} is expressed as $\Lambda_{HBr} = \Lambda^* \exp.(-\Delta E/RT)$.

The potential generated by cell Pt(+), HBr(M_{HBr}) + Br_2(M_{Br_2}), HBr(M_{HBr}), Pt(−), H_2 was determined for various values of the molali-

Publication Date: January 1, 1969 | doi: 10.1021/ba-1965-0047.ch015

ties M_{HBr} and M_{Br_2}. Measurements were made at 30° C. and 60° C. The resulting emf. are given in Table III and cross-plotted in Figures 6 and 7.

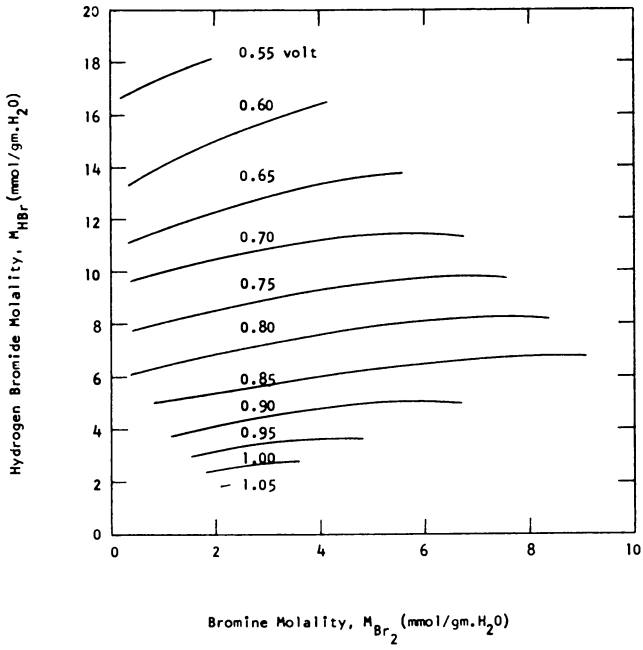

Figure 7. Potential vs. hydrogen electrode at 60° C.

The electropotential data showed that the potential (with reference to a hydrogen electrode) of a platinum electrode immersed, in hydrogen bromide–water–bromine electrolyte depended primarily on the hydrogen bromide–water ratio and only to a very minor degree on the amount of bromine present. Again, most of the bromine seemed to act as a diluent. Apparently the bulk of the bromine is complexed with the bromide and does not affect any of the electrochemical properties of the system.

Membrane Problems

The membrane must permit the ready transport of hydrogen ions and prevent the transport of species containing bromine (Br^-, Br^-_3, Br^-_5, or Br_2). Different membranes were tried in test cells. Samples of the most promising membrane were subjected to prolonged contact with various electrolyte solutions, and the resulting physical and chemical changes were evaluated.

The transport of bromine-containing species through the membrane is undesirable because (1) this would cause reaction to occur without

Publication Date: January 1, 1969 | doi: 10.1021/ba-1965-0047.ch015

electro-chemical benefit, and (2) the bromine would gradually degrade the catalytic platinum black electrode. Early cells did, in fact, suffer from such bromine diffusion. Their average life was of the order 100 hours with a maximum of about 250 hours. In an attempt to minimize bromine transport, cells were made up using a "tight" membrane—that is, one with a low water content of only 33 wt.%. This membrane made bromine diffusion relatively slight—less than 1 micromole of bromine per hour per square centimeter—and has permitted cell life to be extended to more than 9000 hours. A drawback, unfortunately, is that the electrical resistance of these tight membranes is quite high; in solutions of interest, the membrane resistance is of the order 4 ohm-sq. cm. leading to a total cell resistance of about 8 ohm-sq. cm.

A study of the action of various hydrogen bromide–water–bromine solutions on this tight membrane of sulfonated polystyrene was made to gain some insight into its mode of action. Samples of the membrane were exposed to various hydrogen bromide–water–bromine solutions at different temperature for various lengths of time.

A similar set of solutions was used as had been employed for the electrolyte studies. Sample immersion times were 1, 7, 14, and 28 days. Immersion temperatures were 30° and 60° C. The ion-exchange capacity, the density of the resin, and the electrical resistance of the membrane in 0.1*N* potassium chloride were followed.

Immersion in water–bromine–hydrogen bromide solutions reduced the resin Na^+ exchange capacity; increased the dry weight of the resin; and increased the electrical conductance of the membrane when equilibrated with 0.1*N* potassium chloride. Figure 8 shows a plot of Na^+ exchange capacity per ml. of wet resin *vs.* dry resin weight (Na-form) per ml. of wet resin. The five control samples of unimmersed membranes indicate the kind of scatter to be expected. Within the framework of such scatter, a single line adequately represents the data. This indicates that all the solutions attacked the membrane in the same way: A given ion exchange capacity corresponded to a given dry resin weight. Specifically, 280 milligrams were gained for each milliequivalent of exchange capacity lost. This weight gain presumably represents bromination of the polystyrene resin matrix.

Figure 9 shows the relation between electrical conductance (in 0.1*N* KCl) and Na^+ exchange capacity. Again a single line adequately represents the data, indicating that all the various solutions effected the same type of change in the membranes; only the rate of attack seems to have varied.

The attack on the membranes continued until approximately two-thirds of the ion exchange capacity was lost. This occurred in about one week at 30° C. and less than one day at 60° C. Elemental analysis of unimmersed "virgin" membranes and "fully brominated" ones showed

Publication Date: January 1, 1969 | doi: 10.1021/ba-1965-0047.ch015

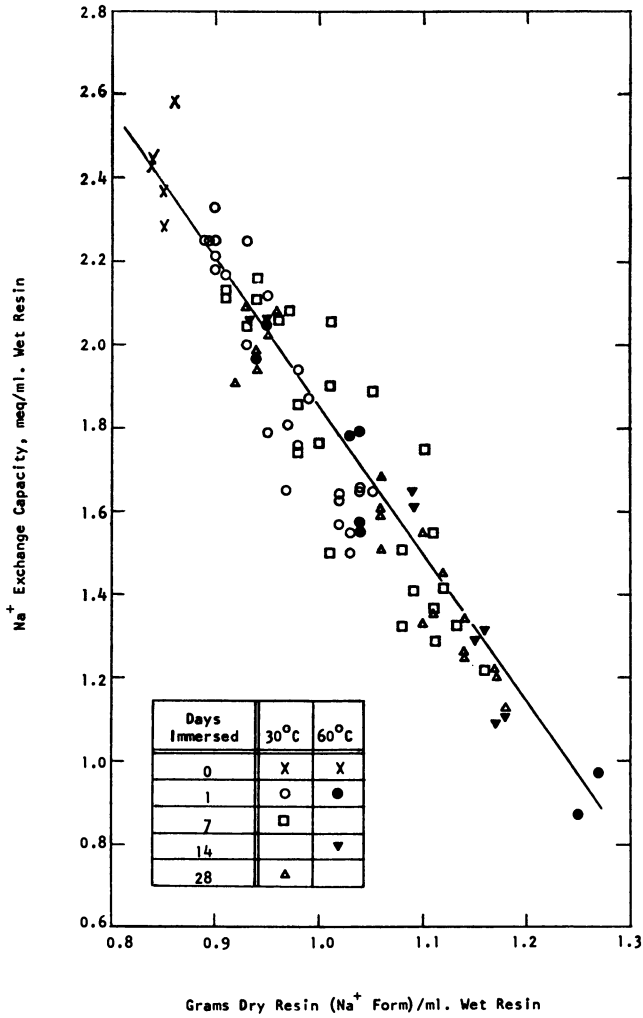

Figure 8. Correlation of capacity and resin density

that about one half the sulfur had been removed from the resin and that approximately 5 atoms of bromine had eventually been added for each atom of sulfur removed. Initially the resin contained roughly one sulfonate group for each two benzene rings. The fact that the capacity loss (down to one third) was greater than the sulfur loss (down to one half) showed that some of the remaining sulfonate groups were not available for ion-exchange sites: presumably they were sterically blocked by the added bromine. The fact that 5 atoms of bromine had been added for each sulfonate group lost showed that the bromine was substituting for hydrogen as well as for the missing sulfonate groups.

Publication Date: January 1, 1969 | doi: 10.1021/ba-1965-0047.ch015

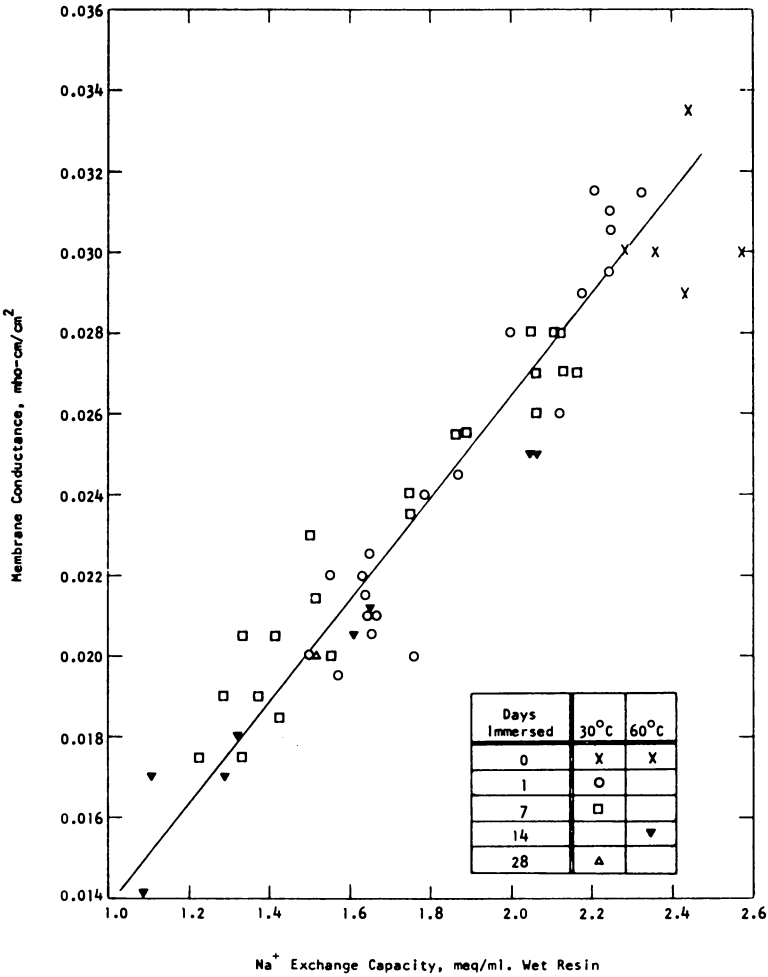

Figure 9. Membrane conductance vs. exchange capacity

Two cells were assembled to check the effect of membrane bromination on cell performance. One cell had a fully brominated membrane and one a virgin membrane. Despite the significant differences in ion exchange capacity and in chemical composition, both cells performed identically. Apparently the membrane acts primarily as an aqueous permeable membrane (with steric hindrance of ions as large as Br^-, Br_3^-, or the like) rather than as a true ion exchange barrier.

Fuel Cell Performance

Fuel cell performance data were obtained over most of the range of hydrogen bromide–water–bromine compositions investigated. Results

Publication Date: January 1, 1969 | doi: 10.1021/ba-1965-0047.ch015

are given in Table IV and plotted in Figures 10 and 11. As expected, cell open-circuit potential paralleled the electropotentials taken *vs.* a hydrogen electrode—that is, depended primarily on the hydrogen bromide–water ratio. Desirable high potential values of about 1 volt were obtained at low hydrogen bromide molalities around 3 moles/kg. H_2O and undesirable low values of about 0.6 volt were obtained at high hydrogen bromide molalities of about 18 moles/kg. H_2O.

Table IV. Fuel Cell Characteristics

Solution[a]	*Open-circuit potential, volt*	*Effective cell resistance,*[b] *ohm-sq. cm.*	
		On charge	*On discharge*
B	0.692	32.5	35.5
C	0.740	14.0	16.75
D	0.833	9.0	9.5
E	1.05	7.5	8.25
G	0.693	11.25	14.75
H	0.850	9.25	9.0
I	0.985	8.25	7.75
J	0.715	11.75	13.5
L	0.855	11.25	12.75

[a] See Table III for composition of solutions.
[b] Slope of voltage *vs.* current density plot.

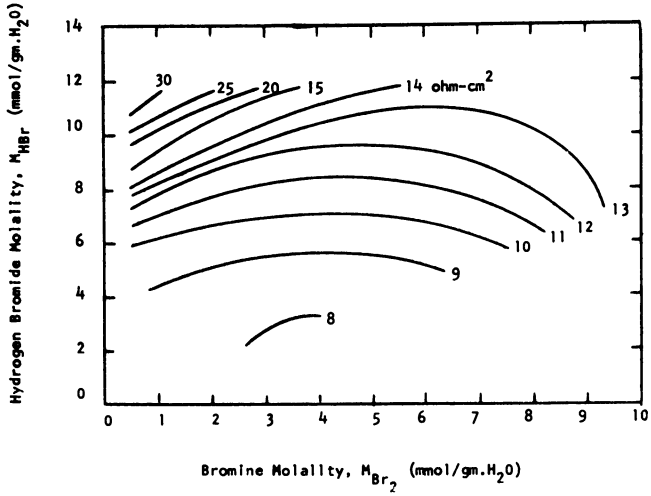

Figure 10. Effective cell resistance while discharging at 30° C.

Effective cell resistances were obtained from the slopes of the voltage *vs.* current density plots. The voltage *vs.* current density lines were quite straight in the range investigated—0.2 volt to 1.8 volts. A single slope thus characterized the effective discharge resistance of a cell, and another single slope characterized the effective charge resistance.

These effective cell resistances showed the same tendencies as the

Publication Date: January 1, 1969 | doi: 10.1021/ba-1965-0047.ch015

open-circuit potentials: more desirable relatively low resistances (around 8 ohms-sq. cm.) at 3 molal hydrogen bromide; and undesirable high resistance (around 20 ohm-sq. cm.) at 12 molal hydrogen bromide. Presence of hydrogen bromide thus lowers the open-circuit potential and increases cell resistance. Unfortunately some hydrogen bromide must be present to solubilize the bromine, and more will be formed by reaction during the discharging of any actual cell. Mission-specific trade-off studies would be required to optimize the hydrogen bromide–bromine–water electrolyte composition and quantity, cell number, and size, and current density to arrive at a weight optimum system.

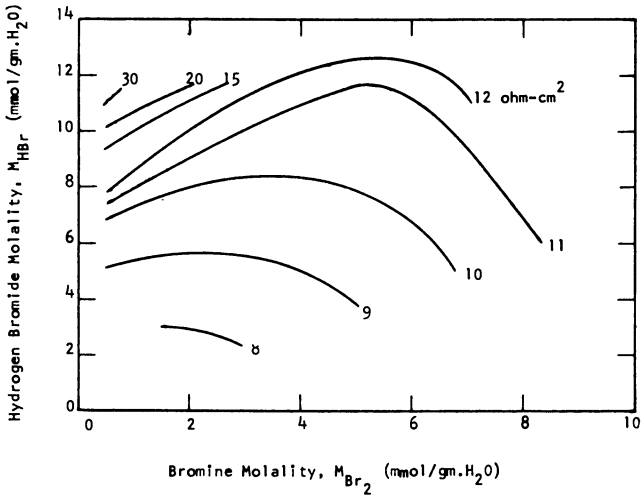

Figure 11. Effective cell resistance while charging at 30° C.

The internal resistance of these hydrogen-bromine cells (~8 ohm-sq. cm.) is very high relative to the state of the art hydrogen–oxygen cells (~1 ohm-sq. cm.). The advantage in power conversion efficiency enjoyed by the hydrogen-bromine system because of its reversibility rapidly disappears when practical current densities of the order 0.1 amp./sq. cm. are considered.

Further work on the hydrogen-bromine fuel cell will therefore be aimed at decreasing internal cell resistance by variations in electrode and membrane structure.

Literature Cited

(1) Berger, C., and Lurie, R. M., "Hydrogen-Halogen Fuel Cell," presented before The Electrochemical Society, Detroit, Mich., October 1961.
(2) Juda, W., Tirrell, C. E., and Lurie, R. M., in "Energy Conversion for Space Power," E. Snyder, editor, Academic Press, New York, 1961.

Publication Date: January 1, 1969 | doi: 10.1021/ba-1965-0047.ch015

(3) Lurie, R. M., and Berger, C., "Regenerable Fuel Cells," presented before the 12th International Astronautical Congress, Washington, D. C., October 1961.

RECEIVED June 22, 1964. The work reported on here was carried out under the sponsorship of the USAF Cambridge Research Laboratories as part of Contract AF 19 (604)-8508.

Publication Date: January 1, 1969 | doi: 10.1021/ba-1965-0047.ch015

16

Hydrogen from Natural Gas for Fuel Cells

JOHN MEEK and B. S. BAKER

Institute of Gas Technology, Chicago, Ill.

Publication Date: January 1, 1969 | doi: 10.1021/ba-1965-0047.ch016

A new multistage process for the production of a hydrogen-rich feed from natural gas for use in an acid electrolyte fuel cell is described. The process, involving no moving parts and operating on a low pressure gas source, is intended for use with on-site fuel cell power generators in the 2- to 100-kilowatt range. The three stages of the process are steam reforming, carbon monoxide shift, and methanation of remaining impurities. Operating parameters are given for each stage. Several possible methods of integrating hydrogen generation and fuel cell systems are presented, and over-all efficiency calculations are made. The economics of the present system are also discussed.

At the beginning of 1963, a low temperature fuel cell program was initiated at the Institute of Gas Technology (IGT) to study the use of reformed natural gas and air in acid fuel cells. This system, based on the use of impure hydrogen, does not appear to have been extensively studied elsewhere. The following considerations motivated this course of study:

1. Natural gas (methane) is difficult to react directly at low temperatures in fuel cells.
2. Hydrogen is known to be a good fuel cell fuel at low temperatures.
3. Natural gas is an easily reformed hydrocarbon fuel.
4. Reformed natural gas will contain about 80 mole % hydrogen.
5. An acid cell, in principle, does not require a high purity hydrogen feed.

This article is concerned with that portion of the IGT program devoted to the production from natural gas of a hydrogen-rich feed which is compatible with economic fuel cell operation.

The objectives set forth for the hydrogen generation system were

In Fuel Cell Systems; Young, G., el al.;
Advances in Chemistry; American Chemical Society: Washington, DC, 1969.

dictated by economic as well as practical feasibility. The project was guided by the following goals:

1. Low-cost components.
2. Maximum methane conversion.
3. Minimum carbon monoxide content.
4. No moving parts.
5. Low system pressure drop.

The need for low cost components with low pressure drop eliminated conventional palladium diffuser purification schemes. The impracticability of having moving parts in small generators (delivering 2- to 100-kilowatt fuel cells) eliminated scrubbing towers, often used in larger hydrogen purification processes. Maximum methane conversion is essential to obtain high efficiency. The desirability of a low carbon monoxide concentration resulted from information derived from the fuel cell portion of the program. All of these goals are based on the needs of on-site generation systems for use in the gas industry.

Publication Date: January 1, 1969 | doi: 10.1021/ba-1965-0047.ch016

Hydrogen Generation System

To achieve the design goals outlined here, a multistage process was necessary. The scheme studied was a three-stage process made up of the following steps:

$$\text{Reforming: } CH_4 + H_2O \rightarrow 3H_2 + CO \quad (1)$$

$$\text{Shifting: } CO + H_2O \rightarrow CO_2 + H_2 \quad (2)$$

$$\text{Methanation: } CO + 3H_2 \rightarrow CH_4 + H_2O \quad (3)$$

The over-all process is shown schematically in Figure 1.

Methane Reforming. Since Reaction 1 is well known, it was the intent of this study to establish operating parameters which might be useful in the construction of small hydrogen generators. Experiments were conducted in reactors capable of providing power for a fuel cell system of a few hundred watts. Since most experience with these reactions is with larger systems, it was believed that scale up in this instance would be relatively straightforward.

A steel reactor 1 inch in diameter and 18 inches long was filled to a 4-inch bed height with Girdler G-56B catalyst, which was reduced in size to give a reactor diameter-to-particle size ratio of about 10:1. The total pressure drop through the reactor at a space velocity of 1000 std. cu. ft. per cu. ft. of catalyst per hour was only 1 inch of water. This reactor and the two subsequent ones operate at slightly above atmospheric pressure. A steam-to-methane mole ratio of 3:1 was chosen, and studies were made at space velocities of 500 and 1000 std. cu. ft. per cu. ft. of catalyst per hour at a variety of temperatures. Effluent gas was analyzed chromato-

graphically for carbon monoxide and methane with a Fischer-Gulf partitioner using a charcoal column. The only other detectable carbon-containing species present, carbon dioxide, was determined from a mass balance.

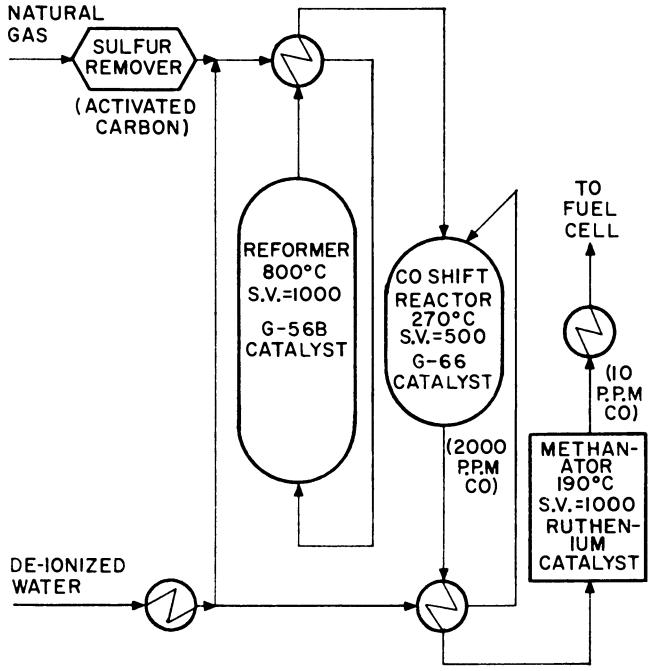

Figure 1. IGT hydrogen generation process

The results of these experiments (Figure 2) show that methane conversion was a strong function of space velocity with respect to the temperature required to achieve complete conversion, higher temperature being required for higher space velocities. For the space velocities studied, complete conversion was obtained at 800° C. and above. The exit gas carbon monoxide content was not a strong function of space velocity, and the effluent carbon monoxide concentration at 800° C. was about 15 mole %. At the lower space velocity, experiments conducted at temperatures up to 100° C. resulted in a further increase in carbon monoxide concentration. Since the ultimate goal is a low carbon monoxide content in the fuel cell feed gas, operating at this high temperature is undesirable. Also, from a thermal efficiency standpoint the lowest possible reforming temperature is most desirable. Having established reasonable operating limits for the reforming stage, the effluent from the reformer was used as the input to the shift reactor.

Publication Date: January 1, 1969 | doi: 10.1021/ba-1965-0047.ch016

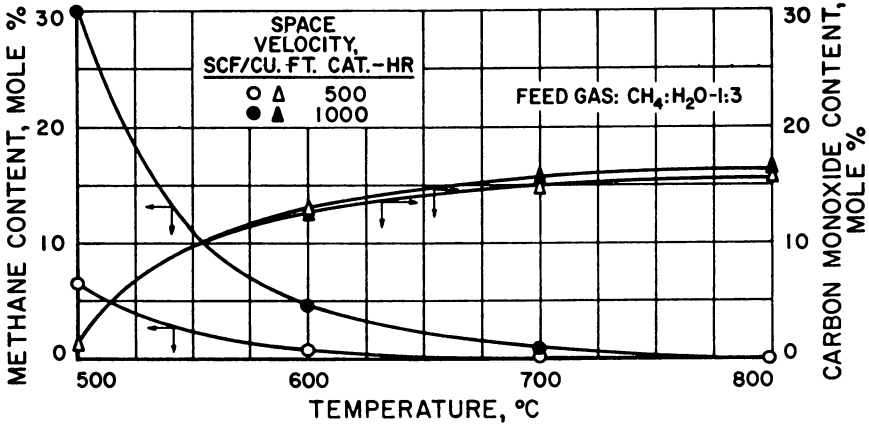

Figure 2. Methane conversion and carbon monoxide composition in reformer

Carbon Monoxide Shift. Conventional shift processes operating between 300° and 500° C. require, to achieve a low carbon monoxide content (3000 p.p.m. or less), the use of a carbon dioxide absorption stage, which is unwieldy for use in small systems. Recently work done by Moe (*1*) indicated that reformed and shifted gases containing 2000 to 3000 p.p.m. carbon monoxide could be achieved without carbon dioxide removal if a low temperature (175° to 300° C.) shift catalyst was used. This relatively new catalyst, Girdler G-66, was placed in a reactor of 1-inch diameter and 18-inch length, filled to a bed height of 8 inches, and the shift reaction was studied with respect to temperature, space velocity, and steam-to-gas ratio. As in the study of the reforming reaction, the carbon monoxide and methane contents of the effluent gas stream were analyzed chromatographically.

The results of this study are shown in Figures 3 and 4. Figure 3 shows the effects of space velocity and temperature on the carbon monoxide content of the effluent gas. At the higher space velocity, 1000 std. cu. ft. per cu. ft. of catalyst per hour, the desired reduction in the carbon monoxide content of the effluent gas could not be obtained. Experiments at still higher space velocities—2000 std. cu. ft. per cu. ft. of catalyst per hour—yielded much poorer results, not reported here. However, at a space velocity of 500 std. cu. ft. per cu. ft. of catalyst per hour, a minimum in the carbon monoxide concentration occurs at about 267° C. Figure 4 shows the strong effect of the steam content of the reaction mixture on the effluent carbon monoxide concentration is indicated. At 250° C., a continuous reduction in the carbon monoxide content is obtained as the steam-to-methane ratio is increased. The maximum ratio tested was 7.3:1, as this ratio readily yielded a carbon monoxide content which was known to be further reducible by methanation. Whether ad-

Publication Date: January 1, 1969 | doi: 10.1021/ba-1965-0047.ch016

ditional steam is desirable will be decided later on the basis of the cost of the steam as well as the fuel cell performance on impure hydrogen feed.

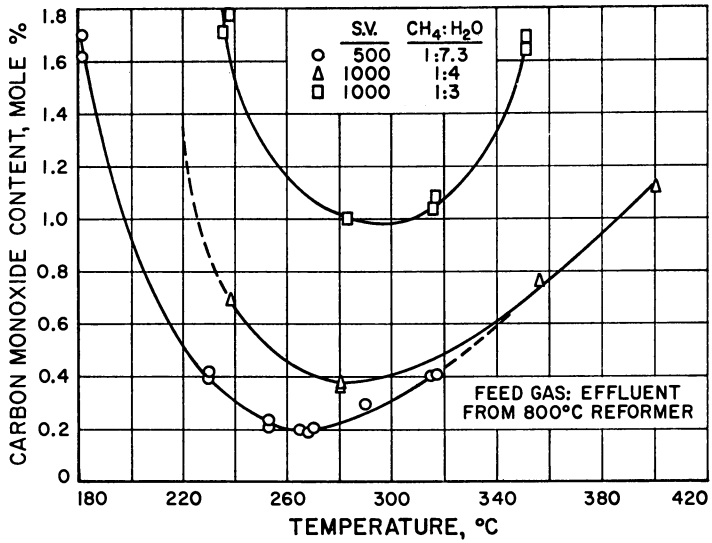

Figure 3. Carbon monoxide conversion in shift reactor

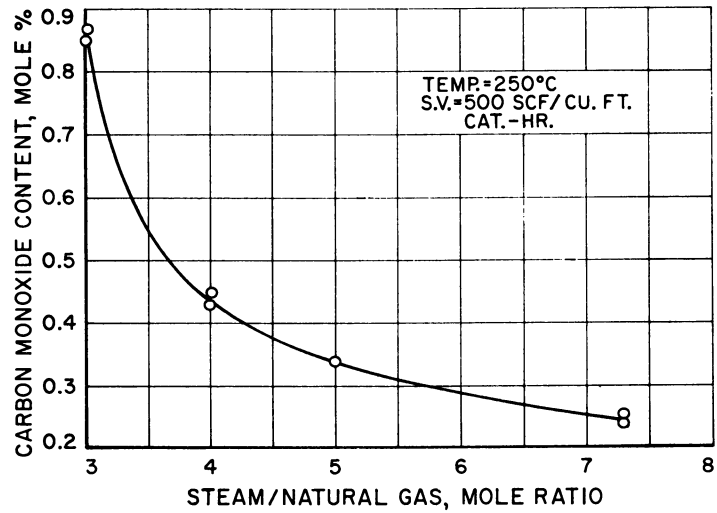

Figure 4. Effect of steam–natural gas ratio on shift reaction

Carbon Monoxide Methanation. Reaction 3, methanation, posed the greatest challenge in the over-all carbon monoxide reduction process. The first attempts at achieving an effective reduction in the carbon monoxide content of a synthetic gas containing 80 mole % hydrogen, 19.7

Publication Date: January 1, 1969 | doi: 10.1021/ba-1965-0047.ch016

mole % carbon dioxide, and 0.3 mole % carbon monoxide, using conventional methanation catalysis, were unsuccessful. Either of two events occurred. At very low temperatures no reactions occurred, while at higher temperatures the water gas shift was promoted along with methanation, and at best only a slight decrease, and in some cases an actual increase, in carbon monoxide was observed.

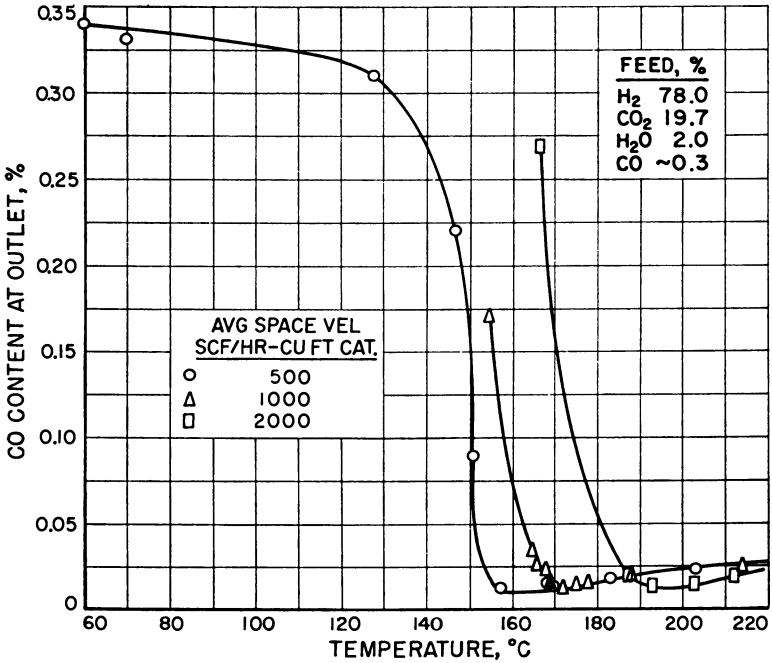

Figure 5. Selective methanation of carbon monoxide at low water content

The problem was to find a catalyst which would permit selective methanation of carbon monoxide in the presence of carbon dioxide, under conditions in which the latter is present in concentrations two orders of magnitude greater than the former. The need for selective methanation is twofold. If appreciable amounts of the carbon dioxide react, the exothermic nature of the reaction almost ensures a complete loss of temperature control in the system. As the temperature rises, more carbon dioxide is methanated, and large amounts of hydrogen are consumed. In the limiting case, all of the hydrogen and carbon dioxide could react to form methane. Equilibrium calculations clearly indicated the desirability of low temperature operation, although even under these conditions the sought-after reduction did not appear achievable.

Using the described gas composition, experiments were conducted

Publication Date: January 1, 1969 | doi: 10.1021/ba-1965-0047.ch016

with a ruthenium-on-alumina catalyst obtained from Englehard Industries, Inc. The effluent gas composition was analyzed with the chromatograph and a Mine Safety Appliances Co. Lira infrared analyzer. With the infrared analyzer, carbon monoxide was determined with an accuracy of about 10 p.p.m. Again, a variety of parameters were studied, including excess water, and the results are shown in Figures 5 and 6. The excess water tests were made to ascertain at what stage in the hydrogen generation system it would be most favorable to remove water.

Figure 5 shows the carbon monoxide content of the exit gas as a function of temperature for 2 mole % water vapor in the feed. It also shows distinct minimums in carbon monoxide content—about 100 p.p.m., dependent on space velocity and temperature. It is interesting that, for increasing space velocity, the same minimum carbon monoxide content is obtained, but at higher temperatures. Figure 6 gives the result of studying the same parameters with a feed gas containing 15% water vapor.

Publication Date: January 1, 1969 | doi: 10.1021/ba-1965-0047.ch016

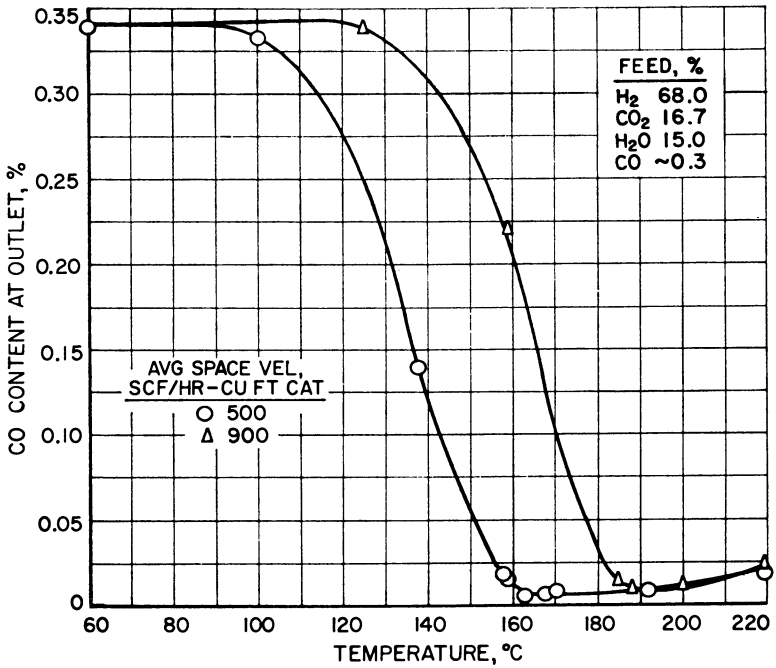

Figure 6. Selective methanation of carbon monoxide at high water content

Again, the same minimum carbon monoxide concentration is obtained, but at slightly higher temperatures. It was also observed that, in the range of minimum carbon monoxide content, no appreciable conversion of carbon dioxide to methane occurred; hence, the reaction can be con-

sidered highly selective. The carbon monoxide reduction process is summarized in Figure 7.

Complete Hydrogen Generation System. After completing the experimental work on the reactions described, reforming, shift, and methanation reactors were connected in series, and the complete system was analyzed. A natural gas containing about 95% methane and 5% higher hydrocarbons was passed through a sulfur-removal cartridge and fed to the first reactor stage, where it was reformed in the presence of excess steam (steam-to-gas mole ratio of 7.3:1) at a space velocity of 250 std. cu. ft. per cu. ft. of catalyst per hour at 800° C. The effluent from this reactor was fed to the shift reactor operating at a space velocity of 500 std. cu. ft. per cu. ft. of catalyst per hour at 270° C. The effluent from this stage was fed to a condenser where a portion of the excess water was removed, and the remaining gas mixture was fed to the methanation reactor operated at a space velocity of 1000 std. cu. ft. per cu. ft. of catalyst per hour and at a temperature of 190° C. The total system pressure drop was 4 inches of water column. Analysis showed the product gas to be 78 mole % hydrogen, 19.7 mole % carbon dioxide, 0.3 mole % methane, 2 mole % water, and 8 p.p.m. of carbon monoxide. The carbon monoxide was analyzed on a special MSA Lira infrared analyzer with a sensitivity of 2 p.p.m.

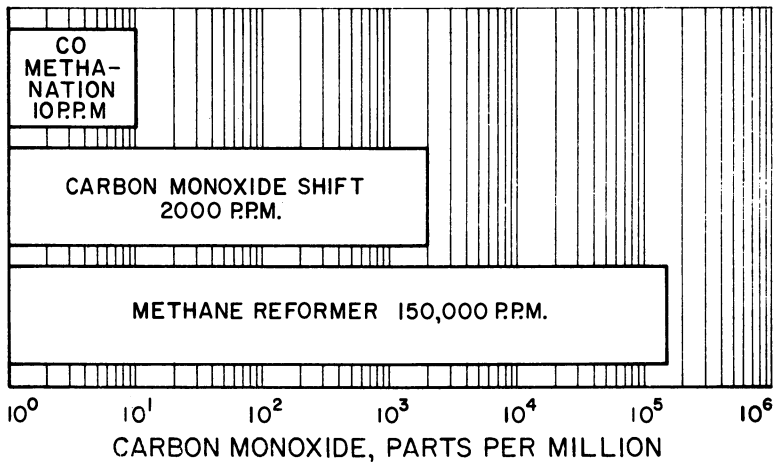

Figure 7. Carbon monoxide reduction in IGT hydrogen generation process

The tenfold improvement in performance compared with the previous experiment is not readily explainable. Some improvement had been anticipated on the basis that the original methanation experiments were performed with a feed gas containing about 3400 p.p.m. of carbon monoxide, while the actual shift reaction reduced that concentration by

Publication Date: January 1, 1969 | doi: 10.1021/ba-1965-0047.ch016

a factor of almost 2. Experiments are being continued to study further the effects of steam-to-methane ratio, space velocity, and catalyst life. Experimental evidence from the fuel cell portion of the program indicates that the carbon monoxide content can be readily tolerated by the hydrogen electrode.

Efficiency and Economics

One of the most attractive features of fuel cells is their potentially high efficiency. When an additional processing stage, such as the one just described, is added to the fuel cell system, a reduction in over-all efficiency may be anticipated. To place the external reformer-fuel cell system in the proper perspective, estimates of the over-all system efficiencies have been made, based on several fuel cell and reforming parameters.

Two models have been chosen for evaluation, and these are shown schematically in Figure 8. In both schemes, it is assumed that the heat required to sustain the reforming reaction is supplied from an external burner—that is, there is no partial combustion in the reformer. Also, both schemes assume single-pass conversion in the fuel cell.

The two schemes chosen for analysis differ only in the effect of recovery of the heat value of recycled spent fuel from the fuel cell. The following parameters have been defined:

η_O = over-all efficiency, electrical energy output based on the heat of combustion of the total amount of methane consumed;
η_V = voltage efficiency, fraction of the theoretical fuel cell potential actually obtained;
η_C = conversion efficiency, fraction of the fuel converted in the fuel cell;
η_R = reactor thermal efficiency, total reformer heat requirement, based on the assumption of nonideal insulation; and
η_E = heat exchanger efficiency, fraction of heat recovered in heat exchangers.

A partial summary of the results of these calculations is shown in Figures 9 and 10. Figure 9 presents a case analyzed for the no-recycle system where reactor thermal efficiency is 80%. A number of arbitrary conversions and voltage efficiencies were chosen as parameters, and the over-all system efficiency was calculated as a function of heat exchanger efficiency. A typical 1-kilowatt fuel cell system using impure hydrogen feed might be expected to operate in the gray zone shown in Figure 9. An over-all system efficiency range from 21.5 to 32.5% can be realistically anticipated. For a pure hydrogen cell, a somewhat higher conversion efficiency and voltage efficiency might be anticipated, and a total system efficiency of 40% is most likely. Figure 10 shows two characteristics using the same parameters for the recycle schemes: First, the over-all system efficiency is less dependent on conversion efficiency because the

Publication Date: January 1, 1969 | doi: 10.1021/ba-1965-0047.ch016

heat of the spent fuel was used. Second, a cutoff point occurs at high heat exchange efficiency and the lowest chosen conversion efficiency. This point indicates where the hydrogen generation system can be operated solely on the spent fuel from the fuel cell. With the same range of heat exchanger efficiency as in the no-recycle case, an over-all efficiency between 26.5 and 35.5% appears likely.

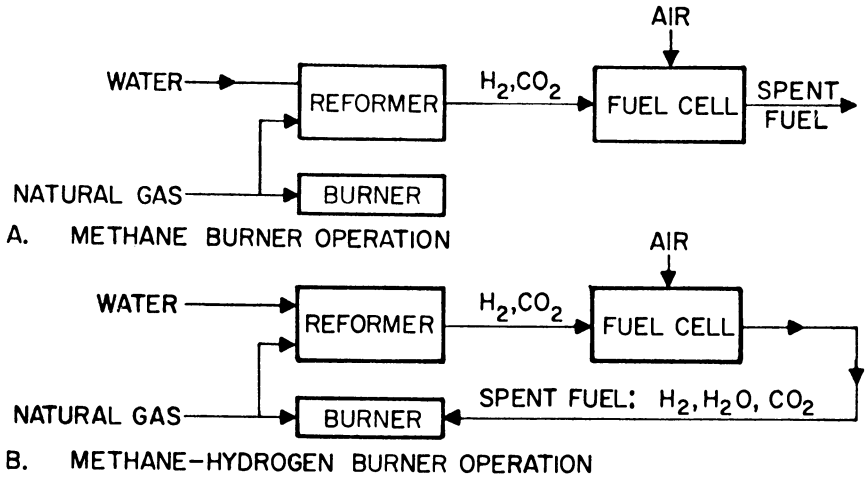

Figure 8. Operational modes for reformer–fuel cell–burner system

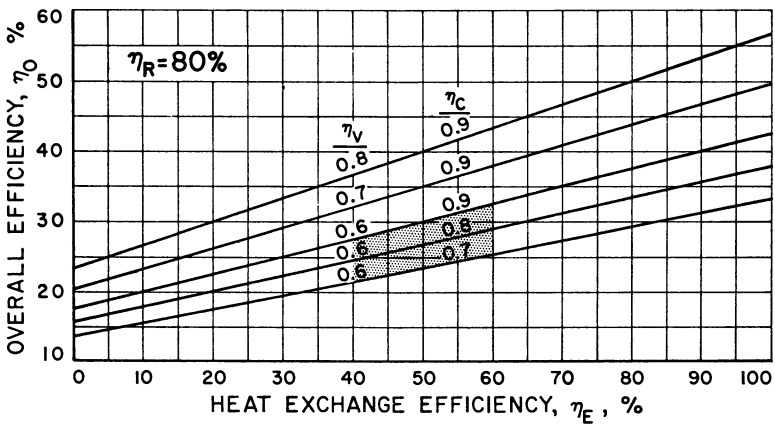

Figure 9. Effect of fuel cell and hydrogen generator parameters on system efficiency

Case 1, no recycle

A more complete analysis, made at IGT, of low temperature fuel cell systems with external reforming places the parameters studied in the following order of importance with respect to over-all efficiency in a recycle

Publication Date: January 1, 1969 | doi: 10.1021/ba-1965-0047.ch016

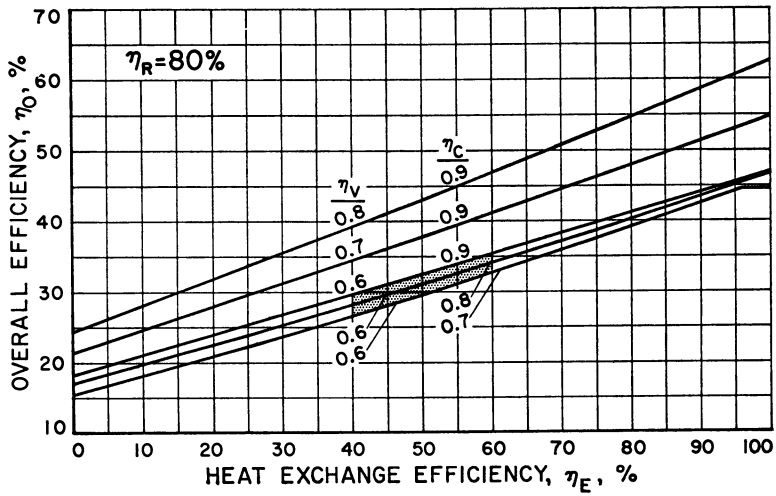

Figure 10. Effect of fuel cell and hydrogen generator parameters on system efficiency

Case 2, recycle

system operating below the cutoff point: (1) voltage efficiency, (2) reactor thermal efficiency, (3) heat exchange efficiency, and (4) conversion efficiency.

The complete economics of the present hydrogen generation system will not be known until more hardware is developed. Present estimates, based on the fuel requirements of the fuel cells under study and the catalysts and conditions described here, indicate the cost of catalysts in the IGT hydrogen generation system would be less than 5 cents per watt.

Acknowledgment

The authors wish to thank the Southern California Gas Co., the Southern Counties Gas Co., and Con-Gas Service Corp., who are sponsoring the low temperature fuel cell project for which this investigation was made. Also, the authors wish to thank Henry Linden of IGT for his helpful suggestions with respect to the conception of the over-all process and Jack Huebler of IGT for his suggestions with respect to the choice of catalysts to be used in these studies.

Literature Cited

(1) Moe, J. M., presented before the 145th National Meeting, Division of Petroleum Chemistry, American Chemical Society, New York, N.Y., September 8–13, 1963; Preprint No. 4-B, Vol. 8, B-29.

Received April 16, 1964. Presented on the Symposium on Gas Generation, Division of Fuel Chemistry, 147th Meeting of the American Chemical Society, Philadelphia, Penn., April 6, 1964.

Publication Date: January 1, 1969 | doi: 10.1021/ba-1965-0047.ch016

In Fuel Cell Systems; Young, G., el al.;
Advances in Chemistry; American Chemical Society: Washington, DC, 1969.

17

Electrode Processes in Molten Carbonate Fuel Cells

ISAAC TRACHTENBERG

Central Research Laboratories, Texas Instruments Inc., Dallas, Tex. 75222

Publication Date: January 1, 1969 | doi: 10.1021/ba-1965-0047.ch017

Current interruption studies of fuel cells using magnesium oxide matrix and a binary eutectic of lithium sodium carbonate as electrolyte show that total cell polarization is a combination of ohmic and concentration factors. No activation polarization has been observed up to 200 amp. per sq. ft. Ohmic polarization is principally the result of electrolyte restrictions at the electrode-electrolyte-matrix interfaces and an oxide film at the cathode. Concentration polarization is the major contributor to the total anode polarization. Based on experimental observations, chemical and electrochemical reaction schemes are presented for both cathodes and anodes. Curves of potential as a function of electrochemically consumed hydrogen are calculated for anodes. Effects of initial hydrogen-carbon dioxide compositions, temperature, and other parameters are considered.

Many of the potential applications of fuel cells require operation on cheap, readily available fuels and air. These fuels in all probability will be hydrocarbons or impure fuel gases readily derived from hydrocarbons. Fuel cells using molten carbonate electrolytes and operating above 500° C. affords an early opportunity for developing rapidly a system capable of satisfying these requirements. This paper presents some of the more fundamental aspects of molten carbonate-magnesium oxide-matrix cells. The causes of electrode polarization are established and measured. Typical data for the effect of fuels on anode polarization are given. Based on the experimental observations, chemical and electrochemical reaction schemes are suggested. Theoretical voltage-fuel composition curves are illustrated and indicate that good utilization of fuel at reasonable voltages can be expected. Cells have actually operated on hydrocarbon fuels and

In Fuel Cell Systems; Young, G., el al.;
Advances in Chemistry; American Chemical Society: Washington, DC, 1969.

air at acceptable power levels continuously over extended time intervals.

Fuel cells using various eutectics of molten alkali carbonates as the electrolyte have been described previously (*1, 2, 5, 8*). Operating characteristics of magnesium oxide matrix cells have also been reported (*6, 7, 9*). These cells have been thermally cycled a number of times and in some instances attained more than 4000 hours of continuous operation at 600° C. Power densities greater than 100 watts per sq. foot at 0.7 volt have been obtained with pure hydrogen fuel and 4:1 air: carbon dioxide mixtures as the cathode gas feed. These results led to design and development work on molten carbonate hydrocarbon fuel cell batteries and systems. However, discussion of these engineering studies is beyond the scope of this paper.

Publication Date: January 1, 1969 | doi: 10.1021/ba-1965-0047.ch017

Experimental

All the experimental work reported here was performed on cells identical to the one shown in Figure 1. This illustration shows the cathode

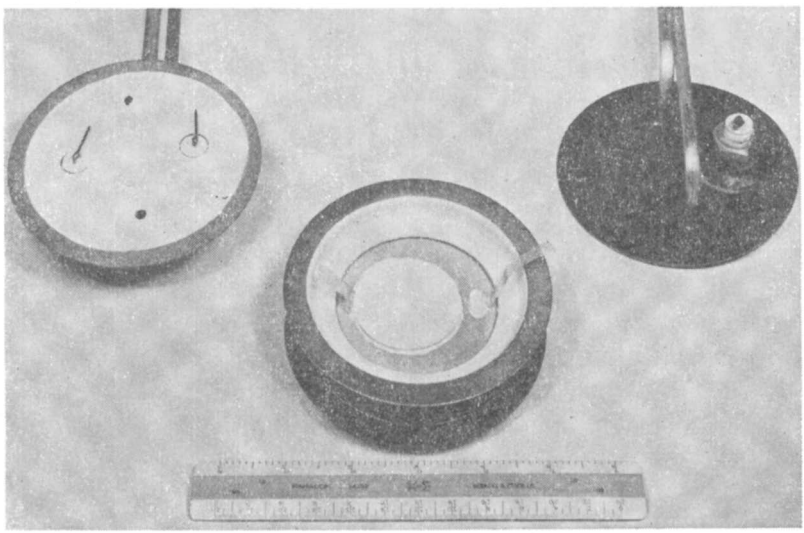

Figure 1. Cathode chamber of a working fuel cell showing third idling electrode

chamber of the cell with the third idling electrode. This small electrode is used to monitor the performance of the individual anode and cathode in a working fuel cell. The large electrode (15.6 sq. cm. or 1/60 sq. foot) is the working cathode and is bonded to the magnesium oxide matrix. The matrix is impregnated with the binary lithium sodium carbonate eutectic (m. p. ca 500° C.). Not shown is the anode bonded on the bottom side of the magnesium oxide matrix. The anode has the same

geometrical configuration and area as the cathode. Cathodes for this study were pure silver; however, substrates of base metals containing catalyst are now being used successfully. The anode is made of either silver or base metal substrates containing a variety of inexpensive catalyst.

Electrical connections are made from the electrodes to the various insulated lead-throughs. The only electrical connection within the cell between the three electrodes is through the electrolyte contained in the magnesium oxide matrix. The lids are then welded on to make each chamber gastight. The cell is placed vertically in a furnace, and the necessary external gas and electrical connections are completed.

Current-voltage traces for the complete working cell and the individual electrodes were obtained with a Moseley Model 3S X-Y recorder. A transistor network is used to give a continuously variable, pure resistive load for the cell. The current passed in this circuit is the *X*-input. The voltage between the non-working electrode and the particular working electrode to be studied, or the terminal voltage of the cell, becomes the *Y*-input. To avoid polarization of the non-working electrode the *Y*-input, or for that matter any voltage measuring device used with the non-working electrode, must have a high input impedance. These current-voltage curves measure the total steady-state polarization of the individual electrodes and the complete cell under working conditions.

To establish the contributions of the various types of polarization — ohmic, activation, and concentration — to the total polarization, it is necessary to resort to a transient method. A single current interruption technique was used for this purpose. The three polarization types of interest may be distinguished according to time intervals after the polarizing load is removed. Ohmic polarization is removed immediately after current interruption for the present investigation in times less than a microsecond. Since removal of activation polarization requires the electrode potential to change, the time required for its decay is governed by the rate of charging of the electrical double layer, or about 10^{-6} to 10^{-4} second. Polarization decay because of concentration effects requires times greater than 10^{-4} second, because appreciable mass transport (either ions in the electrolyte or molecules in gas phase) must occur.

Figure 2 schematically shows the interruption circuit. The heart of this circuit is the mercury wetted Clare relay and its make before break operating feature. This latter feature permits triggering and use of the sweep delay circuits of the Tektronix 545 A oscilloscope. Voltage time curves are recorded from the oscilloscope from 10^{-6} to 1 second (9).

Current-Voltage Curves for Operating Cell

The specific results presented are typical examples of the data obtained from a large number of experiments on many similar cells. Figure

Publication Date: January 1, 1969 | doi: 10.1021/ba-1965-0047.ch017

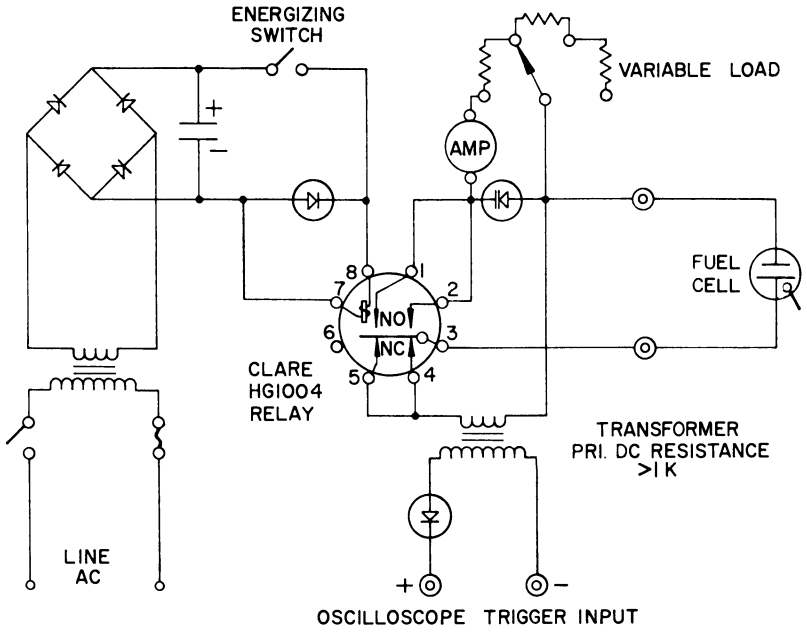

Figure 2. Interrupter circuit

3 shows current-voltage curves for a cell operating at 600° C. on pure hydrogen fuel on the 25th day of operation. The cathode is supplied with a 4:1 mixture of air: carbon dioxide. The curve V_T represents the terminal voltage of the operating cell. The open circuit voltage is 1.40 volts. V_A and V_C curves are the voltage of the anode and cathode, respectively, *vs.* the non-working electrode. The values of R_A and R_C, the ohmic resistances as determined by current interruption, were measured at several pre-interruption currents and were found to be constant. Correction for the ohmic polarization is made, and the curves $V_A + IR_A$ and $V_C - IR_C$ are the current-voltage curves due to concentration polarization. It is interesting to note that $R_A + R_C < R_T$. This difference is assumed to be the bulk electrolyte resistance, R_E. In addition to the ohmic resistance at the electrode-electrolyte-matrix interface, R_A and R_C contain the resistance of the individual electrode leads to the terminals just outside of the furnace. For the particular case of cell 117R at 600° C., R_A, R_C, and R_T are 0.075, 0.10, and 0.21 ohms, respectively; the lead resistance of the individual electrodes is about 0.025 ohm. R_E is calculated to be 0.035 ohm. The calculated resistance based on electrolyte conductivity, electrode size, and separation is 0.011 ohm. These calculations imply a factor of about 3 due to porosity and tortuosity of the magnesium oxide disc.

The V_T curve indicates a power density equivalent to 60 watts per

Publication Date: January 1, 1969 | doi: 10.1021/ba-1965-0047.ch017

sq. foot at 0.7 volt. If all ohmic factors except the bulk electrolyte resistance, R_E, could be removed, this cell would produce an equivalent of 120 watts per sq. foot at 0.7 volt.

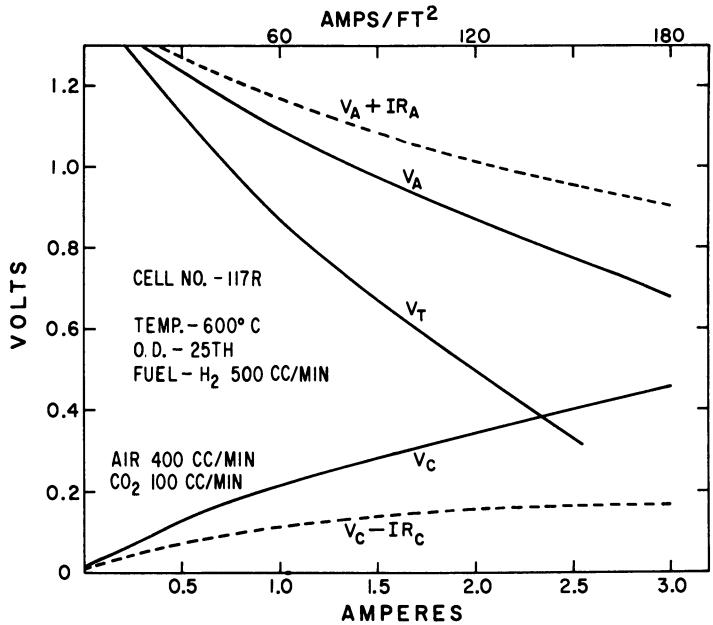

Figure 3. Typical polarization curves for a cell and individual electrodes operating on H_2 and air-CO_2

Several features concerning the polarization of the individual electrodes should be pointed out. Limiting currents are not being approached, even at current densities of 200 amps per sq. foot. Ohmic polarization is a more important factor at the cathode, where oxide films may be formed. Concentration polarization is greater at the anode, since products must back-diffuse.

Figure 4 shows additional current-voltage curves for cell 117R. To obtain these data, 200 cc. per minute of carbon dioxide were added to the original hydrogen fuel supply. This fuel represents a reformed hydrocarbon. The cathode conditions were unchanged, and the same polarization curves were obtained for it as those in Figure 3. The effect of additional flow rate by itself is negligible. (Hydrogen rate was raised to 700 cc. per minute with no measurable change in the current-voltage curve.) The effect of adding carbon dioxide was observed immediately even at open circuit. Considerable amounts of water were obtained in the fuel effluent. The values of R_A, R_C and R_T were not altered by the change in fuel composition. However, the open circuit voltage is markedly reduced and can be attributed to the introduction of carbon dioxide and the for-

Publication Date: January 1, 1969 | doi: 10.1021/ba-1965-0047.ch017

mation of water from the water-gas shift equilibrium. These substances are products from the over-all anode process.

The terminal power output is equivalent to 42 watts per sq. foot at 0.7 volt, and if all ohmic factors excluding bulk electrolyte resistance were eliminated, an equivalent power of about 84 watts per sq. foot at 0.7 volt could be obtained. It should be noted in comparing Figures 4 and 3 that the concentration polarization, 0.18 volt, at an equivalent of 100 amp. per sq. foot for reformed hydrocarbon fuel is considerably lower than that of the pure hydrogen fuel, 0.35 volt, at the same current density. However, the open circuit voltage and the operating voltage are lower for the reformed fuel, 1.06 volts open circuit compared to 1.40 volts open circuit for the pure hydrogen fuel.

Publication Date: January 1, 1969 | doi: 10.1021/ba-1965-0047.ch017

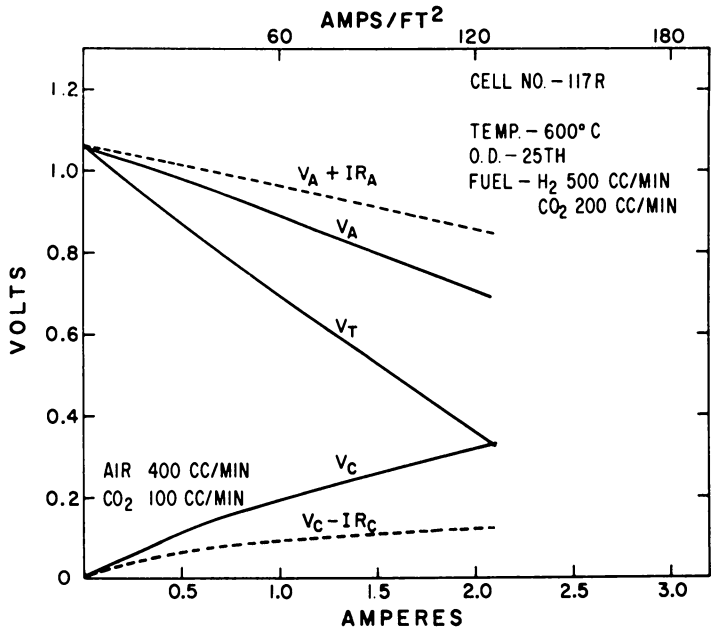

Figure 4. Typical polarization curves for a cell and individual electrodes operating on a simulated reformed hydrocarbon and air-CO_2

What has been referred to as concentration polarization until now is really total polarization minus ohmic polarization. From data such as these and current interruption studies, no activation polarization or evidence of any could be detected. As might be expected, the system is subject to less concentration polarization as product concentration of the incoming fuel increases.

Current Interruption Studies

As previously mentioned, the various types of polarization — ohmic, activation, and concentration — may be distinguished and measured by voltage decay as a function of time after interruption of a steady state current. A previous publication (9) was concerned only with pure hydrogen fuel in this system. Comparison of hydrogen with simulated reformed hydrocarbon fuels is presented here.

Figure 5 illustrates anode current-voltage curves corrected for ohmic polarization. Open circuit voltage decreases with decreasing flow rate and increasing product carbon dioxide and water concentration. However, polarization at any given current density decreases with increasing product concentration of the incoming fuel. The lower open circuit voltage of curve *B* compared to curve *A* is related to the amount of carbon dioxide continuously escaping from the electrolyte and the relative concentration of carbon dioxide, water and hydrogen (see proposed reaction scheme).

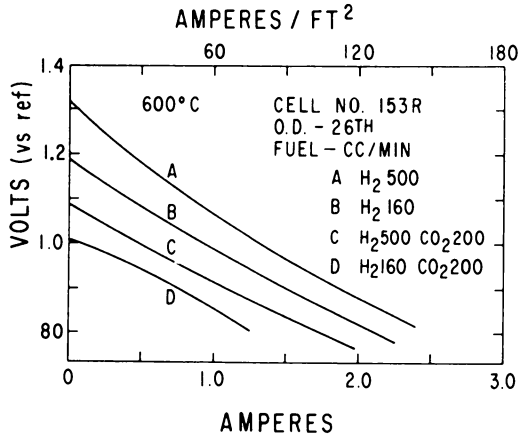

Figure 5. Anode polarization curves corrected for ohmic polarization. Data obtained from operating cell

Current interruption experiments were completed with the fuels indicated in Figure 5. All measurements were made at a pre-interruption current equivalent to a current density of 60 amp. per sq. foot. Figure 6 illustrates the voltage-time curves for the two high fuel flow rates. The two straight lines are characteristic of this type of measurement. The steady state polarization is represented by the symbols through the ordinate. The initial drop is the same for all fuels and flows studied. Data in the 10^{-6} range are somewhat distorted by the ring-back voltage which develops when the current drops instantly. The horizontal line

Publication Date: January 1, 1969 | doi: 10.1021/ba-1965-0047.ch017

in the 10^{-5} to 10^{-4} second range indicates no measurable activation polarization. The polarization decay in times greater than 10^{-4} is attributed to concentration effects. The two curves are almost parallel. At the high flow rates used, any effect of flow rate has been removed. Since polarization for the hydrogen–carbon dioxide fuel is less than that for pure hydrogen, the hydrogen–carbon dioxide open circuit voltage is attained more rapidly.

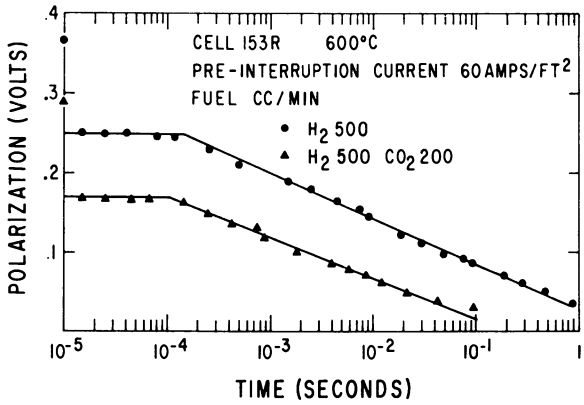

Figure 6. Anode polarization-time curves after interruption of 1.0 amp.

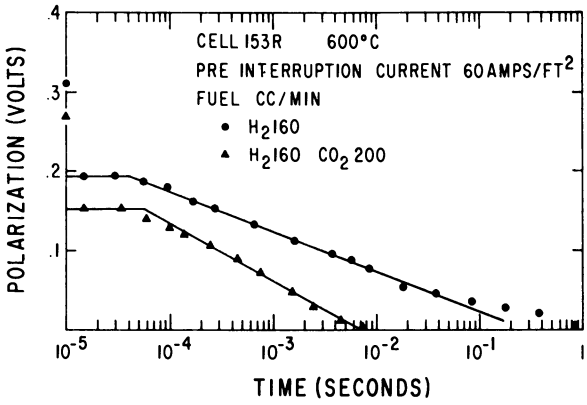

Figure 7. Anode polarization-time curves after interruption of 1.0 amp.

Figure 7 illustrates the voltage–time curves for the lower flow rates of Figure 5. The same characteristic features are observed here as in Figure 6. The ohmic polarization is constant, and there is no measurable activation polarization. However, there is an effect of flow rate. The total flow of 360 cc. per minute for hydrogen–carbon dioxide case in-

Publication Date: January 1, 1969 | doi: 10.1021/ba-1965-0047.ch017

creases the rate of decay of concentration polarization over that observed for pure hydrogen at 160 cc. per minute.

The effect of flow rate on anode polarization curves was studied in another series of experiments. The Figure 8 anode polarization curves are corrected for ohmic polarization for various fuels and flow rates. Curve I illustrated that cells operating on reformed hydrocarbons at high flow rates perform better than on pure hydrogen, even though the open circuit voltage is higher for the pure fuel. The introduction of an inert gas to aid sweep, Curve III, leads to high open circuit voltage but polarizes much more rapidly (compare Curves II or III) when placed under load.

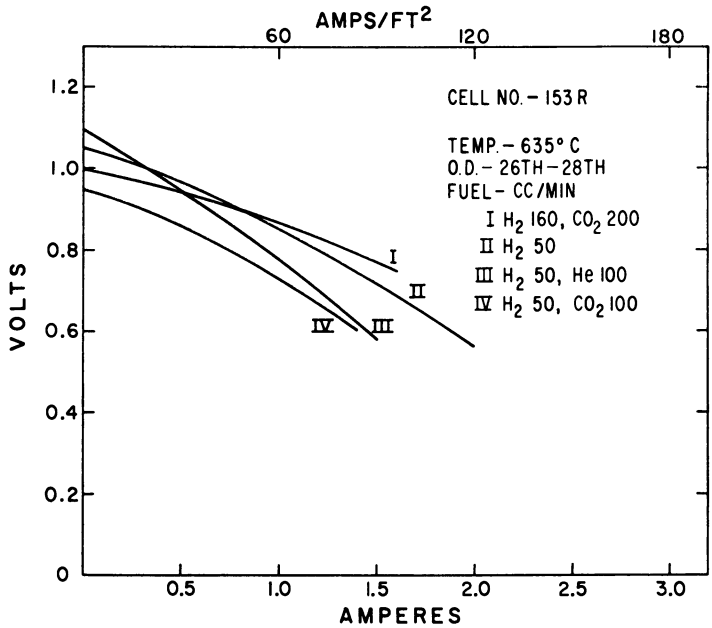

Figure 8. Anode polarization curves corrected for ohmic polarization. Data obtained from operating cell varying fuel composition and flow rate

All data relating to flow rates indicate that the benefits of high open circuit voltage obtained by high flows of pure hydrogen or hydrogen diluted with inert gases are lost when significant quantities of the fuel are consumed. The effect of the high flow rates of gases is to reduce the concentration of non-electrochemically produced carbon dioxide and water. When the electrochemical processes are functioning, this effectiveness of gas sweeping is greatly reduced.

Interruption studies were made on cathodes. Figure 9 is a typical voltage-time plot for a cathode operating on a 4:1 mixture of air: carbon dioxide. The curves are very similar to those obtained for anodes.

Publication Date: January 1, 1969 | doi: 10.1021/ba-1965-0047.ch017

Cathodes exhibit higher ohmic polarization than anodes and less concentration polarization, and they are not as sensitive to gas flows. Since concentration polarization is small, electrode steady state is rapidly attained.

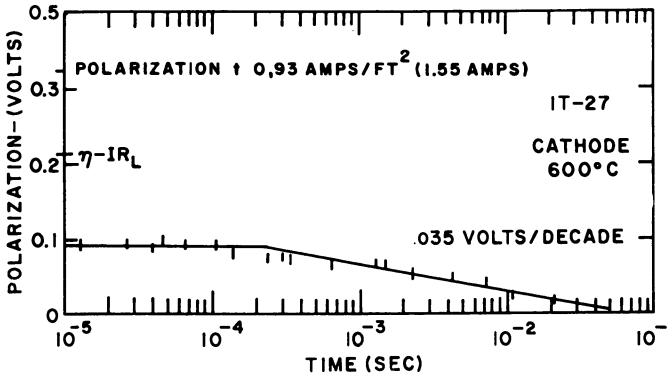

Figure 9. Cathode polarization-time curve for typical cathode after interruption of 1.55 amp.

Ohmic Polarization and Electrolyte Resistance

Ohmic resistance at the individual electrodes is calculated from the initial (10^{-6} second) voltage decay and the pre-interruption current. The values determined include lead resistance (0.025 ohm). Bulk electrolyte resistance is determined by subtracting the sum of the anode and cathode resistance from the total cell resistance.

The temperature coefficients of the various resistances were measured. The coefficient of the anode was nearly identical with that of the bulk electrolyte while the coefficient of the cathode was much higher (resistance decreased more than would be predicted on the basis of changes in electrolyte conductivity alone).

The relatively high ohmic polarization at the anode, the consequence of ohmic resistance, may be attributed to electrolyte restriction at the electrode–matrix interface. It is very unlikely that all pores of the electrode match the pores in the matrix. In fact, there is a great deal of masking. This masking greatly reduces the thickness and number of electrolyte paths between the active electrode sites and the bulk electrolyte and increases the ohmic resistance. Since the temperature coefficient of the ohmic resistance at the anode is the same as the bulk electrolyte, it is reasonable to assume that all the ohmic polarization at this electrode is due to the electrolyte. Its relatively large value is directly attributable to the degree of electrolyte restriction.

At the cathode a similar situation exists. However, there is an addi-

Publication Date: January 1, 1969 | doi: 10.1021/ba-1965-0047.ch017

tional contribution to the ohmic resistance which has a larger temperature coefficient. Although silver oxide is thermally unstable at 600° C., there is a finite amount present on the electrodes. This oxide layer introduces some additional ohmic resistance. As the temperature is increased, the amount of oxide is reduced and the ohmic polarization decreases.

Reaction Scheme for Over-All Electrode Processes

The foregoing experiments and results suggest that all reaction kinetics are very fast and equilibria are established. The observed polarization is attributed to ohmic resistances and mass transport limitations. At the anode the same types of polarization exist for hydrogen fuel as for a variety of hydrogen–carbon dioxide fuels which represent reformed and partially consumed reformed hydrocarbon fuels.

Two chemical reactions are assumed to be always in equilibrium:

$$H_2 + CO_2 \rightleftarrows H_2O + CO \quad (1)$$

$$CO_3^{=} \rightleftarrows CO_2 + O^{=} \ (3,4) \quad (2)$$

The oxide ion is the active potential determining species present in the electrolyte. The electron-transfer reaction becomes

$$M + O^{=} \rightleftarrows MO + 2e^{-} \quad (3)$$

where M represents the active metal catalysts. Fuel is consumed in the chemical reduction of the metal oxide by hydrogen.

$$MO + H_2 \rightleftarrows M + H_2O \quad (4)$$

thus regenerating the active metal catalysts. At 600° C. and higher this latter reaction proceeds rapidly and is always in equilibrium, the equilibrium being shifted very far toward metal-water.

On the basis of this model the anode potential may be represented as

$$E_A = E_A^0 - \frac{2.3\,RT}{nF} \log \frac{[a_{H_2O}][a_{CO_2}]}{[a_{H_2}]} \quad (5)$$

where a_i represents the activity of the various reactants and products. The various activities are represented in terms of a contribution from electrochemical and chemical reaction. For example,

$$a_{H_2O} = \Theta_{H_2O}\,(x + y) \quad (6)$$

where Θ_{H_2O} is a proportionality constant, x is partial pressure of water obtained from electrochemical conversion, and y is the partial pressure of water obtained by shift conversion.

Figure 10 illustrates anode potential curves obtained assuming Θ_{H_2O} and Θ_{CO} equal to 1. The initial fuel is pure hydrogen. The potential

Publication Date: January 1, 1969 | doi: 10.1021/ba-1965-0047.ch017

is plotted as a function of the hydrogen electrochemically consumed. The potential scale is meant to be a relative scale, since E_A^0 was assumed to be standard potential for the reaction

$$H_2 + 1/2\ O_2 \rightleftarrows H_2O \qquad (7)$$

at the appropriate temperature. The dashed line is the same plot neglecting the shift reaction.

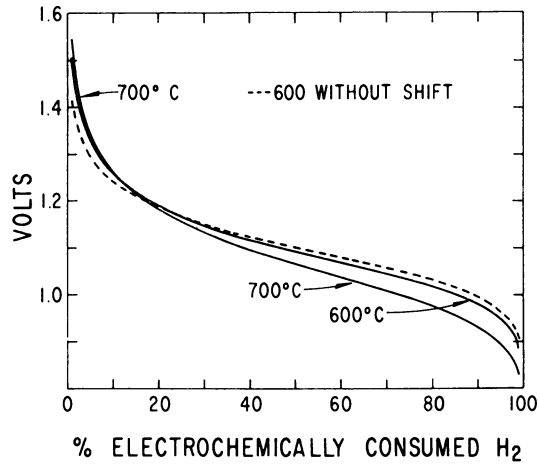

Figure 10. Calculated potential-fuel consumption curves for anodes

In Figure 11 the value of θ_{H_2O} was varied, and a family of curves with the same potential variation with hydrogen consumption was obtained. In all of these curves the cathode is invariant. θ_{H_2O} represents a weighting factor for surface coverage. Since carbon dioxide pressure effects the potential by establishing the equilibrium concentration of $O^=$, its weighting factor is always unity. However, there is competition for metal sites between hydrogen and water. The weighting factor indicates the ratio of water-coverage to hydrogen-coverage when the partial pressure of the two components is equal. As Figure 11 indicates, θ_{H_2O} merely changes the absolute anode potential for a given E_A^0. This value of θ_{H_2O} for an electrode will depend on the metal catalyst.

Figure 12 illustrates the effect of starting with fuels obtained from various hydrocarbon treating processes. Curves *A* and *B* represent steam reforming with limited purification of the raw reformate. Curve *C* represents completely reformed and shifted natural gas. Curve *D* represents partial oxidation of hydrocarbons of the class C_nH_{2n}. Curve *E* is an 80% consumed fuel in which all the water is removed. At low consumption there is appreciable benefit in initially supplying pure hydrogen. How-

Publication Date: January 1, 1969 | doi: 10.1021/ba-1965-0047.ch017

ever, at more than 50% electrochemical consumption of the starting fuel there is very little advantage in using pure hydrogen, and various partially oxidized hydrocarbons may be used with equal effectiveness.

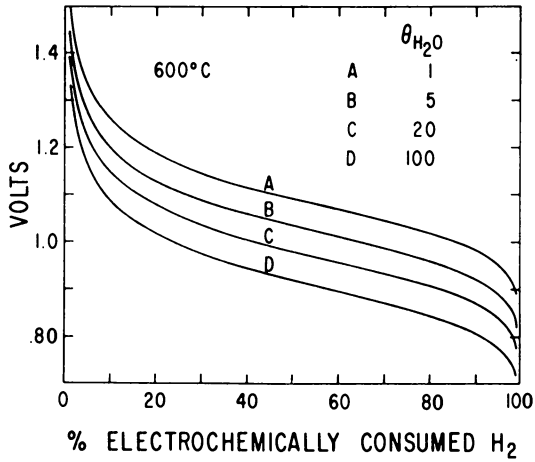

Figure 11. Calculated potential-fuel composition curves for anodes assuming various ratio of H_2O:H_2 adsorption

The proposed reaction scheme for cathodes (9) is similar to that for anodes. The first step in the scheme is the adsorption of oxygen.

$$O_2 + n\text{Ag} \rightleftarrows 2\text{Ag}_{n/2}\text{O} \tag{8}$$

This oxide formation is responsible for the additional ohmic resistance observed at the cathode. The electrochemical reaction is

$$2\text{Ag}_{n/2}\text{O} + 4e^- \rightleftarrows n\text{Ag} + 2O^= \tag{9}$$

and finally the equilibrium between CO_2 and $O^=$,

$$2CO_2 + 2O^= \rightleftarrows 2CO_3^= \tag{10}$$

is established at the cathode. The potential of the cathode may be written as

$$E_C = E_C^0 - \frac{2.3\,RT}{nF} \log \frac{1}{(a_{O_2})(a_{CO_2})^2} \tag{11}$$

where a_{O_2} and a_{CO_2} are the activities (partial pressures of oxygen and carbon dioxide).

According to Equation 11, substitution of oxygen for air should increase the over-all cell voltage about 30 mv. This predicted result has been verified experimentally.

Publication Date: January 1, 1969 | doi: 10.1021/ba-1965-0047.ch017

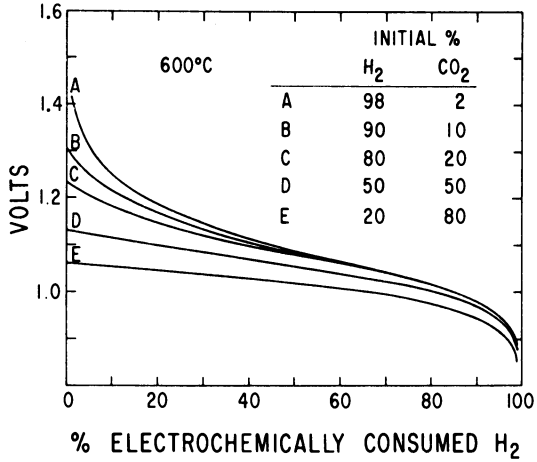

Figure 12. .Calculated potential-fuel composition curves for anodes varying composition of starting fuel

Conclusion

Fuel cells employing molten carbonate electrolytes can be operated successfully on air and a wide variety of fuels readily derived from hydrocarbons. At current densities up to 200 amp. per sq. foot there is no kinetic limitation other than mass transport.

When hydrocarbon-derived fuels are initially supplied to the anode, open circuit voltage is lower than when pure hydrogen is supplied. However, under appreciable load, anode polarization on impure fuel is much lower. Cathodes perform well on mixtures of air and carbon dioxide.

Although all the electrodes investigated showed no activation polarization, electrode potential under operating conditions is dependent on the product-reactant adsorption equilibrium of the particular catalyst-electrode.

Acknowledgment

In part, the work reported here received financial support from the U. S. Army Engineer Research and Development Laboratories, Fort Belvoir, Va.

Literature Cited

(1) Broers, G. H. J., "High Temperature Galvanic Fuel Cells," Thesis, University of Amsterdam, 1958.
(2) Broers G. H. J., Ketellaar, J. A. A. in "Fuel Cells," Young, G. J., ed., pp. 78–93, Reinhold, New York, 1960.
(3) Djordjevic, S., Hills, G. J., *Trans. Faraday Soc.* **56**, 269 (1960).
(4) Flood, H., Forland, T., Motzfeldt, K., *Acta. Chem. Scand.* **6**, 257 (1952).

Publication Date: January 1, 1969 | doi: 10.1021/ba-1965-0047.ch017

(5) Kronenberg, M. L., *J. Electrochem. Soc.* **109,** 753 (1962).
(6) Peattie, C. G., Barbee, B. H., Kreiselmaier, K. W., Parker, S. G., Trachtenberg, Isaac, White, A. H., "Performance Data for Molten-Electrolyte Fuel Cells Operating on Several Fuels," *Conference Proceedings 1962, Pacific Energy Conversion Conference*, San Francisco, Calif., Aug. 12–16, 1962.
(7) Peattie, C. G., Trachtenberg, Isaac, Barbee, B. H., Kreiselmaire, K. W., Parker, S. G., White, A. H., *Progr. Astron. and Aeron.* **XI,** pp. 269–278 Academic Press, New York, 1963.
(8) Sandler, Y. L., *J. Electrochem. Soc.* **109,** 1115 (1962).
(9) Trachtenberg, Isaac, *J. Electrochem. Soc.* **111,** 110, (1964).

RECEIVED February 17, 1964.

Publication Date: January 1, 1969 | doi: 10.1021/ba-1965-0047.ch017

In Fuel Cell Systems; Young, G., el al.;
Advances in Chemistry; American Chemical Society: Washington, DC, 1969.

High Temperature Natural Gas Fuel Cells

B. S. BAKER, L. G. MARIANOWSKI, JOHN MEEK, and H. R. LINDEN

Institute of Gas Technology, Chicago, Ill.

Publication Date: January 1, 1969 | doi: 10.1021/ba-1965-0047.ch018

A substantial operating lifetime (seven months) at a reasonable average power density (12 mw. per sq. cm.) was achieved with reformed natural gas as fuel and flue gas containing excess air as oxidant. Studies with a number of electrode types for immobilized molten carbonate electrolyte fuel cells are described, including metal foil, vacuum deposited film, painted film, sintered powder, and sintered fiber electrodes. The development of multiple-cell batteries of open cathode, natural convection design is discussed. Present work is directed at the development of economically feasible battery configurations. The economics of high temperature fuel cell hardware is presented in a detailed analysis of component costs.

Fuel cell research at the Institute of Gas Technology (IGT) began in 1959. Using the work done by Broers (2) on the molten carbonate high temperature fuel cell as a starting point, IGT has concentrated a large portion of its effort on further development of this system from both a fundamental and an engineering viewpoint. Background material and earlier work from this laboratory, through 1960, have been described elsewhere (*11*).

During the past two years the research and development effort of IGT on a natural gas–operated, molten carbonate fuel cell system has been in five areas:

Electrode evaluation and design
Paste electrolyte development
Natural gas reforming
Battery design and scale-up
Economic evaluation

American Chemical Society
Library
1155 16th St., N.W.
Washington, D.C. 20036

In Fuel Cell Systems; Young, G. J., et al.;
Advances in Chemistry; American Chemical Society: Washington, DC, 1969.

The results in these five areas are summarized here. All five areas are strongly interrelated and interdependent, and each combination of electrode, electrolyte, reformer, and battery design gives rise to different fundamental requirements for one or more of the individual components. Any given design will affect the economics of the fuel cell system.

In an economic analysis of domestic fuel cell systems, Von Fredersdorff (*12*) has indicated some of the limitations on fuel cell hardware costs. An important part of this research has been to establish the feasibility of economic hardware for natural gas operation.

Electrode Evaluation and Design

Almost all fuel cell electrodes must possess the same general characteristics of high electrocatalytic activity, good mass transport properties, and long-term physical and chemical stability. In the high temperature molten carbonate system, the activity criterion is alleviated by the elevated operating temperatures, and the mass transfer problems are not unlike those associated with other types of fuel cells. However, the stability problems are in many respects unique because of the properties of the molten carbonate electrolyte and the operating temperatures.

At IGT a number of different types of electrodes have been studied from both a structural and chemical viewpoint in the last two years. Metal foil, thin film, sintered powder, and sintered fiber structures have been explored. Materials used in these investigations have been platinum, nickel, silver, palladium, and alloys of silver and palladium.

Metal Foil Electrodes. Hydrogen permeable metal foils have been used for some time in conjunction with commercial hydrogen purification processes, and much technical literature on these materials is available (4, 7). IGT was attracted to the concept of a metal foil anode early in its program as an expedient means for solving two problems associated with the molten carbonate fuel cell—electrode flooding and corrosion. The first foils studied were alloys of palladium and silver, for which typical performance is shown in Figure 1. Complete details of the IGT palladium foil fuel cell have been published (*9*). Since the anode in this cell is not permeable to the reaction products, the mass transport processes are very different from those associated with more conventional molten carbonate fuel cells. A variety of experiments indicated that the over-all anode reaction is strongly limited by the diffusion of reaction products (carbon dioxide and water) away from the electrode. The fact that diffusion of hydrogen through the foil did not appear to be limiting led to experiments with pure palladium foils of poorer hydrogen diffusion characteristics. Somewhat better cell performance was observed (Figure 1), although a direct comparison could not be made because improvements in other cell components were incorporated at the same time.

Publication Date: January 1, 1969 | doi: 10.1021/ba-1965-0047.ch018

Silver-palladium diffusion foil electrodes have operated continuously under 25 ma. per sq. cm. load for over seven months without apparent damage to the anodes. Unfortunately, these palladium diffusion foil electrodes are too expensive for gas industry use. At present other, less expensive, hydrogen permeable foil electrode materials are being investigated.

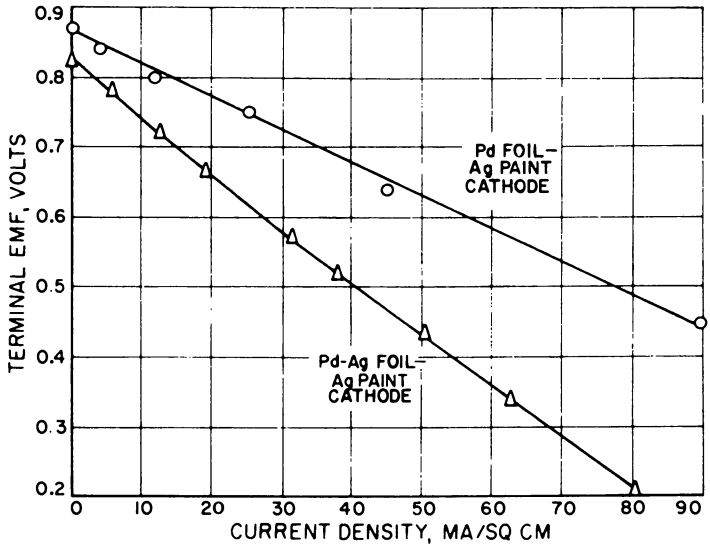

Figure 1. Comparison of performance of pure palladium and palladium-silver anode high temperature fuel cells at 600° C.

Thin Film Electrodes. The use of metal film electrodes is economically attractive, especially in those cases where noble metals are needed. With semisolid electrolyte molten carbonate fuel cells it is possible to use the electrolyte, which at suboperating temperature is a solid, as the support for applying the thin film. Electrodes were applied by vacuum deposition and simple painting techniques. In the latter, the metal to be deposited exists as a finely dispersed particle in an organic binder. All solutions used for the process were commercially available.

The first experiments were directed toward development of a thin film silver cathode. The major anticipated difficulty in this instance was the dissolution of the silver in the electrolyte. Douglas (5), Broers (3), and Janz (8) have discussed this problem. Silver film electrodes (0.001 cm. thick) prepared from commercial silver paints have performed over 4000 hours at 600° C. without apparent loss in performance, although some dissolution of silver in the electrolyte did occur. This relatively long lifetime is attributed to the fact that the cells were operated at lower temperatures than those used in the work of others and were continuously

Publication Date: January 1, 1969 | doi: 10.1021/ba-1965-0047.ch018

under load; the oxygen electrode is always cathodically polarized, suppressing the dissolution reaction. Moreover, cathodes were not physically flooded to any significant extent.

The successes with the silver film cathodes led to experimentation with other metals in an effort to develop a similar type of anode structure. Little success was achieved in this area, primarily because of electrode flooding. Results of various experiments are summarized in Table I. The best results were achieved with vacuum-deposited palladium; however, the cell lifetimes obtained were only about 300 hours.

Table I. Performance of Porous Noble Metal Anode Films

Anode material	*Preparation method*	*Performance decay,[1] hours*		*Cell lifetime, hours*
		90%	*75%*	
Pt	Paint	15	85	108
Ag-Pt	Paint	4	17	41
Pt	Paint	40	57	66
Pd	Paint	26	60	138
Pd	Paint	17	42	95
Pd	Paint	15	45	72
Pd	Vacuum-deposited	100	Not determined	293

[1] Time to reach 90% and 75% of initial performance with respect to power output at constant current.

Since performance decreases with increasing load, anode flooding could have been caused either by carbonate ion transport or by drag forces exerted on the electrolyte by the escaping reaction products. However, the reaction products do not cause cathode flooding when they are forced to escape through a film cathode (by using a foil anode, which is impermeable to the reaction products). Hence, flooding must be associated with the directional character of ionic transport phenomena. A more detailed investigation of these effects is now in progress.

Sintered Metal Electrodes. Two types of sintered metal electrodes have been investigated: (1) conventional nickel and silver powder electrodes available from Clevite Corp.; and (2) nickel and palladium fiber metal electrodes obtained from IIT Research Institute. Early in the study, it was observed that similar performances were obtained from bulk sintered silver and silver film cathodes, and further research with the former was abandoned in favor of the more economic silver film electrode.

The high cost of palladium foil anodes indicated that a new look at nonnoble metals was required. Early IGT attempts to use sintered nickel powder (*11*) indicated that severe corrosion problems existed. The most serious difficulty arises from direct contact of the anode with the oxygen from the cathode because of air leakage through the electrolyte. A second problem arises when the anode is operated at polarization conditions such that electrochemical consumption of the nickel is possible. At 600° C., this polarization value is about 200 mv. below the hydrogen con-

Publication Date: January 1, 1969 | doi: 10.1021/ba-1965-0047.ch018

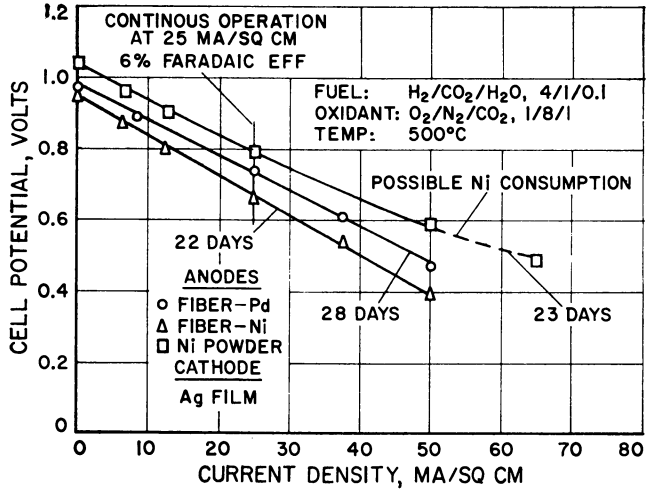

Figure 2. Effect of different anodes on high temperature fuel cell performance

sumption potential. This phenomenon has been discussed recently in some detail by Broers (*3*) for nickel and iron electrodes and by Bloch (*1*) for these and other electrode materials. The most recent IGT experiments with nickel metal electrodes and improved electrolyte structures have been conducted at 500° C. for more than 1500 hours at current densities between 15 and 25 ma. per sq. cm. without serious nickel corrosion. The lower operating temperature alleviates the direct chemical corrosion problem but reduces the polarization zone in which the anode can be safely operated.

To determine the effect of electrode structure on cell performance, a number of recent experiments with sintered fiber metal electrodes have been made. Typical results comparing sintered powder and fiber metal electrodes are shown in Figure 2. So far, performance of fiber metal electrodes seems inferior to that of the sintered powder types. However, the possibilities of fiber metal structures have been only superficially explored, and more extensive research is now in progress.

The conclusions concerning electrode development are:

Hydrogen permeable palladium-silver metal foil electrodes can be used for long periods (more than seven months) without apparent deterioration.

Thin film silver cathodes, at 600° C., are relatively stable and make excellent low cost structures for the molten-carbonate type fuel cells.

Thin film anode structures are unstable, becoming rapidly flooded in proportion to the current drain on the cell.

Sintered powder nickel anodes can be operated for at least 1500 hours without appreciable corrosion under the proper conditions.

Publication Date: January 1, 1969 | doi: 10.1021/ba-1965-0047.ch018

Paste Electrolyte Development

In molten carbonate fuel cells, the electrolyte can exist:

As a free liquid between appropriate electrode structures
Contained in a presintered porous inert matrix
Mixed with an inert powder to form a pasty structure above the melting point of the carbonate mixture

Because of technological problems associated with sealing, stability, contacting, and fabrication techniques, the first two approaches have been abandoned in favor of the paste electrolyte.

Paste electrolytes for the molten carbonate fuel cells can be prepared by cold-pressing, hot-pressing, hot injection or extrusion, and other special techniques, some of which have been described in some detail by other workers (*10*). Only variations in cold-pressing techniques are explored here, since these constituted the bulk of the IGT effort.

Binary and ternary eutectics of sodium-lithium carbonates and sodium-lithium-potassium carbonates were used in all experiments. The ternary eutectic melts at about 100° C. below the binary mixture and thus allows the construction of lower temperature cells. Typical 1000-cycle cell resistivities of 9 and 7 ohm-cm. were obtained for 50 weight % mixtures of ternary carbonate in magnesium oxide at 500° and 600° C., respectively. Thirty weight % mixtures of binary carbonate eutectic exhibited cell resistivities in the neighborhood of 11 ohm-cm. at 600° C. For the most part, cell resistances were dependent only on electrolyte mixtures and not on the electrode structure employed.

The electrolyte matrix employed was determined by the anode structure. In the hydrogen-permeable foil anodes, 30 weight % molten carbonate disks were prepared with 70% coarsely grained magnesium oxide as inert constituent. This cold-pressed disk had a density of 70% of the theoretical after firing. Denser electrolyte compositions showed better open-circuit potential, but under load they polarized more heavily than the 70% density disk. Thus, in the foil anodes, where reaction products must escape through the electrolyte via the cathode, densification of electrolyte would be detrimental.

With the sintered metal electrodes, especially those consisting of nonnoble metals, densification of the electrolyte is important and increases both lifetime and performance characteristics of the fuel cell. Initial experiments with nickel electrodes and 70% density paste electrolyte exhibited lifetimes of the order of 100 hours. By increasing the density of paste electrolyte to about 80% of the theoretical, IGT has achieved lifetimes of 1500 hours. Increasing electrolyte density also increases both the load and open circuit potential by about 200 mv. Electrolyte densification can be achieved by repeated crushing and grinding procedures if care is taken to avoid metallic contamination. Also, it is advantageous

Publication Date: January 1, 1969 | doi: 10.1021/ba-1965-0047.ch018

to increase the total carbonate content of the mixture by the use of small grained (less than 1 micron) magnesium oxide, which has a greater melt retention capacity.

Recent experiments, in which cold-pressed and fired disks are heated within 5° of the melting point of the carbonate eutectic and then hot-pressed at moderate pressures, indicate that disks with 96% of the theoretical density can be prepared.

The conclusions concerning paste electrolytes are:

High density electrolyte pastes are detrimental to the performance of fuel cells using hydrogen-permeable foil anodes.

In all other cases, high density pastes are essential for achieving reasonable cell lifetimes.

Cold-pressed disks can achieve a maximum density of about 85% by repetitive crushing and grinding techniques.

Hot-pressing previously cold-pressed disks at a few degrees below the melting point causes significant densification to take place.

Natural Gas Reforming

Four modes of operation are theoretically possible for natural gas utilization in a molten carbonate fuel cell system:

1. Direct electrochemical oxidation of methane.
2. In situ reforming of methane and steam on the anode and electrochemical oxidation of the carbon monoxide and hydrogen thus formed.
3. In situ catalytic reforming of methane and steam in the anode chamber and electrochemical oxidation of the carbon monoxide and hydrogen thus formed.
4. External catalytic reforming of methane and steam, followed by electrochemical oxidation of hydrogen or hydrogen–carbon monoxide mixtures in the fuel cell.

Scheme 1 has been found unacceptable because of the electrochemical inertness of methane in the presence of nonnoble metal electrodes even at relatively high temperatures and the occurrence of carbon deposition when methane alone is present at these temperatures.

Scheme 2 is undesirable because the temperature required for the reforming (750° C.) is higher than that needed for electrochemical oxidation of hydrogen. This places an undesirable high operational temperature handicap on the fuel cell. Moreover, the presence of excess steam reduces the electrode performance (*6*). Finally, it is very difficult to design an electrode which is effective both as an electrochemical element and as a reforming catalyst.

Scheme 3 is relatively unexplored but would be characterized by the same drawbacks as Scheme 2, except that the electrode would not be required to function both electrochemically and as a reforming catalyst.

Scheme 4 has been adopted by IGT as the most feasible, since it

Publication Date: January 1, 1969 | doi: 10.1021/ba-1965-0047.ch018

permits separate optimization of fuel cell and reformer units. It permits accurate control of the composition of the input gas to the fuel cell and allows the cell to be operated effectively at substantially lower temperatures (between 500° and 600° C.). The lower operating temperatures for the fuel cell enhance electrode stability and the lifetimes of the materials of construction.

The drawback of separate fuel cell and reformer units is a reduction in the over-all system efficiency when the fuel cell is operated at a lower temperature than the reformer. Theoretically, this reduction can be shown to be about 13 percentage points for a reformer operating at 750° C. and a fuel cell operating at 500° C. The loss in efficiency for the dual-temperature system arises from the unavailability of the low quality waste heat of the fuel cell for supplying the heat of reaction for the reforming operation. In actual practice other losses might be incurred when two units are used because of the inefficiency of the heat transfer processes.

The higher voltage efficiencies experimentally achieved in the IGT system with the reformed mixture more than compensate for the engineering and theoretical losses resulting from the dual system mode of operation. Figure 3 compares the performances of a fuel cell at 500° C., supplied with externally reformed natural gas, and of a fuel cell at 750° C. with the equivalent methane-to-water ratio for in situ reforming. Also

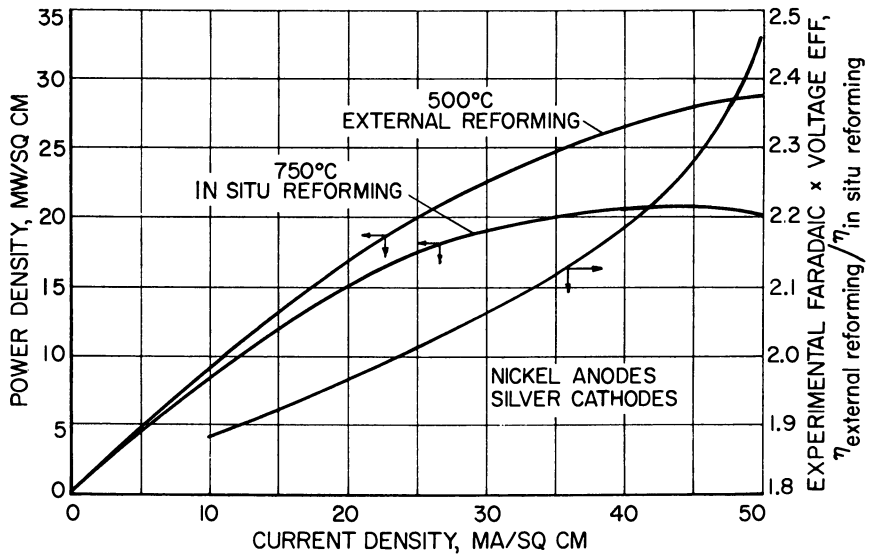

Figure 3. Comparison of external and in situ reforming on fuel cell performance

shown in this figure is the experimentally observed ratio of efficiencies of the two systems. This ratio was computed from the products of the

Publication Date: January 1, 1969 | doi: 10.1021/ba-1965-0047.ch018

experimental Faradaic efficiency and voltage efficiency of the two cells. Thermal inefficiency is not considered in Figure 3. It is significant that with external reforming, performance in terms of efficiency is almost 2.5 times greater at practical current densities.

Reformer design for natural gas is well known, and many excellent reforming catalysts are commercially available. The costs of these catalysts and the corresponding reformer units are only a small fraction of fuel cell hardware costs. The incorporation of the reformer into the natural gas fuel cell system is readily achieved.

Publication Date: January 1, 1969 | doi: 10.1021/ba-1965-0047.ch018

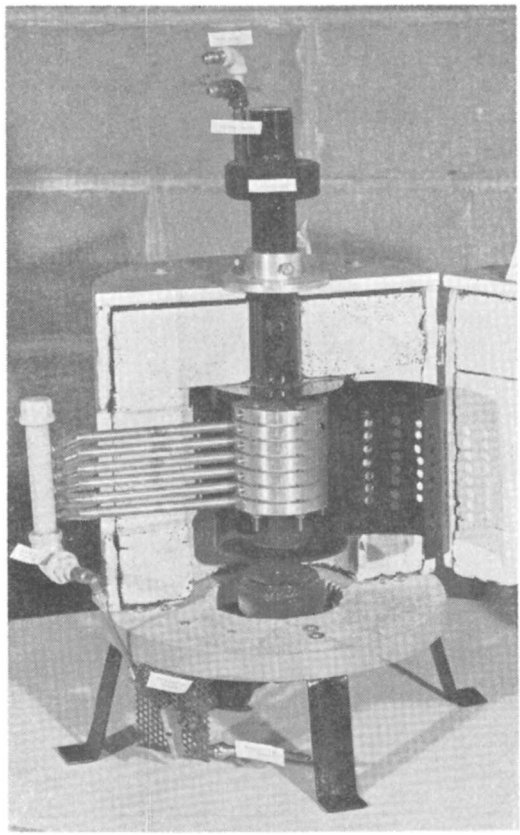

Figure 4. Laboratory size IGT high temperature fuel cell battery

It may be concluded that the use of external reforming with natural gas molten carbonate fuel cells seems justified on the basis of the improved experimental performance of this system over in situ reforming, as well as the more moderate operating temperatures it imposes on the fuel cell.

Battery Design and Scale-Up

The progress made in other areas of the molten carbonate fuel cell development indicated that some attention should be given to the problems associated with battery design and scale-up. The first step in the process was the assembly of a battery consisting of several small laboratory cells in series (Figure 4). No difficulties were encountered in this relatively simple transition, and next the more formidable problem of scale-up was attacked. The long-life performance of the silver film cathode and palladium-silver foil anode indicated that these particular compounds were the best adapted for scale-up techniques. The greatest problems were expected with increasing the size of the electrolyte disks from the 3-inch diameter laboratory disks to the 6-inch square dimensions chosen for the battery development program. In order to achieve the same electrolyte properties developed with the smaller cells, a 1-million-pound press was required for the paste electrolyte fabrication. Special die fixtures were designed, and the larger electrolyte bodies were fabricated without difficulty.

Publication Date: January 1, 1969 | doi: 10.1021/ba-1965-0047.ch018

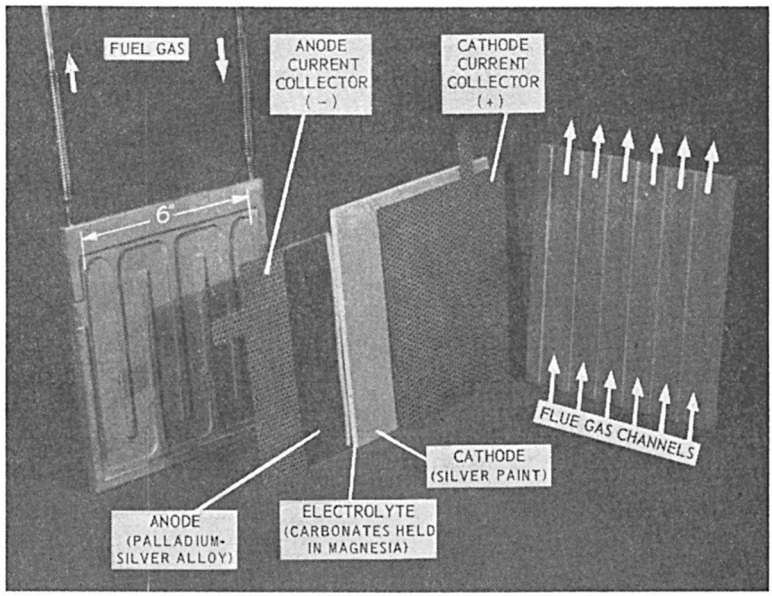

Figure 5. Components used in construction of scaled-up IGT fuel cell battery

Components for the new battery are shown in Figure 5, and a 10-cell battery built from the components is shown in Figure 6. The battery is assembled at room temperature and moderately tightened. It is then heated to 600° C., and the final sealing is accomplished when the paste

electrolyte is in a semisolid state. The battery can now be thermally cycled between ambient and operating temperatures without damage or further adjustment. A 100% leaktight assembly has not yet been achieved, but this represents only a slight loss in fuel efficiency. Complete sealing is anticipated in future designs.

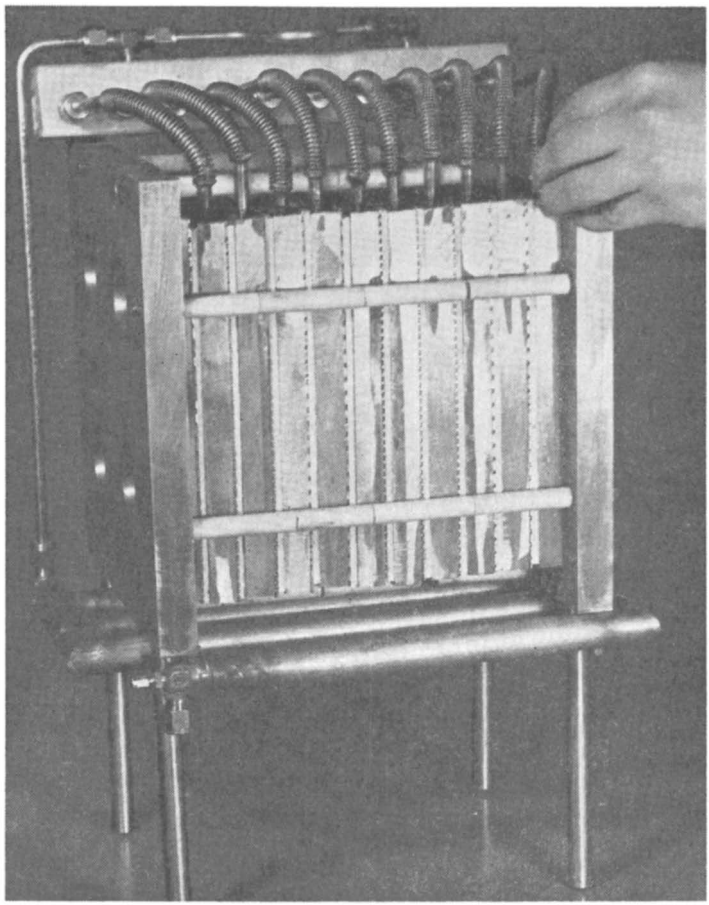

Figure 6. IGT high temperature fuel cell battery and reformer

As shown in Figure 5, the cathode compartment is open to the atmosphere. This design feature is essential for any practical molten carbonate fuel cell system. The mode of operation of the battery is a direct carryover from the laboratory models and is shown schematically in Figure 7. A portion of the incoming methane is burned directly in a burner underneath the fuel cell battery. Another portion of the methane is passed through activated carbon to remove sulfur compounds and, after steam addition, through the reformer containing commercial nickel catalyst.

Publication Date: January 1, 1969 | doi: 10.1021/ba-1965-0047.ch018

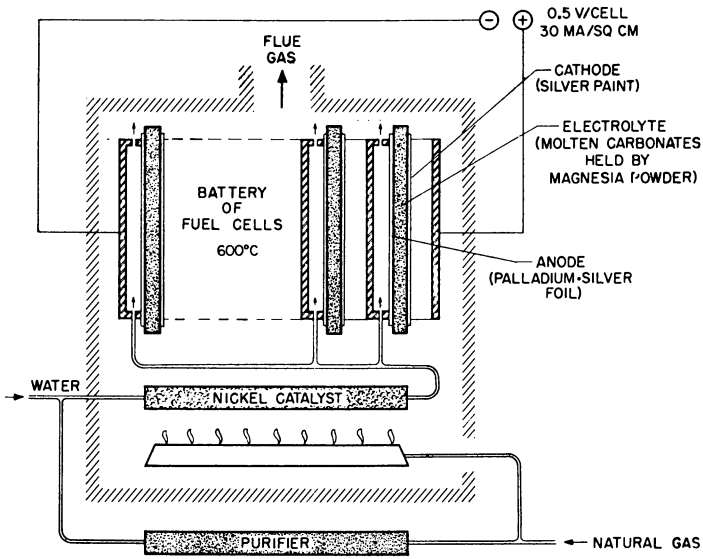

Figure 7. Schematic representation of IGT high temperature natural gas fuel cell system

The hot flue gas, containing excess air, carbon dioxide, and water, rises by natural convection; in passing by the reformer, the flue gas drops in temperature to sustain the endothermic reforming reaction. The flue gas then enters the open cathode chambers, rises through the fuel cell, and supplies the oxygen and carbon dioxide needed to maintain the cathodic reaction. The water vapor in the flue gas has no adverse effect on the fuel cell reaction. To conserve fuel and carbon dioxide, the spent anode gases should be recycled to the burner.

Battery performance is shown in Figure 8. Faradaic efficiencies as high as 40% have been achieved in this apparatus although complete system efficiencies, as might be expected in such a small battery, are very low.

Some conclusions arrived at in battery design are: operation of a multiple-cell battery molten carbonate fuel cell has been demonstrated, and a mode of operation comprising a gas burner-reformer-open cathode fuel cell has been defined.

Economic Evaluation

To evaluate the economics of a fuel cell system, both its application and design must be considered. Von Fredersdorff (*12*) has outlined the economics of the domestic fuel cell application in considerable detail. The cost of fuel cell hardware depends on the cost of materials and cost of manufacturing. Since manufacturing costs are difficult to estimate at this

Publication Date: January 1, 1969 | doi: 10.1021/ba-1965-0047.ch018

early stage of development, only the material costs for the recent IGT design are evaluated here. The design model is similar to that described (Figure 7), with two significant changes. Nickel electrodes are used in

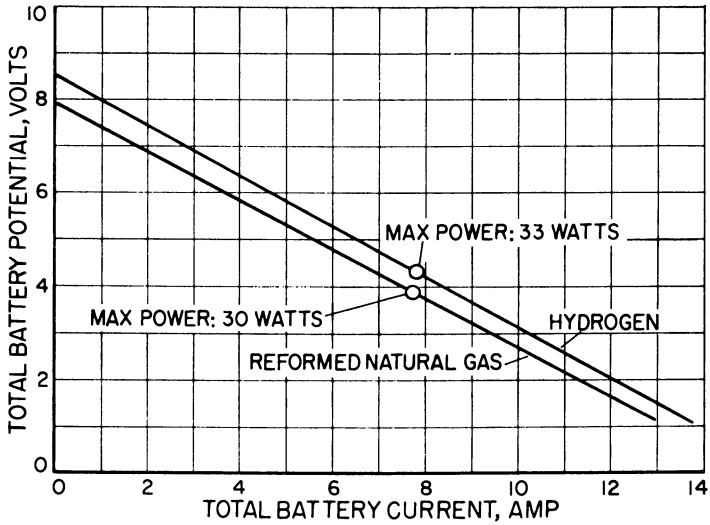

Figure 8. Performance of 10-cell high temperature fuel cell battery

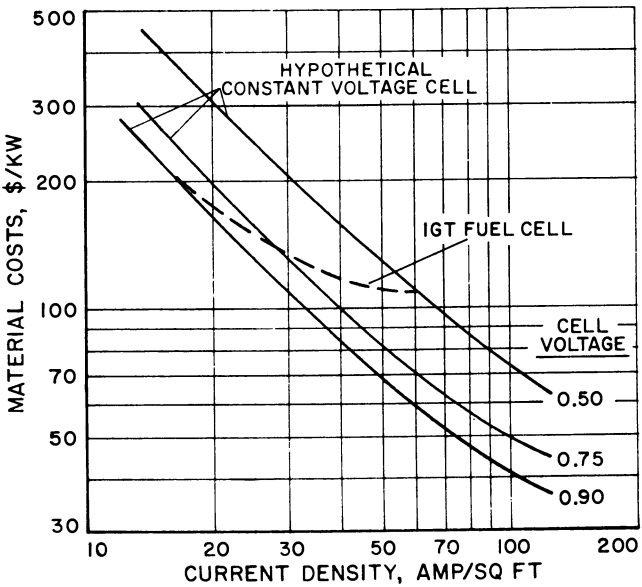

Figure 9. Economics of IGT high temperature molten carbonate fuel cell for constant battery voltage

Publication Date: January 1, 1969 | doi: 10.1021/ba-1965-0047.ch018

place of the expensive silver-palladium foil, and a parallel, dual element geometry is chosen in place of the bipolar flange. The effect of this last change is to eliminate the flange completely from the fuel cell design, using the electrode itself as a structural element.

Table II gives the itemized cost of the various materials used in the IGT battery. These costs, plus the costs of fittings and an additional 10% of the total to cover miscellaneous materials, were used to compute the curves in Figure 9. In this figure, battery material costs are plotted as a function of current density at constant voltage for various single-cell potentials. The dashed line represents the IGT fuel cell performance curve. Since fully manufactured batteries at $300 per kilowatt are reasonable for domestic fuel cell applications, material costs at least are within a reasonable range. It may be concluded that only moderate improvements in voltage-current characteristics of the molten carbonate fuel cells, but considerable improvement in life, are required to bring them within the economic framework of domestic applications.

Table II. Fuel Cell Hardware Costs

Material	*Cost*
Electrolyte paste, 100 mil thick (MgO–Na_2CO_3–K_2CO_3–Li_2CO_3), per sq. ft.	$0.37
Nickel anode, 25 mil thick, per sq. ft.	0.14
Silver cathode, 0.4 mil thick, per sq. ft.	0.43
Carbon steel anode current collector, 18 ga., per sq. ft.	0.16
Stainless steel cathode current collector, 18 ga., per sq. ft.	1.18
Stainless steel frame, 125 mil thick, per ft.	0.14

Publication Date: January 1, 1969 | doi: 10.1021/ba-1965-0047.ch018

Acknowledgement

The Institute of Gas Technology work on development of high temperature fuel cells discussed in this paper was sponsored by the General Research Planning Committee of the American Gas Association under the association's PAR (Promotion-Advertising-Research) Plan.

Literature Cited

(1) Bloch, O., and Degobert, P. *Bull. Soc. Chim. France*, **1962**, 1887–92.
(2) Broers, G. H. J., Ph.D. Thesis, University of Amsterdam, The Netherlands, 1958.
(3) Broers, G. H. J., and Schenke, M., "High-Temperature Galvanic Fuel Cells," Final Rept., File No. **DA-91-591-EVC-1701** (April 1962).
(4) deRosset, A. J., *Ind. Eng. Chem.* **52**, 525–28 (1960).
(5) Douglas, D. L., in "Fuel Cells," G. J. Young, ed., Vol. 1, 129–49, Reinhold Publ. Corp., New York, N. Y., 1960.
(6) Eisenberg, M., and Baker, B. S., Electrochemical Society, Boston, Mass., Sept. 16–20 1962; Extended Abstract No. **46**, Battery Division.

(7) Hurlbert, R. C., and Konecny, J. O., *J. Chem. Phys.* **34,** 655–58 (1961).
(8) Janz, G. J., and Neuenschwander, E., "Corrosion Studies in Molten Alkali Carbonates," Part I "Silver Metal," Tech. Rept. **16, AD-289005,** U. S. Dept. Commerce, Office of Technical Services, Washington, D. C., 1962.
(9) Marianowski, L. G., Meek, J., Schultz, E. B., Jr., and Baker, B. S., "New Concepts on High Temperature Hydrocarbon Cells," Proc. 17th Annual Power Sources Conference, 72–75. PSC Publications Committee, Red Bank, N. J., 1963.
(10) Schenke, M. and Broers, G. H. J., "High Temperature Galvanic Fuel Cells," Final Rept., File No. **DA-91-591-EUC-1398,** February 1961.
(11) Shultz, E. B., Jr., Vorres, R. S., Marianowski, L. G., and Linden, H. R., in "Fuel Cells," G. J. Young, ed., Vol. II, 24–36, Reinhold Publ. Corp., New York, N. Y., 1963.
(12) von Fredersdorff, C. G., *Ibid.*, pp. 50–67.

RECEIVED February 17, 1964.

Publication Date: January 1, 1969 | doi: 10.1021/ba-1965-0047.ch018

In Fuel Cell Systems; Young, G., el al.;
Advances in Chemistry; American Chemical Society: Washington, DC, 1969.

19

Methanol Fuel Cells with Dissolved Oxidants

D. B. BOIES and A. DRAVNIEKS

IIT Research Institute,[1] Chicago, Ill.

Publication Date: January 1, 1969 | doi: 10.1021/ba-1965-0047.ch019

Sodium chlorite has low equivalent weight and favorable electrode potential that combine to make it an interesting oxidant for fuel cell use. It gives useful current densities in alkaline solution at silver-containing electrodes. A methanol-chlorite fuel cell can operate at a current density in excess of 100 ma./sq.cm. The easy storability of the fuel and oxidant for such cell results in favorable energy-to-weight ratios.

Among the desired characteristics of both fuel and oxidant for fuel cells are storability and high energy content per unit weight. The weight must include that of the container. Therefore, the best high energy fuel and oxidant—hydrogen and oxygen—lose much of their advantage in transportable cells, especially if oxygen cannot be taken directly from the air. One of the most easily stored fuels is methanol, and recently the authors developed high current density electrodes for the electrochemical oxidation of methanol in alkaline solution *(1)*. Since methanol is soluble in the electrolyte, no multiple porosity is required in the electrode, and the active layer may be only 0.01 to 0.02 cm. thick. Thus, as far as fuel is concerned, compact cells are feasible. Matching oxidant electrodes are, however, needed.

The customary porous carbon electrode that is operated with oxygen or air as the oxidant performs very poorly in the methanol containing caustic since its waterproofing fails in the presence of methanol. In some applications, air may not be available at all, and then the weight of bottled oxygen is a handicap; one gram equivalent (8 grams) of oxygen requires an additional 30 to 80 grams in the container weight.

Even though all other oxidants have higher equivalent weights, many can easily be stored in solid, dissolved, or liquid form in light containers. Some also have higher oxidizing potentials. Oxidants supplied in dissolved form to the fuel cell cathode should require only a thin porous

[1] Formerly Armour Research Foundation of Illinois Institute of Technology.

In Fuel Cell Systems; Young, G., el al.;
Advances in Chemistry; American Chemical Society: Washington, DC, 1969.

layer of an electrocatalyst and no porous bulk electrode in addition to this layer. Thus, compact fuel cells should be possible if a sufficiently electrochemically active alkaline oxidant/electrode system were available.

To find an appropriate system, several oxidants and electrodes were investigated as half-cells. Complete methanol fuel cells were constructed with the most promising oxidant—chlorite.

Selection of Oxidants—Theoretical

The following requirements were formulated for the selection of soluble oxidants:

1. High positive electrode potential to provide high cell potential when coupled with the negative methanol electrode.
2. Low weight per ampere-hour.
3. Storability in concentrated form.
4. Freedom from obnoxious fumes.
5. Solubility of reduction products.
6. Lack of gas formation in reduction.
7. Electrochemical reactivity.
8. Low polarization.

The first six requirements can be checked by using literature data. The high positive electrode potential expected may not be realized when the electrode is not a good electrocatalyst. Hence the reactivity and low polarization requirements need experimental study.

Table I gives soluble oxidants with high positive Gibbs electrode potentials, V^0 (3). The weights are calculated on the basis of sodium

Table I. Soluble Oxidants for Fuel-Cell Cathode in Alkaline Solution (2)

Reaction	V^0, standard electrode potential[a] vs. SHE	Weight relations	
		Amp-hr./lb.	G./amp-hr.
$ClO^- + H_2O + 2e \rightarrow Cl^- + 2OH^-$	0.89	325	1.4
$HO_2^- + H_2O + 2e \rightarrow 3OH^-$	0.88	700	0.65
		210	2.15[b]
$ClO_2^- + 2H_2O + 4e \rightarrow Cl^- + 4OH^-$	0.77	525	0.86
$ClO_3^- + 3H_2O + 6e \rightarrow Cl^- + 6OH^-$	0.62	670	0.67
$BrO_3^- + 3H_2O + 6e \rightarrow Br^- + 6OH^-$	0.61	470	0.98
$ClO_4^- + 4H_2O + 8e \rightarrow Cl^- + 8OH^-$	0.55	780	0.59
$IO_3^- + 3H_2O + 6e \rightarrow I^- + 6OH^-$	0.26	360	1.26
$O_2 + 2H_2O + 4e \rightarrow 4OH^-$	0.4	1500	0.3
$O_2 + H_2O + 2e \rightarrow OH^- + HO_2^-$			
$2HO_2^- \rightarrow 2OH^- + O_2$	−0.08	1500	0.3
$AgO + H_2O + 2e \rightarrow Ag + 2OH^-$	0.45	200	2.34

[a] SHE = standard hydrogen electrode.
[b] For 30% solution.

salts of the corresponding anions, except for HO_2^- in which hydrogen

Publication Date: January 1, 1969 | doi: 10.1021/ba-1965-0047.ch019

Table II. Experimental

Temperature, 23° C.

Oxidant	*NaClO*	*NaClO*	H_2O_2
Concentration, %	3.8	3.8	3.0
Open-circuit potential, volts *vs.* SHE	0.48	0.29	0.10
Electrode surface	Carbon	Raney Ni–Ag	Sprayed Ag
Current density, ma./sq.cm. Volt *vs.* SHE			
+ 0.30	1.2	...	...
+ 0.20	4.7	41	...
+ 0.10	13.2	55	90
+ 0.00	23.0	57	133
− 0.10	38.0	...	140
− 0.20	...	...	140

Publication Date: January 1, 1969 | doi: 10.1021/ba-1965-0047.ch019

peroxide is the oxidant. Since water is generated at the anode, the weight of water is not included in the calculation. Data for oxygen, with the theoretical V^0 for the four-electron process and for the more realistic two-electron Berl's reaction, are also listed. For comparison, data are shown for silver oxide, the best solid oxidant used in commercial cells. Oxygen needs a container, and hence the weight per ampere-hour would actually be several times higher. Hypochlorite cannot be stored except in dilute form or as CaCl(ClO); hence its weight index is much poorer than shown. Storage of hydrogen peroxide in concentrated form under normal conditions is undesirable. With the usual easily storable 30% peroxide solution, the weight index is much poorer.

Table I indicates that selection of soluble oxidants of an inorganic nature is rather limited. The open-circuit potential for our methanol electrodes in 5*N* potassium hydroxide is −0.79 volt. Therefore, iodate with $V^0 = +0.26$ is the last that may be considered in the descending potential series if the complete cell must have a voltage of 1 volt or higher.

Selection of Oxidants—Experimental

Although the theoretical electrode potentials for a given oxidant can be high, active low polarization electrodes for the corresponding reactions may not exist. Soluble oxidants shown in Table I were studied experimentally in half-cell arrangements. Conventional half-cell polarization techniques, similar to those which have been reported previously, were used. A saturated calomel electrode was used for reference, with a Luggin-type capillary bridge using a potassium hydroxide–soaked asbestos string.

Polarization characteristics were measured potentiostatically by observing current densities that could be obtained at electronically controlled, preselected, polarized potentials. Electrodes included carbon and

In Fuel Cell Systems; Young, G., el al.;
Advances in Chemistry; American Chemical Society: Washington, DC, 1969.

Evaluation of Oxidants

Electrolyte, 5*N* KOH

$NaClO_2$	$NaClO_3$	$KBrO_3$	$NaClO_4$	KIO_4
3.0	3.0	5.0	3.0	3.0
0.29	0.28	0.28	0.15	0.22
Sprayed Ag	Raney Ni–Ag	Raney Ni–Ag	Raney Ni–Ag	Raney Ni–Ag
...	...	...	...	...
30	...	23	...	...
53	0.1	27	...	2.5
83	0.2	28	0.1	7.0
108	0.3	29	0.1	10.0
137	0.4	30	0.1	...

Publication Date: January 1, 1969 | doi: 10.1021/ba-1965-0047.ch019

flame-sprayed thin layers of Raney nickel with or without further platinizing, flame sprayed Raney nickel-silver, and silver. The aluminum-rich phase of alloys was extracted by electrochemical leaching. The platinized Raney nickel corresponded to the high-performance methanol electrodes (*1*). The bases for the sprayed layers were either nickel sheets or porous sintered-nickel powder plates. Representative results are shown in Table II. None of the oxidants reached the theoretical electrode potentials. Only chlorite and hydrogen peroxide supplied practical current densities at acceptable polarization. Because the chlorite is easily stored and handled, this chemical was selected for further study.

Exploration of Chlorite Electrodes

Open-circuit potentials and polarization characteristics of flame-sprayed and other electrodes were measured in alkaline chlorite solutions. The effects of chlorite concentration and temperature were studied at the most promising electrodes, flame-sprayed silver, and flame-sprayed Raney nickel-silver. Representative data are summarized in Table II and Figure 1.

The highest values of the open-circuit potential of the chlorite electrode were +0.27 to +0.30 volt, much lower than the theoretical value of +0.77 (Table I). The theoretical value for the silver oxide–silver electrodes in 5*N* potassium hydroxide is +0.306; hence, it is likely that the reaction mechanism involves chemical oxidation of silver to silver oxide by chlorite and electrochemical reduction of silver oxide. In anodic polarization of the Raney nickel-silver electrode in chlorite solution, heavy currents were accepted with low polarization, apparently with formation of silver oxide. When current was then reversed to begin reduction, approximately equivalent high currents at low polarization could be drawn for a limited time. At continued cathodic polarization, the curves re-

turned to the normal shape of Figure 1. This behavior indirectly supports the silver oxide–silver mechanism of the alkaline chlorite electrode.

The data in Table III show that the flame-sprayed silver and Raney nickel-silver gave comparable results. However, the silver electrode appeared to be susceptible to poisoning, as the performance often fell after a period of time and could only be restored by electrolytic evolution of hydrogen from the surface. The Raney nickel–silver electrodes were not affected in this manner and were therefore chosen for the methanol-chlorite full-cell tests.

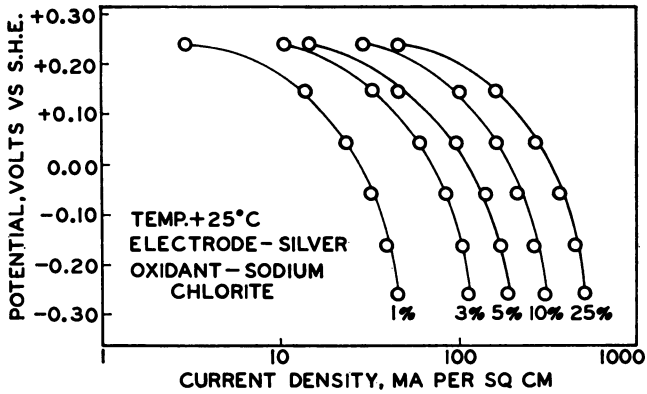

Figure 1. Effect of concentration

Table III. Experimental Evaluation of Chlorite Electrodes

Electrolyte: 10% $NaClO_2$ in 5*N* KOH
Temperature: 23° C.

Electrode	*Sprayed Raney Ag–Ni*	*Sprayed silver*	*Platinized sprayed Raney Ni*[1]	*Platinized Platinum*[1]	*Carbon*
Open-Circuit Potential, volts	0.26	0.27	0.30	0.30	0.10
Current density, ma./sq.cm.					
+ 0.20	35	48	1.1	3	...
+ 0.10	92	118	6	13	...
0.00	170	172	25	50	...
− 0.10	280	215	90	104	0.03
− 0.20	...	245	...	200	0.08

[1] These electrodes are electrochemically active also with methanol.

Since chloride is the end product of chlorite reduction the effect of this material on the electrode operation was studied. An electrolyte containing 10% sodium chlorite and 20% sodium chloride was tested and, at 55°C., showed only a slight decrease in performance due to the chloride. However, at 23°C., the solubility limit was exceeded, and a severe (75%) decrease in performance was noted.

Addition of small amounts (5%) of methanol to a chlorite half-cell did not decrease its performance. However, the presence of 5% chlorite

Publication Date: January 1, 1969 | doi: 10.1021/ba-1965-0047.ch019

reduced the performance of a methanol half-cell in a manner similar to that previously noted for chloride *(1)*. It is probable that the chlorite is immediately reduced to chloride by the methanol and then acts as such. Because of this reduction of chlorite at the methanol electrode it was necessary to separate the anode and cathode compartments with a membrane.

Exploration of Methanol-Chlorite Fuel Cell

Experimental Work. Full-cell tests were conducted with the following conditions:

Fuel solution: 160 grams of methanol/liter; 270 grams of potassium hydroxide/liter
Fuel electrode: Flame-sprayed Raney nickel, platinized
Oxidant solution: 370 grams of sodium chlorite/liter; 270 grams of potassium hydroxide/liter
Oxidant electrode: Flame-sprayed Raney nickel-silver
Temperature: 55°C.

The fuel and oxidant compartments were 3 mm. thick and were separated by a dialysis membrane (D-30, Nalco Chemical Co., Chicago, Ill.). The fuel and oxidant were circulated through the cell and were heated externally.

The results of a full-cell test are shown in Figure 2. For comparison, the predicted performance is also given based on the combined best methanol and chlorite half-cell data for similar electrodes. The lower performance of the full cell is due to the IR drop in the electrolyte and membrane and possible variations in electrodes. The cell output was 144 ma./sq.cm. at 0.6 volt.

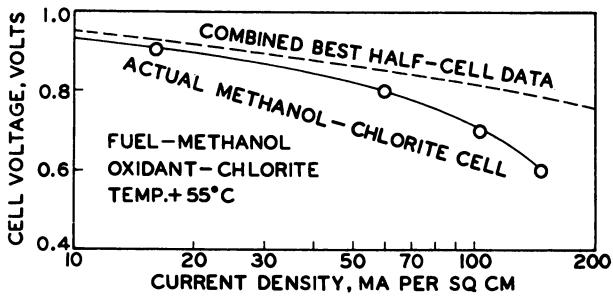

Figure 2. Fuel cell polarization curves

The efficiency of methanol utilization in this cell was studied in long term tests. It was found that the number of electrons obtained per methanol molecule approached four at high current densities and fell as current density lowered. This drop is caused by an approximately con-

Publication Date: January 1, 1969 | doi: 10.1021/ba-1965-0047.ch019

stant loss of methanol by chemical reaction with the chlorite as a result of diffusion of these across the membrane. At lower current densities this loss became an appreciable part of the total methanol consumption and thus led to a lowered current efficiency for both chlorite and methanol. The fact that a maximum of four electrons could be obtained per methanol molecule is in accord with previous results *(1)*, which showed that the formate-carbonate step was comparatively slow under these conditions.

Weight Projections. Based strictly on the equimolar portions of methanol, sodium chlorite, and sodium hydroxide required and 0.7-volt working voltage, the theoretical four electron power output of this system would be 210 watt-hours/pound of reactants. Several factors would combine to reduce this power-to-weight ratio in a practical cell, including the weight of water initially needed to form the electrolyte; the weight of water, methanol, and chlorite that would have to be rejected along with the waste sodium formate and chloride; and loss of reactants due to chemical reaction by diffusion across the membrane. It is difficult to estimate these factors in the present state of development, but there would appear to be a reasonable possibility of the development of fuel cells based on the methanol-chlorite system which would be competitive on a power-output basis with currently available sources. For comparison, conventional cells range from the lead acid storage cells at 10 to 20 watt-hr./lb. to the silver-zinc cell at 65 watt-hr./lb. Currently reported air-breathing fuel cells operate on bottled or chemically generated hydrogen at up to 100 watt-hr./lb. of reactants.

Publication Date: January 1, 1969 | doi: 10.1021/ba-1965-0047.ch019

Acknowledgment

This work was conducted under a contract with the K. W. Battery Co., and Joslyn Manufacturing and Supply Co. Their permission to publish this material is gratefully acknowledged. The authors wish to thank Mr. F. Child who performed much of the experimental work.

Literature Cited

(1) Boies, D. B., and Dravnieks, A., presented at Boston, Mass., meeting of the Electrochemical Society, Sept. 1962; at press, *J. Electrochem. Technol.*
(2) Latimer, W. M., "Oxidation States of Elements," Prentice Hall, New York, 1952.
(3) Lewis, Gilbert N., and Randall, Merle, "Thermodynamics," 2nd Ed. (revised by Kenneth S. Pitzer and Leo Brewer), p. 356, McGraw-Hill Book Co., New York, 1961; cf. de Bethune, *J. Electrochem. Soc.* **102**, 288C (1955).

RECEIVED February 17, 1964.

20

Anodic Oxidation of Derivatives of Methane, Ethane, and Propane in Aqueous Electrolytes

I. Galvanostatic Investigations

H. BINDER, A. KÖHLING, H. KRUPP, K. RICHTER, and G. SANDSTEDE

Battelle-Institut e.V., Frankfurt(Main), Germany

Publication Date: January 1, 1969 | doi: 10.1021/ba-1965-0047.ch020

Anodic potential/current density plots of a Raney platinum electrode were measured galvanostatically with alcohols, aldehydes, ketones, and carboxylic acids up to 800 mv. (vs. hydrogen electrode in the same solution) at 25° and 80°C., the electrolyte being 5N potassium hydroxide and 5N sulfuric acid. Acetic acid and propionic acid cannot be oxidized in potassium hydroxide solution but are active in sulfuric acid. With methanol, ethanol, glycol, and glycerol in 5N potassium hydroxide at 200 ma./sq.cm. potentials from 300 mv. to 350 mv. observed, while in 5N sulfuric acid the potentials range from 500 to 650 mv. under the same conditions.

Organic substances may be used as electrochemical fuels provided that they can be oxidized both easily and rather completely. It is therefore interesting to determine the reaction rate and the reaction mechanism of suitable compounds.

Derivatives of hydrocarbons are not only potential intermediates in the anodic oxidation of hydrocarbons, but they themselves might be used as fuels. A number of papers (*1*, *2*, *4-8*) mainly dealt with the mechanism of anodic methanol oxidation. The reactivities of additional organic compounds were examined particularly by Pavela (*5*) and Schlatter (*7*).

In a previous paper (*3*) we reported on the application of electrodes containing Raney-type transition metals as catalysts in the electrochemi-

In Fuel Cell Systems; Young, G., el al.;
Advances in Chemistry; American Chemical Society: Washington, DC, 1969.

cal oxidation of hydrogen and methanol in aqueous electrolytes. Raney platinum proved to be a very active catalyst.

We have now studied the anodic behavior of alcohols, aldehydes, ketones, and carboxylic acids with 1 to 3 carbon atoms in potassium hydroxide solution and sulfuric acid at different temperatures. Galvanostatic potential/current density plots were measured, and a coulometric-potentiostatic method was employed for quantitative analysis.

Experimental Conditions

Reactants and Electrodes. We selected the following 12 substances for our experiments:

Methanol	Ethanol	1-Propanol
Formaldehyde	Acetic acid	2-Propanol
Formic acid	Glycol	Propionic acid
	Oxalic acid	Acetone
		Glycerol

These reactants were dissolved in the electrolyte. In general, the individual substances were used in concentrations of 2 moles/liter, the solvent being aqueous solutions of 5*N* sulfuric acid or 5*N* potassium hydroxide. In the carboxylic acids, equivalent quantities of potassium hydroxide were added when the solvent was basic.

The electrodes were prepared in the form of porous disks by compressing a mixture of gold powder (99.96%, particle size < 60 micron) forming the electrode skeleton, the powdered Raney platinum aluminum alloy and sodium chloride as an auxiliary substance to obtain macropores. Subsequently, the aluminum of the Raney alloy was dissolved by treating the electrode first with dilute and then with concentrated potassium hydroxide solution, at a final temperature of 80°C. The Raney platinum-aluminum alloy was $PtAl_4$.

In some runs with methanol and formic acid, we used electrodes with Raney palladium; in these cases the Raney alloy was $PdAl_4$.

The Raney alloys were prepared by heating an intimate mixture of the catalyst powder and aluminum powder in the form of compressed disks. Then the alloys were powdered and sieved and the 25 to 40 micron size fraction of the powdered alloy was used in an amount of 35% by volume in the test electrode.

The electrode was suspended by a platinum wire in the electrolyte. The current densities mentioned here always refer to the projected surface area of the electrode.

Measuring Setup. Figure 1 shows the half-cell arrangement for the galvanostatic measurements. The test electrode is the Raney platinum anode. A platinum wire served as counter electrode. As reference electrode we used an "autogenous" hydrogen electrode, as we would like

Publication Date: January 1, 1969 | doi: 10.1021/ba-1965-0047.ch020

to call this type of hydrogen electrode. In our experiments this electrode is a Raney platinum electrode suspended by a platinum wire in a glass tube, which has a capillary tube attached to it. On this Raney platinum electrode, hydrogen is being evolved at a cathodic current density of about 1 ma./sq.cm. At this current density the overvoltage for hydrogen evolution is negligibly small on this electrode, so that it may be used as an accurate hydrogen reference electrode. For every solution and temperature employed the potential of the electrode is assumed to be zero.

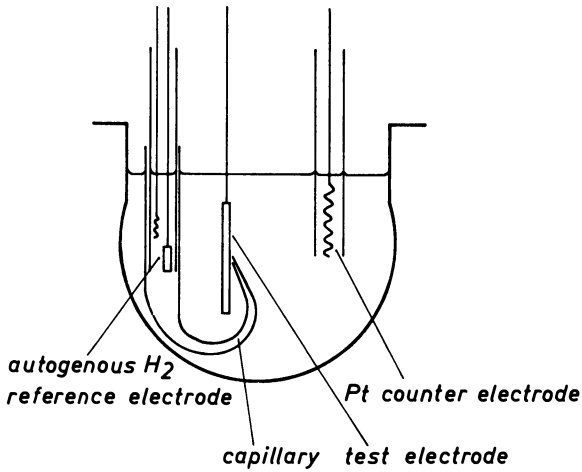

Figure 1. Half-cell arrangement

Hence, the potentials of the anode depicted in the following figures relate to the potential of a hydrogen electrode in the same solution. The ohmic drop between capillary and electrode is not accounted for. All values were taken under quasi steady-state conditions; they remained constant during the measuring period of sometimes more than 24 hours. The plots were taken first at decreasing and then at increasing current densities. This implies that a certain proportion of the reaction products is present in the electrolyte.

Measurements in 5N KOH Solution

Methane Derivatives. Figure 2 shows the results of the measurements with methanol, formaldehyde, and formic acid in 5*N* potassium hydroxide at 25°C. The larger rate of oxidation is obtained for methanol and formaldehyde, while formic acid furnished inferior results.

The peculiar shape of the curve for formaldehyde at small current densities is caused by formaldehyde dehydrogenating on the Raney

Publication Date: January 1, 1969 | doi: 10.1021/ba-1965-0047.ch020

platinum catalyst. In this case, therefore, we are dealing with the oxidation of hydrogen, rather than the conversion of formaldehyde. Only at larger current densities, where the dehydrogenation rate is no longer large enough, is the formaldehyde converted directly.

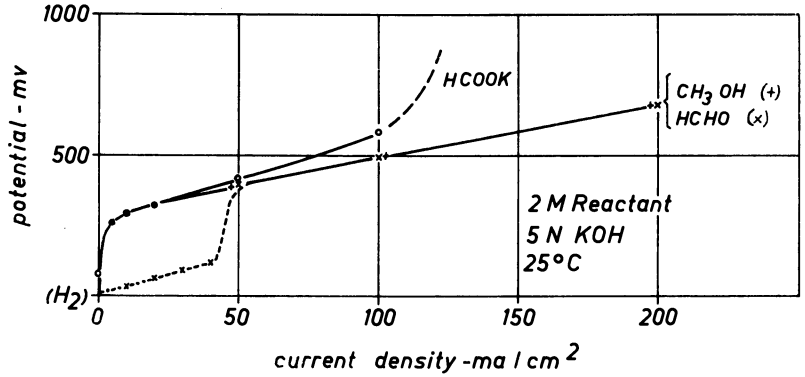

Figure 2. Potential/current density plots of a Raney platinum electrode with methane derivatives in 5N KOH at 25°C.

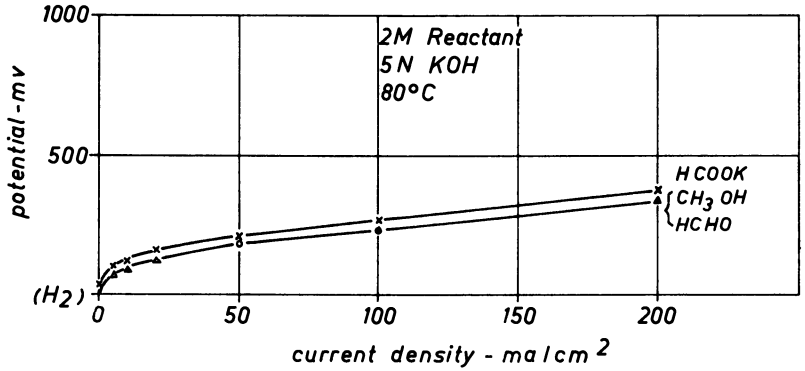

Figure 3. Potential/current density plots of a Raney platinum electrode with methane derivatives in 5N KOH at 80° C.

During the oxidation process of formic acid a distinct limiting current is observed. The current densities that can be realized are below 150 ma./sq.cm. In his measurements on platinized platinum, Vielstich (*8*), too, observed a considerable deviation of the potential/current density plot towards more positive potentials compared with the plot obtained on use of methanol.

At 80°C. (Figure 3) for formic acid, a limiting current is no longer observed in the range examined. At this temperature all of the reactions take place at larger rates, and polarization, consequently, is smaller in all cases.

Publication Date: January 1, 1969 | doi: 10.1021/ba-1965-0047.ch020

At 80°C. the potential/current-density plot for formaldehyde is identical to that of methanol, even at small current densities. This suggests that formaldehyde is not dehydrogenated at the Raney platinum electrode, as was observed at 25°C. It must be assumed that formaldehyde, immediately after having been added to the 80°C. potassium hydroxide solution, undergoes dismutation to give formic acid and methanol by Canizzaro reaction; the rate of this reaction is much larger than that of the dehydrogenation. Consequently, the oxidation of methanol is the rate-determining step.

Figure 4 shows potential/current-density plots at 80°C. with formic acid and methanol, the concentration being used as a parameter. If the concentration of formic acid is 0.2*M*, a limiting current is observed. Even at current densities as small as 50 ma./sq.cm., the potential is no longer constant. This is in satisfactory agreement with the results of our coulometric examinations.

Publication Date: January 1, 1969 | doi: 10.1021/ba-1965-0047.ch020

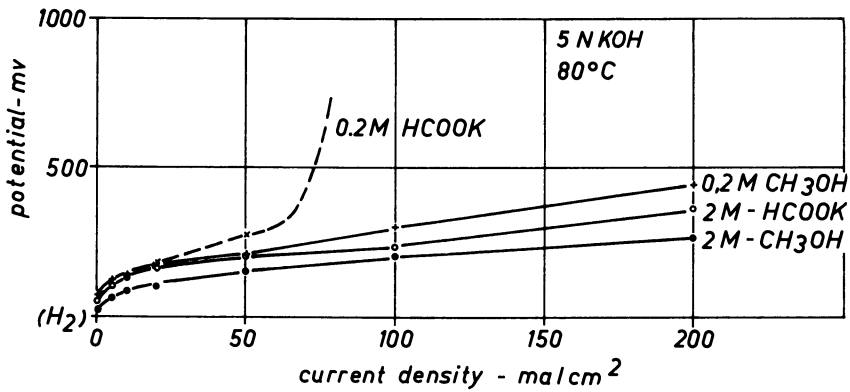

Figure 4. Effect of reactant concentration on potential/current density plots of a Raney platinum electrode with methanol and potassium formate in 5N KOH at 80° C.

In accordance with all results reported previously the oxidation rate of formic acid in potassium hydroxide solution with platinum as catalyst is smaller than that of methanol under equivalent conditions. It is, therefore, interesting to examine the results obtained with electrodes containing Raney palladium (Figure 5). In this case it turned out that the conversion of methanol is the rate-determining step so that formic acid does not become enriched as intermediate during methanol oxidation. The same applies to measurements at 25°C.

Ethane Derivatives. Figure 6 shows the conversion of ethane derivatives in potassium hydroxide solution at 25° and 80°C. Only ethanol and glycol can be converted at fair current densities.

Neither acetic acid nor oxalic acid shows electrochemical oxidation

under these conditions, the current density observed being smaller than 1 ma./sq.cm. This applies to both temperatures.

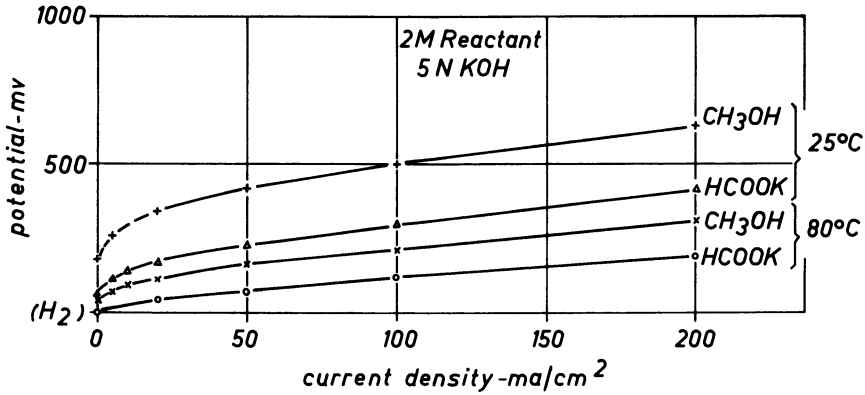

Figure 5. Potential/current density plots of a Raney palladium electrode with methanol and potassium formate in 5N KOH at 25° C. and 80° C.

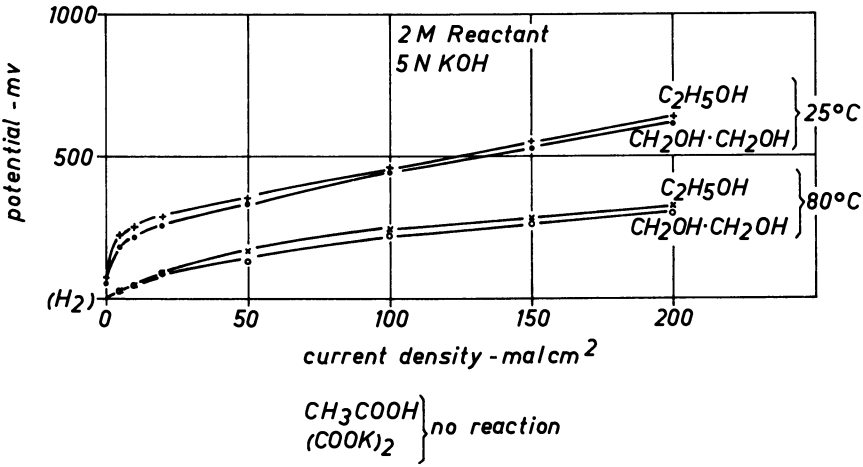

Figure 6. Potential/current density plots of a Raney platinum electrode with ethane derivatives in 5N KOH at 25° C. and 80° C.

Propane Derivatives. Among the propane derivatives (Figure 7) only glycerol is converted at 25°C. to give fairly large current densities. Limiting currents are observed with both of the propyl alcohols. However, the solubility of 1-propanol in 5*N* potassium hydroxide solution is poor.

Acetone is not converted at this temperature, but at higher temperatures (Figure 8), it can be oxidized. The maximum current density obtainable at the Raney platinum electrode amounts to 50 ma./sq.cm. at 60°C. In the experiments with acetone, we chose a limiting tempera-

Publication Date: January 1, 1969 | doi: 10.1021/ba-1965-0047.ch020

ture of 60°C. because of the escape of this relatively volatile compound.

Propionic acid is not oxidized even at 80°C.

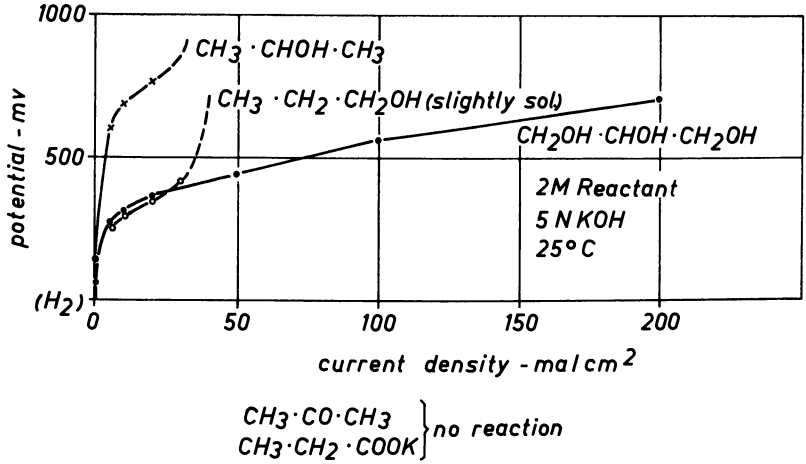

$CH_3 \cdot CO \cdot CH_3$
$CH_3 \cdot CH_2 \cdot COOK$ } no reaction

Figure 7. Potential/current density plots of a Raney platinum electrode with propane derivatives in 5N KOH at 25° C.

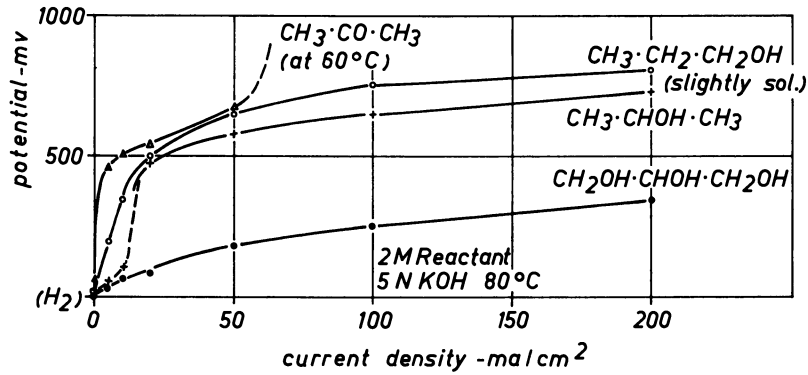

$CH_3 \cdot CH_2 \cdot COOK$
no reaction

Figure 8. Potential/current density plots of a Raney platinum electrode with propane derivatives in 5N KOH at 80° C.

Relatively high current densities can be achieved at 80°C. with *n*-propyl and isopropyl alcohols, but this involves substantial polarization. With isopropyl alcohol under these conditions, dehydrogenation takes place similar to that observed with formaldehyde at 25°C.

For glycerol, polarization is small even at as large a current density as 200 ma./sq.cm.

Comparison of the Alcohols. Figure 9 shows the potential/current-

Publication Date: January 1, 1969 | doi: 10.1021/ba-1965-0047.ch020

density plots of all the alcohols examined on oxidation in 5*N* potassium hydroxide solution at 25°C.

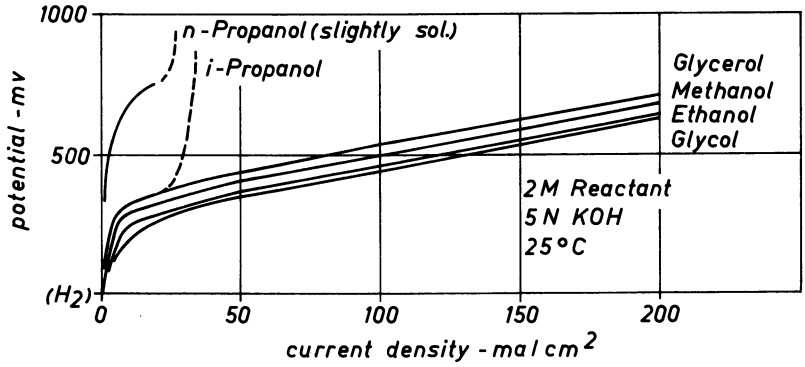

Figure 9. Potential/current density plots of a Raney platinum electrode with C_1 to C_3 alcohols in 5N KOH at 25° C.

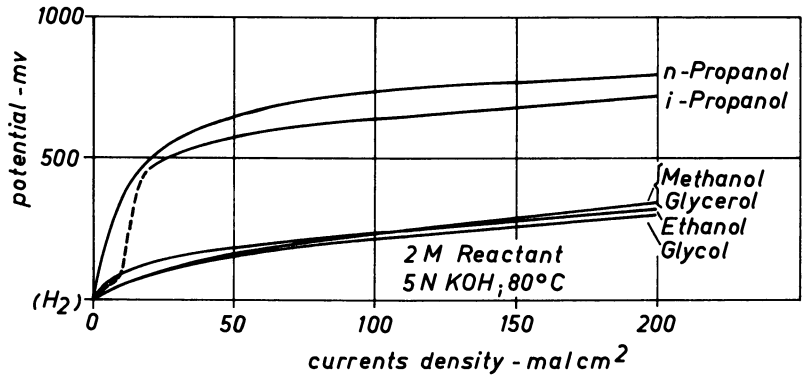

Figure 10. Potential/current density plots of a Raney platinum electrode with C_1 to C_3 alcohols in 5N KOH 80° C.

Glycol proves to be the most active alcohol, followed by ethanol. Methanol ranges third, followed by glycerol. As regards this order, one must, of course, take into account that only methanol is completely oxidized to carbonate, as is shown by coulometric investigations. The propyl alcohols show limiting currents.

At 80°C. the order is nearly the same (Figure 10), all substances, of course, being much more active than at 25°C.

Measurements in 5N Sulfuric Acid

Methane Derivatives. Figure 11 shows the conversion of methanol, formaldehyde, and formic acid in 5*N* sulfuric acid at 25°C. In methanol,

Publication Date: January 1, 1969 | doi: 10.1021/ba-1965-0047.ch020

polarization is much larger than in potassium hydroxide solution. This applies to the oxidation on both Raney platinum and on platinized platinum—for example, (6). In formic acid, however, which yielded a limiting current when converted in 5*N* potassium hydroxide solution, polarization is smaller. In the acid medium the oxidation of formic acid, therefore, involves smaller polarization than the oxidation of methanol under these conditions and the order of the plots is changed. The plot for formaldehyde ranges between those of methanol and formic acid.

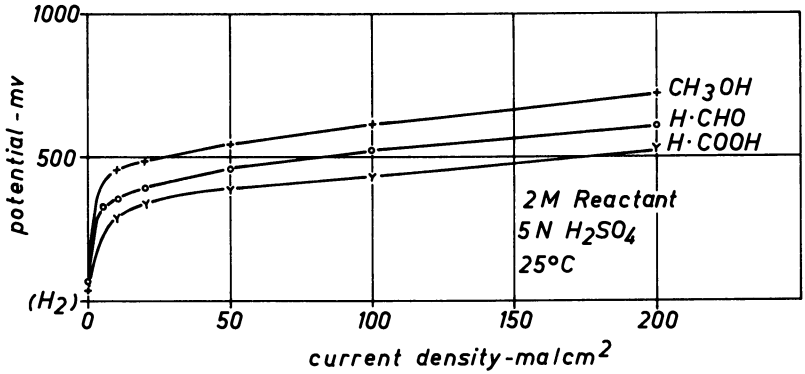

Figure 11. Potential/current density plots of a Raney platinum electrode with methane derivatives in 5N H_2SO_4 at 25° C.

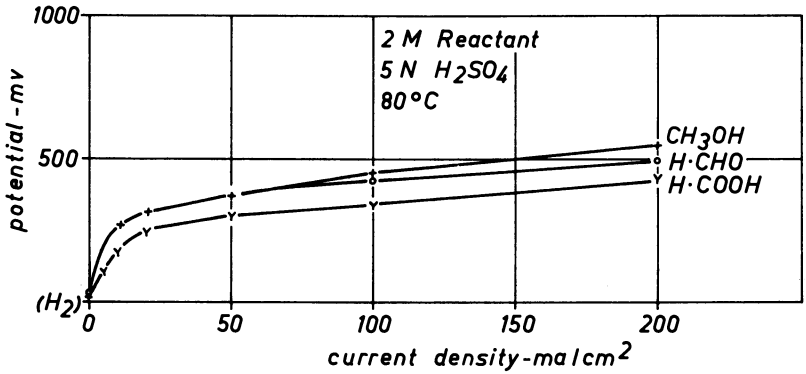

Figure 12. Potential/current density plots of a Raney platinum electrode with methane derivatives in 5N H_2SO_4 at 80° C.

Polarization, of course, is smaller for each of the three compounds at 80°C.(Figure 12), but the order of the curves remains unchanged. At a current density of 100 ma./sq.cm. with methanol a potential of 450 mv. is observed.

Ethane Derivatives. With ethane derivatives polarization is somewhat larger than with methane derivatives. At 25°C. (Figure 13), acetic

Publication Date: January 1, 1969 | doi: 10.1021/ba-1965-0047.ch020

acid can be converted only at extremely small current densities. With oxalic acid a current density of 50 ma./sq.cm. is obtained, but polarization is large. With ethanol and glycol a current density of 200 ma./sq.cm. is reached but at relatively high potentials.

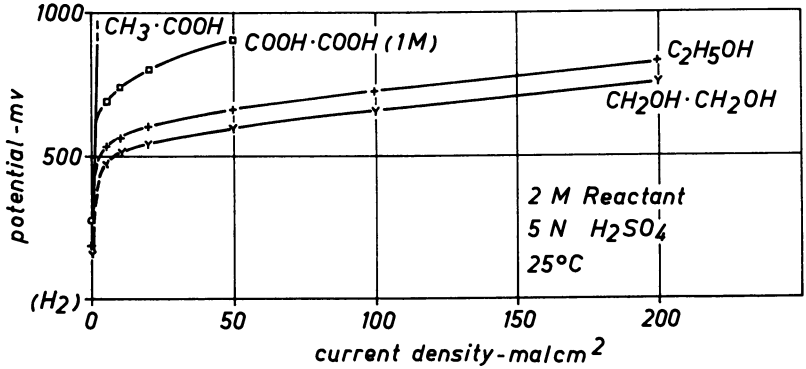

Figure 13. Potential/current density plots of a Raney platinum electrode with ethane derivatives in 5N H_2SO_4 at 25° C.

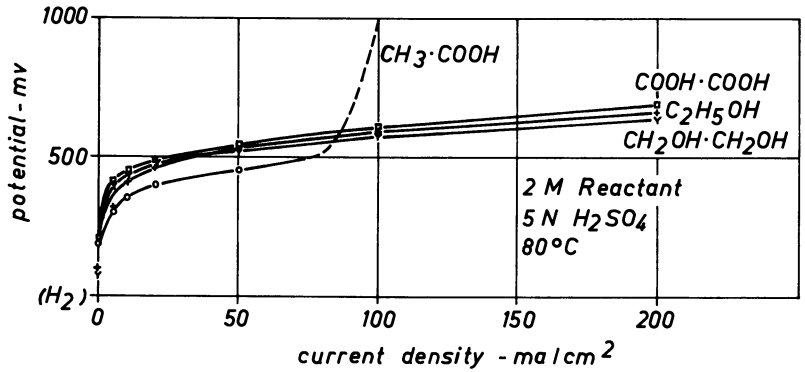

Figure 14. Potential/current density plots of a Raney platinum electrode with ethane derivatives in 5N H_2SO_4 at 80° C.

If the temperature is raised to 80°C. (Figure 14), the polarization with the alcohols at a current density of 50 ma./sq.cm. is about 100 mv. smaller than at 25°C.

Worth noting is the highly improved activity of oxalic acid, particularly of acetic acid. In acetic acid, however, a limiting current is still observed.

Propane Derivatives. The conversion of propane derivatives at 25°C. is even more difficult than that of ethane derivatives (Figure 15). With all substances a comparatively small limiting current is observed.

Publication Date: January 1, 1969 | doi: 10.1021/ba-1965-0047.ch020

As far as propionic acid and acetone are concerned there is practically no conversion worth mentioning.

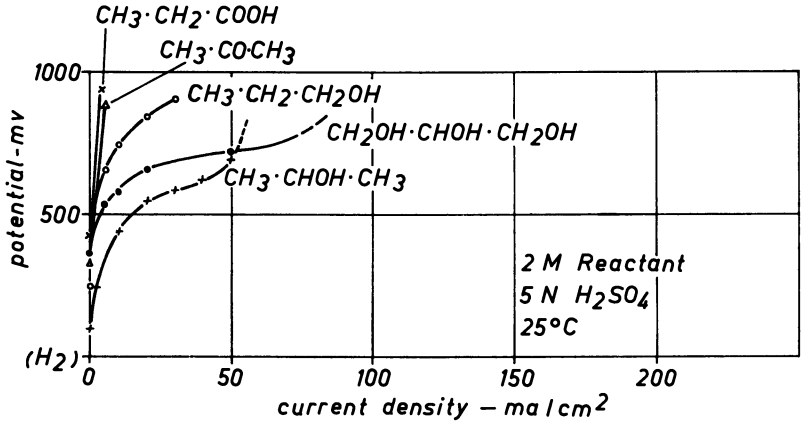

Figure 15. Potential/current density plots of a Raney platinum electrode with propane derivatives in 5N H_2SO_4 at 25° C.

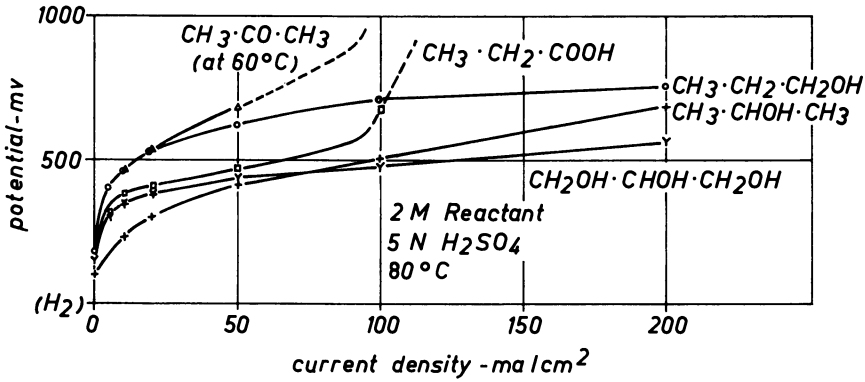

Figure 16. Potential/current density plots of a Raney platinum electrode with propane derivatives in 5N H_2SO_4 at 80° C.

However, at 80°C. (Figure 16), it is possible to convert glycerol and isopropyl alcohol fairly readily; and even with propionic acid the potential is still below 500 mv. at a current density of 50 ma./sq.cm. A limiting current, however, is observed with this acid.

At 60°C. even acetone can be oxidized in acid.

Comparison of the Alcohols. Figure 17 shows the potential/current-density plots of all the alcohols examined on oxidation in 5*N* sulfuric acid at 25°C. Methanol proved to be the most active alcohol, glycol is more active than ethanol, and the derivatives of propane show limiting currents.

Publication Date: January 1, 1969 | doi: 10.1021/ba-1965-0047.ch020

At 80°C. the order of the plots is somewhat different (Figure 18). At this temperature, methanol again is the most active alcohol, while glycerol, which was less active at 25°C., now ranges second, followed by glycol and ethanol.

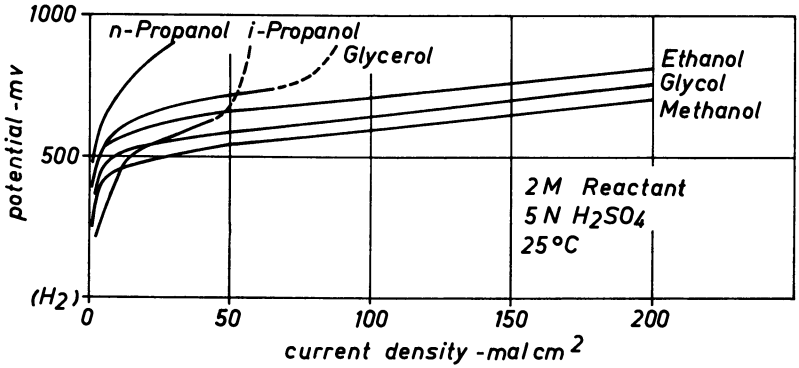

Figure 17. Potential/current density plots of a Raney platinum electrode with C_1 to C_3 alcohols in 5N H_2SO_4 at 25° C.

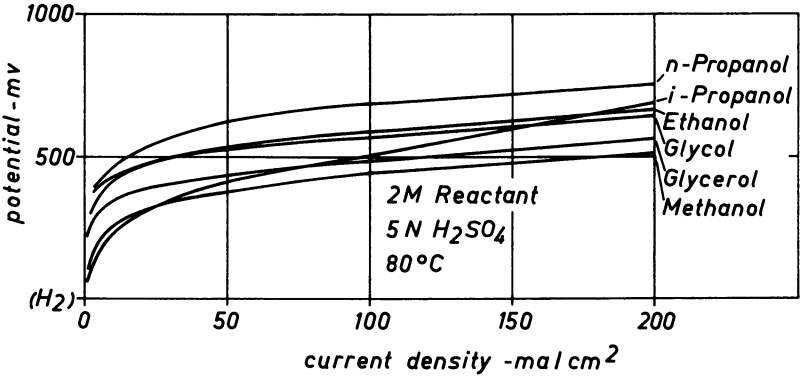

Figure 18. Potential/current density plots of a Raney platinum electrode with C_1 to C_3 alcohols in 5N H_2SO_4 at 80° C.

The smaller polarization at small current densities in the case of isopropyl alcohol may be because this compound, being a secondary alcohol, can be dehydrogenated much more readily than the other alcohols investigated.

In our experiments with Raney platinum electrodes, however, we did not observe a blocking effect by consecutive products, as described by Prigent (*6*) or Yeager (*9*), who used platinized carbon electrodes. This applies to both methanol in acid and to isopropyl alcohol in basic solution.

Publication Date: January 1, 1969 | doi: 10.1021/ba-1965-0047.ch020

Result

Alcohols, aldehydes, and ketones of the first three members of the series of saturated hydrocarbons can be oxidized anodically on a Raney platinum electrode, the electrolyte being sulfuric acid or potassium hydroxide solution.

In sulfuric acid also the corresponding carboxylic acids are converted. In this medium the oxidation is accompanied by the evolution of carbon dioxide.

In alkaline solution no carboxylic acid, except formic acid, can be converted. This is true for potentials below +800 mv. We did not examine the possible oxidation at higher potentials because at +800 mv. an oxygen sorption layer begins to form on platinum.

Hence, the end product of the oxidation of alcohols, aldehydes, or ketones in a base should be a carboxylic acid (excluding formic acid), whereas the oxidation in acid should be complete.

In sulfuric acid the rate of oxidation of carboxylic acid is somewhat larger than that of the corresponding alcohol, but invariably—except with formic acid—a distinct limiting current is observed.

With methanol, ethanol, glycol, and glycerol in 5*N* potassium hydroxide solution at 80°C. and 200 ma./sq.cm., potentials between 300 and 350 mv. can be reached, while in 5*N* sulfuric acid potentials from 500 to 650 mv. are observed under the same conditions.

Publication Date: January 1, 1969 | doi: 10.1021/ba-1965-0047.ch020

Acknowledgment

This work was conducted under a contract and in co-operation with the Robert Bosch GmbH, Stuttgart, Germany. Its permission to publish these results is gratefully acknowledged. We greatly appreciate the interest and the valuable suggestions by Drs. Ilge, Neumann, Herrmann, and Jahnke, members of the sponsoring company. Furthermore we wish to acknowledge the valuable assistance of Miss K. Spurk, member of Battelle-Institut, Frankfurt (Main), Germany.

Literature Cited

(1) Breiter, M. W., and Gilman, S., *J. Electrochem. Soc.* **109,** 622, 1099 (1962); *Ibid.* **110,** 449 (1963).
(2) Buck, R. P., and Griffith, L. R., *Ibid.* **109,** 1005 (1962).
(3) Krupp, H., Rabenhorst, H., Sandstede, G., Walter, G., and McJones, R., *Ibid.* **109,** 553 (1962).
(4) Müller, E., and Tanaka, S., *Z. Electrochem.* **34,** 256 (1928).
(5) Pavela, T. O., *Ann. Acad. Sci. Fennicae,* Ser. **A. II,** No. 59 (1964).
(6) Prigent, M., Bloch, O., and Balaceanu, J.-C., *Bull. Soc. Chim. France,* **1963,** p. 368.

(7) Schlatter, M. J., in "Fuel Cells," Vol. II, G. J. Young, editor, Reinhold Publishing Co., New York, 1963.
(8) Vielstich, W., *Chem. Ing. Tech.* **35,** 362 (1963).
(9) Yeager, J. F., Electrochemical Society Meeting, Indianapolis, Ind., April 1961, Abstract 104.

RECEIVED May 25, 1964.

Publication Date: January 1, 1969 | doi: 10.1021/ba-1965-0047.ch020

In Fuel Cell Systems; Young, G., el al.;
Advances in Chemistry; American Chemical Society: Washington, DC, 1969.

Anodic Oxidation of Derivatives of Methane, Ethane, and Propane in Aqueous Electrolytes

II. Coulometric-Potentiostatic Investigations

H. BINDER, A. KÖHLING, G. SANDSTEDE

Battelle-Institut e.V., Frankfurt(Main), Germany

Publication Date: January 1, 1969 | doi: 10.1021/ba-1965-0047.ch021

Coulometric-potentiostatic measurements show that in alkaline solutions using Raney platinum as catalyst only the derivatives of methane can be oxidized completely to carbonate and water. With derivatives of ethane and propane oxidation stops at the stage of the carboxylic acid. In sulfuric acid all derivatives investigated can be oxidized completely to carbon dioxide at 80° C., if provisions are made to prevent loss of volatile intermediates. From the results with methanol in sulfuric acid it may be concluded that on the Raney platinum electrode at +700 mv. the oxidation of methanol is diffusion-controlled only at concentrations smaller than 0.3 mole per liter.

In fuel cell research the anodic behavior of many organic substances is of great interest. Above all, the derivatives of hydrocarbons are considered to be potential fuels in a fuel cell or possible intermediates during anodic oxidation reactions of hydrocarbons.

Beside the fact that a compound to be used as fuel must be readily oxidized, it should be oxidized rather completely to carbon dioxide and water. Therefore, numerous investigations have been concerned with the anodic behavior of methanol (*2, 3, 5, 6, 7, 8, 9*) and various other compounds (*6*) (*8*). Yet, a survey of the anodic oxidation of potential fuels under conditions similar to those existing in a fuel cell is not yet available. Such a comparison should, of course, include quantitative measurements about the degree of conversion of all substances considered.

In Fuel Cell Systems; Young, G., el al.;
Advances in Chemistry; American Chemical Society: Washington, DC, 1969.

Part I of this communication (*1*) dealt with the electrochemical activity of various partially oxidized hydrocarbons on anodes containing Raney platinum as catalyst. These galvanostatic measurements enabled us to select proper experimental conditions for coulometric measurements which should furnish the necessary data about the degree of conversion.

These coulometric investigations were carried out by a potentiostatic method. We determined the quantity of electricity required for complete oxidation of a given quantity of the substance to be examined and compared it with the theoretical quantity necessary for complete conversion up to the carbon dioxide stage. Potentiostatic measurements are more suitable than galvanostatic methods, because the former method does not involve the risk that the reaction mechanism changes during the experiment.

Publication Date: January 1, 1969 | doi: 10.1021/ba-1965-0047.ch021

Apparatus

The apparatus shown in Figure 1 was used in our experiments. The Raney platinum electrode is situated in the lower part of a tube approximately 4 cm. in diameter. The counter electrode which is likewise contained in a tube is introduced from the side through a nozzle. It is separated from the anode compartment by a diaphragm made of porous glass or porous gold disks for acid and alkaline solution, respectively; this is to prevent the hydrogen evolved at the counter electrode from mixing with the anolyte. The hydrogen can escape to the top. Furthermore, the rising gas bubbles cannot entrain parts of the test substance and, moreover, there is no danger of cathodic reduction of the test substance.

Above the actual reaction vessel there is a cold finger where the vaporized parts of the test substance or of the intermediates condense again and drip back into the anolyte. However, this cold finger could not completely prevent the escape of highly volatile intermediates, such as aldehydes.

The reference electrode—again an autogenous hydrogen electrode —is contained in a separate tube, which is connected to the reaction vessel via a capillary tube.

In general the initial concentration of the test substance was about 2 mole per liter. The total amount of test substance necessary for this starting concentration was not added until the desired potential was reached in the test cell.

The Wenking potentiostat used is designed for loads up to 1 amp.

The decision on the electrode potential to be used was based on the following factors:

A sufficient current density has to be applied to keep the conversion period short; this minimizes losses of the test substance and of the intermediates by vaporization and diffusion. This requirement may be

In Fuel Cell Systems; Young, G., el al.;
Advances in Chemistry; American Chemical Society: Washington, DC, 1969.

moderated to some extent if provisions are made to prevent vaporization of fuel or intermediate in the test cell.

The potential of the Raney platinum electrode against the hydrogen electrode in the same solution should not exceed, say, +700 mv., because above this limit a sorption layer of oxygen begins to form on the platinum. This might inhibit the conversion process or change the reaction mechanism.

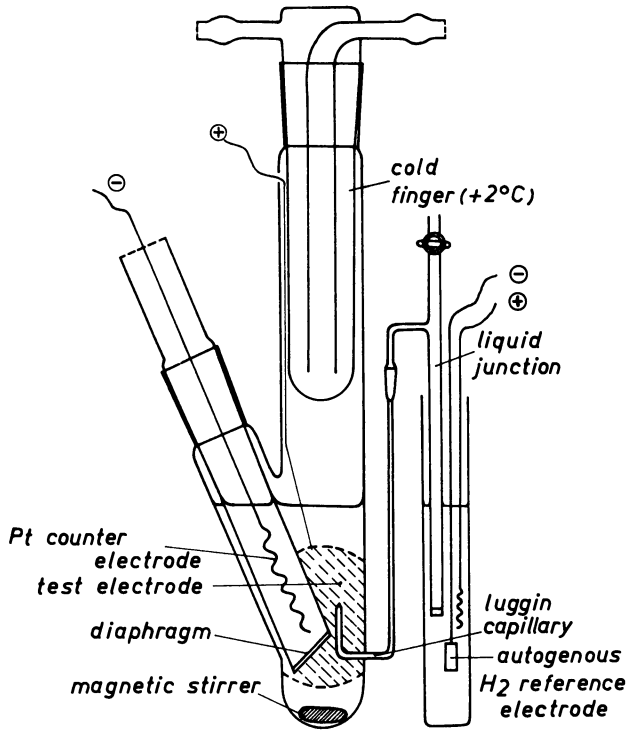

Figure 1. Apparatus for coulometric determination of the degree of conversion during anodic oxidation

The electrode potential should not exceed the potential existing in a fuel cell under extreme conditions, in order to ensure that the conversion is governed by the same mechanism.

Results and Discussion

As an example, Figure 2 shows the results obtained with formic acid at two different potentials; the current density is plotted *vs.* the electrochemical consumption, that is *vs.* the number of faradays transferred per mole of the test substance.

Publication Date: January 1, 1969 | doi: 10.1021/ba-1965-0047.ch021

With decreasing concentration the current density decreases only slightly, especially so at a potential of 500 mv.; only after conversion of about 80% of the initial amount the current density decreases more rapidly. As mentioned above a similar variation of the current density with decreasing concentration of formic acid in the electrolyte was already observed in the galvanostatic measurements (cf. Part I, Figure 4). The current density reaches zero after transport of about 2 faradays of electricity per mole. This corresponds to a 100% oxidation of formic acid to carbonate.

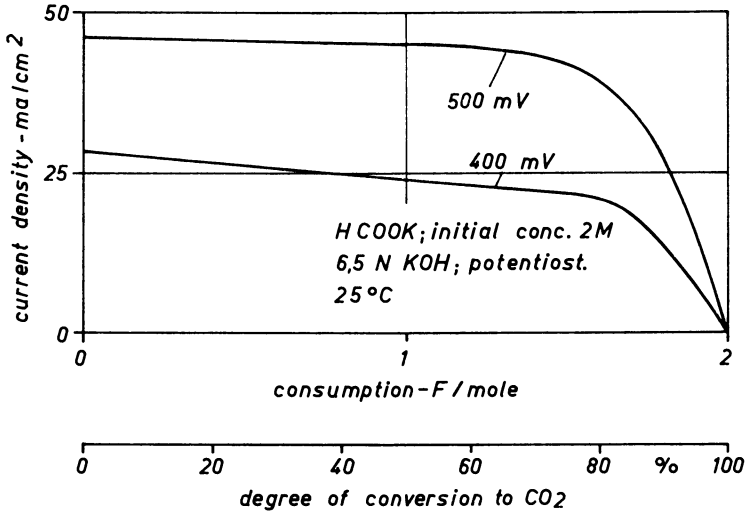

Figure 2. Decay of current density as a function of decreasing concentration of potassium formate during potentiostatic oxidation in 6.5N KOH at 25°C. and potentials of 400 mv. and 500 mv.

A further example is the conversion of methanol in sulfuric acid at 75° C. (Figure 3). In this case the current density remains nearly constant even up to a consumption of 90% of the quantity of methanol used, and then drops rapidly to zero. The measured passage of 6 faradays per mole of methanol likewise corresponds to a complete conversion to carbon dioxide. The peculiar shape of this plot suggested that the rate of oxidation is diffusion-controlled only at bulk concentrations smaller than 0.3 mole per liter. This assumption was confirmed by the use of 0.2 mole per liter as initial concentration. Then the curve drops directly to zero right from the start.

All substances that had shown sufficient activity in the galvanostatic experiments were examined in this way. In general the initial concentration of the test substance was about 2 mole per liter.

Results in Alkaline Medium. Results of the conversion in potassium

Publication Date: January 1, 1969 | doi: 10.1021/ba-1965-0047.ch021

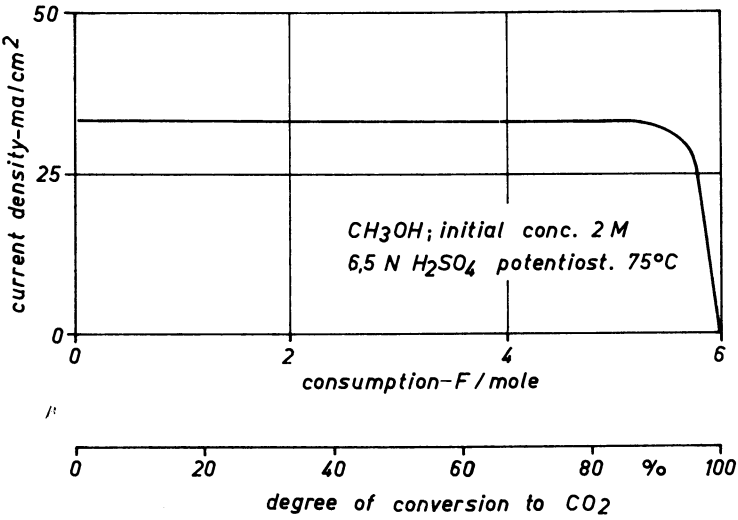

Figure 3. Decay of current density as a function of decreasing concentration of methanol during potentiostatic oxidation in 6.5N H_2SO_4 at 75°C.

hydroxide solution are summarized in Table I. Column 4 of this table indicates the computed degree of conversion in terms of per cent of conversion to carbon dioxide and water. Column 5 shows the degree of conversion if the reaction product is that indicated in this column.

Table I. Coulometric Investigations in 6.5N KOH

Reactant	*Temperature °C.*	*Potential[a] mv.*	*Degree of Conversion, %*	*Notes*
Methanol	25	300	98.0	
	80	300	97.5	
Formic acid	25	500	99.7	
Ethyl alcohol	25	600	33.3	$CH_3COOH \triangleq 33.3\%$
	80	300	33.5	
Glycerol	25	600	81.5	$(COOH)_2 \triangleq 80\%$
	80	300	84.0	
n-Propyl alcohol	25	600	21.9	$C_2H_5COOH \triangleq 22.2\%$
	80	600	22.9	
Isopropyl alcohol	25	600	9.5	$(CH_3)_2CO \triangleq 11.1\%$
	25–60	700	44.5[b]	
Acetone	60	700	34.0	$CH_3COCOOH \triangleq 37.5\%$
Glycerol	25	400	52.5	$CH_3COOH = 43\%$
	80	300	51.6	$(COOH)_2CHOH = 57\%$

[a] *vs.* Hydrogen electrode in the same solution
[b] Estimated

Of all the substances examined, only methanol and consequently also formic acid can be oxidized up to the carbonate stage.

The electrochemical oxidation of all the other alcohols yields the re-

Publication Date: January 1, 1969 | doi: 10.1021/ba-1965-0047.ch021

spective carboxylic acid as final product. This confirms the results of the galvanostatic measurements (Part I) in the course of which no conversion of carboxylic acids was observed. In the case of isopropyl alcohol the degree of conversion measured at 25° C. corresponds to the oxidation to acetone. The somewhat larger degree of conversion at 80° C. corresponds to the subsequent oxidation of acetone. As indicated before, the oxidation of acetone was likewise observed during the galvanostatic measurements. If, however, acetone becomes oxidized one should expect a degree of conversion larger than the observed value of 14%; the next oxidation step to the stage of acetol would result in a degree of conversion of about 22% (with respect to the starting compound isopropyl alcohol). The conclusion is that the apparent degree of conversion of 14% is due to the fact that during oxidation of isopropyl alcohol at a temperature of 80° C. nearly all of the first consecutive product—viz. acetone—had escaped despite the cold finger.

We therefore chose 60° C. for the oxidation of acetone itself. Under these conditions the degree of conversion of acetone is about 34%. This would correspond fairly well to an oxidation to pyruvic acid, CH_3-COCOOH, as principal end product. Pyruvic acid therefore should also be the final product upon oxidation of isopropyl alcohol in alkaline solution provided that the temperature is not raised above 60° C.

For glycerol there are several potential final products, acetic acid — CH_3COOH—and, to a greater extent, tartronic acid—$HOCH(COOH)_2$ —being the most probable ones. A chemical analysis of the conversion product has not been made so far.

Results in Acid Medium. Table II shows the results of conversion in sulfuric acid. At 25° C. and 80° C. methanol is converted quantitatively to give carbon dioxide. At 80° C. complete conversion is achieved at a potential of no more than 300 mv. The same applies to formic acid.

At 25° C. ethanol is oxidized only up to the acetic acid stage. However, a current of 0.2 ma. per sq. cm. is still observed at this stage, which corresponds to the continued oxidation of the acetic acid. The value of 39.6%, instead of 33.3%, shows that even before this stage was reached by all the ethanol involved, the acetic acid itself continued reacting to a certain extent. The oxidation rate of the acetic acid can be increased by subsequent heating of the electrolyte to 90° C. Then, the total amount of ethanol is oxidized to carbon dioxide. Hence, for complete conversion of ethanol to carbon dioxide it is necessary to oxidize it first to acetic acid at 25° C. and then to continue the oxidation at 90° C. If the reaction is carried out at 90° C. right from the start under the conditions mentioned above, the conversion of ethanol to carbon dioxide is not complete. A certain proportion is lost in the form of the highly volatile acetaldehyde, an intermediate of the reaction.

Publication Date: January 1, 1969 | doi: 10.1021/ba-1965-0047.ch021

Table II. Coulometric Investigations in 4.5N H_2SO_4

Reactant	Temperature °C.	Potential[a] mv.	Degree of Conversion %	Notes
Methanol	25	400	98.5	
	70	700	99.2	
	80	300	98.2	
Formic acid	25	500	98.5	
	80	300	99.3	
Ethyl alcohol	25	500	39.6	still 0.2 ma./sq. cm.
	90	700	86.3	
	40–90	700	94.4	
	25–90	700	98.2	
Acetic acid	90	700	99.8	
Glycol	25	500	87.5	still 0.1 ma./sq. cm.
	25	700	98.0	
	75	500	97.6	
Oxalic acid	80	600	97.5	
n-Propyl alcohol	75	500	94.5	
	80	600	89.5	
	25–80		100[b]	
Isopropyl alcohol	25	500	12.8	Acetone ≙ 11.1%
	80	600	58.0	
	25–90		100[b]	
Acetone	60	700	40.0	→ 90° C. further oxidation
	60–90		100[b]	
Diacetone alcohol	80	600	85	
	60	700	100[b]	
Propionic acid	80	500	99.8	
Glycerol	25	700	97.9	
	80	500	100.0	

[a] *vs.* Hydrogen electrode in the same solution
[b] Estimated

In the oxidation of glycol at 25° C. a value of only 87.5% is obtained because the experiment was stopped early. Similar to ethanol, the oxidation continues at first up to the stage of the corresponding carboxylic acid, which at this temperature and at a potential of 500 mv. reacts at such a small rate that exact measurements are no longer possible because of its unavoidable escape from the reaction vessel.

At a potential of 700 mv. or at elevated temperatures glycol is converted completely to carbon dioxide. At 80° C. accordingly we observed complete oxidation of oxalic acid, too.

In the case of *n*-propyl alcohol the apparent degree of conversion is lower at 80° C. than at 75° C. We suppose that this is due to the escape of propionaldehyde, and that complete oxidation will be achieved by oxidizing *n*-propyl alcohol first at 25° C., thus preventing the escape of propionaldehyde, and by further oxidation at 90° C. This would be in agreement with the results obtained on use of ethanol.

At 25° C. isopropyl alcohol is oxidized only to acetone, as was observed in alkaline solution, too. At 80° C. a degree of conversion of only 58% is observed. This may seem puzzling because on the basis of the above results one might expect that all the consecutive reaction products should be converted as well.

Publication Date: January 1, 1969 | doi: 10.1021/ba-1965-0047.ch021

Again the conclusion is that at 80° C. the first consecutive product, i.e. acetone, has escaped. On use of acetone at 60° C. acetic acid is obtained first, which can be oxidized more rapidly at 90° C. (cf. Table II).

Hence, it is evident that isopropyl alcohol, too, may be oxidized to carbon dioxide if special provisions are made.

It is assumed that acetone is converted via its condensation products, such as diacetone alcohol. The presence of diacetone alcohol was identified so far only by its smell. On use of diacetone alcohol itself the degree of conversion is about 85%, probably because of some acetone escaping.

Conclusions

Our investigations show that in potassium hydroxide solution, using Raney platinum as catalyst, only the derivatives of methane can be oxidized to carbon dioxide or, strictly speaking, to the carbonate.

In sulfuric acid all the alcohols and carboxylic acids investigated can be oxidized completely to carbon dioxide. With respect to the oxidation of ethanol and both of the propyl alcohols, special provisions have to be made in order to achieve complete conversion.

The escape of a volatile intermediate and the observation that at a temperature of 25° C. the oxidation stops at the stage of acetic acid, propionic acid, and acetone, respectively, agrees with the observations and suggestions by Schlatter (*8*). This author stated that during the oxidation of alcohols, for example, the possible intermediates need not remain adsorbed on the electrode but are released into the electrolyte.

We did not observe, however, the escape of an intermediate if it was more active than the starting compound. For example, methanol can be oxidized quantitatively in sulfuric acid even at 80° C. since formaldehyde is by far more active than methanol under these conditions so that it cannot accumulate in the electrolyte in concentrations leading to noticeable rates of escape.

Ethanol, isopropyl alcohol and *n*-propyl alcohol, however, cannot be oxidized quantitatively at 80° C. because the respective aldehyde and ketone are less active than the alcohol, so that they do escape. On the other hand, acetic acid which is more active than ethanol at 80° C., accumulates in the electrolyte during oxidation at 25° C. since it is less active at this temperature. This is true also for the oxidation of acetone because acetic acid again is the less active intermediate at 25° C.

An explanation of the fact that in alkaline solution carboxylic acids, except formic acid, cannot be oxidized either on Raney platinum or on platinized platinum while they are oxidizable in the acid medium, may be based on the assumption that it is the undissociated molecule of the acid that is oxidized anodically. Almost no undissociated molecules are left in a strong base (5*N* KOH) and, as is known, the anions are more

Publication Date: January 1, 1969 | doi: 10.1021/ba-1965-0047.ch021

stable because of the resonance energy of 5–7 kcal. per mole, which is due to the resonance structure mainly between the following extremes:

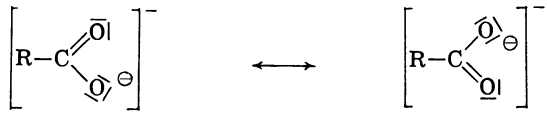

Beyond this, because of the strong dipole moment of the anion, the carboxyl group becomes adsorbed onto the positively polarized electrode in such a manner that further oxidation does not occur.

The only exception is formic acid which may be regarded as a direct hydrogenation product of carbon dioxide, so that, inversely, the oxidation of formic acid may involve a dehydrogenation mechanism.

Nevertheless, from a chemical point of view the anodic oxidation of the other carboxylic acids at such a low potential is remarkable in view of the stability of these acids, even against strong oxidants, such as chromic oxide.

Publication Date: January 1, 1969 | doi: 10.1021/ba-1965-0047.ch021

Acknowledgement

This work was conducted under a contract and in cooperation with the Robert Bosch GmbH, Germany. Their permission to publish these results is gratefully acknowledged. We greatly appreciate the interest and the valuable suggestions by Drs. Ilge, Neumann, Herrmann, and Jahnke, members of the sponsoring company.

Literature cited

(1) Binder, H., Köhling, A., Krupp, H., Richter, K., Sandstede, G., ADVAN. CHEM. SER. **47**, 269 (1965)
(2) Breiter, M. W., Gilman, S., *J. Electrochem. Soc.* **109**, 622, 1099 (1962); **110**, 449 (1963)
(3) Buck, R. P., Griffith, L. R., *Ibid.* **109**, 1005 (1962)
(4) Krupp, H., Rabenhorst, H., Sandstede, G., Walter, G., Mc Jones, R., *Ibid.* **109**, 553 (1962)
(5) Müller, E., Tanaka, S., *Z. Electrochem.* **34**, 256 (1928)
(6) Pavela, T. O., *Ann. Acad. Sci. Fennicae, Ser. A. II*, No. 59 (1954)
(7) Prigent, M., Bloch, O., Balaceanu, J.-C., *Bull. Soc. Chim. France*, **1963**, 368.
(8) Schlatter, M. J., in "Fuel Cells," **II**, Young, G. J., ed., p. 190, Reinhold, New York, 1963
(9) Vielstich, W., *Chemie Ing. Techn.* **35, 362 (1963)**
(10) Yeager, J. F., Electrochemical Society Meeting Abstracts, Indianapolis, April 1961, Abstract 104.

RECEIVED May 25, 1964.

In Fuel Cell Systems; Young, G., el al.;
Advances in Chemistry; American Chemical Society: Washington, DC, 1969.

22

Oxidation of Olefins and Paraffins in Low Temperature Fuel Cells

M. J. SCHLATTER

California Research Corp., Richmond, Calif.

Publication Date: January 1, 1969 | doi: 10.1021/ba-1965-0047.ch022

Low molecular weight paraffins and olefins can be completely oxidized at platinized porous carbon anodes in low temperature acid electrolyte fuel cells. These two classes of hydrocarbons do, however, show substantial differences in electrochemical behavior. The paraffin-depolarized electrodes are readily poisoned by air or oxygen; olefin-depolarized electrodes are much less affected. The paraffins give more favorable cell voltages at low currents but fall off badly under load. The olefins can support high currents as the anode potential approaches that of the oxygen electrode.

We concluded that low temperature hydrocarbon fuel cells might be feasible when we found that current could be drawn from an ethylene or propane depolarized platinized porous carbon electrode for a sustained period at 80° C. and that under these conditions the hydrocarbon was completely oxidized (*7*). Similar results with these and some other hydrocarbons have since been reported from other laboratories (*4, 5*).

Further studies of the behavior of hydrocarbons on platinized porous carbon electrodes in aqueous sulfuric acid electrolytes are discussed here. Results from rotating disk and small platinum foil electrodes have been reported by other members of our group (*3*).

We chose to use platinized porous carbon electrodes for hydrocarbon product studies in order to make enough product for quantitative determination. Porous carbon and graphite are electrically conducting, resistant to acidic and basic electrolytes, and are available in a variety of porosities and surface areas. Further modification by chemical treatment is also possible.

The use of porous electrodes for electrochemical measurements and for electrocatalyst studies does result in some problems. These difficulties

In Fuel Cell Systems; Young, G., el al.;
Advances in Chemistry; American Chemical Society: Washington, DC, 1969.

are shared by those working with "practical" fuel cell electrodes. The theory of porous electrodes is inadequate at present. However, it is receiving much attention because it is probable that practical fuel cell electrodes will be porous structures. This is necessary if large electrocatalyst surface areas and high fuel cell power densities are to be attained.

Time-dependent polarization leading to unstable current-potential behavior complicates the use of current-potential measurements in the evaluation of porous electrodes which are depolarized with saturated hydrocarbons. These difficulties can be avoided by using pseudo steady-state currents after step changes in electrode potential. This procedure gives current-potential curves similar to those obtainable by potential-sweep methods with small electrodes and shows promise for use in the detailed comparison of very different electrodes and systems. From these curves, large differences in behavior of olefins and paraffins can be seen. It is clear that the unstable current-potential behavior with paraffins at high constant currents is not due to inadequate mass transfer immediately adjacent to the electrode but rather to the lower currents that can be supported by paraffins as the electrode potential is polarized above peak current potentials. Electrode poisoning occurs in this potential region with the formation of an oxygen film on the electrode. This could inhibit adsoprtion of the paraffins and reduce the number of effective catalyst sites for the paraffin oxidation. The potential at which this effect will dominate over the tendency for the current to increase with increasing potential differs with different fuels and probably depends on their ability to inhibit formation of the oxygen film or to remove it as it is formed. With olefins, the potential of peak current is more positive than that of an oxygen counterelectrode.

Hydrocarbon depolarized electrodes were also much more sensitive to inhibiting influences than electrodes depolarized with more reactive fuels. The term "electrode inhibition" as used here refers to any influence of materials which, when formed on a fuel cell anode or when introduced into a fuel cell, act to decrease the electrical output from the cell. This does not necessarily require that the rate of oxidation of the fuel itself be diminished. Different types of inhibition by air and oxygen and by extreme polarization of a fuel cell anode were observed and interpreted. When carbon monoxide was injected into the feed stream to a propane or propylene depolarized electrode, an improvement of performance resulted. No effect was evident when carbon dioxide was injected in this way. Preliminary experiments were made to evaluate the possibility of using inhibition data in the study of porous electrode activity and behavior. However, the factors affecting the shape and size of these inhibition peaks are complex, and more study will be required before they are completely understood or before significant application of these techniques can be expected.

Publication Date: January 1, 1969 | doi: 10.1021/ba-1965-0047.ch022

Apparatus and Methods

Product Studies. The apparatus used for our new hydrocarbon product studies is shown in Figure 1. It differs slightly from that described before (7). Fritted-glass separators fused in place are used instead of ion exchange membranes to separate the three cell compartments. A means of equalizing pressure is provided to minimize flow of electrolyte from one compartment to another. The Ascarite "carbon dioxide" absorption tube is preceded by a condensate trap and Drierite and Anhydrone tubes to remove sulfuric acid spray and water. Ascarite and Drierite follow the Ascarite "carbon dioxide" absorption tube to exclude moisture and atmospheric carbon dioxide.

Publication Date: January 1, 1969 | doi: 10.1021/ba-1965-0047.ch022

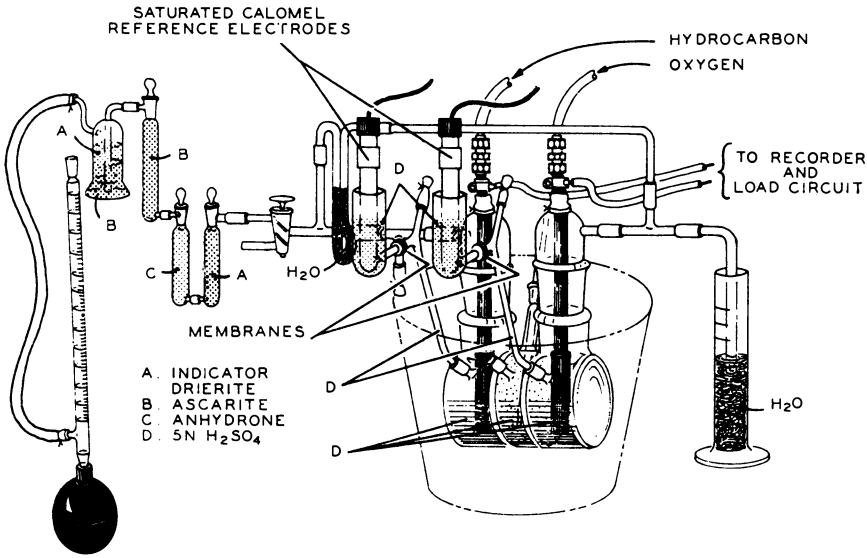

Figure 1. Apparatus for hydrocarbon product studies

The apparatus was thoroughly flushed with the hydrocarbon used before weighing the Ascarite tube at the beginning of each experiment. At the end of an experiment, hydrocarbon flow was continued until at least 2 liters of gas passed through the anode in order to remove all carbon dioxide product from the cell. Additional flushing for an equal period gave changes in the weight of the Ascarite tube of the order $\pm$ 0.5 mg.

Constant cell currents were maintained by automatically varying the load resistance as was previously described (7).

Current and anode potential versus saturated calomel electrode (SCE) at 25° C. were recorded on a calibrated dual-pen Varian recorder. The reference electrode was a Beckman saturated calomel electrode main-

tained at room temperature (25° C.) and connected to a Luggin capillary through a long, small-diameter bridge filled with the fuel cell electrolyte. The anode potential versus SCE was sensed by a Keithley Model 600A electrometer with recorder output. Potentials are reported versus the normal hydrogen electrode (NHE) with the sign of the oxygen electrode positive relative to the hydrogen electrode. These reported potentials differ from those measured versus SCE by 0.242 volt.

Potential-Step Voltammetry. In its simplest form the apparatus used for potential-step voltammetry consisted of a cell like that used for the product studies but modified for half-cell studies by substituting a platinum gauze cathode for the oxygen electrode. Current through the cell was provided by a storage battery in series with variable resistors. Anode potential was controlled by manually adjusting these resistors. Current and potential were sensed and simultaneously recorded as previously described.

Recently we have used one function of a versatile two-stage constant potential/constant current d.c. power source in place of the manually controlled system. The preregulator uses a magnetic amplifier and controlled rectifiers. The second regulator stage uses power transistors with an adjustable gain amplifier for control.

In the constant potential mode, the potential difference between the fuel cell anode and a reference electrode is sensed by an electrometer amplifier. The output of this is compared with an adjustable reference voltage. The difference is then used, through an operational amplifier, to maintain the anode at constant potential.

Slow response of the fuel cell anode potential with changes in cell current requires time delay circuits to limit the rate of change of the power supply output. This is accomplished through variable capacitor feedback to the operational amplifier which controls the power to the test cell.

Air and Oxygen Inhibition Experiments. The apparatus used was similar to that for potential-step voltammetry. Current was supplied to the cell from a storage battery through variable resistors. Control circuits provided for automatic constant-current operation.

Inhibition data were obtained by injecting 2.48-ml. portions of air, oxygen, and other gases into the fuel gas stream before it passed through a platinized porous carbon anode. This was done by means of a Wilkins XA-202 gas sampling valve (Wilkins Instrument and Research, Inc., P.O. Box 313, Walnut Creek, Calif.). Propane and propylene were each used as fuels. Flow rates were measured on the exit gas from the anode compartment using a soap film flowmeter.

Electrodes. The electrodes used were similar in form to those previously described (7). Each consists of a porous carbon cylinder $2^1/_2$ inches long, $^3/_4$-inch o.d., and $^1/_2$-inch i.d. which is fitted tightly to a

Publication Date: January 1, 1969 | doi: 10.1021/ba-1965-0047.ch022

1/2-inch o.d. impervious graphite tube. This tube serves as electrical conductor and gas conduit. The lower end of the cylinder is closed with a graphite plug, and the joints are sealed with an Epon resin (Epon 828-Z, Shell Chemical Co.).

As used in the experiments described here, the electrodes were sometimes new; in other cases they had been used extensively with various fuels and electrolytes at different conditions.

The platinum was applied to the electrode by two general methods:

A. The electrode was electroplated for 20 minutes at ambient temperature and at a current density of 40 ma./sq.cm. in a 1.25- or 1.5-inch diameter graphite cup which served as the counter electrode. The plating solution was drawn into and forced out of the electrode every two minutes during the plating period. Sometimes this procedure was repeated. Different plating solutions were used as shown in Table I.

More active electrodes were obtained by Method B:

B. The porous carbon electrode blank was impregnated with chloroplatinic acid solution containing 10 weight % platinum. It was dried on a rotating graphite mandrel in an air oven at 140°C. and was reduced for three hours in a stream of hydrogen at 400°C. It was then mounted and sealed.

The preparation and geometric areas of the electrodes are summarized in Table I.

Table I. Preparation and Geometric Areas of Some Platinized Porous Carbon Electrodes

Electrode	*Carbon Base Material*[1]	*Geometric Area, sq. cm.*	*Platinum Solution (H_2PtCl_6)*		*Method*	*Number of Times Plated*
			Wt. % Pt	*Other Components*		
A	139	29.9	0.5	0.12 *N* HCl	A	6
B	139	31.8	0.5	0.12 *N* HCl	A	1
C	139	30.0	0.5		A	2
D	139	30.6	0.5		A	2
E	139	35.4	0.5	0.12 *N* HCl	A	3
			0.5		A	2
			0.5	0.12 *N* HCl	A	1
F	FC-14	24.0	10.0		B	1
G	139	33.0	0.5	0.04 wt. % Pb acetate	A	1

[1] No. 139, Stackpole Carbon Co. St. Mary's Pa.; No. FC-14, Pure Carbon Co., St. Mary's Pa.

New Product Studies

Product data which we reported previously (7) showed that ethylene and propane can be completely oxidized in fuel cells at 80° C. New data for propane reconfirm this result, but data from *n*-butane suggest that incomplete oxidation of this hydrocarbon can occur under some conditions that give complete oxidation with propane.

The new results were obtained using a platinized porous carbon

Publication Date: January 1, 1969 | doi: 10.1021/ba-1965-0047.ch022

electrode (electrode A, Table I) with sulfuric acid at 80°C. In this series, the cell was operated at 25.2 ma. (0.84 ma./cm.). A slow decrease in cell voltage occurred with time. When the cell voltage dropped close to the point where the current could no longer be maintained, a short period at open circuit restored the electrode activity for further operation under load. Initial anode potentials for propane and *n*-butane under load were of the order 0.45 to 0.50 volt (versus NHE) increasing with time to 0.74 to 0.84 volt.

The present series consisted of two propane experiments followed by three *n*-butane experiments and another propane experiment. The product results are summarized in Table II.

Table II. Carbon Dioxide Produced by Fuel Cell Oxidation of Hydrocarbons

						Carbon Dioxide		
Expt. No.	*Fuel*	*Current, ma.*	*Current Density, ma./ sq. cm.*	*Time, hours*	*Energy, amp.-hour*	*Theory, mg.*	*Found, mg.*	*Per cent of theory*
1	Propane	25.2	0.84	18.37	0.463	114.2	113.7	99.4
2	Propane	25.2	0.84	18.00	0.453	111.8	112.3	100.5
3	*n*-Butane	25.2	0.84	6.53	0.169	42.6	45.4	106.6
		10.0	0.33	0.40				
4	*n*-Butane	25.2	0.84	41.75	1.053	266.0	287.7	108.2
5	*n*-Butane	25.2	0.84	14.17	0.356	90.3	96.7	107.1
6	Propane	25.2	0.84	14.67	0.369	91.0	90.1	99.0

Propane: $C_3H_8 + 5O_2 \rightarrow 3CO_2 + 4H_2O$ (20-electron change) 3/20 mole CO_2 per faraday = 246.5 mg. CO_2 per amp.-hour.
Butane: $C_4H_{10} + 6^1/_2O_2 \rightarrow 4CO_2 + 5H_2O$ (26-electron change) 4/26 mole CO_2 per faraday = 252.7 mg. CO_2 per amp.-hour.

The "carbon dioxide" values for *n*-butane are 6 to 8% above theory based on the ampere-hours produced during the experiments. This excess could come from direct chemical oxidation of *n*-butane by oxygen transported through the electrolyte from the cathode chamber or from some electro–oxidation of the electrode carbon. This would give more carbon dioxide per coulomb than can be obtained from the hydrocarbon. However, similar oxygen transport or carbon oxidation would be expected in the propane experiments which gave the theoretical amount of "carbon dioxide." It has been suggested that more oxidation of the carbon of the electrode might have occurred in butane, because of greater polarization of the electrode during operation with this less reactive fuel. Inspection of the potentials continuously recorded during the product experiments shows that the average anode potentials during the butane experiments were slightly more positive (0.05 to 0.1 volt) than with propane. Individual differences between the three butane experiments and between the two propane experiments were, however, greater than this. Thus, while some oxidation of electrode carbon may have complicated the results obtained, we believe the effect to have been small with our relatively inactive electrodes at comparatively low temperature and low

Publication Date: January 1, 1969 | doi: 10.1021/ba-1965-0047.ch022

acid concentration. The differences in behavior in propane and *n*-butane reported here may only be detectable with comparatively inactive electrodes under marginal operating conditions.

Partial oxidation products absorbed from the fuel cell exit gas stream with the carbon dioxide could also account for a high "carbon dioxide" value. Calculations were made for experiment 4 (Table II) which gave 108.2% of the theoretical amount of carbon dioxide." Cases were considered where the partial oxidation product was butanol, butanone, butyric acid, or acetic acid. Assuming complete recovery of the products, values of 9 to 14 weight % of partially oxidized *n*-butane in the "carbon dioxide" product were calculated. As it is improbable that all of the partially oxidized materials reached and were retained in the Ascarite tube, even higher percentages of partially oxidized products are possible.

Publication Date: January 1, 1969 | doi: 10.1021/ba-1965-0047.ch022

Evaluation of Hydrocarbon Depolarized Electrodes

As part of a program to improve the performance of platinized porous carbon electrodes, propane was chosen as a test material. With this hydrocarbon we had considerable difficulty in using conventional potential-current plots because of time-dependent polarization.

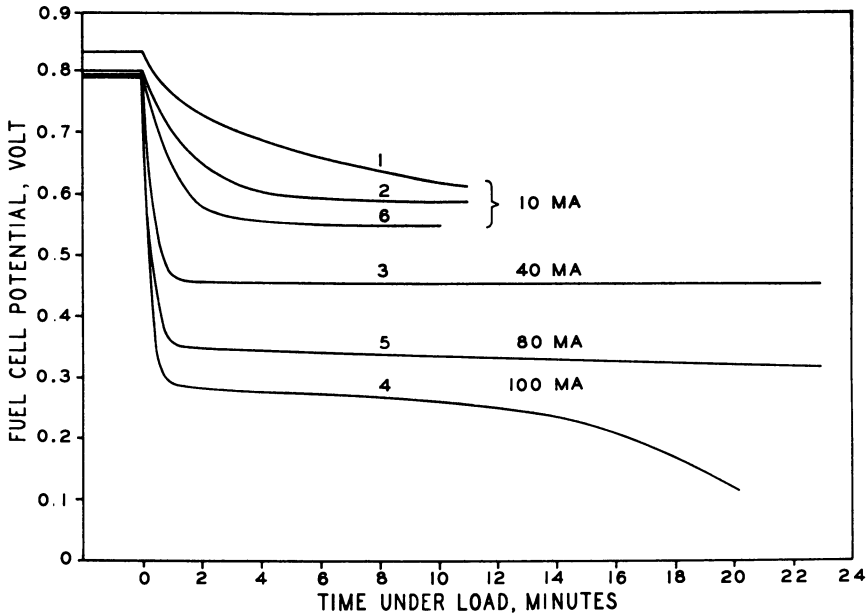

Figure 2. Propane-oxygen fuel cell polarization with time as a function of load
Platinized porous carbon electrodes (Table I, Anode B; Cathode C); 5N sulfuric Acid electrolyte; 80° C.

The nature of these difficulties can be seen more clearly from curves

showing the change in electrode potential with time at constant current (Figure 2). Here the over-all cell voltage is plotted against time. Sequence numbers and current are shown on each curve. Curves 1 and 2 were both recorded at 10 ma. current and show the effect of the removal of active products from pre-electrochemical reactions. Curve 6, also at this current, may illustrate further removal of active materials or the formation of inhibitors during the intermediate experiments. The rapid decrease in potential at the end of the 100-ma. curve is characteristic of time-potential curves at higher currents and would be accentuated at still higher currents.

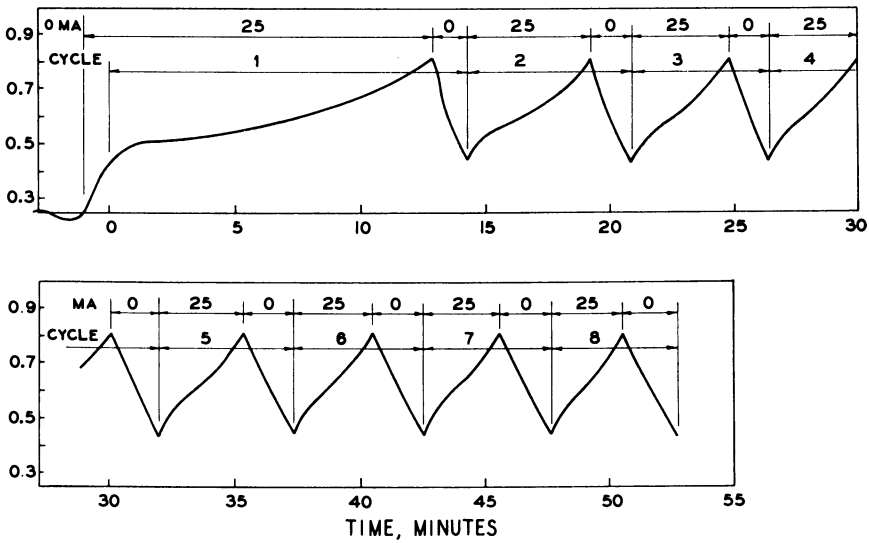

Figure 3. Fuel cell anode polarization data with propane at 80° C. Platinized porous carbon anode (Table I, electrode C); 5N Sulfuric acid electrolyte

Another example of the effect of pre-electrochemical reactions on time-dependent polarization is seen in Figure 3. Here an attempt to remove impurities and intermediates from an electrode was made by use of a repetitive test cycle. The anode was caused to cycle from 0.44 to 0.84 volt under load with return from 0.84 to 0.44 volt at open circuit. In the course of several cycles, it was expected that impurities would be removed and reproducible cycles obtained. In practice, variations in treatment of the electrode immediately before test caused more change in the first few cycles than later; but a continuing decrease in polarization time and increase in recovery time occurred as each series progressed. Preliminary tests were made in order to select appropriate current ranges for each cycle test series. The curves in Figure 4 are derived from these data. The upper curve represents the time in minutes for the anode to

Publication Date: January 1, 1969 | doi: 10.1021/ba-1965-0047.ch022

polarize from 0.44 to 0.84 volt plotted against the number of test cycles. The lower curve shows the corresponding data for recovery times from 0.84 to 0.44 volt.

Data like these were used by us in some cases for comparing electrodes or for investigating the effects of pretreatments on the behavior of a particular electrode.

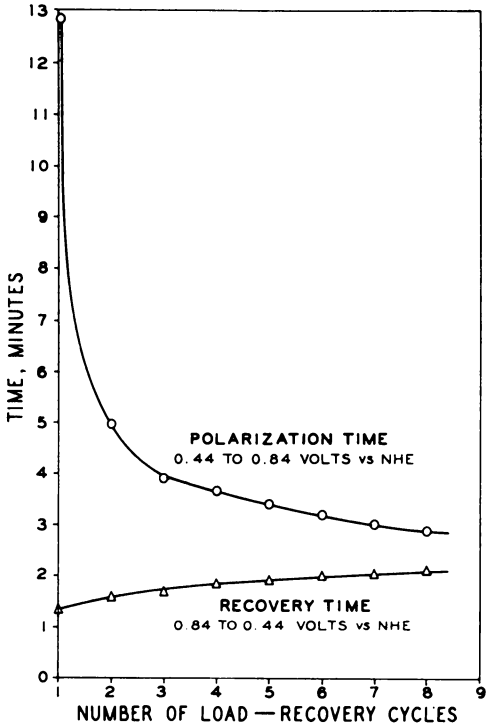

Figure 4. Effect of number of load-recovery cycles on polarization time and recovery time of a propane depolarized electrode at 80° C.

Platinized porous carbon anode (Table I, electrode C); 5N sulfuric acid electrolyte

Potential-Step Voltammetry

In an effort to simplify the interpretation of electrochemical data from porous electrodes, we attempted to establish steady-state conditions by prolonged operation of bubbling hydrocarbon depolarized electrodes at a series of fixed potentials.

If no change in the catalytic activity of a fuel cell anode occurs, it should be possible to establish a steady-state current at constant potential

Publication Date: January 1, 1969 | doi: 10.1021/ba-1965-0047.ch022

for each set of conditions. In this situation current would be determined by the catalytic activity of the electrode surface and the steady state concentrations of reactants and products at the electrode surface.

With our platinized porous-carbon anodes depolarized with propane, this steady state is not reached in four hours at 80° C. at 0.74 volt; though in many cases the current was decreasing very slowly at this time. A curve obtained using automatic potential control is shown in Figure 5.

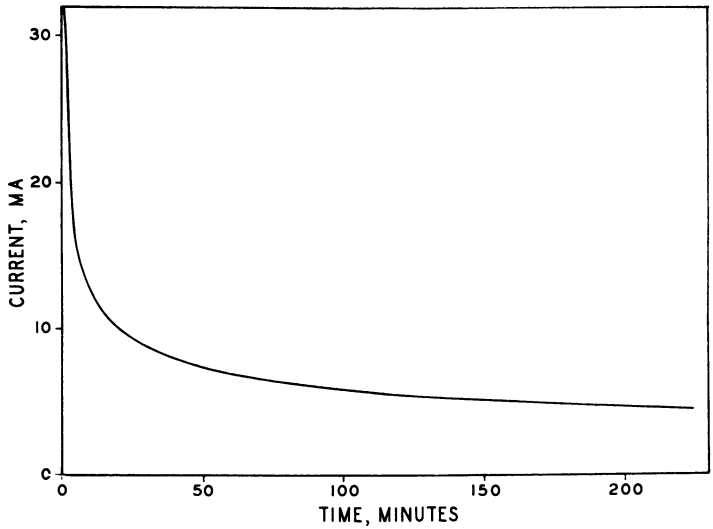

Figure 5. Current decrease with time for propane-depolarized fuel cell anode at constant potential

Potential automatically controlled at 0.74 volt vs. NHE. Platinized porous carbon anode (Table I, electrode D); 5N sulfuric acid electrolyte; 80° C.

Many experiments were carried out to determine the reproducibility of constant potential-current data and to provide a basis for selecting test sequences which would give satisfactory, comparable data in the least time. These curves appear to consist of two sections. In the first part, the current is changing rapidly. This section of the curve appears to be affected considerably by recent electrode history and is sometimes difficult to reproduce. After a period which varies in length, depending on the recent history of the electrode, a steady state is approached. With some fuels, such as ethylene and propylene, the current will remain constant for long periods; with others, such as propane, a gradual, slow decline in current is observed. With the electrodes listed in Table I, 20 to 60 minutes was ordinarily used at each controlled anode potential.

Publication Date: January 1, 1969 | doi: 10.1021/ba-1965-0047.ch022

Fuel Cell Oxidation of Propane, Isobutane, Propylene, Ethylene, and Hydrogen in 5N H_2SO_4 at 80° C.

The anode current densities corresponding to different anode potentials were measured by a constant-potential technique for propane, isobutane, and propylene (Figure 6). The points shown correspond to current densities 20 minutes after the indicated potential was established. A current-potential curve for hydrogen on this electrode is included for reference.

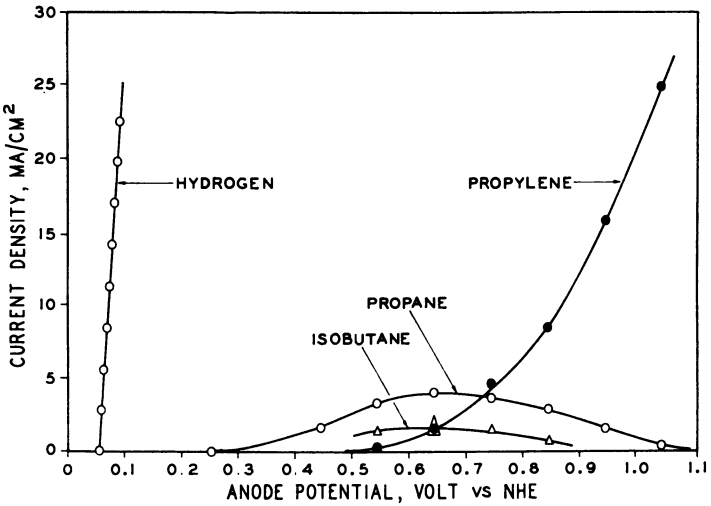

Figure 6. Effect of anode potentials on fuel cell "steady state" current densities for hydrogen, isobutane, propane, and propylene

Platinized porous carbon anode (Table I, electrode E); 5N sulfuric acid electrolyte; fuel rate, 10 ml./minute, 80° C.

Curves showing ethylene and propylene performances are plotted in Figure 7. These data were taken from constant-current experiments, but in these cases the rates of polarization with time were so slow that the data actually were obtained at nearly constant potentials. The ethylene curve is similar to the propylene curve but is displaced slightly toward more favorable lower anode potentials.

The shapes of the propane and ethylene curves correspond fairly closely with potential-sweep data obtained using a platinum-foil electrode and 2*N* sulfuric acid electrolyte (Figure 8).

Figure 6 shows that with the saturated hydrocarbons, propane and isobutane, the anode current increases to a maximum between 0.6 to 0.7 volt and then decreases as the anode is polarized further. This type of behavior appears to be general for saturated hydrocarbons. It is also found with saturated hydrocarbons that at anode potentials above those

Publication Date: January 1, 1969 | doi: 10.1021/ba-1965-0047.ch022

for maximum current, the rate of decay of current increases as the anode potential increases; and "steady-state" currents require more time to establish. Up to a point it is possible to draw more current temporarily by decreasing the load resistance but at the expense of rapidly increasing polarization. Thus, with the constant-current methods ordinarily used in determining electrode current-dependent polarization, a "limiting" current is found beyond which unstable electrode behavior is observed.

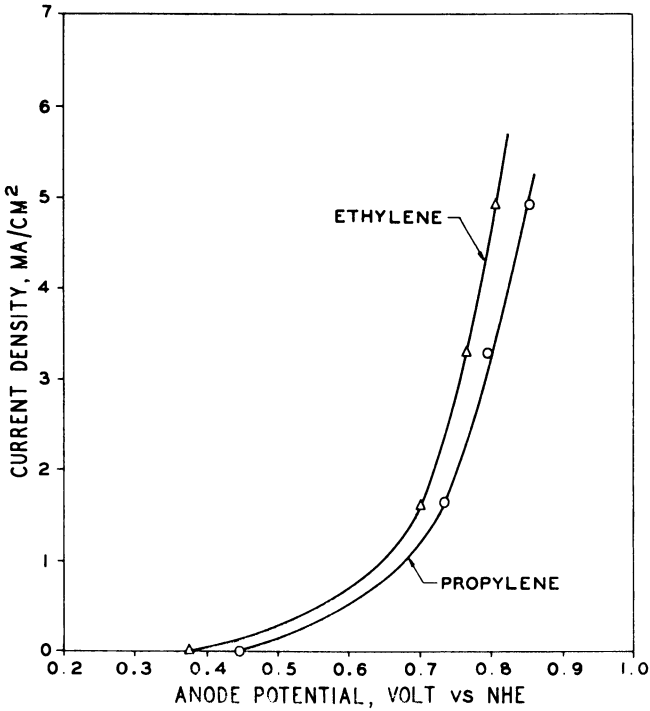

Figure 7. Effect of anode potentials on fuel cell "steady state" current densities for ethylene and propylene
Platinized porous carbon anode (Table I, electrode D); 5N sulfuric acid electrolyte; fuel rate, 10 ml./minute; 80° C.

Olefins differ from paraffins in their current-potential behavior (Figures 6, 7). They give higher "steady-state" currents as the potential is increased beyond the region of interest for hydrocarbon-oxygen fuel cells. Therefore, they do not give the "limiting" currents found with saturated hydrocarbons.

The results reported here are for comparatively inactive electrodes operating under marginal conditions. The relative shapes of the curves may be expected to change as electrodes and operating conditions are changed.

Publication Date: January 1, 1969 | doi: 10.1021/ba-1965-0047.ch022

Air and Oxygen Inhibition of Hydrocarbon-Depolarized Electrodes

The study of hydrocarbon-depolarized electrodes is complicated by their susceptibility to various inhibiting influences. Such effects were much less apparent with hydrogen, methanol, and other more active fuels.

Inhibition of hydrocarbon fuel cell anodes by air was found to be troublesome, and this led to further investigation. Some other inhibiting influences were also observed which resemble and probably are forms of oxygen inhibition.

There is always some possibility that air or oxygen may contact a fuel cell anode. The inhibiting effects of these substances are therefore of practical interest. Our results show, however, that such inhibition is readily overcome. It is probable also that it will be much less evident with electrodes and conditions giving practical performance with hydrocarbons.

Publication Date: January 1, 1969 | doi: 10.1021/ba-1965-0047.ch022

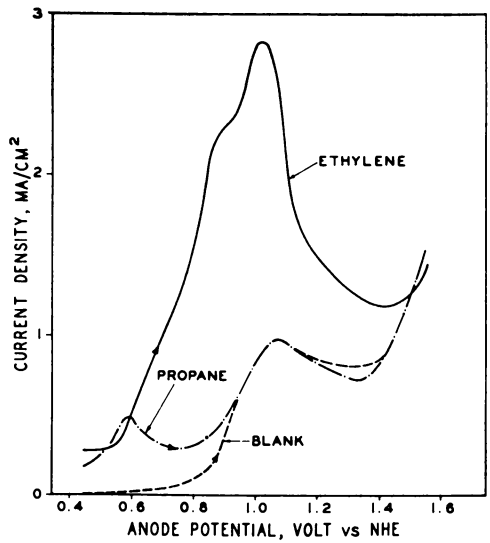

Figure 8. Current potential curves for anodic oxidation of propane and ethylene on platinized platinum foil

Saturated solutions; 2N sulfuric acid electrolyte; sweep rate, 16.7 mv./sec.; 80° C.

Typical inhibition behavior is observed when a little air enters the feed line to a hydrocarbon fuel cell anode. A severe polarization occurs resulting in a very sharp increase in anode potential. This change in potential can amount to several tenths of a volt, and the electrode potential can approach that of an oxygen cathode. (In our equipment, open-circuit potentials of 1.058 to 1.081 volts were observed with platinized porous

carbon electrodes at 80° C. in 5*N* sulfuric acid electrolyte with oxygen at 1 atm. pressure. Lower potentials are, of course, obtained under load.) Recovery of the original anode potential may require a minute or two or several minutes, depending on the hydrocarbon involved, the amount of air admitted, and the temperature.

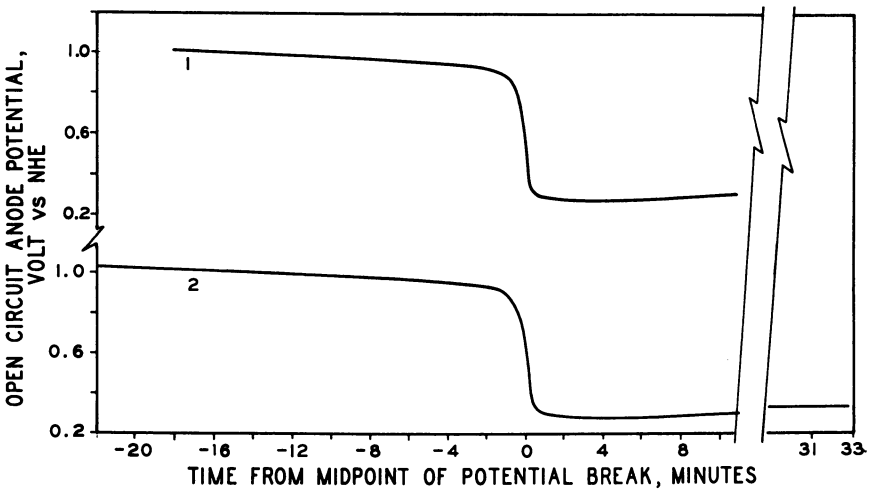

Figure 9. Induction periods before establishing propane open-circuit potential of an air-poisoned platinized porous carbon electrode (Table I, electrode A); 5N sulfuric acid electrolyte; 80° C.

Variable "induction" periods which often occur on start-up with saturated hydrocarbons are also probably due to air inhibition. Examples with propane are shown in Figure 9. Curves 1 and 2 were obtained on successive days with electrode A (Table I). The exposure to air differed, and curve 1 shows less inhibition than curve 2. In other cases "induction" periods from a few minutes to several hours have been observed. All of the curves show a gradual initial drop in potential followed by a rapid transition to a potential minimum and then a gradual increase to a constant open-circuit potential. These open-circuit potentials, although reasonably constant in a particular experiment, do vary a little from one experiment to another.

Similar behavior is noted when enough oxygen is injected into the propane stream to bring the potential of the electrode above 0.8 volt. Inhibition curves obtained with electrode F (Table I) resulting from the injection of different amounts of oxygen are shown in Figure 10. Here the transitions are less abrupt than those in Figure 9. The electrodes are quite different, but there may also be some differences in the nature of the inhibition.

Polarization of a propane-depolarized platinized porous carbon elec-

Publication Date: January 1, 1969 | doi: 10.1021/ba-1965-0047.ch022

trode under load until potentials above approximately 0.94 volt are attained also inhibits the electrode. Operation at open circuit then gives a gradual initial drop in potential followed by a rapid transition to open-circuit potential. The effect of the electrode potential on the potential recovery curves at open circuit for electrode G (Table I) is shown in Figure 11. In these experiments the cell was operated at 100 ma. until the anode polarized to the test potential. The current was then manually adjusted as required to hold this potential for seven minutes. The circuit was then opened, and the potential recovery curve was recorded. The single exception to this is the highest potential case. Here the circuit was opened as soon as the 1.14-volt potential was reached.

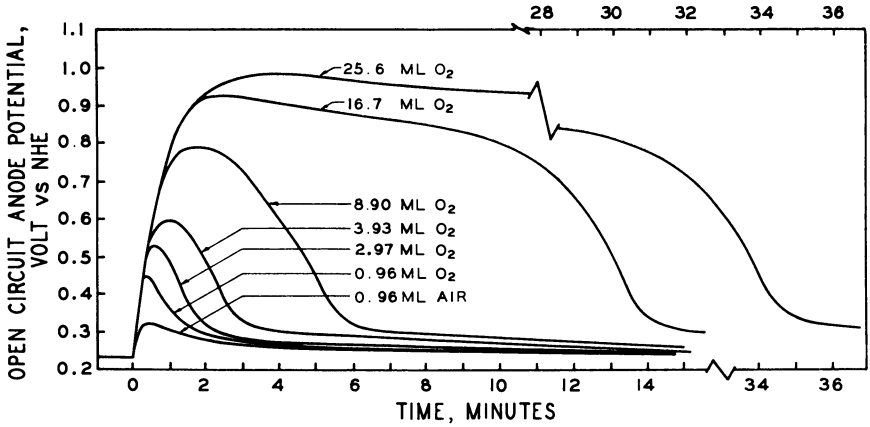

Figure 10. Oxygen inhibition of a propane-depolarized electrode
Platinized porous carbon electrode (Table I, electrode F); 1N sulfuric acid; 80° C.

A slight convex shape of the recovery curve is seen after operation at potentials as low as 0.64 volt. Pronounced effects, however, are not observed until 0.94 volt or more is reached.

There is some possibility that hydrocarbon fuel cell anodes can be inhibited by polarization in a practical situation. With present oxygen-propane fuel cells, anode recovery at open circuit is rapid even after brief short circuit because the potential of the anode cannot exceed the relatively low potential of the polarized oxygen counterelectrode. However, if oxygen electrode efficiencies are improved, their potentials could be high enough to substantially inhibit some saturated hydrocarbon depolarized anodes. These potentials can also be attained in a multiple fuel cell arrangement or in a fuel cell where the anode half cell is coupled with a halogen-depolarized electrode or other high potential system.

The inhibited electrode is restored by contact with propane in due time. The activity toward propane can also be restored rapidly by in-

Publication Date: January 1, 1969 | doi: 10.1021/ba-1965-0047.ch022

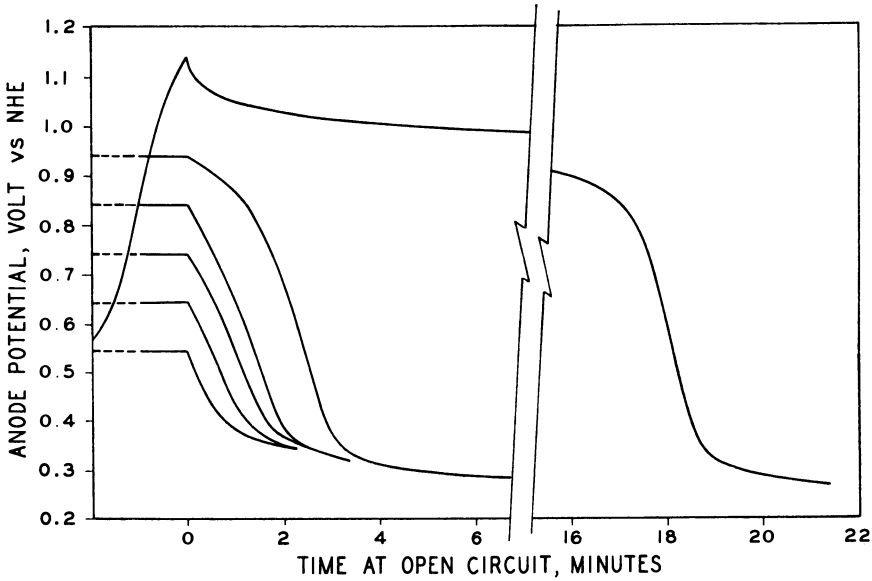

Figure 11. Effect of anode potential of a propane depolarized anode on recovery at open-circuit

Platinized porous carbon electrode (Table I, electrode G); 5N sulfuric acid electrolyte; 80° C.

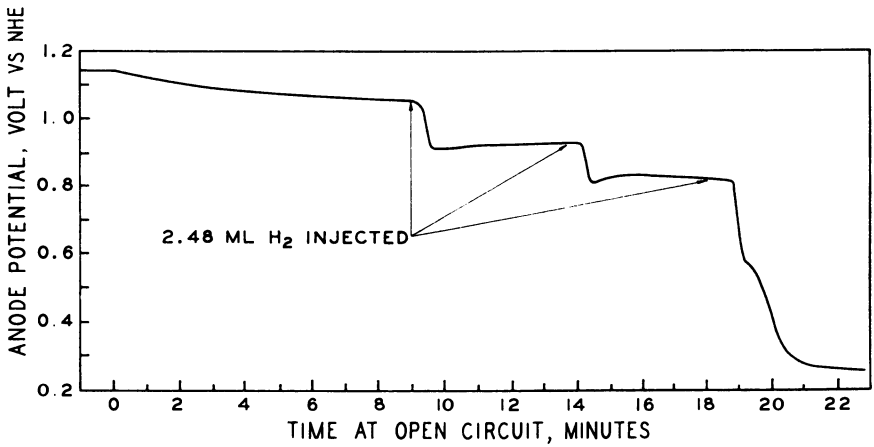

Figure 12. Effect of injected hydrogen on recovery of a propane-depolarized anode at open-circuit

Platinized porous carbon anode (Table I, electrode F); 1N sulfuric acid; 80° C.

jecting small amounts of more reactive fuels into the propane stream. Reactivation of electrode F (Table I), which had been polarized under

Publication Date: January 1, 1969 | doi: 10.1021/ba-1965-0047.ch022

load, is shown in Figure 12. Here hydrogen was used as the reactive fuel.

The experiments described in the following section were carried out to obtain more information about the characteristics and the nature of the air and oxygen inhibition. In this series some factors were maintained constant. The same seasoned electrode (electrode D, Table I) was used in all experiments. The air or oxygen volume injected into the hydrocarbon feed stream was 2.48 ml. in each case. The electrolyte was nominally 5*N* sulfuric acid. It was changed at intervals, but some variation in concentration occurred because of evaporation of water by the gases passing through the anode compartment.

Some variables studied are temperature (40 to 80° C.), hydrocarbon fuel (propane, propylene), and hydrocarbon flow rate (5 to 15 ml./min.).

Publication Date: January 1, 1969 | doi: 10.1021/ba-1965-0047.ch022

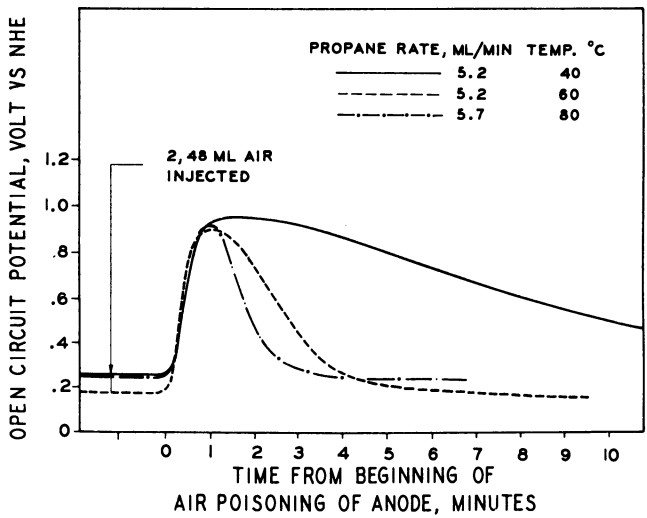

Figure 13. Effect of temperature on air inhibition of a propane depolarized anode

Platinized porous carbon electrode (Table I, electrode D); 5N sulfuric acid electrolyte

Temperature Effects

The effect of temperature on the inhibition of propane-depolarized anodes was studied by repeated injections of air into the propane feed stream at 40° C., 60° C., and 80° C. at flow rates of 5, 10, and 15 ml./min. Single representative curves are shown in Figure 13. These data show that the rate of inhibition is so rapid that any effects of temperature are masked by other factors which control the shape of the ascending inhibition part of the anode potential curve. The slightly slower increase of the 40° C. curve suggests that inhibition may be more rapid at higher

In Fuel Cell Systems; Young, G., el al.;
Advances in Chemistry; American Chemical Society: Washington, DC, 1969.

temperatures, but this observed difference is within the limits of experimental error. The inhibition peak potentials are close to the same value in these series. The height and shape of the peaks do differ, however, with different electrodes and with changing activity of the same electrode.

After the initial break, the anode potential recovers logarithmically with half recovery at 8.0, 1.72, and 0.82 minutes at 40° C., 60° C., and 80° C., respectively.

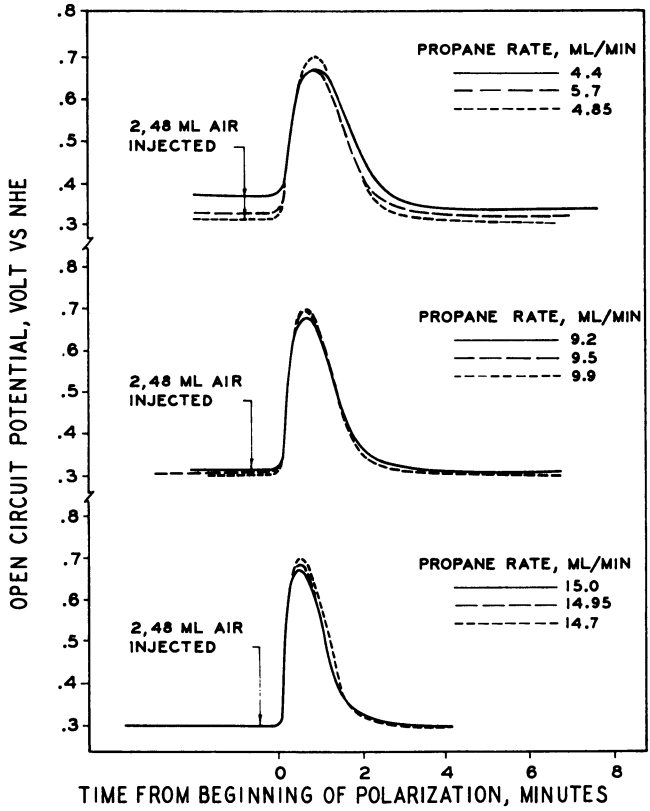

Figure 14. Effect of propane feed rate on air inhibition of a fuel cell anode

Plantinized porous carbon electrode (Table I, electrode D); 5N sulfuric acid electrolyte 80° C.

Hydrocarbon Flow Rate through Anode. The effects of hydrocarbon flow rate through the anode on the inhibition and recovery of propane anode potential were investigated at 40° C., 60° C., and 80° C. The data for the series at 80° C. are typical and are shown in Figure 14. Figure 15 gives corresponding curves for propylene. Oxygen gave higher peaks but otherwise similar behavior.

Publication Date: January 1, 1969 | doi: 10.1021/ba-1965-0047.ch022

One effect of the threefold increase in hydrocarbon flow rates in these experiments is to increase rate of inhibition of the electrode. The time from the beginning to maximum inhibition is very little more than the time required to sweep the air or oxygen into the electrode. The

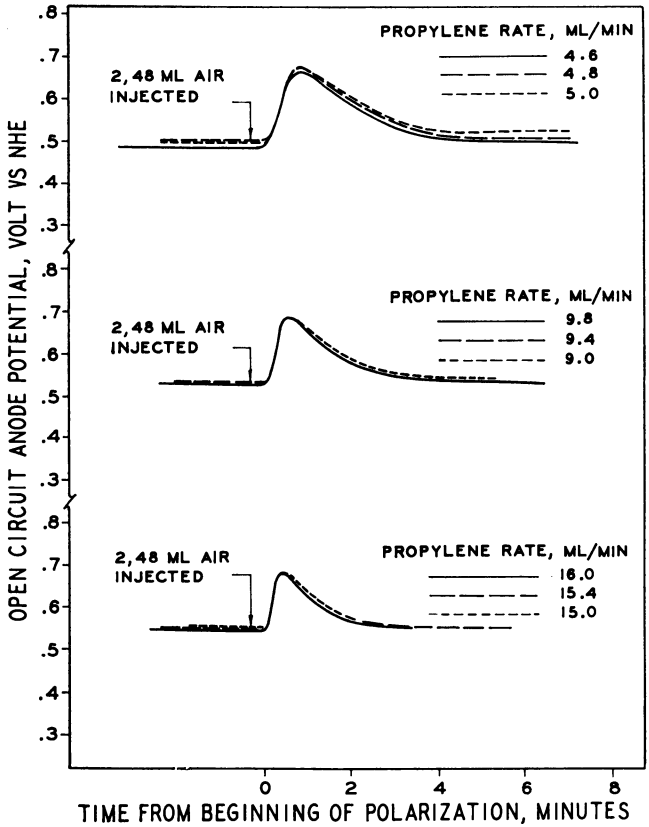

Figure 15. Effect of propylene feed rate on air inhibition of a fuel cell anode

Platinized porous carbon electrode (Table I, electrode D); 5N sulfuric acid electrolyte; 80° C.

amount of inhibition in a given series was not affected by flow rate to any great extent. This is shown by the relatively constant height of the peaks in the anode potential curves. The greatest variations occurred in the experiments at the lowest flow rates. These were the first experiments in each series, and they were often carried out before the propane open-circuit potential had stabilized. The variations of this potential are seen at the extreme left on the curves. The recovery times, as well as the rates of the initial inhibition of the anode, are decreased by increasing the rate of hydrocarbon flow through the anode. Data illustrating this are

Publication Date: January 1, 1969 | doi: 10.1021/ba-1965-0047.ch022

plotted in Figure 16. These data were taken from curves such as those shown in Figures 14 to 15. A decrease in recovery time with increase in hydrocarbon rate is common to all of the experiments. The effect is less with propane than with propylene. Decreasing the temperature of a propane-depolarized anode from 80° to 60° C. slowed the recovery time after air poisoning. However, the two curves showing the recovery time as a function of propane flow rates through the electrode are parallel and show a comparatively small effect. Recovery times after poisoning with oxygen are much more dependent on the propane flow rate. This is most pronounced as the rate is increased from 5 to 10 ml./min.

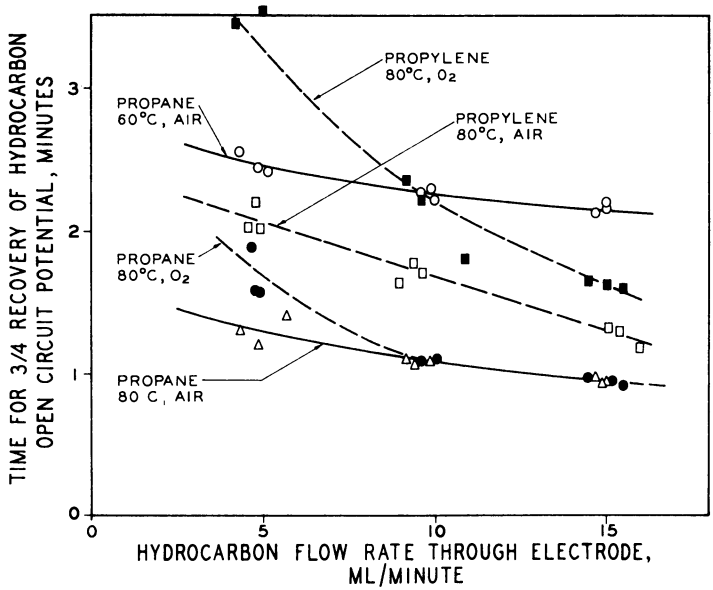

Figure 16. Effect of hydrocarbon flow rate on recovery times for a fuel cell anode after inhibition with air or oxygen
Platinized porous carbon electrode (Table I, electrode D); 5N sulfuric acid electrolyte; 80° C.

Oxygen Compared With Air and Amount of Oxygen in Anode Poisoning. Data showing the effects of amount of oxygen and air injected on the height of the inhibition peaks are plotted in Figure 20. The effect on the shape of the curves is seen in Figure 10. With this electrode, when the inhibition peak potentials get above 0.54 volt, there is a residual effect from one oxygen injection on the next. In a series of four injections of 4 ml. of oxygen at 20-minute intervals, the peak potentials increased successively from 0.54 to 0.60 volt, even though the electrode potential returned to the same value between injections. The scatter of points in Figure 17 is due largely to such residual effects as the points were ob-

Publication Date: January 1, 1969 | doi: 10.1021/ba-1965-0047.ch022

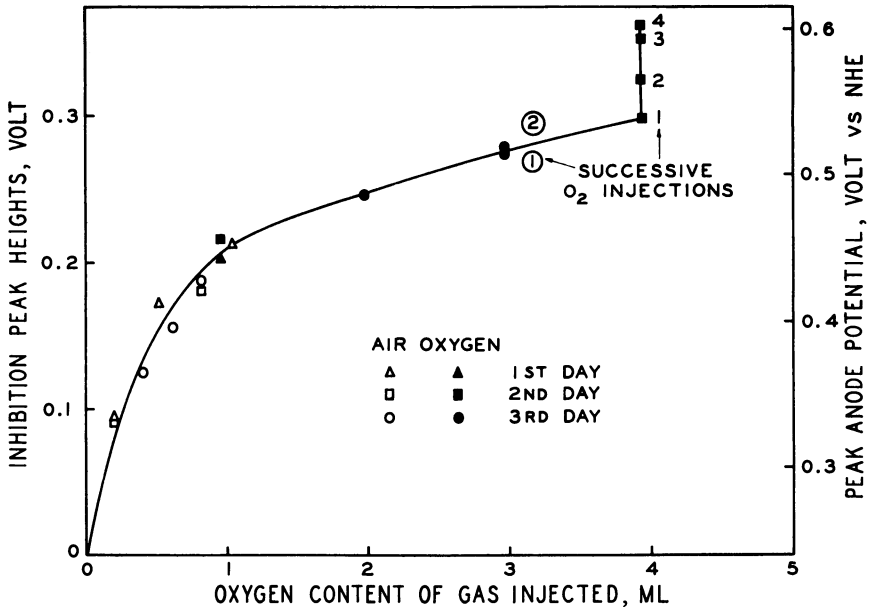

Figure 17. Effect of amount of air or oxygen injected on inhibition of a propane-depolarized fuel cell anode

Platinized porous carbon electrode (Table I, electrode F); 1N sulfuric acid electrolyte; 80° C.; propane rate, 10 ml./minute

tained at different times and in different sequence over a period of three days.

Discussion

Products from Hydrocarbon Oxidation. The new product work reported here confirms our earlier conclusion that propane can be completely oxidized in a fuel cell at 80° C. The *n*-butane data suggest, however, that hydrocarbon oxidation need not be complete and that higher molecular weight hydrocarbons may have a greater tendency to give isolatable intermediates. We have also observed odors tentatively identified as acetic acid and acetaldehyde from some ethylene "fuel cell" oxidations at potentials approximating those of the oxygen electrode. Such odors have also been reported by Young and Rozelle (*8*).

Small amounts of side products would not be detectable by our analytical method, but we have ample electrochemical evidence for pre-electrochemical reactions at open circuit with saturated hydrocarbons. We also see effects of a buildup of some inhibitors on our electrodes after prolonged experiments with various hydrocarbons. These can often be largely removed by drawing hot distilled water through the electrode, cleaning the cell, and using fresh electrolyte.

Publication Date: January 1, 1969 | doi: 10.1021/ba-1965-0047.ch022

It is apparent that more product work should be done, especially at constant anode potentials and with some higher hydrocarbons. There appears to be a good chance of isolating intermediates which may provide clues to the hydrocarbon oxidation reaction mechanisms.

Oxygen Electrode Potentials. Although we are concerned here mainly with the hydrocarbon fuel cell anode, oxygen and oxide films play an important part in inhibition behavior and in affecting hydrocarbon electrode performance at high polarizations.

The over-all oxygen half-cell reaction in acid is:

$$O_2 + 4H^+ + 4e \rightarrow 2H_2O; E^\circ = 1.229 \text{ volt.}$$

The equilibrium potential for this reaction can only be established on platinum when extreme care is used in preparing the electrode surface and in eliminating impurities from the test cell (*1, 6*). Usually, mixed potentials are obtained which give open-circuit voltages of the order 1.06 to 1.09 volts versus NHE. In our equipment we have observed open-circuit potentials of 1.058 to 1.081 volts at 80° C. in 5*N* sulfuric acid. At the present state of development of the oxygen electrode in acid, therefore, there is an inherent loss of at least 0.18 volt before any current is drawn.

By present standards an oxygen electrode that will operate at 0.85 volt at 100 ma./sq. cm. would be considered quite good. This corresponds to a 35% loss in efficiency attributable to the oxygen electrode alone in a hydrocarbon-oxygen fuel cell.

Hydrocarbon Electrode Potentials. Reaction potentials calculated from free energy changes for the complete oxidation of some hydrocarbons with oxygen are shown in the following table. Theoretical reversible half-cell potentials were calculated from thermodynamic data.

	Theoretical Reversible Potential for Complete Oxidation, Volts	*Hydrocarbon Half-Cell Potential,[1] Volt Versus NHE*
Ethane	1.079	0.150
Ethylene	1.136	0.093
Propane	1.091	0.138
Propylene	1.127	0.102

[1] Calculated O_2 half-cell potential in acid, 1.229 volts *vs.* NHE.

With ethane and propane the actual half-cell potential may go as low as or even lower than the calculated values. The actual processes occurring at the anode, however, are different from those represented by the theoretical reversible hydrocarbon half cells. Thus, the saturated hydrocarbon potentials are probably determined largely by the concentration of hydrogen atoms resulting from dissociative adsorption of the hydrocarbons on the electrocatalyst. The open-circuit potentials ob-

Publication Date: January 1, 1969 | doi: 10.1021/ba-1965-0047.ch022

served with the olefins are always more positive than those from the paraffins. It may be that with olefins the adsorbed hydrogen atoms react to hydrogenate unsaturated species, giving paraffins which are then displaced by the more strongly adsorbed olefins (4). During our air and oxygen inhibition experiments, when the feed to the electrode was changed from propane to propylene, the open-circuit potential gradually changed from about 0.29 volt to 0.50 to 0.55 volt. The reverse change occurred when propane was applied to the electrode again.

Under load the polarization behavior of olefins and paraffins is very different. Even structures as closely related as ethane and propane can show large differences. This is revealed clearly by comparison of plots of pseudo steady-state current densities at constant potential (Figure 6). At low potentials the paraffins will often support higher currents than the olefins. With the paraffins, "steady-state" currents increase to maxima between 0.6 and 0.7 volt. This is well below the potential of an oxygen fuel cell cathode. With olefins, the current rises rapidly with potential beyond the fuel cell range. These differences are probably due to differences in the relative rates of reactions of paraffins and olefins at or with the oxygen film on platinum. All electrodes are not alike in their detailed behavior, and we believe that pseudo steady-state current-potential curves should be valuable in more searching evaluations of electrodes, in studying the behavior of different fuels, and in determining the effects of operating variables.

The importance of oxygen and oxide films in determining the behavior of platinized porous carbon electrodes is also seen when inhibition behavior is considered.

Air and Oxygen Inhibition of Hydrocarbon Depolarized Electrodes. Three general types of inhibition of hydrocarbon depolarized porous carbon electrodes have been described here. These are (1) inhibition of hydrocarbon oxidation at an oxygen or air saturated electrode; (2) inhibition of a hydrocarbon saturated electrode by injected oxygen or air; and (3) inhibition of a hydrocarbon depolarized electrode by extreme inhibition of a hydrocarbon saturated electrode by injected oxygen or catalytically inactive oxide films, yet they differ in detail. Recovery of electrode activity depends on the removal of the inhibitor. The rate at which this occurs will depend on the nature of the inhibitor but also on the fuel and operating conditions.

It appears likely that, initially, when two electrochemically active species contact different sites on the surface of an electrode, potentials characteristic of the processes involved tend to develop at these two points. This would cause electrons to move in the conducting electrode in order to equalize the potential of the electrode surface. If a net transfer of electrons from one species to the other can occur, reactions will proceed

Publication Date: January 1, 1969 | doi: 10.1021/ba-1965-0047.ch022

and are accelerated as local polarization to more favorable potentials for the reactions occurs.

The net anode potential observed will be intermediate between the open-circuit potentials that would be observed for the two reactants separately. Its magnitude will depend on the polarization of the two processes which, in turn, will be determined by the polarizability and effective "current density" as determined by relative surface coverage for each reactant. To a lesser extent, it will depend on the geometry of the electrode, on the way in which the two species are distributed on the surface, and on the location of the connections of the potential-measuring device to the electrode.

If this picture is correct, it follows that the coupled oxidation-reduction of a hydrocarbon and oxygen at a platinized electrode in contact with electrolyte can be purely "electrochemical." There need be no direct contact of the reacting species. In this sense this oxidation-reduction differs from direct chemical reaction. It differs also from heterogeneous catalytic oxidation-reduction processes where an electrolyte is not present. These, in general, are believed to require that the reactants contact or at least be adsorbed close to one another. Direct chemical reaction can, of course, also be involved in the electrode recovery process.

Publication Date: January 1, 1969 | doi: 10.1021/ba-1965-0047.ch022

Oxygen is known to adsorb rapidly and completely to give a 1:1 ratio of oxygen atoms to surface platinum atoms (2). On the other hand, coulometric methods show that only about 10% of the surface platinum atoms which will adsorb oxygen are covered with propane at 1 atm. pressure in the presence of dilute sulfuric acid electrolytes. Similar coverages are obtained with ethane. Only slightly higher coverages were obtained with ethylene and probably with propylene (3). Thus, when an electrode is exposed to air or oxygen before contacting with hydrocarbon, the catalyst sites which can catalyze the electrochemical oxidation of propane or propylene are probably covered. When placed in an electrolyte, this electrode develops the oxygen potential. When propane or propylene is passed through this electrode, the potential is not affected to any extent at first. Gradually, a few molecules of oxygen may leave the electrode surface and are removed by the hydrocarbon stream; or they are removed by a catalyzed chemical reduction. This allows the hydrocarbon access to the catalyst sites. The amount of hydrocarbon reacting increases as oxygen is removed; and then suddenly, as the amount of oxygen is reduced to a low level, the hydrocarbon potential resulting from chemisorption becomes dominant; and there is a sudden decrease in net anode potential. After the oxygen layer has been removed (approximately 0.55 volt), the potential approaches the open-circuit potential logarithmically with time. The rate is determined by the rate of oxidation of the hydrocarbon and by the capacitance of the ionic double layer.

Following inhibition of this kind (Figure 9), the potential drops

below the open-circuit hydrocarbon potential and then gradually rises to the open-circuit potential. This may be due to formation of a particularly active catalyst surface as the oxygen film is reduced. This may survive long enough to dissociate more propane than the usual catalyst, giving a higher hydrogen atom concentration than is normal for the electrode surface.

Behavior after polarization under load to the oxygen potential is very similar to that from oxygen inhibition after standing for several hours in the presence of air and absence of propane (Figure 11). Recovery after polarization and presumably after the other similar inhibition processes can be assisted by injecting hydrogen into the hydrocarbon feed (Figure 12).

Inhibition to the oxygen potential by oxygen injection into a propane stream passing through the electrode does have some different characteristics (Figure 10). This type of inhibition requires a comparatively large amount of oxygen. The propane adsorbed on this electrode must be displaced by oxygen, and this may be a comparatively slow process. More than a monolayer of oxygen may also be retained on the platinum or loosely adsorbed on the graphite. This may result in the more gradual transition to the open-circuit propane potential observed with this system.

If inhibition results from injection of a small amount of air or oxygen which is added to a stream of hydrocarbon passing through an electrode, the effect is immediate because open sites on the catalyst surface are available. If the amount of air or oxygen is not enough to displace all of the hydrocarbon, electrochemical reduction and elimination of the added oxygen begins immediately and hydrocarbon potential is soon established again.

A detailed understanding of the factors which determine the shape, height, and inhibition peak potentials might lead to useful methods for evaluating and studying the behavior of porous electrodes. However, the situation is complex; and more study will be required before complete understanding or useful application of inhibition techniques can be expected.

Publication Date: January 1, 1969 | doi: 10.1021/ba-1965-0047.ch022

Acknowledgment

The author gratefully acknowledges the support of the Army Materiel Command, Harry Diamond Laboratories, and the Advanced Research Projects Agency, Washington, D. C., and wishes to thank Drs. G. H. Denison, D. R. Rhodes, L. R. Griffith, and R. T. Macdonald for helpful discussions of this work.

Literature Cited

(1) Bockris, J. O'M., and Huq, A. K. M. S., *Proc. Roy. Soc. London* **237A**, 277 (1956).
(2) Breiter, M., Knorr, C. A., and Völkl, W., *Z. Elektrochemie* **59**, 681 (1955).

(3) Griffith, L. R., and Rhodes, D. R., "Fuel Cells," CEP Technical Manual, American Institute of Chemical Engineers, 345 East 47 St., New York 17, N. Y., 1963, pp. 32–39.
(4) Grubb, W. T., "Low Temperature Hydrocarbon Cells," 17th Annual Power Sources Conference, Atlantic City, N. J., May 21–23, 1963.
(5) Heath, C. E., and Worsham, C. H., in "Fuel Cells," Vol. II, G. J. Young, ed., Reinhold Publishing Corp., New York, 1963, Chapter 14.
(6) Hoare, J. P., Extended Abstracts of the Theoretical Division, Electrochemical Society, April 15–18, 1963, Abstract No. 165.
(7) Schlatter, M. J., "Fuel Cells"; Vol. II, G. J. Young, ed., Reinhold Publishing Corp., New York, 1963, Chapter 15.
(8) Young, G. J., and Rozelle, R. B., in "Fuel Cells," G. J. Young, ed., Reinhold Publishing Corp., New York, 1960, Chapter 3.

RECEIVED February 17, 1964.

Publication Date: January 1, 1969 | doi: 10.1021/ba-1965-0047.ch022

23

Hydrogen-Generating Plant Based on Methanol Decomposition

Design for Submarine Fuel-Cell Use

W. H. HEFFNER, A. C. VEVERKA, and G. T. SKAPERDAS

The M. W. Kellogg Co., New York, N. Y.

Publication Date: January 1, 1969 | doi: 10.1021/ba-1965-0047.ch023

A design study of a hydrogen-generating plant based on the decomposition of methanol and intended as a source of hydrogen for fuel cells to be used in submarine propulsion is reported. The plant is designed to supply 20 pounds per hour of hydrogen normally (70 pounds per hour maximum) and is optimized on the basis of minimum volume, weight, oxygen consumption, hazard, maintenance, and cost, and maximum efficiency, simplicity and reliability. Total impurities in the hydrogen product are guaranteed to be less than one part per million. For 10 days of continuous operation at normal capacity, the hydrogen-generating equipment and fuels (methanol and oxygen for combustion) represent a combined specific weight of about 1.0 lb./kw.-hr. and a specific volume of 0.018 cu. ft./kw.-hr.

A design study has been made of a compact, mobile plant for generating hydrogen from methanol. The plant is intended as a source of fuel for a hydrogen-oxygen fuel cell battery to be used for submarine propulsion. For this application, criteria of satisfactory design and performance differ from those usually encountered in an industrial context, or at least they receive different emphasis. In this study the hydrogen-generating system is optimized on the basis of the following factors, in approximately the order listed: minimum weight and volume; minimum oxygen consumption; maximum over-all efficiency; maximum simplicity and reliability; minimum noise; minimum hazard; minimum maintenance; and minimum cost.

In Fuel Cell Systems; Young, G., el al.;
Advances in Chemistry; American Chemical Society: Washington, DC, 1969.

The hydrogen-generating system is designed to produce 5 to 70 pounds per hour of pure hydrogen, the normal rate being 20 pounds per hour (which is enough to supply a 200-kilowatt fuel cell installation). The system shall operate continuously for a period of 10 days, and maximum hydrogen production will be required for a total of 10 hours during the 10-day span. Temperature and pressure of the pure hydrogen to be delivered are set by the requirements of the fuel cell at 140° F. (maximum) and 6 p.s.i.g., respectively. The purity of the hydrogen is also determined by fuel-cell performance. Carbon monoxide, sulfur, and ammonia are poisons to the cell membrane, while methane and carbon dioxide are inerts. Water is beneficial to the operation of the cell, so the gas may be saturated at the delivery conditions.

Publication Date: January 1, 1969 | doi: 10.1021/ba-1965-0047.ch023

Description of Process

Methanol and steam react catalytically at about 500° F. to produce hydrogen and carbon dioxide. The reaction is believed to take place in two steps: the decomposition of methanol to hydrogen and carbon monoxide, follwed by the reaction of carbon monoxide with steam to produce carbon dioxide and more hydrogen.

$$CH_3OH \rightarrow CO + 2H_2 \quad (1)$$

$$CO + H_2O \rightarrow CO_2 + H_2 \quad (2)$$

A side reaction produces some methane, which will be present in small amounts in a product that is a mixture of hydrogen, carbon dioxide, carbon monoxide, and steam.

A process flow sheet (Figure 1) shows the hydrogen-generating system and flow rates and duties for the normal rate of hydrogen production. Methanol, which is stored in tanks outside the pressure hull of the submarine, and water, which is a product of the fuel cell reaction, are pumped to approximately 300 p.s.i.a., mixed in a mole ratio of 1/1, and heated to 278° F. in exchanger *C*-1 against the product hydrogen stream. After being heated to its boiling point, 352° F., by the system purge gas in exchanger *C*-2, the liquid feed flows to the reactor, *D*-1 (Figure 2). The methanol-water mixture is vaporized and superheated as it flows upward in the jacket surrounding the reactor shell. At the top of the jacket, it enters the chamber above the catalyst tubes by means of openings in the shell wall. The gases are then heated to the reaction temperature as they flow downward through the catalyst tubes and react at about 525° F. to produce the required amount of hydrogen. Heat for the endothermic reaction is supplied by hot flue gas which flows through the baffled shell of the reactor. From the reactor the crude product gas is sent to the purification unit, *L*-1.

The purification unit contains 96 diffusion cells or chambers, each

Publication Date: January 1, 1969 | doi: 10.1021/ba-1965-0047.ch023

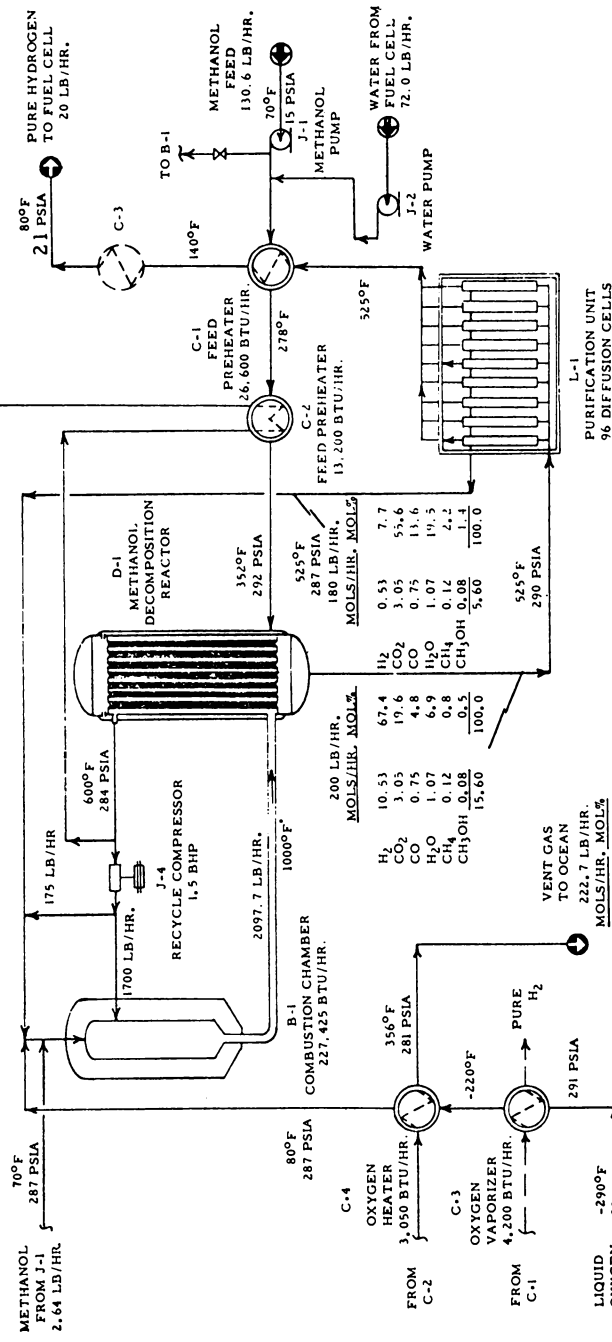

Figure 1. Process flowsheet for hydrogen from methanol

of which contains a number of palladium-silver alloy coils. This alloy has the property of allowing only hydrogen to diffuse through it and hence can be used to produce ultrapure hydrogen from impure hydrogen sources. The product gas from the reactor, containing about 67.5 mole % hydrogen, is fed into the palladium-silver coils at about 290 p.s.i.a. The hydrogen diffuses through the coils into the outer chambers and is manifolded into a single line which carries it to the fuel cell. Using this method of purification, hydrogen recovery is about 95%. Before going to the fuel cell, the pure hydrogen is used to heat the methanol-water feed mixture in exchanger *C*-1, as described previously, and then is further cooled in exchanger *C*-3 against the vaporizing liquid oxygen used for combustion. The dry ultrapure hydrogen, at about 25 p.s.i.a. and 80° F., is now ready for delivery to the fuel cell. The undiffused gas, or bleed gas, from the diffusion unit contains appreciable amounts of carbon monoxide and hydrogen as well as some methane and unreacted methanol and so is suitable for use as fuel in the combustion system. This gas is therefore sent from the purification unit to the combustion chamber, *B*-1.

Liquid oxygen is pumped to about 300 p.s.i.a., vaporized in exchanger *C*-3 as mentioned before, heated to about 80° F. in exchanger *C*-4 by means of the system purge gas, and finally sent to the combustion chamber, *B*-1. Before entering the combustion chamber, however, the oxygen is mixed with recycled flue gas to form a "synthetic air," recycle gas replacing the nitrogen found in air. Bleed gas from the diffusion unit is then burned under pressure with the synthetic air, cooled by dilution with more recycle gas, and sent into the reactor as the heating medium. These hot flue gases enter the baffled reactor shell at 1000° F. and exit at 600° F. Upon leaving the reactor, the flue gas is split into two streams—the system purge gas and the recycle gas used in combustion. The recycle gas is compressed by *J*-4 to make up for pressure drop through the combustion system. During periods of normal operation the bleed gas from the purification unit does not have a high enough heating value to supply the heat required, and an auxiliary fuel is supplied. This auxiliary fuel is methanol, which is split from the feed stream pumped by *J*-1 and is burned in the combustion chamber along with the primary fuel. In periods of maximum operation, however, the heating value of the primary fuel, because of poorer hydrogen recovery, is high enough to supply the necessary heat, and no auxiliary fuel is required.

Before being purged to the ocean, the reactor flue gas is utilized as a heating medium. The gas at 600° F. flows first to exchanger *C*-2, where it is used to heat the incoming methanol-water feed mixture to its boiling point, and then to exchanger *C*-4, where it heats the vaporized oxygen to about 80° F. At purging, the gas is at 281 p.s.i.a., which corresponds to a depth of about 600 feet of sea water.

Publication Date: January 1, 1969 | doi: 10.1021/ba-1965-0047.ch023

To produce hydrogen at the maximum rate, 70 pounds per hour, the following major changes in process conditions are made:

1. Reaction temperature is raised to 575° F. to increase the rate of reaction. According to data presented by Christiansen and Huffman (*1*), this 50° F. rise in reaction temperature should be sufficient to increase the rate of reaction by a factor of 3.5. Permissible space velocity as a function of temperature must be determined experimentally to verify this design.
2. Flue gas temperature is raised to 1500° F. at the reactor inlet and 700° F. at the outlet to increase the rate of heat transfer.
3. Hydrogen recovery in the diffusion unit is reduced to 83% to create a greater driving force for diffusion.
4. All flow rates are increased accordingly.

The system as described is designed for operation with pure oxygen, but it could, with minor changes, be operated on the ocean surface using air instead.

The suggested arrangement of equipment in the submarine is shown in Figure 3.

Hydrogen Purification

In choosing a purification system, prime consideration was given to space requirements and ease of operation. Carbon monoxide poisons the fuel cell membranes; therefore, the first problem was to find a system that would effectively remove carbon monoxide from the product gas. Gross reduction could be accomplished in the reactor by increasing the steam-methanol ratio to shift carbon monoxide to carbon dioxide, but further reduction would be difficult. One possibility was absorption in a regenerable solvent, such as an aqueous solution of copper-ammonium salts. This system would be bulky, however, requiring two towers plus a number of heat exchangers, and its operation would be affected by the roll and pitch of the submarine.

Although the removal of carbon dioxide was not as important, since it is inert to the membranes of the fuel cell, a system for gross reduction still had to be provided. Several systems were available, including absorption in water, ethanolamines, and aqueous potassium carbonate. Adsorption on solids such as silica gel and alumina was also possible. A previous study (*3*) had shown that the towers required for the absorption processes would not be easily adaptable to the space available on the submarine and would be affected by the roll and pitch of the ship. The adsorption systems, while not affected by the motion of the ship, would require time-cycling and, in order to keep the time cycle reasonable, would of necessity be bulky.

Owing to the size and relative unsuitability of the preceding systems for submarine use, it was decided to consider purification of the hydrogen by diffusion through palladium-silver alloy, even though the extremely

Publication Date: January 1, 1969 | doi: 10.1021/ba-1965-0047.ch023

high purity obtained was not required. After study and consultation with the manufacturers of such units, it was concluded that purification of

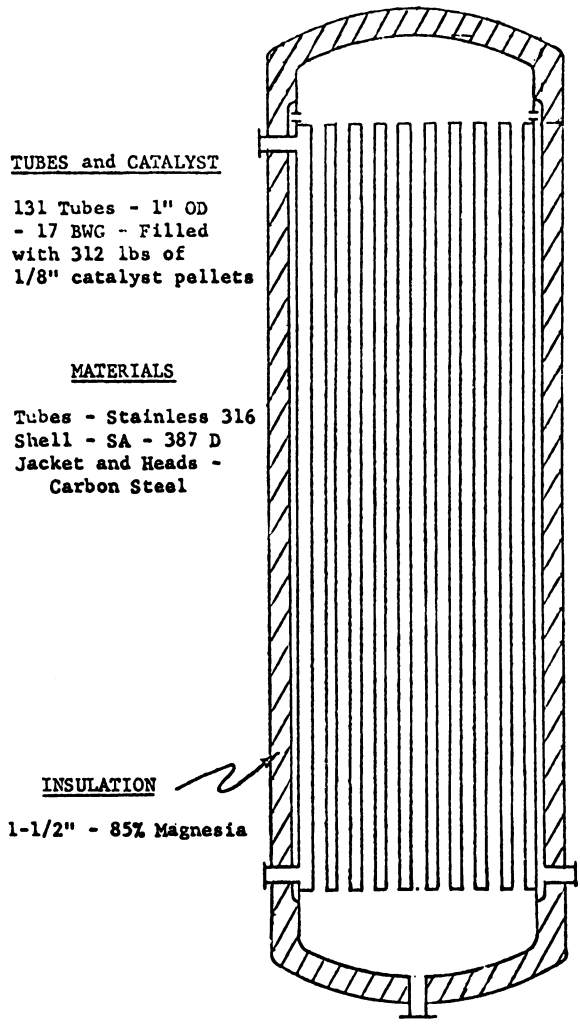

Figure 2. Methanol Decomposition Reactor

hydrogen by palladium-silver diffusion is ideally suited to this particular application. The primary reasons for this choice are:

1. The system requires less space than the others.
2. Carbon monoxide is completely removed, even without gross reduction first.
3. The system is completely unaffected by any motion of the submarine.

Publication Date: January 1, 1969 | doi: 10.1021/ba-1965-0047.ch023

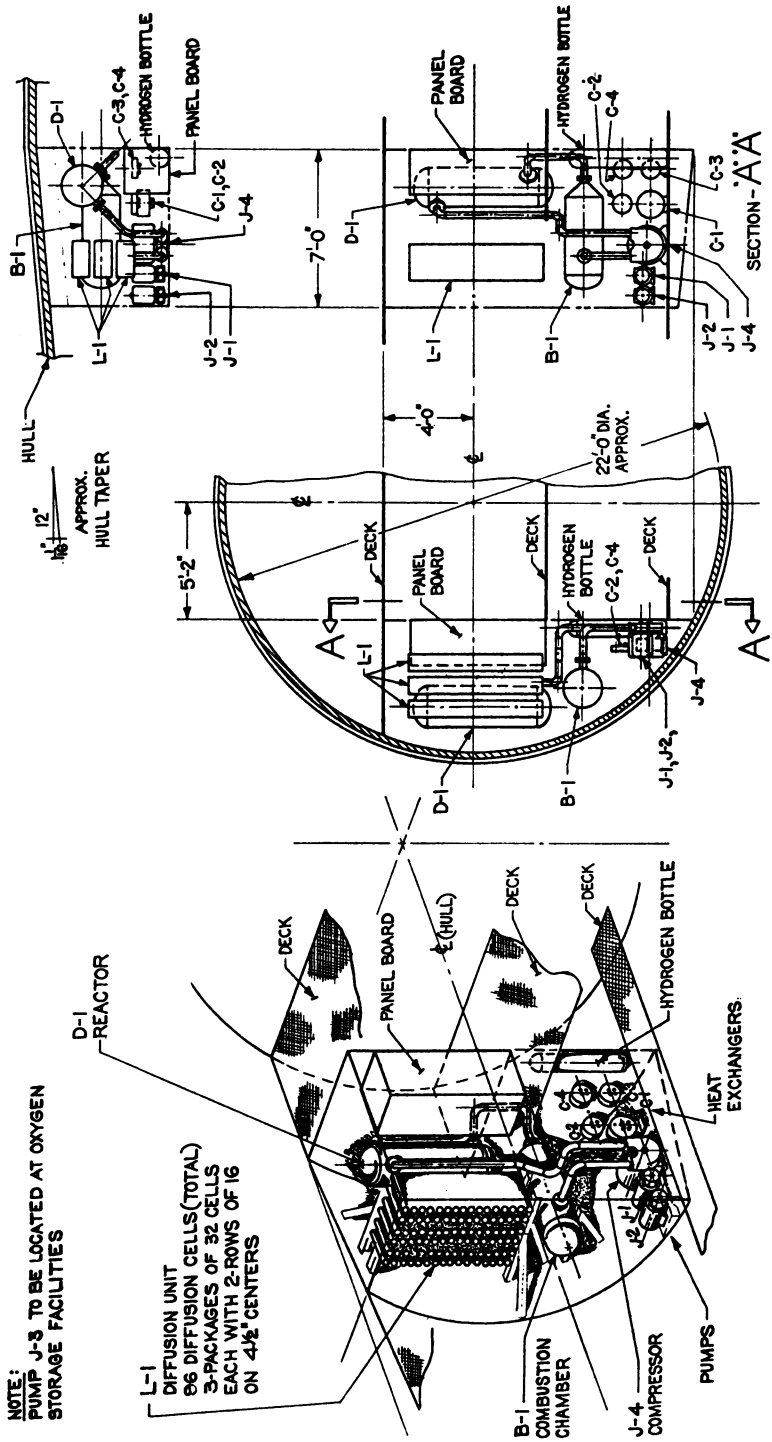

Figure 3. Proposed arrangement for hydrogen generating plant

Publication Date: January 1, 1969 | doi: 10.1021/ba-1965-0047.ch023

Publication Date: January 1, 1969 | doi: 10.1021/ba-1965-0047.ch023

Steam-Methanol Ratio vs. *Oxygen Consumption*

A thorough search of the literature revealed that a steam-methanol ratio of 3/1, or higher, was used in previous installations for producing hydrogen via the decomposition of methanol. A ratio of only 1/1 is required by stoichiometry, hence a large quantity of heat would have to be supplied to vaporize the excess water in addition to that required for vaporizing the stoichiometric amounts of water and methanol. If the excess water was present merely to ensure the maximum conversion of carbon monoxide to carbon dioxide, then a lower ratio should be considered. On the other hand, the excess steam may have been used for reasons of operability—to prevent carbon deposition, for example.

Recent improvements in catalysts used for steam reforming of hydrocarbons have permitted reductions in steam-carbon ratio to the region of 2/1. It seems reasonable that the decomposition of methanol, because it occurs at lower temperature and pressure, should be operable at even lower steam-carbon ratios. The disadvantages of a low steam-methanol ratio are that a substantial quantity of carbon monoxide is then present in the reactor effluent, and more methanol, compared to a high ratio case, is required to produce the same amount of hydrogen.

The hydrogen recovery system can handle either carbon monoxide or carbon dioxide, so the carbon monoxide present affords no real disadvantage. The second objection, the increase in methanol consumption, is more than offset by the decrease in oxygen used for combustion when less water must be vaporized. Oxygen consumption was one of the foremost considerations in this study; hence it was decided to use a 1/1 steam-methanol ratio. Operability under these conditions will have to be verified experimentally.

Effect of Hydrogen Recovery on Reactor, Purification Unit, and Oxygen Volumes

In designing the purification unit, the normal recovery of hydrogen (95%) in periods of maximum production could be achieved only by making the unit three and a half times larger than normal. It was felt that, because maximum production is maintained for such a small part of the operating time, the purification unit would be unnecessarily large. By decreasing the percentage recovery of hydrogen, the diffusion rate could be increased by the greater driving force and hence the size of the purification unit decreased, but this would require greater hydrogen production in the reactor and thus more oxygen would be consumed.

To determine the optimum point, the volumes of the reactor, purification unit, and oxygen needed during overload operation were calculated for various percentages of hydrogen recovery. The increase in volume over that needed for normal operation is shown as a function of hydrogen

recovery in Figure 4. The optimum recovery of hydrogen at maximum production appears to be about 83%, and the purification unit must be three times the size required for normal operation.

Fuel vs. *Oxygen Consumption*

The over-all reaction between steam and methanol is endothermic, and heat must be supplied to the reactor. In evaluating various fuels for this application, the criterion used was minimum oxygen consumption.

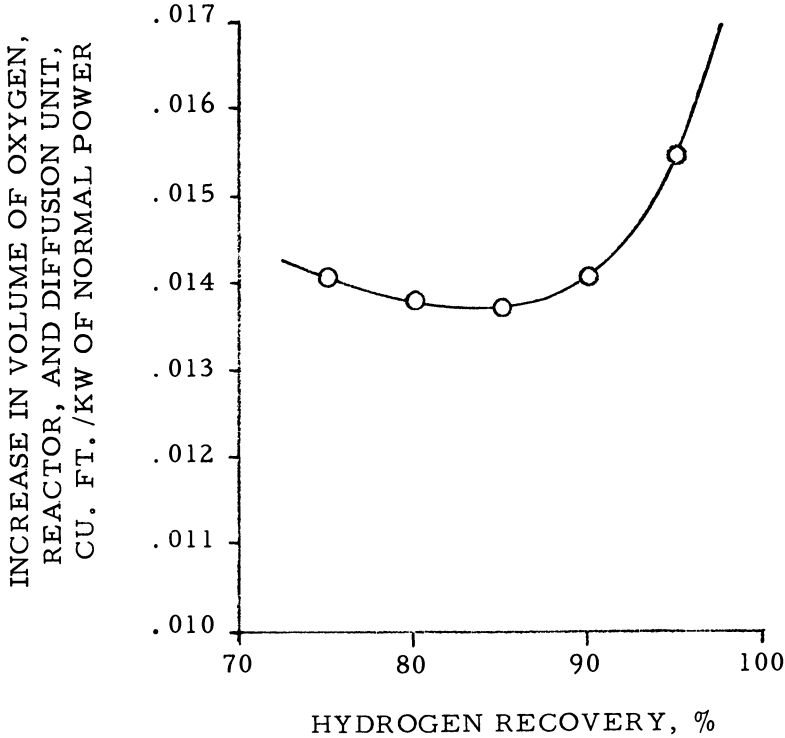

Figure 4. Increase in system volume required to meet overload conditions as a function of hydrogen recovery

Three fuels were evaluated—fuel oil, methanol, and the bleed gas from the diffusion cells. The latter is attractive because it does not need to be stored but has the disadvantage of requiring an auxiliary fuel during normal operation, as well as for start-up. It does, however, require less oxygen per B.t.u. released than the other fuels, and it was therefore chosen as the primary fuel for the design study. Methanol was selected as the auxiliary fuel, using less oxygen than fuel oil and being already available on the submarine.

Publication Date: January 1, 1969 | doi: 10.1021/ba-1965-0047.ch023

Publication Date: January 1, 1969 | doi: 10.1021/ba-1965-0047.ch023

Estimated Weight and Volume

Estimated weight and volume of the equipment in the hydrogen-generating plant is presented in Table I. The weight of catalyst is included, based on data quoted by the Girdler Division of Chemetron Corp. for typical operation of mobile hydrogen producers made during World War II (5). The catalyst had a copper-manganese base and was manufactured in the form of $^1/_8$-inch pellets by Du Pont, as is described in the patent literature (4). The only information available on catalyst life indicates that it is in excess of 400 hours (5). Actual catalyst life under recommended operating conditions will have to be determined experimentally. It has been reported, however, that the presence of about 0.2 wt. % ethanol in the methanol feed materially shortens the life of the Du Pont catalyst. Use of specially refined methanol containing not more than 0.1 wt. % ethanol is recommended (2). Estimated volume occupied by the hydrogen-generating plant in the submarine is also presented in Table I.

Table I. Estimated Weight and Volume of Hydrogen-Generating Plant[1]

Equipment No.	*Description*	*Weight[2], Lb./Kw.*	*Volume[2], Cu. Ft./Kw.*
B-1	Combustion chamber	6.15	0.048
C-1	Primary feed heater	0.98	0.005
C-2	Secondary feed heater	0.46	0.001
C-3	LOX vaporizer	0.46	0.001
C-4	Oxygen heater	0.46	0.001
D-1	Reactor (incl. insulation)	5.75	0.071
J-1	Methanol feed pump	1.00	0.005
J-2	Water feed pump	1.00	0.005
J-3	LOX pump	2.00	0.080
J-4	Recycle gas circulator	0.75	0.016
L-1	Purification unit	8.25	0.172
	Catalyst in reactor	1.56	...
	Instrumentation (control panel)	9.00	0.120
	Piping, valves, fittings, etc.	4.00	...
	Totals	41.82	0.525

[1] Total volume of compartment containing hydrogen-generating plant (excluding J-3, which is with oxygen storage facilities) = 2.10 cu ft./kw.-hr.
[2] Calculated on the basis of normal hydrogen production rate. Divide by 3.5 to change basis to maximum hydrogen rate.

Table II is a summary of the specific weight and volume of methanol, oxygen, and hydrogen-generating equipment. The oxygen listed is only that required to supply the hydrogen-generating plant and does not include that consumed directly by the fuel cell. Water needed for the process is supplied by the fuel cell, so no storage facilities for water are provided.

Because of the possibility of an explosion if the hydrogen contained in the generating system were to leak out, an estimate was made of the volume of this contained hydrogen. To stay below the lower combustible

limit, the maximum allowable hydrogen concentration is about 3% by volume. A slow hydrogen leak could be dealt with by circulating the submarine atmosphere through a catalytic hydrogen burner. A catastrophic leak, however, could release as much as 150 standard cubic feet of hydrogen into the 400–cubic foot compartment. Emergency measures would be required in such an event, but these are beyond the scope of this study.

Table II. Summary of Specific Weight and Volume of Oxygen, Methanol, and Equipment for Hydrogen-Generating System

	Specific Weight, Lb./Kw.-Hr.	*Specific Volume, Cu. Ft./Kw.-Hr.*
Methanol (feed)[1]	0.64	0.0129
Methanol (fuel)[1]	0.01	0.0002
Oxygen[2]	0.20	0.0029
Hydrogen-generating equipment[3]	0.17	0.0022
Totals	1.02	0.0182

[1] Stored outside the pressure hull.
[2] Stored in oxygen storage facilities with oxygen for fuel cell.
[3] Depends on length of operation. This calculation was based on 10 days at normal fuel cell capacity (energy output = 48,000 kw.-hr.).

Some approximations have been made of the change in hydrogen-generating equipment volume with change in hydrogen capacity. If the normal capacity were raised from 20 pounds of hydrogen per hour to 100 pounds per hour, the volume of the equipment would increase by approximately a factor of three. Similarly, if the normal capacity were lowered to 10 pounds per hour, the volume would be approximately three fourths of the present volume.

Estimated Power Consumption

Estimated normal power consumption by the pumps and compressor of the hydrogen-generating system is 1.4 kw. or less than 1% of the power produced by the fuel cell.

Material and Energy Balances

Material and energy balances for the hydrogen-generating system are presented in Table III.

Time Required for Start-up, Shutdown, and Minimum-to-Maximum Operation

Based on the time necessary to heat the reactor and purification unit to operating temperature, it is estimated that approximately one-half hour will be required to put the hydrogen-generating unit on stream from a cold start. Start-up would be accomplished essentially as follows: Hot

Publication Date: January 1, 1969 | doi: 10.1021/ba-1965-0047.ch023

flue gas is produced in the combustion chamber from methanol, oxygen, and water and is circulated to both the reactor shell and the diffusion chambers. As these vessels approach operating temperature, water is fed to the reactor jacket and steam is generated. This steam is used to purge the diffusion chambers of air so that a reaction between hydrogen and oxygen does not occur at the palladium-silver alloy surface. When the purging is completed, the feed to the reactor is changed to the methanol-water mixture, and the unit is placed on automatic control.

Table III. Material and Energy Balances

Datum for energy balance: 60°F.

	Lb./Hr.	*B.t.u./Hr.*
Input		
Methanol		
Feed	128	1,255,000
Fuel	2.6	27,000
Water	72.0	6,000
Oxygen	40.1	−7,000
Totals	242.7	1,281,000
Output		
Hydrogen	20.0	1,223,000
Vent gas		
CO_2	179.2	12,000
H_2O	38.7	46,000
O_2	4.6	...
Ar	0.2	...
Totals	242.7	1,281,000

The start-up time given is valid only when the catalyst is in a reduced state. Catalyst reduction would require about 8 hours and would consume about 500 gallons of a 0.5 wt. % solution of methanol in water (2). Therefore it is recommended that the catalyst be charged to the reactor in a reduced state and that precautions be taken to keep the catalyst from oxidizing. Such a precaution is given in the following paragraph on plant shutdown.

It is estimated that shutdown of the unit could be accomplished in about three minutes, although hydrogen production can be stopped almost instantly. The additional few minutes is required to purge the reactor and blanket it with hydrogen from a compressed gas cylinder that is carried on board the submarine for this purpose. This prevents air from coming in contact with the catalyst and oxidizing it. If this procedure is followed, catalyst reduction is not needed during subsequent start-up.

The time required to go from minimum to maximum operation is approximately one and a half minutes, largely because the reactor must be heated to a higher temperature for maximum operation. If a shorter response time is desired, the reaction system could be redesigned so that the time to go from minimum to maximum operation would depend only on the response time of the instruments—that is, of the order of 20 seconds.

Publication Date: January 1, 1969 | doi: 10.1021/ba-1965-0047.ch023

However, there will be some penalty in the form of an increase in system weight and volume. The over-all hydrogen-generating system was initially optimized on the basis of weight and volume rather than response time. The change from minimum to normal hydrogen production could be accomplished in about 20 seconds.

Conclusions

A mobile hydrogen-generating plant based on methanol decomposition is feasible for submarine service. Because different criteria of design and performance are applied, process sequence and operating conditions differ from those which would be chosen for industrial use. All process heat must be provided by combustion supported by oxygen carried in liquid form on board the submarine, which means that such heating must be minimized and conducted as efficiently as possible. For this reason a lower steam/methanol ratio is recommended than has been used industrially.

If carbon monoxide cannot be tolerated in the hydrogen product, the best method of purification is by diffusion through a palladium-silver alloy. Even if small quantities of carbon monoxide are permissible, the diffusion unit might still be chosen because it is simple to operate, is very compact, and is not affected by motion of the submarine. The sole disadvantage of the diffusion unit is its high cost.

A hydrogen-generating plant capable of producing from 5 to 70 pounds of pure hydrogen per hour (equivalent to 50 to 700 kw. of electricity from a hydrogen-oxygen fuel cell) would weigh about 8400 pounds and would occupy about 420 cubic feet in the submarine. For 10 days of continuous operation at 20 pounds of hydrogen per hour, specific weight and volume of methanol, oxygen, and equipment combined would be about 1.0 lb./kw.-hr. and 0.018 cu. ft./kw.-hr., respectively.

Rate of hydrogen production is controlled by varying the reaction temperature and the degree of hydrogen recovery in the diffusion unit, in addition to the usual control of flow rates. About 1.5 minutes will be required to increase hydrogen production from the minimum (5 lb./hr.) to the maximum (70 lb./hr.). Power equivalent to less than 1% of the hydrogen produced is consumed by the hydrogen-generating plant.

Experimental work is required to verify several assumptions made during the study:

1. That a catalyst can be developed which will produce 2000 standard cubic feet of hydrogen per hour per cubic foot of catalyst at 525° F. with a steam-methanol feed ratio of one mole per mole.
2. That the above catalyst will have a useful life of at least 240 hours.

Acknowledgment

The work reported here was conducted under contract with the

Publication Date: January 1, 1969 | doi: 10.1021/ba-1965-0047.ch023

Bureau of Ships, Department of the Navy, U. S. Department of Defense. Valuable assistance in the selection of palladium-silver diffusion as the optimum method of hydrogen purification was rendered by J. Bishop and Co., Englehard Industries, Inc., and The Milton Roy Co.

Literature Cited

(1) Christiansen, J. A., and Huffman, J. S., *Z. Physik. Chem.* **A 151,** 269-304 (1930).
(2) Christl, R. J., Memorandum Report **D-129-C,** Operating Manual, GRX unit, E. I. du Pont de Nemours and Co., Nov. 13, 1942.
(3) Kellogg Co., The M. W., Report No. **CE-59-193,** "Hydrogen-Oxygen Primary Battery for Submarine Application," April 30, 1959.
(4) Larson, A. T. (to E. I. du Pont de Nemours and Co., Inc., Wilmington, Del.) U. S. Patent 2,425,625 (Aug. 12, 1947).
(5) Weir, J., Girdler Division, Chemetron Corp., to Heffner, W. H., M. W. Kellogg Co., private communication, July 16, 1962.

RECEIVED April 22, 1964. Presented on the Symposium on Gas Generation, Division of Fuel Chemistry, 147th Meeting of the American Chemical Society, Philadelphia, Penn., April 6, 1964.

Publication Date: January 1, 1969 | doi: 10.1021/ba-1965-0047.ch023

24

Westinghouse Solid-Electrolyte Fuel Cell

D. H. ARCHER, J. J. ALLES, W. A. ENGLISH, L. ELIKAN, E. F. SVERDRUP, R. L. ZAHRADNIK

Westinghouse Electric Corp., Research & Development Center, Pittsburgh 35, Pa.

Publication Date: January 1, 1969 | doi: 10.1021/ba-1965-0047.ch024

Solid-electrolyte fuel batteries have been constructed. Cell dimensions have been selected to maximize the power/volume ratio. Three-cell batteries weigh 6 grams, occupy 6 cc, and produce 2.1 watts at maximum power operating around 1000°C. on hydrogen and oxygen; the current density at these conditions exceeds 750 ma./sq. cm. This performance is equivalent to 150 watts/pound and 9500 watts/cu. ft. of battery components. The measured load curves of these batteries check the predictions based on simple theory. Large power systems can be constructed by joining large numbers of optimized cells with the techniques used in constructing the three-cell batteries. Studies show that systems larger than 0.5 kilowatt can maintain their operating temperature without auxiliary heating; they will weigh less than 50 pounds/kilowatt and occupy less than 0.3 cu. ft./kilowatt.

The basic component of the Westinghouse solid-electrolyte fuel cell is the $(ZrO_2)_{0.85}$ $(CaO)_{0.15}$ [or $(ZrO_2)_{0.9}$ $(Y_2O_3)_{0.1}$]electrolyte. This material is an impervious ceramic which has the ability to conduct a current by the passage of $O^=$ ions through the crystal lattice. The ease with which these ions pass through the electrolyte is measured by the electrical resistivity, ρ_b, of the electrolyte. Values of ρ_b for both $(ZrO_2)_{0.85}$ $(CaO)_{0.15}$ and $(ZrO_2)_{0.9}$ $(Y_2O_3)_{0.1}$ as functions of temperature (T) are given in Figure 1(4). The resistance of a disk of $(ZrO_2)_{0.85}$ $(CaO)_{0.15}$ electrolyte, 2 inches in diameter and 15 mils thick, is about 0.1 ohm at 1000° C.

In Fuel Cell Systems; Young, G., el al.;
Advances in Chemistry; American Chemical Society: Washington, DC, 1969.

Publication Date: January 1, 1969 | doi: 10.1021/ba-1965-0047.ch024

Fabricating the Cell

To fabricate a cell from such a disk, porous platinum electrodes are applied to both sides. On the lower electrode of Figure 2, a molecule of oxygen from the surroundings acquires four electrons and forms two $O^=$ ions, which enter the crystal lattice of the ceramic. At the upper electrode, two $O^=$ ions emerge from the electrolyte, give up four electrons, and recombine to form oxygen. The lower electrode is positively charged; the upper is negatively charged if oxygen in the form of $O^=$ ions flows upward in the electrolyte as indicated in Figure 2.

The most direct method for bringing about this flow is to construct one chamber around the lower electrode in which oxygen is kept at a high partial pressure and another chamber around the upper electrode in which the partial pressure of oxygen is maintained at a low value. In this case, the observed open-circuit voltage of the cell, E_t, can be computed from

$$E_t(4F) = RT \ln (P_{O_2,H}/P_{O_2,L}) \quad (1)$$

where $4F$ = 4 (the Faraday number) = quantity of charge transferred per mole of O_2 passing through the electrolyte, 386,000 coulombs/mole
R = universal gas constant, 8.134 watt-sec./°K mole
T = absolute temperature of cell, °K.
$P_{O_2,H}$;$P_{O_2,L}$ = O_2 partial pressures in lower and upper chambers.
$RT \ln (P_{O_2,H}/P_{O_2,L})$ = work per mole obtained from reversible, isothermal expansion of a gas at temperature, T, watt-sec./mole.

Utilization as Fuel Cell

The device can be utilized as a fuel cell (*2, 6, 7*) by flowing oxygen or air to the lower chamber. If atmospheric air is used, the oxygen partial pressure in the lower chamber is maintained at about 0.2 atm. Fuel flows through the upper chamber, combines with any oxygen present, and reduces the oxygen partial pressure in the fuel chamber to about 10^{-16} atm. (The total pressure in both chambers is 1.0 atm.) The calculated value of E_t in this instance is approximately 1.0 volt. The oxygen partial pressure—$P_{O_2,L}$—in equilibrium with any fuel and its combustion products can be computed from their partial pressures in the fuel chamber and from the equilibrium constant for the overall combustion process. The voltage developed by the cell can be, in turn, related to the free energy of combustion for the fuel. This specific relationship has been derived for hydrogen-oxygen reactants elsewhere (*1*).

When a current (I) is drawn from the terminals, the voltage (V) of the cell drops below the open-circuit voltage (E_t) because of resistance losses in the electrolyte and electrodes.

$$V = E_t - IR \quad (2)$$

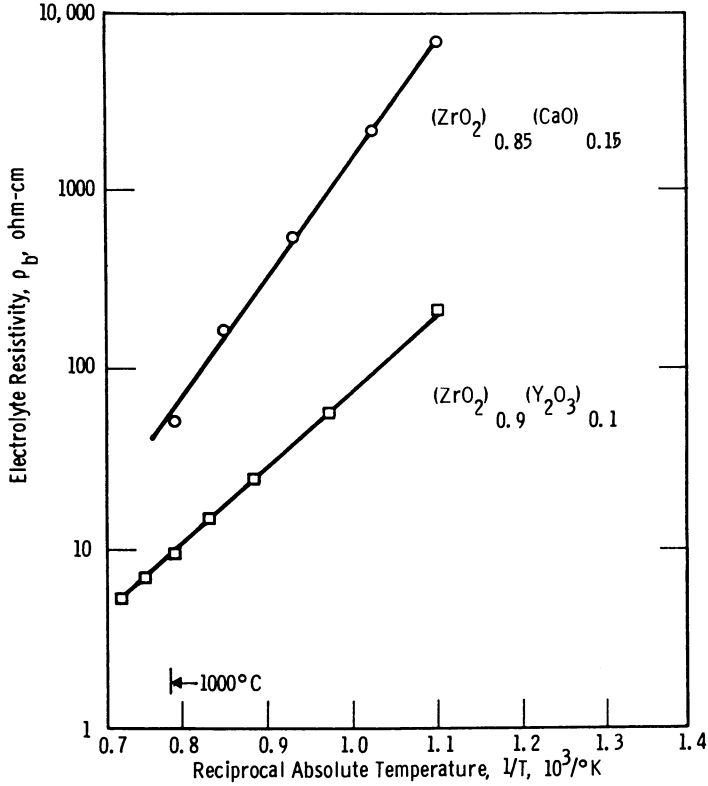

Figure 1. Electrolyte resistivity-temperature characteristics (CaO and Y_2O_3 stabilized ZrO_2)

where E_t is the voltage computed from Equation 1, and R is the ohmic resistance of electrodes and electrolyte. An approximate expression for the resistance (R) of a cell is

$$R = \rho_b\delta_b/A_b + (\rho_e/\delta_e)(L_e/P_e) \quad (3)$$

where δ_b = electrolyte thickness
A_b = active cell area
ρ_e/δ_e = resistivity-thickness quotient for the cell electrodes (Figure 3). This quantity has been determined experimentally by an adaption of a method developed by van der Pauw (5) for the measurement of surface conductivity.
L_e = mean distance traveled by the electronic current in the electrodes passing from the plus to the minus terminal of the cell
P_e = mean width of the electrode perpendicular to the direction of electronic current flow

For a cell operating at 1000° C. using a $(ZrO_2)_{0.85}$ $(CaO)_{0.15}$ electrolyte, 5 cm. in diameter and 0.04 cm. thick,

Publication Date: January 1, 1969 | doi: 10.1021/ba-1965-0047.ch024

$$R \cong \frac{(60\Omega - \text{cm.})\ (0.04\ \text{cm.})}{(4\pi)\ (5\ \text{cm.})^2} + (0.44\ \text{ohm})\ \frac{(2.5\ \text{cm.})}{(2\pi)\ (2.5\ \text{cm.})}$$

$$\cong 0.12 + 0.07 = 0.19\ \text{ohm}$$

If the electrodes of the cell are sufficiently porous, the *IR* loss—as indicated in Equation 2—is the only voltage loss in the cell; there are no appreciable voltage drops in the solid-electrolyte cell attributable to the slowness of diffusion or chemical reaction.

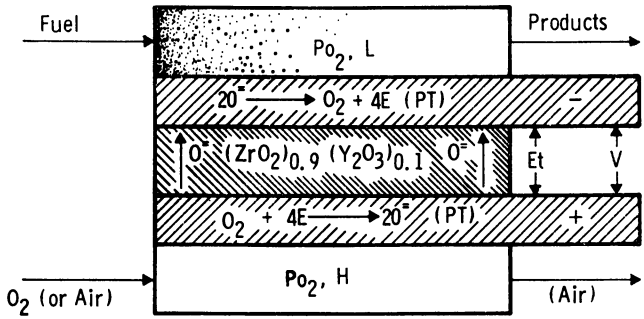

Figure 2. Solid electrolyte fuel cell

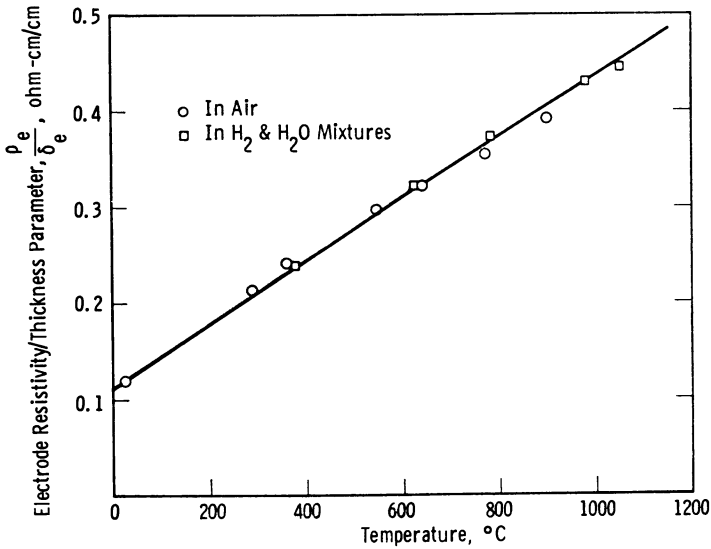

Figure 3. Characteristics of air-sprayed platinum electrodes

Characteristics of Single Cells

A number of single cells based on these principles have been constructed and tested. The components of a disk cell with an effective

Publication Date: January 1, 1969 | doi: 10.1021/ba-1965-0047.ch024

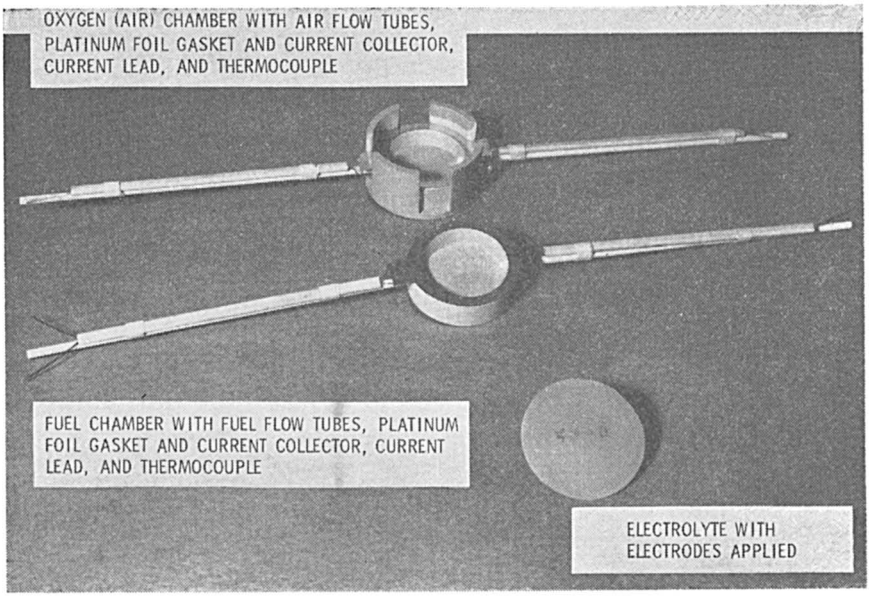

Figure 4. Single cell test assembly

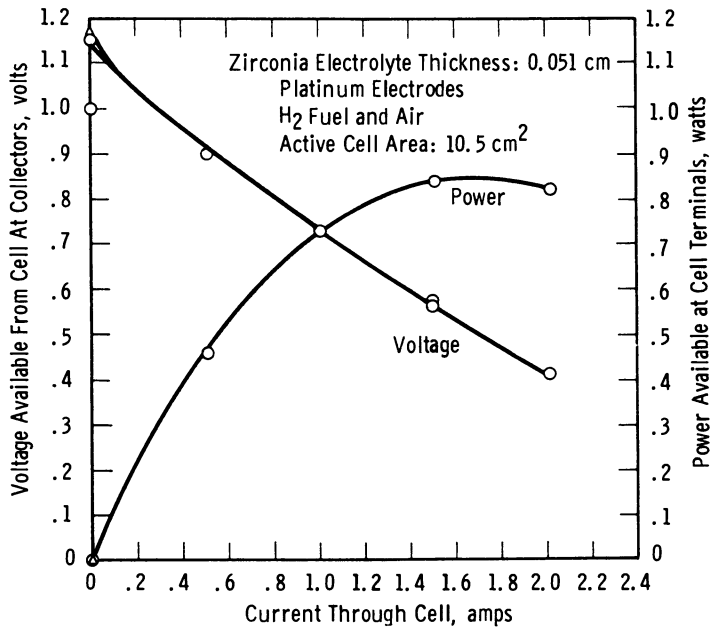

Figure 5. Voltage and power output of Westinghouse solid electrolyte fuel cell

diameter of 1.3 inches are shown in Figure 4, and the performance of such a cell is shown in Figure 5. The open-circuit voltage of the cell with

Publication Date: January 1, 1969 | doi: 10.1021/ba-1965-0047.ch024

hydrogen fuel is 1.15 volts; its resistance is about 0.4 ohm at the operating temperature, 1010° C. The maximum power delivered by the device is 0.85 watt, and the current density at these conditions is 150 amp/sq. ft. No variation in temperature with load current was observed in testing this cell.

Solid-Electrolyte Fuel Cell Batteries

Solid-electrolyte fuel cell batteries have been investigated. One type of battery is constructed of short, cylindrical electrolyte segments shaped so that they can be fitted one into the other and connected into a long tube by bell-and-spigot joints. Figure 6 shows an electrolyte segment. A mathematical analysis has been carried out to determine the active cell length (L) which maximizes the power per unit of cell volume for given values of $\rho_b\delta_b$, electrolyte resistivity-thickness product; ρ_e/δ_e, the electrode resistivity-thickness quotient (Figure 3); l, the seal length; and R_{eo}, the electrical resistance of the metal alloy joint which both makes the seal and connects the individual cell segments electrically in series.

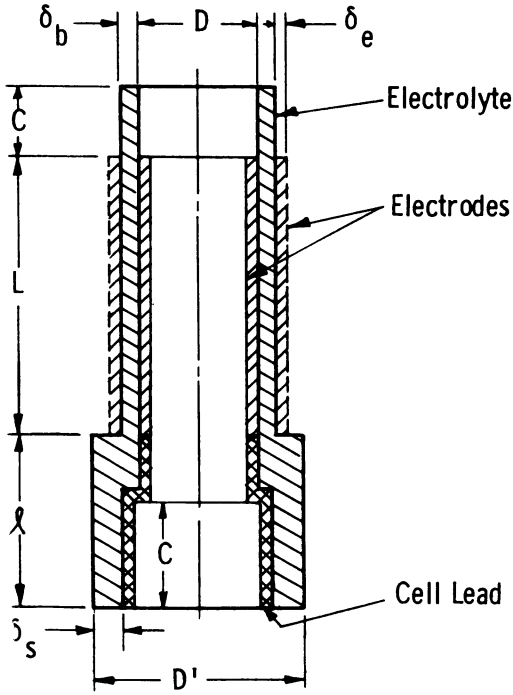

Figure 6. Cross section of basic cell unit for bell-and-spigot design

An optimized three-cell battery with bell-and-spigot joints is shown in

Publication Date: January 1, 1969 | doi: 10.1021/ba-1965-0047.ch024

Figure 7. One of the platinum wires at each end of the cell stack is the current lead to the battery; the other wires are probes for measuring potentials throughout the battery.

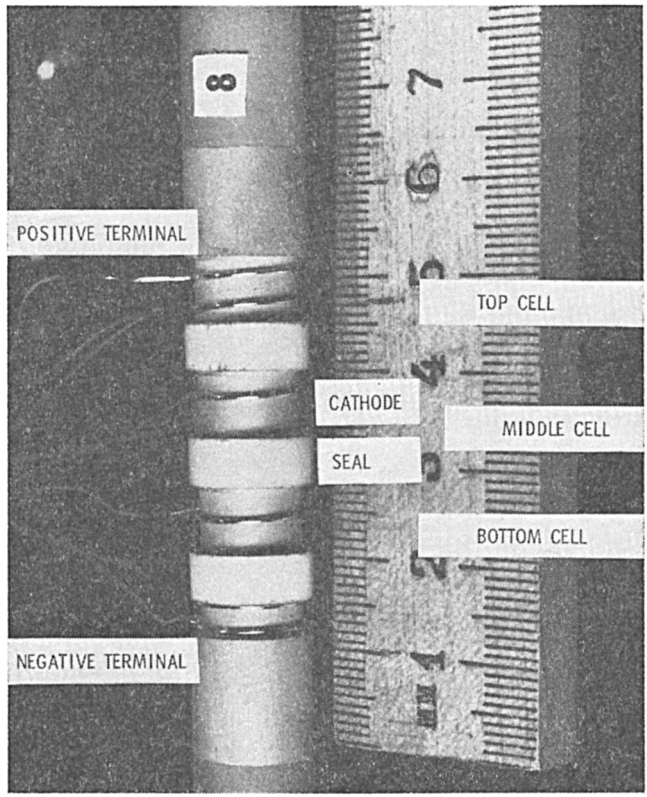

Figure 7. Three-cell segmented tube battery with bell-and-spigot design

Publication Date: January 1, 1969 | doi: 10.1021/ba-1965-0047.ch024

Performance of Battery on Hydrogen Fuel and Air

The performance of the battery on hydrogen fuel saturated with water at 20° C. and air is shown in Figure 8. The fuel gas flow rates were sufficiently large so that in no case did the mole fraction of water in the fuel gas stream leaving the battery exceed 0.15. Under these conditions the measured voltages developed by each cell in the three-cell battery did not differ significantly. For this reason only the over-all battery voltages are given. The open-circuit voltage of the device is below the expected 3.3 volts because of some shorting of the cells occuring in the seal region.

The electrolyte in the seal region—designated by "*l*" in Figure 6—acts as a high resistance shunt between successive anodes of cells in the series-

connected battery. As a result, circulating currents occur in the individual cells of the battery. Such shorting has been determined to draw about 100 ma. in each cell (3); improved seal design will minimize this loss. In spite of this problem, a current density greater than 450 ma./sq. cm. has been achieved in this battery at the maximum power point— about 1.2 watts. Three of the four joints required in the fabrication of the battery (Figure 8) have been demonstrated to be tight with a helium leak detector. The leak was determined to pass between the oxygen surrounding the battery directly to the hydrogen inside through a small passage in the brazing metal filling the joint. The oxygen leak rate through the fourth joint was less than the oxygen added to the fuel by a current flow of 20 ma.

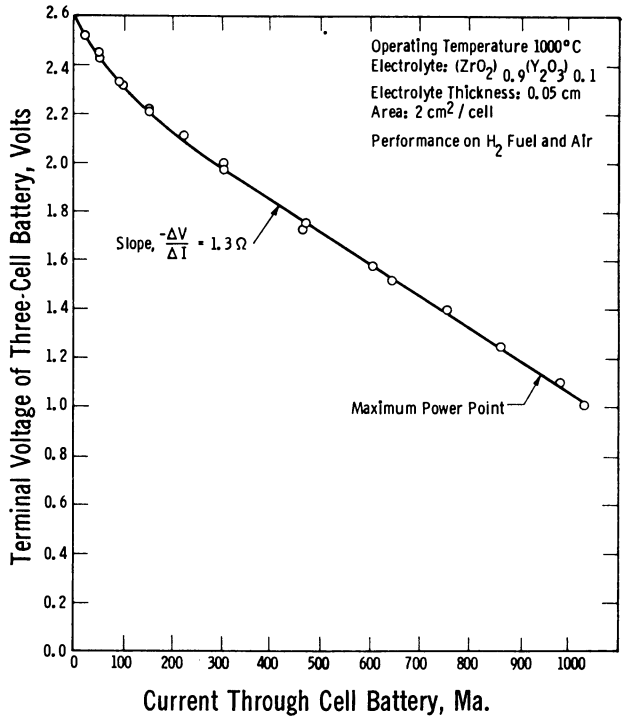

Figure 8. Voltage-current characteristics of three-cell segmented tube battery with bell-and-spigot joints (hydrogen fuel and air)

Performance of Battery on Hydrogen and Pure Oxygen

The performance of this same three-cell battery with hydrogen fuel and pure oxygen is shown in Figure 9. The open circuit voltage is 2.9 volts. The current density at maximum power was 750 ma./sq. cm. At the maximum power point, the battery produces 2.1 watts; and each cell segment, 0.7 watt—about the same as an ordinary flashlight battery.

Publication Date: January 1, 1969 | doi: 10.1021/ba-1965-0047.ch024

The segmented-tube bell-and-spigot battery gives promise of providing a compact, lightweight power system.

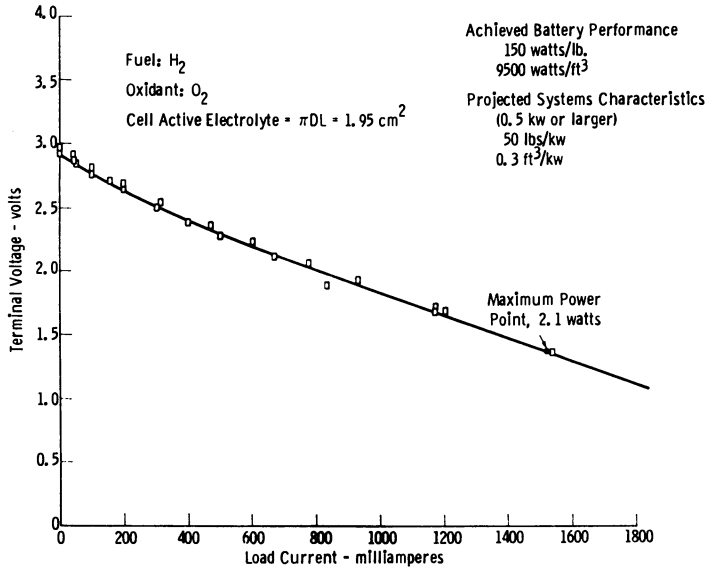

Figure 9. Voltage-current characteristics of three-cell segmented tube battery with bell-and-spigot joints (hydrogen fuel and oxygen)

Cell Segment Characteristics

The characteristics of the cell segments which make up this battery are:

Over-all length, $(L + l) = 0.58 + 0.53 = 1.11$ cm.
Mean diameter, $D = 1.07$ cm.
Electrolyte material: $(ZrO_2)_{0.9}$ $(Y_2O_3)_{0.1}$
Electrolyte resistivity-thickness parameter at 1000°C., $\rho_b\delta_b = 0.4$ ohm-sq. cm.
Electrode material: porous platinum
Electrode resistivity/thickness at 1000°C. $(\rho_e/\delta_e) = 0.43$ ohm-cm./cm.
Segment weight (including one joint = 1.97 grams
Segment volume (including one joint) = 2.0 cc.

The electrodes of the cell are quite light, and the total weight of the cell is also small—about 2.0 grams. If the cells are operated at maximum power, the power produced is equivalent to 160 watts/lb. of electrolyte and electrodes. (This figure does not include battery casing, insulation, and auxiliaries.) The power per unit volume of the cell unit is 9.5 kw./cu. ft. These performance figures can still be improved by developing electrodes with lower ρ_e/δ_e values, using electrolyte materials with lower ρ_b values, and optimizing the seal dimensions. More power/volume can also be obtained by using smaller diameter cells.

Publication Date: January 1, 1969 | doi: 10.1021/ba-1965-0047.ch024

Publication Date: January 1, 1969 | doi: 10.1021/ba-1965-0047.ch024

Solid-Electrolyte Fuel Cell Systems for Space

In order to provide a useful power source it is necessary not only to combine the unit cells into batteries but also to provide manifolding, casing, and insulation. All these components must be integrated into a system. A series of 500-watt solid-electrolyte fuel cell systems have been designed for use in space. Stacks of cells connected by bell-and-spigot joints are contained in an insulated cylindrical can which is maintained at the 1027° C. operating temperature by the heat generated in operating the system at the design power. The hydrogen fuel flows inside each tube stack and the oxygen oxidant fills the can housing the stacks (Figure 10). The gas stream emerging from the stacks is water vapor with 4 mole % or less unburned hydrogen; this gas is exhausted to the surroundings.

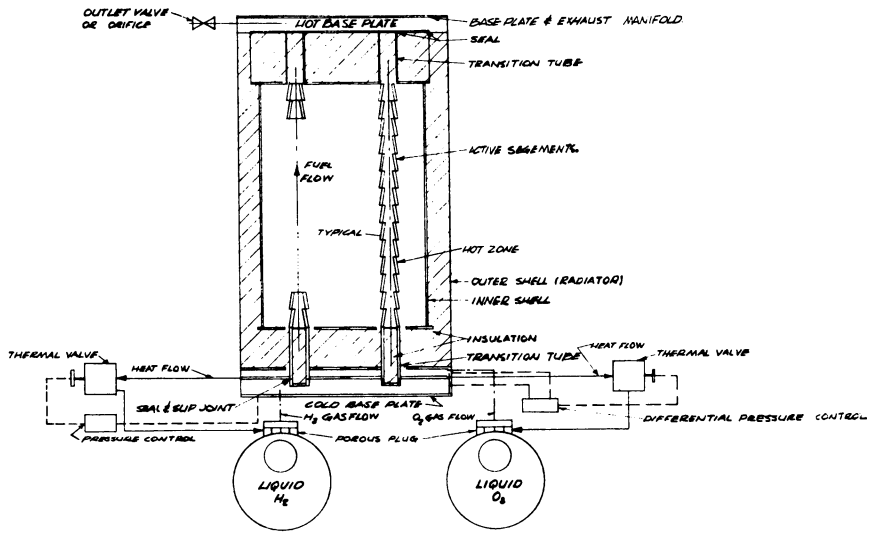

Figure 10. Diagram of over-all cell system

Minimum-weight 500-watt systems have been determined for 10-hour, 100-hour, and 1000-hour total mission lengths using 1-inch diameter stacks. A choice of 1/2-inch diameter stacks would have resulted in a smaller, lighter device. For a 100-hour mission, the estimated weight of the fuel-cell system (including the cell battery, casing, manifolding, insulation, radiator, and controls) is 25 pounds; the estimated weight of hydrogen and oxygen reactants and reactant storage system is 115 pounds. For the 1000-hour mission, the estimated minimum fuel cell system weight is 47 pounds; the reactant and reactant storage weight is 643 pounds.

Advantages of Solid-Electrolyte Fuel Cells

Although particular solid electrolyte fuel cell systems have been considered, modifications can be made to meet other specific requirements. In addition to their light weight, solid-electrolyte fuel cell systems have distinct advantages over other fuel cells: They are compact; their high operating temperature enables the heat generated in operating the cell to be radiated to the surroundings without weighty, complex cooling systems and radiators; the electrolyte is physically and chemically stable; there is no difficulty in removing water from the cell (it flows from the system in vapor form); and the system operates independently of gravitational forces.

For all these reasons, the solid-electrolyte fuel cell system is a promising candidate for generating power in space.

Publication Date: January 1, 1969 | doi: 10.1021/ba-1965-0047.ch024

Literature Cited

(1) Archer, D. H., and Sverdrup, E. F., "Solid Electrolyte Fuel Cells," *Proc. 16 Annual Power Sources Conference,* pp. 34–39, PSC Publications, Red Bank, N. J. (1962).
(2) Archer, D. H., Sverdrup, E. F., English W. A., and Carlson, W. G., "An Investigation of Solid-electrolyte Fuel Cells," *Technical Documentary Report* **ASD-TDR-63-448,** USAF Aero-Propulsion Laboratory, Wright-Patterson Air Force Base, Ohio (1963).
(3) Archer, D. H., Zahradnik, R. L., Severdrup, E. F., English, W. A., Elikan, L., and Alles, J. J., "Construction and Performance of 20-Cell Solid-electrolyte Batteries," *Proc. 18th Power Sources Conference,* PSC Publications, Red Bank, N. J. (1964).
(4) Strickler, D. W., and Carlson, W. G., *J. Am. Ceramic Soc.* **47,** 3, p. 122–27 (1964).
(5) van der Pauw, L. J., *Phillips Research Reports* **13,** pp. 1–9, (1958).
(6) Weissbart, J., and Ruka, R., in "Fuel Cells," vol. 2 (edited by George J. Young) pp. 37–49, Reinhold, New York (1963).
(7) Weissbart, J., and Ruka, R., *J. Electrochem. Soc.* **108,** 8, pp. 723–26 (1962).

RECEIVED February 17, 1964.

A Coal-Burning Solid-Electrolyte Fuel Cell Power Plant

R. L. ZAHRADNIK, L. ELIKAN, and D. H. ARCHER

Westinghouse Research Laboratories, Pittsburgh, Pa.

Publication Date: January 1, 1969 | doi: 10.1021/ba-1965-0047.ch025

A plant is proposed which combines a coal-gasification unit with a high temperature solid-electrolyte fuel cell battery to produce an efficient power generation system. The special requirements imposed on the gasifier by its coupling with a fuel cell battery are discussed and two avenues of investigation—one experimental, one analytical—are proposed. The results of a computer simulation of the over-all plant are presented and preliminary projections of plant economics and characteristics are reported. The many research and development problems, which must be solved before such plants are technically and economically feasible, are pointed out, and the progress made towards their solution is discussed.

The direct conversion of the energy of coal into useful electrical power has long commanded the serious attention of many investigators. This paper describes how in principle a coal gasification unit can be combined with a high temperature solid electrolyte fuel cell battery to produce just such a direct energy conversion system.

Solid Electrolyte Fuel Cell

The basic component of the Westinghouse solid electrolyte fuel cell is the zirconia-calcia or zirconia-yttria electrolyte. This material is an impervious ceramic which has the unique ability to conduct a current by the passage of $O^=$ ions through the crystal lattice. The ease with which these ions pass through the electrolyte is measured by the electrical resistivity of the electrolyte. Values of this resistivity for both types of electrolyte

In Fuel Cell Systems; Young, G., el al.;
Advances in Chemistry; American Chemical Society: Washington, DC, 1969.

as functions of temperature have been published in several places (*4*, *9*).

Fuel cells have been made by applying porous platinum electrodes to this material (*16*). The operating principles of the resultant cells have been discussed (*5*), and optimized batteries constructed from such cells have been described, (*3*). In brief these batteries operate at about 1000° C. and consist of short, cylindrical electrolyte segments of about 15 mils thickness shaped so that they can be fitted one into the other and connected into long tubes by bell-and-spigot joints, as shown in Figure 1.

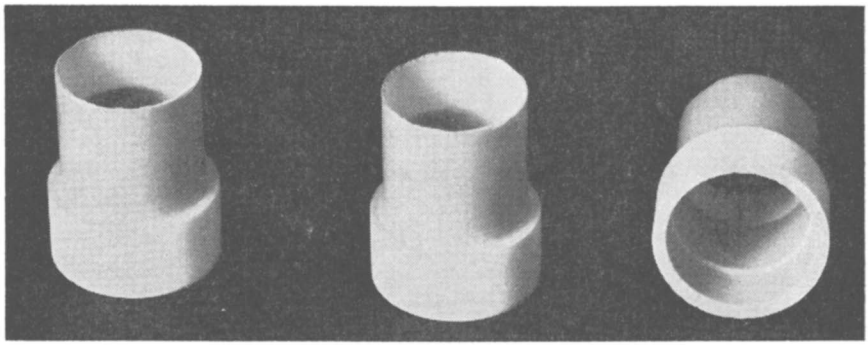

Figure 1. Bell-and-spigot segments

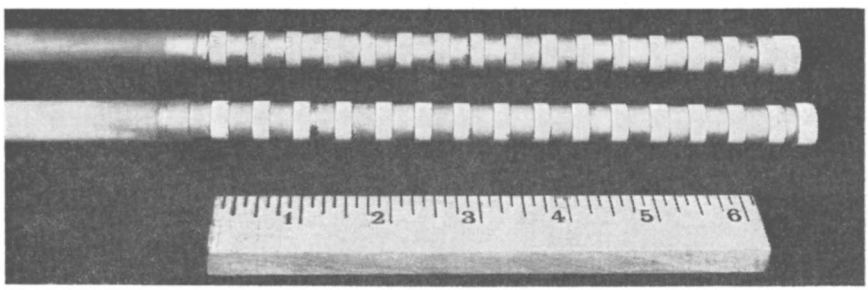

Figure 2. Two 15-cell solid electrolyte fuel cell batteries without leads

The over-all length of an individual segment is 1.1 cm. with a mean diameter of 1.07 cm. and an active length of 0.6 cm. The segment weighs 2 grams and occupies a volume of 2.0 cc. Electrodes are applied to the inside and the outside of these segments which then have an over-all resistance of about 0.2 to 0.3Ω. The inner electrode of one segment is attached to the outer electrode of the adjacent segment, in this way connecting the individual segments electrically in series. Gaseous fuel passes through the center of the resultant, segmented tube, and oxygen or air is supplied on the outside. Figure 2 shows two 15-cell batteries constructed on this principle.

The performance of this and similar batteries has been evaluated for a

Publication Date: January 1, 1969 | doi: 10.1021/ba-1965-0047.ch025

variety of fuels, using either air or pure oxygen as the oxidizing agent. With hydrogen fuel and pure oxygen, a three-cell battery has produced an open circuit voltage of 2.9 volts. The current density at maximum power was 750 ma./sq. cm. At the maximum power point the battery produced 2.1 watts, and each cell segment 0.7 watt—about the same as an ordinary flashlight battery (*1, 6*).

System Configuration

In order to utilize such batteries in the production of electrical power from coal, it is necessary to devise a reasonable over-all system for the purpose. As far as the present type cell is concerned, a gaseous fuel is required for cell operation. In order to provide such a fuel to the fuel cell batteries, the scheme shown in Figure 3 has been devised.

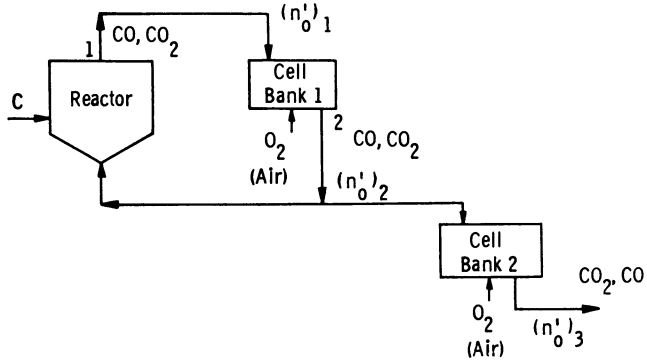

Figure 3. Simplified coal burning fuel cell system

Essentially, coal (indicated as carbon on the figure) is introduced into a reactor, into which recirculating gases from cell bank *1* also enter. Cell bank *1* consists of a number of fuel cell batteries of the kind just described. The gases from this cell bank consist primarily of carbon monoxide and carbon dioxide (along with hydrogen and water in some definite ratio). In the reactor, some carbon dioxide and water is reduced to hydrogen and carbon monoxide by reacting with the coal. This results in a gas composition leaving the reactor which has higher CO/CO_2 and H_2/H_2O ratios than that of the entering gas. The gas leaving the reactor is then cleaned and passed, without cooling, into the fuel cell bank *1*. There it serves as fuel for the cell unit, combining with oxygen which has been ionically transported through the cell electrolyte, resulting in power generation. The gases leaving this cell bank are split into two streams. One stream is recirculated to the reactor at a given recycle rate, completing the major system loop. The second stream is sent to fuel cell bank

Publication Date: January 1, 1969 | doi: 10.1021/ba-1965-0047.ch025

2, which completes the combustion of carbon monoxide to carbon dioxide and hydrogen to water.

The reason for this system configuration is that it allows all of the oxygen which enters the system to react with the coal to pass through the electrolyte and thereby contribute to the electrical energy output of the system. In addition, by limiting the degree of oxidation in cell bank *1*, the concentrations of carbon dioxide and water entering the reactor are only slightly removed from their equilibrium values. This means the bed operates under more nearly reversible conditions, so that over-all the maximum electrical energy output from the coal-oxygen reaction is recovered. To obtain such recovery, however, an over-sized coal reactor, excessively large cell banks relative to the power produced, and high recycle rates would have to be employed. A compromise must be effected between the desire to obtain high recovery and the desire to avoid large and expensive equipment. Much of the work to date on this system has been geared to locate those optimum conditions which best effect this compromise.

Publication Date: January 1, 1969 | doi: 10.1021/ba-1965-0047.ch025

Reactor Considerations

Because the reactor must contribute to an over-all system optimum, certain of its design features must be tailored specifically to the task of gasifying coal in a rather unusual way. In most conventional gasifiers, oxygen is introduced at some point directly into the reactor. The fuel-cell power plant has been so designed, however, that oxygen is introduced into the reactor only in the form of carbon dioxide, water, and carbon monoxide. The coal may be considered to be gasified primarily by the two reactions:

$$C + CO_2 \rightarrow 2CO \quad (1)$$

$$C + H_2O \rightarrow H_2 + CO \quad (2)$$

which proceed at rather slow rates compared to the direct oxidation reaction:

$$C + O_2 \rightarrow CO_2 \quad (3)$$

Moreover, Reactions 1 and 2 are endothermic, as compared to Reaction 3 which is quite exothermic, meaning that heat will have to be supplied to the reactor where 1 and 2 occur. The problem of supplying this heat considerably complicates the over-all reactor design.

Because Reactions 1 and 2 proceed at relatively slow rates, it is advantageous to take steps to increase the rate of these reactions. Two such steps which may be taken are the maintenance of a high reaction temperature or the use of a highly reactive fuel. The temperature level of the reactor is limited, however, because the reactions

which occur there are endothermic. This means that heat must be supplied to the reactor from an external source—for example the fuel-cell banks where exothermic oxidation reactions are taking place, and internal battery heating as a result of I^2R losses is occurring. This transfer may be accomplished either directly through the walls of the gasifier or indirectly in the sensible heat of the recirculating gases. However, some finite temperature gradient will be required to transfer this heat, constraining the reaction temperature to less than the source temperature. If the source is the cell banks, an upper temperature limit is imposed by the mechanical and structural properties of the cells. This is reflected in an upper temperature limit on the reactor of about 1000° C.

At this temperature, many of the fuels, which appear attractive for fuel cell use because of the clean nature of their gasified products, become unusable because of their low reactivity. On the other hand, those fuels which are reactive at this temperature produce quantities of tars, pitches, and other impurities which may have a deleterious effect on cell operation. The presence of such undesirable gasification by-products is increased even further in the absence of a direct supply of oxygen in the reactor. The issue is complicated by the fact that cell performance is most efficient when the fuel contains high concentrations of either carbon monoxide or hydrogen. In the reactor, however, large quantities of carbon monoxide and hydrogen inhibit Reactions 1 and 2, retarding their reaction rate. This effect compounds the problem of striking an effective compromise between a reasonable reactor size and highly efficient cell operating conditions.

To study the effect of these factors on the over-all system performance, two avenues of investigation have been pursued. A small test reactor has been built to which a stream of gases containing carbon monoxide, carbon dioxide, hydrogen, and water can be added, simulating the recycle gases in the proposed design. Second, a systems study of the proposed plant has been undertaken, culminating in a computer simulation of both reactor and cell banks. The purpose of this study was to demonstrate the engineering feasibility of such a plant, to assess its economic desirability, and to point out areas where further development effort would be most beneficial.

Test Reactor

The test reactor is shown in Figure 4. It consists of a $1^3/_8$-inch i.d. Inconel tube located in a commercial four-zone furnace. This reactor itself is of conventional fixed bed design with the exception of two small fuel cells which are located near its inlet and outlet. (The inlet cell is barely visible in Figure 4). The open circuit voltages of these cells are used to determine the compositions of the inlet and outlet streams, thereby

American Chemical Society
Library
1155 16th St., N.W.
Washington, D.C. 20036

In Fuel Cell Systems; Young, G. J., et al.;
Advances in Chemistry; American Chemical Society: Washington, DC, 1969.

Publication Date: January 1, 1969 | doi: 10.1021/ba-1965-0047.ch025

providing a measure of the extent of gasification which occurs in the reactor. The use of the cells as measurement devices allows a rapid and convenient analysis of the gases to be obtained immediately upon their exit from the fuel bed, without cooling or tampering with the gas stream in any way. Initial runs using this setup have been entirely satisfactory, and a report from this laboratory on the observed gasification kinetics is being prepared.

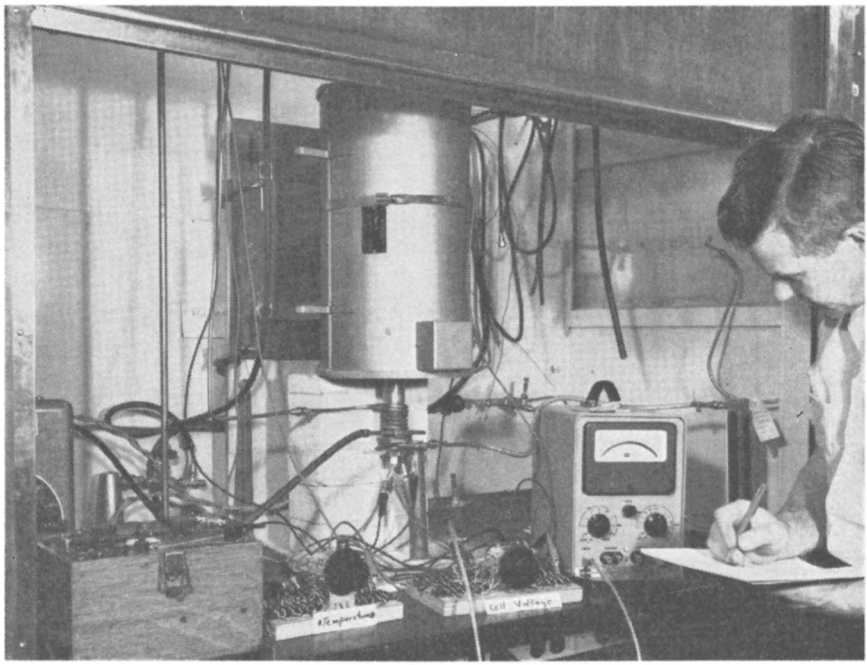

Figure 4. Test reactor

Publication Date: January 1, 1969 | doi: 10.1021/ba-1965-0047.ch025

In addition to providing kinetic data for the various coals of interest, the test reactor serves several other purposes. It is being used to study not only the inhibiting effect of high carbon monoxide and hydrogen concentrations on the gasification but to examine the effects of operating very near to the equilibrium gas compositions, which yield the highest cell efficiency. The problems of cleaning and filtering the reactor output gases are being examined, and the effects of such materials as fly-ash, pitches, and tars on cell performance are being explored. Over-all, the test reactor is used to supply necessary engineering information for the computer simulation so that optimum system operating conditions and general feasibility can be determined.

System Simulation

Some preliminary results of this simulation may be of interest at this time. The simulation includes both fixed and fluidized bed conditions, operated either isothermally, or adiabatically. It includes both the reactor and cell banks *1* and *2*. In the reactor, the surface reactions between carbon and steam and carbon dioxide are assumed to be controlling. In the gas phase, the "water gas" equilibrium is assumed to hold. Rate expressions of the Langmuir-Hinshelwood type were adopted for the surface reactions, and published data for the specific constants were employed in the simulation (*7*, *10*, *11*, *14*). In the cell banks, equilibrium conditions were assumed to prevail as far as the gas composition was concerned, with the generated voltages modified to account for losses due to both internal cell resistance and cell polarization.

Figure 5 illustrates how the gas composition varies in its passage through the main system loop, as predicted by the computer simulation. As carbon dioxide and water react with the carbon, their percentages decrease, while the percentage of carbon monoxide and hydrogen increase.

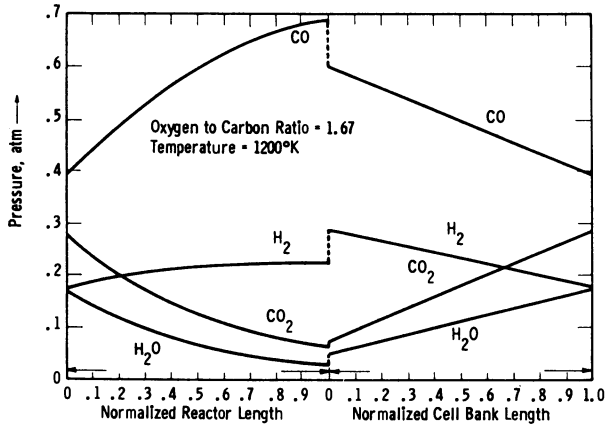

Figure 5. Simulated reactor and cell bank concentration profiles

In the gas space immediately adjacent to the coal bed, provision has been made for some volatile material to enter the gas stream; this is indicated by the sharp change in composition indicated by the dotted lines. In the cell banks as oxidation occurs, the percentage of carbon monoxide and hydrogen decrease while carbon dioxide and water increase. In the example shown in Figure 5, the hydrogen to carbon ratio (H/C) is 1.0. The oxygen to carbon ratio (O/C) at the inlet to the reactor is 1.67, and the system is considered to be isothermal at 1200° K.

Publication Date: January 1, 1969 | doi: 10.1021/ba-1965-0047.ch025

In addition to predicting the change in gas composition as it moves through the system the simulation predicts the size reactor needed to generate sufficient gaseous products to attain an assigned power level, if a particular fuel, an inlet O/C ratio, a recycle rate (moles of carbon monoxide and carbon dioxide flowing through cell bank *1* per mole of carbon consumed in reactor), a per cent fuel burn up, and a system temperature are specified.

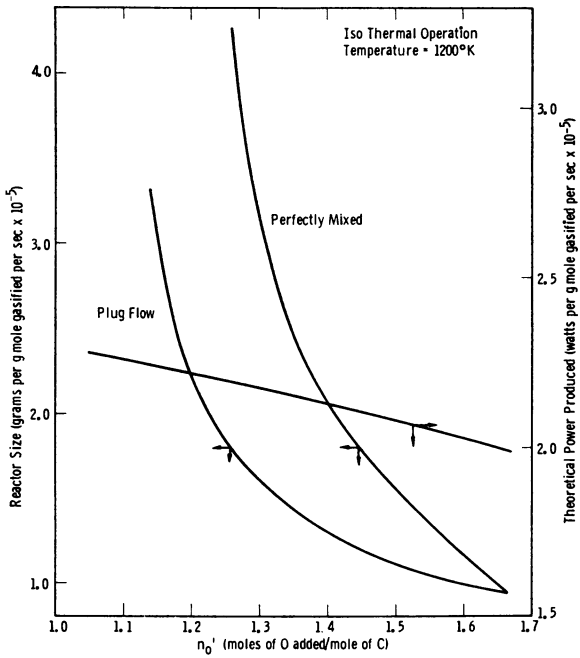

Figure 6. Reactor size and system power vs. conversion

Figure 6 shows how the reactor size required to gasify a gram-mole/sec. varies with conversion, for an inlet n'_0 value of 1.67 and temperature of 1200° K. Plotted on the same figure is a curve which represents the total theoretical power output of the system per gram-mole/sec. gasified and also as a function of conversion. Two cases are illustrated on the figure for reactor size: One corresponds to plug flow conditions in the reactor; the other corresponds to perfectly mixed conditions. The reactivity of the carbon in the bed itself was taken to be that for retort coke, and published rate data for this material were used to construct Figure 6 (*10, 11*).

Figure 7 shows how a normalized gasifier size depends upon degree of conversion. Here the size of the reactor in grams per 100 theoretical

Publication Date: January 1, 1969 | doi: 10.1021/ba-1965-0047.ch025

watts produced by the system is plotted against the oxygen to carbon ratio, n'_0. This figure is obtained from the data on Figure 6 by dividing reactor size by power produced, each per gram-mole gasified per second. The case presented in Figure 7 is for isothermal operation at 1200° K. Two inlet (n'_0) values, 1.25 and 1.67, are illustrated for both plug flow and perfectly mixed reactors. The gas flow in the cells is assumed to be plug flow in all cases. The size of a reactor for a particular configuration

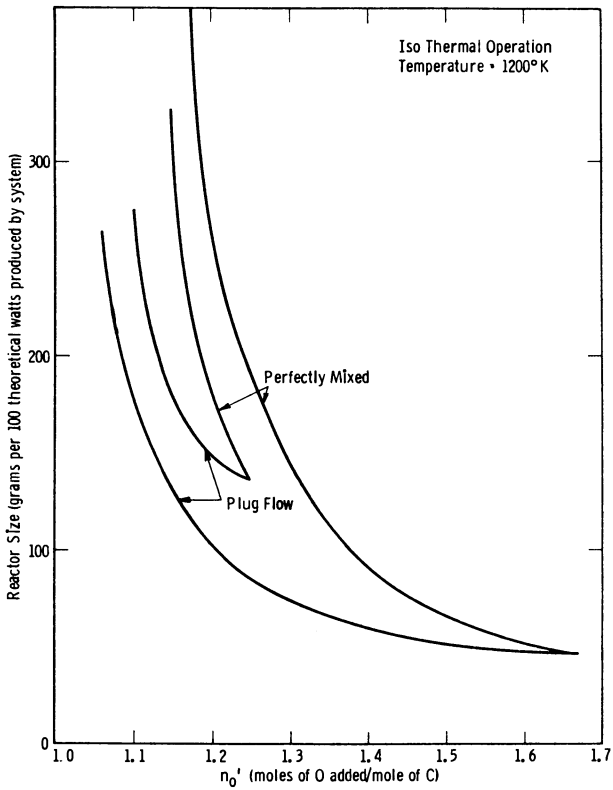

Figure 7. Effect of conversion on normalized reactor size

and inlet condition is obtained by locating the desired (n'_0), value on the abscissa and reading the ordinate for the appropriate curve. To demonstrate the effect of temperature on reactor size, Figure 8 shows a plot of reactor size against the reciprocal absolute temperature for an inlet (n'_0) of 1.67 and an outlet (n'_0) of 1.25.

In addition to such results obtained for isothermal operation, the simulation predicts system size and behavior under adiabatic conditions. In this case the net heat release by the exothermic reactions and I^2R

Publication Date: January 1, 1969 | doi: 10.1021/ba-1965-0047.ch025

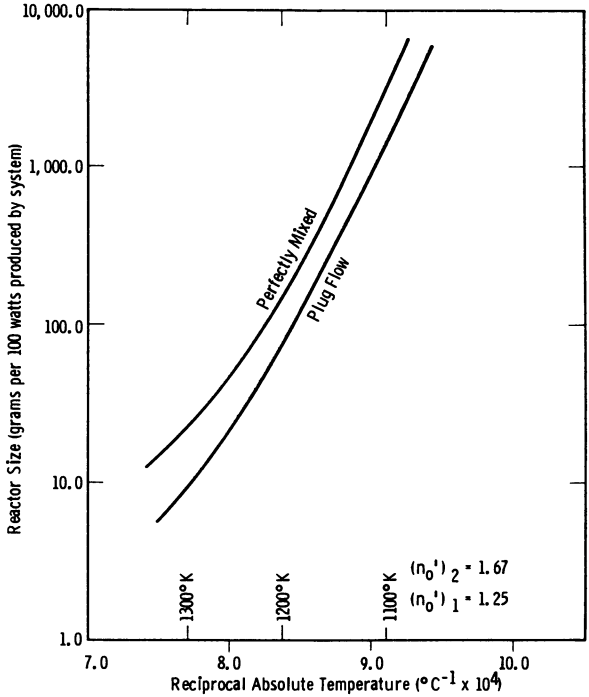

Figure 8. Influence of temperature on reactor size

losses in the cell banks contributes to increasing the sensible heat of the circulating gases. The heated gases then pass through the reactor, losing heat to the endothermic reactions which occur there. The simulation has shown that, depending on conversion and recycle rate, the temperature rise in the cells may exceed, balance, or be less than the temperature drop in the reactor, and careful design will be required to adjust effectively the various system parameters to attain a proper thermal balance.

Discussion

On the basis of the investigations both with present-day laboratory equipment and with the over-all system simulation certain key problems have emerged which require solution before the proposed plant can be considered as a feasible power generation system. There is considerable incentive to seek out these solutions, however, because of the many desirable features such a plant would have—for example, high over-all efficiency even for small sized plants, inherently simpler operation without moving parts, and compact over-all size.

Problems connected with the suggested coal gasifier center around the fact that heat must be supplied to the reactor and that the gasification

Publication Date: January 1, 1969 | doi: 10.1021/ba-1965-0047.ch025

temperature is not spectacularly high. Both of these factors indicate that a rather large scale reactor may be required compared to the idealized size obtained from the isothermal simulation. However Jolley, Poll, and Stanton (*8*), reporting on the fluidized gasification of noncaking coals with steam in a small pilot plant, have shown that reasonably good heat transfer through the walls of the gasification chamber can be attained with as little over-all temperature driving force as 100°C. This is encouraging in that it means that much of the heat which is generated in the cell banks can be transferred directly to the reactor by conduction through separating walls. Moreover, the temperature gradient required to do this is not excessive.

In addition to this external heating of the gasifier, some measure of internal heating will be accomplished by means of the recycle stream, which serves as a heat-carrying fluid as well as a gasification agent. Preliminary indications are that the recycle molar flow rate will be three to six times larger than the amount of coal gasified per unit time. This means that a good portion of the endothermic heat of reaction can be provided by the recirculating gases.

The final solution to this problem remains to be engineered, but for the reasons given here, there is some indication that a reasonable answer may be found, resulting in a reactor size per theoretical watt approaching that given in Figure 7.

The fuel cell batteries themselves are not finished products, to be sure, and still require considerable development effort. Essentially this effort is directed towards extending the life of the devices, minimizing associated electrode polarization losses, and reducing cell costs. Considerable progress has been made on these problems and reports concerning this progress have been published by this laboratory (*2*).

If these and other problems can be solved, the over-all plant described here provides an attractive method for the gasification and utilization of coal. Because it uses air as the oxidizing agent, this raw material cost is negligible. However, because only oxygen enters the major system process stream, the gasification step proceeds as if pure industrial oxygen had been used, with no nitrogen dilution of the gasified products. It is reported that the cost of oxygen represents 40 to 60% of the raw material costs of gasification processes using industrial oxygen (*15*). Thus, if viewed only as a gasification unit, the process offers the possibility of reducing a major portion of the raw material costs.

In addition to this savings, however, the attractiveness of the proposed scheme comes from the fact that the plant utilizes the gasified coal products in an extremely efficient manner. It has been estimated that the over-all efficiency of the proposed plant in converting coal to electricity will be about 60% (*13*). Present-day stations operate at efficiencies of 38 to 42%, with very large installations required to attain

Publication Date: January 1, 1969 | doi: 10.1021/ba-1965-0047.ch025

the higher figure (*12*). Since fuel costs represent 40 to 50% of the cost of generating electricity by present-day techniques, the improved efficiency of the proposed plant represents a highly desirable improvement.

To attain this efficiency, however, certain demands on system performance must be met. Table I gives the projected system characteristics and operating conditions based on an economic optimization of the system as currently envisioned (*13*). On the basis of this study, it has been suggested that if bell-and-spigot cells with internal resistance of 0.25 Ω can be made and fabricated into banks for 10 cents a cell and if a minimum payout time of five years can be used to recover the investment, return a profit, pay taxes, and provide maintenance (the cell life must obviously exceed five years), then coal-burning solid-electrolyte fuel cell power systems can produce electrical energy at 5 mils/kw.-hr.; the system efficiency will be 60%, and the current density in the cell banks, will be 700 ma./sq. cm.

Table I. Coal-Burning Solid-Electrolyte Fuel Cell Power System

Projected system	*Characteristics*
Over-all efficiency, %	60–70
Cell banks	
Current density, ma./sq. cm.	700
Cubic feet per kilowatt	0.3
Reactor volume, cu. ft./kw.	0.1–5.0
System	
Recycle ratio, moles recirculated per mole gasified	3–6
Fuel burn up, %	95–98

Cells have already been built which have an internal resistance of 0.3 Ω. The cost of materials for these cells is about 0.004 cent for zirconia and 0.03 cent for platinum, and effort is being expended to find suitable replacements for platinum to further reduce this raw material cost. Cells have operated at 750 ma./sq. cm. for short periods of time on hydrogen fuel. These facts indicate that solutions to the cell problems may be in the making. If they can be attained, along with reasonable solutions to the coal reactor problems, the proposed plant would offer much promise as a power generation station of the future.

Literature Cited

(1) Archer, D. H., *et al.*, ADVAN. CHEM. SER. **47**, 332 (1964).
(2) Archer, D. H., *et al.*, "Application of the Westinghouse Solid Electrolyte Fuel Cell to Use in Space," 17th Annual Proceedings, Power Sources Conference, May 1963.
(3) Archer, D. H., *et al.*, "An Investigation of Solid-electrolyte Fuel Cells," Tech. Doc. Rept. No. **ASD-TDR-63-448.**
(4) *Ibid.*, Third Quarterly Progress Report," **AF 33(657)-8251; BPS 2-3-3145-60813-17.**
(5) Archer, D. H., and Sverdrup, E. F., "Solid Electrolyte Fuel Cells," 16th Annual Proceedings, Power Sources Conference, May 2–24, 1962.

Publication Date: January 1, 1969 | doi: 10.1021/ba-1965-0047.ch025

(6) Archer, D. H., Sverdrup, E. F., and Zahradnik, R. L., "Coal Burning Fuel Cell Power System," 53rd National AIChE Meeting, Feb. 2–5, 1964.
(7) Gadsby, J., Hinshelwood, C. N., and Sykes, K. W., *Proc. Roy. Soc.* (*London*) **A187**, 129–51 (1946).
(8) Jolley, L. J., Poll, A., and Stanton, J. E., in "Gasification and Liquifaction of Coal," AIME Publ., New York, 1953.
(9) Kingery, W. D., *et al.*, *J. Am. Ceram. Soc.*, **42**, 394 (1959).
(10) Lewis, W. K., Gilliland, E. R., and McBride, G. T., Jr., *Ind. Eng. Chem.*, **41**, 1213–26 (1949).
(11) May, W. G., Mueller, R. H., and Sweetser, S. B., *Ibid.*, **50**, 1289–96 (1958).
(12) Olmstead, L. M., *Elec. World* (Oct. 7, 1963).
(13) Sverdrup, E. F., Zahradnik, R. L., and Archer, D. H., "Fuel Cell Power Generation Systems: An Appraisal," IEEE Winter Power Meeting, Feb. 3–7, 1964.
(14) Von Fredersdorff, C. G., *Inst. Gas. Technol. Research Bull*, No. **19**, (1955).
(15) Von Fredersdorff, C. G., and Elliot, M. A., in "Chemistry of Coal Utilization," John Wiley & Sons, New York, 1963.
(16) Weissbart, J., and Ruka, R., in "Fuel Cells, Vol. **2**, Reinhold Publishing Corp., New York, 1963.

RECEIVED March 31, 1964. This work was sponsored by the Office of Coal Research, Department of the Interior, Contract 14-01-0001-303. Presented on the Symposium on Gas Generation, Division of Fuel Chemistry, 147th Meeting of the American Chemical Society, Philadelphia, Penn., April 6, 1964.

Publication Date: January 1, 1969 | doi: 10.1021/ba-1965-0047.ch025

INDEX

Publication Date: January 1, 1969 | doi: 10.1021/ba-1965-0047.ix001

Publication Date: January 1, 1969 | doi: 10.1021/ba-1965-0047.ix001

In Fuel Cell Systems; Young, G., el al.;
Advances in Chemistry; American Chemical Society: Washington, DC, 1969.

Publication Date: January 1, 1969 | doi: 10.1021/ba-1965-0047.ix001

Publication Date: January 1, 1969 | doi: 10.1021/ba-1965-0047.ix001